# nature

THE INTERNATIONAL WEEKLY JOURNAL OF SCIENCE

## SILVER SERVICE

Metallic nanoparticles shine in the quantum size regime PAGES 417 & 421

BIOCHEMISTRY

### JURASSIC LAB

*Resurrecting ancient proteins to track evolution*

PAGE 390

MICROBIOLOGY

### THE FLU VIRUS AS MIMIC

*Histone-like protein hijacks host antiviral response*

PAGES 416 & 428

PALAEONTOLOGY

### OUT OF THE SHADOWS

*The mammals that thrived when dinosaurs ruled*

PAGE 457


NATURE.COM/NATURE

22 March 2012 £10

Vol. 483. No. 7390

9 770028 083095 12

# Introducing the new BioMed Central

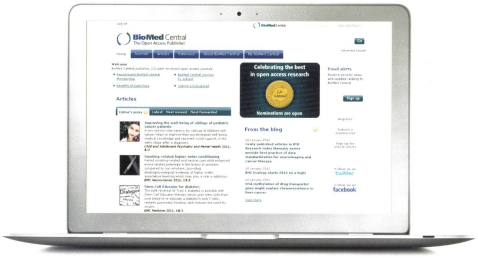


- A new look for the leading open access publisher
- Easy to navigate new website
- Over 220 open access journals across all areas of biology and medicine
- Streamlined online submission system
- Rigorous and efficient peer review
- Immediate archiving of articles in PubMed Central
- Excellent Impact Factors
- Editorial decisions handled by leading researchers
- Integrated support for audio, video and data files

## Discover for yourself at www.biomedcentral.com

BioMed Central
The Open Access Publisher

# nature OUTLOOK

**Published in the 1 March 2012 issue of *Nature* and available free online for six months**

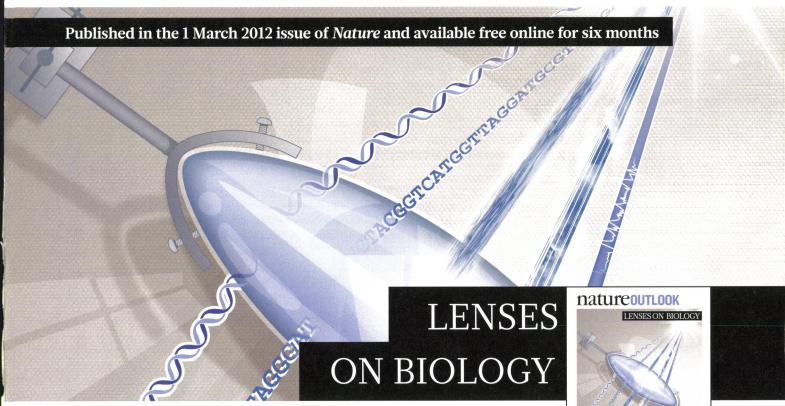

## LENSES ON BIOLOGY

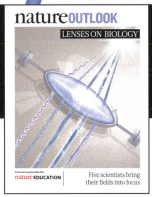


Immersed in the details of the latest laboratory advances, it's easy to lose track of the enormous impact biological sciences are having on our world. In this special edition of *Nature Outlook*, five top scientists explain how research in their specialties — cancer, climate change, stem cells, oceanography and synthetic biology — has changed our lives.

**Access** the Outlook free online for six months.
nature.com/nature/outlook/lenses_biology

Produced in partnership with:
nature EDUCATION
Publishers of *Principles of Biology*

Scan this tag to access the Outlook on your smartphone

nature publishing group npg

wpi World Premier International Research Center Initiative

# Upstart centers lead Japan in new directions

## Six success stories show how innovative policies lead to innovative science.

In Japan, not many females or foreigners head major institutes. Nor are there many researchers with joint positions overseas. And who would think to force physicists and mathematicians to have tea together? For the country's World Premier International Research Center Initiative (WPI), such oddities are becoming commonplace. And they are unleashing a creative burst of science.

Japan has long tried to get more impact from its formidable scientific achievements. Various programs have promoted research excellence, interdisciplinary studies, internationalization, or administrative reform. Usually these are empty words. "Internationalism, interdisciplinary—these things are easy to say but very hard to achieve," says Toshio Kuroki, WPI program director at the Japan Society for the Promotion of Science.

Through innovative approaches, the WPIs are integrating these concepts tightly into a research base that is churning out highly cited publications, swooping up awards, and amassing international collaborators.

**Japan's six WPI centers**

**AIMR on material science:**
**Tohoku University**

**Kavli IPMU on physics and mathematics:**
**The University of Tokyo**

**iCeMS on materials science and stem cells:**
**Kyoto University**

**IFReC on immunology:**
**Osaka University**

**MANA on nanotechnology:**
**National Institute for Materials Science**

**I²CNER on carbon-neutral energy:**
**Kyushu University**

Five WPI center projects were selected in the initial round in 2007 and one, the International Institute for Carbon-Neutral Energy Research (I²CNER), was launched in 2010 at Kyushu University. All are generously funded and all are centered at top universities, except for the International Center for Materials Nanoarchitectonics (MANA) based at the National Institute for Material Sciences in Tsukuba.

WPI centers are expected to create a fundamentally new science by fusing approaches from different fields. Osaka University's Immunology Frontier Research Center (IFReC), for example, took a strong hand in overcoming the significant barriers between its imaging, immunology, and bioinformatics experts by establishing a funding mechanism for interdisciplinary projects that would otherwise have difficulty finding support. The University of Tokyo's Kavli Institute for the Physics and Mathematics of the Universe (Kavli IPMU) forces its scientists to have tea together at three every afternoon—a sternly pleasant practice that has produced many fruitful collaborations between mathematicians, astronomers, and theoretical physicists. Kyoto University's Institute for Integrated Cell-Material Sciences (iCeMS), which counts the renowned discoverer of induced pluripotent stem (iPS) cells, Shinya Yamanaka, among its faculty, takes a similar bottom-up approach, letting researchers find each other at happy hours and annual retreats with poster sessions.

iCeMS' deputy director Susumu Kitagawa says the open atmosphere has helped spur interdisciplinary success, including his own fabrication of a flexible porous coordination polymer that selectively adsorbs oxygen and nitric oxide, both of which are important in cell biology, and promises to ease the integration of the porous material for applications in living cell systems. "The informal discussions that result from such meetings provide a means for everyone to learn something about other projects underway and have already led to numerous collaborative efforts," says Kitagawa.

When the chance for revolutionary change is spotted, decisions are quickly made. At the Advanced Institute for Materials Research (AIMR) at Tohoku University in Sendai, researchers in the fields of bulk metallic glasses, material physics, soft materials, and device construction were all excelling in their own fields, but they weren't creating "a new kind of material sciences," says Kuroki.

From April, Tohoku University's Motoko Kotani, a female mathematician, will become director, and a reborn AIMR will merge these four fields through a "mathematically oriented material science." "They each have their own theories, principles, and language to understand phenomena, so it was not easy to deepen ties," she says. "We did, however, find a way."

Study groups are taking on "target projects," including non-equilibrium materials based on mathematical systems, topological functional materials, and multi-scale hierarchical material based on discrete geometric analysis. "Mathematics has a long history of acting as the most fundamental science among different disciplines and providing a common language to science and technology," she says. "It is not an easy way, but people are excited with ideas and working together well," says Kotani.

The WPI centers are expected to ensure new blood through international exchange. "Japan has so many excellent researchers, yet Japan's universities are mostly just for Japanese. Less than 5% are foreigners. We are trying to change that," says Kuroki. The target is to have 10-20%

Advertiser retains sole responsibility for content

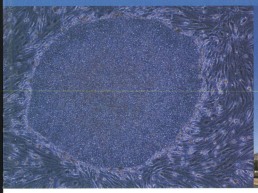

of principal investigators and 30% of research staff from overseas.

Most are already well beyond that. At MANA, 30% of principal investigators, 56% of staff, and 86% of postdoctoral researchers are non-Japanese. With its all-English instruction and bilingual email and documents, MANA has created an exceptional environment. MANA director-general Masakazu Aono credits the staff for making it "the perfect environment for providing swift administrative services to all researchers." But there's a lot more to it, including the foundry, 4-probe STM, and other equipment bought by its multimillion dollar equipment budget.

The Kavli IPMU has rewritten the book on internationalizing science in Japan. For example, it requires that postdoctoral researchers travel for one to three months during their first year. The US$6,000 in support is low intentionally; it forces postdocs to seek local funds by giving seminars. "There is a fear in the US and Europe that working in Japan will make people lose exposure back home and be 'forgotten,' either getting stuck in Japan or losing their academic career altogether," says Kavli IPMU's director, Hitoshi Murayama. "We had to wipe out this perception." Now, for 20 positions offered, the institute gets a thousand applications. It helps that the institute is also involved in major international projects including Super-Kamiokande, KamLAND, XMASS, and the HyperSuprimeCam on the Subaru telescope.

The strategies have paid off. Over four years, the five original WPIs together had nearly 2500 papers. "That's a respectable amount. But what stands out is the impact," says Kuroki. WPI papers average 14 citations, and 5.1% of them are in the "top 1%" of all papers, putting the program in league with some of the most successful overseas organizations like Rockefeller University, Stanford University and the California Institute of Technology. Of IFReC's 700 papers, for example, 12 have over 150 citations and 4 have been cited more than 300 times. "We started out with great researchers, but we want to stimulate their productivity, to make them aim even higher," says Kuroki.

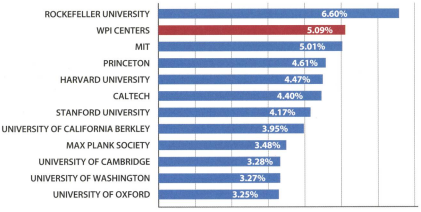


**Cream of the crop:** percentage of papers from each institution published between 2007 and 2010 that are ranked in the top 1% in terms of citations. Of 2,497 papers published by the five WPI centers, 127 (5.09%) are among top 1%. Data: provided by Thomson Reuters.

To make the program work, the WPIs were given freedoms almost unknown in Japan. Murayama and others, like iCeMS researcher John Heuser, have half-time posts that allow them to keep a position elsewhere. And the I²CNER picked the University of Illinois' Petros Sofronis—as a foreigner, another rarity among Japanese institute heads—to lead the organization.

WPI salaries can be raised freely to compete on the international job market, hiring decisions can made independently of Japan's rigid bureaucracy, and retirement ages are flexible. Kotani was able to outbid a competitor, in a quick decision, to land a European researcher. She also gives raises to staff that win prizes. "This encourages all the members to work with high motivation," she says. The freedom to augment salaries has been critical, says Aono, who was able to lure a prominent materials pioneer Enrico Traversa from the University of Rome as a full-time principal investigator. Murayama did extensive human resource market research to find out just what he needed to offer to get the best talent. Kuroki hopes that young, foreign principal investigators especially will see the opportunities. "They should stay for five years and launch their careers. The WPI centers will be an important step for them."

Restructuring scientific activity has been reinvigorating the science, and Kuroki says it will continue. Three more WPI centers will be established this year. "We want to reform the administration systems, the environment, the culture," he says.

Japan Society for the Promotion of Science
www.jsps.go.jp/english/e-toplevel/

Advertiser retains sole responsibility for content

## How being bigger helps you grasp even the most fragile things.

When you're big enough to see everything at once, it's easier to pick out the right answer. Research the smart way, and stand on the shoulders of some of the big minds in the research community. Like Professor van Loosdrecht. His advice helps you spot those things you have not yet grasped. Fragile ideas that can make a huge impression on the academic world. Discover how big you can become at **Biggerbrains.com**.

Stand a chance to win an Apple® iPad®
Raise your level at www.biggerbrains.com/game

BIGGERBRAINS™

# CONTENTS

22 March 2012 / Vol 483 / Issue No 7390

## THIS WEEK


### EDITORIALS

373 BIOETHICS
**Incidental benefits**
Volunteers who have their genes screened should be told of relevant health information gleaned

373 ANIMAL RESEARCH
**Flight risk**
Scientists cannot remain silent over threats to the availability of lab animals

374 PHYSICS
**Mass appeal**
The Higgs by any other name ... would still be the Higgs

### WORLD VIEW

375 **Change the approach to sustainable development**
*Mark Stafford-Smith*
A global system is needed for tackling environmental assessments

### RESEARCH HIGHLIGHTS

376 SELECTIONS FROM THE SCIENTIFIC LITERATURE
Storing hydrogen / Silicon sliced / A test tube with guts / Testosterone-fuelled conflict / Bacteria that hide / Better local weather forecasts

### SEVEN DAYS

378 THE NEWS IN BRIEF
China tackles scientific misconduct / Spanish researchers up in arms over cuts / Neutrinos slow down to below light speed


## CAREERS


499 RESEARCH
**Postdoc or not?**
Alternative routes to a career in research — for physicists at least

501 TURNING POINT
Think about your research as a brand, says ecologist Jessica Hellman

501 CAREER BRIEFS

NATUREJOBS ADVERTISING FEATURE
Spotlight on physics


## NEWS IN FOCUS


381 ANIMAL RESEARCH
Pressure from activists hampers transport of lab animals


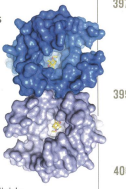


383 CRYSTALLOGRAPHY
Structures of opioid receptors revealed

384 FUNDING
Science faces up to disappointment in India's budget

385 PHYSICS
Synchrotron bridges divide between Middle Eastern foes

387 BIOETHICS
DNA donors in line to get medically relevant information

388 TECHNOLOGY
Shared approach promises boost for photonic chips

389 TRANSLATIONAL RESEARCH
Parallel clinical trial using mice yields insights into human response to drugs

### FEATURES

390 MOLECULAR BIOLOGY
**Raising the dead**
How Joe Thornton breathes new life into proteins extinct for millions of years


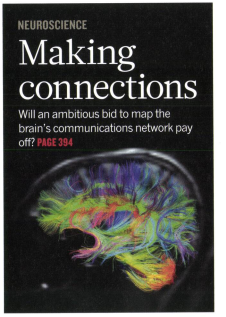


## COMMENT


397 NEUROSCIENCE
**Observatories of the mind**
*Christof Koch & R Clay Reid*
A cell-by-cell map of the mouse cerebral cortex could galvanize brain research

399 ECOLOGY
**Think big for marine conservation**
*Phil Weaver & David Johnson*
Bigger is better, when it comes to marine conservation zones

400 PHYSICS
**A century of cosmic rays**
*Michael Friedlander*
Exotic particles from the depths of the Universe right here on Earth

### BOOKS & ARTS

402 CLIMATE SCIENCE
**At the storm front**
*Simon Lewis*

403 BOOKS IN BRIEF

404 NUTRITION
**Chew on this**
*Anthony King*

405 Q&A
**The maths raconteur**
Barry Mazur's essays add imagination to the realm of mathematics

### CORRESPONDENCE

407 Not-so-open government in the United States / Science in China — and the role of Confucius / Gas-field methane emissions

### OBITUARY

408 **Renato Dulbecco (1914–2012)**
*Inder M. Verma*

### FUTURES

504 **Visiting Bob**
*John Gilbey*

# SCIENTIFIC AMERICAN™

Gain complete online access to the latest in science, technology and medicine **at your institution**

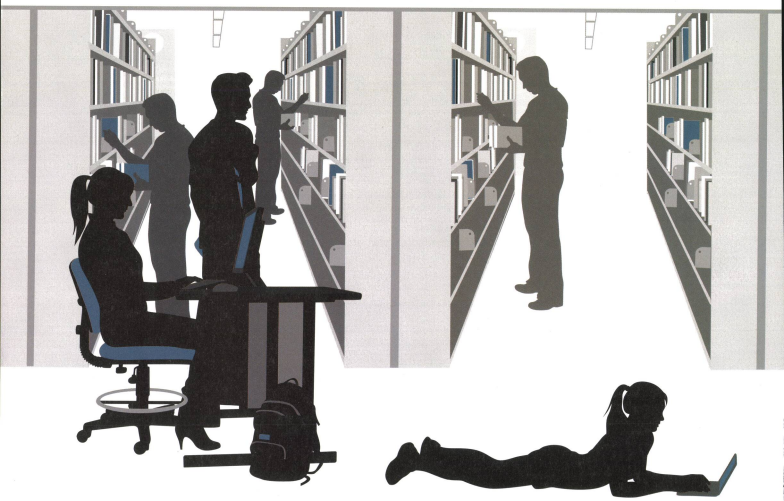

Recommend site license access to your library today!
**www.nature.com/scientificamerican**

™ Scientific American, Inc.

nature publishing group npg

# CONTENTS

22 March 2012 / Vol 483 / Issue No 7390

## RESEARCH

### NEW ONLINE

409 Papers published this week at nature.com

### NEWS & VIEWS

410 EVOLUTIONARY BIOLOGY
**Life imperfectly imitates life**
Weak selection pressure may explain imperfect Batesian mimicry
*David W Pfennig & David W Kikuchi*
SEE LETTER P.461

411 BIOLOGICAL PHYSICS
**Swarming microtubules**
Microtubules propelled by dynein proteins self-organize into vortices
*Tamás Vicsek* SEE LETTER P.448

412 MOLECULAR BIOLOGY
**How to duplicate a DNA package**
The interplay between nucleosome assembly and DNA replication
*Alysia Vandenberg & Geneviève Almouzni*
SEE ARTICLE P.434

413 GEOCHEMISTRY
**Bubbles from the deep**
Global warming and gas release from sedimentary basins during the Eocene
*Henrik Svensen*

416 VIROLOGY
**Influenza's tale of tails**
Virus mimics histone sequence to suppress antiviral gene expression
*Alexei L Krasnoselsky & Michael G Katze*
SEE ARTICLE P.428

417 MICROSCOPY
**Plasmons go quantum**
Observing collective electron waves in metal nanoparticles
*F Javier García de Abajo*
SEE ARTICLE P.421

418 NEURODEGENERATION
**Trouble in the cell's powerhouse**
Mitochondrial dysfunction as the basis for a rare hereditary ataxia
*Derek P Narendra & Richard J Youle*

### ARTICLES

421 MATERIALS SCIENCE **Quantum plasmon resonances of individual metallic nanoparticles**
*J A Scholl, A L Koh & J A Dionne*
SEE N&V P.417

428 IMMUNOLOGY **Suppression of the antiviral response by an influenza histone mimic**
*I Marazzi* et al. SEE N&V P.416

434 MOLECULAR BIOLOGY **Intrinsic coupling of lagging-strand synthesis to chromatin assembly**
*D J Smith & I Whitehouse* SEE N&V P.412

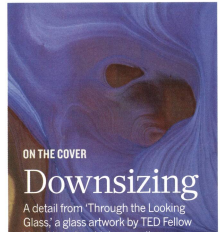

ON THE COVER

**Downsizing**

A detail from 'Through the Looking Glass,' a glass artwork by TED Fellow Kate Nichols, which uses silver nanoparticles as 'paint'. Scholl *et al.* investigate the plasmonic properties of individual silver nanoparticles in the quantum size regime. **PAGES 417 & 421**

KATE NICHOLS, ALIVISATOS LAB, UNIV. CALIFORNIA, BERKELEY. WWW.KATENICHOLSSTUDIO.COM / PHOTO: DONALD TEDTA

### LETTERS

439 PHYSICS **Resonant quantum transitions in trapped antihydrogen atoms**
*C Amole* et al.

444 APPLIED PHYSICS **Electron tomography at 2.4-ångström resolution**
*M C Scott* et al.

448 BIOPHYSICS **Large-scale vortex lattice emerging from collectively moving microtubules**
*Y Sumino* et al. SEE N&V P.411

453 CLIMATE SCIENCE **Collapse of polar ice sheets during the stage 11 interglacial**
*M E Raymo & J X Mitrovica*

457 EVOLUTION **Adaptive radiation of multituberculate mammals before the extinction of dinosaurs**
*G P Wilson* et al.

461 EVOLUTION **A comparative analysis of the evolution of imperfect mimicry**
*H D Penney, C Hassall, J H Skevington, K R Abbott & T N Sherratt* SEE N&V P.410

465 NEUROSCIENCE **MEGF10 and MEGF11 mediate homotypic interactions required for mosaic spacing of retinal neurons**
*J N Kay, M W Chu & J R Sanes*

470 STEM CELLS **Control of ground-state pluripotency by allelic regulation of *Nanog***
*Y Miyanari & M-E Torres-Padilla*

474 CELL BIOLOGY **IDH mutation impairs histone demethylation and results in a block to cell differentiation**
*C Lu* et al.

479 GENOMICS **IDH1 mutation is sufficient to establish the glioma hypermethylator phenotype**
*S Turcan* et al.

484 CANCER **Transformation by the (*R*)-enantiomer of 2-hydroxyglutarate linked to EGLN activation**
*P Koivunen* et al.

489 BIOPHYSICS **Crystal structure of a concentrative nucleoside transporter from *Vibrio cholerae* at 2.4Å**
*Z L Johnson, C-G Cheong & S-Y Lee*

494 STRUCTURAL BIOLOGY **Identification and characterization of a bacterial hydrosulphide ion channel**
*B K Czyzewski & D-N Wang*

498 CORRIGENDUM **Functional complementation between FADD and RIP1 in embryos and lymphocytes**
*H Zhang* et al.

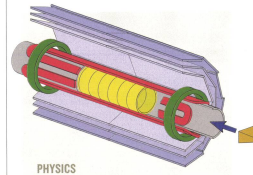

PHYSICS

**Anti matters**

The ALPHA experiment at CERN keeps antihydrogen in its place. **PAGE 439**

# nature

22 March 2012 / Vol 483 / Issue No. 7390



## EDITORIAL

**LONDON, MUNICH, WASHINGTON DC, NEW YORK, BOSTON, PARIS, SAN FRANCISCO, TOKYO** nature@nature.com

**EDITOR-IN-CHIEF:** Philip Campbell

**EXECUTIVE EDITOR:** Nick Campbell

**PUBLISHING EXECUTIVE EDITOR:** Maxine Clarke **EXECUTIVE EDITOR:** Véronique Kiermer

**CHIEF MAGAZINE EDITOR:** Tim Appenzeller

**THIS WEEK/NEWS/FEATURES:** Alison Abbott, David Adam, Ananyo Bhattacharya, Geoff Brumfiel, Declan Butler, Ewen Callaway, Erika Check Hayden, Daniel Cressey, David Cyranoski, Natasha Gilbert, Eric Hand, Heidi Ledford, Corie Lok, Brendan Maher, Emma Marris, Richard Monastersky, Brian Owens, Helen Pearson, Mark Peplow, Eugenie Samuel Reich, Ivan Semeniuk, Quirin Schiermeier, Jeff Tollefson, Richard Van Noorden, Meredith Wadman, M Mitchell Waldrop **COMMENT:** Sara Abdulla, Joanne Baker, Rosalind Cotter, Barbara Kiser, Alison McCook, Lucy Odling-Smee, Sarah Tomlin **NATURE PODCAST/VIDEO:** Adam Rutherford, Eric Olson, Kerri Smith, Charlotte Stoddart **NEWS AND VIEWS:** Sadaf Shadan, Ana Lopes, Andrew Mitchinson, Cesar Sanchez, Marian Turner **RESEARCH:** Ritu Dhand, Karl Ziemelis, Francesca Cesari, I-han Chou, Tanguy Chouard, Rosamund Daw, Alex Eccleston, Angela Eggleston, Joshua Finkelstein, Henry Gee, Patrick Goymer, Noah Gray, Marie-Thérèse Heemels, Magdalena Helmer, Karen Howell, Claudia Lupp, Barbara Marte, Andrew Mitchinson, Juliane Mössinger, Deepa Nath, Leslie Sage, Magdalena Skipper, Clare Thomas, John VanDecar, Liesbeth Venema, Ursula Weiss, Michael White **INSIGHTS/REVIEWS/PERSPECTIVES:** Ursula Weiss **CAREERS:** Gene Russo, Karen Kaplan **TECHNOLOGY FEATURES:** Monya Baker **FUTURES:** Henry Gee **SUPPLEMENTS:** Herb Brody, Michelle Grayson, Tony Scully **SUBEDITORS:** Colin Sullivan, Sarah Archibald, Nicola Bailey, Anne Blewett, Nicolas Fargeot, Isobel Finlayson, Paul Fletcher, Afsaneh Gray, Dinah Loon, Anna Novitzky, Yukie Ozawa, Katherine Perry, David Price, Jenny Rooke, David Winters, Anna York **PRODUCTION:** Jenny Henderson, Leonora Dawson-Bowling, Dan Foley, Stewart Fraser, Susan Gray, Simon Gribbin, Hazel Mayhew, James McQuat, Emilia Orriss, Yvonne Strong, Robert Sullivan, Roberta Tarran, Charles Wenz **ART AND DESIGN:** Kelly Buckheit Krause, Wesley Fernandes, Madeline Hutchinson, Barbara Izdebska, Paul Jackman, Jasiek Krzyszotfiak, Annthea Lewis, Chris Ryan, Nik Spencer, Claire Welsh, Mark Wood **JAPAN EDITION:** Eiji Matsuda, Mika Ishida, Sayaka Ayame **PRESS OFFICE:** Ruth Francis, Neda Afsarmanesh, Lisa Boucher, Rachel Twinn, Rebecca Walton **ADMINISTRATION:** Paul Sng, Liz Bankes, Roseann Campbell, Ffion Cleverley, Faye Fornasier, Ashlee Gagui, Amy Invernizzi, Diane Kempinski, Katie McGoldrick, Jenny Meyer, Rina Nozawa, Anastasia Panoutsou, Kenneth Simpson, Claire Smith

## PUBLISHING

**LONDON** feedback@nature.com

**MANAGING DIRECTOR & PUBLISHER:** Steven Inchcoombe

**ASSOCIATE PUBLISHER:** Arash Hejazi

**PUBLISHING PROJECT MANAGER:** Christian Manco

**TOKYO** feedback@natureasia.com

**REGIONAL MANAGING DIRECTOR — ASIA-PACIFIC:** David Swinbanks

**DIRECTOR — ASIA-PACIFIC:** Antoine E Bocquet

**OPERATIONS DIRECTOR — ASIA-PACIFIC:** Hiroshi Minemura

## DISPLAY ADVERTISING, SPONSORSHIP & NATUREJOBS

**GLOBAL HEAD:** Andrew Douglas a.douglas@nature.com

**DISPLAY ADVERTISING AND SPONSORSHIP**

**GLOBAL HEAD:** Gerard Preston g.preston@nature.com

**ASSISTANT SPONSORSHIP MANAGER:** Reya Silao Tel: +44 (0)20 7843 4977 (r.silao@nature.com)

**EUROPE/REST OF WORLD display@nature.com Tel: +44 (0)20 7843 4960**

**GERMANY/SWITZERLAND/AUSTRIA:** Sabine Hugi-Fürst Tel: +41 52761 3386

**UK/IRELAND/SCANDINAVIA/SPAIN/PORTUGAL:** Evelina Rubio Hokenson Tel: +44 (0)20 7843 4079

**FRANCE/BELGIUM/THE NETHERLANDS/LUXEMBOURG/ITALY/OTHER EUROPE:** Nicola Wright Tel: +44 (0)20 7843 4959

**NORTH AMERICA** display@natureny.com

**NEW ENGLAND/ EASTERN CANADA:** Sheila Reardon Tel: +1 617 494 4900

**NEW YORK/MID-ATLANTIC/SOUTHEAST:** Jim Breault Tel: +1 212 726 9334

**MIDWEST:** Mike Rossi Tel: +1 212 726 9255

**WEST COAST/ WESTERN CANADA:** George Lui Tel: +1 415 781 3804

**WEST COAST NORTH:** Kayla McCutchan Tel: +1 415 403 9038

**ASIA-PACIFIC** display@natureasia.com

**ASIA-PACIFIC HEAD:** Kate Yoneyama

**JAPAN:** Ken Mikami Tel: +81 3 3267 8765

**GREATER CHINA/SINGAPORE:** Gloria To Tel: +852 2811 7191

**INDIA:** Vikas Chawla Tel: +91 124 288 1057

**SPONSORSHIP**

**BUSINESS DEVELOPMENT MANAGER:** David Bagshaw Tel: +1 212 726 9215

**BUSINESS DEVELOPMENT MANAGER:** Patrick Murphy Tel: +1 617 475 9216

**NATUREJOBS** naturejobs@nature.com

**EUROPEAN HEAD OFFICE, LONDON:** Tel: +44 (0)20 7843 4961

**EUROPEAN SALES MANAGER:** Nils Moeller (n.moeller@nature.com) **BUSINESS DEVELOPMENT MANAGER, MIDDLE EAST:** Jon Giuliani (j.giuliani@nature.com) **ADVERTISING PRODUCTION MANAGER:** Stephen Russell **NATUREJOBS ONLINE PRODUCTION:** Dennis Chu

**US HEAD OFFICE, NEW YORK:** naturejobs@natureny.com **US SALES MANAGER:** Ken Finnegan

**JAPAN HEAD OFFICE, TOKYO:** Tel: +81 3 3267 8765 **ASIA-PACIFIC HEAD:** Kate Yoneyama

**ASIA-PACIFIC SALES & BUSINESS DEVELOPMENT MANAGER:** Yuki Fujiwara **BUSINESS DEVELOPMENT MANAGER, GREATER CHINA, SINGAPORE:** Gloria To Tel: +852 2811 7191

**INDIA:** Vikas Chawla Tel: +91 1242881057 (v.chawla@nature.com)

## MARKETING & SUBSCRIPTIONS

**USA/CANADA/LATIN AMERICA** subscriptions@us.nature.com

Tel: (USA/Canada)+1 866 363 7860; (outside USA/Canada) +1 212 726 9223

**MARKETING:** Sara Girard **FULFILMENT:** Karen Dawson

**JAPAN/CHINA/KOREA** subscriptions@natureasia.com

Tel: +81 3 3267 8751 **MARKETING:** Sachiyo Ikeda **FULFILMENT:** Masayo Tanaka

**EUROPE/REST OF WORLD** subscriptions@nature.com

Tel: +44 (0)1256 329242

**MARKETING:** Elena Woodstock, Marcus Parker, Hannah Phipps **FULFILMENT:** Jean Burrows

**INDIA** npgindia@nature.com

Tel: +91 124 2881053/54

**HEAD OF BUSINESS DEVELOPMENT, INDIA:** Debashish Brahmachari **MARKETING:** Harpal Singh Gill

**ANNUAL SUBSCRIPTIONS (UK/Europe, including post and packing)**

**FULL RATE:** £1,400

**PERSONAL RATES:** UK £135; Europe €209; Rest of World £210

**STUDENT RATES:** UK £79; Europe €122; Rest of World £125

Individual rates apply to payments by personal cheque or credit card. Back issues: £20.00.

**ANNUAL SUBSCRIPTIONS (USA, including post and packing)**

**INSTITUTIONAL/CORPORATE RATE:** $2,730 ; **PERSONAL RATE:** $199; **STUDENT RATE:** $99;

**POSTDOC RATE:** $119

Printed in USA. Individual rates available only to subscribers paying by personal check or credit card. Orders for student/postdoc subscriptions must be accompanied by a copy of student ID. Rates apply to USA, Canada, Mexico/Central & South America. Add 7% GST tax in Canada (Canadian GST number 140911595). **BACK ISSUES:** US$20.00.

**ANNUAL SUBSCRIPTIONS (Asia, including post and packing)**

**JAPAN:** **年間購読料金：** *Nature* のみ 437,800 円 +21,890 円 (消費税) =459,690 円 (合計)
*Nature* + *Nature Digest* 466,550 円 +23,328 円 (消費税) =489,878 (合計)

お問い合わせ: 日本出版貿易株式会社 国内営業 1 部
〒101-0064 東京都千代田区猿楽町1-2-1 Tel: 03-3292-3767 Fax: 03-3292-8766

**個人/学生購読について**

NPG オナチャーアジア・パシフィック フルフィルメント & カスタマーサービス
〒162-0843 東京都新宿区市谷田町2-37 千代田ビル Tel: 03-3267-8759 Fax: 03-3267-8752

**CHINA:** www.natureasia.com/cn/subscribe; **KOREA:** www.natureasia.com/korea/subscribe

## NATURE ONLINE WWW.NATURE.COM/NATURE

**CHIEF TECHNOLOGY OFFICER:** Howard Ratner **ASSOCIATE DIRECTOR, NATURE.COM:** Daniel Polnick

**PLATFORM DEVELOPMENT:** Jeremy Macdonald **WEB PRODUCTION:** Alexander Thurrell, Deborah Anthony **WEB DESIGN:** Juan-Carlos Sobrino, Luke Stavenhagen **PLATFORM INTERFACES:** Amanda Ward

## SITE LICENCES, FULFILMENT & CUSTOMER SERVICES

**SITE LICENCES:** npg.nature.com/librairies feedback@nature.com

**CHIEF OPERATIONS OFFICER:** John Carroll **ASSOCIATE DIRECTOR OF OPERATIONS:** Dominic Pettit

**CUSTOMER SERVICE:** Liz Davidson **ORDER PROCESSING OPERATIONS:** Steve Poulter

## NATURE PUBLISHING GROUP OFFICES

**LONDON:** The Macmillan Building, 4 Crinan Street, London N1 9XW Tel: +44 (0)20 7833 4000 Fax: +44 (0)20 7843 4596/7

**BASINGSTOKE:** Nature Publishing Group, Subscriptions, Brunel Road, Basingstoke, Hants RG21 6XS, UK Tel: +44 (0)1256 329242

**WASHINGTON DC:** 968 National Press Building, 529 14th St NW, Washington DC 20045-1938 Tel: +1 202 737 2355

**NEW YORK:** 75 Varick St, 9th Floor, New York, NY 10013-1917 Tel: +1 212 726 9200

**BOSTON:** 25 First Street, Suite 104, Cambridge, MA 02141 Tel: +1 617 475 9275

**SAN FRANCISCO:** 225 Bush Street, Suite 1453, San Francisco, CA 94104 Tel: +1 415 403 9027

**MUNICH:** Nymphenburger Strasse 14, D-80335 München Tel: +49 89 549057-13

**PARIS:** Moulin de Malicorne, Sainte Maure de Touraine, Paris 37800 Tel: +33 2 47 35 72 15

**TOKYO:** Chiyoda Building, 2-37 Ichigayatamachi, Shinjuku-ku, Tokyo 162-0843 Tel: +81 3 3267 8751

**INDIA:** Nature Publishing Group, 3A, 4th Floor, DLF Corporate Park, Gurgaon 122002 Tel: +91 124 2881053/54



*Nature*® (ISSN 0028-0836) is published by Nature Publishing Group, a division of Macmillan Publishers Ltd (The Macmillan Building, 4 Crinan Street, London N19XW). Registered as a newspaper at the British Post Office. North and South American orders to subscriptions@nature.com (Tel: +1 866 363 7860). Other orders to subscriptions@nature.com (Tel: +44 (0)1256 329242; Fax +44 (0)1256 812358). Authorization to photocopy material for internal or personal use, or internal or personal use of specific clients, is granted by *Nature* to libraries and others registered with the Copyright Clearance Center (CCC) Transactional Reporting Service, provided the relevant copyright fee is paid direct to CCC, 222 Rosewood Drive, Danvers MA 01923, USA. Identification code for *Nature*: 0028-0836/03. CPC PUB AGREEMENT #40032744. In the US, *Nature* (ISSN 0028-0836) is published weekly on Thursday, except the last week in December by Nature Publishing Group, 75 Varick St, 9th Fl, New York NY 10013-1917, USA. US Periodicals postage paid at New York NY, and additional mailing post offices. US POSTMASTER: send address changes to *Nature*, Subscription Dept, 75 Varick St, 9th Fl, New York NY 10013-1917, USA. Published in Japan by NPG Nature Asia-Pacific, Chiyoda Building, 2-37 Ichigayatamachi, Shinjuku-ku, Tokyo 162-0843, Japan. ©


2012 Macmillan Publishers Limited. All rights reserved.

nature EDUCATION

ANNOUNCING

# Principles of Biology

**An interactive textbook solution by Nature Education**

A learning solution designed to bridge students from the classroom to the lab.

| | | | |
|---|---|---|---|
| 200 customizable mini-chapters created by dozens of scientists, instructors, and editors | 200+ online interactive exercises to give students a hands-on way to apply their knowledge | 50 Science Techniques units cultivating real scientific skills, including data analysis | 3000+ assessment questions integrated into lessons |
| Synopses and links to milestone research papers from *Nature* and other journals | Affordably priced for all students | Optional color print companion | Access on all devices: |

Learn more at **www.nature.com/principles**

nature publishing group npg

NEW ENGLAND
BioLabs Inc.
enabling technologies in the life sciences

# Mix it up.

## RE-Mix™ Restriction Enzyme Master Mixes

Restriction enzyme digests are now even easier! The same high quality restriction enzymes that you have come to trust from New England Biolabs are now available in master mix format, including enzyme, buffer and loading dye; simply add your DNA and digest.

With RE-Mix Master Mixes take advantage of:

- Simplified and shortened protocols
- Fast digestion in 15 minutes (Time-Saver qualified)
- High product quality with reproducible results

RE-Mix Master Mixes – just add your DNA and mix

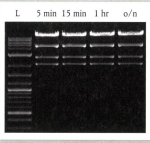


*pXba DNA was digested with EcoRV-HF™ RE-Mix™ according to the recommended protocol. Lane L is the TriDye™ 2-Log DNA Ladder (NEB #N3270). The same results are obtained whether incubated for 5–15 minutes, 1 hour or overnight.*

GTAGC CT
TCUTGA AT
AGTITC G
TTTOUTT
GT ACTACG

To experience the new restriction enzyme challenge from NEB, visit **www.NEBcutitout.com**

For more information, visit
**www.NEBREMIX.com**

*Blue-footed Booby (Sula nebouxii)*
*© Tui De Roy*

# THIS WEEK

EDITORIALS

**HIGGS** Would a boson by another name smell as sweet? **p.374**

**WORLD VIEW** Rio summit demands a different science approach **p.375**

**TASTELESS** Bottlenose dolphins get little flavour from food **p.377**

# Incidental benefits

*Scientists who screen the genes of volunteers for research should tell participants if they find information relevant to their health.*

All research studies on humans can uncover facts relevant to a volunteer's health — at initial screening, during the study itself, or even after the study finishes, when other researchers review the data or conduct their own analyses.

For the most part, researchers have opted not to reveal these potentially important 'incidental findings' to participants. This has been to protect the research process, and to prevent coercing people into studies by unwittingly eliciting the 'therapeutic misconception' — the incorrect assumption on the individual's part that participating in a study will help their own health.

But the emergence of high-throughput genomics, with its ability to catalogue vast amounts of information that may have a bearing on a person's health, has prompted a rethink of this convention.

A working group funded by the US National Institutes of Health (NIH) in Bethesda, Maryland, has recommended that biobanks and archives that house large genetic data sets introduce policies to encourage the return of incidental findings to research subjects (see page 387).

The impact of these recommendations should not be underestimated. As genetics invades every branch of medicine, no field is likely to be exempt from ethical standards introduced to cover genetic data. The recommendations are likely to have their most immediate influence in discussions on the topic now under way at the US Department of Health and the NIH.

There is a precedent for returning information to the subjects of a study. In imaging studies, for instance, a radiologist often reviews patients' scans for incidental findings before they are analysed by researchers. Support is growing for the idea that genetics researchers should similarly review a selected set of genes with known impacts on health before undertaking their own research.

Implementing this will not be easy. Defining appropriate sets of genes is problematic, and any list will need to be constantly updated. And to return the information to an individual in a way that avoids unnecessary anxiety and medical expense is a huge issue. Opponents of the idea point out that it contravenes standard practice in medicine itself, because doctors do not routinely sift through patients' records for old test results that may carry new significance in the light of more recent research.

Perhaps the most visible example of the need for this debate comes not from science, but from commerce. Companies routinely mine vast quantities of consumer information to influence marketing decisions. Governments have not been able to keep pace with standard business practices, and most consumers are unaware of the breadth and depth of information that companies gather on them from Internet searches, social networks and supermarket purchases.

In testimony before the US Presidential Commission on Bioethics in February, John Wilbanks, who runs the project Consent to Research, noted that this pattern is likely to repeat itself in the era of electronic medical records and genomics. "My sad realization is that whether it's your genome or your health information, anyone who really wants to screw you will probably be able to get a copy of the data they need to do so, and the people who are least likely to get a copy are the people who can do something amazing with it, like researchers," he said. Companies are lining up to market products to consumers on the basis of their genomes. Law-enforcement agencies already use DNA left at crime scenes to find suspects and their relatives, and are funding programmes to create physical profiles of suspects on the basis of their DNA. In other words, people now have incomplete protection for their own DNA, and this lack of privacy is likely to increase in the future.

***"No field is likely to be exempt from ethical standards introduced to cover genetic data."***

In this free market, how sure can researchers be that they are truly doing no harm to their study participants when they take a cheek swab? People thinking of entering a study will assess the risks of how their volunteered genetic information might be used, and this might make them more reluctant to participate. Researchers could help to counter this by offering them medically relevant information back in exchange. ■

# Flight risk

*As the campaign against animal research intensifies, so must the response.*

Picture a crowd of scientists waving placards plastered with photographs of stroke victims and sufferers of Parkinson's disease. They are demonstrating outside the corporate headquarters of British Airways, Lufthansa and Delta, demanding that the airlines stop impeding the biomedical research that could deliver big advances against these and other diseases.

Seem far-fetched? Maybe. But if scientists want continued access to animals as research models, they will have to appear on the front line with every bit as much visibility, determination, organization and persistence as animal-rights activists now muster.

In a renewed campaign targeting transportation companies, protestors have found a public pressure point so effective that only a few major airlines still agree to transport non-human primates bound for research labs (see page 381). Nor is the focus confined to primate transportation: earlier this year, the last ferry company that was willing to carry research rodents into the United Kingdom stopped doing so. Such blocks, scientists warn, could shift much animal work to countries where regulations are more lax.

But there is a silent majority for whom the activists do not speak.

This includes most scientists, many ordinary citizens and millions of patients and their families touched by disease and injury. This constituency must mobilize in the defence of human health if the gains enabled by future primate research — and, ultimately, all animal research — are not to be thrown away.

Scientists and their allies must, of course, continue to be open about the price animals pay in research. They must openly acknowledge, immediately correct and do everything they can to prevent lapses in the care of the animals in their charge. At the same time, scientists must make every effort to use lower animal, and non-animal, models where possible, as regulations already require. And alongside all of that, they must emphasize the tangible and compelling improvements to human life that animal research has made possible.

Consider stroke, which affects some 795,000 people in the United States alone each year — 1 person every 40 seconds — at a cost in excess of US$40 billion. More than 1,000 experimental treatments aimed at protecting brains cells in acute stroke have been developed in cells and rodents; none has been effective in humans. So a possible advance in a paper published last month is significant (D. J. Cook *et al. Nature* **483,** 213–217; 2012). Using macaques — animals whose neuroanatomy, genetics and behaviour are far closer to humans than are those of rodents — the study showed that a drug called a PSD-95 inhibitor reduced the volume of brain tissue killed by the stroke and significantly preserved neurological function. It has now moved into human trials, where early results are promising.

Many other advances have been made possible by primate research. Trials of brain–machine interfaces that allow quadriplegics to control robotic limbs with their minds, for example, and of gene therapy for haemophilia B. And deep-brain stimulation to alleviate the symptoms of advanced Parkinson's disease. Primates have also helped the development of antiviral therapies to prevent mother-to-child transmission of HIV; of Rituxan (rituximab), a key drug against non-Hodgkin's lymphoma; and of Benlysta (belimumab), the first new lupus treatment in 50 years. Primates are making possible strides towards a vaccine against Ebola, and they have affirmed that the diabetes drug pioglitazone can slow early Parkinson's disease — a therapy now being taken into human trials.

***"Silence from the research community will mean lost access to research animals."***

Future advances of this kind cannot be allowed to stall. The scientific community and its allies in patient and research advocacy groups should mount a vigorous, coordinated campaign to lobby major airlines. They should vocally support companies such as Air France that continue to fly research primates. They should confront others with the human cost of their alignment with animal activists. And to those airlines that are wavering, they should make a pointed, persuasive case.

An apt target in the last category is United Airlines, which merged with Continental in 2010. Continental was the last major US airline carrying non-human primates for research. The now-merged airline, still under the name of United, says it is "in the process of integrating" the former United and Continental policies on transporting research primates, for publication this autumn. Only a powerful and visible public campaign urging United to transport research primates will give the firm the political cover it needs to take such a position.

Urgent and dramatic action is necessary. It is increasingly clear that silence and passivity from the research community will lead to only one result: lost access to research animals in the countries best equipped for their responsible, humane and justified use. ■

# Mass appeal

*As physicists close in on the Higgs boson, they should resist calls to change its name.*

The naming of the Higgs boson as such is clearly a simplification — physicists besides Peter Higgs contributed to the theory that predicts it. But it is far from the most extreme example.

The relationship between the velocity of recession of galaxies and their distance from Earth that we call Hubble's law was first formulated by Belgian cosmologist Georges Lemaître. The quantity known as Avogadro's number was first calculated by Austrian chemist Johann Josef Loschmidt. Higgs, a physicist at the University of Edinburgh, UK, at least has the strongest claim to credit for the boson. And for the arcane world of particle physics, simplification is often a good thing.

In 1964, Higgs was the first to postulate the existence of a massive particle arising from the mechanism of electroweak symmetry breaking, in which a unification of electromagnetism and the weak nuclear force fails in such a way as to give some force-carrying particles masses while others remain without. Yet moves are afoot to rename the Higgs. Earlier this month, some speakers at the Moriond particle-physics conference in La Thuille, Italy, chose to describe progress on the search for the BEH scalar boson (after the physicists Robert Brout, François Englert and Higgs) or the SM scalar boson (where SM stands for standard model).

It is not hard to guess why. Experiments at the Large Hadron Collider at CERN, Europe's premier particle-physics laboratory near Geneva in Switzerland, have reported tentative signals of the Higgs. If these are real, data collected in 2012 should see CERN claim a discovery. A Nobel prize is in the offing, and one that should arguably go not just to the experimentalists, but also to the theorists whose efforts inspired the successful search. But who — besides Higgs — should be included?

The name Higgs boson was supposedly coined by Korean-born physicist Ben Lee, some time between 1966 and 1972. According to journalist Ian Sample, Lee learned about the mass-giving mechanism from Higgs, and later coined the term as a shorthand. Yet several others played an important part in developing the theory that gives rise to the Higgs.

Belgian physicists Brout and Englert were the first to publish on the subject in 1964, building on ideas from condensed-matter physics developed by physics Nobel laureate Phil Anderson and others. Higgs published the same year; his paper contains the first mention of the boson. Tom Kibble, Gerald Guralnik and Carl Hagen followed with a third account that is generally considered more complete. One interpretation of this history is reflected in the American Physical Society's joint award, in 2010, of the J. J. Sakurai Prize for Theoretical Particle Physics to Brout, Englert, Higgs, Guralnik, Hagen and Kibble.

This provides plenty for physicists to argue about. In 2010, a row over credit erupted when Brout, Englert and Higgs were acknowledged in an advertisement for a conference on the particle but Guralnik, Hagen and Kibble were not (see *Nature* http://doi.org/ctz988; 2010). Meanwhile, 2011 saw a dispute over editing of the Wikipedia article 'Higgs boson' between one editor who supported Guralnik's view that his paper with Hagen and Kibble proposed a boson and another who was pro-Higgs.

Particle physicists should not rename the Higgs. And the reason would be obvious to anyone in business: branding. There are already relatively few concepts in their subject that have achieved widespread recognition without crossing one of them out. In business, it would be considered destructive to take a well-known name and replace it with a long-winded, technical-sounding alternative that no one has heard of.

Correct allocation of credit is important, and authoritative accounts of the history of science are useful and enlightening, but both must be balanced with science's need for consistent conventions, brevity, and public communication and outreach, especially when taxpayer's expenditures, such as the US$6.5 billion for the Large Hadron Collider, are at stake. Renaming the Higgs boson in the year when it is most likely to be found gets the balance wrong. (And anyway, Higgs is a better name than the God particle, isn't it?) ■

➲ **NATURE.COM**
To comment online, click on Editorials at:
go.nature.com/xhumqv

CSIRO

# Change the approach to sustainable development

*Conventional environmental assessments are not enough — it is time for some joined-up global thinking, says* **Mark Stafford Smith.**

As the world heads towards the next big environmental summit — the United Nations Conference on Sustainable Development (Rio+20) in Rio de Janeiro, Brazil, in June — officials and politicians are calling for further assessments of our global ecological plight.

In January, for example, a panel on global sustainability set up by UN secretary-general Ban Ki-moon recommended a "periodic global sustainable development outlook report that brings together information and assessments currently dispersed across institutions and analyses them in an integrated way".

This is a response to research that shows how global society is increasingly interconnected and interdependent. The cascading effect on land availability and food security of a switch to biofuels, for example, demonstrates how actions to address carbon dioxide emissions can rebound on other goals.

But, in these difficult times, can the thinly stretched scientific community support a new assessment process? And is that really what policy-makers need from research?

Scientists are already busy on policy-makers' behalf. There is the Intergovernmental Panel on Climate Change (IPCC), the Millennium Ecosystem Assessment, assessments of international waters, mountains and fresh water, the Global Marine Assessment and the important new Intergovernmental Platform on Biodiversity and Ecosystem Services. Each has a crucial role in consolidating knowledge about individual sectors. But how to connect the dots?

In many areas, the rates of global environmental change are accelerating but decision-making processes are stuck in low gear. It is not clear that another conventional assessment will catalyse swifter action. So, although the research community should rally behind an integrated analysis, it must be done differently.

**THE FOCUS MUST SHIFT FROM DOCUMENTING PROBLEMS TO SUPPORTING SOLUTIONS.**

First, the focus must shift from documenting problems to supporting solutions. This requires strong and continual interaction between those working in strategic applied research and decision-makers in policy, industry and civil society, both on specific decisions (such as how to frame a particular trade agreement) and on the wider context (interactions between national well-being, environmental outcomes and economic flows).

Second, the process must promote responses at all scales, from national governments and regional groups to UN institutions. Appropriate solutions will differ from region to region, be they specific technologies for energy production or carbon sequestration, or analyses that jointly address water, energy and food.

Finally, the process must work across sectors, through simultaneous analysis of the impact of a migration policy on environmental and social well-being, for example. To do this comprehensively, the research must also become more integrated, encompassing natural and social sciences and the humanities to understand the implications of changes.

How could this be done? Two proposals already on the table for Rio+20 could help: a UN Sustainable Development Council (UNSDC), directly answerable to the UN General Assembly, and a set of sustainable-development goals (SDGs).

A UNSDC could commission strategic analyses of global sustainability and set up and coordinate decision-specific panels — small mixed working groups that include non-scientific members, appointed to report quickly on specific issues. Such panels would work across sectors, independent from but jointly owned by global bodies such as the Food and Agriculture Organization of the UN, the World Trade Organization, the UN Environment Programme and the World Bank.

This model must be replicated at regional and national levels, driven by local needs, with local ownership. Light-touch coordination by the UNSDC would ensure good communication and exchange of ideas, and would make sure that activities in one region did not lead to perverse global outcomes — perhaps by causing people to move, distorting prices or over-using resources.

The SDGs could ensure that these activities integrate the three pillars of sustainability — environmental, economic and social — instead of dealing with each in isolation, as the UN's current Millennium Development Goals do. They should connect sectors, aiming for example to improve well-being without environmental damage, ensure food security without undermining local livelihoods and develop habitable urban environments without increasing resource use.

All of this builds on existing trends in the activities of bodies such as the IPCC, but we need a rapid step change in the evolving relationship between science and decision-making.

Countries such as Australia already talk about 'national innovation systems' — the totality of their pure and applied research efforts and the interactions of these with decision-making in industry and government. It is time to embrace a global innovation system to support better-coordinated and more nimble decision-making on global sustainability at all scales. Much work needs to be done on the details, but if science is to be genuinely useful to society, this is what we must fight for. ■

➲ NATURE.COM
Discuss this article online at:
go.nature.com/79fhuu

**Mark Stafford Smith** *is science director of the Commonwealth Scientific and Industrial Research Organisation Climate Adaptation Flagship in Canberra, and co-chair of the Planet Under Pressure conference, which will be held in London next week.*
*e-mail: mark.staffordsmith@csiro.au*

# RESEARCH HIGHLIGHTS

*Selections from the scientific literature*

CHEMISTRY

## Hydrogen can be stored as acid

Hydrogen gas holds promise as a carbon-free fuel, but is difficult to store and transport because it is highly flammable, diffuse and has a low energy density. Jonathan Hull at Brookhaven National Laboratory in New York and his colleagues have found a possible way to store hydrogen as an aqueous solution of formic acid (HCOOH), which has a higher energy density.

At ambient temperature and pressure, an iridium catalyst dissolved in water causes $H_2$ to react with carbon dioxide to form the acid under mildly basic conditions. Acidifying the solution triggers the release of pure pressurized $H_2$ gas. Because of the mild conditions needed for the reactions, the work could eventually lead to a mechanism for $H_2$ storage.

***Nature Chem.*** **http://dx.doi.org/10.1038/nchem.1295 (2012)**

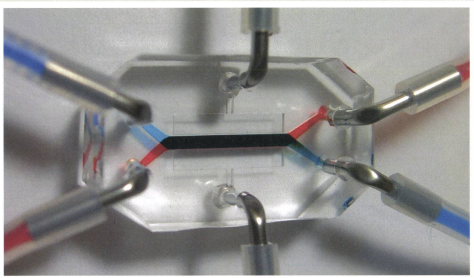

R. SOC. CHEM.

BIOENGINEERING

## A pulsating gut on a chip

A coin-sized device created by a team at Harvard University mimics the structure and physiology of the human intestine by supporting gut microbes and imitating the organ's rhythmic motion.

Donald Ingber and his colleagues at the Wyss Institute in Boston, Massachusetts, built the chip (**pictured**) out of a clear polymer. It contains two microscopic fluid channels separated by a porous, flexible membrane. Human gut epithelial cells, which line the gut's surface, cover the membrane and supported the growth of a common gut bacterium, *Lactobacillus rhamnosus*. The researchers simulated gut contractions, or peristalsis, by applying suction through two side chambers. In response, the epithelial cells formed folds similar to the finger-like protrusions, or villi, that line the inner intestinal wall.

The gut tissue layer blocked the flow of small molecules between the channels, and this barrier function improved with the presence of the bacteria. The authors say that their device is a better intestinal mimic than cells in static culture and suggest that it could be used for drug screening and toxicity tests.

***Lab Chip*** **http://dx.doi.org/10.1039/C2LC40074J (2012)**

MATERIALS

## Slicing silicon with less waste

Cutting silicon blocks into thin wafers for solar cells and other applications generates a lot of wasted metal because of the width and vibration of the mechanical sawing wire typically used. Sungho Jin at the University of California, San Diego, and his colleagues report a way to etch silicon into various intricate shapes that produces an order of magnitude less waste than conventional approaches.

The authors adapted a common etching technique, depositing a catalytic gold and iron layer on top of certain sections of a silicon wafer and using other chemicals to dissolve those parts of the silicon away. Strong neodymium magnets guide the chemical etching, allowing the researchers to slice silicon in any desired direction, forming sheets, microneedles, nanowires (**pictured**) and tunnels. Magnetically guided chemical etching makes thinner cuts than mechanical sawing, thus reducing waste.

***Nano Lett.*** **http://dx.doi.org/10.1021/nl300141k (2012)**

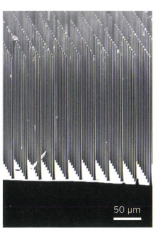


AM. CHEM. SOC.

ZOOLOGY

## All the better to see whales with

The giant eyes of the world's largest squid seem to be specially adapted to spot approaching predatory sperm whales.

Dan-Eric Nilsson at Lund University in Sweden and his colleagues examined a photograph of an adult giant squid (*Architeuthis* sp.) and a full-size colossal squid

(*Mesonychoteuthis hamiltoni*) specimen, and found both animals' eyes to measure about 27 centimetres in diameter — the largest eyes of any species. The researchers created a mathematical model relating eye size to vision. They found that the only advantage of such large eyes over smaller ones is an enhanced ability to detect large, luminous objects below ocean depths of about 500 metres.

The authors suggest that these squid evolved such eyes to detect the bioluminescence that can be created by the movement of hunting whales.

***Curr. Biol.*** **http://dx.doi.org/10.1016/j.cub.2012.02.031 (2012)**

MICROBIOLOGY

## Bacteria signal to survive

Bacterial cells that are genetically identical to members of their population that succumb to antibiotics can survive in a dormant state, thanks to chemical communication between bacteria.

Surviving 'persister' cells have been implicated in chronic infections such as tuberculosis. James Collins and his team at Boston University in Massachusetts gave *Escherichia coli* the chemical indole, which the bacteria produce as a signalling molecule. Indole-treated *E. coli* were able to withstand higher levels of several antibiotics than untreated bacteria. Moreover, the individual bacterial cells in a culture that were most responsive to indole were also those most resistant to antibiotics.

Indole activates genes involved in responding to stress, and *E. coli* strains lacking stress-response genes produce fewer persisters.

***Nature Chem. Biol.*** **http://dx.doi.org/10.1038/nchembio.915 (2012)**

CLIMATE MODELLING

## Predicting realistic rains

A high-resolution climate model has produced the most accurate representation yet of rainfall in the southern United Kingdom, bolstering confidence in the potential of detailed regional modelling.

A team led by Elizabeth Kendon at the Met Office Hadley Centre in Exeter, UK, used a regional model with a 1.5-kilometre grid to conduct detailed simulations from 1989 to 2008. The authors analysed the duration, extent and intensity of rainfall and compared the results of their model with those produced by a less-detailed 12-kilometre regional climate model.

The results suggest that the 1.5-kilometre model significantly improves the representation of heavy rains and reduces long-standing inaccuracies that produced too much light rain.

***J. Clim.*** **http://dx.doi.org/10.1175/JCLI-d-11-00562.1 (2012)**

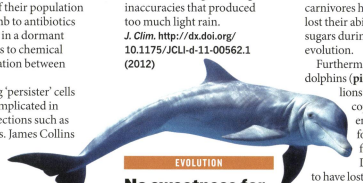

D. PERRINE/NATUREPL.COM

EVOLUTION

## No sweetness for meat-eaters

Many meat-eating animals have lost their ability to taste sugars, having lost a working copy of a gene that encodes a taste receptor for sugar.

Peihua Jiang and Gary Beauchamp at the Monell Chemical Senses Center in Philadelphia, Pennsylvania, and their co-workers sequenced DNA from 12 members of the order Carnivora, including spotted hyenas and several sea mammals. Seven of the species carried a malfunctioning copy of the *Tas1r2* gene that encodes a sweet taste receptor. However, the exact mutations differed from one species to another, suggesting that carnivores have independently lost their ability to detect sugars during the course of evolution.

Furthermore, bottlenose dolphins (**pictured**) and sea lions lack working copies of the gene encoding receptors for tasting savoury flavours, or umami. Dolphins also seem to have lost a receptor that senses bitter compounds. The authors say taste may not affect what these creatures eat as sea lions and dolphins tend to swallow their food whole.

***Proc. Natl Acad. Sci. USA*** **http://dx.doi.org/10.1073/pnas.1118360109 (2012)**

For a longer story on this research, see go.nature.com/y4tzk7

## COMMUNITY CHOICE

*The most viewed papers in science*

BEHAVIOURAL SCIENCE

## Testosterone hinders collaboration

HIGHLY READ on rspb.royalsocietypublishing.org in February

Women taking testosterone pills collaborate less effectively than those given a placebo.

Nicholas Wright and his colleagues at University College London asked 17 pairs of women to decide individually if a set of striped circles on one screen was brighter than those on a second screen. If the women within a pair disagreed, they had to collaborate to come up with a joint decision.

The team found that the women were generally more accurate when they collaborated than when working alone. However, testosterone decreased this boost in the women's performance compared with placebo, even though the hormone did not affect the accuracy of the decisions made individually. The authors suggest that the hormone causes individuals to place much more weight on their own judgment than on that of others.

***Proc. R. Soc. B*** **http://dx.doi.org/10.1098/rspb.2011.2523 (2012)**

CLIMATE CHANGE

## Coming surge in storm surges

As the climate warms and sea levels rise, the frequency of local extremes in storm surges will increase along much of the US coastline.

To assess changes in local flood risk, Claudia Tebaldi at Climate Central in Princeton, New Jersey, and her colleagues combined projections from a model of global sea-level rise with long-term records from 55 tidal gauges around the United States. The team estimates that by 2050, one-third of gauge locations will see an increase in the frequency of extreme high-water levels that are currently expected to occur only about once a century. Some locations can expect to see these extremes, on average, every ten years, others even annually.

In a separate study, Benjamin Strauss, also at Climate Central, and his colleagues assessed US communities' topographic vulnerability to sea-level rise. Given that sea level could increase by one metre or more during this century, the team estimates that 3.7 million people live within one vertical metre of local mean high tide.

***Environ. Res. Lett.*** **7, 014032; 014033 (2012)**

NATURE.COM
For the latest research published by *Nature* visit:
www.nature.com/latestresearch

# SEVEN DAYS *The news in brief*

RESEARCH

## No faster than light

Neutrinos don't travel faster than light, according to results from the ICARUS experiment at the Gran Sasso National Laboratory near L'Aquila, Italy. The experiment found no light-busting speed when it timed 7 neutrinos as they travelled about 730 kilometres from CERN, Europe's particle-physics lab near Geneva, Switzerland — contradicting last September's results from the OPERA experiment, also at the Gran Sasso lab. OPERA had recorded neutrinos travelling faster than light, but has since uncovered possible problems with its measurement. The ICARUS report was posted to the preprint server arXiv.org on 15 March (M. Antonello *et al.* http://arxiv.org/abs/1203.3433; 2012). See go.nature.com/go4247 for more.

## Early drug screening

The newest centre at the US National Institutes of Health — the National Center for Advancing Translational Sciences (NCATS) in Bethesda, Maryland, which aims to speed new drugs to market — has announced its first major deal. NCATS will partner with drug firm Eli Lilly, based in Indianapolis, Indiana, to screen around 3,800 approved and investigational medicines to find potential new uses. The two organizations announced on 13 March that the screening will take place over the next 12–18 months and the results will be posted publicly at http://tripod.nih.gov/npc. See go.nature.com/rgudpy for more.

## LHC restarts

The world's most powerful particle accelerator has begun warm-up stretches for its 2012 run. On 14 March, beams of protons again began to circulate in the Large Hadron Collider (LHC) at CERN, Europe's particle-physics lab near Geneva, Switzerland. Full-scale collisions at 8 teraelectronvolts should begin in April, and scientists could confirm the detection of the long-sought-after Higgs particle by the end of the year.

E. SARKISOV/CORBIS

# Scientists join protest over Spanish cuts

Scientists have warned Spain's government that its planned budget cuts and hiring freeze could be fatal for national research. Along with widespread general protests (pictured, in Madrid) this month against budget cuts and labour reforms, more than 36,000 people (including three Nobel laureates) and 65 organizations have signed an 'open letter for science in Spain', which was presented to members of parliament at the Spanish Royal Academy of Sciences in Madrid on 16 March. Research minister Carmen Vela says that the government is planning to cut €743 million (US$978 million) from the science budget, a fall of 9% from last year; a draft budget is due on 30 March. See go.nature.com/hcarmz for more.

## Children's study row

Two advisers to the US National Children's Study — which aims to track environmental influences on the health of 100,000 children — have resigned in less than a fortnight. Ellen Silbergeld, an environmental scientist at Johns Hopkins Bloomberg School of Public Health in Baltimore, Maryland, resigned on 5 March, followed on 16 March by biostatistician Jonas Ellenberg of the University of Pennsylvania's Perelman School of Medicine in Philadelphia. They and other scientists are complaining about an abrupt change in sampling design, in which the study will recruit subjects from the offices of physicians rather than taking a representative sample of the US population. See go.nature.com/wb9sh8 for more.

## Biomedical awards

The Howard Hughes Medical Institute in Chevy Chase, Maryland, is investing US$200 million to fund up to 30 US biomedical researchers for five years. The 15 March announcement marks the first time the institute has held a general competition for its coveted investigator awards since 2007. See go.nature.com/j2a3xt for more.

BUSINESS

## Academic pharma

In the latest union between academia and industry, drug giant Merck has announced that it will create a non-profit research entity called the California Institute for Biomedical Research (Calibr), to be located in San Diego, California. The institute plans to hire about 150 scientists and will be headed by chemist and serial entrepreneur Peter Schultz, currently at the Scripps Research Institute in La Jolla, California.

D. GRAY/REUTERS

Academics from around the world will be able to submit proposals for research at Calibr. See go.nature.com/26fj7 for more.

## UK venture capital

The Wellcome Trust, the world's largest non-governmental funder of biomedical research, announced on 20 March that it would launch a £200-million (US$371-million) business to invest in health-care and life-sciences companies. The charity — which awards around £600 million in research grants each year — says that in the past it has invested in biotech companies, and that £148 million of £2.7 billion it invested in venture-capital firms in the year to 30 September 2011 already goes to life-sciences and health-care businesses. But the new fund marks its largest direct effort to invest in biotech start-ups.

POLICY

## Rare-earth trade

The United States, Europe and Japan have jointly complained to the World Trade Organization that China is restricting exports of rare-earth elements. The elements are quite plentiful, but miners in China (**pictured**, smelting lanthanum) produce more than 90% of the supply. They

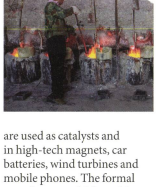

are used as catalysts and in high-tech magnets, car batteries, wind turbines and mobile phones. The formal complaint — which could result in sanctions — was made on 13 March, and follows years of disputes about China's export quotas.

## Misconduct in China

China's education ministry has launched an effort to curb scientific misconduct at universities. Rules announced on 14 March require universities to create mechanisms for inspecting original data, and for getting departing scientists to hand over materials produced in experiments. Universities must also create committees with five or more experts to investigate academic misconduct, and arrange ethics training. Various Chinese organizations have previously issued guidelines to stem scientific misconduct, but many scientists complain that the measures are not implemented and cheaters remain unpunished. A few universities, notably Zhejiang University in Hangzhou, have stepped up efforts to be stringent (see *Nature* **481**, 134–136; 2012).

## SESAME funding

A US$110-million synchrotron is still on track for construction near Amman, Jordan, despite political upheaval in the Middle East. Iran and Israel announced on 13 March that they had joined Jordan and Turkey in committing funding to the project, known as SESAME (Synchrotron-light for Experimental Science and Applications in the Middle East). Partners have now promised $20 million in total, and SESAME is looking for $15 million more to complete its first four beamlines by 2015. See page 385 for more.

## Animal shipments

UK scientists warned last week that pressure from animal-rights activists has led all ferry companies and many airlines to stop transporting research animals (including mice) into the United Kingdom. Less than 1% of UK experiments use animals from abroad. Science minister David Willetts said that the government is working with airlines and ferry companies to try to tackle the problem, perhaps by getting researchers and industry to agree on codes of conduct for animal transportation. For more on the issue of airlines and primate transport, see pages 373 and 381.

## COMING UP

**25–29 MARCH**
The 'chemistry of life' — including topics such as the biochemical basis of epigenetics — is the key topic at the American Chemical Society's spring meeting in San Diego, California.
go.nature.com/ystib8

**26–29 MARCH**
'Planet under Pressure' will see scientists and policy-makers meet in London to discuss the latest research on ecosystems and planetary stewardship.
go.nature.com/xtqrnh

**28 MARCH**
Swiss drug firm Novartis's six-year legal fight with India's government, which began when the firm was denied a patent on a cancer drug, goes to India's supreme court. The ruling could set precedents for patented drugs in India and many developing countries.
go.nature.com/aliuqr

## Indian budget

Researchers in India were not impressed by a moderate increase in the country's science budget, announced on 16 March. Rises varied between 2% and 18% for scientific departments, but, with inflation running at 7%, there will be little extra real spending power — even though Prime Minister Manmohan Singh had promised in January that there would be a "major increase" in research spending. See page 384 for more.

SOURCE: CSTP

## TREND WATCH

Junior researchers are being squeezed out of Japanese universities by government policies that have trimmed hiring. The claim is made in a draft report on Japan's science and technology activities from the Council for Science and Technology Policy, the nation's top advisory body on science. It points out that the number of faculty members under 35 has plunged from more than 10,000 to 6,800 in the past 30 years (see chart). See go.nature.com/bide1g for more.

### GOING GREY

Despite a growth in the number of university faculty members in Japan, there are fewer opportunities for young researchers.

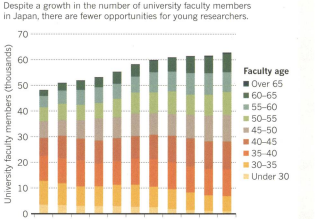


NATURE.COM
For daily news updates see:
www.nature.com/news

# nature MIDDLE EAST
Emerging science in the Arab world

twitter facebook google+

The Arab world has a rich history of scientific breakthroughs. Ensure you're part of the scientific and medical community gaining access to a regularly updated list of **science jobs and local events in the Middle East**.

From the latest news, in-depth features, expert commentaries and research highlights to regional jobs, event listings and alerts direct to your inbox – ***Nature Middle East*** is your free comprehensive portal keeping you at the centre of science in the Arabic speaking Middle East.

**nature.com/nmiddleeast**

Download the free app for your phone at http://gettag.mobi

Sponsored by

nature publishing group npg

# NEWS IN FOCUS

**CRYSTALLOGRAPHY** Opioid receptors revealed in double exposure **p.383**

**PHOTONIC CHIPS** Giving researchers the right tools for the job **p.388**

**TRANSLATIONAL MEDICINE** Teaming mice and men for better clinical trials **p.389**

**PROFILE** Joe Thornton, the man who resurrects extinct proteins **p.390**

CHRISTOPHER J. MORRIS/AP

Protesters make their mark at an Animal Transportation Association meeting in Vancouver on 18 March.

ANIMAL RESEARCH

# Activists ground primate flights

*Supply of research monkeys to Western labs under threat as airlines react to animal-rights campaign.*

BY MEREDITH WADMAN

Each year, thousands of macaques and other monkeys are flown into Europe and North America to supply academic and industrial research labs — more than 18,000 to the United States in 2011 alone. But in a campaign that could affect scientists across the West, the few major air carriers that still transport non-human primates are coming under unprecedented pressure to halt the practice.

One key route under threat is from China, which last year shipped more than 70% of the research primates sent to the United States (see 'Up in the air'). On 14 March, animal breeders in China met with officials of China Southern Airlines to implore them to resume flights into Los Angeles International Airport, the largest US port of entry for research primates. Last August, China Southern cancelled a shipment from Guangzhou of 80 crab-eating macaques (*Macaca fascicularis*) destined for Los Angeles, after a social media, e-mail and telephone campaign by pressure group People for the Ethical Treatment of Animals (PETA), based in Norfolk, Virginia. China Southern has not flown research primates into Los Angeles since then.

"This was part of our larger campaign to disrupt the flow of primates to US labs," says Justin Goodman, associate director of the laboratory investigations department at PETA in Washington DC. The group complains that imports are supplementing an already-burgeoning primate population in US labs (see 'Frequent flyers').

Two other airlines are also in the public spotlight. Air France faces mounting pressure as the last major European carrier to transport research primates. And Air Canada is petitioning the Canadian Transportation Agency, the body that regulates Canadian air carriers, for the required permission to refuse to transport research primates in the future. With news breaking last week that ferry companies have entirely ceased transporting all research animals — including sophisticated mouse disease models — into the United Kingdom, researchers fear that this is the start of a larger trend.

Michael Hsu, president of animal-breeding company Shared Enterprises in Richlandtown, Pennsylvania, says that activism is affecting companies such as his, which maintains a macaque breeding colony in Shanghai and relies on flights into Los Angeles to get its animals to its clients. China Southern, he says, was easily the biggest carrier serving Los Angeles ▶

## UP IN THE AIR

In 2011, some 97% of the 18,044 non-human primates imported into the United States for use in research came from a handful of countries. Airlines are facing pressure to stop such shipments.

SOURCE: PETA/FWS

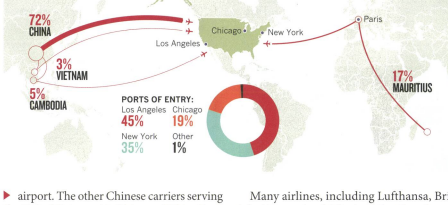


▶ airport. The other Chinese carriers serving the United States — Air China and China Eastern — have lower capacity, creating a bottleneck for breeders lining up to ship animals. The situation, says Hsu, "is causing a big backlog. It's costing us money. We've been producing these animals for these markets, and if we can't ship them, it's very difficult for us to sustain them."

Breeding the animals in the United States instead would be problematic: infrastructure and labour costs are much higher than they are in Asia, and colonies are much more likely to become the targets of animal activists. And moving the animals by sea is a non-starter because of the deleterious effects of the six-week trans-Pacific journey on the animals' health.

Martin Paré, an associate professor at the Centre for Neuroscience Studies at Queen's University in Kingston, Ontario, worries not only about his own access to primates, but about a slippery-slope effect. "If Air Canada was permitted to stop transporting non-human primates, what would be next? Stopping all animal transportation for research, which is what's happening in the UK?"

Many airlines, including Lufthansa, British Airways and Virgin Atlantic, already refuse to carry research primates. In fact, the China Southern shutdown at Los Angeles resulted in part from PETA putting pressure on Lufthansa, which unloads planes for China Southern at the airport. Activists pointed out to Lufthansa that unloading research primates for the Chinese carrier was at odds with its policy on the transport of non-human primates. Within 24 hours, the China Southern macaque shipment was cancelled. Goodman speculates that "Lufthansa was anticipating a really bad PR situation". Lufthansa says that it cannot comment on matters involving another carrier.

At the time that it merged with United Airlines in 2010, Continental Airlines was the last remaining US carrier that still transported research primates. United is preparing to publish a policy for the merged airline later this year.

"Nearly every major airline rejects the transport of primates to laboratories," says Goodman. "The handful that are still doing it are facing more intense opposition and scrutiny than they ever have before. Because it's not in their best interest to continue doing so, I am sure that they will stop."

## SEVERED LINKS

The next several months could prove crucial. After last week's meeting, China Southern is still deciding whether it will resume transporting research primates through Los Angeles. If Air Canada's petition to stop shipping primates is successful, Canadian researchers would be inconvenienced, but not entirely cut off — around 1,700 non-human primates were imported from the United States last year, mostly driven across the border. The Public Health Agency of Canada and Queen's University are challenging the airline's move, and a decision from the transportation agency is expected later this year.

"The research that Queen's University performs has significant benefits for the health and welfare of Canadians," says Steven Liss, the university's vice-principal for research. He adds that the humane treatment of the animals is "always" the university's priority. "Air travel is simply the fastest and least stressful way of transporting them."

Air France issued a statement last September declaring that "nothing allows the airline to decide on the merits of the use of animals in biomedical research", which it called "important and scientifically justified". Nonetheless, after it was bombarded with PETA-orchestrated e-mails, phone calls and Facebook postings, the airline cancelled a scheduled 1 February shipment from Mauritius of 60 monkeys bound for a private laboratory in Everett, Washington.

The apparent success of the public campaign has alarmed breeders, importers and biomedical researchers. "It's unfortunate that some airlines have chosen to capitulate to a small number of individuals with an agenda who aren't truly representative of the general public," says Matthew Bailey, vice-president of the National Association for Biomedical Research in Washington DC, a trade organization that lobbies on lab-animal policy for drug firms and research universities.

Tipu Aziz, a professor of neurosurgery at the University of Oxford, UK, has used macaques to study Parkinson's disease. He believes that restricting transport of animals will not have the desired effect. "My gut feeling is that more and more scientists will go elsewhere to do primate research," he says. "I have no qualms about going abroad to do my work. There are quite a few countries that have good facilities: there are centres in India, Singapore, Malaysia, China."

***"More and more scientists will go elsewhere to do primate research."***

Others say that the drug industry — a major user of research primates — may also be inclined to relocate activities if the flight barrier becomes insurmountable.

"Let's say [the activists] get their wish and no animal comes into the United States," Hsu argues. "Merck is not going to say: 'Okay, fine.' They are going to go to other countries where animal care might not be as good, and start doing research there."

Still, expert observers say that the pressure on the airlines is significant. "The public tide is turning against the use of non-human primates in general, and researchers must either find alternatives or convince the public there is a compelling reason to continue such research," says Paul Root Wolpe, director of the Center for Ethics at Emory University in Atlanta, Georgia, which is home to the Yerkes National Primate Research Center. If scientists don't make a louder, more persuasive public case, he says, "more companies — not only in transportation — will choose the side of animal-rights advocates". SEE EDITORIAL P.373

## FREQUENT FLYERS

The United States has increased imports of non-human primates (NHPs) over the past decade, supplementing a growing lab population.

SOURCE: PETA/FWS/USDA

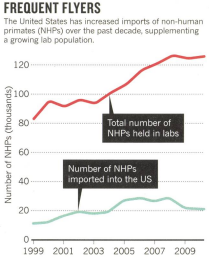

CRYSTALLOGRAPHY

# Opioid receptors revealed

*Two more structures join the parade of once-intractable proteins.*

BY LIZZIE BUCHEN

On a small table in his office at the Scripps Research Institute in La Jolla, California, Ray Stevens spreads out a sheet of paper covered with colourful branched lines, each sprouting and thinning before terminating in an esoteric code. "This is the dream," he declares.

The intricate diagram represents the largest family of receptor proteins encoded in the genome — the G-protein-coupled receptors (GPCRs), ubiquitous cell-surface molecules that are activated by light, odours, hormones and neurotransmitters. Stevens wants to determine the atomic structures of receptors on all branches of the tree. This week, that goal moved two receptors closer: Stevens's group has solved the atomic structure of the κ-opioid receptor (κ-OR)[1], and a team led by Brian Kobilka at Stanford University in California has solved the medically crucial μ-opioid receptor (μ-OR)[2]. The structures, published in *Nature*, bring the tally of GPCR structures solved this year alone up to five.

Ten years ago, Stevens's dream would have seemed a hopeless fantasy — the complex, dynamic molecules had confounded relentless attempts to expose their atomic secrets by X-ray crystallography. But in 2007, several technological breakthroughs brought the drought to an end[3], and the structures began to trickle out, with one or two solved nearly every year. Now, it seems the flood is approaching. Stevens's and Kobilka's groups each have another structure ready to go, on top of the five GPCRs they have already published this year[4–6]. Stevens predicts several more from his lab by the end of the year.

The opioid receptors are hot targets. Opioid drugs, including morphine, codeine and oxycodone, are invaluable in medicine for their powerful painkilling and sedative effects. But they are also highly addictive, an enormous liability that limits their medical use. Their ability to produce a strong sense of euphoria also leads to rampant recreational use of prescription drugs and their more potent and deadly derivative, heroin. The majority of their effects, including analgesia, euphoria and sedation, are mediated by the μ-OR, although most opioid drugs are promiscuous, activating κ-OR and other opioid receptors as well. Understanding the molecular structure of these receptors is crucial for designing drugs that exert the beneficial actions of opioids but lack the unwanted side-effects.

But opioid receptors, like other GPCRs, had long dodged the scrutiny of X-ray crystallography. The technique requires relatively large amounts of purified protein; for proteins nestled in cell membranes, such as GPCRs, that means carefully extracting the molecules from their fatty environment while maintaining their delicate shapes. Identical copies of the protein must then be packed so tightly that they form a crystal. This step is particularly difficult for GPCRs, which have floppy loops that are resistant to staying in place and conforming to a regular crystal lattice.

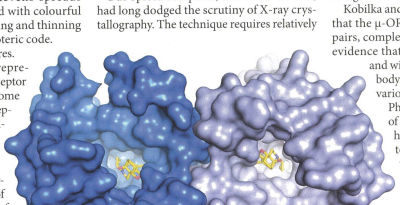

KOBILKA LAB

When crystallized with a ligand (yellow), μ-opioid receptors form an intimate pair.

But one by one, the bottlenecks were circumvented. Kobilka, who had worked on crystallizing the $\beta_2$-adrenergic receptor ($\beta_2$AR) for more than 20 years, discovered that he could quiet the most restive loop by replacing it with a protein called T4L. In 2007, he and Stevens both crystallized the $\beta_2$AR using T4L and a medium called the lipidic cubic phase[7,8]. Since then, all but one of the solved GPCRs have been cracked using this approach.

The μ-OR and the κ-OR structures reveal that the binding pockets of both receptors are large and gaping, which Stevens suggests could explain how the κ-OR recognizes such a diverse set of molecules. Kobilka and his colleague Sébastien Granier, now a molecular pharmacologist at the French National Institute of Health and Medical Research in Montpellier, say that the openness of the μ-OR binding site may also explain why the actions of opioids can turn on so quickly and be rapidly reversed. Heroin overdoses, for example, can be quickly treated with opioid antagonists such as naloxone.

Kobilka and his colleagues also discovered that the μ-OR crystallized in tightly linked pairs, complementing several other lines of evidence that the receptor pairs with itself and with other opioid receptors in the body. These pairings may mediate the various effects of opioid drugs.

Philip Portoghese at the University of Minnesota in Minneapolis, who has been studying opioid receptors since the 1960s, is thrilled with the structures. "When I first started in the opioid field, crystallographic determination of any receptor was viewed as science fiction," he says. "Never in my wildest dreams did I think I would live to see the coordinates of not one, but two opioid receptors." Portoghese points out, however, that both receptors were crystallized in their inactivated states, which he says may limit the value of the structures in the hunt for safer painkillers.

Nor are crystal structures the be-all and end-all for rational drug design. GPCRs are not static; they writhe and twist, and crystal structures don't capture this crucial dynamism, which may be critical for designing drugs that can join in this dance. Kobilka, Stevens and many others are complementing crystallography with techniques that can capture protein movement, such as nuclear magnetic resonance and molecular-dynamics modelling.

On Stevens's website, where the tree of dreams is prominently displayed, 14 victorious red flags mark solved GPCRs, and more will follow very soon. It took at least 20 years of dogged devotion to solve the $\beta_2$AR — but today, when someone visits Stevens's lab to learn about crystallography, he has them crystallize the once-uncrystallizable protein as an introductory exercise. It takes three days. ■


1. Wu, H. *et al. Nature* http://dx.doi.org/10.1038/nature10939 (2012).
2. Manglik, A. *et al. Nature* http://dx.doi.org/10.1038/nature10954 (2012).
3. Buchen, L. *Nature* **476,** 387–390 (2011).
4. Haga, K. *et al. Nature* **482,** 547–551 (2012).
5. Kruse, A. C. *et al. Nature* **482,** 552–556 (2012).
6. Hanson, M. A. *et al. Science* **335,** 851–855 (2012).
7. Rosenbaum, D. M. *et al. Science* **318,** 1266–1273 (2007).
8. Cherezov, V. *et al. Science* **318,** 1258–1265 (2007).

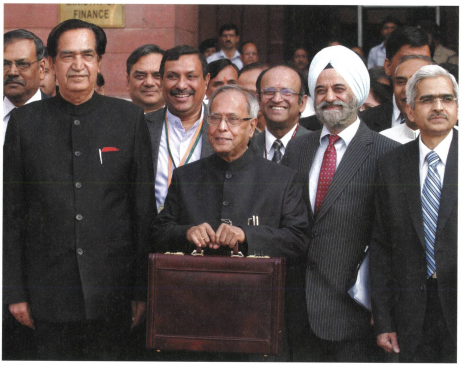


V. MAHESH/REUTERS

Finance minister Pranab Mukherjee (centre, with other ministers) didn't deliver hoped-for increases.

FUNDING

# Indian budget disappoints

*Downturn finally ends run of increases for science.*

BY K. S. JAYARAMAN IN BANGALORE

India's remarkable growth in science funding — notching up annual increases of about 25% over the past five years — seems finally to have been hit by the global economic downturn.

Last week, the government's budget for 2012–13 promised increases of between 2% and 18% for most of its scientific departments, disappointing researchers who note that the country's 7% inflation rate will consume most of the extra cash (see table). An apparent increase of 52% in the space-science budget was actually caused by a roll-over of unused funds from last year.

Researchers had been expecting a major funding boost this year, after assurances from Prime Minister Manmohan Singh. In a speech at the annual Indian Science Congress in Bhubaneswar in January (see *Nature* http://dx.doi.org/10.1038/nature.2012.9750; 2012), Singh lamented that China's progress in science has overshadowed India's, and he promised a "major increase" in research and development spending, from the current 1% of the gross domestic product to at least 2% by 2017. He also backed plans from the Department of Science and Technology (DST) for a 50-billion-rupee (US$1-billion) supercomputing facility in Bangalore; a 13.5-billion-rupee neutrino observatory near Pudukkottai in Theni district, Tamil Nadu; and a 3.5-billion-rupee project to improve monsoon forecasting.

But on 16 March, finance minister Pranab Mukherjee's budget dashed scientists' hopes. The country's economic growth has slowed over the past year, prompting a cautious budget. "Less funding for science agencies will mean fewer research grants for university scientists," says Ajay Sood, a physicist at the Indian Institute of Science in Bangalore, and president of the Bangalore-based Indian Academy of Sciences.

Vishwa Mohan Katoch, secretary for the Department of Health Research, says that although he had requested 30 billion rupees for 2012–13, his department had been allocated only 9 billion, an 18% increase on last year. Kanikaran Satyanarayana, deputy chief of the Indian Council of Medical Research, says that as a result, plans to increase funding for virology laboratories and establish a nationwide disease-surveillance network will have to be put on hold.

"If we want to bring in quality changes we need big money," says Katoch. "But what can the government do if they do not have resources?"

Thirumalachari Ramasami, secretary for the DST, is confident that the relative austerity of this year's budget will not set a precedent. "I am optimistic that funding will be restored [in 2013] once the 12th five-year plan, for 2012–17, is finalized by the planning commission," he says. That plan is expected by next month. Ramasami adds that the big DST projects outlined in Singh's speech should not be affected by the disappointing increases.

There is ample evidence that India's previous budgets have helped to advance science in the country, says Lingadahalli Shashidhara, a developmental biologist at the Indian Institute of Science Education and Research in Pune. "We have quadrupled the number of research faculty members in just ten years," he says. "The quality of projects coming to funding agencies is going up, and India is publishing research papers in high-impact journals more frequently."

But some researchers feel that Indian science needs reform much more than it needs extra cash. Rajesh Kochhar, a historian of science at the Indian Institute of Science Education and Research in Mohali, says that research institutions must be more strictly audited to divert funding away from poorly performing centres and give more to the most productive researchers. Increased funding cannot help to advance science "unless the weeds are ruthlessly removed so that the flowering plants can flourish", he says. ■

**DISCOURAGING RESULT**

Budget allocations in billions of rupees.

| | 2011–12 | 2012–13 | % increase |
|---|---|---|---|
| Atomic energy | 67.24 | 76.51 | 13.8 |
| Department of Health Research | 7.70 | 9.08 | 17.9 |
| Department of Science and Technology | 26.06 | 28.73 | 10.3 |
| Department of Scientific and Industrial Research | 32.17 | 34.84 | 8.3 |
| Department of Biotechnology | 13.77 | 15.00 | 9.0 |
| Department of Agricultural Research | 50.08 | 53.92 | 7.7 |
| Oceanographic research | 6.99 | 7.13 | 1.8 |

PHYSICS

# Clashing nations back SESAME

*Participants put politics aside to find cash for construction of Middle-East synchrotron.*

BY GEOFF BRUMFIEL

Israel and Iran can agree on little these days, but they have found common ground in a scientific project.

Despite brinkmanship over Iran's nuclear programme, the two nations have joined with Jordan and Turkey to commit crucial funding to the construction of Synchrotron-light for Experimental Science and Applications in the Middle East (SESAME). Under an agreement announced on 13 March, the partners have promised a total of US$20 million towards the construction of the project. SESAME is now looking for a further $15 million from other partner nations to complete the synchrotron's first four beamlines in 2015.

"The fact that we could get such an agreement given the political situation is kind of remarkable," says Chris Llewellyn Smith, the president of SESAME's governing council and a past director-general of CERN, Europe's particle-physics lab near Geneva, Switzerland.

Based in Allan, outside Amman, Jordan, SESAME aims to build scientific expertise in its member countries and bolster cultural ties between them. When completed, the $110-million machine would be the Middle East's only source of high-intensity synchrotron X-rays, which are used in fundamental research ranging from molecular biology to materials science.

The project mirrors the organization of CERN, but Amman is a long way from Geneva — metaphorically as well as literally. In recent years, SESAME has had to contend with the assassination of two members of its Iranian delegation and huge political upheavals in partner countries including Egypt.

Despite the tensions, scientists involved with the project say that SESAME is succeeding because it has something to offer all the participants. Israel, for example, gets a world-class research facility on its doorstep and an opportunity to show its willingness to collaborate with neighbours, says Eliezer Rabinovici, director of the Institute for Advanced Studies at the Hebrew University of Jerusalem, and a member of SESAME's council. Other member states see an opportunity to educate a young and rapidly growing science base. "Turkey is also interested in developing similar laboratories and SESAME would be a very good experience," says Zehra Sayers, a physicist at Sabancı University in Istanbul and head of SESAME's scientific advisory committee.

Llewellyn Smith is optimistic that the remaining money can be found. Now that local partners have committed funding, the project is more likely to gain support from outsiders such as the United States and the European Union. And other partners in the Middle East, notably Egypt, may yet provide cash, although political turmoil could make commitments difficult.

Rabinovici says that SESAME shows the strength of scientific collaboration, even under the most difficult circumstances. "This is an existence proof that scientists can, at least for a period of time, transcend the politics around them," he says. ■

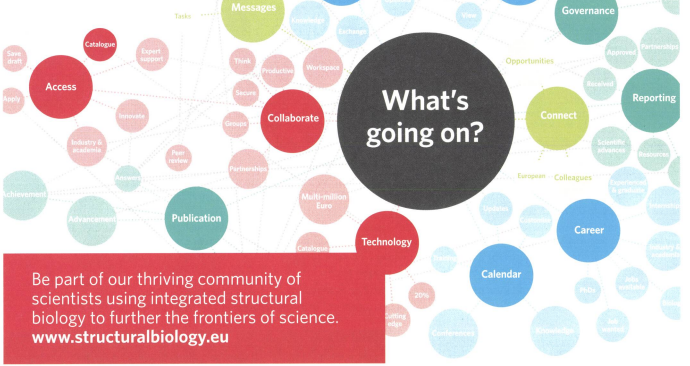

BBSRC
bioscience for the future

## Delivering the Age of Bioscience

# DIRECTOR OF SCIENCE

## BIOTECHNOLOGY AND BIOLOGICAL SCIENCES RESEARCH COUNCIL

With an annual budget of circa £0.5 billion, the Biotechnology and Biological Sciences Research Council supports world-class research in some of the most exciting areas of contemporary science. As the UK's principal funder of basic and strategic biological research, it helps to ensure that the UK has at its disposal the science which is required to meet the complex multi-disciplinary needs of industry, policy makers and other stakeholders. The continuing strength of its bioscience research is recognised as a major factor in multi-national companies' decisions to locate their businesses and invest in the UK.

The role of Director of Science is central to the activity of BBSRC and the post-holder will play a major role both internally and externally. Reporting to the Chief Executive, Professor Douglas Kell, you will work closely with him, other members of the BBSRC Executive and the BBSRC Council in the development of the scientific strategy and will be responsible for its formulation. This will include input into the overall direction of the basic science programme; strategic science policy advice; the development of priorities for consideration by Council and the identification of opportunities for close collaboration with other funders, including other Research Councils, in areas of multi- and inter-disciplinary research.

You will combine a strong personal research record and breadth of understanding across the biological sciences with the strategic leadership and communication skills that will be essential for this key and high profile role.

The post will command a salary of circa £100,000 (more may be available for an exceptional candidate). There is a performance related bonus scheme.

A defined benefit pension scheme (analogous to the Civil Service Pension Scheme) or a "partnership" scheme is available. The post will be based in Swindon. Candidates taking a leave of absence from their current employer would be considered.

**Further information, including how to apply, may be obtained from Carbon-NfP, who would be happy to have an informal and confidential telephone discussion.**
**Please contact Sharon Taylor by email sharon.taylor@carbon-nfp.com in the first instance.**

**The closing date for applications is Friday 20th April 2012.**

U222703R

www.carbon-nfp.com

CARBON-NfP

# Chair and Members of the Emerging Science and Bioethics Advisory Committee

DH Department of Health

The Department of Health is seeking to appoint a Chair and up to 14 Members to the Emerging Science and Bioethics Advisory Committee (ESBAC). ESBAC will be the main UK advisory body on the wider implications of developments in bioscience and its impact for health when it is established as an expert committee on 1 May 2012. It will provide advice to UK Health Departments on emerging healthcare scientific developments and their ethical, legal, social and economic implications.

## Chair

*Ref: DH1225*

The Chair of ESBAC will be an outstanding individual with a first-class reputation and strong leadership skills able to command the confidence of the public, professional healthcare providers, commissioners of services, educational institutions and Ministers. The Chair will have significant experience of successfully leading a complex, high-profile committee, and a commitment to the values of accountability, probity and the Government's best practice principles on transparency, timeliness and exchange of information.

## Up to 14 Members

*Ref: DH1492*

Members will need a broad spectrum of expertise, not only in health related biosciences and biotechnology, but also in medical, social, ethical, legal, commercial and public engagement issues. Most importantly, those appointed to the Committee must be fully committed to the satisfactory discharge of its functions. Those recommended for appointment need to be good communicators with a good track record of committee experience.

The Chair will be appointed for a term of 3 years and the Members will be appointed for a combination of 2 to 3 year terms.

The Chair and Members will be paid expenses in line with Department of Health policy and it is envisaged that the full committee will meet up to 3 times a year.

**For more information, please visit our website www.dh.gov.uk/appointments. If you require an alternative format such as braille, large print or audio please call Holly Wainwright on 0113 254 6135 quoting the relevant reference number.**

**The closing date for applications for all positions is midday on 4 April 2012.**

**Interviews for the Chair role are likely to take place on 19 April 2012.**

**Interviews for the Member roles are likely to take place w/c 7 or 14 May 2012.**

We value and promote diversity and are committed to equality of opportunity for all and appointments are made on merit.

U222723R



To advertise here please contact — US tel. +1 800 989 7718, naturejobs@natureny.com or Europe/ROW tel. +44 20 7843 4961, naturejobs@nature.com

BIOETHICS

# DNA donor rights affirmed

*NIH committee urges that genome study subjects be told of medically relevant results.*

BY ERIKA CHECK HAYDEN

It is a familiar scenario in genetic research: a subject's DNA is collected for one study, deposited in a database or biobank and then analysed by other researchers for separate studies. But what happens when a later study stumbles on something that could be of significance for the donor, such as an allele for familial hypercholesterolaemia — a treatable genetic disorder that causes progressive atherosclerosis — or some other health-related variation? Do researchers conducting secondary studies and biobanks have a duty to share such revelations with the original research subjects?

They do, when possible, according to a detailed consensus statement from a working group funded by the US National Institutes of Health (NIH) in Bethesda, Maryland, and published this week (S. M. Wolf *et al. Gen. Med.* http://dx.doi.org/10.1038/gim.2012.23; 2012). The statement's 26 signatories consulted dozens of other researchers and biobank managers over a two-year period. They conclude that biobanks "shoulder significant responsibility" for addressing how to deal with 'incidental findings' — those research results that could have medical consequences for the donors of genetic material.

Genetics researchers are divided on the matter of incidental findings. Conventional research ethics holds that participants should not be told of their individual results, to keep them from expecting to benefit personally from the study. What's more, reporting such findings can be a logistical challenge because many studies strip identifying information from donated samples. But, increasingly, geneticists are embracing the idea that research participants have a right to know of any unwelcome surprises in their genome. "If we really believe this is medically valuable and useful data, then we have to act on it," says Leslie Biesecker of the US National Human Genome Research Institute in Bethesda, who contributed to the discussions that led up to the consensus statement but is not a signatory.

S. WILTON/BLOOMBERG VIA GETTY

Genetic testing is increasingly coming up with 'incidental findings'.

The need to establish policies for the return of results has grown with the proliferation of whole-genome sequencing, says James Evans, editor-in-chief of *Genetics in Medicine*, which is publishing an entire issue on the return of results in genetic research, along with the consensus statement.

In the past, says Evans, medically significant incidental findings were an exception in genetic studies, but "when you do whole-genome sequencing you will regularly come up with findings that have some medical import". Yet less than half of US biobanks return results to participants, according to a study done for the working group by Mao Thao of the University of Minnesota in Twin Cities and colleagues. The working group, coordinated by Susan Wolf of the University of Minnesota Law School in Minneapolis, urges biobanks to take the lead in changing that ethos. The group recommends that each biobank sets up a committee to oversee the return of results and also that a single central advisory body be created that would foster consistency among biobank research systems. Wolf led a previous NIH working group that in 2008 published recommendations proposing that primary researchers — those responsible for collecting data — should report some incidental findings back to research participants (S. M. Wolf *et al. J. Law Med. Ethics* **36**, 219–248; 2008).

But some researchers warn that keeping track of incidental results and re-identifying participants so that they can be informed could prove costly and pose ethical and legal difficulties. "It's unfortunate that the authors of the consensus statement didn't discuss the cost implications of what they're proposing, because what they have in mind is going to be expensive and difficult, particularly at a time when funding success is as low as it's ever been," says Ellen Wright Clayton, a paediatrician and lawyer at the Center for Biomedical Ethics and Society at Vanderbilt University in Nashville, Tennessee.

Wolf counters that some biobanks already do return results, so it does not need to be prohibitively costly or difficult. For instance, Biesecker runs a study called ClinSeq, which has enrolled around 900 people whose exomes (the protein-coding part of the genome) are being sequenced. The participants are told about any findings that could have implications for their health care. Biesecker says that there is an increasing tension in the field between studies such as his that underscore the usefulness of genetic medicine and an assumption that it is too costly and difficult to use the results of such studies to help improve patients' lives. "I don't think, as a field, that we can continue to say both things at the same time," Biesecker says. ■ SEE EDITORIAL P.373

S. FISCH

## MORE ONLINE

TOP STORY

One researcher's genome shows personalized genomic medicine in action go.nature.com/rwgs6z

OTHER NEWS

- Satellites expose 8,000 years of civilization go.nature.com/2ejdri
- Rare autism spectrum disorder partially caused by faulty immune cells in the brain go.nature.com/oekimu
- Spurned flies turn to booze go.nature.com/oxshcm

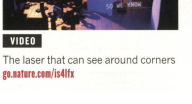

VIDEO

The laser that can see around corners go.nature.com/is4lfx

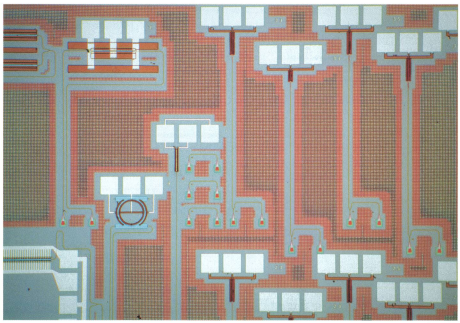

N. HARRIS

Optical components including modulators, waveguides and photodetectors crowd a silicon chip.

TECHNOLOGY

# Photonic chips made easier

*Shared-production system aids academics and start-ups.*

BY KATHERINE BOURZAC

If you want to speed up computers much more, you will need a faster messenger. That is the idea behind silicon photonics, which whizzes data around a silicon chip using light instead of sluggish old electrons.

Photons already carry data in fibre-optic cables for telecommunications. But using light in computing means carving transistors and lasers out of the same wafer of silicon, which needs an advanced manufacturing 'foundry'. Only large companies and a few research institutions with deep pockets have these facilities, and some researchers worry that lack of access is slowing progress in photonics.

A project called Optoelectronic Systems Integration in Silicon (OpSIS) now promises a solution. Based at the University of Washington in Seattle and at the University of Delaware in Newark, OpSIS provides design support for researchers in silicon photonics; organizes shared production runs; and arranges low-cost access to advanced foundries so that academics and start-up companies can create prototype devices. The US Air Force is the project's biggest funder, with more support coming from Intel, based in Santa Clara, California, and design-automation company Mentor Graphics in Wilsonville, Oregon.

OpSIS will make its first batch of silicon photonics prototype chips at the Institute of Microelectronics' foundry in Singapore this month. Its customers are some 25 groups working on high-speed communications circuits, portable medical diagnostic devices and photonics basic research.

Users will pay US$1,500 for one square millimetre of wafer space, with projects requiring anywhere from 10 $mm^2$ to 40 $mm^2$. Researchers going it alone would have to pay for a complete production run at the foundry — at a cost many times higher. OpSIS offers much lower prices by putting many different projects into a single run and splitting the cost.

Michael Hochberg, a photonics researcher at the University of Delaware who co-founded and leads OpSIS, knows how expensive it can be to translate silicon photonics technology from university lab into product. In 2001, he co-founded Luxtera, in Carlsbad, California, the first company to offer integrated electronics and optics on chips, which are now used commercially in data centres and supercomputers. Luxtera spent more than $100 million to develop and produce its first product, released in 2010. "I want to make it possible to do what Luxtera did for an order of magnitude less cost," says Hochberg. OpSIS will soon also have access to foundries owned by Luxtera and by UK aerospace company BAE Systems, headquartered in London.

The history of the silicon chip suggests that OpSIS could be hugely influential. Its shared-production model is based on the University of Southern California's Metal Oxide Semiconductor Implementation Service (MOSIS), which has been operating since 1981 in Marina del Rey and has helped the semiconductor industry to grow rapidly. Electronics pioneers, including Carver Mead at the California Institute of Technology in Pasadena, pushed for academics and small companies to gain access to fabrication facilities ('fabs') to build the integrated circuits they needed to test their ideas and train students. At the time, academics were restricted to making simple devices in the lab, doing theoretical work or — as Mead did — having friends at Intel sneak their students' designs into production runs. "You have to have access to a fab to build the real thing," says Mead.

Silicon photonics now is at a similar stage to the electronics industry in the early 1980s, says Mario Paniccia, director of the photonics technology lab at Intel. Today's photonics researchers have better access to foundries than Mead did decades ago, but most are still excluded from the cutting-edge facilities that can make more complicated devices.

A data-processing photonic chip, for example, must integrate lasers, waveguides and electrical transistors in complex systems that are completely reliable. Making such devices in advanced fabrication facilities ensures that they are of acceptable quality, says OpSIS user S. J. Ben Yoo, director of the Center for Information Technology Research in the Interest of Society at the University of California in Davis.

A service similar to OpSIS has been offered since 2008 by the ePIXfab initiative, funded in part by the European Union. But OpSIS has access to more advanced foundries, says Lukas Chrostowski, an electrical engineer at the University of British Columbia in Vancouver, Canada.

Chrostowski has 20 designs in the first OpSIS run. Several are prototype versions of optical sensors for a hand-held medical-diagnostic device that could analyse blood samples to detect disease biomarkers. Previous versions of this system were far from being hand-held: Chrostowski had to attach an external laser and a detector to an optical chip he made using ePIXfab. Through OpSIS, he will now be able to integrate all the building blocks onto one chip in a more realistic prototype.

This sort of innovation cannot be left only to well funded companies, says Paniccia. "We need more people experimenting, learning, and innovating with silicon photonics." ■

NATURE.COM
For more on silicon photonics, see Focus at: go.nature.com/ywdaa

TRANSLATIONAL RESEARCH

# Mice guide human drug trial

*Parallel approach to cancer study provides genetic insights.*

BY HEIDI LEDFORD

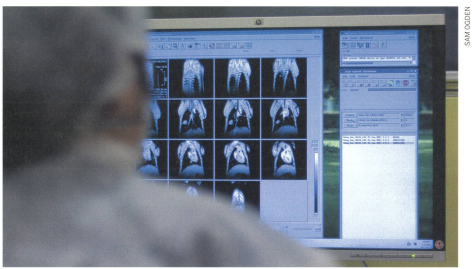

SLOAN KETTERING

A genetically engineered mouse lung-cancer model offers clues to its human analogue.

The mouse hospital at the Dana-Farber Cancer Institute in Boston, Massachusetts, boasts resources rivalling those offered to human patients, including state-of-the-art medical-imaging facilities, round-the-clock nursing staff and access to cutting-edge cancer drugs. The goal is not to cure mice, of course, but to gain insight into clinical trials of those drugs in humans.

The roughly 5,000 rodent residents at Dana-Farber are pioneers in an approach known as a co-clinical trial, in which a human clinical trial is partnered with animal studies designed to reveal clues about why some patients respond to a treatment and others fail to do so. The first findings from the Dana-Farber project, published online on 18 March (Z. Chen *et al. Nature* http://doi.org/hrr; 2012), suggest that adding an experimental drug called selumetinib to standard chemotherapy may help to shrink lung tumours in patients with mutations in a gene called *KRAS*. The parallel study in the mouse revealed, however, that the drug may fail in those who also carry a mutation in a tumour-suppressor gene called *LKB1*.

"Normally, very little scientific interrogation occurs during the conduct of a human cancer trial," says David Tuveson, a cancer researcher at the University of Cambridge, UK, who was not involved in the study. "This is a logical and badly needed path forward."

It is standard for new drugs to undergo animal studies before they reach the clinic. But early-stage animal trials can be misleading because they often fail to mimic the conditions of subsequent human trials, says Andrew Kung, an oncologist at Dana-Farber and an author on the mouse study. By contrast, a co-clinical trial is designed to closely match a parallel trial in human subjects.

Selumetinib, developed by Array BioPharma of Boulder, Colorado, and London-based AstraZeneca, is a member of a hotly pursued class of cancer drug that inhibits a crucial biochemical step promoting tumour-cell proliferation and survival. Full results of the human trial, which enrolled 87 patients with *KRAS* mutations, have yet to be published. Array BioPharma announced last year that, when given with standard chemotherapy, the drug slowed the progress of the cancer. Effects on overall patient survival were not statistically significant.

➲ NATURE.COM
For ways to fix the clinical trial, see: go.nature.com/wy6bns

Like the human subjects, the hundreds of mice used for the co-clinical trial carried a mutated form of *Kras*, but some also contained mutations in the tumour-suppressor genes *p53* and *Lkb1*. Mice treated with selumetinib and standard chemotherapy benefited if they had the additional mutation in *p53* alone, but the *Lkb1* mutation seemed to render the drugs ineffective. Outcomes of the mouse trials were measured using methods similar to those for the human subjects, which meant relying on non-invasive imaging techniques, rather than simply killing the animals and measuring tumour volume, as is often done in animal studies.

***"It is a new way to use mice as a looking glass into the human condition."***

Overall, the mouse study suggests that, in future trials of selumetinib, patients should be screened for the presence of *LKB1* mutations, says Kung. That would allow researchers to determine whether a genetically identifiable subset of patients resistant to the drug may be affecting their results.

The results in mice also suggest that an imaging technique called FDG-PET can measure short-term tumour responses to selumetinib. The method could be a boon for human studies, because patients generally cannot be subjected to repeated tumour biopsies.

The co-clinical approach could speed up drug development as oncology increasingly embraces complex treatment regimens involving multi-drug cocktails and tailored for specific genotypes, says Hugues de Thé, a cancer researcher at the Paris Diderot University. He has used a similar approach in a trial of drugs for a form of leukaemia, but says that the new work is a "technical tour de force" because of the genetic complexity of the tumours studied.

Many other centres are developing facilities for co-clinical trials, but the experiments can be prohibitively expensive. The drugs often need to be given daily, which requires more personnel to handle the animals, and the technology used to image tumours in living animals can be costly. Mouse hospitals will probably have to invest heavily in generating trial-specific mouse models of cancer, cautions Tuveson, who has been using the approach to tackle pancreatic cancer. "You need the infrastructure to breed these animals and then to follow them just like you would in a hospital, and most laboratories do not have that."

But funders are aware of the approach's promise. In 2009, the US National Cancer Institute in Bethesda, Maryland, awarded US$4.2 million to Pier Paolo Pandolfi, a cancer researcher at Harvard Medical School in Boston who is a co-author on the *Nature* study, to establish the co-clinical trial project in lung and prostate cancer. Additional grants from Stand Up To Cancer, a project of the Entertainment Industry Foundation charity, based in Los Angeles, California, are funding co-clinical trials in breast and ovarian cancer. It is a new way, says Tuveson, "to use mice as a looking glass into the human condition". ■

# RAISING THE DEAD

*To dissect evolution, Joe Thornton resurrects proteins that have been extinct for many millions of years. His findings rebut creationists and challenge polluters.*

BY HELEN PEARSON

Halfway through breakfast, Joe Thornton gets a call from his freezer. A local power cut has triggered an alarm on the −80 °C appliance in his lab at the University of Oregon in Eugene, and it has sent out an automatic call. Thornton breaks off our conversation and calls his senior research scientist, Jamie Bridgham, to make sure that the back-up generator has kicked in. If the freezer starts warming up, a lot could be lost — not least a valuable collection of proteins that had been extinct for hundreds of millions of years until Thornton and his team brought them back from the dead.

One deep-frozen vial holds the more-than-600-million-year-old ancestor of the receptors for oestrogen, cortisol and other hormones, which Thornton brought to life[1] nine years ago. Other tubes house proteins more than 400 million years old, which Thornton resurrected a few years later to show how an ancient receptor had changed its preferences — and how the march of evolution cannot be reversed[2–4]. In another corner of the freezer rest the ancient protein components of a sophisticated cellular machine that acquired a more complex form through random mutations rather than selection for superior function, as the group showed in *Nature* this January[5]. The sheer awe of working with long-dead proteins doesn't fade, says Thornton. "It's amazing. The ability to do this type of time travel is fantastic."

Thornton is a leader in a movement to do for proteins what the scientists in *Jurassic Park* did for dinosaurs: bring ancient forms back to life, so that they can be studied in the flesh. "Instead of passively observing things as most evolutionary biologists do, you actively go in and test the hypotheses experimentally," says Antony Dean, a molecular biologist at the University of Minnesota in St Paul who heads another major group in the field. "His is one of the leading labs, no doubt." And Thornton is tackling some important questions, says Kenneth Miller, a molecular biologist at Brown University in Providence, Rhode Island. "He's helping to put some flesh on the bones of speculation about how complexity arises."

What isn't so widely known is that evolutionary biology is Thornton's second career: in his first, he was an activist for Greenpeace, campaigning vigorously against the release of toxic chemicals. He wrote a controversial book on organochlorines: industrial chemicals that include dioxins, polychlorinated biphenyls (PCBs) and pesticides such as DDT. That activist legacy bleeds into his work today, for example in his focus on the oestrogen receptor, which is corrupted by many pollutants. The grubby, sea-green tiles under Thornton's lab benches were carefully sourced to be free of polyvinyl chloride (PVC), one of the organochlorines that worries him most. His activist past also helps to explain why he has been fearless — almost enthusiastic — about highlighting the challenge that his work presents to a creationist argument called intelligent design: the claim that complex molecular systems can only have been created by a divine force. Thornton shows how evolution did the job, leaving no need for a designer.

## ENVIRONMENT TO EVOLUTION

Thornton says that his activist days — during which he saw that many risk-assessment models were shot through with assumptions and biases — left him "intensely committed to methodological reductionism and experimentalism", which he now uses to break evolution down into detailed steps that he can test. "If you're doing science, I think it ought to be as strong and decisive as possible," he says. "If you're doing politics, go ahead, but don't try to disguise it as science."

Thornton's unconventional career path started with an obsession with *Moby Dick*, which led him to study English at Yale University in New Haven, Connecticut. But the course, with its focus on the philosophy of criticism rather than literary texts, left him with a hunger for reality, and nothing seemed more real than politics and activism. He dropped out of college, signed up with Greenpeace and spent several months doorstepping to canvass people for money and support.

In the early 1990s, Greenpeace was campaigning against sources of toxic pollution, and Thornton was drawn in. He became the 'science guy', translating the scientific literature into reports and other material that communities and Greenpeace could use to make their case. "You could rely on Joe when you didn't have enough knowledge of an issue," says Charlie Cray, a research specialist at Greenpeace in Washington DC, who worked with Thornton. His reports "put a challenge out there that industry couldn't answer". One campaign that Thornton helped to organize, against plans to build more than 100 hazardous-waste incinerators across the United States, climaxed in May 1993 when Greenpeace parked a truck dressed up as an incinerator outside the White House and some 60 people chained themselves to it. The next day, the Environmental Protection Agency announced a moratorium on new hazardous waste incinerators.

But Thornton was growing older, and yearning to "develop my own body of work". His time with Greenpeace had taught him the power of science to influence society, and his ambitions turned to research. First, he had to deal with the small matter of graduating from Yale. Then living in New York, he did that by accruing course credits at Columbia University — attending his first molecular-biology classes aged 30 — only to find himself rejected from almost every graduate programme he applied to, in part because of his unusual CV.

Of the seven friends and colleagues of Thornton's who spoke to *Nature*, six called him intense. The seventh described him as "beyond intense". But only a little of that

**NATURE.COM**
Hear more about protein resurrection on *Nature*'s podcast:
go.nature.com/5tlcza

SHAWN RECORDS

intensity is apparent at his Wednesday morning lab meeting in Eugene. The freezer crisis has blown over: the power came back after half an hour and the thermometer rose to only −76 °C. Now graduate student Dave Anderson gets a friendly grilling during a practice talk outlining his thesis proposal: to trace the evolution of the DNA-binding domain of an ancient hormone receptor. The meeting stretches on for 2.5 hours — not uncommon in this lab, everyone says.

### A BINDING FASCINATION

Since his Greenpeace days, Thornton has been fascinated by the steroid hormone receptors: in vertebrates, six proteins that sit in the cell nucleus and control the activity of genes. By binding specific 'ligands' — hormones ranging from oestrogens and androgens to cortisol — the receptors trigger "these remarkable cascades of biological activity during development and physiology", Thornton says. "Their affinity for their hormones is just stunning. A drop of hormone in a railroad tank car of serum is enough" — and yet, as Thornton learned at Greenpeace, they can be waylaid by toxic substances. "I wanted to know where that system came from," he says.

When he was finally accepted for a PhD at Columbia, he set about comparing receptor genes from living organisms to piece together a detailed history of how the receptor family had evolved[8].

Just as Thornton completed his first year of graduate study, however, MIT Press called to ask if he would write a book on organochlorine pollution. He worked in the lab during the day and wrote at night, in a tiny room in his Brooklyn apartment, encircled by towers of papers that eventually formed the nearly 1,200 references and 611 pages of *Pandora's Poison*, which came out in 2000. "I was shocked when I saw the book," says Rob DeSalle, who studies molecular evolution at the American Museum of Natural History in New York, and co-supervised Thornton's PhD. "He could've been writing *War and Peace* and I wouldn't have known it."

The book caused a stir. Drawing on arguments that he had formulated at Greenpeace, Thornton made the case that regulatory policy should focus on managing classes of toxic chemicals rather than tens of thousands of substances, one by one — and that the priority should be organochlorines. These substances, generated by the use of chlorine gas in the chemical and paper-making industries, have properties of stability and solubility that make them desirable to industry but problematic to the environment because they are long-lived and accumulate in animal tissues. *Nature*'s review called *Pandora's Poison* a "landmark" and another review compared it to Rachel Carson's famous 1962 treatise on pollutants, *Silent Spring*. The Chlorine Chemistry Council in Washington DC, however, decried Thornton's "hyperbole and faulty risk analysis".

But Thornton was already gearing up to make a different kind of splash, with his first paper in *Science*[1]. He and his team trampled the assumption that only vertebrates have steroid hormone receptors by cloning one from the sea slug *Aplysia californica*. The finding implied that the origin of the receptor gene was far more ancient than anyone had realized. "I would've hated to be a fellow grad student. He was writing a book and publishing in *Science* and having two children at the same time," says Darcy Kelley, a biologist at Columbia and Thornton's other PhD co-supervisor.

The approach that Thornton took in the 2003 study is one that he has loosely followed ever since. Starting with the genes for steroid hormone receptors from a slew of living organisms, he clambered backwards through the evolutionary tree to deduce the most likely sequence of the common ancestor of all such receptors, which existed some 600 million to 800 million years ago, in the common ancestor of "you and a snail", as he puts it. Instead of stopping there, as most evolutionary biologists would have done, he then built the gene and inserted it into cells that could manufacture the ancient protein.

Resurrecting the protein, says Thornton, allowed his team "to experimentally test hypotheses about evolution that would otherwise be just speculation". They went on to show[1] that the ancestral receptor was sensitive to oestrogens but not to related hormones — supporting the idea that the family of receptors evolved through a series of gene duplications

**"HE'S HELPING TO PUT SOME FLESH ON THE BONES OF SPECULATION ABOUT HOW COMPLEXITY ARISES."**

and that the copies gradually evolved affinities for other ligands (see 'Receptors, resurrected').

By the time his paper came out in *Science*, Thornton had taken a faculty position in Eugene, an old hippy town that pays as much homage to bicycles as it does to cars. He built a house (no PVC, sustainable bamboo floors) and set to work building up his protein-resurrection lab.

Thornton wanted to delve deeper into the puzzle of how complex systems with tightly interacting molecular parts evolve. It was a long-standing conundrum. As Charles Darwin wrote in *On the Origin of Species*: "If it could be demonstrated that any complex organ existed which could not possibly have been formed by numerous, successive, slight modifications, my theory would absolutely break down." And what was an evolutionary puzzle to biologists was a target for evolution's critics. Michael Behe, a biochemist at Lehigh University in Bethlehem, Pennsylvania, and a senior fellow at the Discovery Institute in Seattle, Washington, proposed in the 1990s that such systems — the blood-clotting cascade, for example, or the molecular motor called the flagellum — are so "irreducibly complex" that they could not have evolved step by step, and can only be the product of intelligent design.

Thornton says that he didn't set out to refute intelligent design, but the prospect of a fight hardly put him off. "Been there, enjoyed that," he says. He chose to explore a pair of steroid hormone receptors: the mineralocorticoid receptor (MR), which binds the hormone aldosterone and regulates salt and water balance; and the closely related glucocorticoid receptor (GR), which binds cortisol and controls stress response. A gene duplication more than 450 million years ago produced the two receptors — but aldosterone didn't arise until many millions of years later. The timing seemed to make the MR a textbook example of irreducible complexity: how could selection drive the evolution of a lock (the MR) to fit a key (aldosterone) that didn't yet exist?

### EVOLUTION AT WORK

Led by Bridgham, Thornton's team found the answer by resurrecting the ancestor of both receptors. To their surprise, it was sensitive to aldosterone, suggesting that it had been activated by an ancient ligand with a similar structure[2]. Once aldosterone had evolved, the team proposed, evolution was able to take advantage of the existing receptor to control a new biological function — a process that Thornton termed molecular exploitation. They also showed how its sister receptor, the GR, was evolving functions of its own.

"Such studies solidly refute all parts of the intelligent design argument," wrote Christoph Adami, an evolutionary biologist at the Keck Graduate Institute of Applied Life Sciences in Claremont, California, in an article entitled 'Reducible complexity'[7]. But Behe dismissed the result. The receptor and ligand are not irreducibly complex, he says, and evolution did not give them any truly new function. "I think his results are quite consistent with my own view that Darwinian processes are poor ones to explain the complexity found in life," Behe told *Nature*.

Thornton turned up more clues to the workings of evolution when his team explored the history of the GR, which became sensitive only to cortisol over the course of about 20 million years. Working with structural biologists at the University of North Carolina, Chapel Hill, the group determined the crystal structure of the common ancestor of the GR and MR. They showed[3] that two crucial mutations together

**RECEPTORS, RESURRECTED**

The vertebrate steroid hormone receptors evolved from a common ancestor that existed 600 million to 800 million years ago (Mya). Resurrecting ancient proteins on its family tree has revealed key events in their evolution.

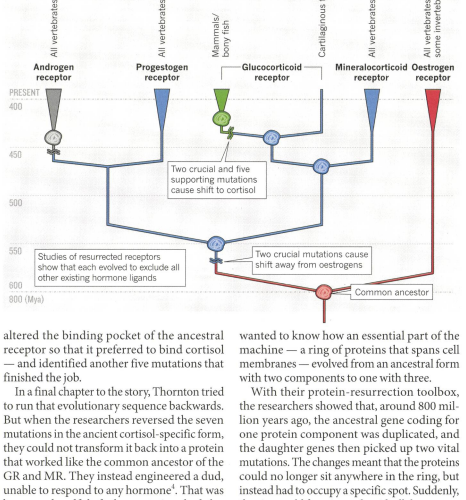


altered the binding pocket of the ancestral receptor so that it preferred to bind cortisol — and identified another five mutations that finished the job.

In a final chapter to the story, Thornton tried to run that evolutionary sequence backwards. But when the researchers reversed the seven mutations in the ancient cortisol-specific form, they could not transform it back into a protein that worked like the common ancestor of the GR and MR. They instead engineered a dud, unable to respond to any hormone[1]. That was because a handful of other mutations had also cropped up on the way to making a cortisol-specific receptor. They played little part in the receptor's new function, but acted as an evolutionary ratchet, preventing it from regaining its old one.

Thornton showed that it was necessary to undo those mutations too, to reverse the change. To him, the work was a powerful demonstration that the path of evolution can be contingent on random events. "Chance plays a very large role in determining what evolutionary outcomes are possible," he says. The study captivated the scientific press — and beyond. "Evolution opens gateways into the future. But it appears to close them — firmly — behind it as well," read an editorial in the *New York Times*.

In the Nature article that was published this year[2], Thornton took a break from hormone receptors, and instead collaborated with Tom Stevens, a geneticist at Eugene, to dissect the evolution of V-ATPase, a molecular machine that pumps protons across membranes to acidify compartments inside cells. The group wanted to know how an essential part of the machine — a ring of proteins that spans cell membranes — evolved from an ancestral form with two components to one with three.

With their protein-resurrection toolbox, the researchers showed that, around 800 million years ago, the ancestral gene coding for one protein component was duplicated, and the daughter genes then picked up two vital mutations. The changes meant that the proteins could no longer sit anywhere in the ring, but instead had to occupy a specific spot. Suddenly, the ring could function only with all three parts. What surprised Thornton was that the three-component ring seemed to work no better than its two-component counterpart. Random mutations that actually corrupted proteins had led to 'irreducible complexity'.

## COMPUTING COMPLEXITY

The study flipped another finger to intelligent-design proponents — but "I'm sort of bored with them", Thornton says. He is more excited by the next scientific story that is about to come out of the lab. His group wanted to explore how the ancestor of the entire steroid hormone receptor family, which was sensitive only to oestrogens, evolved into forms sensitive to other hormones. And this time, he found no clues in the crystal structures of resurrected proteins from before and after the change.

The answer can be found on a computer screen at the end of Thornton's lab. Mike Harms, a postdoc who joined the lab three years ago, used his expertise in biophysics and some immense computational power to simulate the movements of every atom in the ancestral receptors, showing how just two mutations drove the transformation. When Harms hits play, an oestrogen molecule snuggles its way into the binding pocket of a receptor roughly 550 million years old. But when he runs a simulation of the same receptor with those two mutations, the oestrogen never finds a comfortable spot.

This evolutionary story also sheds light on why the oestrogen receptor is now vulnerable to the threats against which Thornton campaigned in his former life. The team worked out that each steroid receptor evolved to be only as specific as it had to be to bind its target ligand and exclude all others that existed at the time. The oestrogen receptor achieves this by binding substances that contain a chemical structure called an aromatized A ring. Because oestrogens are the only steroid hormones to have such a ring, that criterion was enough to ensure that the receptor bound only oestrogens for many millions of years. Until, that is, the chemical industry started pumping out hundreds of substances containing such aromatized rings, which the oestrogen receptor unwittingly bound. "The endocrine disrupters are taking advantage, unfortunately, of the promiscuity that is the result of the evolutionary history of receptors," Thornton says.

Thornton does see progress on the issues on which he once campaigned. Production of toxic chemicals in the United States has fallen since his days with Greenpeace, and in 2007 the European Union enacted REACH (Registration, Evaluation, Authorisation and Restriction of Chemicals), which emphasizes elimination of the most dangerous substances. That law puts the onus on the chemical industry to show that a chemical is safe rather than on regulators to prove it is dangerous — the approach for which Thornton argued in *Pandora's Poison*.

Does he miss having something to campaign against? Yes and no. "I'm less able to convince myself that the world has to be exactly as I envision it. So it's harder for me to occupy that activist persona." Besides, he says, "My kids take all that energy now."

Or almost. His creations need tending too. Back in his office, we listen to the tinny voicemail message left by the freezer on his phone earlier that day. "The past is calling," Thornton says. ■

**Helen Pearson** *is* Nature*'s chief features editor.*

1. Thornton, J. W., Need, E. & Crews, D. *Science* **301,** 1714–1717 (2003).
2. Bridgham, J. T., Carroll, S. M. & Thornton, J. W. *Science* **312,** 97–101 (2006).
3. Ortlund, E. A., Bridgham, J. T., Redinbo, M. R. & Thornton, J. W. *Science* **317,** 1544–1548 (2007).
4. Bridgham, J. T., Ortlund, E. A. & Thornton, J. W. *Nature* **461,** 515–519 (2009).
5. Finnigan, G. C., Hanson-Smith, V., Stevens, T. H. & Thornton, J. W. *Nature* **481,** 360–364 (2012).
6. Thornton, J. W. *Proc. Natl Acad. Sci. USA* **98,** 5671–5676 (2001).
7. Adami, C. *Science* **312,** 61–63 (2006).

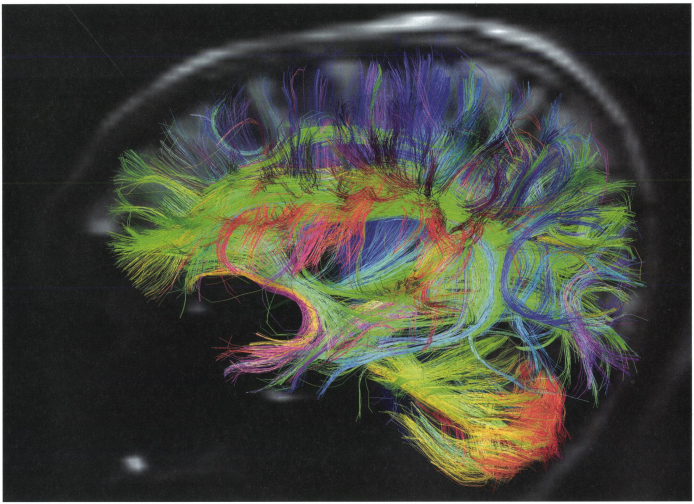

MGH HUMAN CONNECTOME PROJECT ACQUISITION TEAM

# Making *connections*

## Is a project to map the brain's full communications network worth the money?

BY JON BARDIN

A building that once housed a Second World War torpedo factory seems an unlikely location for a project aiming to map the human brain. But the Martinos Center for Biomedical Imaging — an outpost of the Massachusetts General Hospital in an industrialized stretch of Boston's riverfront — is home to an impressive collection of magnetic resonance imaging machines. In January, I slid into the newest of these, head first. The operator ran a few test sequences to see whether I experienced any side effects from the unusually rapid changes in this machine's magnetic field. And, when I didn't — no involuntary muscle twitches or illusory flashes of light in my peripheral vision — we began. The machine hummed, then started to vibrate. For 90 minutes, I held still as it scanned my brain.

That scan would be one of the first carried out by the Human Connectome Project (HCP), a five-year, US$40-million initiative funded by the National Institutes of Health (NIH) in Bethesda, Maryland, to map the brain's long-distance communications network. The network, dubbed the 'connectome', is a web of nerve-fibre bundles that criss-cross the brain in their thousands and form the bulk of the brain's white matter. It relays signals between specialized regions devoted to functions such as sight, hearing, motion and memory, and ties them together into a system that perceives, decides and acts as a unified whole.

The connectome is bewilderingly complex and poorly understood. The HCP proposes to resolve this by using new-generation magnetic resonance imaging (MRI) machines, like that used to scan my brain, to trace the connectomes of more than 1,000 individuals. The hope is that this survey will establish a baseline for what is normal, shed light on what the variations might mean for qualities such as intelligence or sociability, and possibly reveal what

**The nerve fibres of the author's brain were traced by diffusion spectrum imaging, and coloured to represent their direction.**

happens if the network goes awry. "We increasingly believe that brain disorders — from schizophrenia to depression to post-traumatic stress disorder — are disorders of connectivity," says Thomas Insel, director of the National Institute of Mental Health (NIMH) in Bethesda and a strong supporter of the HCP. "So it is of vital importance that we have ways of detecting and quantifying these connections."

Yet many wonder whether the NIH is making a mistake. Researchers have yet to prove that MRI techniques can produce a reliable picture of normal connectivity, never mind the types of abnormal connection likely to be found in brain disorders, and some researchers argue that the techniques have not been adequately validated. "I would do the basic neuroscience before I started running lots of people through MRI scanners," says David Kleinfeld, a physics and neurobiology researcher at the University of California, San Diego.

## THE GRAND CHALLENGE

Proponents counter that the HCP is a calculated risk. "No one thinks this is going to produce a wiring diagram like you might have for the electricity in your house," says Insel. But so little is known about the connectome, he says, that even crude maps would represent a major scientific advance.

The decision to take that risk was made by the NIH's Blueprint for Neuroscience Research, set up in 2004 as a collaboration among the 15 NIH institutes, centres and offices with an interest in nervous-system research. In 2009, after five years of funding smaller projects, the group asked officials from across the NIH to submit ideas for 'grand challenges' in neuroscience: large-scale programmes that, Insel says, "would be both extremely high-impact, and virtually impossible with traditional grant mechanisms".

The Blueprint group received a dozen submissions, including one from Michael Huerta, then a programme officer at the NIMH and a member of a Blueprint subcommittee. Huerta, now at the NIH's National Library of Medicine, began his research career studying the organization of mammalian brains using old-school anatomical and neural-tracing techniques, which typically require the injection of a tracer compound that migrates along nerve fibres and reveals their routes. So he was all too familiar with the barriers to such studies in humans. For ethical reasons, tracers can only be used post-mortem — when they don't migrate far enough to trace a fibre's full length. "The studies just never panned out," says Huerta.

In 2007, Huerta became fascinated by two new non-invasive imaging methods that might finally allow researchers to study the finer details of connectivity in the brains of living humans. The first was diffusion-spectrum imaging (DSI), developed in 2005 by Van Wedeen, a radiologist at the Martinos Center, and his colleagues[1]. DSI is a refinement of the two-decades-old diffusion tensor imaging technique, which exploits MRI's ability to detect the direction in which water molecules are moving at each point in the brain. Because most of those molecules move along the lengths of nerve fibres, like water through a pipe, the data can be used to reconstruct each fibre's location and trajectory. What DSI adds is a more sophisticated form of signal analysis that allows researchers to continue tracing fibre bundles even when one slice, he showed neurons that originated in the left cortex, then branched out and sent fibres to areas on both the left and the right side of the brain. "The brain is not made up of point-to-point connections," he said. "It's made up of trees."

This level of connectome structure is invisible to even the most advanced diffusion-imaging methods, says Mitra, who heads the Mouse Brain Architecture Project, a parallel version of the HCP, funded by the NIH and the W. M. Keck Foundation of Los Angeles, that seeks to generate a whole-brain wiring diagram for the mouse using staining techniques. And the problem is

> *"We increasingly believe that brain disorders are disorders of connectivity."*

seems to pass behind another, a situation that posed serious problems for the older technique.

The second method that caught Huerta's attention was resting-state functional MRI (rs-fMRI), in which people think about nothing in particular while their brain activity is measured. This is quite different from conventional functional-imaging studies, in which participants are asked to carry out a specific cognitive task and researchers look for the brain regions that are activated in the process. In rs-fMRI, there is no task, and researchers look for correlations among the activity levels in different areas. The presumption is that any two regions with a consistently high correlation are linked — perhaps by an actual bundle of nerve fibres, but certainly by working together in some way.

The application of both DSI and rs-fMRI had already led to a number of high-profile publications. But Huerta realized that few groups were applying both methods in the same subjects, and most studies used small samples, limiting their generalizability. So he proposed that the Blueprint group fund a Human Connectome Project that would apply both methods to hundreds of people. This would allow the first large-scale comparison to be made between structural connectivity, as determined by DSI, and functional connectivity, as determined by rs-fMRI. "No single neuroimaging approach would give you the type of gold-standard connectivity data you need," says Huerta, recalling his argument for the dual data sets.

The Blueprint group was intrigued, but was not blind to the problems inherent in these techniques. One obvious issue is DSI's spatial resolution: each fibre bundle in the image contains thousands of neurons, meaning that it would miss a great deal of structure on smaller scales.

Partha Mitra, a neuroscientist at Cold Spring Harbor Laboratory in New York, illustrated the problem to me by displaying a series of high-resolution digital pictures of mouse brain slices, each of which had some of its neurons coloured with a dark brown dye. On one such made even worse when the data are converted into a 'connectivity matrix', which seeks to quantify how much every point in the brain is connected to every other point — but can't tell the difference between, say, two separate fibres and one fibre with two branches.

The Blueprint group was also aware of concerns about resting-state scans. As with the more familiar form of fMRI, what is actually measured isn't neural activity itself, but blood flow. The general presumption is that the two quantities are closely related — that blood flow increases in a region of the brain whenever the neurons there are active and need to be supplied with more oxygen. But recently, Kleinfeld points out, several studies have called that assumption into question, showing that some increases in blood flow in the brain occur without an increase in neuronal activity[2]. "There is no simple one-to-one relationship," he says.

## A REMAINING CONCERN

That makes rs-fMRI studies particularly hard to interpret, Kleinfeld adds, if only because the brain's resting-state activity may fluctuate on the same timescales that its blood vessels do. A recent review[3] of rs-fMRI admits that this vascular fluctuation "remains a concern". Other studies show that even something as simple as a subject's pattern of breathing[4] or slight movements of the head[5] can significantly confound rs-fMRI measurements.

Even leaving the technical challenges aside, there was no assurance that collecting the connectomes of hundreds of individuals would lead to interesting generalizations. "You could certainly imagine situations in which everyone's wiring diagrams are quite different," says Gregory Farber, the programme officer at the NIMH who manages the connectome project. Nonetheless, the Blueprint group was swayed by the argument that imperfect data are better than no data. "The committee asked, 'Will we have better methods in five years?'," recalls Huerta. "I'm sure we would. But if we followed

## SCANNING THE CONNECTOME

The Human Connectome Project aims to trace the brain's long-range communication network using two main techniques, both of which rely on magnetic resonance imaging (MRI) to obtain data from living people.

**Mapping structure**
Diffusion spectrum imaging detects the movement of water molecules that flow along nerve fibres in the brain. The result is a map of the brain's neuronal network.

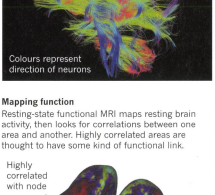


MGH HUMAN CONNECTOME PROJECT ACQUISITION TEAM

**Mapping function**
Resting-state functional MRI maps resting brain activity, then looks for correlations between one area and another. Highly correlated areas are thought to have some kind of functional link.

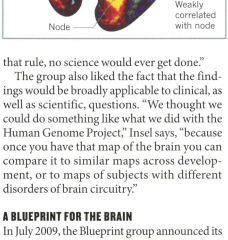


M.F. GLASSER & D.C. VAN ESSEN, THE HUMAN CONNECTOME PROJECT

The brain has many areas specialized for specific functions, some of which are shown here.

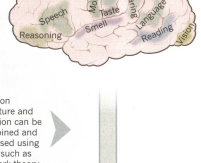


Data on structure and function can be combined and analysed using tools such as network theory.

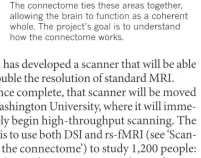

The connectome ties these areas together, allowing the brain to function as a coherent whole. The project's goal is to understand how the connectome works.

that rule, no science would ever get done."

The group also liked the fact that the findings would be broadly applicable to clinical, as well as scientific, questions. "We thought we could do something like what we did with the Human Genome Project," Insel says, "because once you have that map of the brain you can compare it to similar maps across development, or to maps of subjects with different disorders of brain circuitry."

### A BLUEPRINT FOR THE BRAIN

In July 2009, the Blueprint group announced its choice of the HCP as one of three grand challenges — the other two focused on pain and on drugs for nervous-system disorders — and simultaneously put out a request for proposals. On 15 September 2010, the NIH announced that it would be funding two HCP proposals.

The larger of the two is a 5-year, $30-million effort led by David Van Essen, a neurobiologist at Washington University in St Louis, Missouri, and Kamil Ugurbil, an fMRI pioneer at the University of Minnesota in Minneapolis. (Another collaborator is Olaf Sporns, a neuroscientist at Indiana University in Bloomington, a co-author on the 2005 review article that coined the term 'connectome'[1].) During phase one, now nearing completion in Minneapolis, this team has developed a scanner that will be able to double the resolution of standard MRI.

Once complete, that scanner will be moved to Washington University, where it will immediately begin high-throughput scanning. The plan is to use both DSI and rs-fMRI (see 'Scanning the connectome') to study 1,200 people: 300 identical twins, 300 non-identical twins and 600 non-twin siblings. This will allow researchers to explore how much of the brain's connectivity is mapped out by genes. Volunteers will also complete behavioural tests and other fMRI, magnetoencephalogram and electroencephalogram protocols, so that brain structure can be further correlated with function. All these data will be made public, allowing unaffiliated researchers to answer their own questions, and Van Essen's group plans to release a set of new data-analysis tools. Connectomics, Van Essen says, "has been a cottage industry. But we expect this project to allow for a much richer, more unified approach".

The smaller HCP project — a 3-year, $8.5-million effort led by Bruce Rosen, a radiologist at the Massachusetts General Hospital, and Arthur Toga, a neurologist at the University of California, Los Angeles — involved building a new fMRI scanner optimized for the collection of fibre-tracking data. The idea was to massively increase the gradient strength of the machine — a measure of how rapidly the MRI's magnetic field varies from point to point in the brain. A more intense gradient is like "a bigger mirror in a telescope", says Wedeen, who is director of connectomics at the Martinos Center. It simultaneously makes the instrument more sensitive to faint signals, and gives it a higher resolution. The machine has now been built — it is the one that collected images of my brain in January — but will require much more tweaking and testing before it is optimized for routine use. But the researchers have already achieved a tenfold increase in sensitivity to the water-diffusion signal, allowing their scanner to trace connections much more precisely than the best off-the-shelf machines.

In a press release announcing the launch of the HCP in July 2009, Insel said that the project would "map the wiring diagram of the entire, living human brain" and that this map could be linked to "the full spectrum of brain function in health and disease". Such lofty ambitions may or may not succeed in five years. But the project still has its place, says Sebastian Seung, a computational neuroscientist at the Massachusetts Institute of Technology in Cambridge, who studies brain connectivity at the cellular level. "I think it is a mistake to think we have to look at every cell in every region of the brain to make scientific progress," says Seung, who is not involved in the HCP.

But he also emphasizes that the HCP's connectivity map will be, at best, a beginning. "That is just going to tell us where to look," he says. "Then we need to study actual cells to learn more", to figure out how the brain's networks actually transmit information.

A week after my visit to the Martinos Center, I received my DSI data. Using free software from the centre, it is easy to explore the architecture of my brain. I can clearly see my hippocampus, and the vast array of fibres projecting from the midbrain sensory hubs up to my cerebral cortex. I am overwhelmed by the visible detail and obvious organization. At present, it is just a pretty picture — a novelty to show friends. But, I wonder: once scientists know what 'average' looks like, and once they understand the variations, what, if anything, will this rainbow-coloured highway map of my brain say about me? ■

**Jon Bardin** *is a freelance writer based in New York.*

1. Wedeen, V. J., Hagmann, P., Tseng, W. Y., Reese, T. G. & Weisskoff, R. M. *Magn. Reson. Med.* **54,** 1377–1386 (2005).
2. Sirotin, Y. B. & Das, A. *Nature* **457,** 475–479 (2009).
3. Kelly, C., Biswal, B. B., Craddock, R. C., Castellanos, F. X. & Milham, M. P. *Trends Cogn. Sci.* **16,** 181–188 (2012).
4. Di, X., Kannurpatti, S. S., Rypma, B. & Biswal, B. B. *Cerebral Cortex* http://dx.doi.org/10.1093/cercor/bhs001 (2012).
5. Power, J. D., Barnes, K. A., Snyder, A. Z., Schlaggar, B. L. & Petersen, S. E. *Neuroimage* **59,** 2142–2154 (2012).
6. Sporns, O., Tononi, G. & Kötter, R. *PLoS Comput. Biol.* **1,** e42 (2005).

# COMMENT

**MARINE CONSERVATION** A broader concept for protecting ocean reserves **p.399**

**PHYSICS** How the discovery of cosmic rays a century ago seeded particle physics **p.400**

**EXHIBITION** Transgenic sushi and the future of food **p.404**

**OBITUARY** Renato Dulbecco, elegant pioneer of cancer biology **p.408**

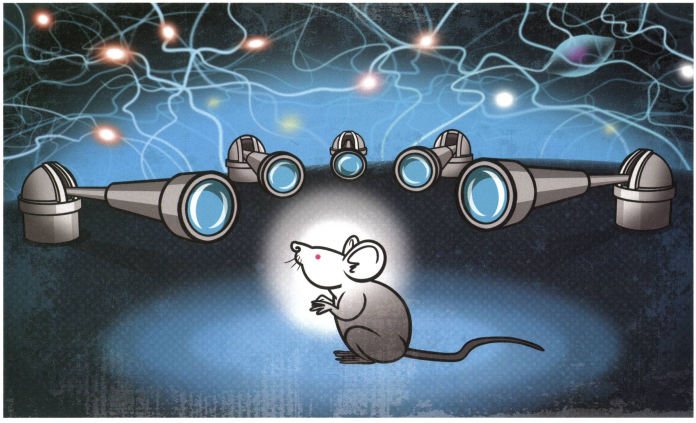

ILLUSTRATION BY PETE ELLIS, DRAWGOOD.COM

# Observatories of the mind

An ambitious project to map the mouse brain at the Allen Institute for Brain Science is a huge undertaking that may unify neuroscience, argue **Christof Koch** and **R. Clay Reid**.

Neuroscience is a splintered field. Some 10,000 laboratories worldwide are pursuing distinct questions about the brain across a panoply of spatio-temporal scales and in a dizzying variety of animal species, behaviours and developmental time-points. At any large neuroscience meeting, one is struck by the pace of discovery, with 50,000 or more practitioners heading away from each other in all directions, in a sort of scientific Big Bang.

Although this independence is necessary, it has prevented neuroscience from entering a more mature phase, which would involve developing common standards and collaborative projects. Neurophysiologists are more likely to use each other's toothbrushes than each other's data and software; physiological results are hoarded and rarely made accessible online; molecular compounds and transgenic animals are shared only after publication. All of this has made comparisons across laboratories difficult and has slowed progress.

At the Allen Institute for Brain Science in Seattle, Washington, we and our colleagues are initiating an experiment in the sociology of neuroscience — a huge endeavour that will involve several hundred scientists, engineers and technicians at the institute. Philanthropist Paul G. Allen, who founded the institute in 2003, has pledged US$300 million for the first four years of an ambitious ten-year plan that will accelerate progress in neuroscience, bringing his total commitment so far to $500 million. Our goal is to attract the best young scientists and build a series of 'brain observatories', with the aim of identifying, recording and intervening in the mouse cerebral cortex, the outermost layer of the brain. Unlike the telescopes that peer at remote events in space ▶

▶ and time, our instruments will track the flow of information in complex, interbraided neural circuits within a layer of tissue one millimetre thick.

The goal is to synthesize knowledge from all relevant disciplines — from genomics, anatomy and physiology to computer modelling — into a comprehensive theory of how the mouse uses its cortex to see. Following Allen's founding mandate for the institute, we will curate and publicly share all data and other resources (such as transgenic animals, probes and neuronal morphologies) for free, even before publication.

We believe that this initiative signals the arrival of large-scale science in a field that is populated by small groups. It will require rewarding the team, rather than a few lead investigators, for its collective effort. We envisage a time in the future when sophisticated, well-equipped brain observatories — 'mindscopes' — will complement the many academic neuroscience labs that will continue to make the bulk of discoveries.

Although the institute's project will focus on visual stimuli in mice, it will capture fundamental aspects of higher brain functions: perception, conscious awareness and decision-making, and how they lead to action. Once neuroscientists know the basic mechanisms in the mouse, they may start to understand more-complex forms of perception in other animals, including humans. In short, we believe that this project has the potential to revolutionize our understanding of the mammalian brain.

## 2020 VISION

The brain observatories initiative focuses on the cerebral cortex — the proverbial 'grey matter' that is one of the hallmarks of mammals, and the seat of cognition and intelligence. For its size, the cortex is the most complex piece of organized matter in the known Universe. But given a grain of cortex, it is not easy to tell from which mammal it came. We all have the same basic hardware — humans just happen to have a thousand times more of it than mice (see 'Man versus mouse').

The project will start with the anatomy of cortical neurons, using molecular techniques to count and catalogue the diverse arrays of cells that transmit information into and out of the visual cortex, as well as those that lie solely within the cortex. Then we will observe and measure the electrical activity of a sizeable fraction of those neurons to learn how the function of the cortex follows from its structure. It is a big question, but less daunting if one considers the cortex as being composed of many copies of a basic local circuit.

Studies of the human brain have been revolutionized by magnetic resonance imaging, which reveals brain regions activated in real time. However, the underlying signals are slow and fuzzy, and brain regions are not the building blocks of the mind — neurons, in their immense complexity, are the atoms of perception and thought.

Fortunately, scientists can now study individual mammalian neurons in living brains, by making neurons fluoresce using genetic engineering. Neurons can be made to emit flashes of light when they are active or, using the most recent optogenetics techniques, can be controlled with light (named Method of the Year in 2010 by *Nature Methods*[1]). In this way, researchers can transiently and reversibly control certain events in specific cell types at defined times. Perturbing the nervous system lets neuroscience move from correlation to causation, from observing that a given circuit is activated whenever the animal makes a decision to inferring that this circuit is necessary for decision-making.

Other technological advances enable neuroscientists to visualize every axon, dendrite and synapse in a circuit using three-dimensional electron microscopy. Another observatory in the visual-brain programme is designed to record the electrical activity of thousands of neurons simultaneously. When all of these techniques are stitched together, one can imagine a full physiological and structural characterization of entire brain regions.

Finally, we will use all of this information to generate realistic and dynamic computer models of the mouse cortex and its associated structures, and use these to build theories of how the visual cortex behaves. The modelling facility will be next door to the labs so that collaborators can mingle easily. This should shorten the time between prediction and experimental validation, a virtuous circle that will be iterated until the model faithfully reproduces the data.

## A CALCULATED RISK

Even though neuroscientists have spent the past 120 years uncovering the constitutive elements of the mammalian brain, we are far from understanding how any higher brain function comes about. Yet such knowledge is vital, especially because of the toll that nervous-system injuries and disorders take on individuals, families and society at large.

Although the challenge may seem daunting, we are not the first to propose such a huge undertaking. For example, the European Human Brain Project, under the leadership of Henry Markram at the Swiss Federal Institute of Technology in Lausanne, hopes to bring together some 150 principal investigators in 22 countries to create working computer models of the mouse, rat, monkey and human brains[2]. The brain observatories programme at the Allen Institute differs in that we are focusing on a single sense, in a single species, in one institution.

We know that such an expensive project will have critics: the resources required could fund hundreds of other projects, so why focus them in this way? Our response is that funding agencies are already spending billions of dollars on many smaller projects across all areas of biomedical research, and the Allen Institute wants to pioneer a new approach. We want to understand one piece of brain tissue by integrating knowledge across techniques and scales, rather than distributing the funds more widely.

There is a risk that this project will not work out as we anticipate, and that the various brain observatories — looking at anatomy, physiology and modelling, for example — will not synergize to form a sophisticated understanding of the mouse visual cortex. There is no guarantee that neuroscience is ready to become big science — but the only way to find out is to try. ■

**Christof Koch** *is at the Allen Institute for Brain Science, Seattle, Washington 98103, USA, and at the California Institute of Technology, Pasadena, California 91125, USA.* **R. Clay Reid** *is at Harvard Medical School, Boston, Massachusetts 02115, USA, and will join the Allen Institute this summer. e-mail: christof@alleninstitute.org*

1. *Nature Methods* **8,** 1 (2011).
2. Waldrop, M. M. *Nature* **482,** 456–458 (2012).
3. Herculano-Houzel, S. *Front. Hum. Neurosci.* **3,** 31 (2009).
4. Herculano-Houzel, S., Mota, B. & Lent, R. *Proc. Natl Acad. Sci. USA* **103,** 12138–12143 (2006).
5. Wang, Q. & Burkhalter, A. *J. Comp. Neurol.* **502,** 339–357 (2007).

**MAN VERSUS MOUSE**

Comparing the human and mouse brain reveals why mapping the mouse brain is easier.

SOURCE: REFS 3–5

| | Human | Mouse |
|---|---|---|
| Mass of brain | 1,500 grams | 0.5 grams |
| Number of brain neurons | 86 billion | 70 million |
| Number of cortical neurons | 16 billion | 14 million |
| Fraction of cortex that is visual | 20% | ~10% |
| Cortical regions involved in vision | 30 | 10 |
| Number of neurons in these areas | 5 billion | 1 million–2 million |
| Axons in optic nerve | 1 million | 45,000 |

➲ NATURE.COM
For more on the European Human Brain Project:
go.nature.com/fjcdtt

# Think big for marine conservation

Err on the side of caution and protect the widest-possible areas of ecologically important deep sea, say **Phil Weaver** and **David Johnson**.

Marine protected areas are key tools for conservation, but they have some serious shortcomings. The Convention on Biological Diversity (CBD) has called for these areas to cover 10% of each of the world's marine and coastal ecoregions by the end of 2020. Even this modest target is proving elusive. So far, less than 2% of the ocean has been designated as protected, and nearly all of these areas are in coastal and continental-shelf regions. This is partly the result of a lack of data from the open ocean, and partly because of pressures from various interest groups, which may resist the management of ocean areas with valuable resources.

There is now an additional option for protecting the marine environment. In 2010, the CBD created a process to officially endorse Ecologically or Biologically Significant Areas (EBSAs) and to convey information to competent intergovernmental organizations, such as the United Nations General Assembly, for further action. The point of EBSAs is to allow scientists to identify areas that are particularly important to the function of marine ecosystems without the requirement for an accompanying detailed management plan. This 'softer' procedure opens the door to labelling a larger swathe of the ocean as important to ecosystem functioning.

An EBSA is defined by a set of criteria established by the CBD in 2008: the area should contain unique, rare or endemic creatures and/or habitats; have a special role in the survival of a given species; be important for the survival or recovery of threatened species; be vulnerable, fragile or slow to recover once harmed; have high biological productivity; and/or have high biological diversity. These are good criteria. Unfortunately, there are vast swathes of ocean about which very little is known, for which these criteria can be hard to prove.

This lack of knowledge is not preventing fishing, deep-sea mining and other exploitation from expanding, however; nor should it stand in the way of designating EBSAs. We believe that EBSAs should be made as large as possible, encompassing all areas within which the criteria are likely to be substantively met, even before that can be proven.

This approach should be widely adopted by the scientific community now, while proposed EBSAs are being drawn up for a first technical evaluation at a CBD meeting in Montreal, Canada, at the end of April, before their political endorsement.

## ATLANTIC BEGINNINGS

The first CBD regional workshop to identify EBSAs was held in September 2011 to consider the northeast Atlantic, which already hosts a number of marine protected areas and precautionary bottom-fisheries closures. This ocean includes the Hatton and Rockall banks and basin area, to the west of Ireland and Scotland. This area, parts of which are heavily fished, hosts many discrete habitats and supports a wide range of animals, including fragile cold-water coral reefs and sponges. It provides feeding grounds for birds such as shearwaters and petrels. And it may harbour turtles and the endangered blue whale (*Balaenoptera musculus*) as well as the critically endangered North Atlantic right whale (*Eubalaena glacialis*). The exact boundaries of any of the habitats and species distributions are yet to be established.

WATERFRAME/ALAMY

Species such as North Atlantic anemones deserve conservation attention.

Initially, there was considerable support among the 25 participating scientists for the designation of small, discrete EBSAs, such as isolated seamounts, in the northeast Atlantic. Experts were focused on their particular specialist habitat or species group, and were conscious that their expert judgement would be scrutinized by their peers. Under such circumstances, it can be difficult to support a large EBSA that extends beyond one's expertise and into areas where there are little data.

Fortunately, the eventual consensus of this meeting was to propose large EBSAs: eight extensive areas (averaging 362,097 square kilometres each) and two smaller international bird areas. For Hatton–Rockall, that meant drawing a line around the entire banks region, measuring 264,322 $km^2$. This stands in stark contrast to the average size of the 276 protected areas in this ocean's national waters, which average just 1,040 $km^2$ each, and the 6 high-seas protected areas, at 47,718 $km^2$ each.

What should happen once an EBSA is defined? We suggest that a marine spatial plan be drawn up for each EBSA and regularly updated. This will articulate a vision, show what activity is taking place in the region (from commercial fishing to tourism) and study the impacts of those activities. In terms of management, we support a three-tier approach whereby areas that historically have been heavily fished and are now degraded remain unprotected; areas with light historical fishing are given full protection; and moderately fished areas are subject to further scrutiny. Marine protected areas could sit comfortably within EBSAs, giving protection to the most critical ecosystems. The main benefit of this system is that it appeals to many different stakeholders: for example, it legitimizes existing fishing activities while preventing them from spreading to vulnerable ecosystems in future.

As scientists meet to rationalize what exactly EBSAs should look like in different parts of the world, we urge them to err on the side of caution and to make the areas large rather than small. This will open the door to broader conservation measures and to sustainable development in future. ■

**Phil Weaver** *is science coordinator of the Global Ocean Biodiversity Initiative and is at the National Oceanography Centre, Southampton, UK.* **David Johnson** *is executive secretary for the Convention for the Protection of the Marine Environment of the North-East Atlantic (OSPAR) in London. e-mail: ppew@noc.ac.uk*

Further reading accompanies this article online at go.nature.com/soxziu

# A century of cosmic rays

High-energy nuclei coming from far beyond the Solar System, and the exotic particles they produce, remain our best window onto the extreme Universe. **Michael Friedlander** reflects on what we have learned.

"Coming out of space and incident on the high atmosphere, there is a thin rain of charged particles known as the primary cosmic radiation." With these words on the nature of cosmic rays, British physicist Cecil Powell began his Nobel prize lecture in 1950.

Powell's prize was awarded for his development of the photographic method of identifying high-speed and short-lived particles that were turning up unexpectedly in cosmic-ray studies as the products of high-energy collisions. At the same time, that photographic method was being used to discover new components of Powell's 'thin rain': heavy atomic nuclei. These two strands — the study of primary cosmic rays and the products of their collisions — continue to be woven into the fabric of today's research.

Although particle collisions are now studied mainly through the use of giant particle accelerators, the only window into the behaviour of the very highest-energy particles comes from examining cosmic rays. The study of the primary cosmic radiation is a part of current astrophysics: by comparing the composition of cosmic rays with that of stars, we can identify their sources and use them to investigate violent stellar processes.

This year, we celebrate the centenary of the discovery of cosmic rays by Austrian–American physicist Victor Hess. Over the decades, cosmic-ray research has spread in directions that he could never have imagined, from the discovery of antimatter to the use of carbon dating in archaeology. It has even played a crucial part in the origins of 'big science'.

## RADIATION SOURCE

Hess's research was carried out in the heady days following the discovery of radioactivity and the electron. In the early 1900s, a prime research tool in the study of radioactivity was the electroscope, a sensitive device for measuring the ionization produced by radiation. It was soon found that the radioactive components of some rocks produced ionization, and most researchers believed that Earth's crust was the source of background levels of radiation. To investigate, scientists lowered electroscopes into lakes and oceans, carried them up mountains and took them to even greater heights in open baskets underneath hydrogen-filled balloons. The results were conflicting, with some showing a decrease in ionization with altitude, others an increase. It was during this confusing time that Hess, in 1911, started his own series of balloon flights.

Physicist Victor Hess on a balloon flight in 1912.

Hess found that the ionization rate at first decreased with altitude, but then started to increase up to a height of 5.3 kilometres, the greatest height he reached. That flight took place from northern Bohemia (now part of the Czech Republic) on 17 April 1912, when a partial solar eclipse was visible from many parts of Europe. Hess detected no decrease in ionization during the eclipse, indicating that whatever the main source of the ionizing radiation coming from above, it was not the Sun.

Born in Austria in 1883 and educated at the University of Graz, Hess was a young assistant at the Radium Institute of the Austrian Academy of Sciences at the time of the flights. His discovery brought him a series of increasingly senior positions and growing professional recognition, culminating in a shared Nobel prize in 1936. With the deteriorating political situation in Europe, Hess was dismissed from his post at the University of Innsbruck in 1938 because he had a Jewish wife. He managed to escape from Austria, taking up a faculty post at Fordham University in New York.

SPL

For some years after these legendary beginnings, the nature of cosmic rays was strenuously debated by physicists. Robert Millikan (who coined the term 'cosmic rays' in 1925) continued to insist that they were electromagnetic 'rays', even after Arthur Compton had established that they were really 'particles', as revealed by the way in which they were deflected by Earth's magnetic field.

The experimental study of cosmic rays has often moved ahead of theory, yielding a host of unpredicted discoveries. One of the most dramatic was the observation of particles of antimatter. Paul Dirac's relativistic quantum theory had foretold the existence of antiparticles, and Dirac speculated that anti-atoms with anti-electrons might exist in distant anti-stars. But he made no predictions as to where to look for them on Earth: certainly not among cosmic rays.

In 1911, a tool for the study of cosmic rays had been developed by Scottish physicist C. T. R. Wilson. Wilson realized that water droplets were formed in the atmosphere by condensation of vapour on ions (an observation inspired by watching mist form on the summit of Ben Nevis in Scotland). He converted this insight into a powerful laboratory-scale device — the cloud chamber — in which the passage of charged particles was made visible by their trails of liquid droplets. In 1932, Carl Anderson was using a Wilson cloud chamber with a large magnet to study cosmic rays when he observed a particle that had the mass of an electron, but a positive charge. The discovery of the positron, as Anderson named the particle, was recognized when Anderson shared the 1936 Nobel prize with Hess.

During the period 1947–56, when cosmic-ray studies resumed after the Second World War, a host of unpredicted subatomic particles including hyperons, pions and kaons was found using photographic emulsions and Wilson cloud chambers. This complex mix of particles, called the particle zoo, forced a complete upheaval in particle theory.

Meanwhile, the study of the primary

cosmic radiation itself was advancing, and nuclei much heavier than helium were discovered. With further recent improvements to experimental techniques, the relative proportions of different cosmic-ray nuclei, and even some of their isotopes, have been precisely determined.

The proportions of the different chemical elements among cosmic rays can be compared with their abundances in the Solar System, in the atmospheres of distant stars and among the remnants of supernova explosions, to identify objects and regions where cosmic rays originate. Researchers also seek to identify the regions in which cosmic rays are accelerated to enormous energies, producing particles that travel close to the speed of light. The largest corresponding kinetic energy measured for a single cosmic-ray particle is comparable to that of a cricket ball or baseball travelling at 160 kilometres per hour. This energy is more than 100 million times larger than that of protons accelerated in the Large Hadron Collider at CERN, Europe's particle-physics laboratory near Geneva, Switzerland.

These ultra-high-energy particles are rare — only a few arrive each century over each square kilometre of Earth. Through their collisions in the atmosphere they generate billions of particles, requiring many detectors spread out over large areas. High-energy γ-rays, also produced in cosmic-ray sources, can similarly be detected by large-area arrays. Their arrival directions can point back to their sources, such as supernova remnants and active galaxies. Continued exploration of these highest-energy particles and photons might tell us about conditions in the early and very hot stages of our Universe.

Cosmic-ray studies have expanded in unanticipated directions. For example, cosmic rays have been identified as the source of the radioactive isotope carbon-14, produced by collisions with atmospheric nitrogen. The amount of carbon-14 produced in the atmosphere depends on the numbers of cosmic rays reaching Earth, which in turn depends on the 11-year cycle of solar activity. Measurement of carbon-14 has revolutionized archaeology by enabling the ages of ancient organic matter to be determined.

## COSMIC CONSEQUENCES

Hess's discovery came from observing the effects of ionization produced by cosmic rays. That same effect is taking place in our bodies as cosmic rays pass through them. Over our lifetimes, we accumulate a radiation dose that causes biological damage, presumably contributing to a basic level of cancer production. Unshielded by the atmosphere, astronauts accumulate radiation doses from cosmic rays that may well exceed those considered safe. This could limit the distances to which astronauts can go as they explore the Solar System.

Today, the scale of physics research has expanded to the point at which it is not unusual for a single scientific paper to have hundreds of authors, crossing international boundaries and using internationally funded equipment. The origin of this revolution can be traced to cosmic rays. The cost and manpower demands of cosmic-ray research in the 1950s, although modest by today's standards, were beyond the capacity of any single group. The 'G-stack' collaboration, for example, of which I was a part (in Powell's research group at the University of Bristol, UK), was created to undertake the flight of a 'giant' stack of photographic detectors beneath a balloon. The special photographic emulsions, made by the photo company Ilford, were processed in Bristol; the balloon was flown in northern Italy; and the measurements and analysis were carried out by groups in Bristol, Brussels, Copenhagen, Dublin, Genoa, Milan and Padua. Our results, including many examples of new and very short-lived particles, were reported in a 1955 paper (J. H. Davies *et al. Il Nuovo Ciménto* **2**, 1063–1103; 1955) that carried the names of 36 scientists, by far the largest number of co-authors up to that time.

This style of large international collaborations is today exemplified by CERN, which was founded in 1954 and houses the largest particle accelerator ever built. Prominent among CERN's founders were many cosmic-ray scientists, including Powell and Edoardo Amaldi, its first director of research.

*"After 100 years, cosmic-ray research is mature but still open to producing surprises."*

One lesson to be learned from cosmic-ray research is the need to examine carefully any rare but apparently strange observations, and not to discard them as part of the background noise that many particle-physics experiments accumulate. The discovery of antimatter rested on the detection of a single track of a lone positron. Similarly, the discovery of some kaons was based on observations of single events. Although some discoveries may emerge from the statistical analysis of large quantities of data, we should remember that important discoveries can still be established by a single observation.

After 100 years, cosmic-ray research is mature but still open to producing surprises. Cosmic rays continue to be studied from balloons, Earth-orbiting satellites and long-range space probes as well as ground-based detectors that cover enormous areas, seeking the sources of the highest-energy cosmic rays. Antiparticles might also be identified. Longer flights and larger areas are permitting the accumulation of more data on particles and cosmic γ-rays, thus increasing the detection of yet more of the rarest events.

There are already suggestions that some of the highest-energy particles and γ-rays come from well-known objects such as some supernova remnants. More data might locate, more firmly, the directions in which their sources are located and should define the acceleration processes. Perhaps the physical conditions are even more exotic than we can imagine at present. This field of astroparticle physics seems sure to produce future Nobel prizewinners. ■

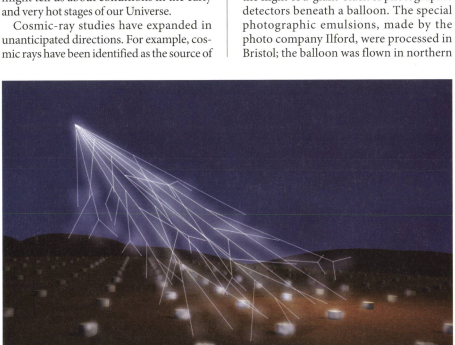

A.SAITOU/ASPERA

**Cosmic-ray collisions create showers of particles, requiring detectors spread out over a vast area.**

**Michael Friedlander** *is emeritus professor in the Department of Physics, Washington University, St Louis, Missouri, USA. His most recent book is* A Thin Cosmic Rain *(Harvard University Press, 2000). e-mail: mwf@wuphys.wustl.edu*

TOM CORHILL

Michael Mann has been harassed personally and politically over his work on climate change.

CLIMATE SCIENCE

# At the storm front

**Simon Lewis** gets to grips with a climate scientist's account of a conflict that began with a graph.

How would you feel if a powerful politician demanded, with apparent legal authority, that you supply him with every piece of scientific data you had ever collected, every computer program you had written, and every detail that would allow his staff to replicate your work? How would you feel if an envelope of suspicious white powder was posted to you — and the police sealed your office? And if your family was threatened with violence?

Michael Mann knows how he would feel: he experienced all this after publishing a scientific paper. His *The Hockey Stick and the Climate Wars* tells the story of one of the most harassed scientists in the United States.

The book begins slowly, moving from happy anecdotes of childhood computer programming to the joys of responsibility-free postdoctoral research. But it becomes riveting when we reach what was in retrospect the turning point in Mann's life: his 1998 paper 'Global-scale temperature patterns and climate forcing over the past six centuries' (M. E. Mann *et al. Nature* **392**, 779–787; 1998).

Mann's study used proxy climate records, such as tree-ring growth and the ratios of oxygen isotopes in corals, to make estimates of surface air temperature extending back to AD 1400 — long before direct thermometer measurements were available. The results showed that in the Northern Hemisphere, temperatures were higher in the last years of the twentieth century than at any time in the previous 600 years, and that the suspected dominant cause was anthropogenic carbon dioxide emissions.

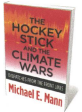


**The Hockey Stick and the Climate Wars: Dispatches from the Front Lines**
MICHAEL E. MANN
*Columbia Univ. Press: 2012. 384 pp. $28.95, £19.95*

Mann's result came to be known as the hockey stick, because the key graph showed a flat 'handle' — the low-level natural oscillations in temperature in the centuries before humans began to create large quantities of greenhouse gases — and a 'blade' representing the sharp uptick in surface air temperature in the twentieth century. The work invoked the ire of lobby groups opposed to political action on climate change, who launched an astonishing decade of attacks on the veracity of the result. The bulk of Mann's book documents this ugly debate.

Mann ably dissects how ideologically driven, industry-funded campaigns attack climate scientists and their work to obstruct the formulation and implementation of policies restricting $CO_2$ emissions. We learn about Mann's bemusement when he is first assailed, and later his resigned anger. After telling how, in 2006, a US National Academy of Sciences panel found no evidence that Mann's hockey stick was flawed, he notes dryly that one "might think that this would have ended such charges once and for all. One would be wrong."

The influence of lobby groups on public perception of scientific issues is covered in more scholarly detail in the 2010 book *Merchants of Doubt* (Bloomsbury) by historians Naomi Oreskes and Erik Conway. However, Mann's shocking first-hand testimony of the repeated attempts to discredit him and his work gives his book power. Mann reports his 'highs', such as when more than 30 scientific organizations declared their support for him after Senator Joe Barton (Republican, Texas) sent him an aggressive letter demanding, among other things, copies of his records. And we get the 'lows' of what Mann calls the "most malicious of the assaults": the publication in November 2009 of a cache of e-mails, including some from Mann, that had been stolen from the University of East Anglia in Norwich, UK.

Although there is little in the book with which I seriously disagree, it left me uneasy. Many scientists will agree with Mann's three basic points: that climate change is a major societal problem; that there are campaigns to convince the public that this is not the case; and that scientists should engage with society and not allow the public to be "confused and misled by industry-funded propaganda".

However, I am unconvinced that presenting the attacks as a "climate war" waged by a "corporate-funded denial machine" is the best way to help scientists to counter misinformation. It makes good copy, but the war metaphor, with its talk of battle scars and front lines, is unlikely to be an ideal communication strategy: it is, by definition, polarizing. Because denial that climate change poses a problem for society is associated mainly with right-wing political views, science communication needs to transcend ideological divides, not reinforce them.

Last year saw the end of a similarly ugly climate-change spat, following an ideology-transcending innovation that Mann does not mention. After years of bitter dispute about estimates of the warming documented by direct thermometer measurements, the Berkeley Earth Surface Temperature project in California brought together vocal critics of past analyses and experts who were unconnected with those previous studies. They collated, processed and published raw data, results and associated computer code.

*"Science communication needs to transcend ideological divides, not reinforce them."*

Unsurprisingly, the results confirmed previous analyses. This reminded the public of an important result, provided a well-publicized vindication of it and, by involving key critics, dealt deftly with those who choose to confuse the public. A comparable effort to estimate the past millennium's surface air temperature could be similarly decisive.

An influential Editorial in *Nature*, cited by Mann, noted that climate scientists are in a "street fight" (*Nature* **464**, 141; 2010) — imagery that I think is more apt than that of war. Street fighting is not about taking sides, and the metaphor describes well the 'anything goes' attacks that scientists can face when publishing or speaking about climate change.

Mann's story is important. However, it is also important to step back from the conflict. Emphasizing a binary war might not be the best way to end it. ■

**Simon L. Lewis** *is a reader in global change science at University College London, UK, and the University of Leeds, UK.*
*e-mail: s.l.lewis@leeds.ac.uk*

# Books in brief

**Opium: Reality's Dark Dream**
*Thomas Dormandy* YALE UNIVERSITY PRESS *376 pp. $40 (2012)*
'Poppy tears' — the sap of the opium poppy — are aptly named: the drug has enslaved multitudes and sparked violence for 6,000 years. Yet opium and derivatives such as morphine and heroin have been stars of medicine and inspired greats such as the Romantic poet Samuel Taylor Coleridge and, more arguably, surgeon William Stewart Halsted. Those stories are threaded through medical historian Thomas Dormandy's engrossing chronicle, but we're never far from the shadows — the dosing of infants in Victorian England, the torments of addiction, and wars in Afghanistan and China.

**Megachange: The World in 2050**
*Edited by Daniel Franklin and John Andrews* PROFILE/WILEY *320 pp. £15/$34.95 (2012)*
*The Economist* editors Daniel Franklin and John Andrews give the "helicopter view" of where the world will be by mid-century. Aiming to pin down the trends forcing "megachange", they offer 20 chapters that make predictions in everything from public health and women's welfare to social networking, climate change and, inevitably, economics. This succinct, pithy resource has surprises: by 2050, China's gross domestic product will be 80% more than the United States's, for instance; and the world's total fertility rate could stabilize.

**Circulation: William Harvey's Revolutionary Idea**
*Thomas Wright* CHATTO & WINDUS *272 pp. £16.99 (2012)*
It is easy to forget that William Harvey's great theory on the circulation of blood was as groundbreaking as Copernicus's on the Solar System. Working mainly from dissections and vivisections, Harvey also drew insight from his observations of networks and systems in transport and technology. Author Thomas Wright's account has a brilliant cast — including John Donne, the great metaphysical poet and dean of St Paul's Cathedral, London, whose interest in anatomy and the human heart drew him to Harvey's work. A classic example of how great science affects culture, language and politics.

**Learning from the Octopus: How Secrets from Nature Can Help Us Fight Terrorist Attacks, Natural Disasters, and Disease**
*Rafe Sagarin* BASIC BOOKS *320 pp. $26.99 (2012)*
How are tide pools linked to national security? Ecologist Rafe Sagarin says that adaptability in nature — particularly in the octopus — exemplifies key defence principles. For example, the cephalopod has both attack and defence capabilities, with a powerful bite and inky camouflage, and its flair for escapology in the lab shows that it can handle a change in environment. Drawing on life science and evidence from the military and emergency services, Sagarin defines adaptability as the "sweet spot" between reaction and prediction.

**Clouds That Look Like Things: From the Cloud Appreciation Society**
*Gavin Pretor-Pinney* SCEPTRE *112 pp. £12.99 (2012)*
Anyone who has spent long minutes staring idly into the blue will relish these bingo moments gathered by Gavin Pretor-Pinney, author of *The Cloudspotter's Guide* and *The Wavewatcher's Companion*, which won the 2011 Royal Society Winton prize for Science Books. From Alfred Hitchcock to flying saucers and a menagerie of beasts, Pretor-Pinney's gallery of evanescence is a reminder of the simple joy of perception.

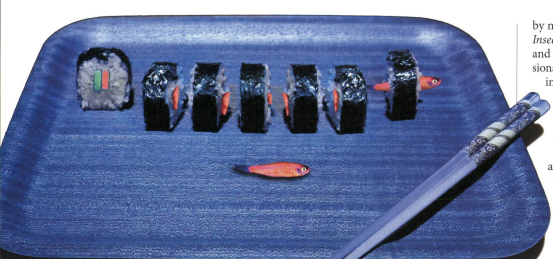

Transgenic sushi is an unusual biotech teaching tool.

GOODMEDIA

NUTRITION

# Chew on this

**Anthony King** savours a surreally varied show on food, from glowing sushi to 1,001 uses for a pig carcass.

Fifty billion chickens are heading to the slaughter at any one time on Earth. What humans eat determines which crops are grown and which animals are reared, with big implications for science, agriculture, the environment and society.

*Edible*, an exhibition at Dublin's Science Gallery, probes our cultivation and consumption choices and their effects in the contexts of time, place, technology and taste. There are serious messages, but much of what is on offer has a zany flavour.

The increasingly globalized agricultural system gets more than a look-in. Artist Christien Meindertsma's photobook on 'pig parts' is a compellingly graphic exploration of the afterlife of a pig carcass. For *PIG 05049* (the number denotes the animal's ear tag), Meindertsma spent three years tracing the products derived from a single animal raised in the Netherlands to build a visual chronicle of the carcass's incredible global journey.

The pig's skin was used for tattoos, chewing gum, injectable collagen, safety gloves and cheesecake, while its bones went into paper, X-ray films, book covers and train brakes. Cigarettes, cooked ham, mink feed and photodynamic therapy accounted for some of its blood, and its gelatine eased cordite into bullets. Meindertsma dissects the pig all over again, depicting the products to scale.

Humanity's over-reliance on a handful of crops is explored in an infographic revealing how rice, wheat, maize (corn) and potatoes make up 50% of what we eat. The exhibition's curators, Cat Kramer and Zack Denfeld — artists with the mobile research institute the Center for Genomic Gastronomy — point out that new crops could gain dominance within a century: "The future of food is much more complex than we can predict," they write.

**EDIBLE: The Taste of Things to Come**
*Science Gallery, Trinity College Dublin. Until 5 April 2012.*

One aspect of that complexity is the need to maintain species diversity as insurance in case of disease; the Food and Agriculture Organization of the United Nations in Rome estimates that crop genetic diversity has fallen by 75% since 1900. *The Edible Heritage Lab* features 12 historically and scientifically important varieties of potato. Part of a haul collected by the Irish Seed Savers Association, which champions non-commercial Irish heritage varietals, they include the lumper potato, which succumbed to successive attacks by the fungal blight *Phytophthora infestans* in the mid-nineteenth century, triggering the great Irish potato famine.

Close by, a stuffed grey squirrel illustrates the question of whether we should eat invasive species. A recipe for Guinness and grey squirrel stew is provided for the brave. Insects give more food for thought; eaten over much of the world, they are seen by many as a part of future food security. *Insects Au Gratin* by designer Susana Soares and her colleagues consists of three-dimensional sculptural shapes printed using milled insect flour. Crickets, we're told, are more efficient than cattle in converting vegetation to protein: 100 kilograms of feed produces 40 kg of the insects, but only 10 kg of beef.

Given the current fashion for foodyism and molecular gastronomy, the science of taste inevitably plays its part. You can learn whether you are a supertaster by gauging the bitterness of a disc infused with bitter compounds, or pinpoint where particular taste buds are concentrated by sprinkling droplets of five solutions onto your tongue.

But with taste, the proof of the pudding is obviously in the eating. A ticketed 'curated dinner' — a molecular-gastronomy evocation of the spirit of Dublin — by chef-for-the-night Pete Williams proved a sensory treat. The recipes, by local company Deasngoat, featured a contemporary take on the traditional Irish coddle, involving a poached pork-mousse sausage with a mashed-potato gel, set carrot foam and a bacon and pork sausage broth in a test tube.

The diners themselves learned to whip up a gin and tonic with a difference. Spheres of cucumber, lime juice and salt were mixed with sodium alginate and sodium citrate, then set in a bath of calcium chloride. The resulting chewable spheres went into the drinks.

Back at the exhibition, a "mutagenic mist" reminds the audience that radiation has been used since the mid-twentieth century to induce mutations in crops. The mist, a palate-cleansing puff of peppermint oil, is made from a varietal approved in the 1970s and bred for disease resistance. Most peppermint oil consumed today is from this variety.

Elsewhere, you can watch *The Glowing Sushi Cooking Show*, a video of Kramer and Denfeld creating an even more startling treat: transgenic, bioluminescent zebrafish sushi. It is an intriguing way to absorb cutting-edge biotechnology. "This will be fun at parties," quips Denfeld.

*"The future of food is much more complex than we can predict."*

There is much more to this feast, from smog tasting to the fun inflated-stomach sculpture *Gas Bag* by artists Andy Best and Merja Puustinen. *Edible* offers a menu of appetizing morsels on the evolution of gastronomy and its influence on our ecological, technological, commercial and political world — something to chew on even if you're not yet ready to snack on a cricket. ■

**Anthony King** *is a writer based in Dublin. e-mail: anthonyjking@gmail.com*

➲ **NATURE.COM**
For more on attitudes to food:
go.nature.com/gtmfyx

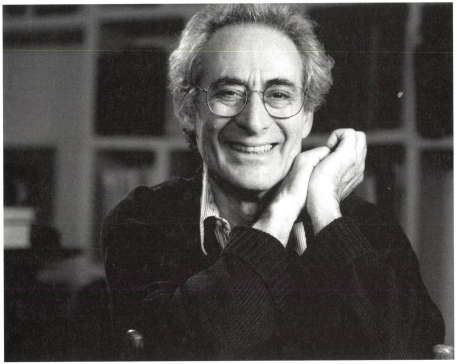

JIM HARRISON

Barry Mazur believes that maths and literature are driven by the same imaginative impulse.

## Q&A Barry Mazur

# The maths raconteur

*Barry Mazur, a mathematician at Harvard University in Cambridge, Massachusetts, has explored the literary side of mathematics. With the publication this month of* Circles Disturbed, *a collection of essays on mathematics and narrative that he edited with writer Apostolos Doxiadis, he talks about the overlapping realms of mathematics and the imagination.*

**How did you get into mathematics?**

Through electronics. At school I read popular works on electromagnetism. I found it baffling that there could be action at a distance that let energy travel through a medium you couldn't touch. As a student at the Massachusetts Institute of Technology in Cambridge, I saw mathematics as a gateway to a more philosophical understanding of electronics. I wanted to understand physical principles, such as conservation of energy, from a Euclidean standpoint: rarified and axiomatic. I later saw that this was impossible, but I became riveted by mathematics. I came to Harvard in 1959, starting in topology then moving to algebraic geometry, which has led me to number theory.

**What inspired you to write your 2003 book, *Imagining Numbers*?**

It began as a letter to a friend. We had been chatting about the difficulties of imagining certain things and he said that he would like to know what imaginary numbers were. It took more than 200 years for mathematicians to become comfortable with them, so I thought it might be instructive not to directly teach this to my friend, but to help him to arrive at his own familiarity with them. I wrote him a letter inviting him to do just that. It expanded, circulated among literary friends, and eventually became the book.

**Circles Disturbed: The Interplay of Mathematics and Narrative**
EDITED BY APOSTOLOS DOXIADIS AND BARRY MAZUR
*Princeton University Press: 2012. 552 pp. $49.50, £34.95*

**And *Circles Disturbed*?**

The concept came from Apostolos Doxiadis. His 1992 novel *Uncle Petros and Goldbach's Conjecture* marries literature and mathematical themes, and his 2008 graphic novel *Logicomix* is about the mathematicians Gottlob Frege, David Hilbert, Henri Poincaré, Ludwig Wittgenstein and Kurt Gödel, and the early-twentieth-century crisis in the foundations of mathematics. Apostolos invited mathematicians, historians and literary scholars to write about mathematics and narrative. They met in Greece in 2007 to discuss their work; this was the origin of *Circles Disturbed*. They interviewed one another to make their contributions more accessible. These interviews are available at www.thalesandfriends.org.

**How can historians tell the story of maths?**

You can recount mathematical lives, as Peter Galison does in the book. His essay contrasts the biographies of John Archibald Wheeler — whose mechanical illustrations of mathematical operations were influenced by his upbringing on a Vermont farm — and Nicolas Bourbaki, the pseudonym of a group of Parisian mathematicians whose vision of mathematical progress was monolithic and structural. Or you can take the meta-historical approach, as Amir Alexander does in his essay, which discusses how the transformation in mathematics in the eighteenth and nineteenth centuries was partly guided by the stories told about it. You can do a close reading of dramatic mathematical texts, as in Federica La Nave's examination of a work on imaginary numbers by sixteenth-century Italian mathematician Rafael Bombelli, who laboured for decades over the question of whether these numbers are fictitious.

**And is it possible to use mathematics for literary purposes?**

Yes, you can reverse roles. A mathematical sensibility is useful for illuminating patterns and structures — such as the structure of narrative, as in our book. A seminal example is French literary theorist Gérard Genette's 1972 modelling of the tangled layers of time in the writings of Marcel Proust.

**Is there a place for dreams in mathematics?**

In Michael Harris's chapter on intuition in *Circles Disturbed*, he recounts how mathematician Robert Thomason had a dream in which a dead friend (not a mathematician) made a mathematical claim. Although the claim was false, it inspired Thomason, once awake, to successfully complete his mathematical project, and to include his friend as a co-author in the published paper.

**What do the pursuits of maths and literature have in common?**

The common thread is urgency. Mathematicians are impelled by an urgent desire to understand. In literature, there is a similar impulse to engage in an all-absorbing imaginative experience. When it comes to mathematical inspiration, the imagination could be considered the ghost in the rational machine of proof-making. ■

INTERVIEW BY JASCHA HOFFMAN

Mirus

The Transfection Experts

# Transfection in 3D!

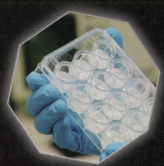
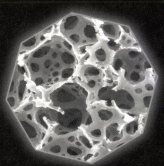
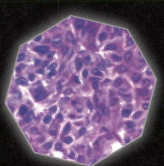
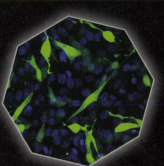

*Introducing the*

## *Trans*IT®-3D Transfection Reagent

Ideal for transfection of cells in 3D cell culture, the *Trans*IT®-3D Transfection Reagent empowers scientists to attain further insight into the complexities of cell function and behavior.

- ▷ **High Efficiency DNA Delivery:** Achieve high expression in a wide range of cell types
- ▷ **Easy-to-Use:** User friendly protocol that requires minimal optimization
- ▷ **Flexible**: Compatible with various 3D matrices

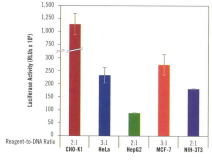


**3D Transfection of Multiple Cell Types.** Cell lines were seeded in alvetex® 3D plates, incubated for 48 hours and transfected with plasmid encoding firefly luciferase using *Trans*IT®-3D Transfection Reagent.

Not sure 3D transfection is right for your work? TRY IT.
Order the Introductory 3D Transfection System* for $300 USD.
*The system includes Mirus Bio *Trans*IT®-3D Transfection Reagent and Reinnervate alvetex® 3D Cell Culture Plates.

Visit www.TheTransfectionExperts.com
Call 888.530.0801 (U.S. only) or +1.608.441.2852 (outside U.S.)

Find us on facebook
Mirus Bio LLC—The Transfection Experts

**www.TheTransfectionExperts.com**

Providing gene delivery expertise since 1995

reinnervate
The REAL 3D Cell Culture Company

*Images courtesy of Reinnervate.*

©2012 All rights reserved Mirus Bio LLC. All trademarks are the property of their respective owners. *Trans*IT is a registered trademark of Mirus Bio LLC.

# Correspondence

## Mixed media policies of US federal agencies

You cite two US government agencies that interact openly with the media (*Nature* **483,** 6; 2012): the National Oceanic and Atmospheric Administration (NOAA) and the National Science Foundation (NSF). Yet these are rare exceptions in my experience as editor of *FDA Webview* and *FDA Review*.

Take the US Department of Health and Human Services (DHHS), which last September proclaimed a repressive media guidelines policy. All journalists are now referred to its press office, which permits access only to selected personnel and may monitor and record interviews (see go.nature.com/xczin6).

Another large US government entity, the Department of Justice, has gone even further. Barely a month after the DHHS move, it proposed a rule that directs federal law-enforcement agencies to respond to requests for particularly sensitive documents under the Freedom of Information Act "as if the excluded records did not exist" (see go.nature.com/gfd8pn).

Recent guidelines on openness from the NSF and NOAA are modest steps in the right direction — albeit on a tiny scale, given the size, scope and complexity of the US federal government.

**James G. Dickinson** *Camp Hill, Pennsylvania, USA.*
*jim@fdaweb.com*

## China: a cultural shift for science

I disagree that the ancient cultural influences of Confucius and Zhuang Zhou are to blame for the problems pervading China's academic research today (*Nature* **481,** 411; 2012). Neither sage encouraged isolation or inhibited intellectual curiosity. I believe that China's problems are exacerbated by insufficient respect for these cultural traditions, which promote such values as objectivity and high moral standards.

China's scientists should be devoting themselves to the advance of research that abides by international scientific standards. Misconduct and other flaws undermine the Chinese government's increased investment in higher education and scientific research.

It is time for the research community in China to rekindle its respect for cultural traditions and to take responsibility for creating a healthy, transparent academic system.

**Keqian Xu** *Nanjing Normal University, Jiangsu, China.*
*xukeqian@njnu.edu.cn*

## China: philosophers sparked good science

Peng Gong misrepresents the thoughts of Chinese philosophers Confucius and Zhuang Zhou by suggesting that they hinder scientific advancement in modern China (*Nature* **481,** 411; 2012).

Confucius encouraged curiosity and practice in teaching and learning. His thoughts are universal and timeless, and have influenced many other Asian countries — including Japan, where sound science thrives.

Zhuang advocated harmony so that we could fulfil our essential connection with nature. This view is pertinent in today's China, where the environment and human health are being damaged by explosive and unbalanced development.

Moreover, Confucius, Zhuang and other ancient Chinese philosophers made significant advances in science, technology, medicine, mathematics, astronomy and architecture, with inventions such as paper and the compass having a large impact on civilization.

**Jianxin Su** *Fujian University of Technology, Fuzhou, China.*
*jianxinsu@gmail.com*
**Cheng Lu** *Newark, Delaware, USA.*

## Work together to crack wildlife trade

There is no single solution to monitoring illegal wildlife trade (L. F. Toledo *et al. Nature* **483,** 36; 2012), which is widespread, adaptive and sophisticated. Extensive reforms are needed to expand government monitoring and reporting, and to include a wider range of detection strategies and non-government stakeholders (J. Phelps *et al. Science* **330,** 1752–1753; 2010).

Government agencies are largely limited to regulating wildlife trade through monitoring and enforcement, mainly confined to checkpoints such as airports. More resourceful research strategies are crucial for keeping up with wildlife trading (see, for example, M. Gastañaga *et al. Bird Conserv. Int.* **21,** 76–85; 2011).

Improving regulation will require broadening collaborations, for example through resource monitoring by local communities, engaging the private sector in point-of-harvest reporting, and forming partnerships with non-governmental organizations and academics. Local networks and expertise would encourage pooling of resources and give governments access to new techniques and methodological support.

Such cooperation would help to resolve taxonomic uncertainties and offer independent review of contentious trade decisions. This is especially relevant to countries where the technical and administrative authorities of the Convention on International Trade in Endangered Species lie within the same government institution.

**Jacob Phelps, David P. Bickford, Edward L. Webb** *National University of Singapore, Singapore.*
*jacob.phelps@gmail.com*

## Colorado methane study not clear-cut

As a partner of the US National Oceanic and Atmospheric Administration, we at Western Energy Alliance provided much of the data for the reported study on methane emissions from a natural-gas field in Colorado's Denver-Julesburg Basin (*Nature* **482,** 139–140; 2012). However, uncertainties remain over the extent of methane leakage from these operations.

For example, this study (G. Pétron *et al. J. Geophys. Res.*, in the press) relied heavily on data from mobile-laboratory samples taken in summer 2008, before regulations reduced emissions of volatile organic compounds to 90%, and before low-bleed pneumatic devices were implemented to reduce methane emissions from the field. Much of the data were collected in an operating environment that no longer exists. Also, the venting you describe is at odds with industry practices.

The authors acknowledge that methane emissions from agriculture are of "comparable magnitude to the estimate from natural gas systems" in Colorado, but do not consider these.

Pétron *et al.* should have noted that methane readings were lower at the Boulder observation tower than at a tower in a Wisconsin forest that is far removed from significant industrial activity.

**Kathleen M. Sgamma** *Western Energy Alliance, Denver, Colorado, USA.*
*ksgamma@westernenergyalliance.org*

**CORRECTION**

A declaration of competing financial interests was omitted from the Correspondence 'Sugar: fruit fructose is still healthy' (*Nature* **482,** 470; 2012). This has been added at http://go.nature.com/xudf1i.

# Renato Dulbecco

## (1914–2012)

Molecular biologist who proved that virus-derived genes can trigger cancer.

Renato Dulbecco, a giant of cancer biology, passed away peacefully on 19 February, just three days shy of his 98th birthday. Through a decade-long series of experiments that began in the late 1950s — first at the California Institute of Technology (Caltech) in Pasadena and then at the Salk Institute in La Jolla, California — he and his co-workers demonstrated that the behaviour of cancer cells could be traced directly to acquired genes. Some viruses can integrate their genomes into host cell DNA, inducing uncontrolled cell growth — the hallmark of a cancer cell. For these early clues to the genetic origins of cancer, Dulbecco shared the 1975 Nobel prize with the late Howard Temin, his former student, and with David Baltimore, my former mentor.

Born in Catanzaro, Italy, on 22 February 1914, Dulbecco grew up during the First World War and its aftermath with his mother and siblings. He entered the University of Turin in 1930 at the age of 16 to study medicine. His interests quickly shifted to biology and he became a laboratory assistant for Giuseppe Levi, learning from him the cell-culture techniques that had a dominant role in Dulbecco's later scientific work. His fellow students included two other future Nobel laureates — microbiologist Salvador Luria and neurobiologist Rita Levi-Montalcini.

After obtaining his doctorate in 1936, Dulbecco was drafted into the Italian army as a physician. He was called to action in 1939, at the outset of the Second World War, to serve first in France and then in Russia. Disaffected by the war and its consequences, he deserted the army and hid in a small village near Turin, becoming physician to the local partisan units resisting the German occupation. After the end of the war, following a short stint as an elected city councillor in Turin in 1945, he returned to scientific research at the University of Turin.

In 1946, Luria invited Dulbecco to join his research group at the University of Indiana in Bloomington to work on bacteriophages — the viruses of bacteria. Dulbecco shared his laboratory with a graduate student, James Watson, who was later to determine the structure of DNA with Francis Crick. Dulbecco's finding that visible light can reactivate phages previously rendered inactive by exposure to ultraviolet light — with repercussions for experimental methods at the time — brought him to wider attention. Phage geneticist Max Delbrück invited Dulbecco to join him at Caltech in 1949 as a research fellow.

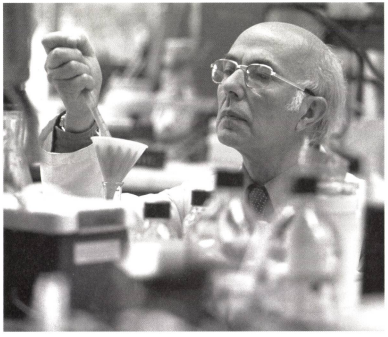

SALK INST.

Dulbecco felt that research into animal viruses would benefit hugely from improved quantitative techniques. In 1952, he developed the plaque assay for Western equine encephalomyelitis virus: a system that allowed researchers to determine the number of biologically active viral particles in a sample by counting the number of discrete plaques, or clear spots, where a single virus and its progeny had killed host cells. Soon Dulbecco was joined by Marguerite Vogt, a German émigré. Their fruitful collaborations led to quantitative assays for the poliomyelitis virus, a scourge at the time, and later for the polyoma virus — a DNA virus that causes many different types of tumours.

In 1963, Dulbecco left Caltech to become one of the first fellows of the Salk Institute, founded by Jonas Salk of polio vaccine fame. He and Vogt continued their research collaborations on tumour viruses, definitively proving the essential role of the viral genes in transforming cells into cancer cells. During this highly productive period, Dulbecco trained some of the top virologists in the world. In 1972, he moved to the Imperial Cancer Research Fund (now Cancer Research UK) in London, where he initiated studies of breast cancer — a subject he continued to pursue after moving back to California in 1977. His last scientific paper, published in 2004, identified tumour-initiating cells in rat mammary cancers. In 1988, Dulbecco assumed the presidency of the Salk Institute, following the illness of long-term president Frederic de Hoffmann, and brought stability during a difficult time.

An experimentalist at heart, Dulbecco loved to work in the laboratory. He was a quiet man, yet did not shy away from making bold visionary statements: in a classic 1986 perspective in *Science* (R. Dulbecco *Science* **231,** 1055–1056; 1986), he argued that the best way to understand cancer would be to sequence the human cancer genome. In 1992, Dulbecco stepped down from the Salk presidency to organize the Italian contribution to the Human Genome Project. He spent a good part of his time in Italy, where he was much revered and helped the careers of many young scientists.

Dulbecco was an elegant man: a dapper dresser, soft spoken, with an ever-present smile. He was comfortable among the nobility, yet adept at changing the oil in his car; at once distant yet approachable. He was a charming host at dinners organized by his wife Maureen, which my wife and I often had the pleasure of attending. In short, he was always the perfect gentleman. ■

**Inder M. Verma** *is the Irwin and Joan Jacobs Chair in Exemplary Life Science and an American Cancer Society professor of molecular biology at the Salk Institute, La Jolla, California 92037, USA.*
*e-mail: verma@salk.edu*

nature REVIEWS GENETICS

ARKITEK STUDIOS

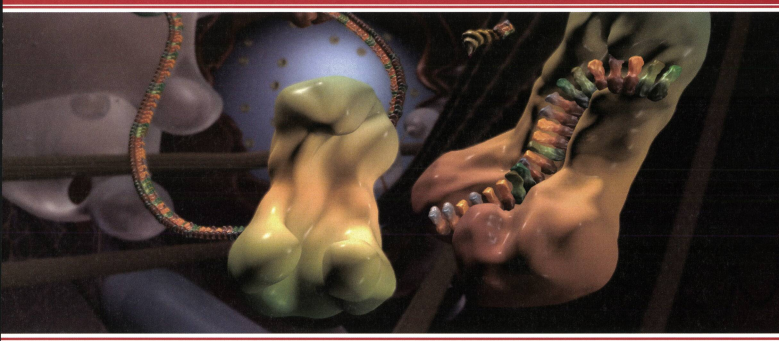

## Animation on RNA interference

RNA interference (RNAi) has enormous scientific implications, from shaping our understanding of how gene expression is regulated to providing new tools for basic and clinical research. Now you can learn about the principles RNAi through an up-to-date animation that introduces you to gene regulation by small interfering RNAs (siRNAs) and microRNAs (miRNAs).

*Nature Reviews Genetics*, in association with Arkitek Studios, has brought RNAi to life in this vivid, audio-visual journey into the cell.

**See RNAi in action by viewing the animation for FREE at:**
**www.nature.com/nrg/multimedia/rnai**

Also, download a **FREE** poster on tools for studying and using small RNAs at:
**www.nature.com/nrg/posters/small-rna**

The Animation and Poster are freely available thanks to support from:

Thermo SCIENTIFIC
Part of Thermo Fisher Scientific

nature publishing group npg

ACTIVE MOTIF®

Enabling Epigenetics Research

NEW DNA Methylation Antibodies 5-hmC 5-fC 5-caC

**Active Motif** develops validated antibodies and assays to enable the discovery and characterization of key epigenetic processes.

Our products are developed in-house and supported by scientists with expertise in chromatin biology. For a complete product listing please visit www.activemotif.com.

## Superior Antibodies & Kits for EPIGENETICS RESEARCH

Visit us at **www.activemotif.com**

**CHROMATIN ANALYSIS**
ChIP kits and ChIP-validated antibodies

**HISTONE MODIFICATION**
Antibodies and ELISAs, HAT/HDAC assays and Histone purification

**DNA METHYLATION**
Methylated DNA enrichment, bisulfite conversion, DNMT assays, whole genome amplification, 5-hmC antibody

# RESEARCH

## NEW ONLINE

*Papers published this week at Nature.com/nature*

**NEWS & VIEWS** The fate of carbon in sedimentary rocks is linked to climate change **p.413**

**LETTER** Why it makes evolutionary sense to create a bad impression **p.461**

**LETTERS** An epigenetic dimension to glioma tumorigenesis **pp.474, 479, 484**

PUBLISHED 18 MARCH 2012

CELL BIOLOGY

## Nuclear positions crucial in muscles

The cells in skeletal muscle contain many nuclei, positioned at regular intervals along the muscle fibre. Improperly positioned nuclei are a hallmark of numerous muscle diseases. Thomas Metzger *et al.* identify the microtubule-associated protein ensconsin (Ens)/MAP7 and kinesin heavy chain/Kif5b as evolutionarily conserved regulators of myonuclear positioning in *Drosophila* and in cultured mammalian myotubes. *Drosophila* larvae with mutant *ens* display decreased locomotion and incorrect myonuclear positioning, and these phenotypes are rescued by muscle-specific expression of Ens. This work provides a system in which to study the genes involved in nuclear positioning, and to screen drugs for the ability to alleviate muscle weakness.

**MAP and kinesin-dependent nuclear positioning is required for skeletal muscle function**
T Metzger *et al.*
doi:10.1038/nature10914

CANCER

## Successful trial separation

'Co-clinical trials' have been proposed as way to evaluate new therapies. In this approach, drugs are tested simultaneously in clinical and preclinical trials. To demonstrate its potential, Zhao Chen *et al.* used genetically engineered mouse models alongside a randomized phase II trial of the chemotherapeutic drug docetaxel, used both alone and in combination with a MEK inhibitor in *KRAS*-driven lung cancer. Mice with *Kras* or *Kras* plus *p53* mutations were more responsive to the combination than to docetaxel alone, whereas mice with a deletion of *Lkb1* and activated *Kras* were unresponsive. These findings suggest that patients in the clinical side of the trial should be tested for the presence of *Lkb1* mutations.

**A murine lung cancer co-clinical trial identifies genetic modifiers of therapeutic response**
Z Chen *et al.*
doi:10.1038/nature10937

MICROBIOLOGY

**Endospore abundance, microbial growth and necromass turnover in deep sub-seafloor sediment**
B A Lomstein *et al.*
doi:10.1038/nature10905

DEVELOPMENTAL BIOLOGY

**Notch-dependent VEGFR3 upregulation allows angiogenesis without VEGF–VEGFR2 signalling**
R Benedito *et al.*
doi:10.1038/nature10908

CHEMICAL BIOLOGY

**Small-molecule inhibitors of the AAA+ ATPase motor cytoplasmic dynein**
A J Firestone *et al.*
doi:10.1038/nature10936

NEUROSCIENCE

**Wild-type microglia arrest pathology in a mouse model of Rett syndrome**
N C Derecki *et al.*
doi:10.1038/nature10907

**Trans-synaptic Teneurin signalling in neuromuscular synapse organization and target choice**
T J Mosca *et al.*
doi:10.1038/nature10923

**Teneurins instruct synaptic partner matching in an olfactory map**
W Hong *et al.*
doi:10.1038/nature10926

PUBLISHED 21/22 MARCH 2012

BIOCHEMISTRY

## Ribosomal spellchecker

The ribosome plays a pivotal part in protein synthesis, translating the genetic code with remarkable accuracy. The structural basis of this accuracy has long been a puzzle. In one proofreading step, conserved residues around the A site, which binds to the incoming aminoacylated transfer RNA (tRNA), ensure that the codon–anticodon pairing is correct before a conformational change in the ribosome occurs. As a model of the decoding process, Natalia Demeshkina *et al.* have solved six X-ray crystal structures of 70S ribosomal complexes with cognate or near-cognate tRNA. They propose that the ribosomal structure forces the first two nucleotides in the A site to adopt canonical Watson–Crick geometry. Wobble base pairs — non-Watson–Crick pairs essential to the secondary structure of RNA — induce distortion elsewhere that causes the near-cognate tRNA to be released.

**A new understanding of the decoding principle on the ribosome**
N Demeshkina *et al.*
doi:10.1038/nature10913

STRUCTURAL BIOLOGY

**Structure of the mitotic checkpoint complex**
W C H Chao *et al.*
doi:10.1038/nature10896

PHYSIOLOGY

**Role of corin in trophoblast invasion and uterine spiral artery remodelling in pregnancy**
Y Cui *et al.*
doi:10.1038/nature10897

PHYSICS

**Spontaneous coherence in a cold exciton gas**
A A High *et al.*
doi:10.1038/nature10903

**An entangled walk of photons**
J C F Matthews & M G Thompson
doi:10.1038/nature11035

PLANT SCIENCE

**Transcription factor PIF4 controls the thermosensory activation of flowering**
S V Kumar *et al.*
doi:10.1038/nature10928

NEUROSCIENCE

**Structure of the human κ-opioid receptor in complex with JDTic**
H Wu *et al.*
doi:10.1038/nature10939

**Crystal structure of the μ-opioid receptor bound to a morphinan antagonist**
A Manglik *et al.*
doi:10.1038/nature10954

**Optogenetic stimulation of a hippocampal engram activates fear memory recall**
X Liu *et al.*
doi: 10.1038/nature11028

## NATURE PODCAST

This week, evolutionary history revealed in ancient proteins, and treating a mouse model of Rett syndrome using bone marrow transplants. And we discuss a new book on natural soundscapes or 'biophonies', and how humans can influence them.
**nature.com/nature/podcast**

EVOLUTIONARY BIOLOGY

# Life imperfectly imitates life

**Some species evolve to resemble another species so as to protect themselves from predation, but this mimicry is often imprecise. An analysis of hoverflies suggests why imperfect imitation persists in the face of natural selection.** SEE LETTER P.461

DAVID W. PFENNIG & DAVID W. KIKUCHI

M. COLE/FLPA

**Figure 1 | A fly in wasp's clothing.** The harmless marmalade hoverfly, *Episyrphus balteatus*, shown here, resembles stinging wasps. Although some species of hoverfly closely resemble wasps or bees, others are poor lookalikes. Penney and colleagues[5] show that the lower selection pressures that come with decreasing abundance and small body size may provide the explanation for how such imprecise mimicry can persist.

One hundred and fifty years ago, the English naturalist Henry Walter Bates[1] discovered a phenomenon that he regarded as "a most powerful proof of the theory of natural selection". Charles Darwin and Alfred Russel Wallace, who had proposed natural selection as the engine of evolution only a few years earlier, agreed. Indeed, Darwin[2] considered Bates's manuscript to be "one of the most remarkable and admirable papers I ever read".

Bates had uncovered a spectacular type of adaptation, now known as Batesian mimicry[3], in which a species (the mimic) that is edible to predators evolves to resemble a conspicuous, inedible species (the model) that predators avoid. These lookalikes are selectively favoured, Bates argued[1], because predators confuse them for the inedible model and thereby avoid them. This idea was so persuasive that Batesian mimicry is still widely used to illustrate the power of natural selection for producing adaptations[3,4]. However, mimics are often poor replicas of their model, and this inexact mimicry poses a challenge for evolutionary theory[3]. On page 461 of this issue, Penney *et al.*[5] discuss possible explanations for why mimics are frequently imprecise.

As Penney and colleagues describe, several non-mutually exclusive hypotheses have been proposed to explain imperfect mimicry. They include: the 'eye-of-the-beholder' or sensory-limitation hypothesis, which asserts that imprecise mimicry is an artefact of human perception; the 'jack-of-all-trades' or multimodel hypothesis, which posits that imperfect mimics persist because they are under selection pressure to resemble more than one model; and the 'kin-selection' hypothesis, which asserts that imperfect mimicry is maintained because it provides benefits for genetically related individuals. Specifically, if mimics are imperfect, then predators will be more discriminatory and occasionally spare a mimic by mistaking it for a model. This will also spare relatives that share the same imperfect trait.

Another theory to explain imperfect mimicry is the 'relaxed-selection' hypothesis, which holds that there is little selective benefit in refining mimetic resemblance beyond a certain point, for example if the model is common or especially noxious. Finally, the 'constraints' hypothesis proposes that either imperfect mimics lack the genes to produce refined mimicry, or that a selective trade-off exists between predator-mediated selection favouring more precise mimicry on the one hand and other agents of selection (such as mate choice) favouring divergence on the other.

Until now, no study had rigorously evaluated these multiple hypotheses within a single system. Penney and colleagues[5] did precisely this by comparing the degree of mimicry in dozens of species of hoverfly. Mimicry is a dominant feature of this large family of harmless Diptera (Fig. 1). About 5,600 species have been described, at least a quarter of which resemble stinging wasps and bees (Hymenoptera)[6]. Although some hoverflies are remarkably accurate mimics, converging both morphologically and behaviourally on their hymenopteran model, many others seem to bear poor resemblance[6]. This variation in mimetic fidelity makes hoverflies ideal for studying imperfect mimicry.

The authors report that birds (which are hoverfly predators) and humans seem to agree on the resemblances between hoverflies and hymenopterans. Thus, in this case, the eye-of-the-beholder hypothesis does not hold. Furthermore, Penney and colleagues' statistical analysis reveals that the mimics' characteristics do not fall somewhere between those of different models, so the jack-of-all-trades hypothesis receives no support either. The kin-selection hypothesis predicts that mimetic precision should decrease with an increasing abundance of mimics, but the authors observed the opposite trend. In fact, this finding is consistent only with the constraints and relaxed-selection hypotheses. In addition to predicting that mimics' precision should increase with their abundance, these two hypotheses predict that mimetic precision should increase with the body size of the mimic, and this is exactly what the authors find.

To understand how the relaxed-selection hypothesis applies when both the abundance and body size of mimics increase, let us consider the problem of discriminating between tasty mimics and nasty models from the predators' perspective. If not all mimics are equally deceptive, a predator must take risks when attacking its prey — if it strikes a mimic, it will reap more reward than regret. When mimics are abundant, the likelihood of attacking a model by mistake decreases. In such conditions, predators should be willing to sample all but the best mimics, which will push selection towards more precise mimicry.

By the same token, when mimics have a larger body size, their potential benefit to predators is greater (larger prey are generally more profitable for predators), so there will be greater selection pressure on them than on their smaller counterparts to become better mimics. Although other studies have found that mimetic precision increases when mimics are abundant[7], Penny and colleagues' demonstration that this pattern also holds when mimics increase in size is an elegant affirmation of an old idea.

We still do not know whether hoverfly mimicry is imprecise because of an absence of selection for refinement once mimicry is 'good enough' (as in the relaxed-selection hypothesis), or whether there is active selection pressure against further refinement because of the costs of producing better mimicry (as in the constraints hypothesis). For example, constraints may be imposed by competition between mimics and their models (over shared resources[8] or reproductive opportunities[9]), which would favour divergence between them and, hence, imprecise mimicry[10]. Future studies are needed to tease apart these two hypotheses.

As we celebrate the 150th anniversary of Bates's discovery of mimicry[1], the topic continues to fascinate the public and scientists alike[3,4]. Penny and colleagues' findings help us to understand why selection sometimes produces precise mimicry, but often does not, and further clarification of this puzzle promises to provide additional insight into the evolutionary process. ■

**David W. Pfennig** *and* **David W. Kikuchi** *are in the Department of Biology, University of North Carolina, Chapel Hill, North Carolina 27599, USA.*
*e-mails: dpfennig@unc.edu; dkikuchi@live.unc.edu*

1. Bates, H. W. *Trans. Linn. Soc.* **23,** 495–556 (1862).
2. Burkhardt, F., Evans, S. & Pearn, A. M. (eds) *Evolution: Selected Letters of Charles Darwin 1860–1870* (Cambridge Univ. Press, 2008).
3. Ruxton, G. D., Sherratt, T. N. & Speed, M. P. *Avoiding Attack: The Evolutionary Ecology of Crypsis, Warning Signals & Mimicry* (Oxford Univ. Press, 2004).
4. Forbes, P. *Dazzled and Deceived: Mimicry and Camouflage* (Yale Univ. Press, 2009).
5. Penney, H. D., Hassall, C., Skevington, J. H., Abbott, K. R. & Sherratt, T. N. *Nature* **483,** 461–464 (2012).
6. Gilbert, F. in *Insect Evolutionary Ecology* (eds Fellowes, M. D. E., Holloway, G. J. & Rolff, J.) 231–288 (CABI, 2005).
7. Harper, G. R. Jr & Pfennig, D. W. *Proc. R. Soc. Lond. B* **274,** 1955–1961 (2007).
8. Alexandrou, M. A. *et al. Nature* **469,** 84–88 (2011).
9. Estrada, C. & Jiggins, C. D. *J. Evol. Biol.* **21,** 749–760 (2008).
10. Pfennig, D. W. & Kikuchi, D. W. *Curr. Zool.* (in the press).

BIOLOGICAL PHYSICS

# Swarming microtubules

**An artificial system of microtubules propelled by dynein motor proteins self-organizes into a pattern of whirling rings. This observation may provide insight into collective motion in biological systems.** SEE LETTER P.448

TAMÁS VICSEK

The spectacle of animals moving en masse is arguably one of the most fascinating phenomena in biology. For example, schools of fish can move in an orderly manner, and then change direction abruptly or, if under pressure from a nearby predator, swirl like a vigorously stirred fluid. The non-living world also has examples of collective motion, in systems that consist of units ranging from macromolecules to metallic rods, or even robots. On page 448 of this issue, Sumino *et al.*[1] describe another, until now unobserved, example of such behaviour: the coordinated motion of hundreds of thousands of subcellular structures known as microtubules, which spontaneously self-organize into a lattice-like structure of vortices. When considered in the context of about half a dozen known universal classes of collective-motion pattern[2], this new structure poses challenges in terms of explaining how it can arise and its relevance to applications.

If two or more moving units such as self-propelled rods interact, their direction of motion is likely to change. When pairwise interactions dominate over multiparty ones, the process of two units approaching each other, then adopting a new direction and leaving the area of interaction, can be interpreted as a collision. In closed systems at equilibrium, such collisions conserve energy and momentum, whereas, for example, when two birds interact and decide which way to fly in the open expanses of the sky, the concept of conservation of momentum is not applicable.

Typically, local interactions between organisms result in a consensus: fish or mammals tend to adopt a common direction of motion. Such 'polar' interactions are widespread and have been observed even for bacteria[3] and locusts[4]. Nonetheless, it was a great achievement when, in 2010, two groups[5,6] observed motional patterns associated with polar interactions on a molecular scale — that is, for a huge number of actin filaments on a layer of immobilized myosin protein heads.

In addition to polar interactions, 'nematic' interactions also occur. In this case, if the directions of motion of two units approaching one another form an angle smaller than 90°, both parts will take the same direction after the approach. But if the units come towards one another from directions that differ by more than 90°, they will leave in opposite directions.

Sumino *et al.*[1] have constructed a biological system in which nematic collisions take place (Fig. 1). The authors achieved this by choosing an assay of moving microtubules propelled by modified motor proteins (one-headed dynein molecules) in which the microtubules cannot, for the most part, cross each other's trajectories and maintain their own trajectory's direction and curvature. The authors find that, in this setting, and for relatively high densities (typically 5 microtubules in 100 square micrometres), the moving microtubules self-organize into a semiregular pattern of whirling rings, or vortices, within which they move either clockwise or anticlockwise. Furthermore, as time goes on, the microtubules jump from one vortex to another and change their rotational direction. The size of the observed pattern is large compared with the 15-micrometre length of each microtubule: the system shows regularities on a millimetre scale.

One of the strengths of the present study is the authors' ability to explain the main features of the microtubules' intricate motion with a simple model. The model draws on studies aimed at understanding the rich, large-scale behaviour that results from simple bilateral interactions between point-like, self-propelled particles.

But Sumino and colleagues' results also prompt several questions. For example, is the observation that individual microtubules have a slight preference to rotate anticlockwise

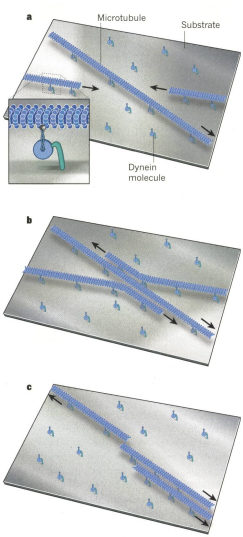


**Figure 1 | Nematic collisions.** Sumino *et al.*[1] have studied a system of microtubules in which nematic collisions occur. The microtubules are propelled by one-headed dynein molecules attached to the surface of a substrate. Three microtubules are shown here: **a**, approaching one another; **b**, colliding; and **c**, after the collision has taken place. Their final direction of motion depends on the angles at which they approach one another. In this case, the two leftmost microtubules adopt the same direction, whereas the rightmost microtubule leaves in the opposite direction.

a necessary condition for the observed semi-regular pattern of vortices? How is the persistence of the curvature of the microtubules' trajectories relevant? Furthermore, it would be interesting to investigate why actin filaments undergo polar interactions, whereas microtubules undergo nematic ones.

Whether the authors' observations are system specific or belong to a new class of collective-motion pattern remains to be seen. But one possibility is that the observed lattice-like structure falls within the group of patterns of vortex formation seen in many systems made up of self-propelled units. Typically, vortex formation can be closely related to the geometry of the confined area within which the collective motion occurs. In the current case, it seems that, owing to the persistence of curvature in the individual microtubules' motion, curved 'walls' of microtubules are spontaneously formed and enforce the formation of the vortices. Indeed, it has been shown[7] that, without such curvature persistence, nematic interactions in a system of self-propelled rods do not result in a similar arrangement of vortices.

Potential applications of Sumino and colleagues' study remain, for the time being, in the realm of speculation. But it is conceivable that the complex fluid currents generated in the stems of various plants relate to the collective motion of microtubules observed by the authors[1]. The streams of energy-supplying and waste materials in a stem have to fulfil a number of criteria, which could be best met through a coordinated action of motor molecules. The authors' demonstration that such action can be attained in a relatively simple assay is a step towards a better understanding of the role of collective motion in plants and other biological systems. ■

**Tamás Vicsek** *is in the Department of Biological Physics, Eötvös University, 1117 Budapest, Hungary.*
*e-mail: vicsek@hal.elte.hu*

1. Sumino, Y. *et al. Nature* **483,** 448–452 (2012).
2. Vicsek, T. & Zafeiris, A. *Phys. Rep.* (in the press); preprint at arxiv.org/abs/1010.5017 (2012).
3. Ingham, C. J. & Jacob, E. B. *BMC Microbiol.* **8,** 36 (2008).
4. Buhl, J. *et al. Science* **312,** 1402–1406 (2006).
5. Schaller, V. *et al. Nature* **467,** 73–77 (2010).
6. Butt, T. *et al. J. Biol. Chem.* **285,** 4964–4974 (2010).
7. Ginelli, F., Peruani, F., Bär, M. & Chaté, H. *Phys. Rev. Lett.* **104,** 184502 (2010).

MOLECULAR BIOLOGY

# How to duplicate a DNA package

**Cells replicate half of their genome as short fragments that are put together later on. The way in which this process is linked to the formation of DNA–protein complexes called nucleosomes is now becoming clearer.** SEE ARTICLE P.434

ALYSIA VANDENBERG & GENEVIÈVE ALMOUZNI

In a typical human cell, about two metres of DNA is wrapped around proteins to form nucleosomes, the basic units of chromatin. When this DNA is duplicated, the nucleosomes that lie ahead of the replication machinery are displaced, or disassembled into their component histone proteins. And after the machinery has passed by, the nucleosomes are reassembled on the two resulting 'daughter' strands, which requires the addition of new histones[1]. To make things more complicated, one of the two DNA strands can be replicated only in short pieces — called Okazaki fragments — that are joined together afterwards, and so its replication lags behind that of the other strand (Fig. 1). This elaborate mechanism is needed because DNA synthesis is unidirectional, whereas the sequences of the two DNA strands run in opposite directions. However, the links between DNA replication and nucleosome dynamics have previously been studied without distinguishing between the two strands. On page 434 of this issue, Smith and Whitehouse[2] uncover the interplay between nucleosome assembly and the synthesis of the lagging strand.

The authors[2] analysed Okazaki fragments from baker's yeast, a unicellular fungus commonly used as a model for eukaryotic cells — those found in organisms such as animals, plants and fungi. Smith and Whitehouse took advantage of an available large catalogue of defined yeast mutants, together with well annotated genomic information that included recently defined nucleosome positions[3]. The researchers developed an elegant method for purifying Okazaki fragments from yeast, then sequenced the fragments and mapped them on the yeast genome. The result is the first high-resolution, genome-wide analysis of Okazaki fragments from live eukaryotic cells. The analysis is a major achievement, as our knowledge of lagging-strand synthesis has been based largely on model studies[4] of the replication of non-chromosomal DNA molecules such as viral DNA.

Smith and Whitehouse discovered that, strikingly, the Okazaki fragments' size and location in the genome depend on where the nucleosomes are located. More specifically, the ends of the Okazaki fragments fall near the nucleosome's dyad axis, which corresponds to the midpoint of the DNA segment wrapped around the chromatin unit. This result contrasts with a common assumption that, during lagging-strand replication, a nucleosome would form as soon as the Okazaki fragment

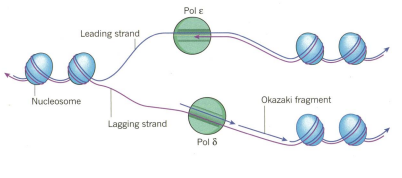


**Figure 1 | Asymmetric DNA replication.** The sequences of the two strands of a DNA molecule run in opposite directions, but during replication the new DNA molecules are synthesized in only one direction. Each strand is therefore duplicated differently. The leading strand is used as a template by a polymerase enzyme (Pol ε, top), which makes a new molecule in a continuous manner. By contrast, duplication of the lagging strand is discontinuous and requires another polymerase (Pol δ, bottom), which synthesizes short DNA pieces known as Okazaki fragments. These fragments are then joined together with the help of other enzymes to form a continuous molecule. During the process, nucleosomes — protein complexes around which DNA is coiled — disassemble from parental DNA to then reassemble, along with additional nucleosome proteins as needed, allowing both DNA duplication and chromatin reorganization. Smith and Whitehouse's analysis[2] of Okazaki fragments illuminates the link between nucleosome assembly and the synthesis of the lagging strand.

was long enough, and then the next fragment would be synthesized. This assumption tallies with the observation that the average length of Okazaki fragments is similar to that of the DNA wound around a nucleosome.

The authors[2] propose an alternative model in which the presence of a nascent nucleosome acts as a roadblock to an advancing polymerase enzyme (Pol δ), which is synthesizing the lagging strand. According to their model, Pol δ and other associated enzymes can invade the nascent nucleosome up to its dyad axis, but then the nucleosome mediates the dissociation of all of these enzymes from the DNA — by doing so, the nucleosome determines the length of the Okazaki fragment.

To test the model, Smith and Whitehouse used yeast strains in which the physiological balance between polymerases and nucleosomes was altered, either because the polymerases were less active or because nucleosome assembly was impaired. For example, they observed[2] that the Okazaki fragments were longer in mutant strains defective in CAF-1, a protein complex known[3] to act as a histone chaperone, which promotes histone deposition on newly synthesized DNA. Therefore, the tight balance between the capacity to form a new nucleosome on the lagging strand and the polymerase's ability to advance is what sets the length of the Okazaki fragment. These findings also suggest that the efficiency of the replication machinery's progression may depend on where the nucleosome forms.

The authors' work provides the basis for research on how other factors involved in histone dynamics and nucleosome movement on DNA — such as histone chaperones[4] and chromatin remodeller enzymes — can affect Okazaki-fragment size and, overall, DNA replication. Moreover, additional proteins involved in chromatin assembly could be identified by screening the available collection of yeast mutants for changes in Okazaki-fragment length. And the technique used for mapping Okazaki fragments offers a means to identify the genomic sites at which DNA replication starts.

It is tempting to postulate that the inherent asymmetry of nucleosome dynamics during DNA replication could contribute to a mechanism for asymmetric cell division, a process by which two different cell types are generated. This hypothesis is supported by the finding[6] that CAF-1 has a role in asymmetric cell division in the worm *Caenorhabditis elegans*. In addition, histones in nucleosomes exist in different forms associated with specific genomic regions, and can be 'marked' with various chemical modifications that reflect functional states, such as activation or repression of gene expression. Whereas some of these modifications are transient, others may be inherited during cell division in an epigenetic fashion — that is, independently of the DNA sequence. But to understand how the chemical modifications of nucleosomes can be inherited during cell division, we must first determine how nucleosomal organization is reproduced during DNA replication. So Smith and Whitehouse's study paves the way for a deeper exploration of the intimate relationship between genetics and epigenetics. ■

**Alysia Vandenberg** *and* **Geneviève Almouzni** *are in Unit UMR218, Institut Curie/Centre National de la Recherche Scientifique, Paris F-75248, France.*
*e-mail: genevieve.almouzni@curie.fr*

1. Saha, A., Wittmeyer, J. & Cairns, B. R. *Nature Rev. Mol. Cell Biol.* **7,** 437–447 (2006).
2. Smith, D. J. & Whitehouse, I. *Nature* **483,** 434–438 (2012).
3. Jiang, C. & Pugh, B. F. *Genome Biol.* **10,** R109 (2009).
4. Anderson, S. & DePamphilis, M. L. *J. Biol. Chem.* **254,** 11495–11504 (1979).
5. Corpet, A. & Almouzni, G. *Trends Cell Biol.* **19,** 29–41 (2009).
6. Nakano, S., Stillman, B. & Horvitz, H. R. *Cell* **147,** 1525–1536 (2011).

GEOCHEMISTRY

# Bubbles from the deep

**A study suggests that hydrocarbons released from sedimentary basins formed part of a climatic feedback mechanism that exacerbated global warming during the Eocene epoch.**

HENRIK SVENSEN

Gas released from sedimentary basins has been proposed to be a key player in many of the rapid climate changes that occurred in the past 250 million years. The types and sources of the released gases are still debated, but they probably included gases formed by the heating of organic matter around hot magma[1], and gases released by the dissociation of gas hydrates (solid compounds that trap gas molecules) found in deep-ocean sediments[2]. The influence of hydrates is greater in a warming world because higher ocean temperatures can melt methane-bearing gas hydrates, releasing the gas. The methane can then be oxidized to carbon dioxide, causing ocean acidification, and can contribute to global warming because both methane and carbon dioxide are greenhouse gases. Writing in *Geophysical Research Letters*, Kroeger and Funnell[3] suggest another way in which global warming can lead to increased gas emissions from the sea floor.

Sedimentary basins have large accumulations of biological, inorganic and clastic deposits (which consist of fragments of pre-existing rocks), and are host to more than 99.9% of the organic carbon in Earth's crust. This amounts to a staggering 15,000,000 gigatonnes (Gt) of carbon; for comparison, 3,300 Gt of carbon are stored in all known hydrocarbon and

# nature podcast

science... wherever you are.

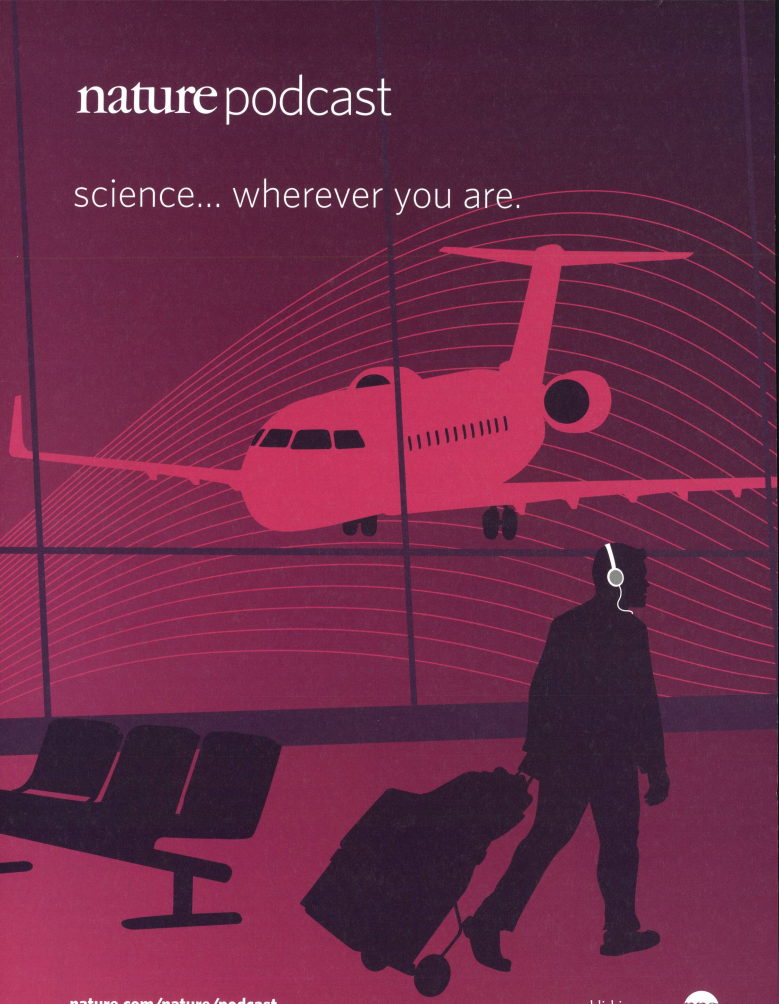

nature.com/nature/podcast

nature publishing group npg

coal reserves[4]. Any viable mechanism for transferring significant quantities of sediment-bound carbon to the atmosphere on a short timescale may thus perturb the global carbon cycle and lead to global warming.

A series of such perturbations has been suggested[5,6] to have happened in the Eocene epoch (which ran from 55.8 million to 33.9 million years ago) to explain several short-lived climatic anomalies that occurred during a period of otherwise steady warming from 58 to 50 Myr ago (Fig. 1). The most prominent of these events was the Palaeocene–Eocene thermal maximum (PETM), which was characterized by global warming of 5–10 °C and subtropical conditions in the Arctic. One cause of the PETM is commonly assumed to have been methane release to the atmosphere that was triggered either by the melting of gas hydrates[7] or by the heating of rocks rich in organic material in sedimentary basins (caused by widespread volcanic activity in the northeast Atlantic region[1,7]).

The extended period of warming during the Eocene culminated in the Early Eocene Climatic Optimum (EECO) 52 to 50 Myr ago, the hottest prolonged climatic episode since the Cretaceous period 145.5 to 65.5 Myr ago. Kroeger and Funnell[3] focus on the EECO in their work. Using computer models of four sedimentary basins in the southwest Pacific, they simulated the increase in hydrocarbon generation in the basins as the warming Eocene oceans transferred heat to the sea floor and to deep-seated, organic-rich rocks.

The sedimentary basins studied by the authors all contained rocks that could produce petroleum given the right temperature conditions and sufficient time. Organic matter within the sedimentary rocks can convert into petroleum at temperatures of 60–120 °C (the oil window), or into predominantly natural gas at temperatures of 100–200 °C (the gas window). On the basis of their models, Kroeger and Funnell estimate that the warming ocean during and after the PETM eventually raised the temperature of a 300-metre-thick layer of sediments into the oil and gas windows. A marked rise in hydrocarbon production would therefore have occurred in the 4 to 5 Myr following the PETM, peaking during the EECO.

The authors' results help us to understand the dynamics and temperature-dependence of hydrocarbon (petroleum and gas) generation in sedimentary basins. But there is more to the story than that. If oil and gas generated during the Eocene somehow escaped the sedimentary basins and leaked out to the ocean and the atmosphere in sufficient quantities, this may have contributed to global warming at the time. In other words, Kroeger and Funnell propose a climate feedback mechanism: global warming causes increased hydrocarbon production that leads to prolonged global warming.

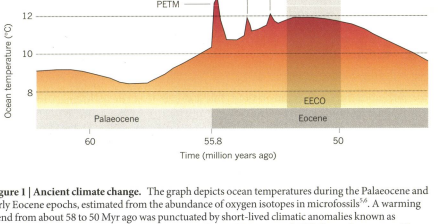


**Figure 1 | Ancient climate change.** The graph depicts ocean temperatures during the Palaeocene and early Eocene epochs, estimated from the abundance of oxygen isotopes in microfossils[5,6]. A warming trend from about 58 to 50 Myr ago was punctuated by short-lived climatic anomalies known as hyperthermals, of which the Palaeocene–Eocene Thermal Maximum (PETM) was the greatest. The warmest climate occurred during the Early Eocene Climatic Optimum (EECO) about 52 to 50 Myr ago, after which climate cooling occurred. The PETM may have been caused in part by the release of methane to the atmosphere, triggered by the melting of gas hydrates (solids that trap gases in ocean sediments) and/or by the heating of organic matter by intruding magma in sedimentary basins. Kroeger and Funnell[3] propose that the production of hydrocarbons (petroleum and natural gas) in sedimentary basins increased during and after the PETM, and that seepage of hydrocarbons from such basins into the ocean and atmosphere contributed to global warming.

The idea that the conversion of organic matter into petroleum following a temperature increase in sedimentary basins may form part of a climate feedback mechanism was first posited[8] by Kroeger and colleagues last year. The modelling in Kroeger and Funnell's present work[3] remarkably predicts and quantifies a peak in hydrocarbon production that overlaps in time with the EECO. The authors' results show that about 37 Gt of oil and 8 Gt of gas were generated from the four basins during this period, which is 50% more than would have occurred in the absence of extra ocean warming. This alone would not have been sufficient to affect the Eocene climate[9], but many other basins around the world would presumably have increased in temperature at the same time. The mass of hydrocarbons generated globally could therefore have been considerably higher than that predicted in the authors' study, although the exact amount is difficult to quantify.

Is hydrocarbon seepage at the sea floor on a climate-changing scale a realistic possibility? Kroeger and Funnell argue that it is, because more oil and gas are generated in sedimentary basins than are trapped[10]. Studies[11] of sedimentary basins around the globe have shown that gas seepage is currently a common phenomenon, and there is no reason why this should not have been the case earlier in Earth's history[12].

But did the hydrocarbons predicted[3] to have been generated during the Eocene really leak out to the ocean and atmosphere, or did they stay trapped in the subsurface? A way to test this is to search for carbonate deposits in old sea-floor sediments, because sea-floor hydrocarbon seepage leaves behind deposits that have distinct geochemical signals that can be attributed to their origin[13]. Unfortunately, the carbonate record is currently too poorly investigated to confirm the extent of seepage from sedimentary basins during the Eocene, and so more studies are needed. Nevertheless, one thing seems clear: the transfer of carbon from sedimentary rocks to the atmosphere is an important component of climate change, both past and future. ■

**Henrik Svensen** *is at the Centre for Physics of Geological Processes, University of Oslo, PO Box 1048, Blindern, 0316 Oslo, Norway. e-mail: hensven@fys.uio.no*

1. Svensen, H. *et al. Nature* **429,** 542–545 (2004).
2. Dickens, G. R., O'Neil, J. R., Rea, D. K. & Owen, R. M. *Paleoceanography* **10,** 965–971 (1995).
3. Kroeger, K. F. & Funnell, R. H. *Geophys. Res. Lett.* http://dx.doi.org/10.1029/2011GL050345 (2012).
4. www.grida.no/publications/other/ipcc_tar
5. Zachos, J. C., Pagani, M., Sloan, L., Thomas, E. & Billups, K. *Science* **292,** 686–693 (2001).
6. Sluijs, A., Bowen, G. J., Brinkhuis, H., Lourens, L. J. & Thomas, E. in *Deep Time Perspectives on Climate Change: Marrying the Signal from Computer Models and Biological Proxies* (eds Williams, M., Haywood, A., Gregory, J. & Schmidt, D.) 267–293 (Geol. Soc. Lond., 2007).
7. Storey, M., Duncan, R. A. & Swisher, C. C. III *Science* **316,** 587–589 (2007).
8. Kroeger, K. F., di Primio, R. & Horsfield, B. *Earth Sci. Rev.* **107,** 423–442 (2011).
9. Cui, Y. *et al. Nature Geosci.* **4,** 481–485 (2011).
10. Kvenvolden, K. A. & Cooper, C. K. *Geo-Mar. Lett.* **23,** 140–146 (2003).
11. Serié, C. S., Huuse, M. & Schødt, N. H. *Geology* http://dx.doi.org/10.1130/G32690 (2012).
12. Berndt, C. *Phil. Trans. R. Soc. A* **363,** 2855–2871 (2005).
13. Mazzini, A., Aloisi, G., Akhmanov, J., Parnell, B. & Murphy, P. J. *Geol. Soc. Lond.* **162,** 815–827 (2005).

VIROLOGY

# Influenza's tale of tails

**Epigenetics is a hot new research field, but it seems that the influenza virus already has it figured out. By mimicking epigenetic regulation in human cells, one flu strain suppresses the expression of antiviral genes.** SEE ARTICLE P.428

ALEXEI L. KRASNOSELSKY & MICHAEL G. KATZE

Influenza virus infections are sometimes severe, or even deadly, but most people recover within a few days, helped by their body's immune system. Yet this apparently simple interaction between the virus and its host is deceptive. Influenza viruses are, in fact, masters at circumventing their hosts' defences — they co-opt cellular protein-synthesis pathways to produce viral proteins, for example, and antagonize aspects of the immune response. On page 428 of this issue, Marazzi *et al.*[1] describe another viral evasion tactic. They show that an influenza protein called NS1 mimics a host-cell histone protein that is involved in regulating gene expression. By hijacking this regulatory machinery, the virus inhibits the cell's production of antiviral proteins*.

Cells tightly regulate the expression of specific genes according to an organism's developmental stage and physiological state, and in response to environmental stimuli such as infection. Gene expression can be altered in various ways, including by transcription-factor proteins, which bind to DNA and regulate the transcription of certain genes, or through epigenetic modification — heritable chemical changes to DNA and associated proteins that do not affect the DNA sequence but alter the rate of transcription. Epigenetics has rapidly become a much-studied topic since these regulatory mechanisms were first reported around 20 years ago.

A common epigenetic alteration is the addition of methyl or acetyl groups to histone proteins, which are the 'building blocks' of chromatin, the scaffold that packages DNA into chromosomes. The four main histone proteins (H2A, H2B, H3 and H4) consist of a globular domain and an unstructured amino-terminal tail region that is dominated by the positively charged amino acids lysine and arginine. These amino acids can be modified by enzymes that add or remove methyl or acetyl groups[2]. Such modifications alter the histone–DNA interaction, which in turn leads to dynamic changes in chromatin that allow specific areas of the chromatin to unfold, or other proteins to be recruited to the site. Thus, by regulating the accessibility of a particular region of DNA, epigenetic modifications can regulate gene expression.

Some epigenetic changes are generally associated with a site of active gene transcription[3]. An example of such a change is methylation at the lysine residue (K) of the amino acid sequence designated ARTK in histone H3 (known as the H3K4 modification). Marazzi *et al.*[1] found that the H3N2 influenza virus contains an amino-acid sequence (ARSK) very similar to the histone's ARTK sequence (Fig. 1). This mimic sequence is found in the virus's NS1 protein, which is not essential for viral structure but is known to have other roles in evading the host's immune system[4]. The authors also show that this sequence similarity is functional — the NS1 tail can serve as a substrate for the histone-modifying enzyme Set1, a lysine methyltransferase.

Marazzi and colleagues also demonstrate that H3N2's histone-mimic tail binds directly to the transcription-elongation complex PAF1C (Fig. 1). PAF1C accompanies the transcription enzyme RNA polymerase II during the formation of messenger RNA, and is thought to recruit the Set1 enzyme that leads to H3K4 methylation[5]. The authors propose that NS1 binding to PAF1C interferes with gene transcription in the host cell. Indeed, the researchers found that when cells from human lung tissue were infected with the H3N2 virus, transcription of rapidly inducible genes was halted. But when the cells were infected with H3N2 viruses that had been mutated so that they could no longer bind PAF1C, transcription of these genes was unaffected. Furthermore, the authors provide compelling evidence that it is specifically the transcription of antiviral genes that is interfered with by the interaction between NS1's histone-like tail and PAF1C. Thus, histone mimicry seems to support viral infection, and may give a selective advantage to viruses that have this ability.

Is this mechanism unique to H3N2 viruses, and could it be a recent evolutionary adaptation? Moreover, does possession of this mechanism have a role in the variation in infectivity and disease severity that is seen among influenza strains? The H3N2 virus is an emerging influenza subtype that has caused only a limited number of human infections during the 2011–12 flu season. However, they seem to cause illness of around the same severity as that induced by standard seasonal influenza viruses, which do not contain the NS1 histone-mimic tail[1]. It will be necessary to assess other emerging influenza strains for histone mimicry to determine whether this mechanism is evolutionarily new, and to study more influenza cases to predict its

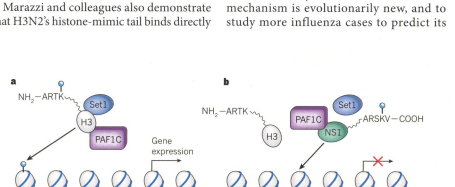


**Figure 1 | Interfering influenza.** Histones are the building-block proteins around which DNA is wound to form chromatin. Epigenetic changes to histones, such as the addition of methyl groups (blue circles), can affect the rate of gene transcription at specific DNA sequences. **a**, The amino-terminal ($NH_2$) 'tail' of the human H3 histone protein contains a string of amino acids (ARTK) that can be methylated at the lysine (K) residue by a methyltransferase enzyme, Set1. This enzyme is recruited by a protein complex called PAF1C, which also promotes elongation of RNA molecules during gene transcription. Methylation of the lysine in ARTK of the H3 histone tail is associated with active gene transcription. **b**, Marazzi and colleagues[1] show that the NS1 protein of the H3N2 influenza virus contains an amino-acid sequence (ARSK, close to the protein's carboxy (COOH) terminus) that mimics the H3 ARTK sequence. Using this sequence, viral NS1 can bind directly to PAF1C, which might direct Set1's methylation activity to NS1 rather than to the H3 histone. The authors also show that NS1 is deposited at the promoter regions of the host's DNA to which methylated H3K4 would typically bind, and that this interference suppresses the expression of antiviral genes.

*This article and the paper[1] under discussion were published online on 14 March 2012.

potential impact on public health. Even if histone mimicry is not widespread and does not dramatically alter disease severity, Marazzi and colleagues' discovery may provide a novel target for antiviral drugs aimed at modulating the host's antiviral response.

The finding raises another intriguing question: what would happen if a person is concurrently infected with H3N2 virus and a more virulent influenza virus, such as the highly pathogenic avian H5N1? Or what might occur if an H5N1 virus acquires the NS1 sequences required for the protein to function as a histone mimic? The combined effect of a suppressed antiviral response and a highly virulent virus might lead to devastating consequences for the host. Alternatively, if an overly active host response is itself the main culprit in causing severe influenza, as has been suggested[6], a suppressed antiviral response could actually reduce disease pathology.

Research aimed at addressing these questions may be hampered by an increasing wariness about generating recombinant H5N1 viruses[7]. But ongoing influenza research remains essential. Although epigenetic gene regulation is new to scientists, other mechanisms of gene regulation no doubt remain to be discovered, and we can be certain that viruses have already evolved to interfere with these regulatory processes, and to use them to their advantage. ■

**Alexei L. Krasnoselsky** *and* **Michael G. Katze** *are in the Department of Microbiology and Washington National Primate Research Center, University of Washington, Seattle, Washington 98195-8070, USA.*
*e-mails: akrasnos@u.washington.edu; honey@u.washington.edu*

1. Marazzi, I. *et al. Nature* **483,** 428–433 (2012).
2. Berger, S. L. *Nature* **447,** 407–412 (2007).
3. Ng, S. S., Yue, W. W., Oppermann, U. & Klose, R. J. *Cell Mol. Life Sci.* **66,** 407–422 (2009).
4. García-Sastre, A. *Virus Res.* **162,** 12–18 (2011).
5. Jaehning, J. A. *Biochim. Biophys. Acta* **1799,** 379–388 (2010).
6. Kash, J. C. *et al. Nature* **443,** 578–581 (2006).
7. Kawaoka, Y. *Nature* **482,** 155 (2012).

MICROSCOPY

# Plasmons go quantum

**Observations of collective electron waves in metal nanoparticles challenge our understanding of how light interacts with matter on small scales and underscore the need to factor quantum effects into nanophotonics.** SEE ARTICLE P.421

F. JAVIER GARCÍA DE ABAJO

Just as water ripples travel along the surface of a pond after a stone is thrown into it, collective oscillations of conduction electrons called plasmons can be produced in a metal and propagate along its surface. Like pond ripples, plasmons can generally be explained in terms of a classical theory — electromagnetism. But if the metal structure on which they reside is very small (less than about 10 nanometres across), quantum-mechanical effects emerge and become relevant, changing the plasmons' oscillation frequency and lifetime. Such changes have so far been poorly understood, particularly on the experimental front. On page 421 of this issue, Scholl *et al.*[1] describe an experiment, and an accompanying theoretical analysis, that addresses this issue.

When light is shone on nanometre-sized particles made of silver and gold, it creates plasmons that have frequencies in the optical and near-infrared parts of the spectrum. The intense colours of the Lycurgus Cup, which dates back to fourth-century Rome and is on display at the British Museum in London, are an example of nanoparticle plasmons at work. Plasmons are unique in their ability to enhance the intensity of incident light and to concentrate the light down to regions much smaller than its wavelength. These features are the main reason that plasmons are finding use in a wide range of applications, including improved photovoltaic devices[2], cancer therapy[3] and catalysis[4].

Much effort is being invested in engineering small metallic structures so as to manipulate plasmons and optimize their performance. As a result, a plasmon taxonomy has been developed that is mostly based on the classical electromagnetic description of structured metals. This classical approach is useful for accurately describing plasmons in structures larger than about 10 nm. But it fails for smaller structures, which are of utmost importance for the applications mentioned above.

Observing plasmons in particles smaller than 10 nm is challenging because they interact only weakly with light. For example, their optical absorption is simply proportional to their volume. It is thus understandable that quantum effects emerging in such particles have been investigated only in ensembles[5]. To make things more complicated, collections of sub-10-nm particles are hard to synthesize with narrow distributions of particle size and shape, so that conventional far-field optical studies have relied only on measurements of averages over such distributions.

Scholl and co-workers[1] circumvent these problems by examining individual particles using an electron microscope. They have excited plasmons by focusing fast electrons on silver nanoparticles with sub-nanometre precision; the electromagnetic interaction between fast electrons and plasmons is analogous to

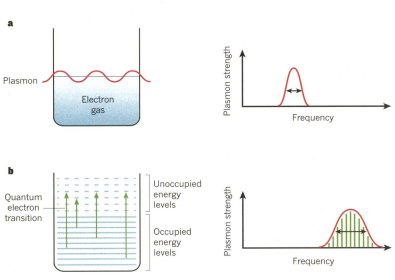


**Figure 1 | Quantum effects in nanoparticle plasmons. a,** In particles larger than about 10 nanometres, plasmons emerge as collective oscillations of a gas of conduction electrons, and have a frequency that is uncertain (double-headed arrow) because of collisions among the electrons and between the electrons and the particles' atomic lattice. **b,** In particles smaller than 10 nanometres, plasmons are associated with quantum electron transitions between occupied and unoccupied energy levels. As a result, the plasmon frequency and its uncertainty, which Scholl *et al.*[1] accurately measured, are larger than those for bigger particles.

the interaction of light with plasmons. Using state-of-the-art electron energy-loss spectroscopy, the authors have measured the plasmon frequencies with sufficient accuracy to separate surface- and bulk-plasmon components and also to resolve tiny changes in the frequency of surface plasmons with particle size. In classical electrodynamics, no size dependence is expected. However, Scholl and colleagues have observed a sizeable increase (about 15%) in the plasmon frequency of their smallest nanoparticles (roughly 2 nm across) compared with larger ones (larger than 10 nm), accompanied by a decrease in the plasmon lifetime of about 50%.

In a simple model, conduction electrons moving at about one million metres per second take approximately $10^{-14}$ seconds to travel across a 10-nm silver particle. This is comparable to the observed plasmon lifetime of such particles, which is about 10 plasmon periods. Under the assumption that reflections of the electrons at the surface contribute to the reduction in the plasmon lifetime, a model has been formulated[5] that is widely used and accounts for the observed lifetime reduction in assemblies of sub-10-nm particles. But the increase in plasmon frequency observed by Scholl *et al.*[1] in their individual sub-10-nm silver particles cannot be explained by this model, and requires quantum-mechanical effects to be understood in detail and carefully accounted for.

In nanoparticles larger than 10 nm, the conduction electrons respond to electromagnetic fields as a classical electron gas. In this gas, the contribution of each electron to the plasmons cannot be observed, and the plasmon frequency is uncertain because of collisions of the electrons with each other and with the metal's atomic lattice (Fig. 1a).

By contrast, in nanoparticles smaller than 10 nm, because there are relatively few conduction electrons participating in the plasmons (about 250 electrons in a 2-nm particle), the electrons appear at a discrete set of energy levels, which are increasingly separated from one another as the particle size is reduced. This produces individual electron transitions between occupied and unoccupied electron energy levels. The frequency jumps of these transitions are centred around a value that is higher than the plasmon frequency of large nanoparticles (Fig. 1b), and the finite separation between the frequency jumps increases the uncertainty about the plasmon frequency and therefore reduces plasmon lifetime[6]. In fact, individual transitions cannot in general be resolved owing to the uncertainty produced by the collisions mentioned previously. Using a simplified model that incorporates the effects of individual electron transitions, Scholl *et al.*[1] have successfully explained their data.

By measuring the plasmon-frequency increase and lifetime reduction in sub-10-nm particles, and by modelling these effects in terms of quantum transitions, Scholl and co-workers[1] have shown that the quantum nature of conduction electrons emerges in plasmons of small nanoparticles. So far, their study has focused on spherical nanoparticles. But it is expected that quantum effects should also have a role in nanometre-sized gaps between metallic nanoparticles and in sharp metal tips. These gaps and tips can create localized plasmon 'hotspots' that are relevant for applications such as nonlinear optics[7] and ultrasensitive, single-molecule detection (for example, through an effect known as surface-enhanced Raman scattering[8]).

Prospects for using plasmons to fabricate quantum-optics devices in robust solid-state systems also depend on the interaction between molecules and plasmon hotspots[9]. In such systems, quantum effects such as non-locality cannot be ignored because they produce sizeable plasmon-frequency shifts and reduced plasmon lifetimes. There are, of course, unknowns on the long road to understanding plasmons at the nanometre scale, but Scholl and colleagues' study is a step in that direction. ■

**F. Javier García de Abajo** *is at the Instituto de Química Física "Rocasolano", CSIC, Serrano 119, 28006 Madrid, Spain.*
*e-mail: j.g.deabajo@csic.es*

1. Scholl, J. A., Koh, A. L. & Dionne, J. A. *Nature* **483,** 421–427 (2012).
2. Atwater, H. A. & Polman, A. *Nature Mater.* **9,** 205–213 (2010).
3. Gobin, A. M. *et al. Nano Lett.* **7,** 1929–1934 (2007).
4. Hirakawa, T. & Kamat, P. V. *J. Am. Chem. Soc.* **127,** 3928–3934 (2005).
5. Kreibig, U. & Vollmer, M. *Optical Properties of Metal Clusters* (Springer, 1995).
6. Thongrattanasiri, S., Manjavacas, A. & García de Abajo, F. J. *ACS Nano* **6,** 1766–1775 (2012).
7. Danckwerts, M. & Novotny, L. *Phys. Rev. Lett.* **98,** 026104 (2007).
8. Stiles, P. L., Dieringer, J. A., Shah, N. C. & Van Duyne, R. P. *Annu. Rev. Anal. Chem.* **1,** 601–626 (2008).
9. Akimov, A. V. *et al. Nature* **450,** 402–406 (2007).

NEURODEGENERATION

# Trouble in the cell's powerhouse

**Studies of rare hereditary disorders are intended to find treatments, but they can also bring other discoveries. One such study links the dysfunction of a protein to that of the cell's energy producers, the mitochondria.**

DEREK P. NARENDRA & RICHARD J. YOULE

In Greek, 'ataxic' (ατάξις) means 'disordered'. In neurological diseases known as ataxias, the lack of order is mainly one of movement: patients cannot coordinate voluntary movements because of the loss of certain neural circuits, making it difficult for them to walk, reach for objects and speak. Increasingly, researchers are finding[1,2] that the underlying cause of some hereditary ataxias is another sort of disorder — that of mitochondria, the intracellular organelles that act as the cell's powerhouses. However, we know very little about the mechanisms that trigger certain other hereditary ataxias, such as the condition known as autosomal recessive spastic ataxia of Charlevoix–Saguenay, or ARSACS. The disease is caused by mutations in the *SACS* gene[3], but the link between the mutations and the neuronal loss has been unclear. Writing in *Proceedings of the National Academy of Sciences*, Girard *et al.*[4] find that mitochondrial dysfunction is just such a link, and in the process provide clues about the cellular role of the *SACS*-encoded protein, sacsin*.

*This News & Views article was published online on 7 March 2012.

The ataxia in ARSACS is due to a progressive loss of neurons called Purkinje cells, which are found in the cerebellum[3], a part of the brain involved in muscle coordination. Affected patients carry mutations in both chromosomal copies of *SACS*, so that their cells lack functional sacsin[3,6]. The disorder was first described[6] in 1978 in patients from the Charlevoix and Saguenay regions of Quebec, Canada, where it is much more common than in the rest of the world. One in 22 of the regions' residents carries a mutation in one of their two copies of *SACS* — probably brought by French immigrants four centuries ago.

To understand sacsin's functions, Girard *et al.*[4] analysed the location of sacsin within various types of cells, including neurons, in culture and observed that the protein co-localizes with mitochondria. Moreover, mitochondria in mouse cells in which sacsin expression had been inhibited, and in cells from patients with ARSACS, had markedly abnormal shapes: they were larger and formed more clumps than mitochondria in normal cells. The authors then generated mice that lacked the protein. These animals progressively lost Purkinje cells as they aged, making them potential models

for studying at least some aspects of ARSACS. Taken together, Girard and colleagues' results suggest that sacsin deficiency results in unusually shaped, large mitochondria, and that this in turn leads to Purkinje-cell loss.

The shape of mitochondria is dynamically controlled by their fission and fusion. But why do unusually shaped mitochondria harm Purkinje cells more than other cells? Each Purkinje cell has many long, branching projections that form an extensive tree-like structure (Fig. 1a), establishing about 150,000 synaptic connections with other neurons[7]. The synapses are energy-demanding because of the need for continual pumping of ions through the cell membrane — to keep the 'lines' clear for neural transmission — and thus they require functional mitochondria to be located nearby. To enter the narrow neuronal projections, small mitochondria need to be pinched off by fission from large ones[7] (Fig. 1b). Moreover, fission has a role in preserving mitochondrial health by eliminating organelles that become damaged by oxidative molecules produced during normal mitochondrial activity[8]. Purkinje cells seem to be highly dependent on the quality and efficient distribution of mitochondria throughout the cell, because their robust activity carries a high oxidative burden and they have a higher number of narrow prolongations than other cells. Indeed, Girard *et al.*[4] find that the clumped, fused mitochondria in sacsin-deficient neurons fail to distribute into the cellular prolongations (Fig. 1c), and that damaged mitochondria seem to be more abundant than in normal cells.

The authors' findings[4] raise several questions. For example, how does sacsin affect the size and distribution of mitochondria? Girard and colleagues propose that the protein may be needed for efficient fission of the organelle. In addition to the abnormal mitochondrial shapes in sacsin-deficient cells, the researchers[4] report that sacsin binds to the Drp1 protein, which is essential for mitochondrial division. During fission, Drp1 polymerizes to form a spiral around the outside of the organelle, constricting it and facilitating its division[9,10].

The hypothesis that sacsin is required for full Drp1 activity is consistent with previous research[11,12] showing that mice with brain-specific Drp1 deficiency display features similar to those observed by Girard *et al.*[4] in sacsin-deficient mice — a loss of Purkinje cells, together with the presence of oversized mitochondria that fail to spread into the neuronal projections. And it has been reported[8] that damaged mitochondria are not efficiently degraded in cultured cells in which Drp1 activity is inhibited. Therefore, the dependence of Purkinje cells on the shape and health of mitochondria may explain why they are preferentially lost in Drp1- and sacsin-deficient mice, and in patients with ARSACS.

Additional questions remain, such as why sacsin binds to Drp1 and how this binding may affect mitochondrial shape. Some portions of the sacsin protein are similar to chaperones (proteins that help other proteins to fold efficiently), so it is tempting to speculate that sacsin may be needed for Drp1 or other proteins involved in mitochondrial division to assume their proper conformation. The link between sacsin and Drp1 also raises the possibility that sacsin regulates the division of peroxisomes, another type of intracellular organelle. Drp1 elimination in mice results in abnormally long peroxisomes[11], and so it would be interesting to test whether the cells of patients with ARSACS contain longer peroxisomes.

Girard and colleagues' study of ARSACS strikes a common theme in research into neurodegenerative disorders: insight from clinical studies reveals new perspectives for cell biology, and vice versa. For instance, the study of families affected by optic atrophy type 1 revealed the protein OPA1 as being essential for mitochondrial fusion[13,14]. And research in the fruitfly revealed that the parkin protein — the dysfunction of which is the leading cause of recessive Parkinson's disease — regulates mitochondrial shape[14]. These examples demonstrate the importance of fostering interaction between the clinic and the lab. Thus, we can continue to learn about neurological disease from model organisms such as the fruitfly, and about mitochondrial biology from people in Quebec who have ataxia. With further collaboration between clinicians and scientists, this understanding might translate into treatments for these devastating disorders in the not-too-distant future. ■

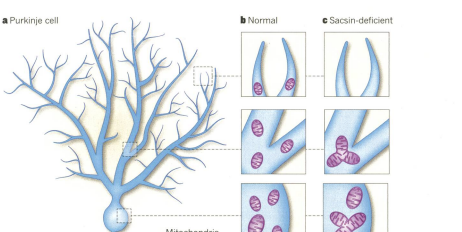


**Figure 1 | Out-of-shape organelles lead to disease.** **a**, Neurons known as Purkinje cells have many long, branching prolongations and are found in the cerebellum, an area of the brain that controls movement. These cells progressively die off in patients with a neurological disease called autosomal recessive spastic ataxia of Charlevoix–Saguenay (ARSACS), which is caused by mutations in the gene encoding the protein sacsin. **b**, Mitochondria are usually found throughout the body of normal neurons, including in the narrow cellular prolongations. **c**, Girard *et al.*[4] find that mitochondria in sacsin-deficient mouse cells and in cells from patients with ARSACS are larger than those in normal cells and accumulate in clumps. Such large mitochondria do not distribute into the cellular prolongations in sacsin-lacking neurons. These results, together with other data from sacsin-deficient mice, suggest that mitochondrial dysfunction is involved in the death of Purkinje cells in patients with ARSACS.

**Derek P. Narendra** *and* **Richard J. Youle** *are in the Biochemistry Section, Surgical Neurology Branch, National Institute of Neurological Disorders and Stroke, National Institutes of Health, Bethesda, Maryland 20892, USA.*
*e-mail: youler@ninds.nih.gov*

1. Babcock, M. *et al. Science* **276,** 1709–1712 (1997).
2. Van Goethem, G. *et al. Neurology* **63,** 1251–1257 (2004).
3. Engert, J. C. *et al. Nature Genet.* **24,** 120–125 (2000).
4. Girard, M. *et al. Proc. Natl Acad. Sci. USA* **109,** 1661–1666 (2012).
5. Kandel, E. R., Schwartz, J. H. & Jessell, T. M. *Principles of Neural Science* (McGraw-Hill, 2000).
6. Bouchard, J. P., Barbeau, A., Bouchard, R. & Bouchard, R. W. *Can. J. Neurol. Sci.* **5,** 61–69 (1978).
7. Li, Z., Okamoto, K., Hayashi, Y. & Sheng, M. *Cell* **119,** 873–887 (2004).
8. Twig, G. *et al. EMBO J.* **27,** 433–446 (2008).
9. Ingerman, E. *et al. J. Cell Biol.* **170,** 1021–1027 (2005).
10. Labrousse, A. M., Zappaterra, M. D., Rube, D. A. & van der Bliek, A. M. *Mol. Cell* **4,** 815–826 (1999).
11. Ishihara, N. *et al. Nature Cell Biol.* **11,** 958–966 (2009).
12. Delettre, C. *et al. Nature Genet.* **26,** 207–210 (2000).
13. Alexander, C. *et al. Nature Genet.* **26,** 211–215 (2000).
14. Greene, J. C. *et al. Proc. Natl Acad. Sci. USA* **100,** 4078–4083 (2003).

nature

22 March 2012 / Vol 483 / Issue No. 7390

# Publication policies, author guidelines and information

**This is a summary of *Nature*'s guide to authors, publication policies and other author information, available in full on the web via our main author information page at www.nature.com/nature/authors.**

## Getting published in *Nature*

Please read www.nature.com/nature/authors/get_published before finalizing any original scientific research manuscripts you intend to submit. This section explains *Nature*'s editorial criteria, and how manuscripts are handled by the editors after submission and before acceptance for publication.

## Formatting guide

Please read www.nature.com/nature/authors/gta before finalizing and submitting your contribution. This section provides instructions for preparing, formatting and writing all types of contribution published by *Nature*.

## Publication policies

This section, at www.nature.com/authors, describes *Nature*'s conditions of publication, including policies on authorship; competing financial interests; duplicate publication; prepublicity and embargoes; materials and data availability; research on animal (including human) subjects; referees; corrections, retractions, errata and addenda to published papers; the complaints procedure and refutations; and copyright/licence to publish. All contributions, for whatever section of the journal, are considered for publication and published on the condition that authors agree to these policies.

## Submissions

These sections, at www.nature.com/nature/authors/submissions, contain our online service for presubmission enquiries and submission and tracking of Articles, Letters and Review-type manuscripts. Authors should read the formatting guide before using this service. Authors who cannot submit online can submit by post, but *Nature* strongly recommends the online service. **Authors must not submit by both methods.** Authors experiencing operational difficulty in using the online submission service can send an enquiry to mtshelp@nature.com, with a brief explanation of the problem.

## Editorial contacts and author services

This section, at www.nature.com/nature/about/contact, provides the addresses of *Nature*'s editorial offices; names of editorial staff; and contact details for advice, reprints, permissions, press office (press@nature.com), and other author-related contact information, including postal addresses for mailed submissions. Short biographies of editors are also available at www.nature.com/nature/about/editors.

## Final submissions

This section, at www.nature.com/nature/authors/submissions/final, applies only if an Article or Letter has been accepted in principle for publication and the author has been asked by the editor for a final version. Authors will need to upload electronic files of the text, production-quality figures and supplementary information (if any) to our database. Authors must include a completed manuscript checklist and all relevant signed forms and declarations as requested by the editor.

## Short version of guide to authors

See www.nature.com/nature/authors for full version. Contributors not used to *Nature*'s format are advised to read some papers in published issues before submission, to familiarize themselves with *Nature*'s style. *Nature*'s main formats for original research are Articles and Letters.

**ARTICLES** are original reports whose conclusions represent a substantial advance in understanding of an important problem and have immediate, far-reaching implications. They do not normally exceed **5 pages** of *Nature* and have **no more than 50** references. (One page of undiluted text is about 1,300 words.)

Articles have a summary for readers outside the discipline, separate from the main text and containing no references, of up to 150 words. The summary does not contain numbers, abbreviations, acronyms or measurements unless essential. It contains a brief account of the background and rationale of the work, followed by a statement of the main conclusions, introduced by the phrase 'Here we show' or its equivalent.

The Article itself typically has about 3,000 words of text, beginning with up to 500 words of referenced text expanding on the background to the work, followed by a concise, focused account of the findings, and ending with one or two short paragraphs of discussion. The text can contain a few short subheadings consisting of about 20 but no more than 40 characters (including spaces) each.

**LETTERS** are short reports of original research focused on an outstanding finding whose importance means that it will be of interest to scientists in other fields. They do not normally exceed **4 pages** of *Nature*, and have **no more than 30** references. They begin with a **fully referenced paragraph** of not more than 300 words, aimed at readers in other disciplines. This paragraph contains a summary of the background and rationale for the work, followed by a one-sentence statement of the main conclusions introduced by the phrase 'Here we show' or its equivalent, and ending with two to three sentences describing the implications in context.

The main text which follows is typically up to 1,500 words long. This text can, if the author requires, start with a further brief paragraph of introductory material. A description of the research then follows. Any discussion at the end of the text should be as succinct as possible.

**FIGURES** in both Articles and Letters are as small as possible: Articles typically have 5 or 6 figures, Letters typically have 3 or 4 figures. Legends and/or methods are additional to the main text. Methods Summaries (which are published in print only) are no longer than 300 words; Methods sections (which are published online) can be up to 1,000 words; legends should not exceed 100 words each and start with a one-sentence title for the figure, followed by a brief explanation of the parts and symbols.

See www.nature.com/nature/authors/gta/others.html for details of other types of contribution to *Nature*, including Brief Communications Arising; Reviews and Perspectives (presubmission enquiries to reviewsandinsights@nature.com); and Correspondence (submit to corres@nature.com).

See Authors and Referees @ NPG (www.nature.com/authors) for details of Nature journals' publication policies, author and referee services, author benefits and for links to Nautilus and Peer to Peer blogs.

ARTICLE

doi:10.1038/nature10904

# Quantum plasmon resonances of individual metallic nanoparticles

Jonathan A. Scholl[1], Ai Leen Koh[2] & Jennifer A. Dionne[1]

**The plasmon resonances of metallic nanoparticles have received considerable attention for their applications in nanophotonics, biology, sensing, spectroscopy and solar energy harvesting. Although thoroughly characterized for spheres larger than ten nanometres in diameter, the plasmonic properties of particles in the quantum size regime have been historically difficult to describe owing to weak optical scattering, metal–ligand interactions, and inhomogeneity in ensemble measurements. Such difficulties have precluded probing and controlling the plasmonic properties of quantum-sized particles in many natural and engineered processes, notably catalysis. Here we investigate the plasmon resonances of individual ligand-free silver nanoparticles using aberration-corrected transmission electron microscope (TEM) imaging and monochromated scanning TEM electron energy-loss spectroscopy (EELS). This technique allows direct correlation between a particle's geometry and its plasmon resonance. As the nanoparticle diameter decreases from 20 nanometres to less than two nanometres, the plasmon resonance shifts to higher energy by 0.5 electronvolts, a substantial deviation from classical predictions. We present an analytical quantum mechanical model that describes this shift due to a change in particle permittivity. Our results highlight the quantum plasmonic properties of small metallic nanospheres, with direct application to understanding and exploiting catalytically active and biologically relevant nanoparticles.**

The remarkable growth of nanotechnology has been driven by the ability to alter material properties as dimensions are reduced towards the atomic scale. Nanomaterials exhibit physical and chemical properties very different from those of their bulk counterparts, often resulting from enhanced surface interactions or quantum confinement. In the past decade, attention has focused on nanoparticles composed of noble metals, because they support localized surface plasmon resonances (LSPRs). These collective oscillations of the conduction band electrons enable strong optical absorption and scattering in subwavelength structures, with spectral properties dependent on the nanoparticle's material, size, shape, electronic charge and surrounding medium[1,2]. LSPRs have enabled applications including photothermal ablation of cancer cells[3] and light concentration in thin-film photovoltaics[4]. Furthermore, the sensitivity of LSPRs to changes in the particle's environment has enabled ultrafine sensing, with applications including biomolecular and gas detection[5–8], catalytic monitoring of reactant adsorption[9,10] and sensing of electron charge-transfer events[11].

Although the plasmon resonances of nanospheres with diameters exceeding 10 nm have been well characterized[12], LSPRs of nanoparticles below this size are poorly understood. In this smaller size regime, plasmon resonances become more sensitive to the quantum nature of the conduction electrons. Experimentally probing this transition has been extremely challenging: optical detection in the far-field is hampered by these particles' diminishing scattering and absorption intensities, which scale as the sixth and third power of a particle's diameter, respectively[13]. Furthermore, the LSPR peaks become broadened and damped as the dimensions of the particle decrease well below the electron mean free path (52 nm for silver[14]). The difficulty in observing such weak signals has led to conflicting results from experiments involving quantum-sized plasmonic particles, with multiple reports of LSPR 'redshifts' or 'blueshifts' as the sphere dimensions are reduced[15]. For example, ensemble studies of glass-embedded silver spheres with sizes ranging from 10 nm to 2 nm have indicated a plasmon resonance blueshift of 0.1 eV (ref. 16). In contrast, ensembles of monodisperse silver nanospheres stabilized with oleylamine ligands have indicated significant LSPR redshifts of 0.3 eV (from 3.1 eV to 2.8 eV) as the mean particle diameter decreases from 18 nm to 2 nm (ref. 17).

To eliminate ensemble heterogeneity effects, other recent experiments have examined single metallic nanoparticles. Confocal heterodyne[18] and photothermal[19] techniques were used to observe the absorption of nanoparticles as their diameter decreased. Citrate-stabilized gold spheres with diameters ranging from 30 nm to 5 nm have exhibited a plasmon-resonance blueshift of approximately 0.05 eV, indicating a transition to quantum-confined effects. However, direct correlation between individual particle geometry, size and spectra was not achieved because the specimens were substantially below the optical diffraction limit.

With such difficulty in experimentally determining the plasmonic properties of small metallic particles, theoretical models to explain the nanospheres' deviations from bulk permittivity values have been equally challenging to develop and validate. Classical approaches have included the addition of size-dependent electron scattering terms in the Drude permittivity model, but the use of these alone results in predictions of redshifts and imperceptible plasmon resonances at small size scales[14] that conflict with experimental findings[16,18,19]. *Ab initio* density functional theory (DFT) approaches have also been used to predict metallic cluster properties[20,21], but are currently limited to particles smaller than 1–2 nm, owing to their high computational demands[22].

If the plasmon resonances of such quantum-sized particles could be understood and used, they would offer unprecedented opportunities in biology, catalysis and quantum optics. For example, their reduced dimensions would enable improved nanoparticle integration into cells for bio-plasmonic imaging or therapeutics[23–26]. Simultaneously, their increased surface-to-volume ratios would make them ideal catalytic centres or sensors[27]. Quantum-sized plasmonic particles would be

[1]Department of Materials Science and Engineering, Stanford University, Stanford, California 94305, USA. [2]Stanford Nanocharacterization Laboratory, Stanford University, Stanford, California 94305, USA.

particularly sensitive to single-molecule adsorbates[6] or to few-photon or few-electron transfer events[28], with potentially profound applications for quantum information transfer[29].

In this Article, we examine the plasmonic properties of individual nanospheres with diameters ranging from 20 nm to less than 2 nm, extending from the classically described regime to the quantum size regime. Rather than relying on optical observation, we use aberration-corrected TEM imaging in conjunction with monochromated scanning transmission electron microscopy (STEM) EELS. Combined, these techniques allow direct morphological and spectral analysis of individual nanoparticles, addressing many of the ambiguities of previous investigations. STEM EELS has recently yielded unprecedented insight into the plasmonic resonances of nanoscale hemispheres[30] as well as larger spheres[31] and prisms[32]. Here, we explore the plasmon modes of silver nanoparticles as their size is reduced to dimensions well below the electron mean free path. To minimize any surface chemical interface effects, the particles are synthesized without ligands. Our experimental results indicate a significant 0.5-eV blueshift in the plasmon resonance as the particle size approaches the quantum regime, with only slight linewidth broadening. The results indicate an increasingly substantial change in nanoparticle permittivity as the diameter is reduced below 10 nm, which can be well described with a computationally light analytical model based on fundamental quantum mechanical principles.

## Nanoparticle synthesis and electron spectroscopy

Figure 1 presents high-resolution micrographs of our particles. The Ag nanospheres were synthesized in solution using silver nitrate as the metallic precursor and sodium borohydride as both the reducing agent and electrostatic stabilizer to prevent agglomeration (see Methods)[33]. The absence of surface ligands on the silver nanoparticles is important to reduce the chemical interface effects on the plasmon resonance, but does present some synthetic challenges: ligands are typically used to prevent particle aggregation and reduce surface energy to counterbalance thermodynamic driving forces, allowing particle size to be more directly controlled. In this synthesis, electrostatic repulsion is used as a substitute for surface ligands to prevent agglomeration. The resulting silver nanoparticles have a mean diameter of 8 nm with sizes ranging from 1 nm up to 20 nm. They retain spherical-like symmetry for diameters just below 2 nm.

Spectroscopic analysis of our silver nanoparticles was performed with a FEI Titan transmission electron microscope at 300 kV in STEM mode, with an imaging spatial resolution of 0.27 nm, a spectral dispersion of 0.01 eV per pixel, and an EELS zero-loss peak (ZLP) full-width at half-maximum of 0.15 eV. Particles were deposited and well-dispersed on ultrathin (3 nm) carbon films to minimize the signal from the substrate during EELS. As a control, we also investigated the plasmon resonances of nanoparticles on 8-nm-thick $SiO_2$ substrates, which yielded very similar results (see Supplementary Information).

During EELS collection, electrons that interact with the particle exhibit an energy loss corresponding to the electromagnetic modes of the structure[32,34–37]. However, not all incident electrons will excite plasmons. In fact, the vast majority of source electrons are able to pass through the sample with minimal energy loss, resulting in a dominant ZLP on the detector. Owing to its relative magnitude and intrinsic Gaussian-like shape, the ZLP contributes a substantial background spanning several electronvolts in energy loss. To extract the plasmon contribution, techniques must be implemented either to deconvolve the ZLP from the collected spectra or to subtract the signal entirely. The former was accomplished through the Richardson–Lucy deconvolution algorithm, using the spectra of the substrate alone as the point spread function and deconvolving it from the particle spectra[38]. Alternatively, the ZLP subtraction was accomplished through two techniques: the 'reflected tail' method and Gaussian plus Lorentzian ZLP curve fitting (see Methods)[31]. Each of the above three strategies separately yielded consistent results in the plasmonic spectra.

Multiple energy loss spectra were collected for each particle, both near the sphere's edge to observe the surface plasmon resonance modes and through its centre to observe the bulk modes. When the electron beam is directed in close proximity to the edge of a particle, the surface electrons collectively oscillate and the LSPR modes are excited[37]. The energy of this resonance is dependent on not only the material's permittivity function but also its size, shape and surrounding medium. The bulk plasmon resonance, in contrast, is the collective oscillation of all the electrons in the material. It indicates the frequency of a metal-to-dielectric transition and is affected solely by the material's permittivity. Although the higher-energy bulk resonance peak can be observed with electron excitation, it cannot be seen in optical measurements, owing to the symmetry of the mode[36].

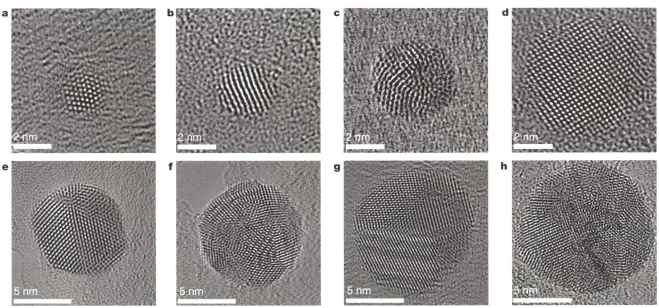


**Figure 1 | Aberration-corrected TEM images of silver nanoparticles synthesized free of stabilizing ligands.** Particles with diameters of 2 nm (**a**), 3 nm (**b**), 4.5 nm (**c**), 6 nm (**d**), 7.5 nm (**e**), 9 nm (**f**), 10.5 nm (**g**), and 12 nm (**h**) are shown. Scale bars: **a**–**d**, 2 nm; **e**–**h**, 5 nm.

First, we used STEM EELS to measure the plasmon resonances of larger, classically described nanoparticles that have been well characterized[31]. Figure 2 illustrates a 20-nm-diameter nanosphere that was excited with the electron beam along the edge and through the bulk of the particle. Both the STEM-acquired particle image and spectra are included. As can be seen, exciting the particle at the edge (position (i)) results in a single spectral peak at 3.3 eV, corresponding to the particle's LSPR. Electron excitation near the particle's interior (positions (ii) and (iii)) results in development of a second spectral peak at 3.85 eV, corresponding to the bulk plasmon of silver. The spectral positions of the surface and bulk plasmon resonances remain unchanged with the location of the electron source. However, the relative weight of the peaks varies, corresponding to the efficiency with which each mode is excited.

We repeated these techniques for individual nanoparticles with diameters ranging from 20 nm down to 1.7 nm. Figure 3a illustrates the STEM image and energy loss spectra of six individual particles with diameters of 11 nm, 8.5 nm, 5.5 nm, 3.5 nm, 2.5 nm and 1.7 nm. These spectra were generated by directing the electron beam at the edge of the particles to excite the LSPR selectively. As the nanosphere diameter is decreased, several trends can be noted. First, signal strength from larger particles is stronger than from smaller spheres, as would be expected on the basis of particle volume. However, even with the smallest observed particles, the plasmon resonance is still significantly above the noise level. Second, the spectral peak widths do show some expansion as particle size is decreased, with a full-width at half-maximum increasing from 0.4 eV to 0.6 eV as the diameter is reduced from 11 nm to 1.7 nm. Nevertheless, this broadening is substantially less than would be expected from ensemble measurements for similarly sized small particles, where the resonance peak becomes so dampened as to be nearly unrecognizable[14]. Finally, and most significantly, the energy of the surface plasmon resonance exhibits a notable increase as the particle size decreases.

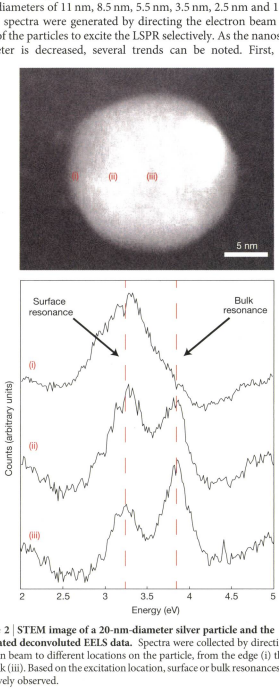


**Figure 2 | STEM image of a 20-nm-diameter silver particle and the associated deconvoluted EELS data.** Spectra were collected by directing the electron beam to different locations on the particle, from the edge (i) through the bulk (iii). Based on the excitation location, surface or bulk resonances can be selectively observed.

Figure 3b plots this plasmon resonance energy shift over a collection of particle sizes, with surface resonance peaks increasing from 3.3 eV to 3.8 eV as the particle size decreases. In contrast, classical Mie theory would predict only a 0.03-eV blueshift over the same size range. Interestingly, the trend towards higher energy resonances is not purely monotonic in the EELS data, with a greater variety in peak locations occurring at the smallest sizes.

In Fig. 3b, two standard deviation (95%) confidence intervals are included, generated by analysing the particle's spectra and fitted peak location data with a bootstrapping technique (see Methods). The confidence intervals indicate that the observed surface resonance peak shift is indeed real and is due to alterations in the permittivity as the particles enter the quantum size regime.

Figure 3b also includes a plot of the bulk plasmon shift with decreasing particle diameter, generated by directing the electron source through the particle's interior. For large particle dimensions, the bulk plasmon peak remains unaltered around 3.85 eV. For diameters smaller than 10 nm, however, a slight blueshift of 0.1 eV can be noticed. Bulk plasmon resonances distinct from LSPRs were observed for particles as small as 6 nm in diameter. Smaller particles exhibited a nearly indistinguishable spectral response for electron excitation both at the edge and at the centre of the particle. As shown below, this small-particle response can ostensibly be assigned to the LSPR.

## Modelling the classical–to–quantum transition

To understand the EELS data of Figs 2 and 3, we have developed an analytic model to describe size-dependent changes in plasmon resonances. The model is rooted in quantum calculations of the metal's electric permittivity $\varepsilon$ as particle dimensions are reduced towards the atomic scale. Though completely analytic, the results are complementary to both *ab initio* DFT calculations[39] and recent developments in predicting a system's electromagnetic response with nonlocal dielectric functions[40–42].

According to the quasistatic approximation of Mie theory for small particles[13,43], the LSPR peak occurs when the particle's polarizability is maximized. For a spherical particle, this condition is satisfied when $|\varepsilon_{\text{particle}} + 2\varepsilon_{\text{medium}}|$ is minimized. The bulk plasmon resonance occurs when the real component of the metal permittivity crosses zero. Thus, the spectral properties of plasmonic nanoparticles depend very sensitively on their dielectric function.

Classically, the frequency-dependent permittivity of metals can be described with a Drude model which determines the material's dielectric response by considering the motion of the free electrons against a background of positive ion cores. The general Drude permittivity is expressed as:

$$\varepsilon(\omega) = \varepsilon_{\infty} - \frac{\omega_p^2}{\omega^2 + i\gamma\omega} \qquad (1)$$

where $\omega$ is the angular frequency of the light, $\omega_p$ is the plasma frequency, a material property that is based on the number density of conduction electrons, $\varepsilon_{\infty}$ is a corrective constant that accounts for the background electron screening at high frequency, and $\gamma$ represents the scattering frequency of the electron as it travels through the metal. To increase the energy range across which the Drude model matches the

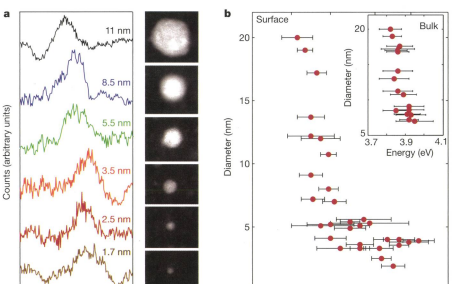


**Figure 3 | Correlating Ag nanoparticle geometry with plasmonic EELS data.** **a**, Collection of normalized, deconvoluted EELS data from particles ranging from 11 nm to 1.7 nm in diameter and the corresponding STEM image of each specimen. The electron beam was directed onto the edge of the particles so that only the surface resonance is shown. **b**, Plot of the surface plasmon resonance energy versus particle diameter, with the inset depicting bulk resonance energies. Horizontal error bars indicating 95% confidence intervals were generated with a curve fitting and bootstrapping technique (see Methods). Vertical error bars are contained within the size of the data points.

empirical literature data[44], we replace the corrective constant $\varepsilon_{\infty}$ with the frequency-dependent term $\varepsilon_{\mathrm{IB}}$. This component accounts for the contribution of d-band valence electrons that undergo an interband transition at high energies (see Supplementary Information).

Although Drude-like permittivity models accurately predict the plasmon spectra for larger nanoparticles (diameters greater than 10 nm), error significantly increases for reduced particle sizes. For nanostructures composed of only a few hundred to a few thousand atoms, both increased surface interactions and quantum confinement will affect the motion of electrons. Surface interactions will cause the scattering frequency $\gamma$ to increase owing to the increased number of electron collisions. Existing classical models of small-particle Drude-based permittivities have described this change with the expression:

$$\gamma = \gamma_{\mathrm{bulk}} + \frac{Av_{\mathrm{F}}}{R} \tag{2}$$

where $R$ is the particle radius and $v_{\mathrm{F}}$ is the Fermi velocity (approximately $1.4 \times 10^6\ \mathrm{m\,s^{-1}}$ in silver[45]). The variable $A$ is a fitting coefficient whose value is still much debated in the literature, spanning an order of magnitude from 0.1 to 2 depending on the experimental data and physical model[15,46,47]. The discrepancies in reported values for this coefficient may indicate that by itself, the classical surface scattering approach is insufficient to model the plasmon resonances of quantum-sized particles accurately. In fact, in contrast to our experimental results, solely increasing the $\gamma$ value with decreasing particle size results in a slight redshift of the plasmon resonance[14].

To fully model small plasmonic particles (diameters of 2–10 nm), quantum mechanical effects must also be considered. For such particles, the energy levels in the conduction band become discretized and only certain electronic or plasmonic transitions are allowed. To account for these transitions, we start with the Drude model of equation (1), but include Lorentzian terms that can be defined quantum mechanically. Following the example of Genzel[16] and Kraus[48], we model the conduction electrons as a free electron gas constrained by infinite potential barriers at the physical edges of the particle. Transition frequencies $\omega_{if}$ thus correspond to the allowed quantum energies of transitions of conduction electrons from occupied states $i$ within the k-space Fermi sphere to unoccupied states $f$ immediately outside it.

The relative magnitude of each of these Lorentzian perturbations is based on the well-established Thomas–Reiche–Kuhn energy-weighted sum rule (also known as the f-sum rule) that are commonly used for absorption processes. Encapsulating significant information about the energy spectrum and eigenfunctions of a system in a compact form, they have enabled experimental confirmation of early quantum theory and have since been widely used in solid-state physics as well as atomic and nuclear spectroscopy[49]. Here, the technique is employed in the form of oscillator strengths ($S_{if}$) that correspond to each transition frequency.

In total, the particle permittivity can be expressed as:

$$\varepsilon(\omega) = \varepsilon_{\mathrm{IB}} + \omega_{\mathrm{p}}^2 \sum_i \sum_f \frac{S_{if}}{\omega_{if}^2 - \omega^2 - i\gamma\omega} \tag{3}$$

where the sum is taken over all initial and final states of the electrons. The frequency of the transitions from the occupied to excited states can be described as:

$$\omega_{if} = \frac{E_f - E_i}{\hbar} \tag{4}$$

where the energy levels $E_f$ and $E_i$ depend on the geometry and potential of the system. We assume that the nanocrystal's physical shape closely approximates a sphere and thus treat the conduction electrons as particles in an infinite spherical well:

$$E = \frac{\hbar^2\pi^2}{8MR^2}(2n + l + 2)^2 \tag{5}$$

Here, $M$ is the mass of the electron, and $n$ and $l$ are the principal and azimuthal quantum numbers respectively. (This assumption of a 'spherical well' potential is justified on the basis of the geometry of the particles seen in Fig. 1.)

The oscillator strength terms, as dictated by the Thomas–Reiche–Kuhn sum rule, collectively sum to unity and are described using the standard harmonic oscillator quantum mechanical definition:

$$S_{if} = \frac{2M\omega_{if}}{\hbar N} |\langle f|z|i\rangle|^2 \tag{6}$$

where $N$ is the number of conduction electrons in the nanoparticle. The matrix element term $\langle f|z|i\rangle$ is determined by the allowed

wavefunctions of the spherical well model. Further details can be found in the Supplementary Information.

Figure 4a illustrates the real and imaginary components of the permittivity, accounting for both quantum mechanical effects and surface scattering. Here, the electron scattering term $\gamma$ was allowed to vary in accordance with equation (2), using $A = 0.25$. This value was chosen based on fits from single-particle experiments of larger spheres on glass substrates[19] and DFT simulations of silver nanoparticles[39], both of which are free of the complicating effects of heterogeneity in ensemble measurements.

As can be seen, the permittivity is highly dependent on the specific size of the spherical particle. For small particle diameters ($<$10 nm), the Lorentzian oscillations occur at higher energies as a result of the allowed electron transition frequencies. These have an $R^{-2}$ dependence according to the allowed energies in a spherical well (equation (5)). As the particle diameter increases beyond the quantum size range ($>$10 nm), the conduction electron transition frequencies decrease into the infrared, and the magnitude of the perturbations, as dictated by the oscillator strength, also decrease. Accordingly, larger particle permittivities converge to bulk experimental data and the classical Drude model based on bulk parameters (see Fig. 4). The choice of a larger $A$ coefficient would result in increased plasmon peak broadening, but does not significantly affect the general energy trends.

Using the permittivity values shown in Fig. 4a as an input to electromagnetic Mie theory, the absorption efficiencies (absorption cross-sections divided by physical cross-sections) of spheres with diameters of 2, 4, 6 and 8 nm are determined. The energies of the dipolar resonances that dominate the particles' optical spectra are the same as when generated through EELS[35,36], allowing direct comparison with our experimental data (see Supplementary Information). Figure 4b illustrates the results, revealing decreasing absorption efficiency and blueshifting LSPR peaks as particle size decreases that agree with experimental findings.

The full trend of calculated LSPR energy versus particle diameter is shown in Fig. 5a. Particle diameter values are displayed in gradations of full metallic monolayers (each adding approximately 0.5 nm), and the corresponding absorption spectra for each size is normalized to the same intensity colour scale. An effective medium refractive index of $n = 1.3$ is used as a weighted average of the carbon substrate ($n = 2$) and the surrounding vacuum ($n = 1$). The precise value of the index was determined by fitting the theory to the resonances of the largest particles (diameters about 20 nm) outside the quantum size regime. For comparison at smaller sizes, the full range of experimental EELS data was then overlaid, showing excellent agreement with the analytic quantum model. Both empirical values and calculations point to quantum size effects beginning to appear at diameters below 10 nm, resulting in a strong blueshift of the LSPR peaks compared to classical Mie theory predictions (dashed line).

The increased variability in experimental resonance energies in this quantum size regime additionally matches the non-monotonic trend in theoretical absorption. In the model, these perturbations are caused by higher-order conduction electron transitions (from deeper within the Fermi sphere to immediately outside it). Although these resonances have a weaker influence on the permittivity than the lowest-order transitions that dominate in Fig. 4a, their effects can be more pronounced for particles of certain diameters: when the radius-dependent transition frequencies overlap the overall dipolar resonance condition of the particle in its environment (that is, $|\varepsilon_{\text{particle}} + 2\varepsilon_{\text{medium}}|$ is minimized), additional spectral resonance peaks may appear and result in apparent shifts in the LSPR. These higher-order transitions have an increasing role for smaller particles because their oscillator strengths are relatively greater than those of larger spheres.

Our analytic model provides a straightforward method of understanding changes in the metal permittivity as nanomaterials approach the quantum size regime. It remains a relatively coarse approximation, however, because three simplifying assumptions are necessary to make the model tractable. First, the wavefunctions and allowed energies are based on an infinite potential barrier model. In experimental systems that involve colloidal particles with stabilizing ligands, the barrier may behave in a more finite manner with spill-out effects[14]. The nanospheres used in this experiment, however, were synthesized without ligands to minimize this phenomenon. Second, the quantum model assumes an essentially spherical particle, which becomes increasingly difficult to synthesize at sizes below 1.5 nm when there are fewer than a hundred atoms. For this reason, we limit the present model and experimental study to particles larger than 1.5 nm in diameter. However, it should be noted that high-symmetry structures approximating spheres can be attained at certain 'magic number' collections of atoms even down to the smallest cluster sizes[39]. Lastly, the model assumes that there is no interaction between the conduction electrons, a common assumption in many analytical quantum models. For a complete understanding of nanoparticle properties, *ab initio* techniques are required.

## Comparing analytic and *ab initio* predictions

As a means of comparison, we have also used Ag permittivities derived from a rigorous DFT model employing a local density approximation[39] to calculate plasmon resonances. In ref. 39, the particle dielectric functions were generated through the analysis of

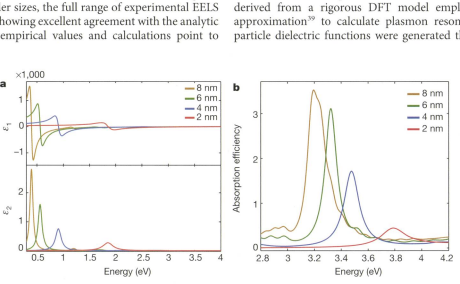


**Figure 4 | Analytic quantum theory of particle permittivity and spectra.** **a**, The real ($\varepsilon_1$) and imaginary ($\varepsilon_2$) components of the dielectric functions of silver nanoparticles with diameters of 2, 4, 6 and 8 nm, calculated using the analytic quantum model of equation (3). **b**, The corresponding absorption spectra of the particles generated by Mie theory. The refractive index of the surrounding medium was set to 1.3. As particle size decreases, reduced absorption efficiencies and blueshifted surface plasmon peak energies are predicted.

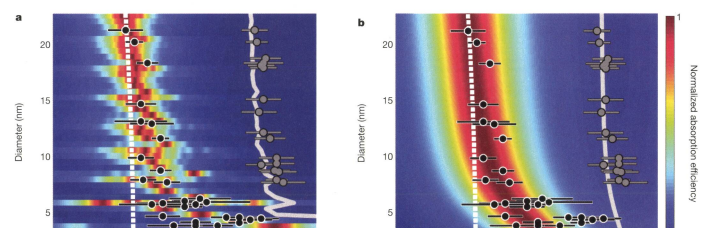


**Figure 5 | Comparison of experimental data with quantum theory.** Experimental, EELS-determined localized surface plasmon resonance energies of various Ag particle diameters are overlaid on the absorption spectra generated from the analytic quantum permittivity model (**a**) and the DFT-derived permittivity model (**b**). The experimental bulk resonance energies are also included (grey dots) along with the theory prediction (grey line). Classical Mie theory peak prediction is given by the dashed white line. The experimental data begin to deviate significantly from classical predictions for particle diameters smaller than 10 nm. Horizontal error bars represent 95% confidence intervals, as calculated through curve fitting and bootstrapping techniques.

high-symmetry silver clusters spanning from $Ag_{13}$ to $Ag_{586}$. Interband (d-band) and intraband (conduction) electron contributions were separated, and it was shown that interband effects on permittivity remain consistent with those seen in bulk while the particles exceed 2 nm in diameter, thus validating our use of a constant $\varepsilon_{IB}$ term in the analytic model. In ref. 39, the intraband contributions to the DFT-calculated permittivities were smoothed by single Gaussians to fit the relevant Drude model parameters, including the plasma frequency $\omega_p$, scattering frequency $\gamma$ and a single resonance frequency $\omega_{if}$. Given that particle sizes larger than $Ag_{586}$ (diameter 2.7 nm) become increasingly computationally demanding using DFT techniques, the trends in these parameters were extrapolated to bridge the quantum to classically described size span.

Using this DFT permittivity model and inserting the values into Mie theory, we similarly generated the absorption efficiency spectra for comparison to our experimental EELS data, as seen in Fig. 5b. The empirical and DFT-derived resonances again exhibit excellent agreement, with blueshifts of 0.5 eV observed as the particle decreases below 10 nm in diameter. It is additionally worth noting that when only the lowest-order electron transitions are allowed in our quantum analytic approach, it presents a trend nearly identical to that seen in the DFT-derived model (see Supplementary Information).

Predictions of the bulk plasmonic resonance energies using the quantum analytic and DFT-derived permittivity data have also been calculated by monitoring the frequency of the metal-to-dielectric transition (where $\varepsilon_1 = 0$). Note that this bulk frequency differs from the plasma frequency $\omega_p$ that is calculated by the simple Drude model, owing to the additional influence of the interband transitions on the permittivity.

The theory data for the bulk frequency, plotted as lines in Fig. 5a and b, shows strong consistency with the experimental values. Both show a blueshift for particles below 10 nm because the permittivity is altered by quantum size effects. We note that the predicted bulk resonance energy is greater than that of the corresponding surface resonance at all particle sizes throughout the modelled range. As the sphere diameter decreases, however, the LSPR frequency experiences a greater shift and the two peaks become harder to distinguish empirically. Additionally, with these smallest-sized particles, the relative surface-to-volume ratio greatly increases and the probability of bulk excitation decreases through a documented *begrenzung* effect[32,34,37]. We therefore predict that the surface resonance peak will dominate the peak from the bulk.

## Discussion

We have, for the first time, systematically observed and thoroughly analysed the plasmonic properties of individual silver nanospheres with sizes entering the quantum size regime. Using STEM EELS in an aberration-corrected electron microscope, we correlate the exact nanoparticle size and geometry with its spectra for colloidally synthesized particles devoid of the surface damping effects of ligands. A substantial blueshift in LSPR resonances is observed as particle size decreases, indicating a transition into the quantum-influenced regime. We develop an analytical quantum model to describe these resonances, which, despite its approximations and relative simplicity, agrees remarkably well with DFT methods. This straightforward theoretical framework can be directly applied to other metals with only the adjustment of the bulk material parameters $\gamma_{bulk}$, $\omega_p$ and $\varepsilon_{IB}$. Additional particle geometries such as rectangular prisms, cylinders and spherical shells can also be analysed through modification of the analytic quantum wavefunctions[48].

The combination of this versatile analytic model with direct plasmon observation in STEM EELS presents numerous opportunities for exploiting the plasmonic properties of quantum-sized particles. We anticipate a number of *in situ* STEM EELS experiments on both metallic and semiconducting plasmonic quantum dots[50]. In particular, real-time EELS monitoring of quantum plasmon resonances may yield dynamic insight into multi-electron redox reactions catalysed by small metallic particles, such as in artificial photosynthesis. Moreover, these quantum plasmon resonances may enable novel quantum devices based on excitation and detection of single photons or plasmons. Ultimately, EELS of quantum plasmonic systems should facilitate new understanding of electronic-scale processes, powerfully complemented by the atomic-scale resolution of aberration-corrected TEM.

## METHODS SUMMARY

Ligand-free silver nanospheres were synthesized according to a previously described technique[51]. 5 ml of 1 mM $AgNO_3$ (>99% Alfa Aesar) were added dropwise over 3 min to 15 ml of 2 mM $NaBH_4$ (Fisher Scientific) that had been chilled in an ice bath. The sodium borohydride solution was stirred during the silver addition to ensure a homogeneous distribution.

Particles were dispersed on either ultrathin carbon or silicon dioxide suspended films. Spectra were collected by directing the electron beam onto the edge and centre of the particle, with ten acquisitions of 30 ms each to prevent saturation of the charge-coupled device (CCD) detector. These collections were aligned

according to their ZLP and summed in post-processing. To reduce the background from the dominant ZLP and improve the energy resolution, the Richardson–Lucy deconvolution algorithm was employed. The point spread function, which indicates the energy spread of the electron source and aberrations in the spectrometer and CCD, was estimated by the acquisition of ten aligned spectra from the nearby substrate alone.

ZLP subtraction can also be used to reveal the plasmon resonance and was accomplished through two different techniques. In the first, 'reflected tail' method, the negative tail of the ZLP was reflected about the 0-eV axis and subtracted from the positive side[31]. In the second method, the ZLP was fitted to the sum of a Gaussian and Lorentzian curve and subtracted from the spectra. We separately applied each ZLP-removal method, which yielded consistent results in the plasmonic spectra.

Confidence intervals for resonance peak energies were generated using a bootstrapping method in which a locally weighted scatterplot smoothing (LOWESS) algorithm was applied to the summed EELS data of each particle. Each curve-fitting relies on a randomly selected subset of the spectral data, producing slight variations in the calculated peak energy. Using 20 iterations of the algorithm, 95% confidence intervals could be generated.

**Full Methods** and any associated references are available in the online version of the paper at www.nature.com/nature.

**Received 12 October 2011; accepted 26 January 2012.**


1. Willets, K. A. & Van Duyne, R. P. Localized surface plasmon resonance spectroscopy and sensing. *Annu. Rev. Phys. Chem.* **58,** 267–297 (2007).
2. Juluri, B. K., Zheng, Y. B., Ahmed, D., Jensen, L. & Huang, T. J. Effects of geometry and composition on charge-induced plasmonic shifts in gold nanoparticles. *J. Phys. Chem. C* **112,** 7309–7317 (2008).
3. Lal, S., Clare, S. E. & Halas, N. J. Nanoshell-enabled photothermal cancer therapy: impending clinical impact. *Acc. Chem. Res.* **41,** 1842–1851 (2008).
4. Catchpole, K. R. & Polman, A. Design principles for particle plasmon enhanced solar cells. *Appl. Phys. Lett.* **93,** 191113 (2008).
5. Bingham, J. M., Anker, J. N. & Kreno, L. E. Gas sensing with high-resolution localized surface plasmon resonance spectroscopy. *J. Am. Chem. Soc.* **132,** 17358–17359 (2010).
6. Anker, J. N. *et al.* Biosensing with plasmonic nanosensors. *Nature Mater.* **7,** 442–453 (2008).
7. Stiles, P. L., Dieringer, J. A., Shah, N. C. & Van Duyne, R. P. Surface-enhanced Raman spectroscopy. *Ann. Rev. Anal. Chem.* **1,** 601–626 (2008).
8. Jeanmaire, D. L. & Van Duyne, R. P. Surface Raman spectroelectrochemistry. Part I. Heterocyclic, aromatic, and aliphatic amines adsorbed on the anodized silver electrode. *J. Electroanal. Chem. Interf. Electrochem.* **84,** 1–20 (1977).
9. Larsson, E. M., Langhammer, C., Zorić, I. & Kasemo, B. Nanoplasmonic probes of catalytic reactions. *Science* **326,** 1091–1094 (2009).
10. Liu, N., Tang, M. L., Hentschel, M., Giessen, H. & Alivisatos, A. P. Nanoantenna-enhanced gas sensing in a single tailored nanofocus. *Nature Mater.* **10,** 631–636 (2011).
11. Novo, C., Funston, A. M. & Mulvaney, P. Direct observation of chemical reactions on single gold nanocrystals using surface plasmon spectroscopy. *Nature Nanotechnol.* **3,** 598–602 (2008).
12. Link, S. & El-Sayed, M. A. Spectral properties and relaxation dynamics of surface plasmon electronic oscillations in gold and silver nanodots and nanorods. *J. Phys. Chem. B* **103,** 8410–8426 (1999).
13. Bohren, C. F. & Huffman, D. R. *Absorption and Scattering of Light by Small Particles* (Wiley, 1983).
14. Kreibig, U. & Vollmer, M. *Optical Properties of Metal Clusters* (Springer, 1995).
15. Kreibig, U. & Genzel, L. Optical absorption of small metallic particles. *Surf. Sci.* **156,** 678–700 (1985).
16. Genzel, L., Martin, T. P. & Kreibig, U. Dielectric function and plasma resonances of small metal particles. *Z. Phys. B* **21,** 339–346 (1975).
17. Peng, S., McMahon, J. M., Schatz, G. C., Gray, S. K. & Sun, Y. Reversing the size-dependence of surface plasmon resonances. *Proc. Natl Acad. Sci. USA* **107,** 14530–14534 (2010).
18. Lindfors, K., Kalkbrenner, T., Stoller, P. & Sandoghdar, V. Detection and spectroscopy of gold nanoparticles using supercontinuum white light confocal microscopy. *Phys. Rev. Lett.* **93,** 037401 (2004).
19. Berciaud, S., Cognet, L., Tamarat, P. & Lounis, B. Observation of intrinsic size effects in the optical response of individual gold nanoparticles. *Nano Lett.* **5,** 515–518 (2005).
20. Bakr, O. M. *et al.* Silver nanoparticles with broad multiband linear optical absorption. *Angew. Chem.* **48,** 5921–5926 (2009).
21. Zhu, M., Aikens, C. M., Hollander, F. J., Schatz, G. C. & Jin, R. Correlating the crystal structure of a thiol-protected Au25 cluster and optical properties. *J. Am. Chem. Soc.* **130,** 5883–5885 (2008).
22. Snoll, D. S. & Steckel, J. A. *Density Functional Theory: A Practical Introduction* (Wiley-Interscience, 2009).
23. Cognet, L. *et al.* Single metallic nanoparticle imaging for protein detection in cells. *Proc. Natl Acad. Sci. USA* **100,** 11350–11355 (2003).
24. Hu, M. *et al.* Gold nanostructures: engineering their plasmonic properties for biomedical applications. *Chem. Soc. Rev.* **35,** 1084–1094 (2006).
25. Jain, P. K., Huang, X., El-Sayed, I. H. & El-Sayed, M. A. Noble metals on the nanoscale: optical and photothermal properties and some applications in imaging, sensing, biology, and medicine. *Acc. Chem. Res.* **41,** 1578–1586 (2008).
26. Sperling, R. A., Gil, P. R., Zhang, F., Zanella, M. & Parak, W. J. Biological applications of gold nanoparticles. *Chem. Soc. Rev.* **37,** 1896–1908 (2008).
27. Templeton, A. C., Pietron, J. J., Murray, R. W. & Mulvaney, P. Solvent refractive index and core charge influences on the surface plasmon absorbance of alkanethiolate monolayer-protected gold clusters. *J. Phys. Chem. B* **104,** 564–570 (2000).
28. Hirakawa, T. & Kamat, P. V. Charge separation and catalytic activity of Ag@TiO2 core-shell composite clusters under UV-irradiation. *J. Am. Chem. Soc.* **127,** 3928–3934 (2005).
29. Akimov, A. V. *et al.* Generation of single optical plasmons in metallic nanowires coupled to quantum dots. *Nature* **450,** 402–406 (2007).
30. Ouyang, F., Batson, P. E. & Isaacson, M. Quantum size effects in the surface-plasmon excitation of small metallic particles by electron-energy-loss spectroscopy. *Phys. Rev. B* **46,** 15421–15425 (1992).
31. Koh, A. L. *et al.* Electron energy-loss spectroscopy (EELS) of surface plasmons in single silver nanoparticles and dimers: influence of beam damage and mapping of dark modes. *ACS Nano* **3,** 3015–3022 (2009).
32. Nelayah, J. *et al.* Mapping surface plasmons on a single metallic nanoparticle. *Nature Phys.* **3,** 348–353 (2007).
33. Solomon, S. D. *et al.* Synthesis and study of silver nanoparticles. *J. Chem. Educ.* **84,** 322–325 (2007).
34. Ritchie, R. H. Plasma losses by fast electrons in thin films. *Phys. Rev.* **106,** 874–881 (1957).
35. Ferrell, T. L. & Echenique, P. M. Generation of surface excitations on dielectric spheres by an external electron beam. *Phys. Rev. Lett.* **55,** 1526–1529 (1985).
36. García de Abajo, F. J. Optical excitations in electron microscopy. *Rev. Mod. Phys.* **82,** 209–275 (2010).
37. Egerton, R. F. Electron energy-loss spectroscopy in the TEM. *Rep. Prog. Phys.* **72,** 016502 (2009).
38. Gloter, A., Douiri, A., Tence, M. & Colliex, C. Improving energy resolution of EELS spectra: an alternative to the monochromator solution. *Ultramicroscopy* **96,** 385–400 (2003).
39. He, Y. & Zeng, T. First-principles study and model of dielectric functions of silver nanoparticles. *J. Phys. Chem. C* **114,** 18023–18030 (2010).
40. García de Abajo, F. J. Nonlocal effects in the plasmons of strongly interacting nanoparticles, dimers, and waveguides. *J. Phys. Chem. C* **112,** 17983–17987 (2008).
41. McMahon, J. M., Gray, S. K. & Schatz, G. C. Nonlocal optical response of metal nanostructures with arbitrary shape. *Phys. Rev. Lett.* **103,** 097403 (2009).
42. David, C. & García de Abajo, F. J. Spatial nonlocality in the optical response of metal nanoparticles. *J. Phys. Chem. C* **115,** 19470–19475 (2011).
43. Mie, G. Beiträge zur optik trüber medien, speziell kolloidaler metallösungen. *Ann. Phys.* **330,** 377–445 (1908).
44. Johnson, P. B. & Christy, R. W. Optical constants of the noble metals. *Phys. Rev. B* **6,** 4370–4379 (1972).
45. Kreibig, U. & Fragstein, C. V. The limitation of electron mean free path in small silver particles. *Z. Phys.* **224,** 307–323 (1969).
46. Alvarez, M. M. *et al.* Optical absorption spectra of nanocrystal gold molecules. *J. Phys. Chem. B* **101,** 3706–3712 (1997).
47. Hövel, H., Fritz, S., Hilger, A., Kreibig, U. & Vollmer, M. Width of cluster plasmon resonances: bulk dielectric functions and chemical interface damping. *Phys. Rev. B* **48,** 18178–18188 (1993).
48. Kraus, W. A. & Schatz, G. C. Plasmon resonance broadening in small metal particles. *J. Chem. Phys.* **79,** 6130–6139 (1983).
49. Palik, E. D. *Handbook of Optical Constants of Solids* (Elsevier, 1998).
50. Luther, J. M., Jain, P. K., Ewers, T. & Alivisatos, A. P. Localized surface plasmon resonances arising from free carriers in doped quantum dots. *Nature Mater.* **10,** 361–366 (2011).


**Supplementary Information** is linked to the online version of the paper at www.nature.com/nature.

**Acknowledgements** We thank S. Sheikholeslami, A. Atre, A. García-Etxarri and A. Baldi for discussions. This research was supported by the National Science Foundation Graduate Research Fellowship Program. J.A.D. acknowledges support from a Stanford Terman Fellowship and a Robert N. Noyce Family Faculty Fellowship.

**Author Contributions** J.A.S. performed the experiment, analysed the data, and developed the model. A.L.K. provided substantial assistance with the STEM EELS procedure. J.A.D. guided and supervised the experiments and analysis. All authors contributed to writing and editing the manuscript.

**Author Information** Reprints and permissions information is available at www.nature.com/reprints. The authors declare no competing financial interests. Readers are welcome to comment on the online version of this article at www.nature.com/nature. Correspondence and requests for materials should be addressed to J.A.D. (jdionne@stanford.edu) or J.A.S. (jscholl@stanford.edu).

ARTICLE

doi:10.1038/nature10892

# Suppression of the antiviral response by an influenza histone mimic

Ivan Marazzi[1], Jessica S. Y. Ho[1], Jaehoon Kim[2], Balaji Manicassamy[3,4], Scott Dewell[5], Randy A. Albrecht[3,4], Chris W. Seibert[3], Uwe Schaefer[1], Kate L. Jeffrey[1], Rab K. Prinjha[6], Kevin Lee[6], Adolfo García-Sastre[3,4,7], Robert G. Roeder[2] & Alexander Tarakhovsky[1]

**Viral infection is commonly associated with virus-driven hijacking of host proteins. Here we describe a novel mechanism by which influenza virus affects host cells through the interaction of influenza non-structural protein 1 (NS1) with the infected cell epigenome. We show that the NS1 protein of influenza A H3N2 subtype possesses a histone-like sequence (histone mimic) that is used by the virus to target the human PAF1 transcription elongation complex (hPAF1C). We demonstrate that binding of NS1 to hPAF1C depends on the NS1 histone mimic and results in suppression of hPAF1C-mediated transcriptional elongation. Furthermore, human PAF1 has a crucial role in the antiviral response. Loss of hPAF1C binding by NS1 attenuates influenza infection, whereas hPAF1C deficiency reduces antiviral gene expression and renders cells more susceptible to viruses. We propose that the histone mimic in NS1 enables the influenza virus to affect inducible gene expression selectively, thus contributing to suppression of the antiviral response.**

Histones are essential regulators of genome function in eukaryotic cells[1,2]. The amino-terminal domain of histones (the histone tail) provides a scaffold for the assembly of protein complexes controlling gene activity[3]. This role of a histone tail is achieved largely by post-translational histone modifications, catalysed by distinct modifying enzymes[4]. The combination of diversely modified histone tails establishes gene-region-specific patterns that, upon recognition by histone-binding proteins, contribute to the regulation of gene replication[5], repair[6] and transcription[7].

The ability of histone tails to guide gene function indicates the possibility of targeted control of gene expression by artificial or naturally occurring molecules that can structurally and/or functionally mimic the histone tail. The former possibility has been demonstrated by studies that show the ability of synthetic compounds to interfere with inducible gene expression by abolishing the interaction between the acetylated histone H4 and the BET family of transcriptional regulators[8,9]. Histone binding to transcriptional regulators could also be interrupted by exogenous cell-permeable histone peptides[10,11]. This approach underscores the possibility of a competition between endogenous and exogenous histone tails for the common binding partners. Indeed, the histone H3 tail-like sequence (histone mimic) within histone methyltransferase G9a can compete, in a modification-dependent fashion, for binding to the histone-bound heterochromatin protein 1 (HP1)[12]. Overall, the 3–5-amino-acid-long sequences that match various parts of the histone tail can be found in numerous eukaryotic and prokaryotic proteins; however, the role of these presumptive histone mimics in the regulation of gene activity remains unknown.

## Influenza virus NS1 carries a histone H3-like sequence

Pathogens have a known ability to interfere with vital processes in the host cells by mimicking regulatory components of host protein networks[13]. In searching for naturally occurring histone mimics with a gene regulatory capability, we screened *in silico* for pathogen-derived proteins that have a known or predicted capacity to accumulate within the nuclei of infected cells, and bear a histone-tail-like unstructured domain at the amino or carboxy termini. One of these proteins was found to be the influenza A virus NS1 protein that suppresses host response to influenza virus[14].

Depending on the viral subtype, NS1 is a 219–237-amino-acid-long protein[14]. NS1 is not essential for formation of the viral particle but is critical for counteracting the antiviral cell response[14,15]. In the absence of NS1, influenza is greatly attenuated[15]. Suppression of antiviral host response by NS1 relies partly on the ability of NS1 to interfere with cytosolic signalling processes that regulate the expression of type I interferon genes[16–19]. Additionally, the NS1 protein can affect host gene expression by interfering with RNA splicing and messenger RNA export[20–23].

We found that NS1 of influenza A (H3N2) virus carries a sequence that resembles the histone H3 tail. Similar to the histone tail, the C terminus of NS1 comprises a non-structured and potentially highly interactive domain[24,25] (Fig. 1a). Although this unstructured C-terminal domain is present in most of the human influenza A variants (Fig. 1a), only NS1 from H3N2 subtype (hereafter defined as NS1) possesses the ARSK sequence (amino acids 226–229) that is chemically analogous to the $^{1}$ARTK[4] sequence that comprises the lysine 4 site (H3K4) of histone H3 (Fig. 1a). The similarity between histone H3 and NS1 tails is further strengthened by the ability of the NS1 tail to serve as a substrate for histone-modifying enzymes *in vitro*. Incubation of the NS1 tail peptide with lysine methyltransferase Set1 complex or Set7/9 in the presence of *S*-adenosylmethionine resulted in incorporation of the methyl mark into the peptide (Fig. 1b, upper panel). Accordingly, substitution of lysine 229 to arginine (K229R) prevented methylation. These results, as well as the ability of histone acetyltransferase TIP60—which acetylates histone H3 lysine 4 in yeast[26]—to acetylate the NS1 peptide at K229 (Fig. 1b, upper panel), support the histone mimicry by NS1. The ability of the H3K4-like sequence within the NS1 tail to serve as a substrate

[1]Laboratory of Immune Cell Epigenetics and Signaling, The Rockefeller University, 1230 York Avenue, New York, New York 10065, USA. [2]Laboratory of Biochemistry and Molecular Biology, The Rockefeller University, 1230 York Avenue, New York, New York 10065, USA. [3]Department of Microbiology, Mount Sinai School of Medicine, One Gustave L. Levy Place, Box 1124, New York, New York 10029, USA. [4]Global Health and Infectious Pathogens Institute, Mount Sinai School of Medicine, One Gustave L. Levy Place, Box 1124, New York, New York 10029, USA. [5]Genomics Resource Center, The Rockefeller University, 1230 York Avenue, New York, New York 10065, USA. [6]Epinova DPU, Immuno-Inflammation Centre of Excellence for Drug Discovery, GlaxoSmithKline, Medicines Research Centre, Gunnels Wood Road, Stevenage SG1 2NY, UK. [7]Department of Medicine, Division of Infectious Diseases, Mount Sinai School of Medicine, One Gustave L. Levy Place, Box 1124, New York, New York 10029, USA.

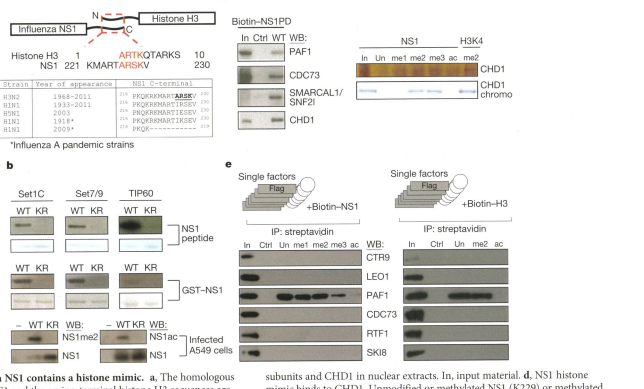


**Figure 1 | Influenza NS1 contains a histone mimic. a**, The homologous carboxy-terminal NS1 and the amino-terminal histone H3 sequences are shown (red letters). The table displays C-terminal NS1 sequences of the influenza A subtypes. **b**, Methylation or acetylation of the NS1 peptide (top panel), the GST–NS1 protein (middle panel) or of the viral NS1 in A549 infected cells (bottom panel) are shown. KR, NS1 substrates where K229 is replaced by arginine. **c**, Association of the NS1 histone mimic with the hPAF1C subunits and CHD1 in nuclear extracts. In, input material. **d**, NS1 histone mimic binds to CHD1. Unmodified or methylated NS1 (K229) or methylated H3 (K4) peptides were incubated with the recombinant CHD1 or the CHD1 double-chromodomain. Binding to NS1 was revealed by silver or Coomassie staining (top and bottom panel, respectively). **e**, Binding of Flag-tagged hPAF1C subunits to NS1 or histone H3 peptides was assessed by western blotting (left and right panels, respectively). IP, immunoprecipitation.

for chosen histone-modifying enzymes has been further confirmed by using recombinant GST fusion NS1 protein (Fig. 1b, middle panel). Finally, the H3K4-like site within NS1 could be methylated or acetylated in virally infected cells. Using a custom-made antibody against dimethylated lysine 229 in NS1 (NS1me2; Supplementary Fig. 1), or acetyl-specific antibody[27], we found the presence of methylated and acetylated NS1 in infected human cells (Fig. 1b, lower panel). Point mutation of the NS1 gene that causes K229R substitution prevented modification (Fig. 1b, lower panel). It is likely that members of the H3K4 methyltransferase and acetyltransferase enzymes, that can modify NS1 *in vitro*, are responsible for NS1 modification *in vivo*. However, in view of the known redundancy between multiple H3K4 modifying complexes[4,28–30], identification of a sole NS1 modifying enzyme seems unlikely.

## NS1 interacts with transcript-elongating proteins

Our experiments show the presence of a histone mimic within the NS1 tail. In histones, the unmodified or modified histone tail contributes to the assembly of chromatin protein complexes[31–33]. The nature of the histone-tail-binding proteins is commonly revealed by the identification of nuclear proteins that bind to immobilized histone peptides during affinity purification[34]. Using this approach (Supplementary Fig. 2), we searched for human nuclear proteins that bind to the NS1 tail peptide (amino acids 220–230). To control for the specificity of binding we used a scrambled peptide with an amino acid composition identical to NS1. Mass-spectrometry analysis of NS1-tail-bound proteins revealed the association of the NS1 tail with polypeptides that belong to the human PAF1 transcription elongation (hPAF1C) and CHD1 chromatin remodelling complexes (Supplementary Fig. 2). Binding of the NS1 tail to human PAF1, parafibromin (CDC73), SNF2l and CHD1 were validated by western blotting (Fig. 1c). In support of the histone mimicry by the NS1 tail, we observed the histone-H3-like pattern of the NS1 tail binding to CHD1 *in vitro*. The chromodomain of human CHD1 binds specifically to di- or trimethylated lysine 4 of histone H3 (ref. 35). Similarly, the full-length CHD1 or the purified double-chromodomain binds selectively to di- or trimethylated NS1 peptide, but not to unmodified or acetylated NS1 tail (Fig. 1d).

To start assessing the role of the NS1 histone mimic in the regulation of chromatin complexes, we focused our attention on hPAF1C. We chose this on the basis of several factors. First, hPAF1C is a potent regulator of RNA elongation[36], a co-transcriptional process that contributes significantly to pathogen-induced gene expression[11,37]. Second, PAF1C has been implicated in the regulation of stress-induced genes in yeast[38] that could be functionally equated to pathogen-induced genes in mammalian cells. Third, opposite to CHD1 that binds to the NS1 tail in a methyl-dependent fashion, purified hPAF1C binds to unmodified as well as modified NS1 tail (Supplementary Fig. 3a, left panel), thus making this interaction potentially more versatile. The interaction of hPAF1C with the NS1 tail is sequence-dependent. Neither NS1 tail of the H5N1 influenza virus, the scrambled NS1 peptide, nor the truncated NS1 tail that lacks the H3K4-like sequence were able to bind to hPAF1C (Supplementary Fig. 3b).

hPAF1C consists of six distinct subunits (PAF1, LEO1, CDC73 (also called parafibromin), SKI8 (also called WDR61), CTR9, RTF1) that have different roles in the interaction between hPAF1C and its binding partners, including RNA polymerase II (RNA Pol II)[36,39,40]. To identify the primary NS1-tail-interacting hPAF1C subunit(s), we tested binding of the NS1 tail to purified recombinant individual hPAF1C subunits. We found that human PAF1 is the primary binder of the unmethylated or methylated NS1 tail, but not the control peptide that lacks the histone mimic (Fig. 1e, left panel). PAF1 does not bind to

acetylated NS1 tail, thus pointing to a possible *in vivo* regulation of NS1 binding to PAF1 by a methyl/acetyl-switch mechanism. Finally, NS1 interacts with PAF1 *in vivo*. Immunoprecipitation of NS1 or PAF1 from infected cell extract revealed the existence of an NS1–PAF1 complex (Supplementary Fig. 3c). Our findings show that direct binding of the NS1 histone mimic to PAF1 is responsible for the association of NS1 with hPAF1C.

Interaction of hPAF1C with the NS1 histone mimic raised the possibility of hPAF1C binding to the histone H3 tail. Although the interaction of hPAF1C with RNA Pol II and other transcriptional regulators is well established[36,39,40], the direct association between hPAF1C and histone H3 has not been documented. We found that unmodified and methylated histone H3 tail peptides, but not the scrambled control peptide, bind to hPAF1C (Supplementary Fig. 3a, right panel) or to purified PAF1 protein (Fig. 1e, right panel). Similar to the NS1 histone mimic, the acetylated histone H3 tail did not bind to either hPAF1C components.

The ability of homologous tails of NS1 and histone H3 to interact directly with hPAF1C indicated a possibility of virus-mediated hijacking of the transcription elongation machinery from the host genes. We found that NS1 accumulates in the nuclei of the infected human cells (Supplementary Fig. 4a), where it reaches approximately $5 \times 10^5$ molecules per nucleus within 12 h after infection (Supplementary Fig. 4b). The salt-extraction profile of NS1 from nuclei of infected cells showed association of NS1 with chromatin (Supplementary Fig. 4c). To assess the position of NS1 on chromatin during viral infection, we generated a recombinant virus (Flag–NS1) that expresses Flag-tagged NS1 protein (Supplementary Fig. 5a, b). Genome-wide analysis of the Flag–NS1 binding at 12 h after infection revealed the presence of NS1 on induced antiviral gene promoters (Supplementary Tables 1 and 2).

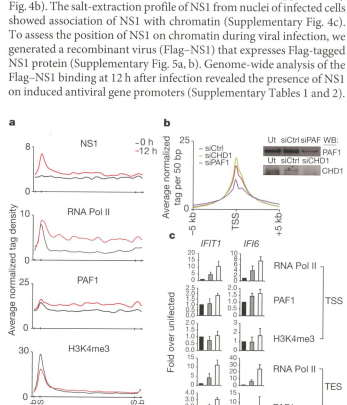


**Figure 2 | Functional interaction between NS1 and PAF1 in infected cells.** **a**, The ChIP-seq profiles show the distribution of indicated proteins at inducible genes before (black line) and after (red line) infection. The induced genes were revealed by RNA-seq and ChIP-seq analysis of infected A549 cells (Supplementary Tables 1 and 2). TSS and TES, the transcriptional start and end sites, respectively. **b**, The NS1 levels at gene promoters in PAF1- or CHD1-deficient cells (blue and green lines, respectively). The scrambled siRNA-treated cells (red line) were used as control. The insert shows knockdown of PAF1 or CHD1 in A549 cells. **c**, PAF1, RNA Pol II and H3K4me3 levels at the TSS and TES of the induced genes in uninfected (ui) cells, cells infected with the wild-type (WT) or PAF1-binding mutant virus (ΔPAF). Data are representative of three independent experiments; error bars show the s.e.m.

In infected cells, NS1 is enriched at promoters characterized by the presence of H3K4me3 and RNA Pol II (Fig. 2a). The pattern of NS1 distribution on its targets parallels the distribution of hPAF1C (Fig. 2a). Collectively, these data revealed a strategic position of NS1 at sites of active antiviral gene transcription.

## NS1 histone mimic controls antiviral gene expression

The interaction between the NS1 tail and hPAF1C has two complementary functions that may support viral infection. The virus probably uses the NS1–hPAF1C interaction to target sites of active transcription. The short interfering RNA (siRNA)-mediated PAF1 deficiency resulted in 30% reduction of NS1 levels at the transcriptional start sites of the NS1-bound genes in infected cells (Fig. 2b). The specific role of PAF1 in recruitment of NS1 was supported by unaltered NS1 binding to its gene targets in cells treated with *CHD1*-specific siRNA (Fig. 2b). These findings revealed a previously unknown ability of the influenza virus to use host PAF1 to position viral NS1 protein at sites of active gene transcription.

Once targeted to transcriptionally active loci, as defined by RNA Pol II levels cross-referenced to the infected cell transcriptome (Supplementary Tables 1 and 2), NS1 interferes with PAF1 and RNA Pol II abundance at target genes. As exemplified by virus-induced *IFIT1* and *IFI6* genes, infection with the wild-type influenza virus resulted in decreased PAF1 and RNA Pol II levels at the transcriptional end sites (TES) and to a lesser extent at the transcriptional start sites (TSS) of the genes, as compared with PAF1-binding mutant virus (ΔPAF) (Fig. 2c). This pattern of PAF1, RNA Pol II and H3K4me3 distribution is indicative of impaired transcriptional elongation.

To determine the impact of the NS1 tail on the dynamics of antiviral gene transcription, we conducted a genome-wide nuclear 'run-on' analysis (global run-on sequencing, GRO-seq)[41] of cells infected with the wild-type or mutant viruses that cannot bind to human PAF1 (ΔPAF). In the absence of infection, we observed accumulation of RNA species that map to the TSS of antiviral genes and low levels of RNAs that map to the gene body (Fig. 3a). Accumulation of TSS-associated short RNAs is a common feature of rapidly inducible genes that maintain a paused/poised state in the absence of an inducer[41].

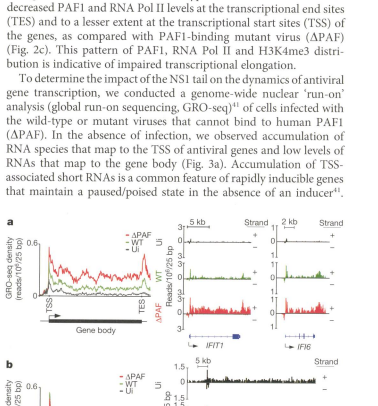


**Figure 3 | NS1 suppresses antiviral gene transcription in infected cells.** **a**, Left: the GRO-seq profile of inducible RNA transcripts in uninfected (ui) A549 cells (black line) or cells infected with wild-type or ΔPAF virus (green and red lines, respectively). Right: GRO-seq profile of *IFIT1* and *IFI6* genes in uninfected and infected cells. **b**, GRO-seq profile of A549-expressed genes that are not affected by virus infection (left panel) or of the *HPRT1* gene (right panel). Reads from either DNA strands are indicated as +/−. The *y* axes display reads per million mapped reads per 25 bp.

Infection with the ΔPAF virus resulted in a marked increase in levels of RNA transcripts that map to the TSS as well as to the downstream gene region. The high abundance of transcripts associated within the gene body is indicative of effective RNA elongation, which has an essential role in regulation of the pathogen-driven host response[11,37]. Compared to cells infected with ΔPAF virus, the cells infected with wild-type virus displayed slightly reduced levels of TSS-associated RNAs but greatly diminished levels of transcripts associated with the gene body and 3′ end region (Fig. 3a). This pattern is indicative of impaired transcriptional elongation and is consistent with defective elongation in other experimental settings[42,43]. The differences between the impact of ΔPAF and wild-type viruses on the global dynamics of antiviral gene transcription are exemplified by differences in transcription of selected antiviral genes (Fig. 3a, right panel). Infection with either wild-type or ΔPAF virus has no effect on transcriptional dynamics of housekeeping genes and genes not affected by viral infection (Fig. 3b).

The ability of NS1 to control directly hPAF1C-dependent transcriptional elongation was further supported by the analysis of the impact of the NS1 tail on hPAF1C-driven RNA elongation *in vitro*. In this assay, a chromatinized DNA template, supplemented with selected transcription factors and histone-modifying enzymes, supports hPAF1C-mediated transcription in a fashion that faithfully reproduces transcriptional elongation *in vivo*[36] (Fig. 4a). We found that NS1 has a negative impact on hPAF1C function (Fig. 4b). The comparison between the amount of *in vitro* synthesized RNA in the absence or presence of hPAF1C shows the ability of hPAF1C to boost RNA synthesis (Fig. 4b). Addition of purified NS1 (Supplementary Fig. 5c) to the transcription reaction reduced the amount of synthesized RNA to background levels (Fig. 4b). Addition of purified NS1 that lacks the PAF1-binding sequence had no effect on RNA synthesis (Fig. 4b). Both wild-type NS1 and NS1 that lacks the PAF1 binding sequence have no impact on transcription of non-chromatinized template *in vitro* (Supplementary Fig. 6). This selective and direct impact of NS1 on virus-induced gene expression has been further supported by a lack of NS1 requirement for the association between the viral and the host RNA polymerases in infected cells[44,45] (Supplementary Fig. 7).

Our findings provide unambiguous proof for the ability of the NS1 tail to interfere directly with hPAF1C-driven transcription of antiviral genes.

## hPAF1C controls antiviral gene expression and infection

The significance of NS1–hPAF1C interaction during infection was evaluated by two independent experimental approaches. Deletion of the hPAF1C binding sequence in NS1 resulted in reduced viral titres of the ΔPAF virus as compared to those of the virus carrying full-length NS1 (Supplementary Fig. 8). This finding is in agreement with the previously reported positive role of the NS1 carboxy terminus in influenza A virulence[46].

We also revealed the central role of hPAF1C in transcriptional response induced by various viruses, as well as by the viral RNA analogue poly(I:C) and type I interferon. To study the impact of PAF1 on influenza-induced antiviral gene expression we used the NS1-deficient influenza virus (PR8/ΔNS1) that elicits an extremely potent antiviral response and is therefore particularly useful to study host factors that regulate the antiviral response[14,15]. Infection with PR8/ΔNS1 of control siRNA-treated cells resulted in a strong upregulation of numerous antiviral genes (Fig. 5a). This response was reduced in PAF1-deficient cells (Fig. 5a, Supplementary Fig. 9, left panel, and Supplementary Table 3). The negative effect of PAF1 deficiency on antiviral response is not a consequence of impaired virus life-cycle caused by a reduction in viral gene expression (Supplementary Fig. 10).

PAF1 deficiency also attenuated the transcriptional response to wild-type influenza A H1N1 (Supplementary Fig. 11, left panel). The general positive role of PAF1 in antiviral gene expression was underscored by reduced expression of antiviral genes in PAF1-deficient cells infected with vesicular stomatitis virus (VSV) as well as cells treated with poly(I:C) (Supplementary Fig. 11 and Supplementary Tables 4–6). PAF1 deficiency also downregulates the transcriptional response to type I interferon that governs the antiviral immunity (Fig. 5b, Supplementary Fig. 9, right panel and Supplementary Table 7). The impaired antiviral response by PAF1-deficient cells contributes to a nearly tenfold increase of NS1-deficient PR8/ΔNS1 virus replication,

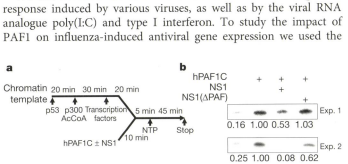


**Figure 4 | NS1 inhibits transcriptional elongation *in vitro*.** **a**, The full-length NS1 protein (NS1) or NS1 lacking the PAF1-binding sequence (NS1(ΔPAF)) (Supplementary Fig. 5c) was added to the RNA elongation reaction as indicated. **b**, The amount of the 390-nt RNA elongation product was quantified by ImageJ. The results of two independent experiments are shown.

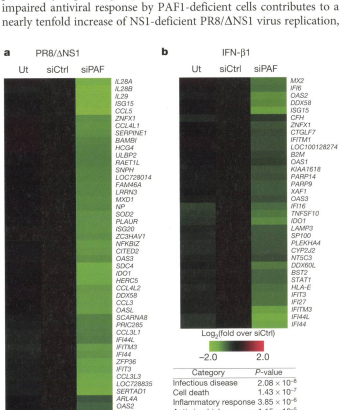


**Figure 5 | PAF1 controls antiviral response.** **a**, **b**, The expression levels of mRNAs in influenza infected (**a**) or IFN-β1-treated (**b**) control (siCtrl) or PAF1-deficient (siPAF) A549 cells. The tables show the siPAF-affected gene categories. Ut, untreated with siRNA. **c**, Dynamics of virus replication in control or PAF1-deficient A549 cells. p.f.u. plaque-forming units. Data are representative of three independent experiments. Error bars show the s.e.m.

as compared to infected control cells (Fig. 5c). The impact of PAF1 deficiency on antiviral gene expression is selective. PAF1 deficiency does not alter the expression of housekeeping genes (Supplementary Fig. 12 and Supplementary Table 8).

## Concluding remarks

We have shown that H3N2 influenza A virus interferes with host gene expression by exploiting the very basic principles of the epigenetic control of gene regulation. By mimicking the histone H3K4 sequence, which has a key role in positive regulation of gene transcription, the influenza virus gains access to histone-interacting transcriptional regulators that govern inducible antiviral gene expression. The histone-like unstructured NS1 tails are present in the majority of human influenza A isolates, but their primary sequence differs between viruses. The presence of potentially reactive amino acid residues within the unstructured NS1 tails and the nuclear localization of NS1 predict a multitude of nuclear proteins interacting with influenza NS1 in a sequence- and/or modification-specific fashion. In extension of the histone code that has provided a conceptual framework for understanding chromatin-based gene regulation[47–49], we propose the existence of the 'NS1 code' that guides influenza virus interference with host chromatin. The interference with chromatin function may complement other immunosuppressive functions of NS1 and provide the influenza virus with an opportunity to affect host gene expression in a highly selective fashion by recognizing and using epigenetic patterns of the host cells. This mechanism may contribute to the influenza-variant-specific pathogenesis and disease progression that differ between viruses carrying the histone-like NS1 tail and those viruses, such as human H1N1 (including pandemic 2009 virus), that lack the NS1 tail[50]. It is possible that by targeting the actively transcribed antiviral genes, the NS1 tail helps influenza to balance its virulence against the preservation of the infected cell function. Such a mechanism could help the virus to maintain its long-term presence within the human population. Our findings could also be applied to the development of novel anti-influenza therapies that will interfere in a highly selective fashion with the NS1 tail binding to its chromatin partners. Finally, identification of hPAF1C as a key mediator of antiviral and pro-inflammatory gene response may pave the way for the development of anti-inflammatory therapies that—similar to the recently described 'epigenetic' therapies[8,9]—will interfere selectively with hPAF1C binding to its partners.

## METHODS SUMMARY

The methylation and acetylation *in vitro* has been performed as described previously[12,26]. The analysis of NS1 methylation or acetylation *in vivo* has been done by using custom-made methyl-specific or commercial acetyl-specific antibodies[27]. Isolation of the NS1 binding proteins, their analysis by mass-spectrometry and western blotting were performed according to a protocol used to identify histone-bound proteins[34]. The recombinant hPAF1C and its individual components were prepared as described before[46]. Interaction between hPAF1C and its individual components with peptides were performed as reported[32,33]. The transcriptional assays have been performed as described[36]. Genome-wide distribution of NS1 and other chromatin-bound proteins were accessed by ChIP-sequencing as previously described[8], and analysed using standard bioinformatic approaches. Recombinant influenza viruses were generated using standard reverse genetics approaches[13,17]. Infection of cells with viruses was performed according to the standard methods[17,46] and viral titres were quantified by plaque assay. Gene expression analysis has been done by microarray using Illumina Human HT-12 v4 Expression BeadChips or by RNA-sequencing and verified by quantitative real-time PCR[9]. GRO-sequencing was performed as described[41]. All methodological details are additionally outlined in Supplementary Information.

**Received 7 September 2011; accepted 23 January 2012.**
**Published online 14 March 2012.**

1. Kornberg, R. D. & Thomas, J. O. Chromatin structure—oligomers of histones. *Science* **184,** 865–868 (1974).
2. Campos, E. I. & Reinberg, D. Histones: annotating chromatin. *Ann. Rev. Genet.* **43,** 559–599 (2009).
3. Taverna, S. D., Li, H., Ruthenburg, A. J., Allis, C. D. & Patel, D. J. How chromatin-binding modules interpret histone modifications: lessons from professional pocket pickers. *Nature Struct. Mol. Biol.* **14,** 1025–1040 (2007).
4. Kouzarides, T. Chromatin modifications and their function. *Cell* **128,** 693–705 (2007).
5. Kelly, A. E. *et al.* Survivin reads phosphorylated histone H3 threonine 3 to activate the mitotic kinase Aurora B. *Science* **330,** 235–239 (2010).
6. Fernandez-Capetillo, O. *et al.* DNA damage-induced G2-M checkpoint activation by histone H2AX and 53BP1. *Nature Cell Biol.* **4,** 993–997 (2002).
7. Li, B., Carey, M. & Workman, J. L. The role of chromatin during transcription. *Cell* **128,** 707–719 (2007).
8. Filippakopoulos, P. *et al.* Selective inhibition of BET bromodomains. *Nature* **468,** 1067–1073 (2010).
9. Nicodeme, E. *et al.* Suppression of inflammation by a synthetic histone mimic. *Nature* **468,** 1119–1123 (2010).
10. Nishiyama, A. *et al.* Intracellular delivery of acetyl-histone peptides inhibits native bromodomain-chromatin interactions and impairs mitotic progression. *Febs Lett.* **582,** 1501–1507 (2008).
11. Hargreaves, D. C., Horng, T. & Medzhitov, R. Control of inducible gene expression by signal-dependent transcriptional elongation. *Cell* **138,** 129–145 (2009).
12. Sampath, S. C. *et al.* Methylation of a histone mimic within the histone methyltransferase G9a regulates protein complex assembly. *Mol. Cell* **27,** 596–608 (2007).
13. Elde, N. C. & Malik, H. S. The evolutionary conundrum of pathogen mimicry. *Nature Rev. Microbiol.* **7,** 787–797 (2009).
14. Hale, B. G., Randall, R. E., Ortin, J. & Jackson, D. The multifunctional NS1 protein of influenza A viruses. *J. Gen. Virol.* **89,** 2359–2376 (2008).
15. Garcia-Sastre, A. *et al.* Influenza A virus lacking the NS1 gene replicates in interferon-deficient systems. *Virology* **252,** 324–330 (1998).
16. Lu, Y., Wambach, M., Katze, M. G. & Krug, R. M. Binding of the influenza virus NS1 protein to double-stranded-RNA inhibits the activation of the protein-kinase that phosphorylates the Elf-2 translation initiation-factor. *Virology* **214,** 222–228 (1995).
17. Gack, M. U. *et al.* Influenza A Virus NS1 targets the ubiquitin ligase TRIM25 to evade recognition by the host viral RNA sensor RIG-I. *Cell Host Microbe* **5,** 439–449 (2009).
18. Pichlmair, A. *et al.* RIG-I-mediated antiviral responses to single-stranded RNA bearing 5′-phosphates. *Science* **314,** 997–1001 (2006).
19. Hale, B. G., Jackson, D., Chen, Y. H., Lamb, R. A. & Randall, R. E. Influenza A virus NS1 protein binds p85b and activates phosphatidylinositol-3-kinase signaling. *Proc. Natl Acad. Sci. USA* **103,** 14194–14199 (2006).
20. Krug, R. M., Yuan, W. M., Noah, D. L. & Latham, A. G. Intracellular warfare between human influenza viruses and human cells: the roles of the viral NS1 protein. *Virology* **309,** 181–189 (2003).
21. Nemeroff, M. E., Barabino, S. M. L., Li, Y. Z., Keller, W. & Krug, R. M. Influenza virus NS1 protein interacts with the cellular 30 kDa subunit of CPSF and inhibits 3′ end formation of cellular pre-mRNAs. *Mol. Cell* **1,** 991–1000 (1998).
22. Das, K. *et al.* Structural basis for suppression of a host antiviral response by influenza A virus. *Proc. Natl Acad. Sci. USA* **105,** 13093–13098 (2008).
23. Satterly, N. *et al.* Influenza virus targets the mRNA export machinery and the nuclear pore complex. *Proc. Natl Acad. Sci. USA* **104,** 1853–1858 (2007).
24. Luger, K., Mader, A. W., Richmond, R. K., Sargent, D. F. & Richmond, T. J. Crystal structure of the nucleosome core particle at 2.8 A resolution. *Nature* **389,** 251–260 (1997).
25. Hale, B. G., Barclay, W. S., Randall, R. E. & Russell, R. J. Structure of an avian influenza A virus NS1 protein effector domain. *Virology* **378,** 1–5 (2008).
26. Xhemalce, B. & Kouzarides, T. A chromodomain switch mediated by histone H3 Lys 4 acetylation regulates heterochromatin assembly. *Genes Dev.* **24,** 647–652 (2010).
27. Becker, P. B. *et al.* Site-specific acetylation of ISWI by GCN5. *BMC Mol. Biol.* **8** (2007).
28. Ruthenburg, A. J., Allis, C. D. & Wysocka, J. Methylation of lysine 4 on histone H3: Intricacy of writing and reading a single epigenetic mark. *Mol. Cell* **25,** 15–30 (2007).
29. Wang, P. F. *et al.* Global analysis of H3K4 methylation defines MLL family member targets and points to a role for MLL1-mediated H3K4 methylation in the regulation of transcriptional initiation by RNA polymerase II. *Mol. Cell. Biol.* **29,** 6074–6085 (2009).
30. Guillemette, B. *et al.* H3 lysine 4 is acetylated at active gene promoters and is regulated by H3 lysine 4 methylation. *PLoS Genet.* **7** (2011).
31. Lachner, M., O'Carroll, N., Rea, S., Mechtler, K. & Jenuwein, T. Methylation of histone H3 lysine 9 creates a binding site for HP1 proteins. *Nature* **410,** 116–120 (2001).
32. Shi, X. B. *et al.* ING2 PHD domain links histone H3 lysine 4 methylation to active gene repression. *Nature* **442,** 96–99 (2006).
33. Lan, F. *et al.* Recognition of unmethylated histone H3 lysine 4 links BHC80 to LSD1-mediated gene repression. *Nature* **448,** 718–722 (2007).
34. Wysocka, J. Identifying novel proteins recognizing histone modifications using peptide pull-down assay. *Methods* **40,** 339–343 (2006).
35. Sims, R. J. *et al.* Human but not yeast CHD1 binds directly and selectively to histone H3 methylated at lysine 4 via its tandem chromodomains. *J. Biol. Chem.* **280,** 41789–41792 (2005).
36. Kim, J., Guermah, M. & Roeder, R. G. The human PAF1 complex acts in chromatin transcription elongation both independently and cooperatively with SII/TFIIS. *Cell* **140,** 491–503 (2010).
37. Ramirez-Carrozzi, V. R. *et al.* A unifying model for the selective regulation of inducible transcription by CpG islands and nucleosome remodeling. *Cell* **138,** 114–128 (2009).

38. Kim, K. Y. & Levin, D. E. Mpk1 MAPK association with the Paf1 complex blocks Sen1-mediated premature transcription termination. *Cell* **144,** 745–756 (2011).
39. Chen, Y. X. *et al.* DSIF, the Paf1 complex, and Tat-SF1 have nonredundant, cooperative roles in RNA polymerase II elongation. *Genes Dev.* **23,** 2765–2777 (2009).
40. Jaehning, J. A. The Paf1 complex: platform or player in RNA polymerase II transcription? *Biochim. Bioiphys. Acta* **1799,** 379–388 (2010).
41. Core, L. J., Waterfall, J. J. & Lis, J. T. Nascent RNA sequencing reveals widespread pausing and divergent initiation at human promoters. *Science* **322,** 1845–1848 (2008).
42. Min, I. M. *et al.* Regulating RNA polymerase pausing and transcription elongation in embryonic stem cells. *Gene Dev.* **25,** 742–754 (2011).
43. Mapendano, C. K., Lykke-Andersen, S., Kjems, J., Bertrand, E. & Jensen, T. H. Crosstalk between mRNA 3′ end processing and transcription initiation. *Mol. Cell* **40,** 410–422 (2010).
44. Loucaides, E. M. *et al.* Nuclear dynamics of influenza A virus ribonucleoproteins revealed by live-cell imaging studies. *Virology* **394,** 154–163 (2009).
45. Engelhardt, O. G., Smith, M. & Fodor, E. Association of the influenza a virus RNA-dependent RNA polymerase with cellular RNA polymerase II. *J. Virol.* **79,** 5812–5818 (2005).
46. Jackson, D., Hossain, M. J., Hickman, D., Perez, D. R. & Lamb, R. A. A new influenza virus virulence determinant: The NS1 protein four C-terminal residues modulate pathogenicity. *Proc. Natl Acad. Sci. USA* **105,** 4381–4386 (2008).
47. Strahl, B. D. & Allis, C. D. The language of covalent histone modifications. *Nature* **403,** 41–45 (2000).
48. Turner, B. M. Histone acetylation and an epigenetic code. *Bioessays* **22,** 836–845 (2000).
49. Jenuwein, T. & Allis, C. D. Translating the histone code. *Science* **293,** 1074–1080 (2001).
50. Yang, Y. *et al.* The transmissibility and control of pandemic influenza A (H1N1) virus. *Science* **326,** 729–733 (2009).

**Supplementary Information** is linked to the online version of the paper at www.nature.com/nature.

**Acknowledgements** We thank P. deGross and A. Rudensky for the mass spectroscopy analysis of the NS1 binding proteins. A. Rojas Soto, D. Reinberg, M. Dobenecker and T. Zhanyun provided us with recombinant CHD1 (A.R.S., D.R.), recombinant Set7/9 (M.D.) and Set1C (T.Z.). F. Casadio, P. Lewis, O. Binda, O. Gozani, N. Levenkova, A. Mele, R. Darnell, L. Core, J. Lis and P. Palese gave us valuable technical advice and help with data analysis. We acknowledge the Rockefeller University Genomics Resource Center for technical support. We thank R. Cadagan, A. Santana, W. Huang, R. Chandramouli and H. Zebronsky for technical assistance, R. Rizzo for help with manuscript preparation and C. Nathan for discussion. L.M.K. for artwork. B.M is supported by NIH/NIAID K99 Pathway to Independence award (1K99AI095320-01). A.G.-S. is partially supported by NIAID grants R01AI046954, U19AI083025 and by CRIP (Center for Research in Influenza Pathogenesis), an NIAID funded Center of Excellence for Influenza Research and Surveillance, HHSN266200700010C. R.G.R. is supported by NIH grant CA129325. J.K. is supported by Charles H. Revson Foundation. I.M. is supported by American Italian Cancer Foundation. J.H. is supported by the Agency for Science, Technology and Research (A*STAR), Singapore. A.T. is supported by the NIH grant R01AI068058 and by Starr Cancer Consortium.

**Author Contributions** I.M. contributed to design, execution, analysis of the experiments and manuscript preparation. J.S.Y.H. studied the role of PAF1 in viral infection and assisted in manuscript preparation. J.K. and R.R. studied the impact of NS1 on hPAF1C and transcriptional elongation. B.M., R.A.A. engineered the recombinant influenza viruses and studied viral infectivity. U.S. was involved in gene expression studies. S.D. performed bioinformatic analysis. C.W.S. generated antibody against viral polymerase. K.L.J. gave technical assistance. R.K.P. and K.L. contributed to manuscript preparation and enabled ChIP-seq and RNA-seq. A.G.-S. supervised and discussed the work with infectious influenza viruses. A.T. conceived and supervised this study and wrote the final manuscript.

**Author Information** Reprints and permissions information is available at www.nature.com/reprints. The authors declare competing financial interests: details accompany the full-text HTML version of the paper at www.nature.com/nature. Readers are welcome to comment on the online version of this article at www.nature.com/nature. Correspondence and requests for materials should be addressed to I.M. (imarazzi@rockefeller.edu) or A.T. (tarakho@rockefeller.edu).

ARTICLE

doi:10.1038/nature10895

# Intrinsic coupling of lagging-strand synthesis to chromatin assembly

Duncan J. Smith[1] & Iestyn Whitehouse[1]

**Fifty per cent of the genome is discontinuously replicated on the lagging strand as Okazaki fragments. Eukaryotic Okazaki fragments remain poorly characterized and, because nucleosomes are rapidly deposited on nascent DNA, Okazaki fragment processing and nucleosome assembly potentially affect one another. Here we show that ligation-competent Okazaki fragments in *Saccharomyces cerevisiae* are sized according to the nucleosome repeat. Using deep sequencing, we demonstrate that ligation junctions preferentially occur near nucleosome midpoints rather than in internucleosomal linker regions. Disrupting chromatin assembly or lagging-strand polymerase processivity affects both the size and the distribution of Okazaki fragments, suggesting a role for nascent chromatin, assembled immediately after the passage of the replication fork, in the termination of Okazaki fragment synthesis. Our studies represent the first high-resolution analysis—to our knowledge—of eukaryotic Okazaki fragments *in vivo*, and reveal the interconnection between lagging-strand synthesis and chromatin assembly.**

During eukaryotic chromosome replication, both genetic and epigenetic information must be accurately duplicated. For chromatin architecture and modifications to be truly epigenetic—that is, heritable despite not being genetically encoded—complete disruption and dissociation of nucleosomes from the replication fork must be prevented to allow the rapid re-deposition of precisely located and appropriately modified histones on the nascent DNA. Histone chaperone complexes govern both nucleosome disassembly and assembly at the replication fork[1].

DNA replication is inherently asymmetric. Okazaki fragment synthesis on the lagging strand necessitates the repeated production of single-stranded DNA and polymerization in the opposite direction to fork progression. Given the delay in lagging-strand synthesis and the rapidity of histone deposition behind the replication fork[2], these two processes may be interlinked. A coordinated series of events occurs each time an Okazaki fragment is synthesized[3]. Each fragment is initiated via an RNA primer[4] and up to 30 nucleotides of DNA, both synthesized by DNA polymerase α (Pol α)-primase[5]; subsequently, the clamp loading factor RFC mediates the replacement of Pol α by the sliding clamp PCNA and the processive polymerase Pol δ (ref. 6). Pol δ extends the nascent DNA chain through the 5′ end of the preceding Okazaki fragment[7,8]; this strand-displacement synthesis generates a 5′ RNA or DNA flap that is cleaved by nucleases such as the flap endonuclease Fen1 (ref. 9). Repeated cycles of extension and DNA cleavage followed by Pol δ idling[10] produce a nick that migrates away from the replication fork and can be sealed by DNA ligase I[11]. Little to no DNA synthesized by the error-prone Pol α remains in the genome after replication[12], suggesting that strand displacement generally replaces at least 30 nucleotides of DNA, but it remains unclear how the replication machinery coordinates the transition from Pol δ to DNA ligase. Indeed, despite their fundamental importance in replication, comparatively little is known about the *in vivo* properties of eukaryotic Okazaki fragments: although they are widely accepted to be shorter than the 1–2 kilobases (kb) observed in prokaryotes, a clear consensus has not emerged[11,13–15]. Moreover, we have little information about how nucleosome assembly may interact with lagging-strand synthesis. A plausible explanation for the difference in size between eukaryotic and prokaryotic Okazaki fragments is that eukaryotic DNA replication occurs within the context of chromatin.

To investigate the relationship between lagging-strand processing and chromatin assembly, we have developed strategies to analyse Okazaki fragments purified from *S. cerevisiae*. We find that Okazaki fragments are heterogeneously sized with a repeat length corresponding to that of nucleosomes. In addition, we find that ligation junctions occur preferentially around known nucleosome midpoints, and that these relationships can be altered by interfering with chromatin assembly or Pol δ processivity. Our data suggest an integrated model whereby nascent chromatin structure facilitates Okazaki fragment processing, which may provide a means to monitor nucleosome assembly behind the replication fork.

## Nucleosome-sized Okazaki fragments

To enrich for ligation-competent Okazaki fragments, we constructed strains of *S. cerevisiae* in which DNA ligase I[11] (*CDC9*) expression is driven from a doxycycline-repressible promoter and the encoded protein tagged with a temperature-sensitive degron[16]. The inability to ligate Okazaki fragments should result in the accumulation of nicked DNA that, after purification, can be radiolabelled using DNA polymerase and α-$^{32}$P dCTP.Ligase inactivation in an asynchronous culture resulted in the accumulation of short heterogeneous DNA species whose abundance increased with duration of ligase inhibition (Fig. 1a). Notably, these fragments displayed an underlying periodicity reminiscent of the nucleosome repeat. Indeed, comparison of the nicked DNA to a nucleosome ladder indicated that a significant fraction of fragments seem to be sized according to the 165-bp nucleosomal repeat length in *S. cerevisiae* (Fig. 1b).

To clarify that we were observing Okazaki fragments, we confirmed that they did not appear in a G1-arrested culture until S-phase release (Fig. 1c). Additionally, we treated purified DNA with recombinant DNA ligase; this repaired the nicks and severely diminished our ability to label fragments (Fig. 1d), showing that our assay predominantly detects nicked DNA rather than species containing single-stranded gaps or flaps resulting from incomplete Okazaki fragment processing. Unrelated control experiments indicated that a 125-nucleotide species previously reported to be Okazaki fragments[14,17] is 5S ribosomal RNA (Supplementary Fig. 2). Thus, we demonstrate that the mono-, di- and

[1]Molecular Biology Program, Memorial Sloan-Kettering Cancer Center, 1275 York Avenue, New York, New York 10065, USA.

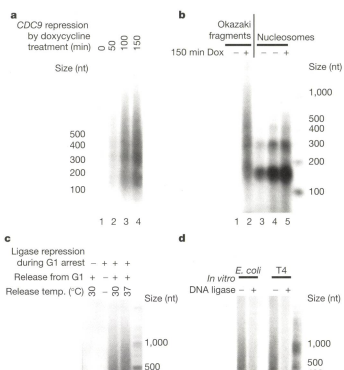


**Figure 1 | DNA ligase I depletion in *S. cerevisiae* leads to the accumulation of Okazaki fragments sized similarly to the nucleosome repeat.** **a**, Transcriptional repression of DNA ligase I (*CDC9*) results in the accumulation of nicked DNA. Cells carrying a doxycycline-repressible allele of the *CDC9* gene were treated with doxycycline (Dox) for the indicated time. Purified genomic DNA was labelled using exonuclease-deficient Klenow fragment and $\alpha$-$^{32}$P dCTP and separated in a denaturing agarose gel. nt, nucleotides. **b**, The size of labelled Okazaki fragments mirrors the nucleosome repeat. Okazaki fragments (lane 2) were labelled as in Fig. 1a; nucleosomes were prepared from wild-type (lane 3) or repressible *CDC9* strains (lanes 4 and 5) by *in vivo* micrococcal nuclease (MNase) digestion. The chromatin digestion patterns in lanes 4 and 5 indicate that *CDC9* repression does not alter global chromatin structure. **c**, Okazaki fragments accumulate during S phase. Cells were arrested in G1 using $\alpha$-factor, during which time *CDC9* transcription was inhibited by the addition of doxycycline, and degradation of the protein stimulated by activation of the degron system using galactose and 37 °C. Okazaki fragments appear upon release of the culture into S phase (lanes 3 and 4). d, Okazaki fragments are bordered by ligatable nicks. Purified DNA was treated (lanes 2 and 4) or mock-treated (lanes 1 and 3) with the indicated ligase, and then labelled as in Fig. 1a. The inability to label fragments after ligase treatment confirms that labelled Okazaki fragments are flanked by ligatable nicks.

trinucleosome-sized fragments observed on ligase inhibition are generated in S phase and bordered by ligatable nicks—the essential properties of ligation-competent Okazaki fragments.

## Global distribution of Okazaki fragments

To explore further the relationship between Okazaki fragments and nucleosomes, we developed a deep sequencing approach to map the strand, position and abundance of fragments across the *S. cerevisiae* genome. To allow yeast to complete S phase in the presence of nicked DNA we inactivated the DNA damage checkpoint by deleting the *RAD9* gene. Additionally, to deplete ligase activity further we deleted the second DNA ligase (*DNL4*). *DNL4* or *RAD9* deletion does not affect Okazaki fragment size (Supplementary Fig. 3). Okazaki fragments were harvested from an asynchronous culture after a ~2.5 h ligase inactivation. Small single-stranded fragments were purified by anion exchange chromatography in alkaline conditions and sequencing primers were ligated directly to each end[18] (Supplementary Fig. 4). Importantly, this method preserves strand identity.

After paired-end deep sequencing, we aligned the data to the *S. cerevisiae* genome and found that use of a single asynchronous culture was sufficient to attain complete coverage (a representative chromosome is shown in Fig. 2a, and a comparison of replicates in Supplementary Fig. 5). Sequencing reads aligning to the Watson or Crick strands showed a complementary distribution with strand bias being particularly pronounced close to replication origins[19]; such asymmetry is expected, given that replication forks proceed bidirectionally from origins (Fig. 2b). The strong strand bias observed around experimentally validated replication origins mapped at high resolution (Fig. 2c)[20] demonstrates preferential sequencing of nascent lagging strands, unequivocally confirming that the DNA species enriched after ligase repression are Okazaki fragments. Detailed analysis of global Okazaki fragment distributions can provide mechanistic insight into replication-fork dynamics (S. McGuffee, D.J.S. and I.W., manuscript in preparation).

## Okazaki fragments terminate within nucleosomes

The periodic size of Okazaki fragments observed in Fig. 1 led us to investigate how the ends of Okazaki fragments relate to nucleosome positions found within the yeast genome. We aligned Okazaki fragment termini to a reference list of all consensus nucleosome midpoints (dyads) in *S. cerevisiae*[21]. Inherent bias towards smaller fragments during purification, library amplification and sequencing result in size distributions that differ substantially between starting material and sequenced fragments (Supplementary Fig. 6); therefore, we randomly selected fragments from our sequencing data to approximate the mononucleosome-sized fragments we detected by electrophoresis (Supplementary Fig. 6). Aligning both the 5′ and 3′ ends of mature (Fig. 3a) mononucleosome-sized fragments against the dyads of

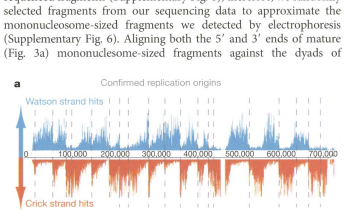


**Figure 2 | Sequenced Okazaki fragments show a pronounced bias towards the lagging strand.** **a**, Distribution of paired-end sequencing hits mapping to either the Watson (blue, above the axis) or Crick (orange, below) strands across *S. cerevisiae* chromosome 10. The locations of replication origins[19] are indicated as grey dashed lines. Data are unsmoothed. **b**, The anticipated distribution of Okazaki fragments surrounding an efficient origin. **c**, Sequenced Okazaki fragments are strongly enriched in regions predicted to be replicated as the lagging strand. $Log_2$ ratio of Watson strand: Crick strand fragments across a 50-kb window around ARS consensus sequences (ACS) confirmed previously[20] to correspond to active origins. Data are smoothed to 200 bp.

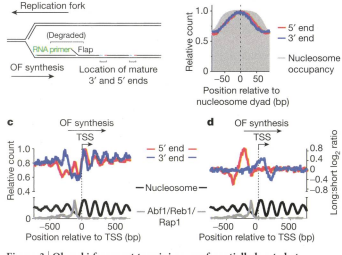


**Figure 3 | Okazaki fragment termini are preferentially located at nucleosome dyads.** **a**, Schematic indicating the mature Okazaki fragment termini sequenced in this study. **b**, Okazaki fragment termini are enriched around nucleosome dyads. The distribution of termini from mononucleosome-sized Okazaki fragments around the top 50% consensus *S. cerevisiae* nucleosome dyad locations[21] is shown. Unless otherwise indicated, all analyses use unsmoothed data normalized to the maximum signal in the analysed range, and area aligned such that Okazaki fragment (OF) synthesis by Pol δ proceeds from left to right. **c**, The distribution of Okazaki fragment termini correlates with nucleosome occupancy[28] around TSSs. Data are aligned to TSSs such that the direction of transcription is from left to right: only Okazaki fragments synthesized in the same direction as transcription are analysed here; equivalent analyses for fragments synthesized in the opposite direction can be found in Supplementary Fig. 7. Data are smoothed to 5 bp. **d**, Okazaki fragments at nucleosome-depleted regions are disproportionately likely to be long. Equal numbers of reads were selected from the top (long), and the bottom three (short) length quartiles of sequenced fragments. The $\log_2$ ratio of long to short fragments is plotted. Data are smoothed to 5 bp.

high-confidence nucleosomes indicated that the highest density of ends occurs at the dyad (Fig. 3b). Alignment of unfiltered data and dinucleosome-sized fragments is comparable to the mononucleosome size-selected subset (Supplementary Fig. 6). Therefore, rather than being overrepresented in the accessible internucleosomal linker DNA, we find that Okazaki fragment termination is most likely to occur at locations corresponding to nucleosome dyads.

## DNA-bound proteins dissociate Pol δ

To confirm that the observed correspondence between nucleosome occupancy and Okazaki fragment end density was not biased by a small subset of nucleosomes, we analysed transcription start sites (TSSs), at which nucleosome positioning follows a well-defined pattern[22]. Alignment of Okazaki fragment termini around ~4,500 TSSs indicated a marked correlation between nucleosome occupancy and the density of Okazaki fragment ends (Fig. 3c and Supplementary Fig. 7) across a broad region surrounding TSSs. Precise nucleosome positioning around TSSs is determined by chromatin remodelling[22,23], allowing us to infer that the correlation refers to remodelled, rather than intrinsically preferred, nucleosome locations.

If the ends of Okazaki fragments are dictated by nucleosomes then nicks should always be in register with positioned nucleosomes, regardless of internucleosomal spacing. Thus, nucleosomes separated by long linker DNA should be associated with longer Okazaki fragments. We took advantage of the differential nucleosome spacing surrounding the nucleosome-depleted region (NDR) at TSSs, comparing the distribution of equal numbers of randomly selected long and short fragments (defined, respectively, as the top quartile of sequenced fragments by length, and the bottom three quartiles). When the ratio of long to short fragments is plotted across this region (Fig. 3d and Supplementary Fig. 7), we find that fragments whose ends map within nucleosomes bordering the NDR are disproportionately long. Thus, Okazaki fragment length reflects nucleosome spacing.

As well as correlating with nucleosome occupancy, Okazaki fragment termini were enriched around known transcription factor binding sites (Fig. 3c)[24,25]. This suggested that, in addition to nucleosomes, sequence-specific DNA binding factors might directly influence the ends of Okazaki fragments. Such correlations would be expected if, following replication-fork passage, some transcription factors rapidly bound to replicated DNA and impeded Pol δ during strand-displacement synthesis, causing the polymerase to dissociate and leave a nick close to the site of collision. Furthermore, this model would also provide an explanation for the observed link between nucleosome occupancy and Okazaki fragment termination: nucleosomes contain numerous weak protein–DNA interactions, whose cumulative strength peaks around the dyad[26]. Polymerases can invade nucleosomes, but experience increasing resistance as they approach the dyad[27,28]. Therefore, if nucleosomes are rapidly re-established on the lagging strand behind the replication fork, and Pol δ invades them during strand-displacement synthesis, the likelihood of polymerase stalling and/or dissociation will increase with proximity to the dyad (see model in Supplementary Fig. 1), producing Okazaki fragments sized according to the nucleosome repeat. Other models that invoke biased Okazaki fragment initiation due to replisome pausing on encountering nucleosomes would produce distinct correlations around NDRs (Supplementary Fig. 8).

If polymerization by Pol δ is inhibited by sequence-specific DNA-bound transcription factors, Okazaki fragment ends should accumulate on the side of the factor that is first encountered by Pol δ. Aligning all transcription factor binding sites[25] indicated a significant enrichment of precisely juxtaposed Okazaki fragment 5′ and 3′ termini around the replication-fork-proximal side of the binding site (Fig. 4a). However, when the Abf1, Reb1 and Rap1 binding sites were considered separately we found that, among transcription factors, these proteins most strongly biased the positioning of Okazaki fragment ends (Fig. 4b, c and Supplementary Fig. 9). Abf1, Reb1 and Rap1 have essential roles in chromatin organization[24,29], and may therefore bind more rapidly and tightly to newly replicated DNA than the majority of transcription factors. We observed a strand-dependent enrichment of Okazaki fragment termini around the 3′ ends of tRNA genes, as well as transcription factor TFIIIB binding sites (Supplementary Fig. 10). Thus, it seems that diverse DNA binding proteins can influence the processing of Okazaki fragments and probably facilitate the dissociation of Pol δ, with tightly bound protein complexes stimulating termination more precisely than those, such as nascent histones, that have more diffuse binding regions.

## Chromatin assembly dictates nick location

Two testable predictions arise from the model that Pol δ dissociates via interaction with nascent nucleosomes: (1) disrupting nucleosome

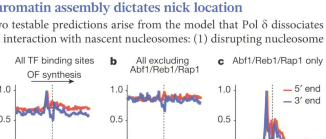


**Figure 4 | Transcription factors with roles in nucleosome positioning stimulate dissociation of Pol δ.** **a**, Okazaki fragment termini are enriched on the replication-fork-proximal side of known transcription factor (TF) binding sites[25]. Mid, midpoint of TF binding site. **b**, **c**, The enrichment of Okazaki fragment termini around transcription factor binding sites can be attributed almost entirely to three factors—Abf1, Reb1 and Rap1—known to have roles in nucleosome positioning.

assembly will impair nucleosome-mediated Okazaki fragment termination and should, therefore, alter the size distribution of the fragments; and (2) reducing Pol δ processivity will result in a shift of Okazaki fragment termination sites away from the dyad, towards the replication-fork-proximal side of nucleosomes.

The deposition of $(H3H4)_2$ tetramers on nascent DNA—the first stage in nucleosome assembly—is mediated in part by CAF-1, a multisubunit histone chaperone complex associated with the replisome via PCNA[30]. We deleted each subunit of CAF-1 individually, and compared the length of Okazaki fragments in the deletion strains to those with wild-type CAF-1 (Fig. 5a). Loss of any CAF-1 subunit abrogated the periodic sizing of Okazaki fragments, significantly increasing their average length. These data are consistent with a global delay in $(H3H4)_2$ deposition following replication, with the resulting paucity of tetrasomes/nucleosomes on the lagging strand leading to increased strand displacement by Pol δ and thus to longer Okazaki fragments.

In *S. cerevisiae*, Pol δ is a heterotrimer whose Pol32 subunit increases processivity and PCNA binding affinity[31]; Pol δ lacking Pol32 shows decreased strand-displacement synthesis *in vitro* and probably *in vivo*[32]. Labelled Okazaki fragments from a *pol32*Δ strain were more heterogeneous but were still generally sized according to the nucleosome repeat (Fig. 5b). When the positions of the 5′ and 3′ termini of mononucleosome-sized fragments (165 ± 15 nucleotides, as per Fig. 3b) from the *pol32*Δ strain were aligned against nucleosome midpoints, a clear shift was observed towards the first edge of the nucleosome encountered by the polymerase (Fig. 5c and Supplementary Fig. 11). Therefore, when Pol δ processivity is perturbed, the polymerase dissociates more rapidly due to an inability to invade nascent nucleosomes assembled on Okazaki fragments. The new maximum end density occurs ~35–40 nucleotides from the dyad, consistent with the extent of DNA protected by $(H3H4)_2$ tetramers[33]; nucleosome assembly occurs step-wise, with assembly of $(H3H4)_2$ tetramers preceding recruitment of H2A/H2B[34]; it is therefore possible that the histone–DNA species encountered by Pol δ is a tetrasome rather than a nucleosome, although our data do not allow us to distinguish between these possibilities. Importantly, the distribution of Okazaki fragment termini around transcription factor binding sites was identical between wild-type and *pol32*Δ strains (Supplementary Fig. 9), allowing us to conclude that the shift towards the edge of nucleosomes does not simply represent a constant decrease of ~35–40 bp in the extent of strand displacement.

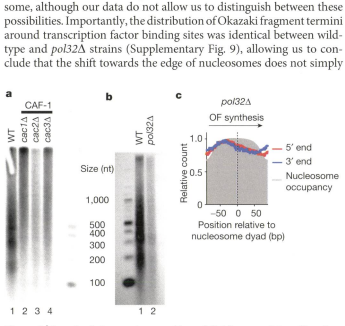


**Figure 5 | Impaired chromatin assembly and Pol δ processivity affect the size of Okazaki fragments and the location of their termini, respectively.** **a**, Deletion of any component of the CAF-1 complex (lanes 2–4) results in Okazaki fragments that are no longer sized according to nucleosomes. WT, wild type. **b**, Deletion of the *pol32* subunit of Pol δ (lane 2) does not abrogate the chromatin-like size distribution of Okazaki fragments. **c**, In the absence of Pol32, the termini of mononucleosome-sized Okazaki fragments are shifted towards the replication-fork-proximal edge of the nucleosome: peak density occurs at a location consistent with the predicted edges of $(H3H4)_2$ tetramers. See also Supplementary Fig. 11.

## Discussion

Our data suggest a mechanism by which Pol δ may reliably remove DNA synthesized by Pol α while avoiding excessive strand-displacement synthesis. Repeated cycles of extension and cleavage can occur during the synthesis of a single Okazaki fragment. After removal of the RNA primer, all DNA flap structures generated by Pol δ are biochemically indistinguishable from one another, and an external mechanism is therefore required to measure the extent of strand displacement already carried out by Pol δ on each fragment. The removal of Pol δ by newly deposited histones represents a simple way to constrain Pol δ extension, and might allow nucleosome assembly to stimulate replication-fork progression directly. Although our data imply that nucleosomes strongly impede Pol δ, we note that both Fen1 and DNA ligase I can act efficiently on nucleosomal substrates[35,36]. We speculate that carrying out Okazaki fragment processing in the context of nucleosomes rather than DNA allows the ligation reaction to outcompete further strand displacement by Pol δ.

CAF-1 is not essential in *S. cerevisiae*, suggesting that other histone chaperones such as Asf1, Rtt106 and HIR[37] allow sufficient replication-coupled or post-replicative nucleosome assembly for viability. Nevertheless, our results are consistent with a temporal delay in nucleosome assembly in CAF-1 mutants, which may give rise to previously reported silencing defects[38]. The importance of replication-coupled chromatin assembly in metazoa is illustrated by the severe phenotypes of CAF-1 or ASF1 disruption in human cell lines: ASF1 depletion leads to replication-fork stalling[39], and CAF-1 depletion also precludes progression through S phase[40].

Our studies demonstrate that the location of Okazaki fragment termini can be determined by interactions between the lagging-strand polymerase and nascent nucleosomes. This observation provides the first direct mechanistic evidence for the coupling of DNA replication to chromatin assembly on the newly replicated daughter genomes. Such coupling is fundamentally important given the part played by chromatin in the regulation of gene expression, as well as the potential for the epigenetic inheritance of precisely located modified nucleosomes. In addition, transcription factors known to have roles in the establishment of chromatin structure are apparently able to re-bind to DNA immediately after replication-fork passage. Unlike histones, which are present in sufficient number to be distributed to both daughter genomes, DNA-bound transcription factors are present at only one local copy per two daughters. Regulation of transcription factor re-binding could thus have a key role in asymmetric epigenetic inheritance.

## METHODS SUMMARY

Genomic DNA was prepared from spheroblasts essentially as described for medium resolution DSB mapping[41], labelled using exo-Klenow fragment (NEB) and α-$^{32}$P dCTP and separated in 1.3% denaturing agarose gels.

Okazaki fragments were purified by binding heat-denatured genomic DNA to Source 15Q (GE Healthcare) at pH 12, 300 mM NaCl, and eluting in 50 mM steps to 1 M. Primers for paired-end Illumina TruSeq sequencing were directly ligated to each end. Following second-strand synthesis and size selection by gel purification, libraries were amplified by PCR, purified from two sequential 2.5% native agarose gels, and sequenced directly. Full details are in Supplementary Fig. 4 and Methods.

**Full Methods** and any associated references are available in the online version of the paper at www.nature.com/nature.

**Received 21 November 2011; accepted 24 January 2012.**
**Published online 14 March 2012.**

1. Corpet, A. & Almouzni, G. Making copies of chromatin: the challenge of nucleosomal organization and epigenetic information. *Trends Cell Biol.* **19**, 29–41 (2009).

2. Sogo, J. M., Stahl, H., Koller, T. & Knippers, R. Structure of replicating simian virus 40 minichromosomes. The replication fork, core histone segregation and terminal structures. *J. Mol. Biol.* **189,** 189–204 (1986).
3. Burgers, P. M. Polymerase dynamics at the eukaryotic DNA replication fork. *J. Biol. Chem.* **284,** 4041–4045 (2009).
4. Kaufmann, G. & Falk, H. H. An oligoribonucleotide polymerase from SV40-infected cells with properties of a primase. *Nucleic Acids Res.* **10,** 2309–2321 (1982).
5. Nethanel, T. & Kaufmann, G. Two DNA polymerases may be required for synthesis of the lagging DNA strand of simian virus 40. *J. Virol.* **64,** 5912–5918 (1990).
6. Waga, S. & Stillman, B. Anatomy of a DNA replication fork revealed by reconstitution of SV40 DNA replication *in vitro*. *Nature* **369,** 207–212 (1994).
7. Ayyagari, R., Gomes, X. V., Gordenin, D. A. & Burgers, P. M. Okazaki fragment maturation in yeast. I. Distribution of functions between FEN1 and DNA2. *J. Biol. Chem.* **278,** 1618–1625 (2003).
8. Bae, S. H., Bae, K. H., Kim, J. A. & Seo, Y. S. RPA governs endonuclease switching during processing of Okazaki fragments in eukaryotes. *Nature* **412,** 456–461 (2001).
9. Kao, H. I., Veeraraghavan, J., Polaczek, P., Campbell, J. L. & Bambara, R. A. On the roles of *Saccharomyces cerevisiae* Dna2p and Flap endonuclease 1 in Okazaki fragment processing. *J. Biol. Chem.* **279,** 15014–15024 (2004).
10. Garg, P., Stith, C. M., Sabouri, N., Johansson, E. & Burgers, P. M. Idling by DNA polymerase δ maintains a ligatable nick during lagging-strand DNA replication. *Genes Dev.* **18,** 2764–2773 (2004).
11. Johnston, L. H. & Nasmyth, K. A. *Saccharomyces cerevisiae* cell cycle mutant *cdc9* is defective in DNA ligase. *Nature* **274,** 891–893 (1978).
12. Pavlov, Y. I. *et al.* Evidence that errors made by DNA polymerase α are corrected by DNA polymerase δ. *Curr. Biol.* **16,** 202–207 (2006).
13. Anderson, S. & DePamphilis, M. L. Metabolism of Okazaki fragments during simian virus 40 DNA replication. *J. Biol. Chem.* **254,** 11495–11504 (1979).
14. Bielinsky, A. K. & Gerbi, S. A. Discrete start sites for DNA synthesis in the yeast *ARS1* origin. *Science* **279,** 95–98 (1998).
15. Blumenthal, A. B. & Clark, E. J. Discrete sizes of replication intermediates in *Drosophila* cells. *Cell* **12,** 183–189 (1977).
16. Dohmen, R. J. & Varshavsky, A. Heat-inducible degron and the making of conditional mutants. *Methods Enzymol.* **399,** 799–822 (2005).
17. Bielinsky, A. K. & Gerbi, S. A. Chromosomal *ARS1* has a single leading strand start site. *Mol. Cell* **3,** 477–486 (1999).
18. Ng, P. *et al.* Gene identification signature (GIS) analysis for transcriptome characterization and genome annotation. *Nature Methods* **2,** 105–111 (2005).
19. Nieduszynski, C. A., Hiraga, S., Ak, P., Benham, C. J. & Donaldson, A. D. OriDB: a DNA replication origin database. *Nucleic Acids Res.* **35,** D40–046 (2007).
20. Eaton, M. L., Galani, K., Kang, S., Bell, S. P. & MacAlpine, D. M. Conserved nucleosome positioning defines replication origins. *Genes Dev.* **24,** 748–753 (2010).
21. Jiang, C. & Pugh, B. F. A compiled and systematic reference map of nucleosome positions across the *Saccharomyces cerevisiae* genome. *Genome Biol.* **10,** R109 (2009).
22. Whitehouse, I., Rando, O. J., Delrow, J. & Tsukiyama, T. Chromatin remodelling at promoters suppresses antisense transcription. *Nature* **450,** 1031–1035 (2007).
23. Hartley, P. D. & Madhani, H. D. Mechanisms that specify promoter nucleosome location and identity. *Cell* **137,** 445–458 (2009).
24. Badis, G. *et al.* A library of yeast transcription factor motifs reveals a widespread function for Rsc3 in targeting nucleosome exclusion at promoters. *Mol. Cell* **32,** 878–887 (2008).
25. MacIsaac, K. D. *et al.* An improved map of conserved regulatory sites for *Saccharomyces cerevisiae*. *BMC Bioinformatics* **7,** 113 (2006).
26. Hall, M. A. *et al.* High-resolution dynamic mapping of histone–DNA interactions in a nucleosome. *Nature Struct. Mol. Biol.* **16,** 124–129 (2009).
27. Bondarenko, V. A. *et al.* Nucleosomes can form a polar barrier to transcript elongation by RNA polymerase II. *Mol. Cell* **24,** 469–479 (2006).
28. Churchman, L. S. & Weissman, J. S. Nascent transcript sequencing visualizes transcription at nucleotide resolution. *Nature* **469,** 368–373 (2011).
29. Bai, L., Ondracka, A. & Cross, F. R. Multiple sequence-specific factors generate the nucleosome-depleted region on *CLN2* promoter. *Mol. Cell* **42,** 465–476 (2011).
30. Shibahara, K. & Stillman, B. Replication-dependent marking of DNA by PCNA facilitates CAF-1-coupled inheritance of chromatin. *Cell* **96,** 575–585 (1999).
31. Johansson, E., Garg, P. & Burgers, P. M. The Pol32 subunit of DNA polymerase δ contains separable domains for processive replication and proliferating cell nuclear antigen (PCNA) binding. *J. Biol. Chem.* **279,** 1907–1915 (2004).
32. Stith, C. M., Sterling, J., Resnick, M. A., Gordenin, D. A. & Burgers, P. M. Flexibility of eukaryotic Okazaki fragment maturation through regulated strand displacement synthesis. *J. Biol. Chem.* **283,** 34129–34140 (2008).
33. Dong, F. & van Holde, K. E. Nucleosome positioning is determined by the (H3–H4)2 tetramer. *Proc. Natl Acad. Sci. USA* **88,** 10596–10600 (1991).
34. Smith, S. & Stillman, B. Stepwise assembly of chromatin during DNA replication *in vitro*. *EMBO J.* **10,** 971–980 (1991).
35. Chafin, D. R., Vitolo, J. M., Henricksen, L. A., Bambara, R. A. & Hayes, J. J. Human DNA ligase I efficiently seals nicks in nucleosomes. *EMBO J.* **19,** 5492–5501 (2000).
36. Huggins, C. F. *et al.* Flap endonuclease 1 efficiently cleaves base excision repair and DNA replication intermediates assembled into nucleosomes. *Mol. Cell* **10,** 1201–1211 (2002).
37. Ray-Gallet, D. *et al.* Dynamics of histone H3 deposition *in vivo* reveal a nucleosome gap-filling mechanism for H3.3 to maintain chromatin integrity. *Mol. Cell* **44,** 928–941 (2011).
38. Zhang, Z., Shibahara, K. & Stillman, B. PCNA connects DNA replication to epigenetic inheritance in yeast. *Nature* **408,** 221–225 (2000).
39. Groth, A. *et al.* Regulation of replication fork progression through histone supply and demand. *Science* **318,** 1928–1931 (2007).
40. Hoek, M. & Stillman, B. Chromatin assembly factor 1 is essential and couples chromatin assembly to DNA replication *in vivo*. *Proc. Natl Acad. Sci. USA* **100,** 12183–12188 (2003).
41. Murakami, H., Borde, V., Nicolas, A. & Keeney, S. Gel electrophoresis assays for analyzing DNA double-strand breaks in *Saccharomyces cerevisiae* at various spatial resolutions. *Methods Mol. Biol.* **557,** 117–142 (2009).


**Supplementary Information** is linked to the online version of the paper at www.nature.com/nature.

**Acknowledgements** We thank S. McGuffee for assistance with data processing; S. Keeney, K. Marians, D. Remus, T. Tsukiyama, members of the Molecular Biology Program and Whitehouse laboratory for discussions and comments on the manuscript. This work was supported by a Louis V. Gerstner Jr Young Investigator Award and an Alfred Bressler Scholars Endowment Award to I.W. D.J.S. is an HHMI fellow of the Damon Runyon Cancer Research Foundation (DRG-#2046-10).

**Author Contributions** D.J.S. and I.W. designed experiments; D.J.S. performed experiments and analysed data; D.J.S. and I.W. interpreted results; the manuscript was drafted by D.J.S. and edited by D.J.S. and I.W.

**Author Information** Raw sequencing data and processed data are available at the Gene Expression Omnibus (http://www.ncbi.nlm.nih.gov/geo/query/acc.cgi?acc=GSE33786) under accession number 33786. Reprints and permissions information is available at www.nature.com/reprints. The authors declare no competing financial interests. Readers are welcome to comment on the online version of this article at www.nature.com/nature. Correspondence and requests for materials should be addressed to I.W. (whitehoi@mskcc.org).

LETTER

doi:10.1038/nature10942

# Resonant quantum transitions in trapped antihydrogen atoms

C. Amole[1], M. D. Ashkezari[2], M. Baquero-Ruiz[3], W. Bertsche[4,5,6], P. D. Bowe[7], E. Butler[8], A. Capra[1], C. L. Cesar[9], M. Charlton[4], A. Deller[4], P. H. Donnan[10], S. Eriksson[4], J. Fajans[3,11], T. Friesen[12], M. C. Fujiwara[12,13], D. R. Gill[13], A. Gutierrez[14], J. S. Hangst[7], W. N. Hardy[14,15], M. E. Hayden[2], A. J. Humphries[4], C. A. Isaac[4], S. Jonsell[16], L. Kurchaninov[13], A. Little[3], N. Madsen[4], J. T. K. McKenna[17], S. Menary[1], S. C. Napoli[4], P. Nolan[17], K. Olchanski[13], A. Olin[13,18], P. Pusa[17], C. Ø. Rasmussen[7], F. Robicheaux[10], E. Sarid[19], C. R. Shields[4], D. M. Silveira[20]†, S. Stracka[13], C. So[3], R. I. Thompson[12], D. P. van der Werf[4] & J. S. Wurtele[3,11]

**The hydrogen atom is one of the most important and influential model systems in modern physics. Attempts to understand its spectrum are inextricably linked to the early history and development of quantum mechanics. The hydrogen atom's stature lies in its simplicity and in the accuracy with which its spectrum can be measured[1] and compared to theory. Today its spectrum remains a valuable tool for determining the values of fundamental constants and for challenging the limits of modern physics, including the validity of quantum electrodynamics and—by comparison with measurements on its antimatter counterpart, antihydrogen—the validity of CPT (charge conjugation, parity and time reversal) symmetry. Here we report spectroscopy of a pure antimatter atom, demonstrating resonant quantum transitions in antihydrogen. We have manipulated the internal spin state[2,3] of antihydrogen atoms so as to induce magnetic resonance transitions between hyperfine levels of the positronic ground state. We used resonant microwave radiation to flip the spin of the positron in antihydrogen atoms that were magnetically trapped[4–6] in the ALPHA apparatus. The spin flip causes trapped anti-atoms to be ejected from the trap. We look for evidence of resonant interaction by comparing the survival rate of trapped atoms irradiated with microwaves on-resonance to that of atoms subjected to microwaves that are off-resonance. In one variant of the experiment, we detect 23 atoms that survive in 110 trapping attempts with microwaves off-resonance (0.21 per attempt), and only two atoms that survive in 103 attempts with microwaves on-resonance (0.02 per attempt). We also describe the direct detection of the annihilation of antihydrogen atoms ejected by the microwaves.**

Magnetostatic trapping of neutral atoms[7] or anti-atoms is accomplished by creating a local minimum of the magnetic field magnitude in free space. The confining force results from interaction of the atomic magnetic moment $\boldsymbol{\mu}$ with the non-uniform magnetic field. Figure 1 shows the expected Breit–Rabi hyperfine level diagram for the ground state of the antihydrogen atom in a magnetic field. We label the four eigenstates $|a\rangle$, $|b\rangle$, $|c\rangle$ and $|d\rangle$ in order of increasing energy. Trapping is possible when the atom is in a 'low-field seeking' quantum state ($|c\rangle$ or $|d\rangle$ in Fig. 1). We employ the Ioffe–Pritchard[7] configuration: the superposition of a magnetic multipole (an octupole) field that confines atoms in the transverse directions and two 'mirror coil' fields for axial confinement[4].

Working at the Antiproton Decelerator[8] facility at CERN, we recently demonstrated magnetic confinement of cold antihydrogen atoms[4] and showed that—once trapped—these atoms end up in their ground state, where they can be held[5] for up to 1,000 s. Here we use the same apparatus, modified to enable injection of microwaves into the trapping volume (Fig. 2a). Antihydrogen atoms are produced near the field minimum (about 1 T, Fig. 2b) by mixing cold plasmas of antiprotons and positrons for about 1 s (Methods). Atoms having kinetic energies corresponding to less than 0.5 K can be trapped. Mixing about two million positrons and 20,000 antiprotons yields approximately 6,000 anti-atoms; on average, approximately one anti-atom is trapped. The trapping field currents can be ramped down with a time constant of 9 ms, releasing trapped atoms in a well-defined time window[4]. The trapping volume is surrounded by a three-layer, 30,720-channel imaging silicon detector[16], which can locate the spatial positions—vertices—of antiproton annihilations.

Our approach was to subject trapped antihydrogen atoms to resonant microwaves to eject them from the trap. A tuned, oscillating magnetic field $\mathbf{B}_1$ applied perpendicularly to the trapping field can drive positron spin-flip transitions between the trappable and the untrappable states, that is, $|c\rangle \rightarrow |b\rangle$ and $|d\rangle \rightarrow |a\rangle$. Untrapped atoms escape and annihilate on the surrounding apparatus. A single experimental cycle or 'trapping attempt' involves producing anti-atoms in

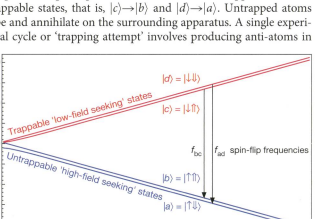


**Figure 1 | Hyperfine energy levels.** The Breit–Rabi diagram, showing the relative hyperfine energy levels of the ground state of the hydrogen (and antihydrogen, assuming CPT invariance) atom in a magnetic field. In the state vectors shown (for the high-field limit), the single arrow refers to the positron spin and the double arrow refers to the antiproton spin.

[1]Department of Physics and Astronomy, York University, Toronto, Ontario, M3J 1P3, Canada. [2]Department of Physics, Simon Fraser University, Burnaby, British Columbia, V5A 1S6, Canada. [3]Department of Physics, University of California, Berkeley, California 94720-7300, USA. [4]Department of Physics, Swansea University, Swansea SA2 8PP, UK. [5]School of Physics and Astronomy, University of Manchester, M13 9PL Manchester, UK. [6]The Cockcroft Institute, WA4 4AD Warrington, UK. [7]Department of Physics and Astronomy, Aarhus University, DK-8000 Aarhus C, Denmark. [8]CERN, Department PH, CH-1211 Geneva 23, Switzerland. [9]Instituto de Fisica, Universidade Federal do Rio de Janeiro, Rio de Janeiro 21941-972, Brazil. [10]Department of Physics, Auburn University, Auburn, Alabama 36849-5311, USA. [11]Lawrence Berkeley National Laboratory, Berkeley, California 94720, USA. [12]Department of Physics and Astronomy, University of Calgary, Calgary, Alberta T2N 1N4, Canada. [13]TRIUMF, 4004 Wesbrook Mall, Vancouver, British Columbia V6T 2A3, Canada. [14]Department of Physics and Astronomy, University of British Columbia, Vancouver, British Columbia V6T 1Z1, Canada. [15]The Canadian Institute of Advanced Research, Toronto M5G-1Z8, Canada. [16]Department of Physics, Stockholm University, SE-10691, Stockholm, Sweden. [17]Department of Physics, University of Liverpool, Liverpool L69 7ZE, UK. [18]Department of Physics and Astronomy, University of Victoria, Victoria, British Columbia V8W 3P6, Canada. [19]Department of Physics, NRCN-Nuclear Research Center Negev, Beer Sheva, IL-84190, Israel. [20]Atomic Physics Laboratory, RIKEN, Saitama 351-0198, Japan. †Present address: Instituto de Física, Universidade Federal do Rio de Janeiro, Rio de Janeiro 21941-972, Brazil.

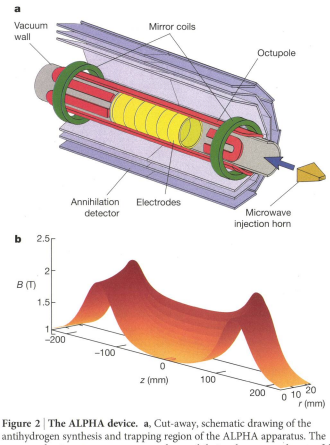


**Figure 2 | The ALPHA device. a**, Cut-away, schematic drawing of the antihydrogen synthesis and trapping region of the ALPHA apparatus. The superconducting atom-trap magnets, the annihilation detector, and some of the Penning trap electrodes are shown. An external solenoid (not shown) provides a 1-T magnetic field for the Penning trap. The drawing is not to scale. The inner diameter of the Penning trap electrodes is 44.5 mm and the minimum-$B$ trap has an effective length of 274 mm. Microwaves are injected along the axis of the trapping volume using a horn antenna, which is located about 130 cm from the trap axial midpoint. **b**, Map of magnetic field strength in the ALPHA antihydrogen trap. The red contour bounds a region up to 0.35 mT (or 10 MHz in microwave frequency equivalent) above the minimum field, to roughly indicate the size of the resonant volume.

the magnetic trap, holding any trapped atoms first for 60 s (during which the magnetic field may be changed) and then for 180 s (during which microwaves may be introduced), and then intentionally releasing any remaining atoms to detect their annihilation.

To select the proper microwave frequencies and magnetic field configurations, we consider (Fig. 3a) the calculated positron spin resonance lineshapes for equal numbers of trapped $|c\rangle$ and $|d\rangle$ state atoms exposed to microwaves. The abrupt low-frequency onsets are associated with the minimum in the static magnetic field near the trap centre; the high-frequency tails reflect the highly inhomogeneous nature of the trapping fields elsewhere. We choose the resonance condition such that transitions are induced as atoms pass close to the magnetic minimum (Fig. 2b). This choice yields higher transition rates than elsewhere in the trap, and it localizes the position in space where transitions occur, and whence the resulting high-field seeking atoms are ejected. We do not know a priori the hyperfine level in which atoms are trapped; for a given magnetic field configuration we need to alternately irradiate the trap at two frequencies (details in Fig. 3 legend) separated by the zero-field hyperfine splitting of 1,420.4 MHz.

We collect two distinct, complementary types of annihilation data. First, at the end of every trapping attempt, we rapidly turn off the confining fields and watch for annihilation events in a 30-ms window from the start of the magnet shutdown. This allows us to determine an effective trapping rate. The ejection of trapped atoms by resonant microwaves will reduce this rate. Rates for application of resonant microwaves, off-resonant microwaves and no microwaves can be compared: these are 'disappearance mode' data. The second data set comes from monitoring annihilation events throughout the entire time that antihydrogen atoms are held in the trap. We look for events from ejected atoms during the time that resonant microwave fields are applied: these are 'appearance mode' data.

Because the duration of the observation window differs significantly between these two modes, we rely on two different cosmic background rejection algorithms (Methods). In the 30-ms 'disappearance window' we use the algorithm developed earlier[4] (the 'default criteria'). The rate at which cosmic ray events are interpreted as annihilations by this selection scheme is $(4.7 \pm 0.2) \times 10^{-2}\,\mathrm{s}^{-1}$. For the much longer 'appearance mode' observation (180 s), we rely on an alternative set of acceptance criteria that, compared to the default criteria, reduces annihilations by 25% but lowers the cosmic background by an order of magnitude. To avoid experimenter bias, the two sets of criteria are optimized and cross-checked using control samples[4,6]: cosmic ray events and annihilation events collected independently of the trapping experiments described here.

We conducted six series of measurements. For series 1, we set the minimum on-axis trapping field $B^{\mathrm{axis}}_{\mathrm{min}}$ to some value $B^{\mathrm{A}}$ (Methods), and then applied resonant microwave fields at frequencies $f^{\mathrm{A}}_{\mathrm{bc}}$ and $f^{\mathrm{A}}_{\mathrm{ad}}$ (Fig. 3b; see the legend for microwave frequency drive details) during the 180-s hold portion of the cycle. For series 2, we shifted $B^{\mathrm{axis}}_{\mathrm{min}}$ to $B^{\mathrm{B}} > B^{\mathrm{A}}$ by increasing the mirror coil currents such that microwave fields oscillating at $f^{\mathrm{A}}_{\mathrm{bc}}$ and $f^{\mathrm{A}}_{\mathrm{ad}}$ are detuned by 100 MHz and are no longer resonant with atoms at the centre of the trap (Fig. 3c). The field was shifted (in about 1 s) after the mixing and initial trapping phase of each trapping attempt, and a waiting period of 59 s was imposed to allow the field to stabilize before microwave introduction. This configuration should eliminate $|d\rangle \rightarrow |a\rangle$ transitions and reduce the rate of $|c\rangle \rightarrow |b\rangle$ transitions. The latter can still occur as atoms pass through regions of space in which the local magnetic field brings them into resonance with microwave fields applied at frequency $f^{\mathrm{A}}_{\mathrm{ad}}$. Series 3 involved operating at the higher field $B^{\mathrm{B}}$ and shifting the microwave frequencies so as to bring both transitions back into resonance (Fig. 3d). Series 4 field and frequency conditions were identical to those of series 2, but series 4 attempts were interleaved with those of series 3. This repetition attempts to minimize possible systematic effects due to time variations in the experimental conditions. Antiproton beam and plasma conditions—and thus the initial trapping rate—can vary from day to day, so on- and off-resonance experiments were interspersed. Thus, series 1 and 2 were taken under very similar conditions, and series 3 and 4 constitute a second, complementary set of measurements. In concert with series 1–4, we measured trapping and annihilation rates with $B^{\mathrm{axis}}_{\mathrm{min}}$ set to $B^{\mathrm{A}}$ or $B^{\mathrm{B}}$ when no microwaves are injected into the apparatus (series 5 and 6, respectively). Apart from changes in magnetic field or microwave conditions, the experimental procedure was identical for each of the six series.

A summary of 'disappearance mode' data appears in Tables 1 and 2. The errors quoted are based on counting statistics only. By comparing the Poisson rate of the process of interest with the rate of the control process, we evaluate the probability ($P$-value) that the observed number of outcomes, or a more extreme one, could have been produced by background fluctuations[11]. We observe a clear decrease in the survival rate for the cases in which microwaves are injected on-resonance, as compared to the equivalent off-resonance measurements, with a $P$-value of $1.0 \times 10^{-5}$.

The two measurement sets (series 1–2; series 3–4) could have different systematic uncertainties. For example, in the former, the mirror field shift might affect the orbit dynamics of the trapped antihydrogen (a hypothesis not supported by numerical simulations), while the latter could suffer from different microwave field characteristics between on- and off-resonance frequencies (again, this is not supported by our detailed off-line measurements with electron plasmas; see Methods). However, both data sets show decreases in the on-resonance rate

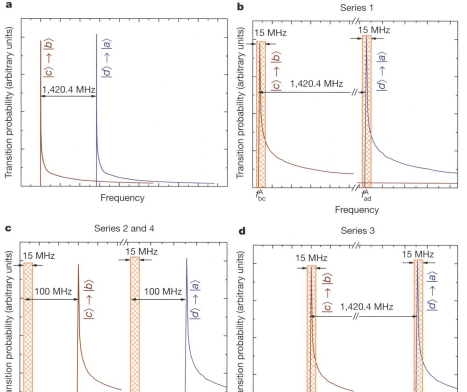


**Figure 3 | Transition lineshapes and resonance conditions. a**, Calculated spin-flip transition lineshapes in the ALPHA antihydrogen trap. Transition probability (arbitrary units) is plotted versus microwave frequency. Only the trapping field inhomogeneity is considered in calculating the lineshape. **b**, Schematic representation of the experimental situation for the on-resonance experiments at magnetic field $B^{\mathrm{A}}$ (series 1). The yellow bands represent the frequency ranges over which the microwaves are scanned. **c**, The situation for off-resonance experiments at magnetic field $B^{\mathrm{B}}$ (series 2 and 4). **d**, The situation for on-resonant experiments at magnetic field $B^{\mathrm{B}}$ (series 3). A two-segment frequency sweep lasting 30 s was used to apply microwave fields. This sweep was repeated six times in each trapping attempt for a total microwave application time of 180 s, beginning 60 s after the end of antihydrogen formation. In each case, the first 15-s scan covers the lower yellow band and the second 15-s scan covers the upper yellow band. The bands span −5 MHz to +10 MHz about the target frequency.

measurements, compared to the associated off-resonance measurements, with $P$-values of $1.6 \times 10^{-4}$ and $1.5 \times 10^{-2}$, respectively, supporting the hypothesis that the difference is due to spin flip.

We note that the survival rates for the no-microwave measurements are higher than for those in which microwaves are present but off-resonance (the $P$-value is $6 \times 10^{-5}$). This difference could be explained by far off-resonant interactions with the $|c\rangle$ state, assuming there is sufficient microwave power to induce spin flips in the long tails of the resonance lineshape (Fig. 3c). (See the discussion of the appearance mode data below.)

We also directly searched for annihilation signals of anti-atoms that are ejected from the trap after a spin-flip transition—the 'appearance mode' described above. Figure 4a shows the time history of events satisfying the alternative acceptance criteria and having $|z| < 6$ cm (Methods). In the first frequency sweep ($0 < t < 30$ s) we observe a significant excess of counts ($P = 2.8 \times 10^{-5}$) in on-resonance (series 1 plus series 3) compared to off-resonance attempts (series 2 plus series 4). Seven of the 19 events appearing in $0 < t < 15$ s (microwaves probing $f_{\mathrm{bc}}$) occur in the first second; for $15 < t < 30$ s (probing $f_{\mathrm{ad}}$) the first second has seven of 18 events. This suggests that the microwave power is sufficient to flip most of the spins during the first 30-s sweep, in agreement with numerical simulations of the transition rate (Methods). An investigation of power dependence indicated that a level as low as one-sixteenth of the nominal 700 mW injected (Methods) was still enough to eject the trapped atoms in the first 30-s sweep, again consistent with the simulations.

In the off-resonant experiments, we observe a mild excess of counts above the no-microwave case (series 5 plus series 6) with an associated $P = 5.6 \times 10^{-2}$. We interpret this excess to be due to the above-mentioned off-resonance interaction with the $|c\rangle$ state. This conclusion is supported by the fact that the events are in $15 < t < 30$ s (Fig. 4a), when the microwaves are probing the upper 15-MHz

**Table 1 | Series summaries for the 'disappearance mode' analysis**

| Series | Relative microwave frequency | Relative magnetic field | Number of attempts | Antihydrogen detected at trap shutdown | Rate | Comment |
|---|---|---|---|---|---|---|
| 1 | 0 MHz | 0 mT ($B^{\mathrm{axis}}_{\mathrm{min}} = B^{\mathrm{A}}$) | 79 | 1 | 0.01 ± 0.01 | On resonance (Fig. 3b) |
| 2 | 0 MHz | +3.5 mT ($B^{\mathrm{axis}}_{\mathrm{min}} = B^{\mathrm{B}}$) | 88 | 16 | 0.18 ± 0.05 | Off resonance (Fig. 3c) |
| 3 | +100 MHz | +3.5 mT ($B^{\mathrm{axis}}_{\mathrm{min}} = B^{\mathrm{B}}$) | 24 | 1 | 0.04 ± 0.04 | On resonance (Fig. 3d) |
| 4 | 0 MHz | +3.5 mT ($B^{\mathrm{axis}}_{\mathrm{min}} = B^{\mathrm{B}}$) | 22 | 7 | 0.32 ± 0.12 | Off resonance (Fig. 3c) |
| 5 | Off | 0 mT ($B^{\mathrm{axis}}_{\mathrm{min}} = B^{\mathrm{A}}$) | 52 | 17 | 0.33 ± 0.08 | No microwaves |
| 6 | Off | +3.5 mT ($B^{\mathrm{axis}}_{\mathrm{min}} = B^{\mathrm{B}}$) | 48 | 23 | 0.48 ± 0.10 | No microwaves |

**Table 2 | Totals for all 'disappearance mode' series**

| | Number of attempts | Detected antihydrogen | Rate |
|---|---|---|---|
| On resonance (1 + 3) | 103 | 2 | $0.02 \pm 0.01$ |
| Off resonance (2 + 4) | 110 | 23 | $0.21 \pm 0.04$ |
| No microwaves (5 + 6) | 100 | 40 | $0.40 \pm 0.06$ |

frequency band (Fig. 3c), and by indications that the nominal power should be sufficient to drive off-resonant transitions. Taken together, the disappearance and appearance analyses constitute a consistent picture of the fate of the trapped antihydrogen atoms.

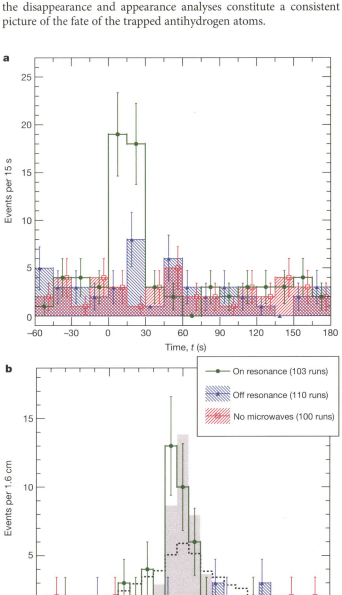


**Figure 4 | Appearance mode data. a**, The number of 'appearance mode' annihilation events satisfying the alternative selection criteria and $|z| < 6$ cm (Methods) as a function of time between the end of antihydrogen production and the trap shutdown. Microwave power is first applied at time $t = 0$. The expected cosmic background per bin per run is $0.026 \pm 0.005$ events. The error bars are due to counting statistics. **b**, The $z$-distribution of annihilation vertices in 'appearance mode' for $0 < t < 30$ s. The grey histogram is the result of a numerical simulation of the motion of spin-flipped atoms ejected from the trap. The dashed black curve is the result of a simulation of trapped antihydrogen annihilating on the residual gas (Methods). Both simulations are normalized to the on-resonant data.

We have considered other processes that could lead to antihydrogen loss in the presence of microwaves but that could not be due to a spin-flip. The only plausible candidate is heating of the trap electrodes by the microwaves, causing desorption from the surfaces of cryo-pumped material, which could then scatter or annihilate the trapped anti-atoms. Indeed, we observe a slight electrode temperature increase from about 8 K to at most 11 K during the 180-s microwave cycle. However, any such thermal effect on the vacuum should be the same for series 1 and 2, which differ only by a slight change in the trapping magnetic field. Further evidence against vacuum deterioration comes from Fig. 4b, which shows the $z$-distribution of appearance-type events ($in\ 0 < t < 30$ s). The distribution is highly localized around the trap centre, as we expect from simulations of how spin-flipped atoms are lost from the trap (Methods). Annihilation or collisional loss of trapped anti-atoms in a compromised vacuum could occur anywhere in the 274-mm-long trapping volume.

We thus conclude that we have observed resonant interaction of microwave radiation with the internal quantum states of trapped antihydrogen atoms. This is a proof-of-principle experiment; we have not yet attempted to accurately localize a resonance or determine a spectroscopic lineshape. We have bounded the resonance between the off-resonance scan value and the maximum of the on-resonance sweep. Roughly speaking, the observed resonance is within 100 MHz of the resonance frequency expected for hydrogen, corresponding to a relative precision of about $4 \times 10^{-3}$. This experiment marks the advent of antimatter spectroscopy and takes a preliminary step towards precision comparison of the spectra of hydrogen and antihydrogen as a test of CPT symmetry. Importantly, it also demonstrates the viability of performing fundamental measurements on small numbers of trapped anti-atoms by combining resonant interaction with the long trapping times and sensitive annihilation detection in ALPHA. In future experiments, the transition $|c\rangle \leftrightarrow |d\rangle$ could be probed by double resonance; the frequency of this transition goes through a broad maximum[12] at a field of 0.65 T, allowing a precision measurement of hyperfine parameters without requiring precise knowledge of the absolute value of $B$ (see Supplementary Information).

## METHODS SUMMARY

The ALPHA apparatus traps antihydrogen atoms synthesized from cold plasmas of positrons and antiprotons. Microwaves from a frequency synthesizer were amplified and injected into the magnetic atom trap using a horn antenna. We use electron cyclotron frequency measurement techniques to set the magnetic field in the device, and to characterize microwave field patterns. We perform numerical simulations of trapped antihydrogen dynamics to model microwave resonant lineshapes and transition rates, atom ejection dynamics, and the spatial distribution of residual gas annihilation. Two distinct analysis methods are used to reduce cosmic ray background in the annihilation detector.

**Full Methods** and any associated references are available in the online version of the paper at www.nature.com/nature.

**Received 9 January; accepted 7 February 2012.**
**Published online 7 March 2012.**

1. Hänsch, T. W. Nobel lecture: Passion for precision. *Rev. Mod. Phys.* **78,** 1297–1309 (2006).
2. Martin, A. G., Helmerson, K., Bagnato, V. S., Lafyatis, G. P. & Pritchard, D. E. RF spectroscopy of trapped neutral atoms. *Phys. Rev. Lett.* **61,** 2431–2434 (1988).
3. Fujiwara, M. C. *et al.* Towards antihydrogen confinement with the ALPHA antihydrogen trap. *Hyperfine Interact.* **172,** 81–89 (2006).
4. Andresen, G. B. *et al.* Trapped antihydrogen. *Nature* **468,** 673–676 (2010).
5. Andresen, G. B. *et al.* Confinement of antihydrogen for 1,000 seconds. *Nature Phys.* **7,** 558–564 (2011).
6. Andresen, G. B. *et al.* Search for trapped antihydrogen. *Phys. Lett. B* **695,** 95–104 (2011).
7. Pritchard, D. E. Cooling neutral atoms in a magnetic trap for precision spectroscopy. *Phys. Rev. Lett.* **51,** 1336–1339 (1983).
8. Bertsche, W. *et al.* A magnetic trap for antihydrogen confinement. *Nucl. Instrum. Meth. A* **566,** 746–756 (2006).
9. Maury, S. The antiproton decelerator: AD. *Hyperfine Inter.* **109,** 43–52 (1997).
10. Andresen, G. B. *et al.* The ALPHA detector: module production and assembly. *J. Instrum.* **7,** C01051 (2012).

11. Przyborowski, J. & Wilenski, H. Homogeneity of results in testing samples from Poisson series. *Biometrika* **31,** 313–323 (1939).
12. Hardy, W. N. *et al.* Magnetic resonance studies of gaseous atomic hydrogen at low temperatures. *Phys. Rev. Lett.* **42,** 1042–1045 (1979).

**Supplementary Information** is linked to the online version of the paper at www.nature.com/nature.

**Acknowledgements** This work was supported by CNPq, FINEP/RENAFAE (Brazil), ISF (Israel), MEXT (Japan), FNU (Denmark), VR (Sweden), NSERC, NRC/TRIUMF, AITF, FQRNT (Canada), DOE, NSF (USA), EPSRC, the Royal Society and the Leverhulme Trust (UK). We thank them for their generous support. We are grateful to the AD team (T. Eriksson, P. Belochitskii, B. Dupuy, L. Bojtar, C. Oliveira, B. Lefort and G. Tranquille) for the delivery of a high-quality antiproton beam. We thank the following individuals for help: M. Harrison, J. Escallier, A. Marone, M. Anerella, A. Ghosh, B. Parker, G. Ganetis, J. Thornhill, D.Wells, D. Seddon, F. Butin, H. Brueker, K. Dahlerup-Pedersen, J. Mourao, T. Fowler, S. Russenschuck, R. De Oliveira, N. Wauquier, J. Hansen, M. Polini, J. M. Geisser, L. Deparis, P. Frichot, J. M. Malzacker, A. Briswalter, P. Moyret, S. Mathot, G. Favre, J. P. Brachet, P. Mésenge, S. Sgobba, A. Cherif, J. Bremer, J. Casas-Cubillos, N. Vauthier, G. Pernic, O. Pirotte, A. Perin, G. Perinic, B. Vullierme, D. Delkaris, N. Veillet, K. Barth, R. Consentino, S. Guido, L. Stewart, M. Malabaila, A. Mongelluzzo, P. Chiggiato, G. Willering, E. Mahner, A. Froton, C. Lasseur, F. Hahn, E. Søndergaard, F. Mikkelsen, W. Carlisle, A. Charman, J. Keller, P. Arnaudruz, D. Bishop, R. Bula, K. Langton, P. Vincent, S. Chan, D. Rowbotham, P. Bennet, B. Evans, J.-P. Martin, P. Kowalski, A. Read, T. Willis, J. Kivell, H. Thomas, W. Lai, L. Wasilenko, C. Kolbeck, H. Malik, P. Genoa, L. Posada, R. Funakoshi, M. Okeane, S. Carey and N. Evetts. We thank former collaborators M. J. Jenkins, G. B. Andresen, R. Hydomako, S. Chapman, A. Povilus, R. Hayano, L. V. Jørgensen and Y. Yamazaki. We are grateful to the CERN Summer Student Program for funding the participation of undergraduate students (C.Ø.R. and S.C.N.) in our experiment.

**Author Contributions** W.B., P.D.B., J.F., M.C.F., J.S.H., N.M. and D.M.S. conceived, designed and constructed the central ALPHA apparatus and participated in all aspects of the experimental and physics programme. The microwave hardware was designed and fabricated by M.D.A., E.B., W.N.H. and M.E.H., who also participated in all aspects of the experimental programme. T.F. developed the electron cyclotron resonance diagnostic and participated actively in all aspects of the experimental programme. S.S. developed the alternative event analysis and participated actively in the experimental and analysis efforts. C.A., M.B.-R., A.C., A.G., A.J.H., J.T.K.M., E.S. and C.S. participated actively in the experimental runs, data taking, on- and offline analysis, and maintenance and modification of the apparatus. D.R.G. and A.O. contributed to all aspects of the detector systems and participated actively in the experimental shift work and analysis efforts. M.C. designed and built the positron accumulator and participated in the experimental shift work, the physics planning effort, and the strategic direction of the experiment. D.P.v.d.W. designed and built the positron accumulator, contributed to the magnetic design of the atom trap, and participated in the experimental programme. F.R., with help from P.H.D., performed the spin-flip simulations reported in this paper and supported the design and experimental programme with simulations and calculations. P.N. led the design of the ALPHA silicon detector. P.P. was responsible for implementing the silicon detector at CERN and participated in the experimental and analysis programme. A.D., C.A.I., C.Ø.R., S.C.N., A.L. and C.R.S. contributed to the experimental shift work. S.J. and J.S.W. contributed theoretical support in the form of atomic or plasma physics calculations and simulations and contributed to the experimental shift work. C.L.C., S.E., S.M. and R.I.T. participated in the experimental programme and the physics planning effort. L.K. and K.O. provided offsite support for detector electronics and database management systems, respectively, and contributed to the experimental shift work. E.B., J.S.H. and M.E.H. wrote the initial manuscript, which was edited, improved and approved by the entire collaboration.

**Author Information** Reprints and permissions information is available at www.nature.com/reprints. The authors declare no competing financial interests. Readers are welcome to comment on the online version of this article at www.nature.com/nature. Correspondence and requests for materials should be addressed to J.S.H. (hangst@phys.au.dk) or M.E.H. (mhayden@sfu.ca).

LETTER

doi:10.1038/nature10934

# Electron tomography at 2.4-ångström resolution

M. C. Scott[1]*, Chien-Chun Chen[1]*, Matthew Mecklenburg[1]*, Chun Zhu[1], Rui Xu[1], Peter Ercius[2], Ulrich Dahmen[2], B. C. Regan[1] & Jianwei Miao[1]

**Transmission electron microscopy is a powerful imaging tool that has found broad application in materials science, nanoscience and biology[1–3]. With the introduction of aberration-corrected electron lenses, both the spatial resolution and the image quality in transmission electron microscopy have been significantly improved[4,5] and resolution below 0.5 ångströms has been demonstrated[6]. To reveal the three-dimensional (3D) structure of thin samples, electron tomography is the method of choice[7–14], with cubic-nanometre resolution currently achievable[10,11]. Discrete tomography has recently been used to generate a 3D atomic reconstruction of a silver nanoparticle two to three nanometres in diameter[12], but this statistical method assumes prior knowledge of the particle's lattice structure and requires that the atoms fit rigidly on that lattice. Here we report the experimental demonstration of a general electron tomography method that achieves atomic-scale resolution without initial assumptions about the sample structure. By combining a novel projection alignment and tomographic reconstruction method with scanning transmission electron microscopy, we have determined the 3D structure of an approximately ten-nanometre gold nanoparticle at 2.4-ångström resolution. Although we cannot definitively locate all of the atoms inside the nanoparticle, individual atoms are observed in some regions of the particle and several grains are identified in three dimensions. The 3D surface morphology and internal lattice structure revealed are consistent with a distorted icosahedral multiply twinned particle. We anticipate that this general method can be applied not only to determine the 3D structure of nanomaterials at atomic-scale resolution[13–15], but also to improve the spatial resolution and image quality in other tomography fields[7,9,16–20].**

Since its introduction in 1968, electron tomography has been primarily used to determine the 3D structure of biological samples[7,9]. In the past decade, electron tomography has been increasingly applied in materials science and nanoscience through the use of scanning transmission electron microscopy (STEM)[8,10,11]. The highest resolution at present achieved by STEM tomography is around 1 nm in three dimensions[10,11], although slightly higher resolution has been obtained in a study of fullerene-like nanostructures with bright-field electron tomography[21]. A general electron tomography method with atomic-scale resolution, however, has not been demonstrated for several reasons. First, aligning the projections of a tomographic tilt series to a common axis with atomic level precision is technically challenging. Second, radiation damage limits the number of projections that can be acquired from a single object[13,22]. Last, specimens cannot usually be tilted beyond $\pm 79^{\circ}$, preventing acquisition of data from the 'missing wedge'[7–11]. Here we demonstrate that these limitations can be overcome or alleviated by applying a novel alignment approach and an iterative tomographic reconstruction method to a tilt series obtained via annular dark field (ADF)-STEM[23,24].

The conventional alignment approach used in electron tomography either relies on fiducial markers such as colloidal gold beads or is based on the cross-correlation between neighbouring projections[7,9]. To our knowledge, neither of these alignment approaches can achieve atomic-level precision. To overcome this limitation, we have developed a method based on the centre of mass, which is able to align the projections of a tilt series at atomic-level accuracy even with noise (Methods). To address the other two difficulties mentioned above, we have implemented a data acquisition and tomographic reconstruction method, termed equally sloped tomography[16,18–20,25] (EST). Compared to conventional tomography, which reconstructs a 3D object from a tilt series of projections with constant angular increments, EST acquires a tilt series with equal slope increments, and then iterates back and forth between real and reciprocal space (Methods). In each iteration, constraints such as the sample boundary (that is, the support) and positivity of the Coulomb potential are applied in real space, while the measured projectional slices (that is, the Fourier transform of the projections) are enforced in reciprocal space. Each iteration is monitored by an error metric, and the algorithm is terminated after reaching a maximum number of iterations.

To test the feasibility of achieving a high-resolution tomographic reconstruction by the centre-of-mass and EST methods, we conducted numerical simulations on an ~5-nm gold nanoparticle with icosahedral symmetry and a total of 3,871 atoms (Supplementary Figs 3a, 4a, c, e). A tilt series of 55 projections was obtained from the particle using multislice STEM calculations[26] (energy, 300 keV; spherical aberration, 1.2 mm; illumination semi-angle, 7.98 mrad; defocus, 48.6 nm; detector inner and outer angles, 13 and 78 mrad). To minimize nonlinear intensity contributions caused by dynamical scattering and electron channelling[27], projections along zone axis orientations were avoided. The tilt angles range from $-72.6^{\circ}$ to $+72.6^{\circ}$ with equal slope increments. To more closely approximate realistic experimental conditions, several additional modifications were made to generate the simulated data. First, the tilt angles were continuously shifted from $0^{\circ}$ to $0.5^{\circ}$ over the process of the tilt series and the magnification of the images was continuously changed from 0 to 0.2%. Second, each projection in the tilt series was arbitrarily shifted along the $x$ and $y$ axes, where the electron beam direction is parallel to the $z$ axis. Last, Poisson noise was added to the projections of the tilt series with a total electron dose of $6.1 \times 10^6$ e Å$^{-2}$. Supplementary Fig. 3 shows a linear projection of the model at $0^{\circ}$ and the corresponding multislice STEM projection. The apparent increase of the atom size in the multislice projection was mainly caused by the nonlinear and diffraction effects in the nanoparticle.

The 55 projections were aligned to a common tilt axis with the centre-of-mass method, and were then reconstructed with the EST algorithm. Supplementary Fig. 4b, d, f shows three 2.5-Å-thick central slices of the 3D reconstruction in the $x$–$y$, $z$–$x$ and $z$–$y$ planes. Although the missing wedge problem is not completely solved (the top and bottom parts in Supplementary Fig. 4f) and the size of the reconstructed atoms is increased mainly due to the nonlinear and diffraction effects, the atomic positions and grain boundaries in the 3D reconstruction are consistent with the model. The simulation results indicate that the centre-of-mass and EST methods can be used

[1]Department of Physics and Astronomy and California NanoSystems Institute, University of California, Los Angeles, California 90095, USA. [2]National Center for Electron Microscopy, Lawrence Berkeley National Laboratory, Berkeley, California 94720, USA.
*These authors contributed equally to this work.

to achieve an atomic-scale resolution reconstruction from a tilt series of 55 projections with a missing wedge, nonlinear effects, Poisson noise and experimental errors.

Next, the centre-of-mass and EST methods were applied to experimental tilt series acquired from gold nanoparticles. Nanoparticles are an important class of materials with properties different from either molecules or bulk solids[13–15], and nano-gold is among the most widely studied of this class of material owing to its broad applications in chemistry, biology, materials science, nanoscience and nanotechnology[16]. In this study, we imaged gold particles with a diameter of ~10 nm because smaller particles are not as stable under an electron beam[13,22]. To reduce the electron dose, we used a low-exposure data acquisition scheme with a 300-keV ADF-STEM (Methods). When focusing an image, a nearby nanoparticle was first viewed (not the particle of interest), thus reducing the unnecessary radiation dose to the particle under study. Using this scheme, we acquired several tomographic tilt series of gold nanoparticles. Supplementary Fig. 5 shows a tilt series of 69 projections and their Fourier transforms, with a total electron dose of $\sim 7.6 \times 10^6$ e Å$^{-2}$. Supplementary Fig. 6 shows three 0° projections and their Fourier transforms measured during the acquisition of this tilt series to monitor the effects of radiation damage. Although some minor shape changes occurred, the crystal lattice structure of the particle remained consistent throughout the experiment.

To investigate the nonlinear effects in the experiment, we simulated an ~10-nm gold particle with icosahedral symmetry and performed multislice STEM calculations on an 11.5-Å-thick slab of this particle[26] (Supplementary Fig. 7). Although the atom size was increased, mainly owing to the nonlinear diffraction and dynamical scattering effects, the multislice STEM projection exhibits a crystal lattice structure consistent with the model. We then calculated a tilt series for a 2.5-Å central slice using the multislice simulations. The tilt series consists of 69 projections with a tilt range of ±72.6°. Supplementary Fig. 8 shows the model and reconstructed slices. The atomic positions and the internal grain boundaries are resolved, except in a very few places owing to the nonlinear effects in the projections.

After investigating the nonlinear effects, we performed post data analysis of the experimental tilt series (Methods), and aligned the projections with the centre-of-mass method. To reconstruct the 3D structure, we first estimated a loose 3D support, defined to be larger than the particle boundary. After 500 iterations of the EST algorithm, the reconstruction was used to determine a tight support (that is, close to the true boundary of the particle). Using the tight support, we ran another 500 iterations and obtained a final 3D structure. To examine the quality of the reconstruction, we calculated 69 projections from the final 3D structure and found the average normalized discrepancy with the measured projections to be 6.7% (Supplementary Methods and Supplementary Table 1). Representative measured and calculated projections at different particle orientations are shown in Fig. 1 and Supplementary Fig. 9. Although there are some minor differences between the two projections, the overall shape and lattice structure agree well. To more rigorously examine the accuracy of the reconstruction, an EST reconstruction was performed from 68 experimental projections by removing the 7.1° projection. The 3D reconstruction was then projected back to calculate the projection at 7.1°, which is consistent with the experimentally measured one (Supplementary Fig. 10).

To estimate the resolution achieved in the reconstruction, we chose a 3.36-Å-thick central slice in the $x$–$y$ plane. Figure 2a, b shows the slice and its Fourier transform, in which the distance between two neighbouring atom columns and the location of the Bragg peaks indicate that a resolution of 2.4 Å was achieved in the $x$ and $y$ directions. To estimate the resolution along the $z$ axis (beam direction), we selected a 3.36-Å-thick slice with the horizontal axis along the $z$ axis (Fig. 2c, d). The resolution close to the $z$ axis was determined to be 2.4 Å. Individual atoms are visible in some regions of the slices, but not all atoms can be identified in the slices. Supplementary Fig. 11 shows two 3.36-Å-thick slices of the nanoparticle in a different orientation,

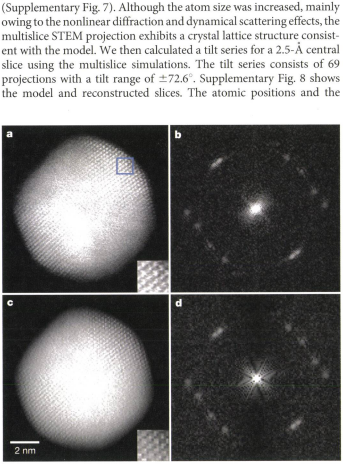


**Figure 1 | Evaluation of the 3D reconstruction quality. a–d**, Representative measured (**a**) and calculated (**c**) projections and their Fourier transforms (respectively **b**, **d**) at tilt angle 7.1°. Insets in **a** and **c** show the projected atomic positions inside the blue square in the main panel. The overall shape of the nanoparticle and the location of the Bragg peaks agree well, indicating a good quality 3D reconstruction. This gold nanoparticle is the same as studied in Figs 2–4.

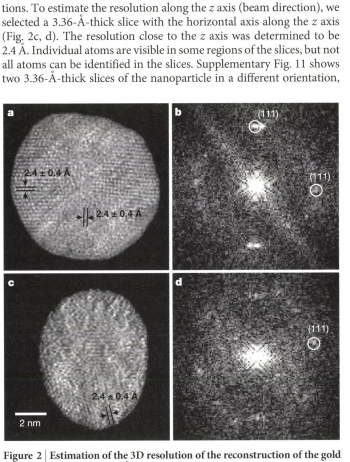


**Figure 2 | Estimation of the 3D resolution of the reconstruction of the gold nanoparticle. a**, **b**, A 3.36-Å thick central slice in the $x$–$y$ plane (**a**) and its Fourier transform (**b**), indicating that a resolution of 2.4 Å corresponding to the gold (111) lattice was achieved along the $x$ and $y$ axes. **c**, **d**, A 3.36-Å-thick slice in the $z$–$y$ plane (**c**) and its Fourier transform (**d**) where the horizontal axis is along the $z$ axis (beam direction). The resolution in the $z$ axis was estimated to be 2.4 Å. Individual atoms are visible in some regions of the slices, but not all atoms can be identified in the slices.

exhibiting crystal lattice structure that is not present in Fig. 2a and c. The apparent flattening of the particle along the beam axis was also observed in the 3D reconstructions (Fig. 2 and Supplementary Movie 1), and was probably caused by the interaction between the nanoparticle and the Si substrate.

To visualize the internal structure and the morphology of the gold nanoparticle, we generated 3D volume and iso-surface renderings of the reconstruction, in which both surface and internal lattice structures are visible (Supplementary Movies 1 and 2). Figure 3a, b shows volume renderings of the nanoparticle and their Fourier transforms (insets) at the two- and three-fold symmetry orientations. The corresponding iso-surface renderings at the same orientations are shown in Fig. 3c and d. The overall 3D shape and facets of the nanoparticle are consistent with an icosahedron (insets in Fig. 3c and d). To identify internal 3D grains, we applied the 3D Fourier transform to the reconstruction. By identifying the Bragg peaks of each major grain and applying the 3D inverse Fourier transform to the selected Bragg peaks, we determined four major 3D grains inside the gold nanoparticle (Methods). Figure 4 and Supplementary Movie 3 show a volume rendering of the four grains in three dimensions, in which grains 1, 2 and grains 3, 4 are related by mirror-reflection across the horizontal interfaces marked by dotted lines. The angle enclosed by close-packed planes across these interfaces was measured to be $69.9^\circ \pm 0.8^\circ$ between grains 1 and 2, and $71.3^\circ \pm 0.8^\circ$ between grains 3 and 4, both of which are consistent with the angle for a face-centred-cubic twin boundary ($70.53^\circ$). By applying the same method to some other Bragg peaks, we identified 3D grains in the top and bottom parts of the particle (Supplementary Fig. 12). The surface morphology and the internal lattice structures suggest that this is a distorted icosahedral multiply twinned particle, typically found for nano-gold in the size range above 10 nm (ref. 29).

By combining the centre-of-mass alignment technique and the EST reconstruction method with an ADF-STEM, we have determined the 3D structure of a ~10-nm gold nanoparticle at 2.4 Å resolution from a tilt series of 69 projections with a missing wedge. Several grains are identified inside the nanoparticle in three dimensions. Although individual

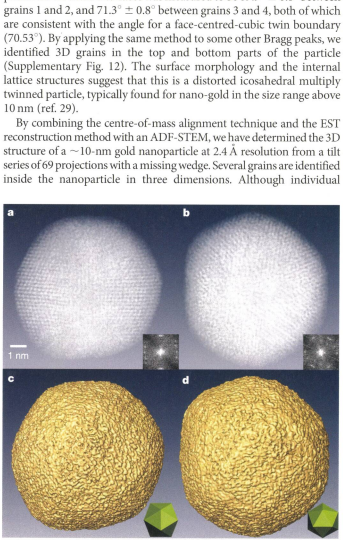


**Figure 3 | 3D structure of the reconstructed gold nanoparticle. a**, **b**, 3D volume renderings of the nanoparticle and their Fourier transforms (insets) at the two-fold (**a**) and three-fold (**b**) symmetry orientations. **c**, **d**, Iso-surface renderings of the nanoparticle at the two-fold (**c**) and three-fold (**d**) symmetry orientations. Insets show a model icosahedron at the same orientations.

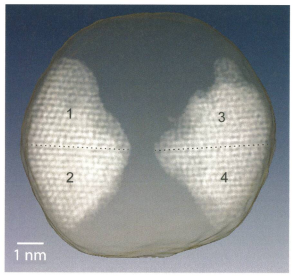


**Figure 4 | Identification of four major grains inside the gold nanoparticle in three dimensions.** Grains 1, 2 and grains 3, 4 are related by mirror-reflection across the horizontal interfaces marked by dotted lines. The angle enclosed by close-packed planes across these interfaces was measured to be $69.9^\circ \pm 0.8^\circ$ between grains 1 and 2, and $71.3^\circ \pm 0.8^\circ$ between grains 3 and 4, both of which are consistent with the angle for a face-centred cubic twin boundary ($70.53^\circ$).

atoms are visible in some regions of the nanoparticle, we cannot definitively locate all of the atoms inside the particle. In order to identify all the atoms in the particle (estimated to be ~23,800) without using atomicity and bond information, a resolution higher than 2.4 Å is needed, which requires future developments. With aberration-corrected STEM[4,23,24], better 3D resolution and image quality should be achievable, but extended depth-of-field techniques may have to be applied to the tilt series before the EST reconstruction can be performed. Compared to atom-probe tomography[30], this non-destructive technique can not only handle isolated nanoparticles, but also provide the 3D local structure of complex nanomaterials at high resolution.

## METHODS SUMMARY

Gold nanoparticles with a size of ~10 nm (Ted Pella) were supported on 5-nm-thick Si membranes (TEMwindows.com), which can withstand plasma cleaning for a longer period than carbon substrates to alleviate carbon contamination. Tomographic tilt series with equal slope increments were acquired from the gold nanoparticles by using an ADF-STEM (FEI Titan 80-300). The tilt angles ($\theta$) were determined by[16,25] $\theta = -\tan^{-1}[(N+2-2n)/N]$ for $n = 1, \ldots, N$ and $\theta = \pi/2 - \tan^{-1}[(3N+2-2n)/N]$ for $n = N+1, \ldots, 2N$ with $N = 32$ or 64 in this experiment. The angles beyond $\pm 72.6^\circ$ were not accessible owing to the geometry of the support grid. To monitor the radiation induced stability effect, several projections at the same particle orientation were measured during the acquisition of each tilt series (Supplementary Fig. 6). To improve the 3D reconstruction and enhance the signal to noise ratio, the background of the projections was subtracted and $2 \times 2$ pixel binning was performed for each projection. After post data analysis, the tilt series was aligned with the centre-of-mass method (Methods). The reconstruction of the aligned tilt series was conducted using the EST method, which iterated back and forth between real and reciprocal space with constraints enforced in real space and measured data in reciprocal space (Methods, Supplementary Methods and Supplementary Fig. 2). To examine the reconstruction quality, the reconstructed 3D structure was projected back to obtain 69 projections, which were compared to the corresponding measured ones. An average $R_{real}$ (Supplementary Methods) was calculated to be 6.7%, indicating a good quality reconstruction (Fig. 1, Supplementary Table 1).

**Full Methods** and any associated references are available in the online version of the paper at www.nature.com/nature.

**Received 18 April 2011; accepted 9 February 2012.**

1. Williams, D. B. & Carter, C. B. *Transmission Electron Microscopy: A Textbook for Materials Science* 2nd edn (Springer, 2009).

2. Spence, J. C. H. *Experimental High-Resolution Electron Microscopy* 3rd edn (Oxford Univ. Press, 2003).
3. Frank, J. *Three-Dimensional Electron Microscopy of Macromolecular Assemblies* (Oxford Univ. Press, 2006).
4. Batson, P. E., Dellby, N. & Krivanek, O. L. Sub-ångstrom resolution using aberration corrected electron optics. *Nature* **418,** 617–620 (2002).
5. Haider, M. *et al.* Electron microscopy image enhanced. *Nature* **392,** 768–769 (1998).
6. Erni, R., Rossell, M. D., Kisielowski, C. & Dahmen, U. Atomic-resolution imaging with a sub-50-pm electron probe. *Phys. Rev. Lett.* **102,** 096101 (2009).
7. Frank, J. *Electron Tomography* (Plenum, 1992).
8. Midgley, P. A. & Weyland, M. 3D electron microscopy in the physical sciences: the development of *Z*-contrast and EFTEM tomography. *Ultramicroscopy* **96,** 413–431 (2003).
9. Lučič, V., Förster, F. & Baumeister, W. Structural studies by electron tomography: from cells to molecules. *Annu. Rev. Biochem.* **74,** 833–865 (2005).
10. Midgley, P. A. & Dunin-Borkowski, R. E. Electron tomography and holography in materials science. *Nature Mater.* **8,** 271–280 (2009).
11. Arslan, I., Yates, T. J. V., Browning, N. D. & Midgley, P. A. Embedded nanostructures revealed in three dimensions. *Science* **309,** 2195–2198 (2005).
12. Van Aert, S., Batenburg, K. J., Rossell, M. D., Erni, R. & Van Tendeloo, G. Three-dimensional atomic imaging of crystalline nanoparticles. *Nature* **470,** 374–377 (2011).
13. Marks, L. D. Experimental studies of small particle structures. *Rep. Prog. Phys.* **57,** 603–649 (1994).
14. Billinge, S. J. L. & Levin, I. The problem with determining atomic structure at the nanoscale. *Science* **316,** 561–565 (2007).
15. Yacamán, M. J., Ascencio, J. A., Liu, H. B. & Gardea-Torresdey, J. Structure shape and stability of nanometric sized particles. *J. Vac. Sci. Technol. B* **19,** 1091–1023 (2001).
16. Lee, E. *et al.* Radiation dose reduction and image enhancement in biological imaging through equally sloped tomography. *J. Struct. Biol.* **164,** 221–227 (2008).
17. Kak, A. C. & Slaney, M. *Principles of Computerized Tomographic Imaging* (SIAM, Philadelphia, 2001).
18. Fahimian, B. P., Mao, Y., Cloetens, P. & Miao, J. Low dose X-ray phase-contrast and absorption CT using equally-sloped tomography. *Phys. Med. Biol.* **55,** 5383–5400 (2010).
19. Mao, Y., Fahimian, B. P., Osher, S. J. & Miao, J. Development and optimization of regularized tomographic reconstruction algorithms utilizing equally-sloped tomography. *IEEE Trans. Image Process.* **19,** 1259–1268 (2010).
20. Jiang, H. *et al.* Quantitative 3D imaging of whole, unstained cells by using X-ray diffraction microscopy. *Proc. Natl Acad. Sci. USA* **107,** 11234–11239 (2010).
21. Bar Sadan, M. *et al.* Toward atomic-scale bright-field electron tomography for the study of fullerene-like nanostructures. *Nano Lett.* **8,** 891–896 (2008).
22. Bovin, J.-O., Wallenberg, R. & Smith, D. J. Imaging of atomic clouds outside the surfaces of gold crystals by electron microscopy. *Nature* **317,** 47–49 (1985).
23. Muller, D. A. Structure and bonding at the atomic scale by scanning transmission electron microscopy. *Nature Mater.* **8,** 263–270 (2009).
24. Pennycook, S. J. & Nellist, P. D. *Scanning Transmission Electron Microscopy: Imaging and Analysis* 1st edn (Springer, 2011).
25. Miao, J., Föster, F. & Levi, O. Equally sloped tomography with oversampling reconstruction. *Phys. Rev. B* **72,** 052103 (2005).
26. Kirkland, E. J. *Advanced Computing in Electron Microscopy* 2nd edn (Springer, 2010).
27. Howie, A. Diffraction channelling of fast electrons and positrons in crystals. *Phil. Mag.* **14,** 223–237 (1966).
28. Daniel, M. C. & Astruc, D. Gold nanoparticles: assembly, supramolecular chemistry, quantum-size-related properties, and applications toward biology, catalysis, and nanotechnology. *Chem. Rev.* **104,** 293–346 (2004).
29. Barnard, A. S., Young, N. P., Kirkland, A. I., van Huis, M. A. & Xu, H. Nanogold: a quantitative phase map. *ACS Nano* **3,** 1431–1436 (2009).
30. Arslan, I., Marquis, E. A., Homer, M., Hekmaty, M. & Bartelt, N. C. Towards better 3-D reconstructions by combining electron tomography and atom-probe tomography. *Ultramicroscopy* **108,** 1579–1585 (2008).


**Supplementary Information** is linked to the online version of the paper at www.nature.com/nature.

**Acknowledgements** We thank E. J. Kirkland for help with multislice STEM calculations, R. F. Egerton, Z. H. Zhou and J. A. Rodriguez for discussions and I. Atanasov for assistance in data acquisition. The tomographic tilt series were acquired at the Electron Imaging Center for NanoMachines of the California NanoSystems Institute. This work was partially supported by UC Discovery/TomoSoft Technologies (IT107-10166).

**Author Contributions** J.M. conceived the overall project; M.C.S., M.M., C.Z., B.C.R. and J.M. designed and conducted the experiments; C.Z., R.X., C.-C.C., P.E. and J.M. did multislice STEM calculations; C.-C.C. and J.M. performed the data analysis and image reconstruction; U.D., J.M., C.-C.C., M.C.S., M.M. and B.C.R interpreted the results, and J.M., M.C.S., C.-C.C. and M.M. wrote the manuscript. All authors commented on the manuscript.

**Author Information** Reprints and permissions information is available at www.nature.com/reprints. The authors declare no competing financial interests. Readers are welcome to comment on the online version of this article at www.nature.com/nature. Correspondence and requests for materials should be addressed to J.M. (miao@physics.ucla.edu).

LETTER

doi:10.1038/nature10874

# Large-scale vortex lattice emerging from collectively moving microtubules

Yutaka Sumino[1]*, Ken H. Nagai[2]*, Yuji Shitaka[3], Dan Tanaka[4]‡, Kenichi Yoshikawa[5], Hugues Chaté[6] & Kazuhiro Oiwa[3,7]

**Spontaneous collective motion, as in some flocks of bird and schools of fish, is an example of an emergent phenomenon. Such phenomena are at present of great interest[1–5] and physicists have put forward a number of theoretical results that so far lack experimental verification[6–8]. In animal behaviour studies, large-scale data collection is now technologically possible, but data are still scarce and arise from observations rather than controlled experiments. Multicellular biological systems, such as bacterial colonies or tissues[9,10], allow more control, but may have many hidden variables and interactions, hindering proper tests of theoretical ideas. However, in systems on the subcellular scale such tests may be possible, particularly in *in vitro* experiments with only few purified components[11–13]. Motility assays, in which protein filaments are driven by molecular motors grafted to a substrate in the presence of ATP, can show collective motion for high densities of motors and attached filaments. This was demonstrated recently for the actomyosin system[14,15], but a complete understanding of the mechanisms at work is still lacking. Here we report experiments in which microtubules are propelled by surface-bound dyneins. In this system it is possible to study the local interaction: we find that colliding microtubules align with each other with high probability. At high densities, this alignment results in self-organization of the microtubules, which are on average 15 μm long, into vortices with diameters of around 400 μm. Inside the vortices, the microtubules circulate both clockwise and anticlockwise. On longer timescales, the vortices form a lattice structure. The emergence of these structures, as verified by a mathematical model, is the result of the smooth, reptation-like motion of single microtubules in combination with local interactions (the nematic alignment due to collisions)—there is no need for long-range interactions. Apart from its potential relevance to cortical arrays in plant cells[16,17] and other biological situations, our study provides evidence for the existence of previously unsuspected universality classes of collective motion phenomena.**

Our experimental *in vitro* motility assay consisted of dynein motor proteins grafted to a glass surface at a density of 750–2,500 molecules per square micrometre and to fluorescently labelled, stabilized microtubules (details can be found in Supplementary Methods). We used inner-arm dynein subspecies c (dynein c) purified from *Chlamydomonas* flagella. This drove the microtubules, with their plus ends leading, at a mean velocity of ~12 $\mu m\,s^{-1}$ *in vitro* at 23 °C in the presence of 1 mM ATP, while rotating them around their longitudinal axis in a clockwise direction as viewed from their minus ends[18,19]. ('Plus' and 'minus' here refer to microtubule polarity.) When introduced in a flow cell, the microtubules did not move and bound to the dynein-c-coated glass surface in the absence of ATP[18,19]. On addition of 1 mM Mg–ATP, they started moving smoothly on the surface at a fairly constant speed. No preferred direction of isolated microtubule motion was observed. The smoothness and isotropy of motion reflect the fact that relatively many, randomly oriented, dyneins were attached at any time to a given microtubule.

Using microtubules at a concentration of 40 $\mu g\,ml^{-1}$, which is a few times greater than in conventional assays[18], we found the density of attached microtubules to be 0.05 $\mu m^{-2}$ (there were five microtubules, 15.6 ± 7.3 μm in length (mean ± s.d., $n = 257$), per 100 $\mu m^2$). On addition of ATP (at 0 min), we observed many aligning collisions (discussed further below) that gradually led to streams along which dozens of microtubules moved in both directions. The size of a stream increased in time (by more than 10 μm in width and more than 100 μm in length) (12 min; Fig. 1a). The streams started to meander over the surface typically after 10 min. At 10–20 min, some vortices appeared (17 min; Fig. 1a and Supplementary Movie 1) and eventually covered the flow cell almost entirely, except for the area less than 500 μm away from the boundaries (Fig. 1b). The shape of the vortices gradually changed over time but their diameters were almost constant, at 400 μm (major axis, 443 ± 64 μm (s.d., $n = 40$); minor axis, 390 ± 59 μm (s.d., $n = 40$)). At this late stage, the vortices showed a tendency to arrange their positions into a hexagonal lattice, although not perfectly. A given vortex consists of a sparse core and a dense peripheral annulus inside which microtubules move both clockwise and anticlockwise in small streams and slide past each other (Fig. 2 and Supplementary Movie 2). That is, the streams show nematic rather than polar order. Microtubules were never trapped in a vortex: they would circulate inside one vortex for some time before moving to a neighbouring one or travelling farther and starting to revolve around a more distant core.

As the first step in understanding vortex formation, we examined the interactions between microtubules. We decreased their density to 0.5–1 $\mu g\,ml^{-1}$ to focus on pair interactions between isolated microtubules. We examined 393 pair collision events. No significant interaction was detected until the pair collided, indicating that long-range, 'hydrodynamic' effects are negligible. On collision, strong interactions due to volume exclusion occurred overwhelmingly (80% of events), leading either to alignment or anti-alignment (70%; Fig. 3a, b) or to the stoppage of one microtubule to prevent it from hitting the other (10%; Fig. 3c). In the remaining fraction of events (20%), the microtubules crossed each other with little effect on their trajectories (Fig. 3d, e; see also Supplementary Movie 3). In aligning and anti-aligning collisions, the trajectory of one microtubule undergoes a sharp turn (Fig. 3a, b) and alignment was observed to be near perfect. We believe that this is due to the leading end of the microtubule being relatively free from attached dyneins by comparison with rest of it: on meeting an obstacle, the tip of the microtubule can then bend more easily. Thus, the outgoing angle is near 0 or $\pi$ in aligning events, irrespective of the value of the incoming angle, $\phi$. In stoppage and crossing events, the orientations of both microtubules remain roughly unchanged. (During stoppage events, one microtubule simply 'waits'

[1]Faculty of Education, Aichi University of Education, Aichi 448-8542, Japan. [2]Department of Physics, Graduate School of Science, The University of Tokyo, Tokyo 113-0033, Japan. [3]Advanced ICT Research Institute, National Institute of Information and Communications Technology, Kobe 651-2492, Japan. [4]Department of Complex Systems Science, Graduate School of Information Science, Nagoya University, Nagoya 464-8601, Japan. [5]Department of Physics, Graduate School of Science, Kyoto University and ICORP, JST, Kyoto 606-8502, Japan. [6]Service de Physique de l'Etat Condensé, CEA-Saclay, 91191 Gif-sur-Yvette, France. [7]Graduate School of Life Science, University of Hyogo, Harima Science Park City, Hyogo 678-1297, Japan.

*These authors contributed equally to this work.

‡Deceased.

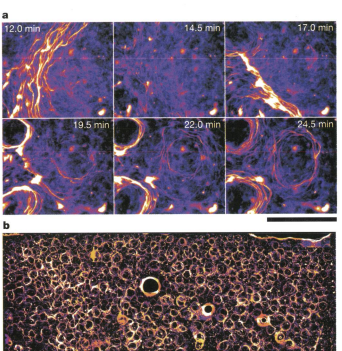


**Figure 1 | Emergence of vortices of microtubules.** False-colour images. **a**, Formation process of vortex pattern: 0 min corresponds to the time of injection of ATP. Streams appeared around 5 min after this injection. At 12 min, streams started to meander. Vortices started to appear around 17 min, when meandering streams contacted one another. Once vortices had formed, they grew steadily (22 min). Scale bar, 500 μm. **b**, Large-scale lattice of vortices. Vortices can be observed everywhere on the surface of the flow cell. Three air bubbles in the flow cell can be seen distinctively owing to their greater size and thicker edges. Scale bar, 2 mm.

until the other has passed (Fig. 3c).) Given that the outcome of each type of collision is well defined, we represented the complete collision statistics in terms of the probability of each collision type as a function of $\phi$ only (Fig. 3d). We observe an overall symmetry around $\phi = \pi/2$, with alignment and anti-alignment occurring mainly for small ($\phi \approx 0$) and large ($\phi \approx \pi$) angles, respectively, whereas stoppage and crossing dominate for $\phi \approx \pi/2$. Thus, we conclude that near-perfect *nematic* alignment is induced by direct collision.

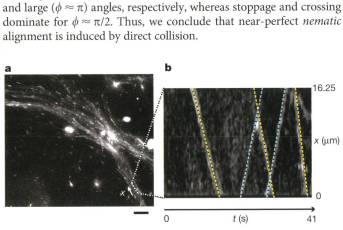


**Figure 2 | Nematic order inside a vortex stream.** In this experiment, the microtubules were all stained fluorescent but approximately 0.1% of microtubules were stained to be more fluorescent than the rest. **a**, Close-up of vortex. Scale bar, 20 μm. **b**, Spatiotemporal diagram of a magnified region of the vortex shown in **a**. Yellow lines indicate microtubules travelling from top to bottom, and blue lines indicate microtubules travelling from bottom to top.

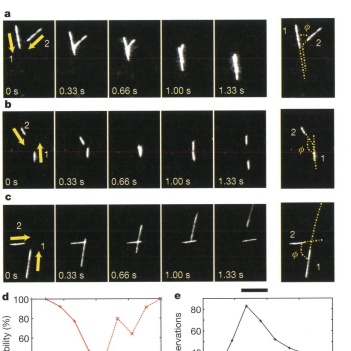


**Figure 3 | Collision between microtubules.** **a**–**c**, Three different types of collision between two microtubules. In **a** and **b**, microtubule 2 collides with the side of microtubule 1 and changes its direction of motion abruptly, leading to almost perfect alignment (**a**) or anti-alignment (**b**). In **c**, microtubule 2 stops until microtubule 1 has passed. Scale bar, 10 μm. **d**, Probability of each interaction type as a function of $\phi$ (see right-most images in **a**–**c**). We analysed 393 events. Red lines represent alignment (solid) and anti-alignment (dotted) events; blue dotted lines represent stopping events; yellow solid lines represent crossing-over events. **e**, Total number of observations in each angular bin.

Constant-speed particles aligning nematically in the presence of noise have been studied recently in mathematical models of self-propelled rods, which were shown to give rise to unexpected collective dynamics but not to vortical structures[20]. Our motility assay has properties not present in simple models of colliding rods. One such feature is the nature of the motion of isolated microtubules: as already mentioned, their reptation-like movement yields smooth but constantly turning trajectories, unlike both straight ballistic motion and the ragged behaviour of random walkers submitted to rotational diffusion, the individual dynamics adopted in rods models[20–22]. We analysed the trajectories of isolated microtubules for durations of up to 350 s (Fig. 4a, left). Here we further decreased their concentration, to 4.8 ng ml$^{-1}$. The speed (tangential velocity) of the microtubules fluctuated in time, with a mean of $v_0 = 8.75$ μm s$^{-1}$. We also measured the direction of motion, $\theta$ (where $\theta = 0$ and $\pi/2$ correspond to the direction of the $x$ and $y$ axes, respectively), and the instantaneous angular velocity, and found them to have no significant correlation with the instantaneous speed. This allowed us to neglect the speed fluctuations and focus on $\theta$.

A closer look at a representative trajectory (Fig. 4a, right) reveals small-amplitude transverse oscillations, which might be caused by the rotation of the microtubule around its axis[18]. After an appropriate filtering, based on the Savitzky–Golay method, to eliminate these oscillations (Supplementary Methods), we obtained the variation of curvature, $\kappa = \mathrm{d}\theta/\mathrm{d}s$, as a function of distance, $s$, along the trajectory and calculated its autocorrelation (Fig. 4b). (With this definition, $\kappa$ can be positive

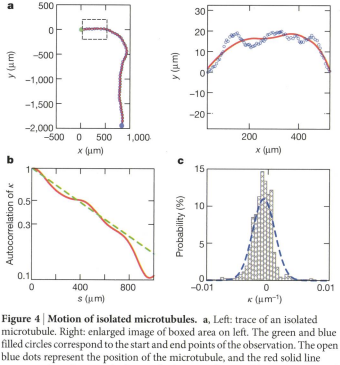


**Figure 4 | Motion of isolated microtubules.** **a**, Left: trace of an isolated microtubule. Right: enlarged image of boxed area on left. The green and blue filled circles correspond to the start and end points of the observation. The open blue dots represent the position of the microtubule, and the red solid line corresponds to the smoothed curve. **b**, Autocorrelation of the trajectory curvature, $\kappa$, with respect to the distance along a trajectory, $s$ (red solid line). The green dotted line is an exponential fit with the correlation length $s_0 = 542 \pm 4\,\mu\text{m}$. **c**, Distribution of $\kappa$ values observed (bars) and Gaussian fit (dashed blue line): mean, $\kappa_0 = -7.1 \times 10^{-4}\,\mu\text{m}^{-1}$; s.d., $\sigma_\kappa = 1.8 \times 10^{-3}\,\mu\text{m}^{-1}$.

(anticlockwise motion) or negative (clockwise motion).) Fitting the result with the exponential function $\exp(-s/s_0)$, we found the persistent length, $s_0$, of curvature to be of the order of 500 μm. The distribution of $\kappa$ values observed is roughly Gaussian with mean $\kappa_0 = -7.1 \times 10^{-4}\,\mu\text{m}^{-1}$ and standard deviation $\sigma_\kappa = 1.8 \times 10^{-3}\,\mu\text{m}^{-1}$ (Fig. 4c). We note that these numbers correspond to length scales that are rather large and of the same order as the vortex diameter, and that the small negative value of $\kappa_0$ indicates a preference for clockwise turning in single-microtubule trajectories, which is probably a consequence of the clockwise rotation around of the microtubules around their axes while in motion[23]. A detailed molecular-level study should confirm this.

We constructed a mathematical model for the collective motion of microtubules in our experimental motility assay by incorporating the few ingredients uncovered in our analysis of the trajectories of single microtubules and of pair collisions. A deliberate choice of minimality was made, to stress that with only these very few features all observed collective phenomena are reproduced, and to allow for numerical simulations of millions of objects: for instance, the dynein motors driving the microtubules are not modelled explicitly; the hydrodynamic interactions induced by the fluid are neglected, in agreement with our observation that only direct contact modifies the microtubules' motion. The microtubules themselves are not represented as flexible polymers: here, in the spirit of ref. 6, they are identical point particles moving at constant speed, $v_0$ (the speed fluctuations are also neglected). In direct agreement with the observations reported in Fig. 4, the free motion of particle $i$, with position $\mathbf{x}_i$ and orientation $\theta_i$, is a biased Ornstein–Uhlenbeck process, $\omega_i(t)$, with correlation time $\tau = s_0/v_0$, acting on the particle's instantaneous angular velocity, $\mathrm{d}\theta_i/\mathrm{d}t$:

$$\begin{aligned} \frac{\mathrm{d}\mathbf{x}_i}{\mathrm{d}t} &= v_0(\mathbf{e}_x \cos\theta_i + \mathbf{e}_y \sin\theta_i) \\ \frac{\mathrm{d}\theta_i}{\mathrm{d}t} &= \omega_i \end{aligned} \tag{1}$$

$$\frac{\mathrm{d}\omega_i}{\mathrm{d}t} = -\frac{1}{\tau}(\omega_i - \omega_0) + \xi(t) \tag{2}$$

where $\mathbf{e}_x$ and $\mathbf{e}_y$ are respectively unit vectors in the $x$ and $y$ directions, $\xi(t)$ is a Gaussian white noise with zero mean and variance $\sigma^2 = 2v_0^2\sigma_\kappa^2/\tau = 2v_0^3\sigma_\kappa^2/s_0$, and $\omega_0 = v_0\kappa_0$ is the preferred non-zero angular velocity induced by the mean curvature, $\kappa_0$. This ensures that all correlation properties of the curvature measured in the experiment are reproduced (Supplementary Methods).

These equations must be complemented with an interaction term. Only the nematic alignment collisions are modelled (because stoppage and crossings do not substantially modify the microtubule orientations). As they were observed to induce much sharper turns in the trajectories (Fig. 3a, b) than the spontaneous curvature changes of free microtubules (Fig. 4a), these collisions are modelled as a nematic alignment term acting directly on the particle orientation $\theta_i$, that is, in equation (1), and not on the angular velocity, $\omega_i$. Following previous studies[6,20], we replaced explicit pair collisions by an effective alignment within an interaction range, $l$, which is naturally chosen to be the typical microtubule length. Equation (1) is thus replaced by

$$\begin{aligned} \frac{\mathrm{d}\mathbf{x}_i}{\mathrm{d}t} &= v_0(\mathbf{e}_x \cos\theta_i + \mathbf{e}_y \sin\theta_i) \\ \frac{\mathrm{d}\theta_i}{\mathrm{d}t} &= \omega_i + \frac{\alpha}{n_i(t)} \sum_{j\sim i} \sin\left(2(\theta_j - \theta_i)\right) \end{aligned} \tag{3}$$

where $\alpha$ is a parameter and the sum is over the $n_i(t)$ particles $j$ within distance $l$ of particle $i$ at time $t$.

Numerical simulations of equations (2) and (3) using experimentally obtained parameters (Supplementary Methods) show the emergence, from disordered initial conditions, of large-scale vortices with a diameter of the same order as those observed in experiments (Fig. 5a and Supplementary Movie 4).

Inside vortices, the simulated particles revolved both clockwise and anticlockwise, with the majority moving clockwise, as expected from the non-zero value of $\omega_0$ used. The number of vortices increased over time and saturated, leading eventually to a regular hexagonal lattice structure. As in our experimental observations, vortices did not form at low densities. To see this more clearly, we calculated $u^2(n)$, the variance of the local density in small boxes containing $n_a$ particles on average, as a function of the rescaled average density, $\rho_a$ (the actual density multiplied by $l^2$; Supplementary Methods), the other parameters being kept fixed (Fig. 5b). For $\rho_a < 0.4$, the system remains disordered and $u^2(n)/n_a$ is almost constant, indicating the absence of density structures (Fig. 5b, right, images (i) and (ii)). However, $u^2(n)/n_a$ increased with $\rho_a$ for $\rho_a > 0.4$, indicating the appearance of a density pattern, which we checked visually to be a vortex lattice (Fig. 5b, right, images (iii) and (iv)). This result is consistent with our experimental observation that the vortex pattern disappears when the density of microtubules is halved (compare with Supplementary Fig. 1). We also performed numerical simulations in which we varied the rescaled correlation time, $\lambda = v_0\tau/l$ (Supplementary Methods), but kept all the other parameters fixed. Global nematic order without a density pattern was observed for $\lambda < 60$, but the system showed vortex formation for $\lambda > 60$ (Fig. 5c). Thus, the large persistence length and time of single-microtubule motion is necessary for the emergence of the vortices. Further information on the phase diagram of our mathematical model can be found in Supplementary Methods and Supplementary Fig. 2.

The study of our mathematical model thus shows that smooth trajectories of single microtubules and their direct collisions inducing sharp bends and nematic alignment—both experimentally observed—are sufficient, when associated with self-propulsion, to account for all observed collective properties. In particular, there is no theoretical reason to invoke, nor is experimental evidence of, long-range 'hydrodynamic' interactions or other 'collective effects' in our system. By

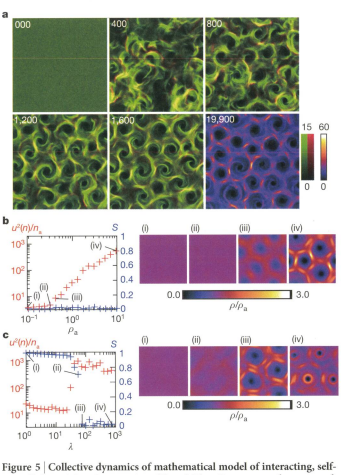


**Figure 5 | Collective dynamics of mathematical model of interacting, self-propelled particles.** See equations (2) and (3). **a**, Spontaneous formation of a vortex reproduced by our model. Each image is averaged for $\Delta T = 10$, where $T$ is simulation time rescaled by $l/v_0$. The brightest area corresponds to a density of 15 particles per unit area. Green and red respectively correspond to the densities of particles moving clockwise ($\omega < 0$) and anticlockwise ($\omega > 0$). Yellow regions indicate areas with clockwise and anticlockwise motion in approximately equal proportions. The area of the figure is $512 \times 512$ simulation cells. The last snapshot, at $T = 19{,}900$, shows the particle densities without differentiating between clockwise and anticlockwise motion, to make comparison with experimental results easy. **b**, Global nematic order parameter, $S$, and variance of the local density, $u^2(n)$ (calculated over boxes 4 simulation cells in linear size and $\Delta T = 10$), divided by the average density for the box, $n_s$, plotted against $\rho_a$. Corresponding density distributions are shown in images (i)–(iv) (each corresponds to a different value of $\rho_a$, as shown, and is a sum over 5,000 snapshots taken at intervals of $\Delta T = 1$ in a $256 \times 256$ system). Here we set the rescaled correlation time, $\lambda = v_0\tau/l$, to $\lambda = 100$. **c**, Same as **b**, but plotted against $\lambda$ with $\rho_a = 10$. The density distributions correspond to different values of $\lambda$, as shown.

contrast, such interactions were relied on to explain some of the collective phenomena observed in the actomyosin system[14]. We believe that our observations are a consequence of using dynein c motors; in fact, when kinesin was used instead of dynein, microtubules mostly crossed each other and vortex formation could not be observed (Supplementary Fig. 3). With dynein, collisions are frequent enough to induce large-scale order. We suppose that this is due to the mechanical properties of dynein molecules and the asymmetry of their molecular structure. The formation of vortices arises from the smoothness and the curvature persistence of trajectories of single microtubules, both of which properties are, we believe, the consequence of having a relatively large number of motors attached at any time (we estimate it to be of the order of 100).

The vortices observed in our motility assay possess unique features: their large scale (relative to the length of microtubules), the irrelevance of hydrodynamic interactions and the dominantly nematic order inside them distinguish them from the polar, small-scale vortices formed by swimming sperm cells confined in quasi-two-dimensional conditions[24]. Their stability in time, and their well-defined diameters also distinguish them from the unstable 'swirling patterns' reported in the actomyosin assay[14]. From a theoretical viewpoint, we are not aware of other models showing a large-scale vortex pattern of the type found here. In our model, the crucial feature introduced is the combination of smooth, reptation-like motion and sharp nematic alignment. This combination can be seen as the signature of a new class in the emerging landscape of universality classes of collective motion phenomena.

Returning to the biological relevance of our findings, we believe that they stress further the message, in various *in vivo* situations and in particular in plant cell cortical arrays[16,17,25,26], that simple physical collisions can induce the reorientation of microtubules, creating large-scale structures even in the absence, here, of crosslinkers[27,28]. Furthermore, there is a striking analogy between our analysis of microtubule collisions and that performed in plant cell cortex[17,26,29], although there is only treadmilling and no actual displacement of microtubules in the cortex. As shown in Fig. 3d, in our system the probability of aligning collisions is high at small incoming angles ($\phi = 0 \bmod \pi$) and decreases monotonically from 0 to $\pi/2$, as for 'zippering' (positive-end entrainment) of cortical microtubules.

Well-controlled *in vitro* experiments of the type reported here present crucial advantages due to the simplicity of the objects involved and the relative ease of collecting large amounts of data: not only can theoretical ideas be tested, but such experiments can reveal the importance of mechanisms previously ignored, and allow for quantitative analysis of features also present *in vivo*. They are and will remain invaluable tools for our understanding of active matter and biological organization processes.

## METHODS SUMMARY

We prepared inner-arm dynein and tubulin using standardized protocols[18]. Cy3-labelled microtubules were polymerized from a mixture of Cy3-tubulin and non-fluorescent tubulin and were stabilized using Taxol. Fractionated dynein c was diluted at various concentrations (27–90 $\mu g\,ml^{-1}$) in buffer solution containing 30 mM HEPES/KOH (pH 7.4), 5 mM $MgSO_4$, 1 mM DTT, 1 mM EGTA and 1 mg $ml^{-1}$ bovine serum albumin. The flow cell was flushed with the diluted dynein solution, incubated for 5 min and then washed using the buffer solution. Solution containing microtubules as well as 1 mM ATP and 1 mM DTT was introduced into the flow cell. Microtubules were visualized on an epifluorescence microscope. The vortex pattern, binary collisions and individual trajectories were observed with solutions of microtubules with respective concentrations of 40 $\mu g\,ml^{-1}$, 0.5–1 $\mu g\,ml^{-1}$ and 4.8 $ng\,ml^{-1}$. For single-trajectory analysis, the position of a microtubule was measured every $\Delta t = 0.68$ s.

**Received 14 October 2011; accepted 17 January 2012.**

1. Ballerini, M. *et al.* Interaction ruling animal collective behavior depends on topological rather than metric distance: evidence from a field study. *Proc. Natl Acad. Sci. USA* **105,** 1232–1237 (2008).
2. Buhl, J. *et al.* From disorder to order in marching locusts. *Science* **312,** 1402–1406 (2006).
3. Katz, Y., Tunstrøm, K., Ioannou, C. C., Huepe, C. & Couzin, I. D. Inferring the structure and dynamics of interactions in schooling fish. *Proc. Natl Acad. Sci. USA* **108,** 18720–18725 (2011).
4. Lukeman, R., Li, Y.-X. & Edelstein-Keshet, L. Inferring individual rules from collective behavior. *Proc. Natl Acad. Sci. USA* **107,** 12576–12580 (2010).
5. Sumpter, D. J. T. *Collective Animal Behavior* (Princeton Univ. Press, 2010).
6. Vicsek, T., Czirók, A., Ben-Jacob, E., Cohen, I. & Shochet, O. Novel type of phase transition in a system of self-driven particles. *Phys. Rev. Lett.* **75,** 1226–1229 (1995).
7. Toner, J., Tu, Y. & Ramaswamy, S. Hydrodynamics and phases of flocks. *Ann. Phys.* **318,** 170–244 (2005).
8. Ramaswamy, S. The mechanics and statistics of active matter. *Annu. Rev. Condens. Mat. Phys.* **1,** 323–345 (2010).
9. Zhang, H. P., Be'er, A., Florin, E.-L. & Swinney, H. L. Collective motion and density fluctuations in bacterial colonies. *Proc. Natl Acad. Sci. USA* **107,** 13626–13630 (2010).
10. Poujade, M. *et al.* Collective migration of an epithelial monolayer in response to a model wound. *Proc. Natl Acad. Sci. USA* **104,** 15988–15993 (2007).
11. Nédélec, F. J., Surrey, T., Maggs, A. C. & Leibler, S. Self-organization of microtubules and motors. *Nature* **389,** 305–308 (1997).

12. Surrey, T., Nédélec, F., Leibler, S. & Karsenti, E. Physical properties determining self-organization of motors and microtubules. *Science* **292,** 1167–1171 (2001).
13. Loose, M., Fischer-Friedrich, E., Ries, J., Kruse, K. & Schwille, P. Spatial regulators for bacterial cell division self-organize into surface waves *in vitro*. *Science* **320,** 789–792 (2008).
14. Schaller, V., Weber, C., Semmrich, C., Frey, E. & Bausch, A. R. Polar patterns of driven filaments. *Nature* **467,** 73–77 (2010).
15. Butt, T. *et al.* Myosin motors drive long range alignment of actin filaments. *J. Biol. Chem.* **285,** 4964–4974 (2010).
16. Yuan, M., Shaw, P. J., Warn, R. M. & Lloyd, C. W. Dynamic reorientation of cortical microtubules, from transverse to longitudinal, in living plant cells. *Proc. Natl Acad. Sci. USA* **91,** 6050–6053 (1994).
17. Wasteneys, G. O. & Ambrose, J. C. Spatial organization of plant cortical microtubules: close encounters of the 2D kind. *Trends Cell Biol.* **19,** 62–71 (2009).
18. Kagami, O. & Kamiya, R. Translocation and rotation of microtubules caused by multiple species of Chlamydomonas inner-arm dynein. *J. Cell Sci.* **103,** 653–664 (1992).
19. Sakakibara, H., Kojima, H., Sakai, Y., Katayama, E. & Oiwa, K. Inner-arm dynein c of *Chlamydomonas flagella* is a single-headed processive motor. *Nature* **400,** 586–590 (1999).
20. Ginelli, F., Peruani, F., Bär, M. & Chaté, H. Large-scale collective properties of self-propelled rods. *Phys. Rev. Lett.* **104,** 184502 (2010).
21. Kudrolli, A., Lumay, G., Volfson, D. & Tsimring, L. S. Swarming and swirling in self-propelled polar granular rods. *Phys. Rev. Lett.* **100,** 058001 (2008).
22. Peruani, F., Deutsch, A. & Bär, M. Nonequilibrium clustering of self-propelled rods. *Phys. Rev. E* **74,** 030904(R) (2006).
23. Kikushima, K. & Kamiya, R. Clockwise translocation of microtubules by flagellar inner-arm dyneins. *Biophys. J.* **94,** 4014–4019 (2008).
24. Riedel, I. H., Kruse, K. & Howard, J. A self-organized vortex array of hydrodynamically entrained sperm cells. *Science* **309,** 300–303 (2005).
25. Tindemans, S. H., Hawkins, R. J. & Mulder, B. M. Survival of the aligned: ordering of the plant cortical microtubule array. *Phys. Rev. Lett.* **104,** 058103 (2010).
26. Allard, J. F., Ambrose, J. C., Wasteneys, G. O. & Cytrynbaum, E. N. A mechanochemical model explains interactions between cortical microtubules in plants. *Biophys. J.* **99,** 1082–1090 (2010).
27. Hess, H. *et al.* Molecular self-assembly of "nanowires" and "nanospools" using active transport. *Nano Lett.* **5,** 629–633 (2005).
28. Schaller, V., Weber, C., Hammerich, B., Frey, E. & Bausch, A. R. Frozen steady states in active systems. *Proc. Natl. Acad. Sci. USA* **108,** 19183–19188 (2011).
29. Dixit, R. & Cyr, R. Encounters between dynamic cortical microtubules promote ordering of the cortical array through angle-dependent modifications of microtubule behavior. *Plant Cell* **16,** 3274–3284 (2004).

**Supplementary Information** is linked to the online version of the paper at www.nature.com/nature.

**Acknowledgements** We thank H. Sakakibara, Y. Uchida and R. Nakamori for the preparation of the material and observations. They as well as H. Kitahata are also thanked for discussions. Y. Sumino is supported by a Grant-in-Aid for Research Activity Start-up (no. 23840019), Grant-in-Aid for Scientific Research (B) (no. 21340023) and Grant-in-Aid for Scientific Research (A) (no. 20244067). K.H.N. would like to acknowledge the support of a fellowship from the JSPS (no. 23-1819).

**Author Contributions** K.O. discovered the phenomenon of vortex lattice formation described here and conceived and performed the experiments with Y. Shitaka. Y. Sumino, K.H.N., D.T. and H.C. conceived and designed the simulations. Y. Sumino, K.H.N. and H.C. performed and analysed the simulations. *In vitro* motility assays were carried out under the directions of K.O. Y. Sumino, K.H.N., Y. Shitaka, H.C., K.Y. and K.O. interpreted the data. Y. Sumino, K.H.N., H.C. and K.O. wrote the paper.

**Author Information** Reprints and permissions information is available at www.nature.com/reprints. The authors declare no competing financial interests. Readers are welcome to comment on the online version of this article at www.nature.com/nature. Correspondence and requests for materials should be addressed to K.O. (oiwa@nict.go.jp).

LETTER

doi:10.1038/nature10891

# Collapse of polar ice sheets during the stage 11 interglacial

Maureen E. Raymo[1] & Jerry X. Mitrovica[2]

**Contentious observations of Pleistocene shoreline features on the tectonically stable islands of Bermuda and the Bahamas have suggested that sea level about 400,000 years ago was more than 20 metres higher than it is today[1–4]. Geochronologic and geomorphic evidence indicates that these features formed during interglacial marine isotope stage (MIS) 11, an unusually long interval of warmth during the ice age[1–4]. Previous work has advanced two divergent hypotheses for these shoreline features: first, significant melting of the East Antarctic Ice Sheet, in addition to the collapse of the West Antarctic Ice Sheet and the Greenland Ice Sheet[1–3]; or second, emplacement by a mega-tsunami during MIS 11 (ref. 4, 5). Here we show that the elevations of these features are corrected downwards by ~10 metres when we account for post-glacial crustal subsidence of these sites over the course of the anomalously long interglacial. On the basis of this correction, we estimate that eustatic sea level rose to ~6–13 m above the present-day value in the second half of MIS 11. This suggests that both the Greenland Ice Sheet and the West Antarctic Ice Sheet collapsed during the protracted warm period while changes in the volume of the East Antarctic Ice Sheet were relatively minor, thereby resolving the long-standing controversy over the stability of the East Antarctic Ice Sheet during MIS 11.**

The stability of ice sheets in the face of continuing global warming is an issue of significant societal concern. Satellite gravity measurements indicate that the Greenland Ice Sheet (GIS) and the West Antarctic Ice Sheet (WAIS), the two ice sheets most susceptible to climate change, are experiencing a net mass loss[6–9], with evidence of an accelerating pace[9–12]. In contrast, the current mass balance of the much larger East Antarctic Ice Sheet (EAIS) is uncertain, even in sign[6,9], though a recent study[11] has inferred EAIS mass loss localized to coastal regions. This uncertainty about the stability of the EAIS in a progressively warming world has been a key motivation for studies of the palaeoclimate record during past warm intervals.

One such study, a statistical analysis of widely distributed sea-level markers related to the last interglacial (MIS 5e; about 120,000 years ago), concluded with 95% confidence that eustatic sea level (ESL; defined as the globally averaged sea-level change) was >6.6 m higher during MIS 5e than at the present day, and with 66% confidence that ESL was >8.0 m higher[13]. (This inference, higher than earlier estimates[14], is supported by a recent analysis of MIS 5e sea-level records from Florida[15].) Estimates of the ESL rise associated with collapse of polar ice sheets range from 3.4 m (ref. 16) to 7 m for the GIS, and from 3.2 m (ref. 17) to 5 m for the WAIS, where the upper bounds refer to the complete disappearance of the ice sheet. Thus, whereas the estimate of peak ESL during MIS 5e implies significant collapse of both the GIS and the WAIS, it also implies that the EAIS remained relatively stable.

It is within this context of assessing potential future instability of the EAIS that the sea-level highstand features found at ~20 m (here and elsewhere, height above present-day sea level is meant) in Bermuda and the Bahamas, and which formed during the MIS 11 interglacial (~424–395 kyr ago), have taken on great significance. MIS 11 spanned two precession cycles and was the longest interglacial of the past 500 kyr (refs 18, 19), including the current interglacial MIS 1 (Fig. 1) and MIS 5e (Supplementary Fig. 4). If the ESL during the MIS 11 interglacial peaked at a level 20 m higher than today[1–3], then at least 8 m of that rise must have come from melting of the EAIS. Geologic evidence for a ~20-m sea-level highstand in Bermuda and the Bahamas is convincing. In Bermuda, reasonably well-dated deposits with thalassinidean shrimp burrows, foraminifera, and gastropods characteristic of littoral and intertidal environments constrain relative sea level at 21.3 ± 1.0 m during MIS 11 (refs. 2, 3). On Eleuthera, in the Bahamas, a gently sloping erosion surface capped with fenestrae-rich intertidal beach deposits provides a maximum sea-level estimate of 20 ± 3 m, and the occurrence of pendant fibrous cements suggests a minimum sea level of 17 ± 2 m (we will henceforth quote a sea-level estimate of 18.5 ± 3.6 m for this site); multiple dating methods suggest that these deposits were formed during MIS 11 (ref. 1).

How do these observations compare to other MIS 11 sea-level indicators or proxies? In a recent survey of MIS 11 sea-level records worldwide (most of which are located in tectonically active regions), Bowen[5] estimated peak MIS 11 sea level using a range of tectonic uplift

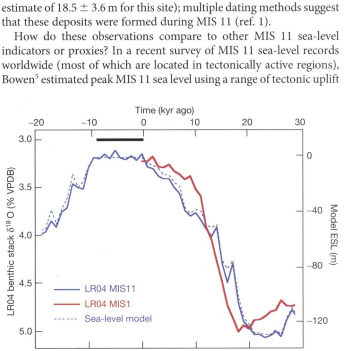


**Figure 1 | Comparison of the duration of the MIS 11 and MIS 1 interglacials.** Plot of the LR04 benthic oxygen isotope stack[28] (left-hand vertical axis) over a time window spanning the MIS 11 (blue; bottom time scale) and MIS 1 (red; top time scale) interglacials. The mean standard error on $\delta^{18}O$ in the LR04 stack is 0.06‰ with an age error of ±4 kyr for the intervals considered here. The juxtaposition illustrates the significantly longer duration of maximum interglacial conditions during MIS 11 relative to MIS 1. ESL associated with the model ice history used to calculate GIA effects during MIS 11 is shown by dashed line (right-hand vertical axis). Note the hiatus in model ice volume changes from 410 to 401 kyr ago (black bar). An analogous comparison between the duration of MIS 11 with MIS 5e can be found in Supplementary Fig. 4.

[1]Lamont-Doherty Earth Observatory, Columbia University, PO Box 1000, 61 Route 9W, Palisades, New York 10964, USA. [2]Department of Earth and Planetary Sciences, Harvard University, 20 Oxford Street, Cambridge, Massachusetts 02138, USA.

corrections based on different assumed ages and elevations of MIS 5e sea-level markers. If we adopt Kopp *et al.*'s[13] recent inference of the age and peak magnitude of ESL during MIS 5e as a constraint on the latter, then Bowen's estimates from far-field sites imply that peak sea level during MIS 11 was 6–9 m above the present-day value, an estimate consistent with marine $\delta^{18}O$ isotopic anomalies[70]. However, Bowen excluded a number of outliers, including the well-studied Bermuda and Bahamas sites, and following McMurtry *et al.*[4], he attributed the anomalously high elevation of shoreline features at those sites to deposition by storms or a mega-tsunami.

The two explanations for the MIS 11 highstand features in Bermuda and the Bahamas—global sea-level rise associated with significant EAIS melting[1–3], or mega-tsunami deposition[4,5]—ignore the potential signal from glacial isostatic adjustment (GIA). The GIA signal may be significant at the two sites, as they both are located on the peripheral bulge of the ancient Laurentian ice complex. As a consequence, they would be subject to local crustal subsidence and sea-level rise of amplitude ~1–2 mm $yr^{-1}$ during any interglacial[21].

To explore the potential contribution from GIA to MIS 11 highstand elevations, we compute global sea-level variations over the past 500 kyr using a gravitationally self-consistent theory valid for spherically symmetric, linear viscoelastic Earth models[22] (see Supplementary Information). As an illustration of the physics of interglacial sea-level trends, we plot the predicted change in sea level across the warmest, most stable interval in MIS 11 (as implied by $\delta^{18}O$ records), a 9-kyr period spanning 410–401 kyr ago that occurred during the second half of MIS 11 (Fig. 2). The predictions adopt an Earth model with upper-mantle and lower-mantle viscosities of $5 \times 10^{20}$ Pa s and $5 \times 10^{21}$ Pa s, respectively (model LM[23,24]; see Supplementary Information).

In the near-field of the former MIS 12 ice sheets, the predicted sea-level change is dominated by radial crustal motions. For example, in regions once covered by ice sheets, post-glacial rebound of the crust produces a sea-level fall of amplitude up to ~1–2 cm $yr^{-1}$, leading to a net fall over 9 kyr that can exceed 100 m (these amplitudes are well off the scale of Fig. 2). Surrounding these regions of uplift are peripheral bulges predicted to subside at rates of up to 0.2–0.3 cm $yr^{-1}$ during the interglacial. This subsidence accounts for the (red) zones of sea-level rise in Fig. 2, with maximum amplitude of ~20 m, that encircle the Laurentian, Fennoscandian and Antarctic ice complexes. In contrast, a sea-level fall of 2–3 m is predicted across most of the far-field of the former ice sheets during MIS 11. This fall is due to a combination of two processes: (1) deglaciation-induced ocean loading effects, which act, near continental margins, to tilt the crust such that continents are deformed upward (that is, sea level falls) and offshore regions downward[21,25]; and (2) the redistribution—or syphoning—of water from ocean basins towards regions of peripheral bulge and offshore subsidence[21].

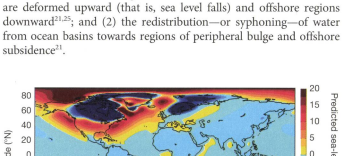


**Figure 2 | Predicted sea-level change across the hiatus in ice volume changes (410–401 kyr ago) spanned by the model MIS 11 interglacial.** The GIA calculation is based on the ice history discussed in Supplementary Information and the LM[23,24] viscosity model. The colour scale saturates in regions within the near-field of the late Pleistocene ice sheets.

Following Fig. 2, we conclude that in the absence of interglacial ice volume changes and steric effects, sea-level highstands will date to the end of the interglacial at sites within the subsiding peripheral bulge of major ice centres, and to the beginning of the interglacial over most of the far-field (Fig. 3). (Of course, any sea-level signal associated with interglacial ice volume variations and with ocean temperature and salinity changes will be superimposed on these predicted GIA trends.) Consider Bermuda: the predicted relative sea-level history for this site (Fig. 3 and Supplementary Fig. 1, solid red line) exhibits a monotonic rise across MIS 11, reaching a level 11.9 m above the present-day value. The predicted highstand for the Bahamas (dashed red line, Fig. 3), lying on the outer flank of the same peripheral bulge, is 7.4 m. It is clear that the amplitude of highstands at Bermuda or the Bahamas, indeed at all sites within a peripheral bulge, will be a strong function of the duration of the interglacial highstand. In this regard, the protracted length of MIS 11, relative to the Holocene (Fig. 1) or MIS 5e (Supplementary Fig. 4), should be manifested by highstands of particularly large magnitude. From this it also follows that simple field comparisons of the relative elevations of Holocene, MIS 5e and MIS 11 sea-level markers on these islands would lead to an erroneous assessment of the difference in ESL between those times.

This result may be stated with more generality. The elevation of an ancient interglacial highstand at any site within a peripheral bulge will be governed by the difference in the state of isostatic disequilibrium at the end of the ancient interglacial relative to the disequilibrium at the present day in that same location. As the MIS 11 interglacial was significantly longer than the current interglacial (or MIS 5e), more subsidence had occurred by the time the final MIS 11 shoreline indicators were emplaced on those islands than during the current (or MIS 5e) interglacial. Further, as the current interglacial proceeds, sites like Bermuda and the Bahamas will be subject to a continuing sea-level rise as the present peripheral bulge continues to subside. Thus, the height of these ancient MIS 11 highstand features will progressively fall as time progresses (even in the absence of any future change in ice volume).

By contrast, the highstand amplitude at sites located in the far field will depend on the difference in isostatic disequilibrium at the beginning of the interglacial relative to the disequilibrium at the present day.

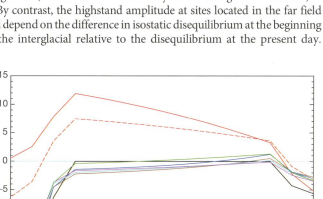


**Figure 3 | Predicted relative sea-level changes across the model MIS 11 interglacial.** The calculations are based on the ice history discussed in Supplementary Information and the LM viscosity model. The top two curves are predictions for Bermuda (solid red line) and the Bahamas (dashed red line) at locations of published data discussed in text. The lower coloured curves, predictions for a number of far-field sites, are included for comparison: the Gulf of Aden, Red Sea (brown), Curacao (green), Coorong, South Australia (magenta), Oahu, Hawaii (blue) and Cape Town, South Africa (cyan). The black line shows the ESL variation associated with the adopted ice history (as in the dashed blue line in Fig. 1 and the black line in Supplementary Fig. 1) and the thin horizontal dashed line references to present-day sea level.

Thus, perhaps counter-intuitively, the current elevation of these highstands does not depend on the duration of the ancient interglacial.

Global predictions of current MIS 11 shoreline elevations within each of the two zones discussed above are shown in Fig. 4a and b: Fig. 4a encompasses sites where the highstand occurred at the end of the modelled interglacial hiatus in ice mass change (for example, 401 kyr ago) whereas Fig. 4b encompasses sites where the highstand occurs at the beginning of the modelled hiatus (410 kyr ago). These results represent the predicted contribution to observed MIS 11 highstands from GIA alone; this contaminating signal should be removed from geological observations before they are used to infer the difference in ESL (or ice volume) between MIS 11 and the present.

As noted above, the GIA contribution to the MIS 11 shoreline elevations in Bermuda and the Bahamas is predicted to be 11.9 m and 7.4 m, respectively (Fig. 3). Correcting the published highstand estimates at these sites for these GIA predictions yields residual MIS 11 sea-level elevations of $9.4 \pm 1$ m for Bermuda and $11.1 \pm 3.6$ m in Eleuthera (Supplementary Table 1). Although additional field observations in the Bahamas could greatly decrease the multi-metre error associated with these sea-level estimates, we conclude that no significant contribution from melting of the EAIS is required to explain the geologic observations at the two sites.

In our analysis, we implicitly assume that melting of the WAIS and the GIS occurred towards the end of the MIS 11 interglacial, such that the contribution of the melt event to sea level at Bermuda and the Bahamas could be added to a coeval GIA-induced highstand. This timing for ice sheet collapse is strongly supported by at least two arguments. First, if the collapse took place at the beginning of the hiatus in MIS 11 melting (that is, at ~410 kyr ago), then the associated ESL rise would have had to be close to 20 m in order to fit the observed highstand elevations at Bermuda and the Bahamas. However, in this case, the predicted highstand elevation at far-field sites would have been even greater than 20 m (that is, an ~20-m melt signal added to the GIA-induced highstand of a few metres; Fig. 3), a situation apparently ruled out by far-field observations[5]. Second, GIA calculations predict a submergence of up to several metres for far-field sites by 401 kyr ago (Fig. 3) and an average submergence of ~1 m at the specific far-field sites considered by Bowen[5]. Therefore, correcting an inferred sea-level peak of 6–9 m for this GIA-induced contamination yields a predicted ESL ~1 m higher (that is, 7–10 m), in accord with the residual highstand elevations at Bermuda and the Bahamas cited above (Supplementary Table 1).

In the Supplementary Information we present results of sensitivity tests related to GIA predictions. First, we extend the duration of the MIS 11 hiatus in ice mass change from 9 to 14 kyr. In this case, the GIA-induced elevation of MIS 11 shorelines at sites within the Laurentian peripheral bulge are predicted to increase by ~1–2 m when viscosity model LM is adopted, yielding residual MIS 11 highstand elevations of $7.0 \pm 1$ m for Bermuda and $9.9 \pm 3.6$ m in Eleuthera (Supplementary Table 1), and thus lowering the inferred peak ESL during MIS 11 by ~1–2 m. Second, we considered an alternative viscosity profile, VM2 (ref. 26), characterized by a lower-mantle viscosity that is a factor of two smaller than model LM. In this case, the predicted GIA contribution to MIS 11 highstand elevations within the peripheral bulge is reduced by a factor of ~2. This reduction yields residual (GIA-corrected) MIS 11 elevations of $15.0 \pm 1$ m and $14.3 \pm 3.6$ m at Bermuda and the Bahamas, respectively, values that appear to be at odds with lower far-field estimates[5]. Last, we performed a Monte Carlo parameter search in which we varied mantle viscosity, lithospheric thickness, and the duration of the modelled hiatus in MIS 11 ice volume changes, and tested for the consistency of the GIA-corrected highstand elevations. This exercise yields a preferred bound on the peak ESL during MIS 11 of 6–13 m.

In summary, observations of MIS 11 highstand features in Bermuda and the Bahamas must be corrected for the significant contaminating signal of GIA before these data are used to infer peak ESL during the MIS 11 interglacial. We conclude that ESL reached ~6–13 m above the present-day value in the late stages of MIS 11. It is unlikely that ocean thermal expansion contributed more than ~1 m to this inference[13,27]. Therefore, although this estimate of peak ESL indicates significant collapse of both the WAIS and GIS during the MIS 11 interglacial, it rules out any significant melting of the EAIS during this unusually prolonged period of ice age warmth.

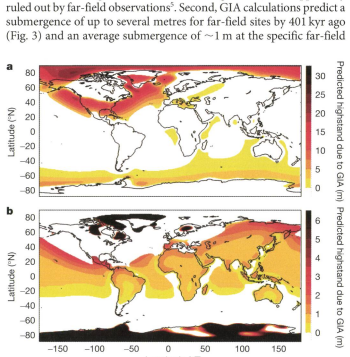


**Figure 4 | Plot of the predicted GIA-induced present-day elevation of MIS 11 highstands that are currently greater than zero.** Elevation is shown for all sites in which sea-level peaks either at the end of the hiatus in ice volume changes spanned by the model MIS 11 interglacial (**a**; that is, at 401 kyr ago; see also Supplementary Fig. 1) or at the beginning of that hiatus (**b**; that is, at 410 kyr ago).

**Received 30 September 2011; accepted 23 January 2012.**
**Published online 14 March 2012.**

1. Hearty, P. J., Kindler, P., Cheng, H. & Edwards, R. L. A +20 m middle Pleistocene sea level highstand (Bermuda and the Bahamas) due to partial collapse of Antarctic ice. *Geology* **27,** 375–378 (1999).
2. Olson, S. L. & Hearty, P. J. A sustained +21 m sea level highstand during MIS 11 (400 ka): direct fossil and sedimentary evidence from Bermuda. *Quat. Sci. Rev.* **28,** 271–285 (2009).
3. van Hengstum, P., Scott, D. B. & Javaux, E. Foraminifera in elevated Bermudian caves provide further evidence for +21 m eustatic sea level during Marine Isotope Stage 11. *Quat. Sci. Rev.* **28,** 1850–1860 (2009).
4. McMurtry, G. M. *et al.* Elevated marine deposits in Bermuda record a late Quaternary megatsunami. *Sedim. Geol.* **200,** 155–165 (2007).
5. Bowen, D. Q. Sea level ~400000 years ago (MIS 11): analogue for present and future sea-level? *Clim. Past* **6,** 19–29 (2010).
6. Velicogna, I. & Wahr, J. Measurements of time-variable gravity show mass loss in Antarctica. *Science* **311,** 1754–1756 (2006).
7. Luthcke, S. B. *et al.* Recent Greenland ice mass loss by drainage system from satellite gravity observations. *Science* **314,** 1286–1289 (2006).
8. Shepherd, A. & Wingham, D. Recent sea-level contributions of the Antarctic and Greenland ice sheets. *Science* **315,** 1529–1532 (2007).
9. Rignot, E. *et al.* Recent Antarctic ice mass loss from radar interferometry and regional climate modelling. *Nature Geosci.* **1,** 106–110 (2008).
10. Thomas, R. *et al.* Accelerated sea level rise from West Antarctica. *Science* **306,** 255–258 (2004).
11. Chen, J. L., Wilson, C. R., Blankenship, D. & Tapley, B. D. Accelerated Antarctic ice loss from satellite gravity measurements. *Nature Geosci.* **2,** 859–862 (2009).
12. Velicogna, I. Increasing rates of ice mass loss from the Greenland and Antarctic ice sheets revealed by GRACE. *Geophys. Res. Lett.* **36,** L19503, http://dx.doi.org/10.1029/2009GL040222 (2009).
13. Kopp, R. E., Simons, F. J., Mitrovica, J. X., Maloof, A. C. & Oppenheimer, M. Probabilistic assessment of sea level during the last interglacial stage. *Nature* **462,** 863–867 (2009).
14. Jansen, E. *et al.* in *Climate Change 2007: The Physical Science Basis* (eds Solomon, S. *et al.*) 433–498 (Cambridge Univ. Press, 2007).

15. Muhs, D. R., Simmons, K. R., Schumann, R. R. & Halley, R. B. Sea-level history of the past two interglacial periods: new evidence from U-series dating of reef corals from south Florida. *Quat. Sci. Rev.* **30**, 570–590 (2011).
16. Otto-Bliesner, B. *et al.* Simulating Arctic climate warmth and ice field retreat in the last interglaciation. *Science* **311**, 1751–1753 (2006).
17. Bamber, J. L., Riva, R. E. M., Vermeersen, L. L. A., & LeBrocq, A. M. Reassessment of the potential sea level rise from a collapse of the West Antarctic Ice Sheet. *Science* **324**, 901–903 (2009).
18. Loutre, M. F. & Berger, A. Marine isotope stage 11 as an analogue for the present interglacial. *Glob. Planet. Change* **36**, 209–217 (2003).
19. Rohling, E. J. *et al.* Comparison between Holocene and Marine Isotope Stage-11 sea level histories. *Earth Planet. Sci. Lett.* **291**, 97–105 (2010).
20. McManus, J., Oppo, D., Cullen, J. & Healey, S. in *Earth's Climate and Orbital Eccentricity: The Marine Isotope Stage 11 Question* (eds Droxler, A. W., Poore, R. Z. & Burckle, L. H.) 69–85 (AGU Geophys. Monogr. Ser. 137, 2003).
21. Mitrovica, J. X. & Milne, G. A. On the origin of postglacial ocean syphoning. *Quat. Sci. Rev.* **21**, 2179–2190 (2002).
22. Kendall, R. A., Mitrovica, J. X. & Milne, G. A. On post-glacial sea level: II. Numerical formulation and comparative results on spherically symmetric models. *Geophys. J. Int.* **161**, 679–706 (2005).
23. Lambeck, K., Smither, C. & Johnston, P. Sea level change, glacial rebound and mantle viscosity for northern Europe. *Geophys. J. Int.* **134,** 102–144 (1998).
24. Mitrovica, J. X. & Forte, A. M. A new inference of mantle viscosity based upon a joint inversion of convection and glacial isostatic adjustment data. *Earth Planet. Sci. Lett.* **225**, 177–189 (2004).
25. Nakada, M. & Lambeck, K. Late Pleistocene and Holocene sea-level change in the Australian region and mantle rheology. *Geophys. J. Int.* **96,** 497–517 (1989).
26. Peltier, W. R. Global glacial isostasy and the surface of the ice-age Earth: the ICE-5G (VM2) model and GRACE. *Annu. Rev. Earth Planet. Sci.* **32,** 111–149 (2004).
27. McKay, N. P., Overpeck, J. T. & Otto-Bliesner, B. L. The role of ocean thermal expansion in Last Interglacial sea level rise. *Geophys. Res. Lett.* 38, L14605, http://dx.doi.org/10.1029/2011GL048280 (2011).
28. Lisiecki, L. E. & Raymo, M. E. A. Pliocene-Pleistocene stack of 57 globally distributed benthic $\delta^{18}O$ records. *Paleoceanography* **20,** PA1003, http://dx.doi.org/10.1029/2004PA001071 (2005).

**Supplementary Information** is linked to the online version of the paper at www.nature.com/nature.

**Acknowledgements** We thank P. Hearty and D. Bowen for discussions of MIS 11 field data, and J. L. Davis for suggestions regarding data analysis. Support for this research was provided by NSF-OCE-0825293 and OCE-1202632 (M.E.R.). Harvard University (J.X.M.) and the Canadian Institute for Advanced Research (J.X.M.).

**Author Contributions** This study was planned, undertaken and written jointly.

**Author Information** Reprints and permissions information is available at www.nature.com/reprints. The authors declare no competing financial interests. Readers are welcome to comment on the online version of this article at www.nature.com/nature. Correspondence and requests for materials should be addressed to M.E.R. (raymo@ldeo.columbia.edu).

LETTER

doi:10.1038/nature10880

# Adaptive radiation of multituberculate mammals before the extinction of dinosaurs

Gregory P. Wilson[1], Alistair R. Evans[2], Ian J. Corfe[3], Peter D. Smits[1,2], Mikael Fortelius[3,4] & Jukka Jernvall[3]

**The Cretaceous–Paleogene mass extinction approximately 66 million years ago is conventionally thought to have been a turning point in mammalian evolution[1,2]. Prior to that event and for the first two-thirds of their evolutionary history, mammals were mostly confined to roles as generalized, small-bodied, nocturnal insectivores[3], presumably under selection pressures from dinosaurs[4]. Release from these pressures, by extinction of non-avian dinosaurs at the Cretaceous–Paleogene boundary, triggered ecological diversification of mammals[1,2]. Although recent individual fossil discoveries have shown that some mammalian lineages diversified ecologically during the Mesozoic era[5], comprehensive ecological analyses of mammalian groups crossing the Cretaceous–Paleogene boundary are lacking. Such analyses are needed because diversification analyses of living taxa[6,7] allow only indirect inferences of past ecosystems. Here we show that in arguably the most evolutionarily successful clade of Mesozoic mammals, the Multituberculata, an adaptive radiation began at least 20 million years before the extinction of non-avian dinosaurs and continued across the Cretaceous–Paleogene boundary. Disparity in dental complexity, which relates to the range of diets, rose sharply in step with generic richness and disparity in body size. Moreover, maximum dental complexity and body size demonstrate an adaptive shift towards increased herbivory. This dietary expansion tracked the ecological rise of angiosperms[8] and suggests that the resources that were available to multituberculates were relatively unaffected by the Cretaceous–Paleogene mass extinction. Taken together, our results indicate that mammals were able to take advantage of new ecological opportunities in the Mesozoic and that at least some of these opportunities persisted through the Cretaceous–Paleogene mass extinction. Similar broad-scale ecomorphological inventories of other radiations may help to constrain the possible causes of mass extinctions[9,10].**

Multituberculate mammals were a taxonomically rich[3,11] and numerically abundant[12] clade that had originated by the Middle Jurassic epoch (approximately 165 million years (Myr) ago) and went extinct in the late Eocene (approximately 35 Myr ago)[3,11]. They were nearly globally distributed[13] and had a distinctive dentition consisting of procumbent incisors, blade-like premolars, molars with longitudinal rows of cusps (Fig. 1) and a predominantly posteriorly directed (palinal) chewing motion[14,15].

Palaeontologists have agreed for a long time that the success of multituberculate mammals was at least partly related to their highly derived dentition. Despite this, there is little consensus on the interpretations of their feeding ecology, perhaps owing to the limitations of previous approaches. For example, toothwear analysis is time intensive

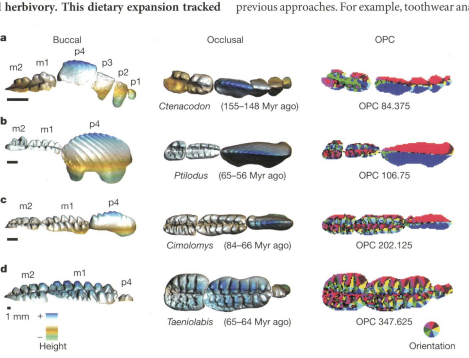


**Figure 1 | Dental and dietary diversity in multituberculate mammals.** **a**–**d**, Three-dimensional buccal–occlusal and occlusal reconstructions of multituberculate lower-right cheek tooth rows for GIS analysis: Late Jurassic plagiaulacid *Ctenacodon serratus* (**a**), Paleocene ptilodontoid *Ptilodus kummae* (**b**), Late Cretaceous cimolomyid *Cimolomys gracilis* (**c**), Paleocene taeniolabidid *Taeniolabis taoensis* (**d**). Surface orientation map of each three-dimensional reconstruction (colour wheel indicates orientation) for OPC measurements (shown by the number of coloured patches). Clumps that are smaller than three grid points (black) are ignored. p, premolar; m, molar. Scale bars, 1 mm.

[1]Department of Biology, University of Washington, Seattle, Washington 98195-1800, USA. [2]School of Biological Sciences, Monash University, Victoria 3800, Australia. [3]Developmental Biology Program, Institute of Biotechnology, University of Helsinki, PO Box 56, FIN-00014, Helsinki, Finland. [4]Department of Geosciences and Geography, University of Helsinki, PO Box 64, FIN-00014, Helsinki, Finland.

and requires high-quality preservation[15], and multituberculates lack living descendants and this hampers comparative studies. Interpretations of multituberculate feeding ecology therefore vary widely; they have been proposed to be broad herbivores, frugivores, granivores, root- and bark-eaters, egg-eaters, insectivores, carnivores and omnivores[15–17].

To obtain a robust and comprehensive view of multituberculate ecomorphological diversity through time, we quantified dental complexity in 41 genera using geographic information systems (GIS) analyses[18] of three-dimensional crown surfaces of lower cheek teeth (Fig. 1; Supplementary Table 1). These analyses do not require cusp and facet homologies to be established, which can be a challenging task when comparing morphologically and phylogenetically divergent taxa. Orientation patch count (OPC), a measure of dental complexity, was calculated as the number of discrete surfaces on the cheek tooth row distinguished by differences in orientation (for example, north, southwest; Fig. 1). Extant rodents, carnivorans and bats demonstrate a robust correlation between OPC and feeding ecology; OPC increases across the dietary spectrum from carnivores to omnivores to herbivores, despite many differences in specific tooth components, body size and chewing mechanics among these taxa[18,19]. For a given clade, the standard deviation of OPC is an effective proxy for the dietary diversification and divergence in feeding function: higher standard deviation means greater dental disparity and a broader range of diets. OPC thus offers promise as a powerful tool for quantifying overall tooth shape and inferring diet in extinct taxa, such as multituberculates, that have highly derived dentitions with uncertain homology with living mammals and imprecise functional analogy.

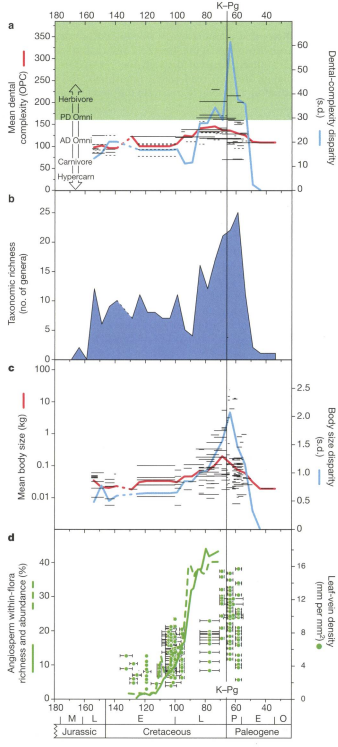


**Figure 2 | Temporal patterns of multituberculate dental complexity, taxonomic richness, body size and angiosperm ecological diversification.** **a**, Dental complexity (measured by OPC) for 41 multituberculate genera (solid black lines) and estimated for 24 additional genera (dashed black lines; see Supplementary Information) with mean dental complexity (OPC; red line) and disparity as standard deviations of OPC (blue line) in 5-Myr bins. Lengths of horizontal lines represent temporal ranges of taxa or uncertainties in ages of fossil localities. Labels for dietary classes are positioned at the lower end of their range based on OPC values in modern mammals[18]. Green shaded area represents plant-dominated omnivory (PD omni) and herbivory. **b**, Taxonomic richness is equal to the number of genera per 5-Myr bin (blue shaded area). **c**, Body-mass estimates for 156 multituberculate species (solid black lines) with geometric means (red line) and disparity (blue line) for each 5-Myr bin. **d**, Angiosperm within-flora richness (solid green line) and relative abundance (dashed green line) from ref. 24 (±7.5-Myr moving averages). Leaf hydraulic capacity of angiosperms as leaf-vein density (green circles) from ref. 25. The 136–131-Myr bin was excluded from all analyses (Supplementary Information). AD omni, animal-dominated omnivory; E, early; Hypercarn, hypercarnivory; M, middle; L, late; O, Oligocene; P, Paleocene.

Among the earliest multituberculates, the 'Plagiaulacida' are a paraphyletic assemblage of taxa with up to four simple blade-like premolars and two multi-cusped molars (Fig. 1a). OPC analyses of 'plagiaulacids' from the Late Jurassic through to the Early Cretaceous epoch (from 156–100 Myr ago) show low and tightly constrained dental complexity (Fig. 2a; OPC, 84–125). Their OPC values correspond to carnivory and the low end of animal-dominated omnivory among extant mammals (for example, eating both insects and fruits). Multituberculates in the early Late Cretaceous (100–84 Myr ago), which include mostly basal members of the suborder Cimolodonta, had a slightly higher mean OPC than did the 'plagiaulacids' but retained the low standard deviation of OPC (Fig. 2a), indicating low morphological disparity. A distinct break occurred 84–66 Myr ago, in the latest Cretaceous, when the mean OPC rose and peaked within the Campanian (mean OPC, 145) and maximum OPC and disparity sharply increased as well (Fig. 2a; OPC, 70–230). Of the 17 taxa for this interval, 5 have OPC values that are greater than 160 and 2 have OPC values that are greater than 200, corresponding to values for plant-dominated omnivory and herbivory among extant mammals, respectively (Fig. 2a).

Finally, in the early Paleocene (66–62 Myr ago) multituberculates maintained high OPC (mean OPC, 138) and disparity peaked (Fig. 2a; OPC, 70–348). The early Paleocene *Taeniolabis* from North America (Fig. 1d) had the highest OPC among multituberculates (OPC, 348), which exceeded OPC values of extant herbivorous rodents and carnivorans[18]. Of the 16 other early Paleocene taxa, 4 have OPC values greater than 160 and 1 has an OPC value greater than 200 (Fig. 2a). Mean OPC and disparity of OPC declined during the remainder of the Paleocene and in the early Eocene (62–49 Myr ago). *Ectypodus*, the only known genus from the middle to late Eocene (49–35 Myr ago), has a low OPC (109), corresponding to the high end of the range for extant mammalian carnivores. This sharp drop in dental ecomorphological

disparity is intriguing in light of the hypothesis that some late Paleocene to early Eocene eutherian lineages (for example, rodents) competitively displaced multituberculates[12].

Variable sampling of fossils through time may influence our inferred patterns of multituberculate radiation. In particular, the relatively depauperate Jurassic and Early Cretaceous taxonomic richness of multituberculates may be partly due to the limited fossil record[3]. To test whether the changes in OPC through time might be sensitive to uneven sampling of fossils, we randomized the OPC value assignments for each genus. The results of 5,000 randomized mean OPC profiles through time indicate that even with additional fossil discoveries, the OPC patterns and ecological inferences that are presented here are likely to be robust (see Supplementary Fig. 8).

The overall trend of increasing multituberculate dental complexity was driven by increases in the number of cusps per molar and the relative size of molars in the cheek tooth row (Supplementary Fig. 1). This evolutionary pathway differs from that taken by ungulates, primates, rodents and lagomorphs, which responded to increased mechanical processing demands (that is, greater plant component) by evolving multi-cusped, molar-like premolars in addition to complex molars[20]. Among several other mammalian lineages with blade-like premolars (for example, carpolestid primates and potoroid marsupials), only sthenurine marsupials re-evolved multi-cusped premolars[21]. Developmental, functional or structural constraints that are associated with the evolution of a blade-like premolar may have inhibited later evolution of more cuspidate premolars.

Patterns of generic richness and conservative estimates of body size for multituberculates (see Methods Summary) mirror the pattern of initially low dental complexity for most of the Mesozoic followed by a marked increase just before the end of the Cretaceous (84–66 Myr ago; Fig. 2b, c). From the Late Jurassic to the early Late Cretaceous, multituberculate generic richness fluctuated between 4 and 16 genera, and body mass ranged between 9 g and 105 g. A marked shift occurred near the end of the Cretaceous, with generic richness increasing from 16 to 21 genera and average body mass increasing from 67 g to 194 g, in particular, *Bubodens magnus* reached an estimated 5.25 kg (for a comparison, the alpine marmot weighs 3–8 kg). Similarly, Cenozoic generic richness and body size patterns parallel changes in dental complexity (Fig. 2b, c). However, it should be noted that body size and dental complexity are not interchangeable as predictors of diet because small multituberculates can have high OPC values, and large multituberculates can have low OPC values (Supplementary Information), conforming to previous analyses of extant taxa[18]. Furthermore, variation in the amount of available fossil-bearing rock through the studied interval could contribute to the pattern of generic richness[22].

It is worth noting that increases in dental complexity (OPC of greater than 160) occurred in five multituberculate lineages: in the Asian Djadochtatheroidea, the North American Eucosmodontidae and Cimolomyidae (just before the end of the Cretaceous), the North American and Asian Taeniolabididae, and the North American Microcosmodontidae (in the early Paleocene). In the absence of a robust multituberculate phylogeny, it is unclear whether this represents a single evolutionary increase in tooth complexity, with multiple reversals to low complexity, or parallel increases in individual lineages or clades. This increase differs from the more commonly observed pattern, in which increased morphologic disparity precedes taxonomic diversification[23], as this increase occurred in step with an increase in multituberculate body size and taxonomic richness.

Overall, the pattern of increasing dental complexity in multituberculate mammals that pre-dates the Cretaceous–Paleogene mass extinction event contrasts with conventional ideas that mammalian evolution was suppressed during the Mesozoic era by selective pressures imposed by dinosaurs. Instead, multituberculates, the mammalian clade that co-existed for the longest time with non-avian dinosaurs, initiated an evolutionary radiation during the acme of dinosaur diversity, approximately 20 Myr before the Cretaceous–Paleogene boundary[22]. This is consistent with the highly specialized adaptations that are found among several new, exceptionally well-preserved Mesozoic mammal specimens[5] and with the timing of increased molecular divergence rates among extant mammalian lineages[6,7], but the multituberculates also show broad taxonomic and ecomorphologic diversification at the intraordinal level.

This adaptive response post-dated the taxonomic radiation of angiosperms but coincided broadly with increases in ecological diversity, abundance and leaf hydraulic capacities of angiosperms in the Late Cretaceous (in the Campanian and Maastrichtian)[8,24,25] (Fig. 2d), suggesting that there is a causal link. Many angiosperms during this time were herbaceous, and had a rapid life cycle and less-effective herbivore defences compared to other seed plants and would consequently have been an attractive, protein-rich food source for herbivores[26]. Some angiosperms had begun inhabiting a broader range of niches (trees, herbs and epiphytes) than most other plant groups and this may have enabled greater partitioning of the herbivore niche. Therefore, the multituberculate adaptive radiation, suggested by the increasing dental complexity, may have been triggered mainly by new niche space that was generated through the evolutionary and ecological radiations of angiosperms, but may have also been influenced by parallel radiations of associated non-angiosperm clades (for example, ferns[27]), insect pollinators, dispersers and herbivores[28]. A trophic link between angiosperms and some multituberculates is supported by our inferred dietary trend towards increased plant-dominated omnivory and herbivory among multituberculates just before the end of the Cretaceous and in the early Paleocene.

Our data also show that the dietary range of multituberculates did not decrease in response to the Cretaceous–Paleogene mass extinction event (Fig. 2a). Despite substantial taxonomic turnover of multituberculates at the Cretaceous–Paleogene boundary[29], they seem to have experienced little change in available food resources during one of the most severe extinction events in Earth's history. This apparent indifference of the multituberculate radiation to the Cretaceous–Paleogene event underscores the ecological selectivity of extinctions and suggests that broad-scale ecomorphological inventories of radiations may help to constrain the possible causes of extinction for other groups at the Cretaceous–Paleogene boundary[9,10].

## METHODS SUMMARY

We scanned 48 dentitions from 41 genera of multituberculates. The three-dimensional scans of lower cheek tooth rows were analysed using GIS to quantify the number of discrete orientation patches using eight orientation directions. The mean of repeated measurements for eight rotations at multiples of 5.625° was used to reduce the effect of slight variations in the orientation of teeth. We compiled generic richness data from recent compendia and the primary literature. We estimated body mass from skull length, whenever available, and a tooth size to skull length regression formula. Detailed methods and calculations of dental complexity, generic richness and estimated body mass, data sets, measurements, calculations, randomization analyses and additional references are provided in the Supplementary Information.

**Received 26 September 2011; accepted 20 January 2012.**
**Published online 14 March 2012.**

1. Alroy, J. The fossil record of North American mammals: evidence for a Paleocene evolutionary radiation. *Syst. Biol.* **48,** 107–118 (1999).
2. Smith, F. A. *et al.* The evolution of maximum body size of terrestrial mammals. *Science* **330,** 1216–1219 (2010).
3. Kielan-Jaworowska, Z., Cifelli, R. L. & Luo, Z.-X. *Mammals from the Age of Dinosaurs: Origins, Evolution, and Structure* (Columbia Univ. Press, 2004).
4. Van Valen, L. M. & Sloan, R. E. Ecology and the extinction of the dinosaurs. *Evol. Theory* **2,** 37–64 (1977).
5. Luo, Z.-X. Transformation and diversification in early mammalian evolution. *Nature* **450,** 1011–1019 (2007).
6. Bininda-Emonds, O. R. P. *et al.* The delayed rise of present-day mammals. *Nature* **446,** 507–512 (2007).
7. Meredith, R. W. *et al.* Impacts of the Cretaceous terrestrial revolution and KPg extinction on mammal diversification. *Science* **334,** 521–524 (2011).
8. Wing, S. L. & Boucher, L. D. Ecological aspects of the Cretaceous flowering plant radiation. *Annu. Rev. Earth Planet. Sci.* **26,** 379–421 (1998).

9. Archibald, J. D. *et al.* Cretaceous extinctions: multiple causes. *Science* **328,** 973 (2010).
10. Schulte, P. *et al.* The Chicxulub asteroid impact and mass extinction at the Cretaceous-Paleogene boundary. *Science* **327,** 1214–1218 (2010).
11. Weil, A. & Krause, D. W. in *Evolution of Tertiary Mammals of North America* Vol. 2 (eds Janis, C. M., Gunnell, G.F. & Uhen, M. D.) 19–38 (Cambridge Univ. Press, 2008).
12. Krause, D. W. in *Vertebrates, Phylogeny, and Philosophy* (eds Flanagan, K.M. & Lillegraven, J.A.) 119–130 (Contributions to Geology, 1986).
13. Rich, T. H. *et al.* An Australian multituberculate and its palaeobiogeographic implications. *Acta Palaeontol. Pol.* **54,** 1–6 (2009).
14. Gingerich, P. D. in *Patterns of Evolution* (ed. Hallam, A.) 469–500 (Elsevier, 1977).
15. Krause, D. W. Jaw movement, dental function, and diet in the Paleocene multituberculate *Ptilodus*. *Paleobiology* **8,** 265–281 (1982).
16. Cope, E. D. The tertiary Marsupialia. *Am. Nat.* **18,** 686–697 (1884).
17. Simpson, G. G. The "plagiaulacoid" type of mammalian dentition. *J. Mamm.* **14,** 97–107 (1933).
18. Evans, A. R., Wilson, G. P., Fortelius, M. & Jernvall, J. High-level similarity of dentitions in carnivorans and rodents. *Nature* **445,** 78–81 (2007).
19. Santana, S. E., Strait, S. & Dumont, E. R. The better to eat you with: functional correlates of tooth structure in bats. *Funct. Ecol.* **25,** 839–847 (2011).
20. Jernvall, J., Gilbert, C. C. & Wright, P. C. in *Elwyn Simons: A Search for Origins* (eds Fleagle, J. G. & Gilbert, C. C.) 335–342 (Springer, 2008).
21. Prideaux, G. J. Systematics and evolution of the sthenurine kangaroos. *Univ. Calif. Publ. Geol. Sci.* **146,** 1–622 (2004).
22. Barrett, P. M., McGowan, A. J. & Page, V. Dinosaur diversity and the rock record. *Proc. R. Soc. B* **276,** 2667–2674 (2009).
23. Foote, M. The evolution of morphological diversity. *Annu. Rev. Ecol. Syst.* **28,** 129–152 (1997).
24. Lupia, R., Lidgard, S. & Crane, P. R. Comparing palynological abundance and diversity: implications for biotic replacement during the Cretaceous angiosperm radiation. *Paleobiology* **25,** 305–340 (1999).
25. Feild, T. S. *et al.* Fossil evidence for Cretaceous escalation in angiosperm leaf vein evolution. *Proc. Natl Acad. Sci. USA* **108,** 8363–8366 (2011).
26. Wing, S. L. & Tiffney, B. H. in *The Origins of Angiosperms and Their Biological Consequences* (eds Friis, E.M., Chaloner, W.G. & Crane, P.R.) 203–224 (Cambridge Univ. Press, 1987).
27. Schneider, H. *et al.* Ferns diversified in the shadow of angiosperms. *Nature* **428,** 553–557 (2004).
28. Grimaldi, D. The co-radiations of pollinating insects and angiosperms in the Cretaceous. *Ann. Mo. Bot. Gard.* **86,** 373–406 (1999).
29. Wilson, G. P. Mammalian faunal dynamics during the last 1.8 million years of the Cretaceous in Garfield County, Montana. *J. Mamm. Evol.* **12,** 53–76 (2005).


**Supplementary Information** is linked to the online version of the paper at www.nature.com/nature.

**Acknowledgements** We thank museums, institutions and individuals that made specimens available for this study (full list is available in Supplementary Information). Funding was provided by the National Science Foundation, Denver Museum, the University of Washington (G.P.W. and P.D.S.), the Australian Research Council, Monash University (A.R.E.), the Academy of Finland (A.R.E., M.F. and J.J.) and the EU SYNTHESYS program (project GB-TAF-4779) (I.J.C.).

**Author Contributions** G.P.W., A.R.E., J.J. and M.F. designed the study. G.P.W., A.R.E, I.J.C. and P.D.S. collected and analysed the data. G.P.W., A.R.E. and J.J. wrote the manuscript. G.P.W., A.R.E., I.J.C., P.D.S., M.F. and J.J. discussed results and commented on the manuscript at all stages.

**Author Information** The three-dimensional scans for this study are deposited in the MorphoBrowser database (http://morphobrowser.biocenter.helsinki.fi/). Reprints and permissions information is available at www.nature.com/reprints. The authors declare no competing financial interests. Readers are welcome to comment on the online version of this article at www.nature.com/nature. Correspondence and requests for materials should be addressed to G.P.W. (gpwilson@u.washington.edu).

LETTER

doi:10.1038/nature10961

# A comparative analysis of the evolution of imperfect mimicry

Heather D. Penney[1], Christopher Hassall[1], Jeffrey H. Skevington[1,2], Kevin R. Abbott[1] & Thomas N. Sherratt[1]

**Although exceptional examples of adaptation are frequently celebrated, some outcomes of natural selection seem far from perfect. For example, many hoverflies (Diptera: Syrphidae) are harmless (Batesian[1]) mimics of stinging Hymenoptera[2]. However, although some hoverfly species are considered excellent mimics, other species bear only a superficial resemblance to their models[3] and it is unclear why this is so. To evaluate hypotheses that have been put forward to explain interspecific variation in the mimetic fidelity of Palearctic Syrphidae we use a comparative approach. We show that the most plausible explanation is that predators impose less selection for mimetic fidelity on smaller hoverfly species because they are less profitable prey items. In particular, our findings, in combination with previous results, allow us to reject several key hypotheses for imperfect mimicry: first, human ratings of mimetic fidelity are positively correlated with both morphometric measures and avian rankings, indicating that variation in mimetic fidelity is not simply an illusion based on human perception[4]; second, no species of syrphid maps out in multidimensional space as being intermediate in appearance between several different hymenopteran model species, as the multimodel hypothesis[5] requires; and third, we find no evidence for a negative relationship between mimetic fidelity and abundance, which calls into question the kin-selection[6] hypothesis. By contrast, a strong positive relationship between mimetic fidelity and body size supports the relaxed-selection hypothesis[7,8], suggesting that reduced predation pressure on less profitable prey species limits the selection for mimetic perfection.**

Much of evolutionary theory relating to mimicry has been based on the assumption that the fidelity of mimicry in any given system is extremely high (reviewed in ref. 9). Of course, if mimicry were poor, one might intuitively expect that signal receivers would learn be able to distinguish mimics from their models and (depending on context) accept or reject them. In reality, however, there are many examples of inaccurate or low-fidelity mimics[3,5,6,8,10]. For example, the relative compositions of key odour compounds of specific non-rewarding orchids differ markedly from the bees they have evolved to resemble[10]. Similarly, although mimetic spiders of the genus *Cosmophasis* bear some resemblance to ants, they are readily visually discriminated by the human observer[11]. Perhaps the best examples of imperfect mimics are found in hoverflies (Diptera: Syrphidae), which are considered Batesian (harmless) mimics of hymenopteran models[2] but seem to vary markedly across species in the degree of mimetic perfection[3,12] (see Supplementary Fig. 1).

Numerous hypotheses have been proposed to explain the evolution and maintenance of 'imperfect' mimicry, but despite calls for study there have been no comparative tests of their validity[6,13]. Common (and interrelated) explanations include the following: first, 'eye of the beholder', such that poor mimics to human eyes remain good mimics to natural predators[4]; second, 'multimodel', such that mimics gain most benefit from imperfect similarity to multiple models[5]; third, kin selection, such that imperfect mimicry is maintained through its benefit to conspecifics carrying the same trait[6]; fourth, constraints such that some factor limits the evolution of more perfect mimicry[14] including trade-offs (for example mimetic perfection versus thermoregulation[14] or camouflage[15]), phylogenetic constraints on body plan, or lack of genetic variation; and fifth, relaxed selection, such that selection for mimicry gradually weakens to a point at which it is readily counteracted by weak selection or mutation[7,8] (see Supplementary Information for additional hypotheses). Here we describe new comparative morphological and genetic data that allow us to evaluate which of these hypotheses are best able to explain the range of mimetic perfection seen in hoverflies.

A long-standing challenge in elucidating the ultimate causes of imperfect mimicry is that of quantifying the extent of mimetic fidelity between mimics and models, which frequently differ in multiple trait dimensions ranging from colour to shape. Previous measures of mimetic fidelity have used human rankings[16], pigeon responses[12,17], pixel mapping[12], neural networks[16] and multivariate analyses[18]. We employed subjective human rankings of mimetic fidelity (hereafter $f_{\mathrm{HR}}$; see Methods) across a range of species that were compared for consistency against a measure derived from a multivariate analysis of trait values (hereafter $f_{\mathrm{MD}}$; see Methods).

Overall, our morphological analysis of 38 syrphid species and 10 hymenopteran model species indicated that there was a clear statistical difference in appearance between the two taxa (Syrphidae and Hymenoptera) (nested multivariate analysis of variance: taxon, $F_{1,427} = 797.77$, $P < 0.001$; species, $F_{47,427} = 11.03$, $P < 0.001$). The first three canonical variates in a generalized canonical discriminant analysis (GCDA) explained 80.6% of the variance between the species in terms of their morphological features (individually: 41.1%, 20.4% and 19.2%). The Mahalanobis distances between each of the syrphid species and each of the Hymenoptera groups were calculated from these three canonical variates. This measure was multiplied by $-1$ to give a quantity, $f_{\mathrm{MD}}$, that is positively related to mimetic fidelity. Syrphids and hymenopterans tend to cluster with their respective orders, largely on the basis of relative length of antennae ($L_{\mathrm{ant}}$), a feature that is thought to be used in discrimination by birds[16]. The multimodel hypothesis[5] would predict that mimics fall between several models, gaining greater benefit from multiple, weaker associations. Our analysis clearly indicates that there are no mimetic phenotypes in our sample that could be considered to be falling morphologically between two or more distinct model phenotypes (Fig. 1).

The eye-of-the-beholder hypothesis recognizes that the natural predators of mimics (such as birds) and humans differ in both their perception and cognitive abilities, and argues that the apparent variation in mimetic perfection is therefore illusory and/or misleading. However, our multivariate measure of mimetic fidelity correlated well with our human ranking ($r = 0.555$, d.f. $= 36$, $P < 0.001$; Fig. 2), whereas similar work indicates that trained pigeons rank mimetic fidelity of hoverfly species in much the same way as humans do (Supplementary Fig. 2). Additional results suggest that behavioural mimicry (antenna waving, mock stinging, wing wagging) occurs only in species that humans classify as high-fidelity mimics (H.D.P., C.H.,

[1]Department of Biology, Carleton University, 1125 Colonel By Drive, Ottawa, K1S 5B6, Canada. [2]Agriculture and Agri-Food Canada, Canadian National Collection of Insects, Arachnids and Nematodes, K.W. Neatby Building, 960 Carling Avenue, Ottawa, K1A 0C6, Canada.

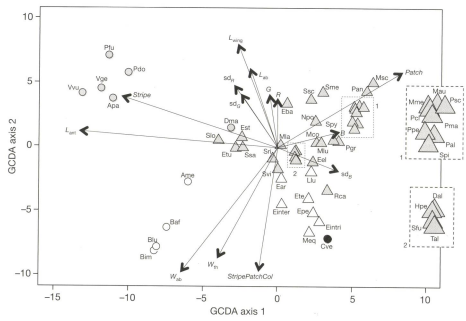


**Figure 1 | GCDA plot of biometrical measurements.** Circles are models (hymenopterans); triangles are mimics (syrphids); grey symbols are wasps or wasp mimics. Open symbols are bees or bee mimics, and the solid black circle is the non-mimetic syrphid *Cheilosia vernalis*. Species codes can be found in Supplementary Table 2; other abbreviations are described in Methods.

J.H.S. and T.N.S., unpublished observations), further suggesting that the human-based quantification of mimetic perfection is ecologically relevant. Taken together, these findings suggest that we can discount the eye-of-the-beholder hypothesis as an explanation for interspecific variation in hoverfly fidelity.

It has been stated frequently that, within hoverflies at least, poor mimics tend to occur at higher population densities than good mimics[3,5,12]. Although this relationship is plausible, it remains entirely anecdotal. The kin-selection hypothesis for imperfect mimicry not only assumes a degree of family grouping (which is unlikely in hoverflies[3]) but also predicts that the evolved degree of mimetic perfection will be lowest when mimics are relatively common and/or relatively beneficial to attack in comparison with their models[6]. This prediction arises from the assumption that predators that are largely unable to distinguish mimics from models will sample those high-fidelity mimics at a greater rate when the incentive to attack is greater. The constraints[14,15] and relaxed-selection[7,8] hypotheses predict the opposite, namely that the evolved degree of perfection will be highest when mimics are relatively common and/or relatively beneficial to attack as a result of the increased selection pressure to avoid predation through mimicry. A meta-analysis of 11 independent studies (Supplementary Table 1) demonstrated no evidence of a strong correlation between relative abundance and either measure of mimetic fidelity in our 38 focal species, either before controlling for phylogenetic autocorrelation ($f_{HR}$, $\bar{r} = 0.065$ (95% confidence interval (CI), −0.052 to 0.181); $f_{MD}$, $\bar{r} = 0.001$ (95% CI, −0.149 to 0.152)) or after controlling for phylogeny by using phylogenetic generalized least-squares regression for a subset of 31 species (Fig. 3) ($f_{HR}$, $\bar{r} = -0.083$ (95% CI, −0.031 to 0.198); $f_{MD}$, $\bar{r} = 0.223$ (95% CI, 0.058–0.389)). Note that this latter correlation between $f_{MD}$ and abundance was significant (the 95% CI did not overlap zero) and positive, indicating that in this case poor mimics tend to be less common. Therefore, on the basis of our sample of species (that is, those sufficiently common to appear regularly in systematic field surveys) we found no evidence that good mimics tend to be rarer (Supplementary Figs 3 and 4).

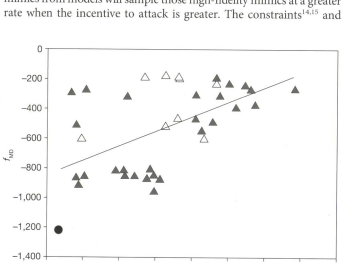


**Figure 2 | The relationship between Mahalanobis distances ($f_{MD}$) and human rankings ($f_{HR}$) measures of mimetic fidelity in hoverflies.** The line shows the fitted linear regression. Filled triangles, wasp mimics; open triangles, bee mimics; filled circle, the non-mimetic syrphid *Cheilosia vernalis*.

The constraints[14,15] and relaxed-selection[7,8] hypotheses suggest that smaller-bodied (and thus less nutritionally profitable[19]) species will endure low levels of predation, even if they are poor mimics, which produces weaker selection for improved mimicry; the kin-selection hypothesis predicts the opposite (see above). Therefore the relationship between the body size of hoverfly species and their mimetic fidelity was assessed. There was a highly significant relationship between body size (principal component 1; −PC1) and $f_{HR}$ both before controlling for phylogeny (Pearson's correlation, $r = 0.680$, d.f. = 36, $P < 0.001$) and after controlling for phylogeny (phylogenetic generalized least-squares regression, $t = 4.693$, $P < 0.001$). The relationship between body size and $f_{MD}$ was also highly significant before controlling for phylogeny ($r = 0.632$, d.f. = 36, $P < 0.001$) and after controlling for phylogeny ($t = 3.005$, $P = 0.005$); see Fig. 4. Finally, our meta-analysis indicates that the relative abundance of hoverfly species was only weakly (negatively) correlated with their body size before controlling for phylogeny ($\bar{r} = -0.132$ (95% CI, −0.239 to −0.024)) and after controlling for phylogeny ($\bar{r} = -0.240$ (95% CI, −0.476 to −0.005)), and it is clear that this relationship is not consistent across studies (Supplementary Fig. 5).

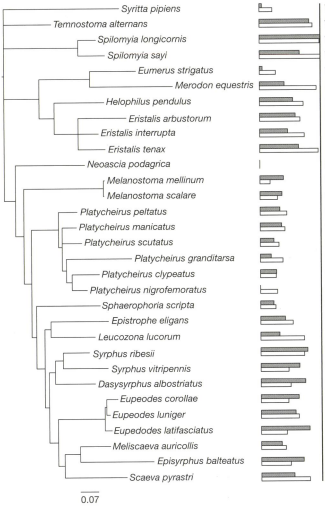


**Figure 3 | Phylogenetic relationships between the 31 hoverfly species (Diptera: Syphidae) for which fidelity and body-size data exist.** Shaded bars show the species' mimetic fidelity ($f_{HR}$), and open bars show the species body size (−PC1). In both cases, the length of the bars is scaled from smallest to the largest score for the species shown. The model for each hoverfly species is shown at the right (W, wasp; B, bee). See the text for details of the tree construction methods, and Supplementary Fig. 6 for the phylogeny of all 81 species for which the cytochrome oxidase c subunit I (*COI*) gene has been sequenced.

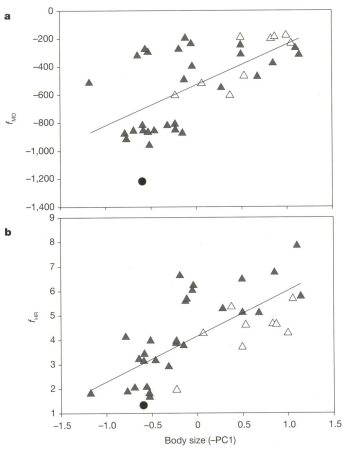


**Figure 4 | Relationship between body size (estimated as −PC1) and two measures of mimetic fidelity. a**, A measure of mimetic fidelity based on Mahalanobis distances ($f_{MD}$). **b**, Human ratings of mimetic fidelity ($f_{HR}$). Lines show the fitted linear regressions. Filled triangles, wasp mimics; open triangles, bee mimics; filled circle, the non-mimetic syrphid *Cheilosia vernalis*.

The constraints and relaxed-selection hypotheses both suggest that larger, more profitable species will tend to achieve a higher degree of mimetic fidelity at equilibrium, as a result of the greater underlying incentive on predators to attack them. Other factors influencing profitability might include evasive flight behaviour, but predation of hoverflies by birds takes place largely on flowers[3]. Of course, the predicted evolutionary trajectory for small and large mimics is less obvious if larger-bodied species are rarer than smaller-bodied species[18,20]; however, as noted above, there is no consistent evidence that this is true. Similarly, our expectation that selection might be less intense on small species because they are less valuable prey might not hold if predators rely heavily on body size as a trait to distinguish mimics from models[21] (hymenopteran models tend to be larger). Thus, if predators were highly sensitive to difference in body size, then depending on conditions there might be a complete relaxation of selection on mimicry in small species (because they are always attacked regardless of mimetic fidelity), leading to the same general outcome we have observed, or even stronger selection mimetic fidelity in small species as a way to counteract size-based discrimination. Nevertheless, there is evidence that predators cannot discriminate perfectly between mimics and models on the basis of body size[21], and so our profitability interpretation seems the most reasonable.

Mimicry provides a textbook example of adaptation, but researchers have long debated why the fidelity of many imperfect mimics is not further improved by natural selection. Our study represents the first attempt to evaluate multiple hypotheses for imperfect mimicry in the group best known for it, and the first to reveal a significant pattern. Of the five primary hypotheses that we evaluated, our comparative study is only consistent with the constraints and relaxed-selection hypotheses while questioning the assumptions and predictions of the kin-selection, eye-of-the-beholder and multimodel hypotheses. Our revelation of a strong positive relationship between body size and mimetic fidelity is readily explained if body size influences predation behaviour and thereby the intensity of selection for more perfect mimicry. Indeed, relationships between body size and the evolution of aposematic coloration in dendrobatid frogs[22] and putative snake mimicry in Lepidoptera[23] may also be explained by the kinds of processes we have invoked. The fact that we can explain the variation in mimetic fidelity on the basis of a relaxation of selection on mimetic fidelity alone, without the need to invoke a specific constraint to generate counter-selection, renders the relaxed-selection hypothesis entirely sufficient to explain the variation we have documented, but we cannot discount the constraints hypothesis. Whether the patterns we have revealed are observed in other mimicry complexes remains to be seen. However, it is clear that the comparative method will be important in evaluating the various explanations not only for imperfect mimicry but for limits to adaptation in general.

## METHODS SUMMARY

We focused on 35 hoverfly species recorded in the most extensive multiannual abundance data set available[24] (see Supplementary Table 2) and three additional high-fidelity mimics. Phenotypic characters relevant to avian perception were measured from photographs of the 38 species. These characters included antenna length ($L_{ant}$), abdomen length ($L_{ab}$), abdomen width ($W_{ab}$), thorax width ($W_{th}$), wing length ($L_{wing}$), all expressed relative to head width ($W_{head}$). The mean red, green and blue colours ($R$, $G$ and $B$) of the abdomen and associated standard deviations ($sd_R$, $sd_G$ and $sd_B$) were estimated. Finally, the number and colour of patches and/or stripes were recorded (*Stripe*, *Patch*, *StripePatchCol*). The Mahalanobis distances between species' centroids when these multivariate data were plotted in multivariate space gave a measure of mimetic fidelity, $f_{MD}$, and a principal components analysis of linear dimensions gave a measure of body size (−PC1, because the first principal component was negatively correlated with size). A sample of the photographs, all dorsal view and of the same apparent size, representing two different individuals of each of the 38 syrphid species, were rated by human volunteers ($n = 21$) for similarity (from 1 (very poor mimic) to 10 (excellent mimic)) to photographs of a wasp, honeybee and bumblebee. The highest average rating provided a second measure of mimetic fidelity, $f_{HR}$.

We calculated the relative abundance of our species from 11 independent studies on the basis of a range of trapping and survey methods. The *COI* gene was sequenced for 77 species of 21 genera of Syrphidae, including 31 species for which we have morphological data, and phylogenetic trees were constructed by using Bayesian methods. Relationships between variables were evaluated with control for phylogenetic autocorrelation (using phylogenetic generalized least-squares regression) and without control for phylogenetic autocorrelation (using Pearson correlations). For the abundance analysis, weighted-mean correlations ($\bar{r}$) and 95% confidence intervals were calculated across all 11 studies.

**Full Methods** and any associated references are available in the online version of the paper at www.nature.com/nature.

**Received 21 December 2011; accepted 17 February 2012.**


1. Bates, H. Contribution to an insect fauna of the Amazon Valley, Lepidoptera: Heliconidae. *Trans. Linn. Soc. Lond.* **23,** 495–566 (1862).
2. Mostler, G. Observations on the question of wasp mimicry. *Z. Morphol. Oekol. Tiere* **29,** 381–454 (1935).
3. Gilbert, F. in *Insect Evolutionary Ecology* (eds Fellowes, M. D. E., Holloway, G. J. & Rolff, J.) 231–288 (CABI Publishing, 2005).
4. Cuthill, I. C. & Bennett, A. T. D. Mimicry and the eye of the beholder. *Proc. R. Soc. Lond. B* **253,** 203–204 (1993).
5. Edmunds, M. Why are there good and poor mimics? *Biol. J. Linn. Soc.* **70,** 459–466 (2000).
6. Johnstone, R. A. The evolution of inaccurate mimics. *Nature* **418,** 524–526 (2002).
7. Duncan, C. J. & Sheppard, P. M. Sensory discrimination and its role in the evolution of Batesian mimicry. *Behaviour* **24,** 269–282 (1965).
8. Sherratt, T. N. The evolution of imperfect mimicry. *Behav. Ecol.* **13,** 821–826 (2002).
9. Ruxton, G. D., Sherratt, T. N. & Speed, M. P. *Avoiding Attack: The Evolutionary Ecology of Crypsis, Warning Signals, and Mimicry* (Oxford Univ. Press, 2004).
10. Vereecken, N. J. & Schiestl, F. P. The evolution of imperfect floral mimicry. *Proc. Natl Acad. Sci. USA* **105,** 7484–7488 (2008).
11. Edmunds, M. Do Malaysian *Myrmarachne* associate with particular species of ant? *Biol. J. Linn. Soc.* **88,** 645–653 (2006).
12. Dittrich, W., Gilbert, F., Green, P., McGregor, P. & Grewcock, D. Imperfect mimicry—a pigeon's perspective. *Proc. R. Soc. Lond. B* **251,** 195–200 (1993).
13. Chittka, L. & Osorio, D. Cognitive dimensions of predator responses to imperfect mimicry. *PLoS Biol.* **5,** e339 (2007).
14. Holen, Ø. H. & Johnstone, R. A. The evolution of mimicry under constraints. *Am. Nat.* **164,** 598–613 (2004).
15. Speed, M. P. & Ruxton, G. D. Imperfect Batesian mimicry and the conspicuousness costs of mimetic resemblance. *Am. Nat.* **176,** E1–E14 (2004).
16. Bain, R. S., Rashed, A., Cowper, V. J., Gilbert, F. S. & Sherratt, T. N. The key mimetic features of hoverflies through avian eyes. *Proc. R. Soc. B* **274,** 1949–1954 (2007).
17. Green, P. R. *et al.* Conditioning pigeons to discriminate naturally lit insect specimens. *Behav. Processes* **46,** 97–102 (1999).
18. Iserbyt, A. *et al.* Frequency-dependent variation in mimetic fidelity in an intraspecific mimicry system. *Proc. R. Soc. B* **278,** 3116–3122 (2011).
19. Sutherland, W. J. Do oystercatchers select the most profitable cockles? *Anim. Behav.* **30,** 857–861 (1982).
20. Harper, G. R. & Pfennig, D. W. Mimicry on the edge: why do mimics vary in resemblance to their model in different parts of their geographical range? *Proc. R. Soc. B* **274,** 1955–1961 (2007).
21. Marples, N. M. Do wild birds use size to distinguish palatable and unpalatable prey types? *Anim. Behav.* **46,** 347–354 (1993).
22. Hagman, M. & Forsman, A. Correlated evolution of conspicuous coloration and body size in poison frogs (Dendrobatidae). *Evolution* **57,** 2904–2910 (2003).
23. Janzen, D. H., Hallwachs, W. & Burns, J. M. A tropical horde of counterfeit predator eyes. *Proc. Natl Acad. Sci. USA* **107,** 11659–11665 (2010).
24. Gilbert, F. S. & Owen, J. Size, shape, competition and community structure in hoverflies (Diptera: Syrphidae). *J. Anim. Ecol.* **59,** 21–39 (1990).


**Supplementary Information** is linked to the online version of the paper at www.nature.com/nature.

**Acknowledgements** We thank W. Knee for help with the Bayesian analysis, and R. Laird, G. Ruxton and M. Speed for comments on the manuscript. The human aspect of this research was approved by the Carleton University Research Ethics Committee and conducted according to the guidelines set out in the Tri-Council Policy Statement on Ethical Conduct for Research Involving Humans; subjects gave informed consent. The work was supported by grants to T.N.S. from the Natural Sciences and Engineering Research Council of Canada (NSERC), the Canada Foundation for Innovation and the Ontario Innovation Trust, and to J.H.S. from Agriculture and Agri-Food Canada, the Canadian Centre for DNA Barcoding and NSERC Canpolin. C.H. was supported by an Ontario MRI Fellowship.

**Author Contributions** H.D.P. photographed and measured specimens, and collected data on human rankings. J.H.S. provided the novel molecular phylogeny. C.H. analysed the data. C.H., K.R.A. and T.N.S. wrote the paper. T.N.S. conceived the project. All authors discussed the results and provided comments on the manuscript.

**Author Information** All new genetic sequences are deposited in GenBank and are listed in Supplementary Table 4. Reprints and permissions information is available at www.nature.com/reprints. The authors declare no competing financial interests. Readers are welcome to comment on the online version of this article at www.nature.com/nature. Correspondence and requests for materials should be addressed to T.N.S. (sherratt@connect.carleton.ca).

LETTER

doi:10.1038/nature10877

# MEGF10 and MEGF11 mediate homotypic interactions required for mosaic spacing of retinal neurons

Jeremy N. Kay[1], Monica W. Chu[1] & Joshua R. Sanes[1]

**In many parts of the nervous system, neuronal somata display orderly spatial arrangements[1]. In the retina, neurons of numerous individual subtypes form regular arrays called mosaics: they are less likely to be near neighbours of the same subtype than would occur by chance, resulting in 'exclusion zones' that separate them[1–4]. Mosaic arrangements provide a mechanism to distribute each cell type evenly across the retina, ensuring that all parts of the visual field have access to a full set of processing elements[2]. Remarkably, mosaics are independent of each other: although a neuron of one subtype is unlikely to be adjacent to another of the same subtype, there is no restriction on its spatial relationship to neighbouring neurons of other subtypes[5]. This independence has led to the hypothesis that molecular cues expressed by specific subtypes pattern mosaics by mediating homotypic (within-subtype) short-range repulsive interactions[1,4–9]. So far, homotypic molecules have been identified that show such activity, so this hypothesis remains untested. Here we demonstrate in mouse that two related transmembrane proteins, MEGF10 and MEGF11, have critical roles in the formation of mosaics by two retinal interneuron subtypes, starburst amacrine cells and horizontal cells. MEGF10 and 11 and their invertebrate relatives *Caenorhabditis elegans* CED-1 and *Drosophila* Draper have hitherto been studied primarily as receptors necessary for engulfment of debris following apoptosis or axonal injury[10–14]. Our results demonstrate that members of this gene family can also serve as subtype-specific ligands that pattern neuronal arrays.**

The retina contains over 70 neuronal subtypes, divided into broad categories of photoreceptors, interneurons and retinal ganglion cells[15]. To seek molecules involved in cell–cell recognition events during retinal circuit assembly, we purified 13 subtypes of retinal neurons from transgenic mice and used microarrays to inventory the genes they expressed[16,17]. We collected cells at postnatal day (P)6, a time at which synapse formation and mosaic refinement are underway. From this data set we identified genes selectively expressed by specific subtypes, including starburst amacrine cells (SACs), an interneuronal subtype that has critical roles in motion detection[18]. The approximately 100 genes that met our criteria for selective SAC expression included most known SAC markers as well as potential new markers (Fig. 1a and Supplementary Table 1). Thirty-one of the novel genes were tested by *in situ* hybridization or immunohistochemistry in combination with SAC markers such as choline acetyltransferase (ChAT) or calbindin[19]. This secondary screen yielded 26 genes (Supplementary Table 1), among which were two homologues, *Megf10* and *Megf11*. These genes encode transmembrane proteins with multiple epidermal growth factor (EGF)-like domains, a single membrane-spanning region, and a cytoplasmic domain with several binding sites for signal transduction components[10,13] (Supplementary Fig. 1). At P5–6, both genes were strongly expressed in SACs (Fig. 1a–c). Both were also expressed in horizontal cells (HCs), which were not part of the data set.

SACs are present in both the inner nuclear and ganglion cell layers, and form independent mosaics in each[5]. These mosaics develop during late embryonic stages, as newborn SACs migrate from the site of their birth, the outer neuroblast layer, to their final laminar locations. SACs begin to exhibit mosaic spacing upon arrival at their destinations, presumably due to contacts with their homotypic neighbours[8,9]. As

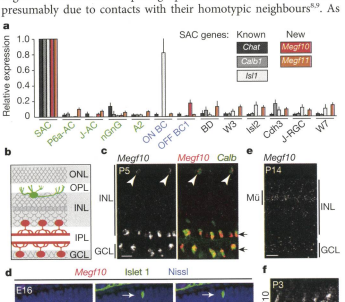


**Figure 1 | Expression of *Megf10* and *Megf11* in SACs and HCs. a**, Relative expression level of *Megf10*, *Megf11* and the known SAC markers *Chat*, *Calb1* (encoding calbindin) and *Isl1* (islet 1) in 13 amacrine (green), bipolar (blue) and retinal ganglion cell (black) subtypes analysed with microarrays. Level in SACs set to 1 for each gene. *Isl1* was also detected in ON bipolar cells as previously reported[21]. Abbreviations for subtypes are defined in Supplementary Table 2. **b**, Schematic of retina. INL, inner nuclear layer with horizontal, bipolar, amacrine, and Müller glial cells; IPL, inner plexiform layer with synapses among bipolar, amacrine and ganglion cells; GCL, ganglion cell layer including displaced amacrine cells; ONL, outer nuclear layer containing photoreceptors; OPL, outer plexiform layer with photoreceptor synapses. SACs (red), HCs (green) and Müller cells (dark grey row) are indicated. **c**, *In situ* hybridization for *Megf10* (left panel; red in right panel) combined with anti-calbindin immunohistochemistry (green in right panel) at P5 shows expression in SACs (black arrows) and HCs (arrowheads). **d**, *Megf10* (red) in E16 retina. Islet 1 (green) marks SACs migrating through the outer neuroblast layer (ONbL) and in the INL[9]. *Megf10* (red) is expressed by migrating SACs as they arrive in the INL (arrowhead), but not at earlier stages of their migration through the ONbL (arrows). **e**, *Megf10* expression appears in Müller glia (Mü) and is lost from SACs and HCs by P14. **f**, Double-label immunostaining for MEGF10 (green) and ChAT (red). MEGF10 protein localizes to the somata and processes of developing SACs (also see Supplementary Fig. 1). Scale bars, 20 μm (**c**–**e**) or 10 μm (**f**).

[1]Center for Brain Science and Department of Molecular and Cellular Biology, Harvard University, 52 Oxford Street, Cambridge, Massachusetts 02138, USA.

new SACs are added to the array, local cellular rearrangements maintain mosaic spacing[14,9]. Mosaic spacing is maintained even as SAC dendrites grow to overlap with those of their neighbours[20]; thus, mosaicism is distinct from the phenomenon called tiling, which minimizes dendritic overlap[15]. Co-staining at embryonic day (E)16 with the early SAC marker islet 1 (refs 9, 21) demonstrated that newborn SACs activated *Megf10* expression as they finished their migration and became integrated into mosaics (Fig. 1d). *Megf10* expression persisted in SACs from E16 to the first postnatal week, and began in HCs at P0 (Supplementary Fig. 1 and data not shown). In the second postnatal week, *Megf10* was downregulated in neurons but appeared in Müller glia (Fig. 1e), consistent with previous reports that *Megf10* is expressed by brain glia[22]. To determine the subcellular localization of MEGF10 in neurons, we generated an antibody to recombinant protein (Supplementary Fig. 1). MEGF10 was present both on the somata of SACs and HCs and on their processes (Fig. 1f and Supplementary Fig. 1). As expected, immunoreactivity levels on SACs and HCs were highest during the first postnatal week, and then declined (data not shown). Thus, *Megf10* is expressed by SACs and MEGF10 protein is present on SAC processes during the time that mosaics form. Because *Megf11* expression was not observed in retina until after SAC mosaics had formed (see later), we focused first on *Megf10*.

To investigate whether MEGF10 is required for SAC development, we generated mutant mice (Supplementary Fig. 2). *Megf10* mutants were viable and fertile and their retinas exhibited no gross abnormalities. Mutant SACs migrated to the inner nuclear and ganglion cell layers as in controls, they were present in normal numbers, and their dendrites projected to appropriate sublaminae of the inner plexiform layer (Fig. 2a–c). Examination of whole mounts showed, however, a marked loss of regular spacing among SAC somata, suggesting that their mosaic arrangement had been disrupted (Fig. 2a and Supplementary Fig. 3).

To assess the degree to which SAC mosaics were disrupted, we measured the exclusion zone—the region surrounding each SAC in which other SACs are rarely found. This parameter is calculated from the density recovery profile, a plot of cell density as a function of distance from each SAC in the array[23] (Fig. 2d). The SAC exclusion zone in mutants was smaller than in wild-type littermates, and was approximately equal to the diameter of a SAC soma (Fig. 2e). As the only limitation on proximity was soma size, SACs seem to be positioned randomly in *Megf10* mutants. This conclusion was supported by two additional measurements of spatial order: the packing factor[23], another index of regularity calculated from the density recovery profile; and an independent measure, the Voronoi domain regularity index, which quantifies variations in the area of the territories nearest to each cell in an array[20,24]. In each case the index calculated for SAC arrays in *Megf10* mutants was similar to that measured for computer-generated random arrays, whereas SAC arrays from wild-type littermates were highly ordered (Fig. 2f, g); heterozygotes showed a mild disorganization (Supplementary Fig. 4). Together these results suggest that MEGF10 acts in SACs to impose a minimal intercellular spacing; in

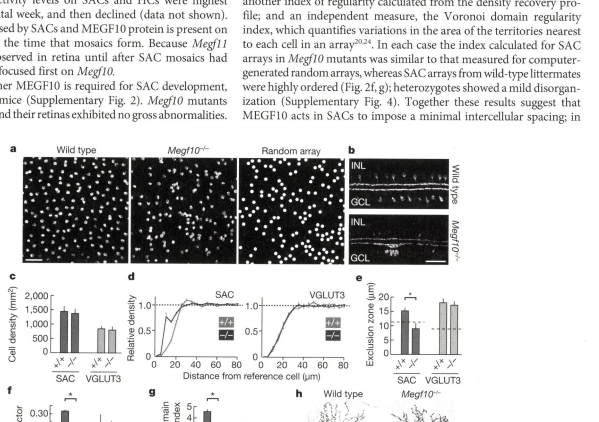


**Figure 2 | Loss of SAC mosaic spacing in *Megf10* mutant mice.** **a**, SAC mosaic in inner nuclear layer (INL) of wild-type (left) and *Megf10*$^{-/-}$ (centre) retina, revealed by whole-mount staining with anti-ChAT. Wild-type mice have evenly spaced SAC somata, whereas mutants exhibit clumps and gaps similar to those seen in a simulation of a random cellular array (right). See Supplementary Fig. 3 for similar results in ganglion cell layer (GCL) SACs. **b**, ChAT-stained retinal sections from wild-type and *Megf10* mutant animals. Laminar positions of SAC somata and processes are normal in mutants, even in regions where somata are clumped. **c**, Density of SACs and VGLUT3$^{+}$ amacrine cells is similar in wild-type (+/+) and *Megf10* mutant (−/−) retina. **d**, Density recovery profiles (DRPs) for the SAC (INL) and VGLUT3$^{+}$ amacrine arrays. Graphs show the density of cells in a ring of radius *x*, relative to the density of cells in the image as a whole. Dashed line, DRP of random point array. The exclusion zone characteristic of mosaic spacing is measured as a dip below this line. **e**, Exclusion zone radius measured from **d**. Dashed line, expected result for an array of cells distributed randomly; that is, the diameter of a single cell. Increases above this minimum indicate spatial order. The mutant SAC exclusion zone radius was similar in size to a SAC cell diameter, and was significantly smaller than wild type (*$P < 0.0001$). VGLUT3$^{+}$ amacrine exclusion zones were unaffected. **f**, **g**, SAC packing factor (**f**) and Voronoi domain regularity index (**g**) were significantly lower in *Megf10*$^{-/-}$ mice than in wild-type littermates (*$P < 0.0001$). Dashed line, mean for arrays of cells distributed randomly. Wild-type SACs and VGLUT3$^{+}$ cells of both genotypes were non-randomly arrayed. The SAC array in mutants was not significantly different from random arrays (**f**, $P = 0.16$; **g**, $P = 0.48$). **h**, Morphology of single GCL SACs, labelled with adeno-associated virus driving membrane-targeted Cherry fluorescent protein, showed no gross abnormalities in *Megf10* mutants ($n \geq 8$ cells each genotype). Data from P15 (**a**–**g**) or P80 (**h**) mice. Scale bars, 50 μm. Error bars, s.e.m.

its absence SACs assume random positions relative to each other. By contrast, other amacrine cell types examined (VGLUT3- (also known as SLC17A8) and tyrosine hydroxylase-positive) as well as bistratified direction-selective retinal ganglion cells, which are prominent synaptic targets of SACs[18], showed normal mosaic spacing (Fig. 2d–g and Supplementary Fig. 3).

In mice lacking the adhesion molecules DSCAM or DSCAML1, certain retinal cell mosaics form normally, then degrade secondary to hyperfasciculation of their neurites[25,26]. To investigate whether MEGF10 acts in a similar indirect fashion, we labelled individual SACs in mutants. Lack of MEGF10 had no obvious effect on SAC dendritic morphology (Fig. 2h). Moreover, soma disorganization was already evident by P0 (Supplementary Fig. 5), shortly after mosaics form, indicating that MEGF10 affected formation of SAC mosaics.

Next we asked whether MEGF10 is also essential for formation of the HC mosaic. Loss of MEGF10 had only a modest effect on HC regularity (Fig. 3). We therefore considered that MEGF11 might have a redundant role. *Megf11* was not expressed in embryonic retina, but it appeared in HCs and SACs during the first postnatal week and persisted into adulthood (Fig. 3a–d). Importantly, SAC mosaics begin to form before P0, but HC mosaics are established postnatally[4,6,9]. We therefore generated *Megf11* mutant mice (Supplementary Fig. 2), which, like *Megf10* mutants, showed no gross retinal abnormalities (Supplementary Fig. 6). Examination of HC arrays in *Megf11* mutants revealed a modest decrease in regularity similar to that in *Megf10* mutants, whereas in *Megf10*$^{-/-}$; *Megf11*$^{-/-}$ double-mutant animals, the HC mosaic was severely disrupted (Fig. 3e–m and Supplementary Fig. 7). By contrast, SACs were unaffected by loss of *Megf11* function, and were no more affected in double mutants than in *Megf10* single mutants (Supplementary Figs 6 and 8). Thus, *Megf11* is dispensable for SAC arrangement, but acts together with *Megf10* to shape the HC mosaic.

To elucidate the cellular mechanisms by which *Megf10* and *Megf11* act, we used a gain-of-function approach in which we introduced MEGF10 into the retina by electroporation of plasmid DNA at P0. We first tested the hypothesis that MEGF10 can act as a signal that repels SACs, creating the exclusion zone that defines mosaic spacing. The electroporation method predominantly transfects dividing cells, leading to expression in neurons that exit the cell cycle postnatally, such as bipolar cells, Müller glia, photoreceptors and late-born amacrine cells[27]. Because SACs and HCs are born embryonically, they are rarely transduced[27], allowing us to surround wild-type SACs and HCs with cells ectopically expressing excess MEGF10. Indeed, electroporation of plasmid encoding a fluorescent protein (FP) or a MEGF10–FP fusion produced retinal patches in which a large fraction of neurons, but no SACs or HCs, were FP$^{+}$ (Fig. 4a and Supplementary Fig. 9). Expression of MEGF10–FP (but not FP alone) resulted in exclusion of SACs and HCs from a swath at the edge of the electroporated patch, whereas spacing of these cells was essentially normal in patch centres (Fig. 4a, b and Supplementary Fig. 10). A truncated MEGF10 lacking the cytoplasmic domain produced an identical phenotype (Supplementary Fig. 10), ruling out the possibility that MEGF10 acts indirectly by triggering production of a repellent factor by the transfected cells. Thus, MEGF10 can act as a ligand that signals to SACs and HCs.

Because MEGF10 relatives have been implicated in cell engulfment[10–13], we asked whether its overexpression formed an exclusion zone by eliminating cells. We found no evidence for cell death at patch edges (no pyknotic nuclei or activated caspase-3 immunoreactivity; data not shown). Instead, cell density was increased at the outer edge of the cell-free swath, indicating that SACs had exited the patch to create the

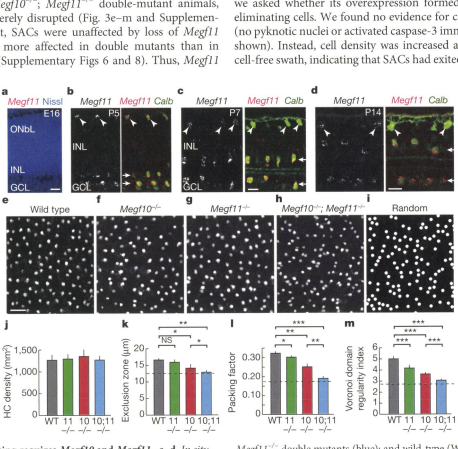


**Figure 3 | HC mosaic spacing requires *Megf10* and *Megf11*.** **a**–**d**, *In situ* hybridization for *Megf11* at ages indicated. *Megf11* (red) was not expressed at E16 (**a**). Calbindin immunostaining (green) labels SACs and HCs, which co-express *Megf11* at P5 (**b**), P7 (**c**) and P14 (**d**). See Fig. 1 for abbreviations. **e**–**i**, Retinal whole mounts stained for calbindin to reveal the HC array. In wild-type mice (**e**), HCs are distributed evenly. *Megf10*$^{-/-}$ mutants (**f**) and *Megf11*$^{-/-}$ mutants (**g**) show subtle changes in the regular spacing of HCs, whereas double *Megf10*$^{-/-}$;*Megf11*$^{-/-}$ mutants (**h**) show marked HC disorganization similar to a simulation of a random HC array (**i**). **j**–**m**, Quantification of HC spacing regularity in *Megf10*$^{-/-}$ (red) or *Megf11*$^{-/-}$ (green) single mutants; *Megf10*$^{-/-}$; *Megf11*$^{-/-}$ double mutants (blue); and wild-type (WT) siblings (grey). In all genotypes, HCs were present at normal density (**j**) but were less regularly spaced relative to wild type based on exclusion zone radius (**k**), packing factor (**l**) and Voronoi domain regularity (**m**) measurements as in Fig. 2. Double mutants showed significantly less order than single *Megf10*$^{-/-}$ or *Megf11*$^{-/-}$ mutants and approach random arrangement, indicated by dashed lines (**k**, mean HC soma diameter; **l**, **m**, computed values for random arrays). *P* values: $*P < 0.01$, $**P < 0.001$, $***P < 0.0001$. NS, not significant. Error bars give s.e.m. Data in **e**–**m** from P15 animals. Scale bars, 20 μm (**a**–**d**; **b**, **c** share scale) or 50 μm (**e**–**i**).

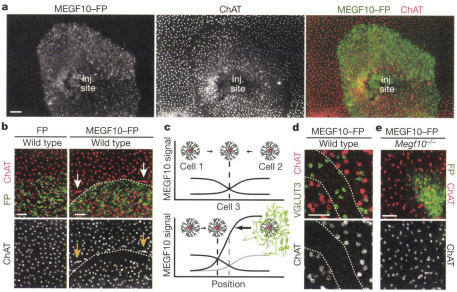


**Figure 4 | MEGF10 acts as both ligand and receptor to trigger SAC repulsion.** **a**, A retinal patch transfected by electroporation with plasmid encoding MEGF10–FP fusion protein, viewed in flat mount. SAC somata in INL, stained with anti-ChAT, are excluded from a swath at the patch edge. SACs are evenly spaced elsewhere, except where the retina was pierced to inject DNA (Inj. site). **b**, Higher-magnification views of patch edges. FP misexpression (left) did not affect SAC spacing, but MEGF10–FP (right) produced a SAC-free zone just inside the transfected region and induced apparent crowding of SACs immediately outside it (arrows). Dashed line, patch edge. See Supplementary Fig. 11 for quantification of cell distribution at patch edges. **c**, Hypothesis for MEGF10 function based on **a**, **b**. In wild-type retina (top), SACs use MEGF10 as a ligand to signal their location to neighbouring SACs. Cell 3 positions itself at the point where repulsive signals on either side (from Cell 1 and Cell 2) are equal. In MEGF10–FP overexpression (bottom), that location is now outside the patch. **d**, MEGF10–FP transfected whole-mount immunostained for ChAT and VGLUT3. Dashed lines mark SAC-free zone (see Supplementary Fig. 10). VGLUT3$^+$ amacrine cells are present in this zone. **e**, MEGF10–FP is incapable of generating a SAC-free zone when misexpressed in *Megf10* mutant retina, indicating that MEGF10 is needed for SAC responses to MEGF10. See Supplementary Fig. 11 for quantification. Scale bars, 100 μm (**a**); 50 μm (**b**–**e**). All retinas are from P10–P15 animals.

SAC-free zone (Fig. 4b and Supplementary Fig. 11). Our interpretation is that SACs and HCs are repelled by MEGF10, but that within MEGF10–FP patches the concentration of MEGF10 is similar in all directions, resulting in no net movement (Fig. 4c). Consistent with this view, SACs and HCs were entirely excluded from small patches (≤5–6 cell diameters; Supplementary Fig. 10). Together these results suggest that MEGF10 can act as a repellent ligand.

We next asked which cells are sensitive to MEGF10 ligand. In *Megf10* mutants, SACs and HCs are selectively affected; this might be because they are uniquely sensitive to MEGF10 or because only these cells encounter endogenous MEGF10 at high concentration. Ectopic expression allowed us to distinguish between these possibilities. None of 13 other amacrine, bipolar or retinal ganglion cell subtypes assayed with cell-type-specific markers was detectably affected by MEGF10–FP (Fig. 4d and Supplementary Table 3). Thus, MEGF10 appears to act as a cell-surface ligand for a receptor specifically expressed by SACs and HCs.

This led us to ask whether MEGF10 might be the MEGF10 receptor. We used cultured epithelial cells (HEK293) to seek evidence for a MEGF10-dependent homotypic interaction. Whereas FP-expressing cells overlapped, MEGF10–FP-expressing cells formed sharp borders with narrow gaps (Supplementary Fig. 12a), consistent with previous results[14]. This 'jigsaw' pattern reflected suppression or elimination of filopodia at points of intercellular apposition (Supplementary Fig. 12b). Jigsaw formation and loss of filopodia required the MEGF10 cytoplasmic domain and did not occur when a MEGF10–FP-expressing cell contacted an untransfected or FP-transfected cell (Supplementary Fig. 12b, c). Although we have been unable to demonstrate MEGF10 homophilic binding using biochemical methods (data not shown), these results suggest that a MEGF10-containing signalling complex mediates a homotypic interaction resulting in intercellular repulsion.

Finally, we tested the idea that MEGF10 serves as both ligand and receptor *in vivo*. To this end, we electroporated MEGF10 into *Megf10* mutant retina. Mutant SACs did not exit MEGF10–FP patches (Fig. 4e and Supplementary Fig. 11b), indicating that *Megf10* gene function is required for SACs to respond to MEGF10 repulsive signals. Together these results suggest a model in which SACs and HCs use MEGF10 as part of a receptor complex that detects MEGF10 on their homotypic neighbours. This repulsive signal positions their somata so as to equalize MEGF10 signals on all sides, thereby creating exclusion zones (Fig. 4c).

The phenomenon of retinal mosaicism implies a molecular system for cell-type-specific recognition. Several potential mechanisms have been proposed, based on imaging and computational studies, one being that short-range repulsive signals regulate tangential movements to establish each cell's territory[3,4,6–9]. So far, however, direct mediators of this phenomenon have not been described. Here we provide evidence that, for SACs and HCs, mosaic spacing requires repellent homotypic interactions mediated by MEGF10 and 11. Signals initiated by MEGF10/11 in growing neurites could lead to repositioning of the soma within the cytoplasm, perhaps by mechanisms resembling those that direct soma translocation in response to signals at the leading process of migrating neurons[28]. The finding that MEGF10 and 11 facilitate formation of three independent mosaics (two for SACs and one for HCs) appears at first to contradict the idea that mosaics are independent of each other and must therefore be regulated by distinct molecules[1,3–5]. However, because the three mosaics occupy distinct cellular planes, they may be exempt from the requirement for molecular individuation. Different molecules are likely to mediate homotypic interactions in other retinal subtypes, some of which may lead to soma translocation and others to the death of cells that violate minimal spacing[24].

We note two broader implications of our results. First, Draper/CED-1/MEGF10 homologues have until now been studied predominantly as receptors for cell engulfment[10–14]. Here we show that they also mediate cell–cell repulsion and can act as ligands as well as receptors, thereby expanding the roles for this gene family. Second, although mosaic arrangements have so far been studied formally only in retina, regularly arranged neuronal arrays are common features of central neural

organization[1,29]. Mechanisms similar to those described here could be involved in promoting this regularity.

## METHODS SUMMARY

Retinal neurons expressing fluorescent proteins were purified and used to generate amplified RNA for hybridizing Affymetrix microarrays as described previously[16,17]. SAC-specific genes were identified using dChip software. *Megf10* and *Megf11* mutant mice were produced from constructs generated by the Knockout Mouse Project and European Conditional Mouse Mutagenesis program (EUCOMM)[30]. Histological methods[16,17] and methods for electroporation of plasmid DNA *in vivo*[17,27] were described previously. HEK293 cells (ATCC) were cultured and transfected by standard methods.

For analysis of spatial statistics, we sampled a 635.9 μm square at 3–4 locations per retina. *X*–*Y* cell coordinates, marked manually, were used to calculate Voronoi domain areas (Fiji) or DRP statistics such as the effective radius (that is, exclusion zone) and packing factor (WinDRP). We generated random arrays matched in density and soma size to real data; these were analysed in parallel with data from mutants. For measurement of SAC crowding in gain-of-function experiments, the Delaunay triangulation[8] was used to define each cell's nearest neighbours.

**Full Methods** and any associated references are available in the online version of the paper at www.nature.com/nature.

**Received 8 October 2011; accepted 17 January 2012.**
**Published online 11 March 2012.**

1. Cook, J. E. & Chalupa, L. M. Retinal mosaics: new insights into an old concept. *Trends Neurosci.* **23,** 26–34 (2000).
2. Wässle, H. & Riemann, H. J. The mosaic of nerve cells in the mammalian retina. *Proc. R. Soc. Lond. B* **200,** 441–461 (1978).
3. Eglen, S. J. Development of regular cellular spacing in the retina: theoretical models. *Math. Med. Biol.* **23,** 79–99 (2006).
4. Reese, B. E. & Galli-Resta, L. The role of tangential dispersion in retinal mosaic formation. *Prog. Retin. Eye Res.* **21,** 153–168 (2002).
5. Rockhill, R. L., Euler, T. & Masland, R. H. Spatial order within but not between types of retinal neurons. *Proc. Natl Acad. Sci. USA* **97,** 2303–2307 (2000).
6. Huckfeldt, R. M. *et al.* Transient neurites of retinal horizontal cells exhibit columnar tiling via homotypic interactions. *Nature Neurosci.* **12,** 35–43 (2009).
7. Poché, R. A. *et al.* Somal positioning and dendritic growth of horizontal cells are regulated by interactions with homotypic neighbors. *Eur. J. Neurosci.* **27,** 1607–1614 (2008).
8. Galli-Resta, L. Local, possibly contact-mediated signalling restricted to homotypic neurons controls the regular spacing of cells within the cholinergic arrays in the developing rodent retina. *Development* **127,** 1509–1516 (2000).
9. Galli-Resta, L., Resta, G., Tan, S. S. & Reese, B. E. Mosaics of islet-1-expressing amacrine cells assembled by short-range cellular interactions. *J. Neurosci.* **17,** 7831–7838 (1997).
10. Wu, H.-H. *et al.* Glial precursors clear sensory neuron corpses during development via Jedi-1, an engulfment receptor. *Nature Neurosci.* **12,** 1534–1541 (2009).
11. MacDonald, J. M. *et al.* The *Drosophila* cell corpse engulfment receptor Draper mediates glial clearance of severed axons. *Neuron* **50,** 869–881 (2006).
12. Reddien, P. W. & Horvitz, H. R. The engulfment process of programmed cell death in *Caenorhabditis elegans*. *Annu. Rev. Cell Dev. Biol.* **20,** 193–221 (2004).
13. Hamon, Y. *et al.* Cooperation between engulfment receptors: the case of ABCA1 and MEGF10. *PLoS ONE* **1,** e120 (2006).
14. Suzuki, E. & Nakayama, M. MEGF10 is a mammalian ortholog of CED-1 that interacts with clathrin assembly protein complex 2 medium chain and induces large vacuole formation. *Exp. Cell Res.* **313,** 3729–3742 (2007).
15. Sanes, J. R. & Zipursky, S. L. Design principles of insect and vertebrate visual systems. *Neuron* **66,** 15–36 (2010).
16. Kay, J. N. *et al.* Retinal ganglion cells with distinct directional preferences differ in molecular identity, structure, and central projections. *J. Neurosci.* **31,** 7753–7762 (2011).
17. Kay, J. N., Voinescu, P. E., Chu, M. W. & Sanes, J. R. Neurod6 expression defines new retinal amacrine cell subtypes and regulates their fate. *Nature Neurosci.* **14,** 965–972 (2011).
18. Demb, J. B. Cellular mechanisms for direction selectivity in the retina. *Neuron* **55,** 179–186 (2007).
19. Haverkamp, S. & Wässle, H. Immunocytochemical analysis of the mouse retina. *J. Comp. Neurol.* **424,** 1–23 (2000).
20. Keeley, P. W., Whitney, I. E., Raven, M. A. & Reese, B. E. Dendritic spread and functional coverage of starburst amacrine cells. *J. Comp. Neurol.* **505,** 539–546 (2007).
21. Elshatory, Y. *et al.* Islet-1 controls the differentiation of retinal bipolar and cholinergic amacrine cells. *J. Neurosci.* **27,** 12707–12720 (2007).
22. Cahoy, J. D. *et al.* A transcriptome database for astrocytes, neurons, and oligodendrocytes: a new resource for understanding brain development and function. *J. Neurosci.* **28,** 264–278 (2008).
23. Rodieck, R. W. The density recovery profile: a method for the analysis of points in the plane applicable to retinal studies. *Vis. Neurosci.* **6,** 95–111 (1991).
24. Raven, M. A., Eglen, S. J., Ohab, J. J. & Reese, B. E. Determinants of the exclusion zone in dopaminergic amacrine cell mosaics. *J. Comp. Neurol.* **461,** 123–136 (2003).
25. Fuerst, P. G., Koizumi, A., Masland, R. H. & Burgess, R. W. Neurite arborization and mosaic spacing in the mouse retina require DSCAM. *Nature* **451,** 470–474 (2008).
26. Fuerst, P. G. *et al.* DSCAM and DSCAML1 function in self-avoidance in multiple cell types in the developing mouse retina. *Neuron* **64,** 484–497 (2009).
27. Matsuda, T. & Cepko, C. L. Electroporation and RNA interference in the rodent retina *in vivo* and *in vitro*. *Proc. Natl Acad. Sci. USA* **101,** 16–22 (2004).
28. Solecki, D. J., Model, L., Gaetz, J., Kapoor, T. M. & Hatten, M. E. Par6α signaling controls glial-guided neuronal migration. *Nature Neurosci.* **7,** 1195–1203 (2004).
29. Budry, L. *et al.* Related pituitary cell lineages develop into interdigitated 3D cell networks. *Proc. Natl Acad. Sci. USA* **108,** 12515–12520 (2011).
30. Skarnes, W. C. *et al.* A conditional knockout resource for the genome-wide study of mouse gene function. *Nature* **474,** 337–342 (2011).

**Supplementary Information** is linked to the online version of the paper at www.nature.com/nature.

**Acknowledgements** We thank B. Tilton, P. Rogers, J. Couget, and the Harvard Genome Modification Facility for technical assistance; S. Sarin and M. Yamagata for critical discussions; the National Institutes of Health (NS029169 and EY022073 to J.R.S.) and Life Sciences Research Foundation (J.N.K.) for funding.

**Author Contributions** J.N.K. and J.R.S. designed experiments and wrote the paper. J.N.K. and M.W.C. performed experiments. J.N.K. performed data analysis. J.R.S. supervised the project.

**Author Information** Data have been deposited at the Gene Expression Omnibus (http://www.ncbi.nlm.nih.gov/geo/) under accession code GSE35077. Reprints and permissions information is available at www.nature.com/reprints. The authors declare no competing financial interests. Readers are welcome to comment on the online version of this article at www.nature.com/nature. Correspondence and requests for materials should be addressed to J.R.S. (sanesj@mcb.harvard.edu).

LETTER

doi:10.1038/nature10807

# Control of ground-state pluripotency by allelic regulation of *Nanog*

Yusuke Miyanari[1] & Maria-Elena Torres-Padilla[1]

**Pluripotency is established through genome-wide reprogramming during mammalian pre-implantation development, resulting in the formation of the naive epiblast. Reprogramming involves both the resetting of epigenetic marks and the activation of pluripotent-cell-specific genes such as *Nanog* and *Oct4* (also known as *Pou5f1*)[1–4]. The tight regulation of these genes is crucial for reprogramming, but the mechanisms that regulate their expression *in vivo* have not been uncovered. Here we show that *Nanog*—but not *Oct4*—is monoallelically expressed in early pre-implantation embryos. *Nanog* then undergoes a progressive switch to biallelic expression during the transition towards ground-state pluripotency in the naive epiblast of the late blastocyst. Embryonic stem (ES) cells grown in leukaemia inhibitory factor (LIF) and serum express *Nanog* mainly monoallelically and show asynchronous replication of the *Nanog* locus, a feature of monoallelically expressed genes[5], but ES cells activate both alleles when cultured under 2i conditions, which mimic the pluripotent ground state *in vitro*. Live-cell imaging with reporter ES cells confirmed the allelic expression of *Nanog* and revealed allelic switching. The allelic expression of *Nanog* is regulated through the fibroblast growth factor–extracellular signal-regulated kinase signalling pathway, and it is accompanied by chromatin changes at the proximal promoter but occurs independently of DNA methylation. *Nanog*-heterozygous blastocysts have fewer inner-cell-mass derivatives and delayed primitive endoderm formation, indicating a role for the biallelic expression of *Nanog* in the timely maturation of the inner cell mass into a fully reprogrammed pluripotent epiblast. We suggest that the tight regulation of *Nanog* dose at the chromosome level is necessary for the acquisition of ground-state pluripotency during development. Our data highlight an unexpected role for allelic expression in controlling the dose of pluripotency factors *in vivo*, adding an extra level to the regulation of reprogramming.**

The development of the naive epiblast in the late blastocyst is orchestrated by pluripotency-associated transcription factors such as NANOG and OCT4. OCT4 is required for establishing and maintaining the pluripotent state[3], and NANOG is essential for the acquisition of pluripotency[1,6]. In ES cells, the pluripotent state is also governed by these core transcription factors. *Nanog* occupies a central position in this network, but the mechanisms regulating its expression are unclear.

To address how pluripotency-associated factors are regulated during reprogramming *in vivo*, we assayed the *de novo* gene expression of *Nanog* and *Oct4* in mouse pre-implantation embryos, by using RNA fluorescence *in situ* hybridization (RNA-FISH), which allows nascent transcripts to be visualized. We found that *Oct4* is actively expressed in a small proportion of 2-cell-stage embryos, but most blastomeres express *Oct4* at the 4- and 8-cell stage (Fig. 1a, b). We detected active *Nanog* expression in about half of all 4- and 8-cell-stage blastomeres, which is consistent with previous reports of heterogeneous *Nanog* expression[7]. Surprisingly, although all of the other genes that we analysed were expressed biallelically, *Nanog* invariably showed monoallelic expression in 2-, 4- and 8-cell-stage embryos (Fig. 1a, b and Supplementary Movie 1). We next addressed whether the monoallelic expression of *Nanog* is random or imprinted, by using allele-specific, single-cell PCR with reverse transcription (RT–PCR) on 8-cell-stage embryos from C57BL/6J × *Mus musculus castaneus* crosses. Consistent with our RNA-FISH results, most blastomeres expressed *Nanog* monoallelically (Fig. 1c and Supplementary Fig. 1). We observed no bias in *Nanog* expression from either the C57BL/6J or the *M. musculus castaneus* allele (Fig. 1c). We conclude that *Nanog* expression is monoallelic and random during early pre-implantation development.

*Nanog* expression becomes restricted to the inner cell mass (ICM) of the blastocyst[1,2], where it is needed for the naive epiblast to attain pluripotency[6]. As expected, the proportion of cells expressing *Nanog* and *Oct4* declined gradually as the expression of these genes became restricted to inner cells (Fig. 2a). Remarkably, the proportion of biallelism in *Nanog*-expressing cells increased progressively from 2% at the 8-cell stage to 70% of the inner cells in the late blastocyst (Fig. 2b and Supplementary Movie 2). This switch to biallelism of *Nanog* is in contrast to the consistent biallelic expression of *Oct4* and *Actb* (Fig. 2a). Sequential RNA-FISH and DNA-FISH confirmed the biallelic expression of *Nanog* (Supplementary Fig. 1). The ICM of the late blastocyst contains two lineages: the extra-embryonic primitive endoderm, and the 'ground-state' pluripotent epiblast[5,8], which gives rise to the embryo. Inner cells expressing *Nanog* biallelically also express *Oct4* but not *Gata4*, a primitive endoderm marker[9], and therefore are epiblast cells (Fig. 2c). This finding suggests that *Nanog* is predominantly expressed from both alleles in the naive epiblast. Furthermore, *Nanog* expression gradually reversed to monoallelic expression after implantation (Supplementary Fig. 2), in line with the downregulation of *Nanog* and concomitant loss of

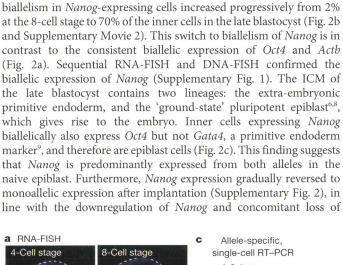


**Figure 1 | *Nanog* expression is monoallelic in early embryos. a**, RNA-FISH for *Nanog* and *Oct4* in 4- and 8-cell-stage nuclei. Scale bar, 2 μm. **b**, Proportion of allelic expression for each gene in 2-cell-stage (2C), 4-cell-stage (4C) and 8-cell-stage (8C) blastomeres. *n*, number of cells analysed. **c**, Summary of single-cell RT–PCR data for *Nanog* in 8-cell-stage blastomeres, according to biallelic, monoallelic (C57BL/6J or *M. musculus castaneus* (*Castaneus*)) and no expression (none).

[1]Institut de Génétique et de Biologie Moléculaire et Cellulaire, CNRS/INSERM U964, Université de Strasbourg, F-67404 Illkirch, Cité Universitaire de Strasbourg, France.

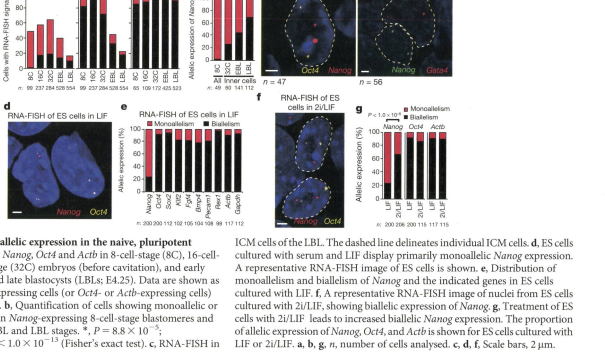


**Figure 2 | *Nanog* shows biallelic expression in the naive, pluripotent epiblast.** **a**, RNA-FISH for *Nanog*, *Oct4* and *Actb* in 8-cell-stage (8C), 16-cell-stage (16C) and 32-cell-stage (32C) embryos (before cavitation), and early blastocysts (EBLs; E3.5) and late blastocysts (LBLs; E4.25). Data are shown as the percentage of *Nanog*-expressing cells (or *Oct4*- or *Actb*-expressing cells) relative to all cells analysed. **b**, Quantification of cells showing monoallelic or biallelic *Nanog* expression in *Nanog*-expressing 8-cell-stage blastomeres and inner cells at the 32-cell, EBL and LBL stages. *, $P = 8.8 \times 10^{-5}$; **, $P = 3.1 \times 10^{-5}$; ***, $P < 1.0 \times 10^{-13}$ (Fisher's exact test). **c**, RNA-FISH in ICM cells of the LBL. The dashed line delineates individual ICM cells. **d**, ES cells cultured with serum and LIF display primarily monoallelic *Nanog* expression. A representative RNA-FISH image of ES cells is shown. **e**, Distribution of monoallelism and biallelism of *Nanog* and the indicated genes in ES cells cultured with LIF. **f**, A representative RNA-FISH image of nuclei from ES cells cultured with 2i/LIF, showing biallelic expression of *Nanog*. **g**, Treatment of ES cells with 2i/LIF leads to increased biallelic *Nanog* expression. The proportion of allelic expression of *Nanog*, *Oct4*, and *Actb* is shown for ES cells cultured with LIF or 2i/LIF. **a**, **b**, **g**, *n*, number of cells analysed. **c**, **d**, **f**, Scale bars, 2 μm.

pluripotency[2]. Thus, *Nanog* expression switches transiently from monoallelic to biallelic during the formation of the pluripotent epiblast *in vivo*, coinciding with the completion of the reprogramming process.

We next investigated the allelic expression of *Nanog* in ES cells. When cultured in medium containing serum and LIF, 60–70% of ES cells express *Nanog* (refs 10, 11) (Supplementary Fig. 4). Under these conditions, *Nanog* is predominantly expressed from a single allele (Fig. 2d, e and Supplementary Movie 3). By contrast, all of the other genes analysed showed biallelic expression, including other pluripotency-associated genes (*Oct4*, *Sox2*, *Klf2* and *Fgf4*), heterogeneously expressed genes (*Pecam1*, *Bmp4* and *Rex1* (also known as *Zfp42*)) and housekeeping genes (*Actb* and *Gapdh*) (Fig. 2d, e). Allele-specific, single-cell RT–PCR with hybrid ES cells showed that *Nanog* expression is independent of parental origin, similarly to the early embryo (Supplementary Fig. 3). Thus, *Nanog* shows random monoallelic expression both in early pre-implantation embryos and in ES cells.

The proportion of monoallelic versus biallelic *Nanog* expression in the naive epiblast is significantly different from that in ES cells, the latter showing much lower biallelism (Fig. 2b, e). We hypothesized that this could reflect the more homogeneous expression of *Nanog* in the naive epiblast compared to ES cells[6,8]. Ground-state pluripotency can be established *in vitro* through pharmacological inhibition (with two inhibitors (2i)) of MEK and GSK3β[12]. ES cells cultured with 2i show increased levels of *Nanog* messenger RNA[6,12] and homogeneous distribution of NANOG protein[13] (Supplementary Fig. 4). Strikingly, we found that culturing ES cells in 2i resulted in a significant increase in biallelic *Nanog* expression (Fig. 2f, g, Supplementary Fig. 3 and Supplementary Movie 4). We confirmed *Nanog* biallelic expression with sequential RNA-FISH and DNA-FISH (data not shown). To address which signalling pathway(s) regulates the allelic expression of *Nanog*, we used combinations of pharmacological inhibitors[6,12,14]. We found that blocking fibroblast growth factor (FGF)–extracellular regulated kinase (ERK) signalling was sufficient to trigger the biallelic expression of *Nanog* (Supplementary Fig. 4). The naive epiblast and ES cells are thought to be maintained in a ground state by preventing the differentiation that is induced through FGF–ERK signalling[8,12]. Thus, collectively these results suggest that ground-state pluripotency might be achieved through the activation of the second allele of *Nanog*.

The above changes in *Nanog* allelic expression upon pharmacological treatment suggest that the *Nanog* alleles are dynamically regulated. To visualize the dynamics of activation of the two *Nanog* alleles in individual cells, we generated an ES-cell reporter in which a gene encoding destabilized Turbo green fluorescent protein (TurboGFP) was inserted immediately downstream of the NANOG-coding region in one *Nanog* allele and a gene encoding destabilized mCherry was inserted similarly into the other *Nanog* allele (Fig. 3a and Supplementary Fig. 5). Both fluorescent proteins dissociate from NANOG by self-cleavage of a 2A peptide and do not alter NANOG function. We observed heterogeneous distribution of TurboGFP or mCherry in ES cells grown in LIF, confirming that the monoallelic expression of *Nanog* is random (Fig. 3b). This is in contrast to the homogeneous distribution in ES cells grown in 2i, in which most cells expressed both fluorescent proteins, reflecting biallelic expression of *Nanog* (Fig. 3b). Using time-lapse analysis, we observed dynamic fluctuation of *Nanog* expression, in agreement with previous reports[10,11] (Supplementary Fig. 6 and Supplementary Movie 5). Moreover, we found that *Nanog* expression can switch between alleles. In most cases, the allelic switch occurred through an intermediate state of biallelic *Nanog* expression or no *Nanog* expression over several cell cycles. In a minority of cases (2%), rapid allelic switching occurred during a single cell cycle (Fig. 3c and Supplementary Fig. 6). This switching is in contrast to other monoallelic genes, including imprinted genes, for which the inactive status of an allele is stably maintained[15].

Given the potential importance of activation of the second *Nanog* allele in establishing ground-state pluripotency, we next addressed the chromatin signatures underlying biallelic activation. We asked whether the allelic expression of *Nanog* obeys any epigenetic feature. We found that *Nanog* replicated asymmetrically in ES cells cultured with LIF alone—a feature of monoallelically expressed genes—but changed its replication pattern towards symmetric replication in ES cells cultured with 2i and LIF (denoted 2i/LIF) (Fig. 3d, e). This pattern is in contrast to the invariable asymmetric replication of imprinted genes (*Snurf* and *H19*; Fig. 3d, e) and is consistent with changes in allelic *Nanog* expression. Replication timing is a distinctive epigenetic fingerprint[5,16,17], thus suggesting that the allelic regulation of *Nanog* could be associated with epigenetic signatures. Indeed, monoallelic expression is accompanied

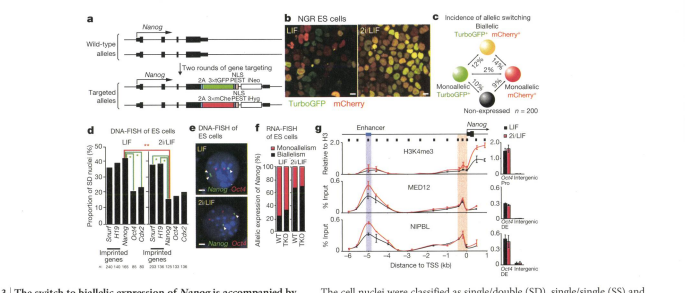


**Figure 3 | The switch to biallelic expression of *Nanog* is accompanied by changes in replication timing and increased recruitment of mediator and cohesin. a**, Schematic of the *Nanog* knock-in reporter NGR. A PEST motif in the carboxy terminus of the fluorescent proteins allows monitoring of dynamic *Nanog* expression. iHyg, internal ribosome entry site (IRES) hygromycin; iNeo, IRES neomycin; mCh, mCherry; NLS, nuclear localization signal; tGFP, TurboGFP. **b**, Representative image of NGR ES cells cultured with LIF or 2i/LIF. Scale bar, 10 μm. **c**, The incidence of allelic switching of *Nanog* expression in ES cells. Cells were classified into four groups: monoallelic (TurboGFP-positive, green), monoallelic (mCherry-positive, red), biallelic (TurboGFP- and mCherry-positive, yellow) and no expression (black). The proportion of cells undergoing a transition between these four groups during a single cell cycle is indicated. Overall, 47% of cells showed a colour change in this period. *n*, number of cells analysed. **d**, The asymmetric replication of *Nanog* in ES cells cultured with LIF changes to symmetric replication upon treatment with 2i. The cell nuclei were classified as single/double (SD), single/single (SS) and double/double (DD) according to DNA-FISH signals[5]. *n*, number of nuclei analysed. *, $P < 4 \times 10^{-7}$; **, $P < 1.4 \times 10^{-5}$ (Fisher's exact test). **e**, Representative image of DNA-FISH for *Nanog* (arrowheads) and *Oct4* in ES cells cultured with LIF or 2i/LIF. Scale bar, 2 μm. **f**, *Nanog* allelic expression is unaffected in the absence of DNA methyltransferase activity. Quantification of RNA-FISH for *Nanog* in wild-type (WT) ES cells and ES cells lacking all three DNA methyltransferases (TKO) cultured with LIF or 2i/LIF. **g**, ChIP for H3K4me3, MED12 or NIPBL along the *Nanog* locus (black line, top) in ES cells cultured with LIF or 2i/LIF. The position of the ChIP amplicons is depicted by the thick boxes below the line, the TSS by an arrow, the first exon by the black box on the line, and the distal enhancer by the blue box on the line. The *Oct4* promoter region (*Oct4* Pro) and distal enhancer (*Oct4* DE) were positive controls (right)[10]. The mean ± s.d. of three independent biological replicates is shown.

by allele-specific DNA methylation and/or histone modifications[15,18]. However, we found that ES cells lacking all three DNA methyltransferases[19] had similar *Nanog* allelic expression to wild-type ES cells (Fig. 3f), indicating that the allelic regulation of *Nanog* is independent of DNA methylation, unlike that of imprinted genes[15].

Next, we assessed allelic histone modifications on *Nanog* by using chromatin immunoprecipitation (ChIP), taking advantage of the fact that ES cells grown in LIF express *Nanog* mainly in a monoallelic manner and those grown in 2i/LIF primarily have two active alleles. ChIP showed a significantly higher enrichment of H3K4me3, a modification of active chromatin, at the transcription start site (TSS) of *Nanog* in ES cells grown in 2i/LIF than those grown in LIF alone (Fig. 3g). This increase is in line with the higher biallelic expression in 2i/LIF than LIF alone. The H3K4me3 enrichment at the *Nanog* TSS was approximately twofold in 2i/LIF, possibly suggesting that H3K4me3 is enriched at the active *Nanog* allele but absent at the inactive one in ES cells expressing *Nanog* monoallelically. We observed significantly higher recruitment of the mediator subunit MED12, as well as the cohesin-loading factor NIPBL, to the *Nanog* enhancer in ES cells grown in 2i/LIF than in ES cells grown in LIF alone (Fig. 3g). This increased recruitment was accompanied by increased RNA polymerase II initiation and elongation upon 2i treatment (Supplementary Fig. 7). Indeed, changes in chromatin architecture mediated through simultaneous binding of mediator and cohesin to the *Nanog* locus facilitate looping between the enhancer and promoter, resulting in *Nanog* gene activation[20]. Collectively, our data suggest that *Nanog* allelic expression might be actively regulated through chromosomal changes over the *Nanog* locus.

Mice that are heterozygous for *Nanog* ($Nanog^{+/-}$) are born at normal Mendelian ratios[1]. We hypothesized that if *Nanog* biallelic expression is important for the formation of the ICM and/or for the acquisition of ground-state pluripotency, then $Nanog^{+/-}$ embryos may show developmental defects at the onset of *Nanog* biallelic expression. To address this, we counted ICM cells in individual $Nanog^{+/-}$ blastocysts by using an anti-OCT4 antibody. Freshly collected embryonic day 3.5 (E3.5) $Nanog^{+/-}$ and $Nanog^{+/+}$ blastocysts had similar ICM cell numbers (Supplementary Fig. 8a). This finding is in agreement with previous reports[6,21] and with our observations documenting *Nanog* monoallelic expression before this embryonic stage. By contrast, we found significantly fewer ICM cells in $Nanog^{+/-}$ blastocysts as the embryo progressed through development to form the nascent epiblast (Fig. 4a), which also showed increased apoptosis in the ICM (Supplementary Fig. 8b). No significant difference in the number of NANOG-positive cells was observed between wild-type ($Nanog^{+/+}$) and heterozygous ($Nanog^{+/-}$) embryos (Fig. 4b, c). However, $Nanog^{+/-}$ embryos showed delayed primitive endoderm formation (Fig. 4b, c). Indeed, primitive endoderm formation depends on a functional epiblast in a non-cell-autonomous manner[21], suggesting that the epiblast in $Nanog^{+/-}$ embryos is functionally impaired. It should be noted that the reduction in primitive endoderm cells does not fatally compromise development, owing to the regulatory capacity of the early post-implantation embryo. Thus, we conclude that the biallelic expression of *Nanog* is necessary for the timely maturation of the ICM into a functional epiblast and the accompanying primitive endoderm.

NANOG has a dose-sensitive action in reprogramming[6]. Overexpression of NANOG is sufficient to prevent ES-cell differentiation[7]; conversely, $Nanog^{+/-}$ ES cells show spontaneous differentiation[22,23], suggesting that the tight regulation of *Nanog* levels is crucial for both reprogramming and differentiation. We found that this dose regulation occurs principally at the allelic level. Monoallelic expression is predominant during the early reprogramming phase in cleavage stages, but it switches to biallelic expression as the ICM matures into the pluripotent epiblast (Fig. 4d). Monoallelic *Nanog* expression in ES cells may be representative of the late ICM or the early post-implantation

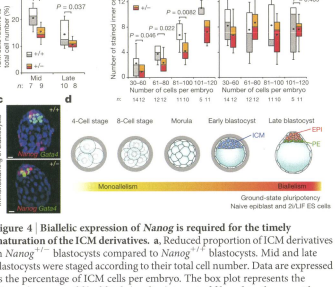


**Figure 4 | Biallelic expression of *Nanog* is required for the timely maturation of the ICM derivatives. a**, Reduced proportion of ICM derivatives in *Nanog*$^{+/-}$ blastocysts compared to *Nanog*$^{+/+}$ blastocysts. Mid and late blastocysts were staged according to their total cell number. Data are expressed as the percentage of ICM cells per embryo. The box plot represents the ninetieth, seventy-fifth, fiftieth (median), twenty-fifth and tenth percentiles, as well as the mean (black dot). **b**, Delayed primitive endoderm (PE) formation in *Nanog*$^{+/-}$ blastocysts. Embryos were staged in groups according to their total cell number. The number of PE (GATA4-positive) and epiblast (EPI; NANOG-positive) cells was determined. **c**, Representative maximal confocal projections of late blastocysts, showing a reduced proportion of ICM derivatives in *Nanog*$^{+/-}$ embryos. Scale bar, 10 μm. **d**, Model for the allelic regulation of *Nanog* and the acquisition of ground-state pluripotency. *Nanog* is expressed monoallelically during the cleavage stages and up to the early blastocyst. Biallelic expression of *Nanog* accompanies the formation of the fully reprogrammed, pluripotent, epiblast. Biallelic expression of *Nanog* also occurs *in vitro* under conditions that mimic the ground-state pluripotency of the naive epiblast (ES cells cultured with 2i/LIF).

epiblast, in which there is a switch back to monoallelic expression. The expression of *Nanog* can switch between alleles, unlike most known monoallelic genes, raising the possibility that the regulation of *Nanog* allelic expression could be unique. Our evidence that such regulation is independent of DNA methylation and does not seem to involve typical repressive modifications (H3K27me3, H3K9me1, H3K9me2 and H3K9me3; data not shown) also supports this possibility. The ground-state pluripotency is facilitated by the suppression of FGF–ERK signalling[6,12]. Our work suggests that the allelic regulation of *Nanog* is involved in this process and that the increased expression of *Nanog* that accompanies the establishment of ground-state pluripotency is achieved through activation of its second allele. The dose regulation of *Nanog* through allelic switching could also contribute to promoting heterogeneity, which could provide a window of opportunity both for establishing ground-state pluripotency in the epiblast and for lineage segregation towards the primitive endoderm. We propose that the regulation of *Nanog* at the allelic level provides a novel mechanism to establish ground-state pluripotency in the naive epiblast. Thus, our work has uncovered an unexpected role for the allelic regulation of key transcription factors, as a novel mechanism in stabilizing pluripotency.

## METHODS SUMMARY

The embryos were from $F_1$ (C57BL/6] × CBA/H) or C57BL/6] × *M. musculus castaneus* crosses. The blastocysts from *Nanog*$^{GAI1+}$ × C57BL/6] crosses[21] were genotyped after immunostaining (47 *Nanog*$^{+/-}$ and 49 *Nanog*$^{+/+}$ were analysed). The ES-cell lines and culture conditions are described in the Methods. Briefly, when referring to LIF, ES cells were cultured in 15% FCS and LIF; when referring to 2i/LIF, ES cells were cultured in 15% FCS, LIF, 3 μM CHIR99021 and 1 μM PD0325901. Embryos and ES cells were fixed with 4% paraformaldehyde in PBS for immunostaining. Images were acquired on a TCS SP5 confocal microscope (Leica). Image analysis was performed with the programs ImageJ, LAS AF Lite (Leica) or Imaris (Bitplane). For single-cell RT–PCR analysis, individual 8-cell-stage blastomeres were mechanically dissociated, and the cells were collected in 3.1 μl Cell Lysis Buffer (Ambion) and processed for RT–PCR then digested with AvaII. All primer sequences are listed in Supplementary Table 1.

**Full Methods** and any associated references are available in the online version of the paper at www.nature.com/nature.

**Received 22 June; accepted 19 December 2011.**
**Published online 12 February 2012.**

1. Mitsui, K. *et al.* The homeoprotein Nanog is required for maintenance of pluripotency in mouse epiblast and ES cells. *Cell* **113,** 631–642 (2003).
2. Chambers, I. *et al.* Functional expression cloning of Nanog, a pluripotency sustaining factor in embryonic stem cells. *Cell* **113,** 643–655 (2003).
3. Nichols, J. *et al.* Formation of pluripotent stem cells in the mammalian embryo depends on the POU transcription factor Oct4. *Cell* **95,** 379–391 (1998).
4. Reik, W. Stability and flexibility of epigenetic gene regulation in mammalian development. *Nature* **447,** 425–432 (2007).
5. Sibinau, J., Hochedlinger, K., Hata, K., Li, E. & Jaenisch, R. Asynchronous replication timing of imprinted loci is independent of DNA methylation, but consistent with differential subnuclear localization. *Genes Dev.* **17,** 759–773 (2003).
6. Silva, J. *et al.* Nanog is the gateway to the pluripotent ground state. *Cell* **138,** 722–737 (2009).
7. Dietrich, J. E. & Hiiragi, T. Stochastic patterning in the mouse pre-implantation embryo. *Development* **134,** 4219–4231 (2007).
8. Nichols, J., Silva, J., Roode, M. & Smith, A. Suppression of Erk signalling promotes ground state pluripotency in the mouse embryo. *Development* **136,** 3215–3222 (2009).
9. Morrisey, E. E., Ip, H. S., Lu, M. M. & Parmacek, M. S. GATA-6: a zinc finger transcription factor that is expressed in multiple cell lineages derived from lateral mesoderm. *Dev. Biol.* **177,** 309–322 (1996).
10. Chambers, I. *et al.* Nanog safeguards pluripotency and mediates germline development. *Nature* **450,** 1230–1234 (2007).
11. Kalmar, T. *et al.* Regulated fluctuations in Nanog expression mediate cell fate decisions in embryonic stem cells. *PLoS Biol.* **7,** e1000149 (2009).
12. Ying, Q. L. *et al.* The ground state of embryonic stem cell self-renewal. *Nature* **453,** 519–523 (2008).
13. Wray, J., Kalkan, T. & Smith, A. G. The ground state of pluripotency. *Biochem. Soc. Trans.* **38,** 1027–1032 (2010).
14. Canham, M. A., Sharov, A. A., Ko, M. S. & Brickman, J. M. Functional heterogeneity of embryonic stem cells revealed through translational amplification of an early endodermal transcript. *PLoS Biol.* **8,** e1000379 (2010).
15. Weaver, J. R., Susiarjo, M. & Bartolomei, M. S. Imprinting and epigenetic changes in the early embryo. *Mamm. Genome* **20,** 532–543 (2009).
16. Shufaro, Y. *et al.* Reprogramming of DNA replication timing. *Stem Cells* **28,** 443–449 (2010).
17. Jørgensen, H. F. *et al.* The impact of chromatin modifiers on the timing of locus replication in mouse embryonic stem cells. *Genome Biol.* **8,** R169 (2007).
18. Magklara, A. *et al.* An epigenetic signature for monoallelic olfactory receptor expression. *Cell* **145,** 555–570 (2011).
19. Tsumura, A. *et al.* Maintenance of self-renewal ability of mouse embryonic stem cells in the absence of DNA methyltransferases Dnmt1, Dnmt3a and Dnmt3b. *Genes Cells* **11,** 805–814 (2006).
20. Kagey, M. H. *et al.* Mediator and cohesin connect gene expression and chromatin architecture. *Nature* **467,** 430–435 (2010).
21. Messerschmidt, D. M. & Kemler, R. Nanog is required for primitive endoderm formation through a non-cell autonomous mechanism. *Dev. Biol.* **344,** 129–137 (2010).
22. Hough, S. R., Clements, I., Welch, P. J. & Wiederholt, K. A. Differentiation of mouse embryonic stem cells after RNA interference-mediated silencing of OCT4 and Nanog. *Stem Cells* **24,** 1467–1475 (2006).
23. Hatano, S. Y. *et al.* Pluripotential competence of cells associated with Nanog activity. *Mech. Dev.* **122,** 67–79 (2005).

**Supplementary Information** is linked to the online version of the paper at www.nature.com/nature.

**Acknowledgements** We thank M. Okano for providing the triple DNA methyltransferase knockout cells, P. Avner and P. Clerc for hybrid ES cells, H. Schöler for the *Oct4* probe (GOF6.1), J. Jaubert for *M. musculus castaneus* mice, R. Kemler and S. Rudloff for the *Nanog*$^{GFP}$ mice, G. Charvin for advice on time-lapse analysis. We also thank M. Koch, A. Dierich, M.-C. Birling, E. Heard and I. Okamoto for advice, and A. Burton, E. Heard and O. Pourquie for critical reading of the manuscript. M.-E.T.-P. acknowledges funding from AVENIR/INSERM, ANR-09-Blanc-0114, Epigenesys NoE and FRM Alsace. Y.M. is a recipient of an EMBO long-term fellowship (ALTF864-2008, 2009) and a JSPS postdoctoral fellowship (2010–2011).

**Author Contributions** Y.M. conceived, designed and performed the experiments in this study and analysed the data; M.-E.T.-P. conceived the project and designed and supervised the study. Y.M. and M.-E. T.-P wrote the manuscript.

**Author Information** Reprints and permissions information is available at www.nature.com/reprints. The authors declare no competing financial interests. Readers are welcome to comment on the online version of this article at www.nature.com/nature. Correspondence and requests for materials should be addressed to M.-E.T.-P. (metp@igbmc.fr).

LETTER

doi:10.1038/nature10860

# IDH mutation impairs histone demethylation and results in a block to cell differentiation

Chao Lu[1,2], Patrick S. Ward[1,2], Gurpreet S. Kapoor[3], Dan Rohle[4,5], Sevin Turcan[4], Omar Abdel-Wahab[4,6], Christopher R. Edwards[7], Raya Khanin[8], Maria E. Figueroa[9], Ari Melnick[9], Kathryn E. Wellen[2], Donald M. O'Rourke[3,10], Shelley L. Berger[7], Timothy A. Chan[4], Ross L. Levine[4,6], Ingo K. Mellinghoff[4,5,11] & Craig B. Thompson[1]

**Recurrent mutations in isocitrate dehydrogenase 1 (IDH1) and IDH2 have been identified in gliomas, acute myeloid leukaemias (AML) and chondrosarcomas, and share a novel enzymatic property of producing 2-hydroxyglutarate (2HG) from α-ketoglutarate[1–4]. Here we report that 2HG-producing IDH mutants can prevent the histone demethylation that is required for lineage-specific progenitor cells to differentiate into terminally differentiated cells. In tumour samples from glioma patients, IDH mutations were associated with a distinct gene expression profile enriched for genes expressed in neural progenitor cells, and this was associated with increased histone methylation. To test whether the ability of IDH mutants to promote histone methylation contributes to a block in cell differentiation in non-transformed cells, we tested the effect of neomorphic IDH mutants on adipocyte differentiation *in vitro*. Introduction of either mutant IDH or cell-permeable 2HG was associated with repression of the inducible expression of lineage-specific differentiation genes and a block to differentiation. This correlated with a significant increase in repressive histone methylation marks without observable changes in promoter DNA methylation. Gliomas were found to have elevated levels of similar histone repressive marks. Stable transfection of a 2HG-producing mutant IDH into immortalized astrocytes resulted in progressive accumulation of histone methylation. Of the marks examined, increased H3K9 methylation reproducibly preceded a rise in DNA methylation as cells were passaged in culture. Furthermore, we found that the 2HG-inhibitable H3K9 demethylase KDM4C was induced during adipocyte differentiation, and that RNA-interference suppression of KDM4C was sufficient to block differentiation. Together these data demonstrate that 2HG can inhibit histone demethylation and that inhibition of histone demethylation can be sufficient to block the differentiation of non-transformed cells.**

The fact that IDH mutations were identified in multiple cancers with disparate tissues of origin suggests that 2HG-producing mutant enzymes probably affect some fundamental cellular processes that facilitate tumour progression. To study the effects of IDH mutations, we collected and performed gene expression microarray analysis on tumour specimens from patients with grade II–III oligodendroglioma. Sequencing results revealed a high frequency of IDH mutations in oligodendroglioma (33 of the samples had the R132 IDH1 mutation, 2 had the R172 IDH2 mutation and 6 were wild type for IDH1/2). Supervised analysis found a statistically enriched gene signature in IDH-mutant samples ($q$ value $<10\%$, fold change $>2$; Fig. 1a and Supplementary Table 1) that was independent of tumour grade and recurrence status and survived multiple testing corrections. Gene-ontology analysis identified the regulation of astrocyte and glial differentiation as the top two functional categories enriched in differentially expressed genes (Supplementary Table 2). We previously reported that IDH mutation may promote leukaemogenesis by expanding the haematopoietic progenitor cell population and impairing haematopoietic differentiation[5], and that such a phenotype could be attributed at least in part to mutant IDH-induced inhibition of TET2, an α-ketoglutarate (αKG)-dependent enzyme potentially involved in DNA demethylation[2,6]. Although DNA hypermethylation has been associated with IDH mutation in glioma samples[6], no mutations in TET family members have been found in this disease. We explored the possibility that IDH mutation may affect additional αKG-dependent enzymes that contribute to the regulation of cell differentiation.

Histone lysine methylation is an integral part of the post-translational modifications of histone tails that are important for chromatin organization and regulation of gene transcription[10–13]. *In vitro* 2HG can competitively inhibit a family of αKG-dependent Jumonji-C domain histone demethylases (JHDMs)[14,15]. To determine whether IDH-associated changes in histone methylation could be observed in cells, we ectopically expressed wild-type or mutant IDH1 or IDH2 in 293T cells and found that mutant IDH1 or IDH2 led to a marked increase in histone methylation compared to the wild-type enzymes. Transient transfection of wild-type IDH2 can also lead to increased 2HG production[2]. In all of the samples, the magnitude of increase in methylation correlated with the intracellular 2HG levels produced by IDH transfection (Fig. 1b and Supplementary Fig. 1). To test whether histone lysine methylation was dysregulated in gliomas with IDH mutation, immunohistochemistry analysis of patient oligodendroglioma samples was performed for several well-characterized histone marks. Compared to tumours with wild-type IDH, there was a statistically significant increase in the repressive trimethylation of H3K9 (H3K9me3) and an increasing trend in trimethylation of H3K27 (H3K27me3) in tumours with IDH1 mutation (Fig. 1c). No statistically significant difference was seen in trimethylation of H3K4 (H3K4me3), a mark associated with active transcription (data not shown). These data suggested that IDH mutations might preferentially affect the regulation of repressive histone methylation marks *in vivo*.

As IDH mutations were associated with glial tumours of the 'pro-neural' phenotype[16], we sought to determine whether the persistence of histone repressive marks promoted by mutant IDH was sufficient to block the differentiation of non-transformed cells. Upon stimulation with a differentiation cocktail, immortalized murine 3T3-L1 cells undergo extensive chromatin remodelling, resulting in their maturation into adipocytes[17]. 3T3-L1 cells transduced with R172K mutant IDH2 produced 2HG whereas cells transduced with either wild-type IDH2 or vector alone did not (Fig. 2a). All three cell types were then

[1]Cancer Biology and Genetics Program, Memorial Sloan-Kettering Cancer Center, New York, New York 10065, USA. [2]Department of Cancer Biology, Perelman School of Medicine, University of Pennsylvania, Philadelphia, Pennsylvania 19104, USA. [3]Department of Neurosurgery, Perelman School of Medicine, University of Pennsylvania, Philadelphia, Pennsylvania 19104, USA. [4]Human Oncology and Pathogenesis Program, Memorial Sloan-Kettering Cancer Center, New York, New York 10065, USA. [5]Department of Pharmacology, Weill Cornell Medical College, New York, New York 10065, USA. [6]Leukemia Service, Department of Medicine, Memorial Sloan-Kettering Cancer Center, New York, New York 10065, USA. [7]Department of Cell and Developmental Biology, Perelman School of Medicine, University of Pennsylvania, Philadelphia, Pennsylvania 19104, USA. [8]Bioinformatics Core, Memorial Sloan-Kettering Cancer Center, New York, New York 10065, USA. [9]Division of Hematology/Oncology, Weill Cornell Medical College, New York, New York 10065, USA. [10]Department of Pathology & Laboratory Medicine, Perelman School of Medicine, University of Pennsylvania, Philadelphia, Pennsylvania 19104, USA. [11]Department of Neurology, Memorial Sloan-Kettering Cancer Center, New York, New York 10065, USA.

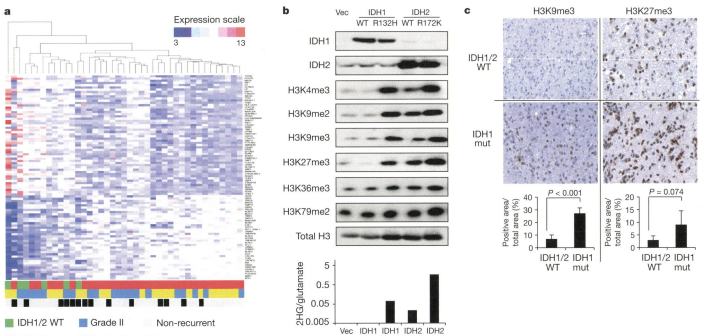


**Figure 1 | IDH mutations are associated with dysregulation of glial differentiation and global histone methylation.** **a**, Heatmap representation of a two-dimensional hierarchical clustering of genes identified as differentially expressed between IDH mutant (mut) patient oligodendroglioma samples and IDH wild-type (WT) samples. Each row represents a gene and each column represents a specimen. IDH mutational status, tumour grade and recurrence of each sample are listed. **b**, 293T cells transfected with empty vector (Vec), wild-type or R132H mutant IDH1, or wild-type or R172K mutant IDH2 for 3 days were lysed and assessed for expression levels of IDH1, IDH2 and histone lysine methylation by western blotting with specific antibodies. Total H3 was used as loading control. Quantification of band intensities is shown in Supplementary Fig. 1. Bottom panel provides quantification of intracellular 2HG to glutamate ratio (2HG/glutamate) as previously reported for these transfectants[7]. **c**, Immunohistochemistry staining with antibodies against H3K9me3 and H3K27me3 in IDH1/2 wild-type and IDH1 mutant oligodendroglioma samples (×40 magnification). Image quantification was performed using Metamorph software (see Methods) and shown in bottom panels. Error bars represent standard deviation (s.d.) of at least three patient samples in each group.

induced to differentiate into adipocytes. After 7 days of differentiation induction, IDH mutant cells had visibly reduced lipid droplet accumulation compared to vector and IDH wild-type cells, as shown by Oil-Red-O staining (Fig. 2b). In separate experiments, stable transfection of R140Q mutant IDH2 also resulted in a block to adipocyte differentiation (data not shown). To determine whether 2HG was sufficient to mediate the effect of mutant IDH on cell differentiation, we synthesized cell-permeable 1-octyl-D-2-hydroxyglutarate (octyl-2HG; Supplementary Fig. 2). Treatment of 3T3-L1 cells with octyl-2HG led to a dose-dependent inhibition of lipid accumulation (Fig. 2c). Gene expression analysis showed that despite exposure to a well-standardized differentiation protocol[18], IDH mutant cells or cells treated with octyl-2HG exhibited a profound defect in the expression of transcription factors essential for executing adipogenesis (*Cebpa* and *Pparg*) and an adipocytic lineage-specific gene (*Adipoq*) (Fig. 2d, e), suggesting that these cells failed to execute adipocyte differentiation.

Cells were harvested for a chromatin immunoprecipitation (ChIP) assay using antibodies against H3K9me3 and H3K27me3, before or after 4 days of differentiation induction. Quantitative polymerase chain reaction (PCR) with primers targeting promoters of *Cebpa* and *Adipoq* revealed that at day 4 there was a statistically significant increase in H3K9me3 and H3K27me3 at promoters of both genes in IDH mutant cells (Fig. 2f). These repressive marks also showed a modest but significant increase at gene promoters before differentiation induction. In contrast, quantitative assessment of DNA methylation at promoters of *Cebpa* and *Adipoq* by MassARRAY failed to reveal any significant difference between IDH wild-type and mutant cells (Supplementary Fig. 3). In addition to gene-specific changes, we detected a global increase in H3K9 methylation and a reciprocal decrease in H3 acetylation (Fig. 2g and Supplementary Fig. 4).

To determine whether IDH mutation was sufficient to induce enhanced repressive histone methylation in central nervous system (CNS)-derived cells and whether it was associated with altered neural gene expression, we retrovirally transduced immortalized normal human astrocytes (NHAs) with either wild-type or R132H mutant IDH1. Compared to parental cells, late-passage cells expressing mutant IDH exhibited elevated levels of a variety of histone methylation marks (Fig. 3a), and this correlated with an enhanced expression of the neural marker nestin (Fig. 3b). IDH mutations have been associated with CpG-island hypermethylation[9] and consistent with this we observed that total CpG methylation was increased in IDH mutant cells (Supplementary Fig. 5). Because histone repressive marks can promote DNA methylation and vice versa[15], we studied the temporal relationship of histone and DNA methylation in IDH-expressing astrocytes (Fig. 3c–e and Supplementary Fig. 5). The first observable change of the histone marks we examined was H3K9me3. H3K9me3 levels were significantly elevated by passage 12 after cells were infected with mutant IDH. Changes in other histone methylation marks were either delayed and of lower magnitude (H3K27me3 and H3K79me2) or were not observed (H3K4me3). Increases in DNA methylation were never observed before passage 17 and the difference in DNA methylation reached statistical significance only at passage 22.

To test whether the IDH1 R132H mutation could interfere with neural differentiation in the absence of prolonged adaptation in culture, primary neurosphere cultures established from the brains of *p16/p19*$^{-/-}$ mice were infected with a retroviral construct containing IDH1 R132H mutant, wild-type IDH1 or the vector alone (Supplementary Fig. 6). After infection the cells were re-plated under conditions that promote astrocyte differentiation and induced to differentiate further by treatment with retinoic acid without further passaging. IDH mutant cells failed to induce expression of the astrocytic marker GFAP and exhibited expression of the neural marker β3-tubulin (Fig. 3f). When the differentiation conditions were supplemented with retinoic acid, enhanced expression of the astrocytic marker GFAP was observed in

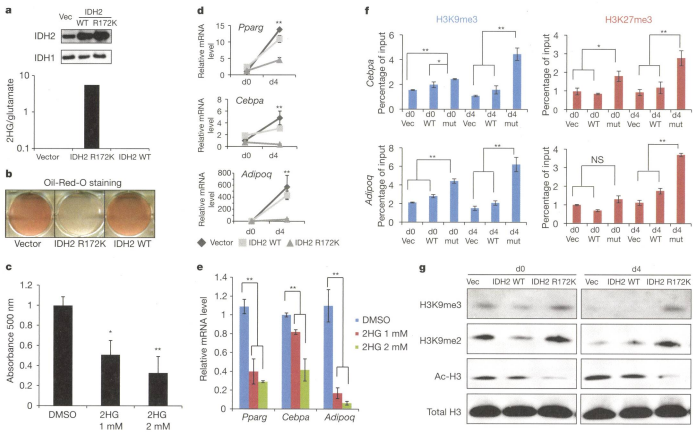


**Figure 2 | Differentiation arrest induced by mutant IDH or 2HG is associated with increased global and promoter-specific H3K9 and H3K27 methylation.** **a**, 3T3-L1 cells stably expressing empty vector, wild-type, or R172K mutant IDH2 were lysed and assessed for expression levels of IDH2 or IDH1 by western blotting. Cells were also extracted for intracellular metabolites, which were then MTBSTFA-derivatized (see Methods) and analysed by gas chromatography–mass spectrometry (GC–MS). The quantification of 2HG signal intensity relative to the intrasample glutamate signal is shown for a representative experiment. **b**, Cells were induced to differentiate into mature adipocytes for 7 days. The accumulation of lipid droplets was assessed by Oil-Red-O staining. Wells from a representative experiment from a total of four independent experiments are shown. **c**, 3T3-L1 cells were induced to differentiate for 7 days in the absence or presence of 1 mM or 2 mM octyl-2HG. Oil-Red-O staining was performed and quantified by measuring absorbance at 500 nm. DMSO, dimethylsulphoxide. **d**, Vector, wild-type or R172K mutant IDH2 transduced 3T3-L1 cells were induced to differentiate for 4 days. At days 0 and 4 (d0 and d4), RNA was extracted. Relative expression of adipocyte-specific gene and transcription factors was assessed by quantitative PCR with reverse transcription (RT–qPCR). **e**, 3T3-L1 cells were induced to differentiate for 4 days in the absence or presence of 1 mM or 2 mM octyl-2HG. RNA was extracted. Relative expression of adipocyte-specific gene and transcription factors was assessed by RT–qPCR. **f**, Vector, wild-type or R172K mutant IDH2 transduced 3T3-L1 cells were induced to differentiate. At days 0 and 4 (d0 and d4), ChIP analysis was performed using antibodies against H3K9me3 and H3K27me3. Immunoprecipitated *Cebpa* and *Adipoq* promoter sequences were analysed by qPCR and shown as percentage of input. **g**, Vector, wild-type or R172K mutant IDH2 transduced 3T3-L1 cells were induced to differentiate for 4 days. At days 0 and 4 (d0 and d4), histones were acid-extracted and levels of H3K9me3, H3K9me2 and acetyl-H3 were assessed by western blotting with specific antibodies. Total H3 was used as loading control. Quantification of band intensities is shown in Supplementary Fig. 4. In **f**, error bars indicate s.d. from triplicate wells and a representative experiment from a total of two is shown. For all other experiments, error bars indicate s.d. from three independent experiments. $*P < 0.05$; $**P < 0.01$; NS, not significant.

IDH wild-type and vector cells but GFAP expression remained repressed in IDH mutant cells.

The enhancement of H3K9 methylation in mutant IDH-expressing cells from multiple tissues of origin led us to investigate whether this H3K9 methylation might be sufficient to block the ability of non-transformed cells to execute differentiation. Support for this hypothesis came with the discovery that KDM4C (also known as JMJD2C), an H3K9-specific JHDM, was induced in 3T3-L1 cells during differentiation (Fig. 4a). An *in vitro* histone demethylase assay with recombinant human GST-tagged KDM4C confirmed that KDM4C effectively removed H3K9me2 and H3K9me3 in the presence of αKG. Importantly, the demethylation reaction was inhibited by 2HG in a dose-dependent manner (Fig. 4b and Supplementary Fig. 7). Given the similarities between 2HG and αKG, the inhibition of KDM4C by 2HG would be predicted to be competitive. Consistently, increasing the concentration of αKG in the reaction mixture reversed the inhibition of H3K9 demethylation by 2HG (Fig. 4c).

Finally, to test the possibility that H3K9 demethylation is a required component of adipocyte differentiation, we examined whether blocking the induction of KDM4C was sufficient to impair the differentiation of 3T3-L1 cells. Treatment with three independent short interfering RNAs (siRNAs) against KDM4C reduced its expression and enhanced H3K9me3 in 3T3-L1 cells (Fig. 4d and Supplementary Fig. 8). After differentiation induction, cells treated with KDM4C siRNAs exhibited reduced ability to differentiate into adipocytes. Thus the inability to erase repressive H3K9 methylation can be sufficient to impair the differentiation of non-transformed cells.

Biochemical studies suggest that 2HG is a universal inhibitor of JHDM family members[14,15]; therefore it was interesting to observe that H3K9 demethylation seemed to be more sensitive to mutant IDH-induced suppression than at least some other histone methylation marks. Future investigation of the sensitivity to 2HG inhibition among JHDM family members and/or cellular feedback mechanisms activated after defective histone demethylation will be needed. In addition to the data presented here, evidence is mounting for a direct role of histone methylation in stem cell maintenance, differentiation and tumorigenesis[16–23] (see Supplementary Discussion). Our findings support a role for αKG-dependent demethylases in cell differentiation

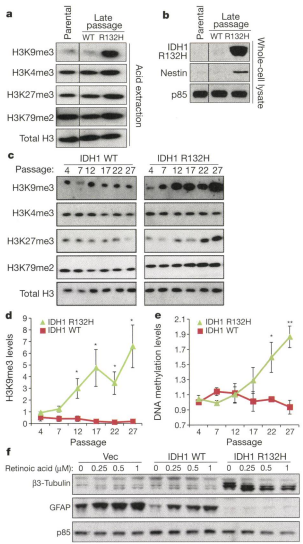


**Figure 3 | IDH mutation induces histone methylation increase in CNS-derived cells and can alter cell lineage gene expression.** **a**, Immortalized NHA cells were retrovirally transduced with constructs containing wild-type or R132H mutant IDH1. Histones were acid-extracted from parental cells or cells expressing wild-type or mutant IDH1 at late (>40) passages. Histone lysine methylation levels were assessed by western blotting with specific antibodies. Total H3 was used as loading control. Images presented are panels from different areas of the same gel. **b**, Parental, IDH1 wild-type and R132H mutant NHA cells at late passages were lysed and assessed for expression levels of nestin by western blotting. p85 was used as loading control. Images presented are panels from different areas of the same gel. **c**, NHA cells were retrovirally transduced with constructs containing wild-type or R132H mutant IDH1. Histones were acid-extracted at different time points as cells were passaged in culture. Histone lysine methylation levels were assessed by western blotting with specific antibodies. Total H3 was used as loading control. Images presented are panels from different areas of the same gel. **d**, Western blot band intensities of H3K9me3 in **c** and two additional independent experiments were quantified using Image J. Red squares indicate IDH1 wild-type cells. Green triangles indicate IDH1 R132H mutant cells. **e**, Total CpG methylation of IDH1 wild-type and R132H mutant NHA cells at various passages was measured by FACS using 5-methylcytosine-specific antibody and shown as normalized mean fluorescence intensity. FACS histograms from a representative experiment are shown in Supplementary Fig. 5. **f**, Neurosphere cultures established from the subventricular zone of brains of *p16/p19*$^{-/-}$ mice were infected with a retroviral construct containing IDH1 R132H mutant, wild-type IDH1 or the vector alone and induced to differentiate. GFAP and β3-tubulin expression levels were assessed by western blotting. p85 was used as loading control. In **d** and **e**, error bars indicate standard error of the mean from three independent experiments. *$P < 0.05$; **$P < 0.01$.

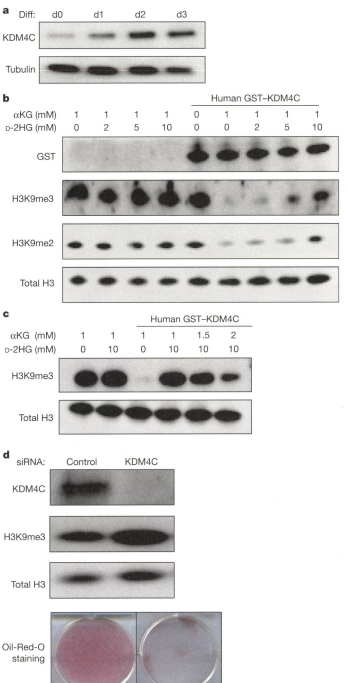


**Figure 4 | 2HG-inhibitable H3K9 demethylase KDM4C is required for cell differentiation.** **a**, 3T3-L1 cells were induced to differentiate (Diff) for 3 days. Before (d0) and each day after differentiation induction, cells were lysed and KDM4C protein levels were assessed by western blotting with specific antibody. Tubulin was used as loading control. **b**, Bulk histones were incubated with purified GST-tagged human KDM4C in the reaction mix with 1 mM αKG and increasing concentrations of D-2HG. Levels of GST tag, H3K9me3 and H3K9me2 were assessed by western blotting with specific antibodies. Total H3 was used as loading control. **c**, Bulk histones were incubated with purified GST-tagged human KDM4C in the reaction mix. 10 mM D-2HG was added to inhibit the demethylation reaction in the presence of increasing concentrations of αKG. Levels of H3K9me3 were assessed by western blotting with specific antibody. Total H3 was used as loading control. **d**, 3T3-L1 cells were transfected with control siRNA or siRNA specific for KDM4C. After 3 days, cells were lysed and assessed for expression levels of KDM4C and H3K9me3 by western blotting with specific antibodies. Total H3 was used as loading control. Cells from the same treatment were induced to differentiate for 7 days. The accumulation of lipid droplets was assessed by Oil-Red-O staining. Wells from a representative experiment from a total of three independent experiments are shown.

that can be impaired through the cellular accumulation of 2HG produced by IDH mutation.

## METHODS SUMMARY

Details about histone extraction, GC–MS and ChIP assay can be found in Methods. In brief, 3T3-L1 cell differentiation, Oil-Red-O staining, and *in vitro* histone demethylase assay were performed as previously described[24,25].

**Full Methods** and any associated references are available in the online version of the paper at www.nature.com/nature.

**Received 3 June 2011; accepted 16 January 2012.**
**Published online 15 February 2012.**

1. Parsons, D. W. *et al.* An integrated genomic analysis of human glioblastoma multiforme. *Science* **321,** 1807–1812 (2008).
2. Yan, H. *et al. IDH1* and *IDH2* mutations in gliomas. *N. Engl. J. Med.* **360,** 765–773 (2009).
3. Mardis, E. R. *et al.* Recurring mutations found by sequencing an acute myeloid leukemia genome. *N. Engl. J. Med.* **361,** 1058–1066 (2009).
4. Amary, M. F. *et al. IDH1* and *IDH2* mutations are frequent events in central chondrosarcoma and central and periosteal chondromas but not in other mesenchymal tumours. *J. Pathol.* **224,** 334–343 (2011).
5. Ward, P. S. *et al.* The common feature of leukemia-associated IDH1 and IDH2 mutations is a neomorphic enzyme activity converting α-ketoglutarate to 2-hydroxyglutarate. *Cancer Cell* **17,** 225–234 (2010).
6. Dang, L. *et al.* Cancer-associated IDH1 mutations produce 2-hydroxyglutarate. *Nature* **462,** 739–744 (2009).
7. Figueroa, M. E. *et al.* Leukemic IDH1 and IDH2 mutations result in a hypermethylation phenotype, disrupt TET2 function, and impair hematopoietic differentiation. *Cancer Cell* **18,** 553–567 (2010).
8. Guo, J. U., Su, Y., Zhong, C., Ming, G. & Song, H. Hydroxylation of 5-methylcytosine by TET1 promotes active DNA demethylation in the adult brain. *Cell* **145,** 423–434 (2011).
9. Noushmehr, H. *et al.* Identification of a CpG island methylator phenotype that defines a distinct subgroup of glioma. *Cancer Cell* **17,** 510–522 (2010).
10. Taverna, S. D., Li, H., Ruthenburg, A. J., Allis, C. D. & Patel, D. J. How chromatin-binding modules interpret histone modifications: lessons from professional pocket pickers. *Nature Struct. Mol. Biol.* **14,** 1025–1040 (2007).
11. Berger, S. L. The complex language of chromatin regulation during transcription. *Nature* **447,** 407–412 (2007).
12. Bernstein, B. E. *et al.* A bivalent chromatin structure marks key developmental genes in embryonic stem cells. *Cell* **125,** 315–326 (2006).
13. Estève, P. O. *et al.* Direct interaction between DNMT1 and G9a coordinates DNA and histone methylation during replication. *Genes Dev.* **20,** 3089–3103 (2006).
14. Xu, W. *et al.* Oncometabolite 2-hydroxyglutarate is a competitive inhibitor of α-ketoglutarate-dependent dioxygenases. *Cancer Cell* **19,** 17–30 (2011).
15. Chowdhury, R. *et al.* The oncometabolite 2-hydroxyglutarate inhibits histone lysine demethylases. *EMBO Rep.* **12,** 463–469 (2011).
16. Verhaak, R. G. *et al.* Integrated genomic analysis identifies clinically relevant subtypes of glioblastoma characterized by abnormalities in *PDGFRA*, *IDH1*, *EGFR*, and *NF1*. *Cancer Cell* **17,** 98–110 (2010).
17. MacDougald, O. A. & Lane, M. D. Transcriptional regulation of gene expression during adipocyte differentiation. *Annu. Rev. Biochem.* **64,** 345–373 (1995).
18. Rubin, C. S., Hirsch, A., Fung, C. & Rosen, O. M. Development of hormone receptors and hormonal responsiveness *in vitro*. Insulin receptors and insulin sensitivity in the preadipocyte and adipocyte forms of 3T3-L1 cells. *J. Biol. Chem.* **253,** 7570–7578 (1978).
19. Krivtsov, A. V. & Armstrong, S. A. *MLL* translocations, histone modifications and leukaemia stem-cell development. *Nature Rev. Cancer* **7,** 823–833 (2007).
20. Hu, Z. *et al.* A novel nuclear protein, 5qNCA (LOC51780) is a candidate for the myeloid leukemia tumor suppressor gene on chromosome 5 band q31. *Oncogene* **20,** 6946–6954 (2001).
21. van Haaften, G. *et al.* Somatic mutations of the histone H3K27 demethylase gene *UTX* in human cancer. *Nature Genet.* **41,** 521–523 (2009).
22. Bilodeau, S., Kagey, M. H., Frampton, G. M., Rahl, P. B. & Young, R. A. SetDB1 contributes to repression of genes encoding developmental regulators and maintenance of ES cell state. *Genes Dev.* **23,** 2484–2489 (2009).
23. Ceol, C. J. *et al.* The histone methyltransferase SETDB1 is recurrently amplified in melanoma and accelerates its onset. *Nature* **471,** 513–517 (2011).
24. Wellen, K. E. *et al.* ATP-citrate lyase links cellular metabolism to histone acetylation. *Science* **324,** 1076–1080 (2009).
25. Ingvarsdottir, K. *et al.* Histone H3K4 demethylation during activation and attenuation of *GAL1* transcription in *Saccharomyces cerevisiae*. *Mol. Cell. Biol.* **27,** 7856–7864 (2007).

**Supplementary Information** is linked to the online version of the paper at www.nature.com/nature.

**Acknowledgements** We thank members of the Thompson laboratory for technical help and critical reading of the manuscript. We thank T. A. Gocke and the genomic core of University of Pennsylvania for their assistance with the microarray study; the molecular cytology core facility of Memorial Sloan-Kettering Cancer Center (MSKCC) for technical help with the immunohistochemistry study; and O. Querfelli and M. K. Spassova at the organic synthesis core of MSKCC for the synthesis of octyl-2HG. This work was supported by grants from the National Cancer Institute and National Institutes of Health. R.L.L. is an Early Career Award recipient of the Howard Hughes Medical Institute and the Geoffrey Beene Junior Chair at MSKCC. D.M.O'R. is supported by the Betsy Cohen Fund of the Abramson Cancer Center at University of Pennsylvania. I.K.M. is supported by NCI-U54CA143798, the Doris Duke Charitable Foundation, and an Advanced Clinical Research Award in Glioma from the American Society of Clinical Oncology.

**Author Contributions** C.L., P.S.W. and C.B.T. designed the study. C.L., P.S.W., G.S.K., D.R. and M.E.F. performed research; S.T., D.R., T.A.C. and I.K.M. contributed research material; C.L., P.S.W., G.S.K., O.A.-W., C.R.E., R.K., M.E.F., A.M., K.E.W., D.M.O'R., S.L.B., R.L.L. and C.B.T. contributed to data analysis and interpretation; C.L., P.S.W. and C.B.T. wrote the manuscript.

**Author Information** Microarray data have been deposited with the ArrayExpress database under accession code E-MEXP-3239. Reprints and permissions information is available at www.nature.com/reprints. The authors declare competing financial interests: details accompany the full-text HTML version of the paper at www.nature.com/nature. Readers are welcome to comment on the online version of this article at www.nature.com/nature. Correspondence and requests for materials should be addressed to C.B.T. (thompsonc@mskcc.org).

LETTER

doi:10.1038/nature10866

# IDH1 mutation is sufficient to establish the glioma hypermethylator phenotype

Sevin Turcan[1]*, Daniel Rohle[1,2]*, Anuj Goenka[1,3]*, Logan A. Walsh[1], Fang Fang[1], Emrullah Yilmaz[1], Carl Campos[1], Armida W. M. Fabius[1], Chao Lu[4,5], Patrick S. Ward[4,5], Craig B. Thompson[4], Andrew Kaufman[1], Olga Guryanova[1], Ross Levine[1], Adriana Heguy[1], Agnes Viale[6], Luc G. T. Morris[1,7], Jason T. Huse[1,8], Ingo K. Mellinghoff[1,2,9,10] & Timothy A. Chan[1,2,3,10]

**Both genome-wide genetic and epigenetic alterations are fundamentally important for the development of cancers, but the interdependence of these aberrations is poorly understood. Glioblastomas and other cancers with the CpG island methylator phenotype (CIMP) constitute a subset of tumours with extensive epigenomic aberrations and a distinct biology[1–3]. Glioma CIMP (G-CIMP) is a powerful determinant of tumour pathogenicity, but the molecular basis of G-CIMP remains unresolved. Here we show that mutation of a single gene, isocitrate dehydrogenase 1 (*IDH1*), establishes G-CIMP by remodelling the methylome. This remodelling results in reorganization of the methylome and transcriptome. Examination of the epigenome of a large set of intermediate-grade gliomas demonstrates a distinct G-CIMP phenotype that is highly dependent on the presence of *IDH* mutation. Introduction of mutant IDH1 into primary human astrocytes alters specific histone marks, induces extensive DNA hypermethylation, and reshapes the methylome in a fashion that mirrors the changes observed in G-CIMP-positive lower-grade gliomas. Furthermore, the epigenomic alterations resulting from mutant IDH1 activate key gene expression programs, characterize G-CIMP-positive proneural glioblastomas but not other glioblastomas, and are predictive of improved survival. Our findings demonstrate that IDH mutation is the molecular basis of CIMP in gliomas, provide a framework for understanding oncogenesis in these gliomas, and highlight the interplay between genomic and epigenomic changes in human cancers.**

The isocitrate dehydrogenase genes *IDH1* and *IDH2* are mutated in >70% of lower-grade gliomas (grades II and III), in some glioblastomas[4,5], and in leukaemias and several other cancers[6,7]. The most common *IDH1* mutations in glioma (>95%) result in an amino acid substitution at arginine 132 (R132), which resides in the enzyme's active site. Mutation of IDH imparts the ability to produce 2-hydroxyglutarate (2-HG), a potential oncometabolite[8–10]. Alterations in the methylation landscape have been shown to have important roles during oncogenesis[11]. CIMP has emerged as a distinct molecular subclass of tumours in a number of human malignancies, including glioblastoma[1–3]. This phenotype is associated with extensive, coordinated hypermethylation at specific loci[1,2,12,13]. In glioblastomas, G-CIMP is associated with the proneural subgroup of tumours and IDH mutation[1]. Exactly how mutant IDH promotes tumorigenesis and causes G-CIMP—or CIMP in any type of human cancer—is unknown.

To determine whether *IDH1* mutation directly causes G-CIMP, we used immortalized primary human astrocytes[14] and constructed isogenic cells expressing either mutant IDH1 (R132H), wild-type IDH1, or neither. These astrocytes are well characterized[14–17]. Introduction of wild-type IDH1 and the R132H IDH1 mutant resulted in equal expression of protein (modest threefold increase) (Fig. 1a). Expression of mutant but not wild-type IDH1 in human astrocytes resulted in the production of 2-HG (Fig. 1b). To determine whether mutant IDH1 altered the methylation landscape, we analysed genomic DNA from these cells using the Illumina Infinium HumanMethylation450 platform. The platform provides genome-wide coverage and is both well validated and highly reproducible[18,19].

Previous data demonstrated that *de novo* DNA methylation in *in vitro* models occurs over extended periods, requiring time to 'lock in' epigenomic changes[12,20]. We thus analysed the methylomes of astrocytes expressing mutant or wild-type IDH1 over successive passages (up to 50). Analysis using self-organizing maps demonstrated that mutant IDH1 progressively remodelled the glial methylome over time (Fig. 1c, d), an effect that was not seen in control astrocytes. Expression of mutant IDH1 caused a marked increase in hypermethylation at a large number of genes, although there was a small group of hypomethylated genes as well (Fig. 1e and Supplementary Fig. 1a and Supplementary Table 1). Surprisingly, expression of wild-type IDH1 also reshaped the methylome but in a manner that differed from effects due to expression of mutant IDH1 (Fig. 1f). Expression of wild-type IDH1 caused hypomethylation at specific loci, suggesting that both the production of 2-HG and the levels of $\alpha$-ketoglutarate can affect the methylome. Unsupervised hierarchical clustering of the methylome data showed that the hypermethylated genes included both genes that underwent *de novo* methylation as well as genes that originally possessed low levels of methylation but subsequently acquired high levels of methylation (Fig. 1e). Control astrocytes did not undergo these methylome changes (Fig. 1c, d). Mutant IDH1-induced remodelling of the methylome was progressive and reproducible, and resulted in significant changes in gene expression (Fig. 1f and Supplementary Fig. 1a, Supplementary Tables 2 and 3).

We sought to define the methylation targets of mutant IDH in astrocytes. Of the 44,334 CpG sites that were differentially methylated in mutant IDH-expressing cells, 30,988 sites were hypermethylated (3,141 unique genes with promoter CpG island methylation changes; Supplementary Table 1). Transcriptional module mapping showed that the genes undergoing methylation changes were highly enriched for polycomb complex 2 (PRC2)-targeted loci (Supplementary Fig. 1b and Supplementary Table 4)[12,21]. These observations demonstrate that mutant IDH1 is sufficient to reshape the epigenome by altering the global methylation landscape.

Lower-grade gliomas (LGGs; World Health Organization grades II and III) and secondary glioblastomas are biologically distinct from primary or *de novo* glioblastomas[22]. Present knowledge of G-CIMP

[1]Human Oncology and Pathogenesis Program, Memorial Sloan-Kettering Cancer Center, New York, New York 10065, USA. [2]Weill Cornell College of Medicine, New York, New York 10065, USA. [3]Department of Radiation Oncology, Memorial Sloan-Kettering Cancer Center, New York, New York 10065, USA. [4]Cancer Biology and Genetics, Memorial Sloan-Kettering Cancer Center, New York, New York 10065, USA. [5]Department of Cancer Biology, University of Pennsylvania School of Medicine, Philadelphia, Pennsylvania 19104, USA. [6]Genomics Core, Memorial Sloan-Kettering Cancer Center, New York, New York 10065, USA. [7]Department of Surgery, Memorial Sloan-Kettering Cancer Center, New York, New York 10065, USA. [8]Department of Pathology, Memorial Sloan-Kettering Cancer Center, New York, New York 10065, USA. [9]Department of Neurology, Memorial Sloan-Kettering Cancer Center, New York, New York 10065, USA. [10]Brain Tumor Center, Memorial Sloan-Kettering Cancer Center, New York, New York 10065, USA.

*These authors contributed equally to this work.

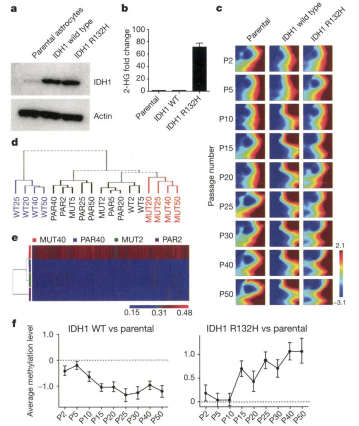


**Figure 1 | Introduction of mutant IDH1 into human astrocytes remodels the methylome. a**, Expression of wild-type and mutant IDH1 (R132H) in immortalized human astrocytes (passage 5). **b**, Overexpression of mutant IDH1 but not wild-type (WT) IDH1 in human astrocytes leads to production of 2-$HG^3$. Error bars show 1 standard deviation (s.d.) ($n = 2$). **c**, Self-organizing map (SOM) analysis of methylome data for wild-type IDH1-expressing, mutant IDH1-expressing (R132H), and parental (control) cell lines shows changes in the methylome in mutant IDH1-expressing and wild-type IDH1-expressing astrocytes, compared to parental cells. Mosaic patterns are pseudo-coloured SOMs from different time points (P indicates passage number). Tile colours indicate methylation level of centroids. **d**, Hierarchical clustering showing divergence of the methylome of IDH1-expressing astrocytes from that of parental astrocytes. MUT, mutant; PAR, parental. **e**, Heatmap showing the 10,678 most significant differentially methylated probes (ANOVA) in IDH1 mutant astrocytes and parental astrocytes (passages 2 and 40). Colour scale indicates $\beta$ values. **f**, Kinetics of differential methylation in mutant and wild-type-expressing astrocytes. Error bars indicate inter-quartile range ($n = 2$).

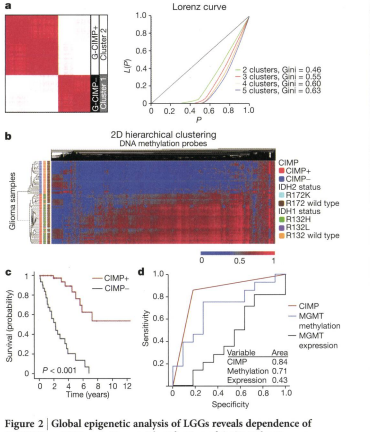


**Figure 2 | Global epigenetic analysis of LGGs reveals dependence of G-CIMP on IDH mutation. a**, Identification of G-CIMP by *K*-means consensus clustering of LGG samples. Unsupervised clustering was performed with the most variant probes (9,711 probes, top 2%). Tumours are listed in the same order along the *x* and *y* axes. G-CIMP status is indicated by the black and white bars. Consensus index values range from 0 to 1, with 0 being dissimilar (white) and 1 being similar (red). $K = 2$ is identified by the Lorenz curve. **b**, Two-dimensional (2D) hierarchical clustering of the same probes as in **a** identified the same two clusters. Each row represents a tumour and each column represents a probe. CIMP and IDH mutation status are indicated by the colour code. The level of DNA methylation ($\beta$ value) for each probe is represented by colour scale (red, methylated; blue, non-methylated). Only cancer-specific events were used[27]. **c**, Kaplan–Meier survival curve of Memorial Sloan-Kettering Cancer Center (MSKCC) patients ($n = 72$) with LGG (grade II and III). **d**, Receiver operating characteristic (ROC) curve comparing the sensitivity and specificity of G-CIMP status compared with MGMT methylation or MGMT expression status, in LGGs. Areas under the curve are noted in the inset. G-CIMP, MGMT methylation and MGMT expression were determined as described in Methods.

is based on the examination of primary glioblastomas in which IDH mutations are infrequent[1,4,5]. To determine the impact of IDH mutation on the methylation landscape in primary LGGs, we generated a high-resolution, genome-wide set of LGG methylome data from patients with complete clinical follow-up using the same Infinium 450K platform as described earlier (72 WHO grade II and III gliomas; Fig. 2 and Supplementary Table 5). We first performed consensus clustering (Fig. 2a and Supplementary Fig. 2a) and unsupervised hierarchical clustering (Fig. 2b and Supplementary Fig. 2b) to identify LGG subgroups. We identified two robust DNA methylation clusters, one encompassing tumours with markedly high methylation levels (cluster 2) and another without the hypermethylated loci (cluster 1). Cluster 2 tumours demonstrated a characteristic DNA methylation profile with high-coordinate cancer-specific methylation at a subset of loci, concordant with the G-CIMP phenotype defined in glioblastomas (Supplementary Fig. 2b and Supplementary Table 6)[1]. The composition of the G-CIMP group in these LGGs was confirmed by two independent clustering methods (*K*-means consensus and two-dimensional hierarchical clustering) (Fig. 2a, b). Probes defining CIMP in LGGs included those in CpG islands and shores (Supplementary Fig. 2c, d) and were enriched for PRC2-target genes (Supplementary Table 7). Global expression profiles showed that G-CIMP+ tumours possessed markedly different transcriptional profiles than G-CIMP− tumours (Supplementary Tables 8 and 9). EpiTYPER (Sequenom) mass spectrometry was used to validate the methylation status of loci in both the astrocyte model and in the tumours (Supplementary Fig. 2e–g)[23].

To determine the mutational status of *IDH1* and *IDH2*, we sequenced the entire coding sequence of the two genes in all the samples above (Fig. 2b). Ninety-eight per cent (49/50) of the G-CIMP+ tumours possessed either an *IDH1* mutation or *IDH2* mutation. Notably, none of the G-CIMP− tumours possessed mutant IDH (Supplementary Fig. 2h). These genomic data show that G-CIMP is highly dependent on the presence of IDH mutation and, in LGGs that are CIMP−, IDH mutations do not occur (0%). Currently, the methylation status of *O*-6-methylguanine DNA methyltransferase (MGMT) is a widely used molecular biomarker for glioblastoma prognosis and response to

temozolomide[24]. In LGGs, G-CIMP associated with markedly better clinical endpoints (Fig. 2c and Supplementary Figs 3–6, Supplementary Tables 10 and 11). Importantly, G-CIMP was significantly superior to MGMT methylation or *MGMT* messenger RNA expression as a predictor of survival (Fig. 2d).

We next sought to define the nature of the methylome differences between IDH mutant and wild-type tumours and characterize the effects of these differences on the LGG transcriptome. Figure 3a shows a principal component analysis (PCA) of methylome and expression data from our tumours. PCA shows that G-CIMP+ and G-CIMP− LGGs methylome subgroups correlate with marked transcriptome differences (Fig. 3a). Of the 140,016 sites that were differentially methylated between IDH mutant and wild-type tumours, 121,660 were hypermethylated (Supplementary Table 6). There were 2,611 unique genes with alterations in promoter CpG islands represented in this group. Consistent with the results in Fig. 2b, a volcano plot showing differentially methylated genes between G-CIMP+ and G-CIMP− tumours was highly asymmetric (Fig. 3b). A starburst plot showing the relationship between DNA methylation and expression is shown in Fig. 3b. Integration of the normalized gene expression and DNA methylation gene sets identified 429 genes with both significant hypermethylation and downregulation and 176 genes that were hypomethylated and upregulated in G-CIMP+ LGGs (Supplementary Table 12). Among these genes are those known to be involved in glioma initiation and outcome, including *CDKN2C* and *GAP43* (refs 25, 26).

As a critical experiment to prove causality between IDH1 mutation and G-CIMP, we performed an in-depth comparison of methylation marks and gene expression alterations between human astrocytes expressing mutant IDH1 and the LGGs with endogenous IDH1 mutation. We first focused on the comparison of methylation marks and found that both sets of methylome alterations targeted similar loci. Gene set enrichment analysis (GSEA) of the mutant IDH1-induced methylation changes in the isogenic astrocyte system (Fig. 1) and the G-CIMP genes demonstrated very significant enrichment and concordance (Fig. 3c and Supplementary Table 13 and Supplementary Fig. 7). Importantly, the genes that were methylated after mutant IDH1 expression correctly classified LGG tumours into CIMP+ or CIMP− groups with very high accuracy (Fig. 3d and Supplementary Table 14). To confirm the impact of these alterations on glioma pathobiology, we used the transcriptomic footprint of mutant IDH to generate an expression signature (mutant IDH repression signature) composed of the most significantly methylated and downregulated genes in both the isogenic astrocyte system and the G-CIMP gene set (17 genes; Supplementary Table 15). As expected, this signature classified an independent LGG cohort (Rembrandt) into two distinct subgroups (Fig. 3e and Supplementary Figs 8–10 and Supplementary Table 16). Together, our findings show that introduction of mutant IDH reprograms the epigenome and generates the foundations of G-CIMP.

IDH mutation is highly enriched in the CIMP+, proneural subgroup of glioblastomas. Using data from The Cancer Genome Atlas (TCGA), we applied the mutant IDH repression signature as a classifier to the transcriptomes of all four subgroups of glioblastomas[27]. The signature segregated IDH mutant and wild-type proneural glioblastomas into two distinct subgroups associated with very different prognoses, but did not do so in other glioblastoma subgroups (Supplementary Fig. 11a, b). These data demonstrate that mutant IDH-induced epigenomic alterations have profound biological implications within the proneural class of glioblastomas that are specific for this subclass. Comparison of gene expression programs that occur in astrocytes expressing mutant IDH1 to those in LGG tumours that harbour the IDH mutation showed remarkable similarity (Fig. 4a and Supplementary Fig. 12). Moreover, introduction of mutant but not wild-type IDH1 into astrocytes resulted in the upregulation of nestin (and other genes associated with stem cell identity) at the time of DNA methylation increase and the adoption of a neurosphere/stem-like phenotype (Fig. 4b and Supplementary

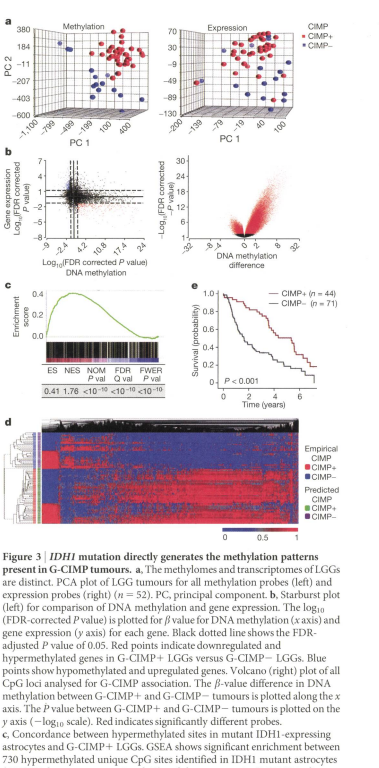


**Figure 3 | *IDH1* mutation directly generates the methylation patterns present in G-CIMP tumours.** **a**, The methylomes and transcriptomes of LGGs are distinct. PCA plot of LGG tumours for all methylation probes (left) and expression probes (right) ($n = 52$). PC, principal component. **b**, Starburst plot (left) for comparison of DNA methylation and gene expression. The $\log_{10}$ (FDR-corrected $P$ value) is plotted for $\beta$ value for DNA methylation ($x$ axis) and gene expression ($y$ axis) for each gene. Black dotted line shows the FDR-adjusted $P$ value of 0.05. Red points indicate downregulated and hypermethylated genes in G-CIMP+ LGGs versus G-CIMP− LGGs. Blue points show hypomethylated and upregulated genes. Volcano (right) plot of all CpG loci analysed for G-CIMP association. The $\beta$-value difference in DNA methylation between G-CIMP+ and G-CIMP− tumours is plotted along the $x$ axis. The $P$ value between G-CIMP+ and G-CIMP− tumours is plotted on the $y$ axis ($-\log_{10}$ scale). Red indicates significantly different probes. **c**, Concordance between hypermethylated sites in mutant IDH1-expressing astrocytes and G-CIMP+ LGGs. GSEA shows significant enrichment between 730 hypermethylated unique CpG sites identified in IDH1 mutant astrocytes (ANOVA between passage 2 and 40) and those present in G-CIMP+ gliomas. GSEA correlation shown in colour scale. ES, enrichment score; FDR, false discovery rate; FEWR, familywise error rate; NES, normalized enrichment score; NOM, nominal $P$ value. **d**, Differential methylation in IDH mutant astrocytes correctly classifies G-CIMP in the human LGGs. Two-dimensional-unsupervised hierarchical clustering of 81 human gliomas with top variant probes ($n = 10{,}000$) from mutant IDH1 astrocytes. Tumours are shown on the $y$ axis, probes along the $x$ axis. Methylation ($\beta$ value) for each probe is represented with the colour scale. G-CIMP classification as determined by the astrocyte-derived data is denoted by the colour bars at the left. **e**, Kaplan–Meier survival curve of 115 patients with grade II or grade III gliomas in the Rembrandt Database grouped by CIMP status. $P$ value calculated by log rank.

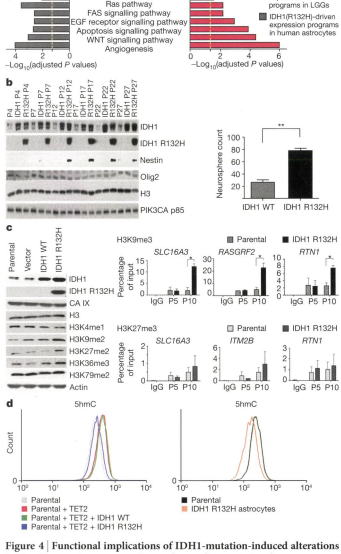


**Figure 4 | Functional implications of IDH1-mutation-induced alterations in the glioma epigenome.** **a**, Concordance of transcriptional programs regulated by mutant IDH1 in astrocytes and G-CIMP in LGGs. *P* value for significance is shown along the *x* axis. Yellow lines indicate threshold of significance ($P = 0.05$). **b**, Mutant IDH1 results in the expression of markers of self-renewal and stem cell identity. Left, mutant IDH1 results in expression of nestin. P indicates passage number. Right, expression of mutant IDH1 promotes the adoption of a neurosphere phenotype. Astrocytes (passage 15) that express IDH R132H or IDH1 wild type were used in the neurosphere assay. Error bars indicate 1 s.d. $^{**}P < 0.01$ (*t*-test). **c**, Alterations in histone marks in IDH1-mutant-expressing human astrocytes. Left, western blot results are shown using the indicated antibodies. Astrocytes are from passage 27. Right, ChIP of the indicated histone marks for representative hypermethylated genes. Error bars indicate 1 s.d. $^{*}P < 0.05$. **d**, Mutant IDH1 inhibits the production of 5hmC in human astrocytes. Left, mutant IDH1 inhibits TET2-dependent 5hmC production in astrocytes. Parental astrocytes were infected with lentivirus directing the expression of TET2 catalytic domain and green fluorescent protein (GFP) ± mutant IDH1. FACS analyses are shown for 5hmC. Right, astrocytes expressing IDH R132H (passage 10) have less 5hmC than astrocytes that do not express the IDH mutant.

Fig. 1)[28]. These data suggest that mutant IDH1 functions by interfering with differentiation state.

Our data show that IDH1 mutation is the mechanistic cause of G-CIMP. To gain further insight, we determined the effects of mutant IDH1 on histone alterations in our astrocyte system. Figure 4c (left) shows that expression of the IDH1 mutant increases levels of H3K9me2, H3K27me3 and H3K36me3, consistent with previous findings[29]. Chromatin immunoprecipitation (ChIP) experiments examining representative genes that undergo hypermethylation show H3K9 and H3K27 methylation are both enriched in cells expressing mutant IDH1 (Fig. 4c, right). As both of these marks can promote DNA methylation, alterations in histone marks may contribute to the accumulation of DNA methylation.

Next, we determined the effects the mutation had on TET2-dependent 5-hydroxymethylcytosine (5hmC) levels. We used a well-established assay[9,29] and first confirmed that we were able to detect TET-dependent alterations in 5hmC (Supplementary Fig. 14). We found that expression of the IDH1 mutant in astrocytes resulted in a significant decrease in 5hmC (Fig. 4d, right). Expression of TET2 in the astrocytes produced 5hmC, which was inhibited by mutant but not wild-type IDH1 (Fig. 4d, left). Because TET-mediated production of 5hmC is a primary mode of DNA demethylation[30], inhibition of this activity in the IDH1-mutant-expressing astrocytes may be a mechanistic basis for accumulation of DNA methylation, ultimately leading to a CIMP pattern.

IDH mutation and the CIMP phenotype are two very common features in cancer, the underlying mechanisms for which are obscure. The fundamental questions regarding these features are (1) how the IDH mutation contributes to oncogenesis, and (2) what the root cause of CIMP is. Our data address these important questions by demonstrating that IDH mutation is the cause of CIMP and leads to the CIMP phenotype by stably reshaping the epigenome. This remodelling involves modulating patterns of methylation on a genome-wide scale, changing transcriptional programs and altering the differentiation state. Our observations suggest that the activity of IDH may form the basis of an 'epigenomic rheostat', linking alterations in cellular metabolism to the epigenetic state. In summary, these data provide a mechanistic framework for how IDH mutation leads to oncogenesis and the molecular basis of CIMP in gliomas. We believe our observations have critical implications for the understanding of gliomas and the development of novel therapies for this disease.

## METHODS SUMMARY

**Cell culture.** Immortalized human astrocytes were a gift from R. O. Pieper (University of California, San Francisco) and were prepared as previously described[14]. Cells were cultured in Dulbecco's modified Eagle's medium (DMEM) plus 10% fetal bovine serum (FBS; Invitrogen). Expression of IDH was accomplished by cloning wild-type or mutant IDH1 (R132H) into the vector pLNCX2. These constructs were used to construct lentiviruses used for infection of target cells. Selection was performed using G418. All experiments were performed in duplicate.

**Tumours.** All tumours ($n = 81$) were obtained following surgical resection at the MSKCC as part of routine clinical care and snap frozen. Tumours were obtained in accordance with Institutional Review Board policies at the MSKCC. Each sample was examined histologically with haematoxylin-and-eosin-stained cryostat sections by a neuropathologist. Before analysis, tumours were sectioned and microdissected. Genomic DNA or RNA was extracted using the DNeasy kit (Qiagen) or RNeasy Lipid Tissue Mini kit (Qiagen) per the manufacturer's instructions.

**Genomic analysis.** Expression analysis of astrocytes and tumours was performed using the Affymetrix U133 2.0 microarray. Genome-wide methylation analysis was performed using the Illumina Infinium HumanMethylation450 bead array. Processing of the arrays was as per the manufacturer's protocol. Methylation data were extracted using GenomeStudio software (Illumina). Methylation values for each site are expressed as a $\beta$ value, representing a continuous measurement from 0 (completely unmethylated) to 1 (completely methylated). This value is based on the following calculation: $\beta$ value = (signal intensity of methylation-detection probe) / (signal intensity of methylation- detection probe + signal intensity of non-methylation detection probe).

**Full Methods** and any associated references are available in the online version of the paper at www.nature.com/nature.

**Received 3 June 2011; accepted 17 January 2012.**
**Published online 15 February 2012.**

1. Noushmehr, H. *et al.* Identification of a CpG island methylator phenotype that defines a distinct subgroup of glioma. *Cancer Cell* **17**, 510–522 (2010).
2. Fang, F. *et al.* Breast cancer methylomes establish an epigenomic foundation for metastasis. *Sci. Transl. Med.* **3**, 75ra25 (2011).

3. Toyota, M. *et al.* CpG island methylator phenotype in colorectal cancer. *Proc. Natl Acad. Sci. USA* **96,** 8681–8686 (1999).
4. Yan, H. *et al.* IDH1 and IDH2 mutations in gliomas. *N. Engl. J. Med.* **360,** 765–773 (2009).
5. Parsons, D. W. *et al.* An integrated genomic analysis of human glioblastoma multiforme. *Science* **321,** 1807–1812 (2008).
6. Sjoblom, T. *et al.* The consensus coding sequences of human breast and colorectal cancers. *Science* **314,** 268–274 (2006).
7. Mardis, E. R. *et al.* Recurring mutations found by sequencing an acute myeloid leukemia genome. *N. Engl. J. Med.* **361,** 1058–1066 (2009).
8. Dang, L. *et al.* Cancer-associated IDH1 mutations produce 2-hydroxyglutarate. *Nature* **462,** 739–744 (2009).
9. Figueroa, M. E. *et al.* Leukemic IDH1 and IDH2 mutations result in a hypermethylation phenotype, disrupt TET2 function, and impair hematopoietic differentiation. *Cancer Cell* **18,** 553–567 (2010).
10. Ward, P. S. *et al.* The common feature of leukemia-associated IDH1 and IDH2 mutations is a neomorphic enzyme activity converting α-ketoglutarate to 2-hydroxyglutarate. *Cancer Cell* **17,** 225–234 (2010).
11. Jones, P. A. & Baylin, S. B. The epigenomics of cancer. *Cell* **128,** 683–692 (2007).
12. Ohm, J. E. *et al.* A stem cell-like chromatin pattern may predispose tumor suppressor genes to DNA hypermethylation and heritable silencing. *Nature Genet.* **39,** 237–242 (2007).
13. Cheng, Y. W. *et al.* CpG island methylator phenotype associates with low-degree chromosomal abnormalities in colorectal cancer. *Clin. Cancer Res.* **14,** 6005–6013 (2008).
14. Sonoda, Y. *et al.* Formation of intracranial tumors by genetically modified human astrocytes defines four pathways critical in the development of human anaplastic astrocytoma. *Cancer Res.* **61,** 4956–4960 (2001).
15. Vivanco, I. *et al.* Identification of the JNK signaling pathway as a functional target of the tumor suppressor PTEN. *Cancer Cell* **11,** 555–569 (2007).
16. Sonoda, Y. *et al.* Akt pathway activation converts anaplastic astrocytoma to glioblastoma multiforme in a human astrocyte model of glioma. *Cancer Res.* **61,** 6674–6678 (2001).
17. Pieper, R. O. Defined human cellular systems in the study of glioma development. *Front. Biosci.* **8,** s19–s27 (2003).
18. Bibikova, M. *et al.* High density DNA methylation array with single CpG site resolution. *Genomics* **98,** 288–295 (2011).
19. Sandoval, J. *et al.* Validation of a DNA methylation microarray for 450,000 CpG sites in the human genome. *Epigenetics* **6,** 692–702 (2011).
20. Mutskov, V. & Felsenfeld, G. Silencing of transgene transcription precedes methylation of promoter DNA and histone H3 lysine 9. *EMBO J.* **23,** 138–149 (2004).
21. Bracken, A. P. *et al.* Genome-wide mapping of Polycomb target genes unravels their roles in cell fate transitions. *Genes Dev.* **20,** 1123–1136 (2006).
22. Furnari, F. B. *et al.* Malignant astrocytic glioma: genetics, biology, and paths to treatment. *Genes Dev.* **21,** 2683–2710 (2007).
23. Docherty, S. J. *et al.* Bisulfite-based epityping on pooled genomic DNA provides an accurate estimate of average group DNA methylation. *Epigenetics Chromatin* **2,** 3 (2009).
24. Hegi, M. E. *et al. MGMT* gene silencing and benefit from temozolomide in glioblastoma. *N. Engl. J. Med.* **352,** 997–1003 (2005).
25. Solomon, D. A. *et al.* Identification of $p18^{INK4c}$ as a tumor suppressor gene in glioblastoma multiforme. *Cancer Res.* **68,** 2564–2569 (2008).
26. Etcheverry, A. *et al.* DNA methylation in glioblastoma: impact on gene expression and clinical outcome. *BMC Genomics* **11,** 701 (2010).
27. The Cancer Genome Atlas Network. Comprehensive genomic characterization defines human glioblastoma genes and core pathways. *Nature* **455,** 1061–1068 (2008).
28. Lendahl, U., Zimmerman, L. B. & McKay, R. D. CNS stem cells express a new class of intermediate filament protein. *Cell* **60,** 585–595 (1990).
29. Xu, W. *et al.* Oncometabolite 2-hydroxyglutarate is a competitive inhibitor of α-ketoglutarate-dependent dioxygenases. *Cancer Cell* **19,** 17–30 (2011).
30. He, Y. F. *et al.* Tet-mediated formation of 5-carboxylcytosine and its excision by TDG in mammalian DNA. *Science* **333,** 1303–1307 (2011).


**Supplementary Information** is linked to the online version of the paper at www.nature.com/nature.

**Acknowledgements** We thank A. Kaysersian, K. Huberman, I. Dolgalev and S. Thomas for technical expertise. We thank C. Sawyers and E. Holland for helpful discussions. This grant was supported in part by the National Institutes of Health (R01CA154767-01) (T.A.C.), the National Cancer Institute (U54-CA143798) (I.K.M.), an Advanced Clinical Research Award in Glioma from the American Society of Clinical Oncology (I.K.M.), the Doris Duke Charitable Fund (I.K.M., T.A.C.), a National Brain Tumor Society Systems Biology Research Grant (I.K.M.), the MSKCC Brain Tumor Center (T.A.C.), the Louis Gerstner Foundation (T.A.C.), the STARR Cancer Consortium (T.A.C.) and the Sontag Foundation (T.A.C., I.K.M.).

**Author Contributions** T.A.C., S.T., A.G. and I.K.M. designed the experiments. S.T., A.G., F.F., D.R., A.H., L.A.W., C.C., E.Y., C.L., P.S.W., A.V., J.T.H., A.W.M.F. and L.G.T.M. performed the experiments. S.T., J.T.H., A.G., F.F., A.K., A.H., E.Y., A.V., P.S.W., C.B.T., T.A.C. and I.K.M. analysed the data. D.R., O.G., R.L. and I.K.M. contributed new reagents. T.A.C., S.T., I.K.M. and A.G. wrote the paper.

**Author Information** Data sets have been deposited in the Gene Expression Omnibus under accession number GSE30339. Reprints and permissions information is available at www.nature.com/reprints. The authors declare competing financial interests: details accompany the full-text HTML version of the paper at www.nature.com/nature. Readers are welcome to comment on the online version of this article at www.nature.com/nature. Correspondence and requests for materials should be addressed to T.A.C (chant@mskcc.org) or I.K.M. (mellinj@mskcc.org).

LETTER

doi:10.1038/nature10898

# Transformation by the (*R*)-enantiomer of 2-hydroxyglutarate linked to EGLN activation

Peppi Koivunen[1]*, Sungwoo Lee[2]*, Christopher G. Duncan[3], Giselle Lopez[3], Gang Lu[2], Shakti Ramkissoon[2,4,5], Julie A. Losman[2], Päivi Joensuu[6], Ulrich Bergmann[7], Stefan Gross[8], Jeremy Travins[8], Samuel Weiss[9], Ryan Looper[10], Keith L. Ligon[2,4,5,11], Roel G. W. Verhaak[12], Hai Yan[3] & William G. Kaelin Jr[2,13]

**The identification of succinate dehydrogenase (SDH), fumarate hydratase (FH) and isocitrate dehydrogenase (IDH) mutations in human cancers has rekindled the idea that altered cellular metabolism can transform cells. Inactivating SDH and FH mutations cause the accumulation of succinate and fumarate, respectively, which can inhibit 2-oxoglutarate (2-OG)-dependent enzymes, including the EGLN prolyl 4-hydroxylases that mark the hypoxia inducible factor (HIF) transcription factor for polyubiquitylation and proteasomal degradation[1]. Inappropriate HIF activation is suspected of contributing to the pathogenesis of SDH-defective and FH-defective tumours but can suppress tumour growth in some other contexts. IDH1 and IDH2, which catalyse the interconversion of isocitrate and 2-OG, are frequently mutated in human brain tumours and leukaemias. The resulting mutants have the neomorphic ability to convert 2-OG to the (*R*)-enantiomer of 2-hydroxyglutarate ((*R*)-2HG)[2,3]. Here we show that (*R*)-2HG, but not (*S*)-2HG, stimulates EGLN activity, leading to diminished HIF levels, which enhances the proliferation and soft agar growth of human astrocytes. These findings define an enantiomer-specific mechanism by which the (*R*)-2HG that accumulates in IDH mutant brain tumours promotes transformation and provide a justification for exploring EGLN inhibition as a potential treatment strategy.**

To study the role of IDH mutations in brain tumours, we stably infected immortalized human astrocytes with retroviral vectors encoding haemagglutinin (HA)-tagged versions of wild-type IDH1, a tumour-derived mutant (IDH1 R132H)[2,3], or an IDH1 R132H variant in which three conserved aspartic acid residues within the IDH1 catalytic domain were replaced with asparagines (R132H/3DN) (Fig. 1a and Supplementary Fig. 1). As expected, (*R*)-2HG levels, but not (*S*)-2HG levels, were markedly increased in the cells producing IDH1 R132H but not in cells producing the R132H/3DN variant (Fig. 1b and Supplementary Fig. 2). In multiple independent experiments the IDH1 R132H cells acquired a proliferative advantage relative to cells producing the other versions of IDH1 beginning around passage 14, manifested as increased proliferation at confluence (Fig. 1c) and the ability to form macroscopic colonies in soft agar (Fig. 1d, e).

Consistent with recent reports, we found that both (*R*)-2HG and (*S*)-2HG inhibit a number of 2-OG-dependent enzymes *in vitro*[4–6], including the collagen prolyl 4-hydroxylases, the TET1 and TET2 methyl cytosine hydroxylases, the HIF asparaginyl hydroxylase FIH1 (also known as HIF1AN) and the JMJD2D (also known as KDM4D) histone demethylase, with (*S*)-2HG being a more potent inhibitor than (*R*)-2HG (Supplementary Fig. 3 and data not shown). (*S*)-2HG was also a micromolar to low millimolar inhibitor of the three mammalian HIF prolyl 4-hydroxylases (EGLN1, EGLN2 and EGLN3) under standard assay conditions, which included 10 μM 2-OG (Supplementary Fig. 4). In contrast, (*R*)-2HG was not an effective EGLN inhibitor (half-maximum inhibitory concentration ($IC_{50}$) values $>5$ mM; Supplementary Fig. 4). Moreover, we discovered unexpectedly that (*R*)-2HG, but not (*S*)-2HG, promoted EGLN1 and EGLN2 activity, and to a lesser extent EGLN3 activity, at tumour-relevant concentrations (low mM) in reactions that lacked exogenous 2-OG (Fig. 2a, c, d and Supplementary Fig. 5a, b). This was specific because (*R*)-2HG did not promote collagen prolyl 4-hydroxylase activity (Fig. 2b) or JMJD2D histone demethylase activity (data not shown). Similar results were obtained with EGLN1 purified from either insect cells or *Escherichia coli* and with a heat-inactivated HIF polypeptide substrate (Supplementary Fig. 6), making it unlikely that the ability of (*R*)-2HG to promote EGLN activity required a contaminating enzyme.

To determine how (*R*)-2HG might promote EGLN activity, we monitored the EGLN1 prolyl 4-hydroxylase reaction using liquid

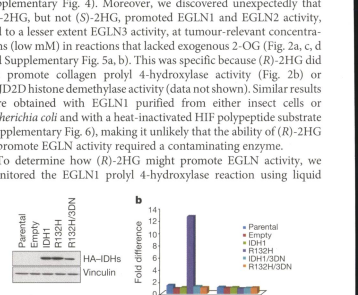


**Figure 1 | Oncogenic properties of IDH1 R132H. a**, **b**, Anti-HA immunoblot (**a**) and LC–MS analysis (**b**) of immortalized human astrocytes (passage 4) infected with retroviruses encoding HA-tagged versions of the indicated IDH1 variants. **c**, **d**, *In vitro* proliferation under standard culture conditions (**c**) or in soft agar (**d**) (passage 23). Scale bars, 0.5 mm. **e**, Number of macroscopic soft agar colonies in **d** (*$P < 0.01$, **$P < 0.005$). Error bars show standard deviation (s.d.); $n = 3$.

[1]Biocenter Oulu, Department of Medical Biochemistry and Molecular Biology, Oulu Center for Cell-Matrix Research, University of Oulu, FIN-90014 Oulu, Finland. [2]Department of Medical Oncology, Dana-Farber Cancer Institute and Brigham and Women's Hospital, Boston, Massachusetts 02215, USA. [3]The Preston Robert Tisch Brain Tumor Center at Duke, The Pediatric Brain Tumor Foundation Institute & The Department of Pathology, Duke University Medical Center, Durham, North Carolina 27710, USA. [4]Department of Pathology, Brigham and Women's Hospital, Boston, Massachusetts 02115, USA. [5]Department of Pathology, Harvard Medical School, Boston, Massachusetts 02115, USA. [6]Department of Chemistry, University of Oulu, FIN-90014 Oulu, Finland. [7]Biocenter Oulu, Mass Spectrometry Core Facility, Department of Biochemistry, University of Oulu, FIN-90014 Oulu, Finland. [8]Agios Pharmaceuticals, Cambridge, Massachusetts 02139, USA. [9]Hotchkiss Brain Institute, Departments of Cell Biology and Anatomy, University of Calgary Faculty of Medicine, Calgary, Alberta T2N 4N1, Canada. [10]Department of Chemistry, University of Utah, Salt Lake City, Utah 84112, USA. [11]Department of Pathology, Children's Hospital Boston, Boston, Massachusetts 02115, USA. [12]Department of Bioinformatics and Computational Biology, University of Texas MD Anderson Cancer Center, Houston, Texas 77030, USA. [13]Howard Hughes Medical Institute, Chevy Chase, Maryland 20815, USA.
*These authors contributed equally to this work.

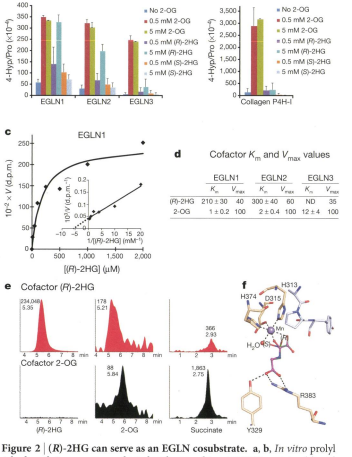


**Figure 2 | (*R*)-2HG can serve as an EGLN cosubstrate. a**, **b**, *In vitro* prolyl 4-hydroxylation assays conducted with recombinant EGLN proteins (**a**) and collagen P4H-I (**b**) in the presence of the indicated amounts of 2-OG or 2HG. 4-Hyp/Pro, ratio of 4-hydroxyproline to proline. L-[2,3,4,5-$^3$H]proline-labelled HIF-1α oxygen-dependent degradation domain (ODDD) (**a**) and [$^{14}$C]proline-labelled protocollagen (**b**) were used as substrates. Enzymes were produced in insect cells using baculoviruses and affinity purified. Error bars, s.d.; $n = 3$–4. **c**, **d**, $K_m$ (in μM) and maximum enzyme velocity ($V_{max}$; percentage of that obtained with 2-OG) values for (*R*)-2HG for EGLN family members. $K_m$ and $V_{max}$ values for 2-OG[21] are included for comparison. d.p.m., disintegrations per minute. N.D., not defined. **e**, LC–MS analysis of succinate, 2-OG and (*R*)-2HG from enzymatic reactions with EGLN1, HIF-1α ODDD polypeptide and either 5 mM (*R*)-2HG (red) or 80 μM 2-OG (black) as cofactors. Numbers next to each peak indicate elution times (bottom) and peak areas (top). No peaks above background were detected in samples in which 2-OG and (*R*)-2HG were both omitted (data not shown). **f**, Model of (*R*)-2HG (green) and (*S*)-2HG (cyan) bound to the active site of EGLN1. *N*-oxalylglycine (magneta) bound in the original structure[29] is shown for comparison. The active-site water molecule, which has been shown to be the $O_2$-binding site[30], is shown in red and the peptide substrate in light blue. Hydrogen bonds are indicated by dash lines.

chromatography–mass spectrometry (LC–MS). 2-OG and succinate were detected when catalytically active EGLN1 was incubated with 5 mM (*R*)-2HG and a recombinant HIF-1α polypeptide, suggesting that EGLN1 can oxidize (*R*)-2HG to 2-OG, which is then decarboxylated to succinate during the hydroxylation reaction (Fig. 2e and Supplementary Fig. 5c). In support of this model, $^{13}$C-labelled succinate was generated in EGLN hydroxylation assays that contained uniformly labelled $^{13}$C-(*R*)-2HG (Supplementary Fig. 5d).

Consistent with the idea that (*R*)-2HG can substitute for 2-OG as a cosubstrate, the addition of increasing amounts of (*R*)-2HG to EGLN1 assays containing 10 μM 2-oxo-[1-$^{14}$C]glutarate progressively decreased the release of $^{14}CO_2$ without decreasing the prolyl hydroxylation of HIF-1α, even at concentrations as high as 100 mM (Supplementary Fig. 7). Modelling of 2HG bound to the active site of EGLN1 predicts that binding of the (*S*)-enantiomer, but not the (*R*)-enantiomer, would prevent the subsequent recruitment of oxygen to the active site, perhaps accounting for the qualitatively different effects of the two enantiomers on EGLN activity (Fig. 2f and Supplementary Fig. 5e).

To investigate whether these findings were relevant *in vivo* we examined HIF levels in IDH1 mutant cells. In keeping with our biochemical results, HIF-1α and HIF-2α protein levels were reproducibly lower in mid-passage (passage 9–15) human astrocytes producing IDH1 R132H relative to control astrocytes (Fig. 3a), due at least partly to increased HIF-1α and HIF-2α hydroxylation and diminished protein stability (Supplementary Figs 8 and 9), and were associated with lower levels of the HIF-responsive messenger RNAs encoding *VEGF*, *GLUT1* and *PDK1* (Supplementary Fig. 10a). Oxygen consumption and reactive oxygen species production, which can also affect HIF levels and the HIF response, were not measurably altered in the IDH1 mutant cells (Supplementary Fig. 11). IDH1(R132H)-expressing cells were relatively resistant to the 2-OG competitive antagonist dimethyloxalylglycine (DMOG), but not to the iron chelator deferoxamine (DFO) (Fig. 3b), consistent with (*R*)-2HG acting as a 2-OG agonist in intact cells. In later passages (more than passage 20), HIF levels in IDH1(R132H)-expressing immortalized human astrocytes began to normalize despite persistent production of the exogenous IDH1 protein and (*R*)-2HG (Supplementary Fig. 12), possibly due to adaptive HIF-responsive feedback loops such as those involving EGLN3 and microRNA miR-155 (refs 1, 7). These cells, however, retained the ability to form colonies in soft agar (data not shown) and remained addicted to EGLN activity (see later).

Similarly, the induction of HIF-1α and HIF-responsive mRNAs by hypoxia was diminished in two independent cell lines derived from two IDH1 R132H, 1p/19q-codeleted oligodendrogliomas compared to a control IDH1 wild-type, 1p/19q-codeleted oligodendroglioma line that had been generated in a similar fashion (Fig. 3c and Supplementary Fig. 10b). Although these three cell lines have similar growth kinetics *in vitro* (data not shown) they are not isogenic. We therefore also tested two HCT116 colorectal cancer cell sublines wherein the R132H mutation was introduced into the endogenous *IDH1* locus by homologous recombination. These sublines also showed a diminished HIF response compared to wild-type cells unless EGLN was pharmacologically (DFO) or genetically (short hairpin (sh)RNA) inactivated (Fig. 3d, e and Supplementary Fig. 13).

Finally, we asked whether IDH mutational status influenced HIF activity in primary patient astrocytoma samples using the TCGA expression data set[8] and a previously defined HIF-responsive gene expression signature[9]. The HIF signature was diminished in proneural tumours—which is the subtype most often associated with IDH mutations[8]—relative to other gene-expression-defined subtypes of brain cancer (Supplementary Fig. 14a, b) and, notably, was diminished in IDH mutant proneural tumours relative to wild-type proneural tumours (Fig. 3f and Supplementary Fig. 14c). Similar results were obtained with other previously published HIF gene sets and with a manually curated data set (Supplementary Fig. 14a, d).

Downregulating HIF-1α with three independent shRNAs promoted soft agar growth by immortalized human astrocytes after approximately 15 passages (Fig. 4a, b and Supplementary Fig. 15), as did overproduction of wild-type, but not catalytic-defective, EGLN1 (Fig. 4c, d and Supplementary Fig. 16). Conversely, downregulation of EGLN1 with multiple shRNAs inhibited the proliferation of late passage IDH1 R132H cells (Fig. 4e, f and Supplementary Fig. 17) unless HIF-1α was concurrently ablated (Fig. 4g, h and Supplementary Fig. 18).

Collectively, these data suggest that EGLN activation by (*R*)-2HG, and subsequent downregulation of HIF-1α, contributes to the pathogenesis of IDH mutant gliomas. Our data do not, however, exclude the possibility that (*R*)-2HG has additional targets, including TET2 and JmjC-containing histone demethylases, which contribute to its ability to transform cells[4–6]. Indeed, we found that downregulation of TET2 in human astrocytes also promotes soft agar growth (Supplementary

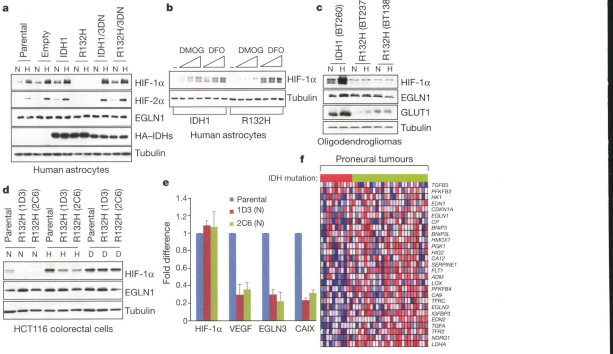


**Figure 3 | HIF activity is diminished in IDH mutant cells. a–d**, Immunoblot analysis of immortalized human astrocytes (passage 10) (**a**, **b**), oligodendroglioma cells (**c**) and HCT116 colorectal cells (**d**) expressing the indicated IDH1 variants grown under 21% (N) or 7.5% (H) oxygen for 24 h before lysis or under 21% oxygen in the presence of DFO (D). Names of cell lines are indicated in brackets. In **b**, cells grown under 21% oxygen were treated with increasing amounts of DMOG or DFO for 16 h before lysis. **e**, Quantitative real-time PCR analysis of cells in **d** under normoxic conditions. Error bars, s.d. $n = 3$. **f**, Heat map depicting expression of HIF target genes (blue, lower expression; red, higher expression) in proneural tumours clustered based on IDH status (in the horizontal bar above the matrix, red indicates mutant; green, wild type).

Fig. 19). Nonetheless, our finding that (*R*)-2HG and (*S*)-2HG are qualitatively different with respect to EGLN might explain the apparent selection for (*R*)-2HG in adult tumours, despite the fact that (*S*)-2HG is a more potent inhibitor of most of the 2-OG-dependent enzymes tested so far. It should be noted, however, that (*S*)-2HG has been linked to neurological abnormalities and brain tumours in children and young adults with germline (*S*)-2-HG dehydrogenase mutations[10–12]. The pathogenesis of (*R*)-2HG-driven tumours linked to somatic IDH mutations in adults and (*S*)-2HG-driven tumours linked to inborn errors of metabolism conceivably differ, with the latter possibly reflecting the perturbation of one or more neurodevelopmental programs during embryogenesis.

Nor are our data incompatible with the finding that HIF-1α protein levels are increased in IDH mutant tumours relative to normal brain[13]. Our data simply suggest that (*R*)-2HG quantitatively shifts the dose–response linking HIF activation to hypoxia, leading to a blunted HIF response for a given level of hypoxia. In support of this idea, HIF elevation in IDH mutant tumours is usually confined to areas of necrosis and presumed severe hypoxia[14].

Although HIF is typically viewed as an oncoprotein it can behave as a tumour suppressor in embryonic stem cells[15,16], leukaemic cells[17] and brain tumour cells[18,19]. For example, HIF-1α has been shown to score as an oncoprotein when transformed murine astrocytes are grown subcutaneously but as a tumour suppressor when such cells are grown orthotopically[19]. This finding, together with our results, raises the possibility that pharmacological inhibition of EGLN activity (and the resulting increase in HIF activity) would impair the growth of IDH1 mutant tumours. A caveat, however, is that IDH mutant tumours tend to be relatively indolent[20]. It is possible that low levels of HIF-1α, although promoting some aspects of transformation, simultaneously suppress other hallmarks of cancer required for aggressive behaviour (such as angiogenesis).

The published 2-OG Michaelis constant ($K_m$) values for the EGLN family members are below the estimated intracellular 2-OG concentration[21,22], suggesting that 2-OG should not be limiting for EGLN activity and that EGLN activity would not be enhanced further by (*R*)-2HG. A caveat is that a considerable amount of intracellular 2-OG appears to be sequestered in mitochondria and might also be bound by other 2-OG-dependent enzymes[22]. Moreover, these 2-OG $K_m$ values were determined under idealized conditions with purified enzymes and substrates in the absence of endogenous inhibitors such as reactive oxygen species, nitric oxide and 2-OG competitive molecules such as succinate and fumarate[1]. Studies in model organisms suggest that many metabolic enzymes are saturated *in vivo* with a mixture of substrate and competitive inhibitors and thus are sensitive to changes in substrate concentrations that are far above their nominal $K_m$ values[23,24]. We confirmed that succinate and fumarate increase the 2-OG requirement for the EGLN reaction and that their inhibitory activity, like that of DMOG (Fig. 3b) and its active derivative 2-oxalyl glycine, is blunted in the presence of (*R*)-2HG (Supplementary Fig. 20).

We have not yet formally proven that (*R*)-2HG is sufficient to downregulate HIF in intact cells. It is possible, for example, that additional metabolic changes in IDH mutant cells sensitize them to the HIF modulatory effects of (*R*)-2HG[25]. Another, potentially related, observation is that both downregulation of HIF and transformation by mutant IDH in immortalized human astrocytes, although highly reproducible, was only noted after multiple passages. HIF activates a number of genes, including genes that participate in feedback regulation of the HIF response and genes that modify chromatin structure[1]. It is possible that modulation of the HIF response over time, perhaps in conjunction with alterations in other enzymes affected by 2-HG, leads to epigenetic changes that ultimately are responsible for transformation. If so, it will be important to determine the degree to which such changes are reversible.

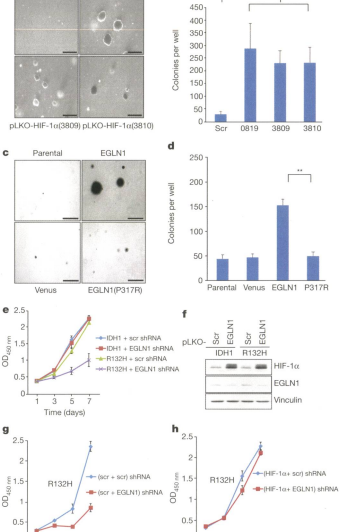


**Figure 4 | Decreased HIF activity contributes to transformation by mutant IDH. a**, **c**, Soft agar colony formation by human astrocytes after stable infection with lentiviruses encoding the indicated HIF-1α shRNAs or scrambled (scr) shRNA (**a**) or lentiviruses encoding EGLN1, EGLN1 (P317R), or venus fluorescent protein (**c**; RNAi Consortium shRNA clone identifiers are indicated in brackets). Scale bars, 0.5 mm. **b**, **d**, Number of macroscopic soft agar colonies in **a** and **c**, respectively. $^{*}P < 0.05$, $^{**}P < 0.005$. Error bars, s.d. $n = 3$. **e**, **f**, Proliferation (**e**) and immunoblot analysis (**f**) of human astrocytes expressing wild-type or R132H IDH1 and an shRNA against EGLN1 (10578) (or scrambled control). **g**, **h**, Proliferation of human astrocytes expressing IDH1 R132H and shRNAs against HIF-1α (0819), EGLN1 (10578), or both.

## METHODS SUMMARY

NHAs immortalized with E6/E7/hTERT have been described elsewhere[26] and were subsequently infected with IDH1 retroviruses. IDH1 R132H HCT116 colorectal cancer cells were made by homologous recombination as previously described[27]. Anaplastic oligodendroglioma cell lines were derived from resection material obtained at surgeries performed at the Brigham and Women's Hospital. Lentiviral shRNA vectors were from the Broad Institute. Immunoblots were performed with anti-HIF-1α monoclonal antibody (BD Transduction Laboratories), anti-HIF-2α polyclonal antibody (NB 100-122, Novus), anti-Flag monoclonal antibody (M2, Sigma-Aldrich), monoclonal anti-HA (HA-11, Covance Research Product), anti-EGLN1 monoclonal antibody (D31E11, Cell Signaling), anti-GLUT1 polyclonal antibody (NB300-666, Novus Biologicals), monoclonal anti-tubulin (B-512, Sigma-Aldrich) or anti-vinculin monoclonal antibody (V9131, Sigma-Aldrich). Metabolite levels were determined by LC–MS as previously described[7]. Enzyme activity assays were performed with affinity-purified human EGLN1, 2 and 3, collagen P4H-I and FIH, and murine Tet1 and Tet2 produced in insect cells using baculoviral vectors. (*R*)-2HG and (*S*)-2HG were from Sigma. (*R*)-2HG was free of contaminating 2-OG as determined by LC–MS under conditions that could detect 0.37 μM exogenous 2-OG in 5 mM (*R*)-2HG (data not shown). Human brain tumour mRNA expression data were obtained from The Cancer Genome Atlas and processed as described[8,28]. Cell proliferation assays were performed using XTT assays (Cell Proliferation Kit II, Roche) according to the manufacturer's instructions or by direct counting of viable cells using an automated cell counter (Invitrogen). For soft agar assays ~8,000 cells were suspended in a top layer of 0.4% soft agar (SeaPlaque Agarose, BMA products) and plated on a bottom layer of 1% soft agar containing DMEM supplemented with 10% fetal bovine serum. For real-time qPCR analysis total RNAs were first extracted with Trizol reagent (Invitrogen). cDNA synthesis and PCR amplification were performed with Superscript One-Step RT–PCR (Invitrogen).

**Full Methods** and any associated references are available in the online version of the paper at www.nature.com/nature.

**Received 26 May 2011; accepted 26 January 2012.**
**Published online 15 February 2012.**

1. Majmundar, A. J., Wong, W. J. & Simon, M. C. Hypoxia-inducible factors and the response to hypoxic stress. *Mol. Cell* **40,** 294–309 (2010).
2. Dang, L. *et al.* Cancer-associated IDH1 mutations produce 2-hydroxyglutarate. *Nature* **462,** 739–744 (2009).
3. Jin, G. *et al.* 2-Hydroxyglutarate production, but not dominant negative function, is conferred by glioma-derived NADP$^{+}$-dependent isocitrate dehydrogenase mutations. *PLoS ONE* **6,** e16812 (2011).
4. Figueroa, M. E. *et al.* Leukemic IDH1 and IDH2 mutations result in a hypermethylation phenotype, disrupt TET2 function, and impair hematopoietic differentiation. *Cancer Cell* **18,** 553–567 (2010).
5. Xu, W. *et al.* Oncometabolite 2-hydroxyglutarate is a competitive inhibitor of α-ketoglutarate-dependent dioxygenases. *Cancer Cell* **19,** 17–30 (2011).
6. Chowdhury, R. *et al.* The oncometabolite 2-hydroxyglutarate inhibits histone lysine demethylases. *EMBO Rep.* **12,** 463–469 (2011).
7. Bruning, U. *et al.* MicroRNA-155 promotes resolution of hypoxia-inducible factor-1α activity during prolonged hypoxia. *Mol. Cell. Biol.* **31,** 4087–4096 (2011).
8. Verhaak, R. G. *et al.* Integrated genomic analysis identifies clinically relevant subtypes of glioblastoma characterized by abnormalities in *PDGFRA*, *IDH1*, *EGFR*, and *NF1*. *Cancer Cell* **17,** 98–110 (2010).
9. Nickols, N. G., Jacobs, C. S., Farkas, M. E. & Dervan, P. B. Modulating hypoxia-inducible transcription by disrupting the HIF-1-DNA interface. *ACS Chem. Biol.* **2,** 561–571 (2007).
10. Aghili, M., Zahedi, F. & Rafiee, E. Hydroxyglutaric aciduria and malignant brain tumor: a case report and literature review. *J. Neurooncol.* **91,** 233–236 (2009).
11. Moroni, I. *et al.* *L*-2-hydroxyglutaric aciduria and brain malignant tumors: a predisposing condition? *Neurology* **62,** 1882–1884 (2004).
12. Ozsoy, Ö. P. A., Akalan, N., Palaoglu, S. & Topcu, M. Medulloblastoma in a child with the metabolic disease *L*-2-hydroxyglutaric aciduria. *Pediatr. Neurosurg.* **37,** 22–26 (2002).
13. Zhao, S. *et al.* Glioma-derived mutations in IDH1 dominantly inhibit IDH1 catalytic activity and induce HIF-1α. *Science* **324,** 261–265 (2009).
14. Williams, S. C. *et al.* R132H-mutation of isocitrate dehydrogenase-1 is not sufficient for HIF-1α upregulation in adult glioma. *Acta Neuropathol.* **121,** 279–281 (2011).
15. Carmeliet, P. *et al.* Role of HIF-1α in hypoxia-mediated apoptosis, cell proliferation and tumour angiogenesis. *Nature* **394,** 485–490 (1998).
16. Mack, F. A. *et al.* Loss of pVHL is sufficient to cause HIF dysregulation in primary cells but does not promote tumor growth. *Cancer Cell* **3,** 75–88 (2003).
17. Song, L. P. *et al.* Hypoxia-inducible factor-1α-induced differentiation of myeloid leukemic cells is its transcriptional activity independent. *Oncogene* **27,** 519–527 (2008).
18. Acker, T. *et al.* Genetic evidence for a tumor suppressor role of HIF-2α. *Cancer Cell* **8,** 131–141 (2005).
19. Blouw, B. *et al.* The hypoxic response of tumors is dependent on their microenvironment. *Cancer Cell* **4,** 133–146 (2003).
20. Christensen, B. C. *et al.* DNA methylation, isocitrate dehydrogenase mutation, and survival in glioma. *J. Natl. Cancer Inst.* **103,** 143–153 (2011).
21. Koivunen, P. *et al.* Inhibition of hypoxia-inducible factor (HIF) hydroxylases by citric acid cycle intermediates: possible links between cell metabolism and stabilization of HIF. *J. Biol. Chem.* **282,** 4524–4532 (2007).
22. Pritchard, J. B. Intracellular α-ketoglutarate controls the efficacy of renal organic anion transport. *J. Pharmacol. Exp. Ther.* **274,** 1278–1284 (1995).
23. Bennett, B. D. *et al.* Absolute metabolite concentrations and implied enzyme active site occupancy in *Escherichia coli*. *Nature Chem. Biol.* **5,** 593–599 (2009).
24. Yuan, J. *et al.* Metabolomics-driven quantitative analysis of ammonia assimilation in *E. coli*. *Mol. Syst. Biol.* **5,** 302 (2009).
25. Reitman, Z. J. *et al.* Profiling the effects of isocitrate dehydrogenase 1 and 2 mutations on the cellular metabolome. *Proc. Natl Acad. Sci. USA* **108,** 3270–3275 (2011).

26. Sonoda, Y. *et al.* Formation of intracranial tumors by genetically modified human astrocytes defines four pathways critical in the development of human anaplastic astrocytoma. *Cancer Res.* **61,** 4956–4960 (2001).
27. Rago, C., Vogelstein, B. & Bunz, F. Genetic knockouts and knockins in human somatic cells. *Nature Protocols* **2,** 2734–2746 (2007).
28. Wang, X. V., Verhaak, R. G., Purdom, E., Spellman, P. T. & Speed, T. P. Unifying gene expression measures from multiple platforms using factor analysis. *PLoS ONE* **6,** e17691 (2011).
29. Chowdhury, R. *et al.* Structural basis for binding of hypoxia-inducible factor to the oxygen-sensing prolyl hydroxylases. *Structure* **17,** 981–989 (2009).
30. Koski, M. K. *et al.* The active site of an algal prolyl 4-hydroxylase has a large structural plasticity. *J. Biol. Chem.* **282,** 37112–37123 (2007).

**Supplementary Information** is linked to the online version of the paper at www.nature.com/nature.

**Acknowledgements** We thank R. P. Hausinger and J. D. Rabinowitz for helpful suggestions and critical reading of the manuscript, C. Schofield and Y. Zhang for reagents, S. Chen and Y. Shi for JMJD2D assays, K. Koski for modelling and T. Aatsinki and E. Lehtimäki for technical assistance. W.G.K. is a Doris Duke Distinguished Clinical Scholar and a Howard Hughes Medical Institute (HHMI) Investigator. Supported by the National Institutes of Health (W.G.K.), HHMI (W.G.K.), Doris Duke Foundation (W.G.K.), Academy of Finland Grants 120156, 140765 and 218129 (P.K.) and S. Juselius Foundation (P.K.).

**Author Contributions** P.K., S.L. and W.G.K. initiated the project, analysed the data and wrote the manuscript. P.K. performed the *in vitro* enzyme assays. S.L. generated astrocyte cell lines stably expressing various IDH1 proteins. C.G.D., G. Lo. and H.Y. generated the HCT116 subclones. S.R., K.L.L. and S.W. provided oligodendroglioma cell lines. G. Lu generated and validated the reporter plasmids encoding HIF-1α–luciferase fusion proteins. P.J., U.B. and S.G. performed the LC–MS analysis. J.T. synthesized $^{13}$C-(9)-2HG and R.L. synthesized and purified different 2-OG and 2-HG derivatives. R.G.W.V. performed the bioinformatics. P.K. and S.L. performed all other experiments with the help of G. Lu, J. A. L. and P.J. All the authors discussed the results and commented on the manuscript.

**Author Information** Reprints and permissions information is available at www.nature.com/reprints. The authors declare competing financial interests: details accompany the full-text HTML version of the paper at www.nature.com/nature. Readers are welcome to comment on the online version of this article at www.nature.com/nature. Correspondence and requests for materials should be addressed to W.G.K. (william_kaelin@dfci.harvard.edu).

LETTER

doi:10.1038/nature10882

# Crystal structure of a concentrative nucleoside transporter from *Vibrio cholerae* at 2.4 Å

Zachary Lee Johnson[1], Cheom-Gil Cheong[1] & Seok-Yong Lee[1]

**Nucleosides are required for DNA and RNA synthesis, and the nucleoside adenosine has a function in a variety of signalling processes[1,2]. Transport of nucleosides across cell membranes provides the major source of nucleosides in many cell types and is also responsible for the termination of adenosine signalling. As a result of their hydrophilic nature, nucleosides require a specialized class of integral membrane proteins, known as nucleoside transporters (NTs), for specific transport across cell membranes. In addition to nucleosides, NTs are important determinants for the transport of nucleoside-derived drugs across cell membranes[3–5]. A wide range of nucleoside-derived drugs, including anticancer drugs (such as Ara-C and gemcitabine) and antiviral drugs (such as zidovudine and ribavirin), have been shown to depend, at least in part, on NTs for transport across cell membranes[4,6–13]. Concentrative nucleoside transporters, members of the solute carrier transporter superfamily SLC28, use an ion gradient in the active transport of both nucleosides and nucleoside-derived drugs against their chemical gradients. The structural basis for selective ion-coupled nucleoside transport by concentrative nucleoside transporters is unknown. Here we present the crystal structure of a concentrative nucleoside transporter from *Vibrio cholerae* in complex with uridine at 2.4 Å. Our functional data show that, like its human orthologues, the transporter uses a sodium-ion gradient for nucleoside transport. The structure reveals the overall architecture of this class of transporter, unravels the molecular determinants for nucleoside and sodium binding, and provides a framework for understanding the mechanism of nucleoside and nucleoside drug transport across cell membranes.**

Humans have three isoforms of concentrative nucleoside transporter (hCNT), and the substrate specificities and tissue distributions of these isoforms are different[14–16]. Knowledge of the mechanism of these transporters would help us not only to understand physiological processes associated with nucleosides but also to provide a framework for future drug design to improve nucleoside drug delivery. The major barrier to achieving a mechanistic understanding is the lack of atomic structures that reveal the origins of nucleoside specificity and the principles of function of CNTs. For structure determination and functional studies we chose a CNT homologue from *Vibrio cholerae* (vcCNT) because of its high sequence homology to hCNTs (39% identical to hCNT3; Supplementary Fig. 1) and optimal biochemical stability.

To test whether vcCNT can transport nucleosides, and if so what ion gradient vcCNT uses, we performed a radioactive nucleoside uptake assay using recombinant vcCNT-reconstituted liposomes. Studies have shown that the human CNTs use $Na^+$ ions and the *Escherichia coli* CNT uses $H^+$ for nucleoside transport[17–19]. Transport activity was measured by monitoring the uptake of [5,6-$^3$H]uridine in both the presence and the absence of a $Na^+$ gradient (Fig. 1a). We chose uridine because all of the CNTs that have been characterized so far transport uridine[4,8,17–19]. When a $Na^+$ gradient was present, vesicles containing vcCNT accumulated radioactive uridine significantly more than the control empty vesicles. When a $Na^+$ gradient was not present ($Na^+$ was replaced with choline in the solution), uridine uptake was significantly decreased.

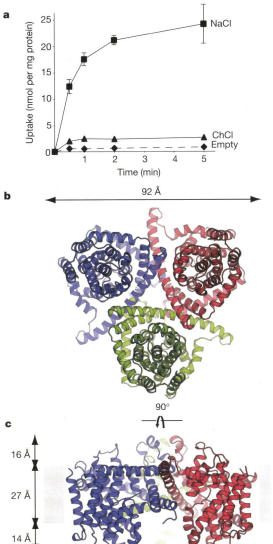


**Figure 1 | vcCNT is a $Na^+$-coupled nucleoside transporter with a trimeric architecture. a**, Time course of the uptake of 2.4 μM [5,6-$^3$H]uridine into vesicles containing vcCNT in the presence of a $Na^+$ gradient (squares, NaCl), in the absence of a $Na^+$ gradient (triangles, choline chloride), and the control empty vesicles in the presence of $Na^+$ (diamonds, empty). Results are means ± s.d. ($n = 3$). **b**, Cartoon representation of the vcCNT trimer viewed from the cytoplasm. Individual protomers are coloured blue, red and green. **c**, Cartoon representation for the vcCNT trimer viewed parallel to the membrane. The putative membrane bilayer is indicated in **c** with grey boxes. The dimensions of the putative membrane bilayer, extracellular region, and intracellular region are shown.

[1]Department of Biochemistry and Ion Channel Research Unit, Duke University Medical Center, 2 Genome Court, Durham, North Carolina 27710, USA.

Further characterization showed that uridine uptake was electrogenic and independent of pH gradients (Supplementary Fig. 2). These data clearly show that vcCNT, like human CNTs, uses a $Na^+$ gradient to transport nucleosides.

We crystallized and solved the structure of vcCNT at 2.4 Å (Supplementary Table 1). Experimental phases to 3.5 Å were obtained by single anomalous dispersion (SAD) from a platinum-soaked crystal (see Methods). The final model contains a single protomer in the asymmetric unit and is of good quality with a free *R* factor of 22.8% (Supplementary Table 1).

vcCNT crystallizes as a homotrimer that is shaped like an inverted triangular basin with its mouth facing the intracellular side and a knob-like structure facing the extracellular side (Fig. 1b, c). The three-fold axis coincides with the crystallographic six-fold axis and is perpendicular to the membrane. When viewed from the intracellular side, each side of the triangle formed by the trimer is about 92 Å, and when viewed parallel to the membrane the trimer is about 57 Å in height (Fig. 1). The membrane-embedded region lies roughly in the middle of the transporter, judging from the positions of three amphipathic helices on each protomer. On the basis of the predicted location of the membrane bilayer, the mouth of the basin penetrates into the membrane plane (Fig. 1c and Supplementary Fig. 3). The presence of several polar amino acids on the basin surface probably allows bulk aqueous solution to reach deep into the membrane bilayer and access this surface of the transporter.

The structure reveals that each protomer contains eight transmembrane helices (TM1–TM8), two re-entrant helix–turn–helix hairpins (HP1 and HP2) with opposite orientations in the membrane, and three interfacial helices (IH1–IH3) that run parallel to the membrane (Fig. 2a). The orientation of the structure relative to the membrane is consistent with previous accessibility studies[20–22] and conforms to the positive-inside rule (Supplementary Fig. 4). hCNTs are predicted to contain three more amino-terminal transmembrane helices than prokaryotic CNTs, suggesting an 11-TM topology for hCNTs[20].

Each protomer can be grouped into two subdomains on the basis of their locations (at the outer and inner regions) relative to the centre of the protomer. TM1, TM2, IH1, EH (a short stretch of extracellular helices), TM3 and TM6 are located at the outer part of the transporter, and they seem to be important for maintaining the overall architecture of the transporter. These helices in the outer region form a scaffold for the transporter (hereafter termed the scaffold domain) (Fig. 2). Trimerization contacts are mediated by part of the scaffold domain: IH1, EH, TM3 and TM6 (Fig. 2b). IH1 is an amphipathic helix 40 Å long that is most probably situated at the water/membrane interface, and TM6 is about 60 Å long and tilted almost 60° with respect to the membrane normal. EH protrudes into the extracellular solution and is about 16 Å in length. Because IH1 is involved in trimerization, is constrained to be at the membrane/water interface and interacts with many TMs (TM2–TM5), it is most probably important in building and maintaining the overall structure of vcCNT.

Surrounded by the scaffold domain, many conserved amino acids implicated in nucleoside transport are localized at the inner domain (hereafter termed the transport domain). The transport domain is composed of two structural groups that are related by an internal two-fold pseudo-symmetry. The first group is composed of IH2, HP1, TM4a/b and TM5 (pink background in Fig. 2a), and the second group is composed of IH3, HP2, TM7a/b and TM8 (cyan background in Fig. 2a). These two groups, separated by TM6 in sequence, can be superimposed with a root mean squared deviation of 3.3 Å, with the two-fold symmetry operator running though the middle of TM6 and

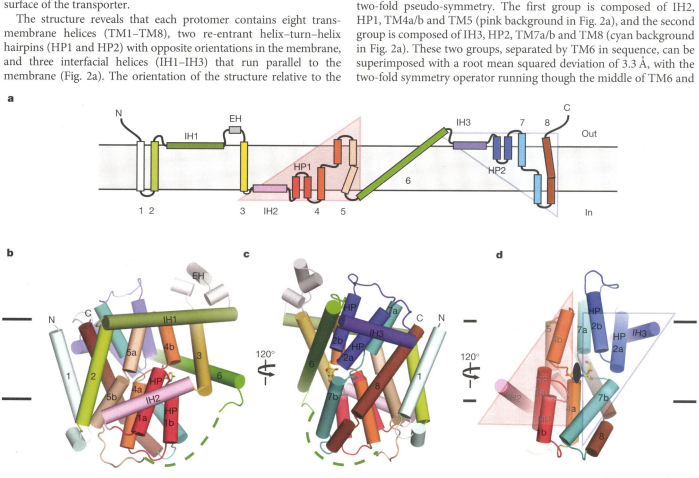


**Figure 2 | Topology and fold of the vcCNT protomer.** **a**, Schematic representation of vcCNT topology. The group of helices under the pink triangular background is related to the group of helices under the cyan triangular background by two-fold pseudo-symmetry, with the symmetry axis parallel to the membrane. **b**, Cartoon representation of the vcCNT protomer fold. Only helices comprising the scaffold domain and the group of helices under the pink triangular background are labelled. **c**, As in **b** but rotated through 120°. Only TM1, TM6 and helices comprising the group of helices under the cyan triangular background are labelled. **d**, As in **c** but rotated through 120°. The scaffold domain has been removed to show the pseudo-two-fold relationship between the two groups of helices, coloured as pink and cyan triangular backgrounds. The two-fold symmetry axis runs through the nucleoside at the centre of the transporter.

parallel to the membrane (Fig. 2d). There is no significant amino-acid sequence homology between these two groups (roughly 10% sequence identity). This two-fold symmetry relationship positions the tips of HP1, HP2 and unwound regions of TM4 and TM7 at the centre of the transport domain, which is located slightly below the middle of the membrane plane (Fig. 2d). Sequence alignment of hCNTs and vcCNT reveals high sequence conservation around HP1, HP2 and the two unwound helices (TM4 and TM7), indicating the functional importance of this region (Supplementary Fig. 1).

To the best of our knowledge, the overall fold of vcCNT is novel, although local structural elements such as helical hairpins and unwound helices have been observed previously[23,24].

The crystal structure suggests that vcCNT adopts a trimeric configuration. To test whether the stoichiometry of vcCNT is trimeric and further validate the physiological relevance of our crystal structure, we performed structure-guided disulphide bridge crosslinking experiments (Supplementary Fig. 5). Our cysteine mutants readily form disulphide-crosslinked trimers in both detergent micelles and cell membranes under oxidizing conditions; therefore our crystal structure reflects a physiologically relevant oligomerization state. Given the sequence conservation of most of the amino acids involved in trimerization, we propose that the stoichiometry of both eukaryotic and prokaryotic CNT family members is trimeric (Supplementary Fig. 1).

The structure contains three deep clefts (one per subunit) at the intracellular side facing the centre of the trimer (Fig. 3a). A simulated-annealing OMIT map clearly shows that the electron density in the cleft is that of uridine (Fig. 3b). The bound uridine in the cleft faces the intracellular basin of the transporter; however, it is not free to be released into the intracellular solution because TM6 and TM7b partly cover the binding site (Fig. 3a, b and Supplementary Fig. 6).

The nucleoside-binding site is located at the centre of the internal two-fold symmetry and lined by the tips of HP1 and HP2 and the unwound regions of TM4 and TM7 (Fig. 3b, c). Inspection of the interactions between uridine and the binding site shows that many polar or charged amino acids from HP1, HP2, TM4 and TM7 interact with the uracil base and ribose. HP1 and TM4b are responsible for interacting with the uracil base. The side chains of Gln 154, Thr 155 and Glu 156 from HP1 interact with the uracil base either directly (Gln 154) or indirectly through a water molecule (Thr 155 and Glu 156; Fig. 3c). Val 188 from TM4b interacts with the uracil base by means of van der Waals interactions. The involvement of these amino-acid residues in the interactions with the nucleoside is consistent with previous mutational studies[25–27]; the residue corresponding to Gln 154, together with that corresponding to Val 188, is important for nucleoside specificity of hCNTs; Glu 156 is critical for $Na^+$–nucleoside coupled transport.

HP2 and TM7 are responsible for the interactions with ribose. The side chains of Glu 332 (HP2), Asn 368 (TM7) and Ser 371 (TM7) interact with the ribose either directly (Glu 332, Asn 368 and Ser 371) or indirectly through a water molecule (Asn 368). Mutation of the residue corresponding to Glu 332 in hCNTs has been shown to have significant functional effects on both nucleoside binding and the rate of transport[21,26].

Because vcCNT is a $Na^+$-coupled transporter, it must contain at least one $Na^+$-binding site. Initial hints regarding the location of the $Na^+$-binding site came from an $F_o - F_c$ map that shows a strong peak

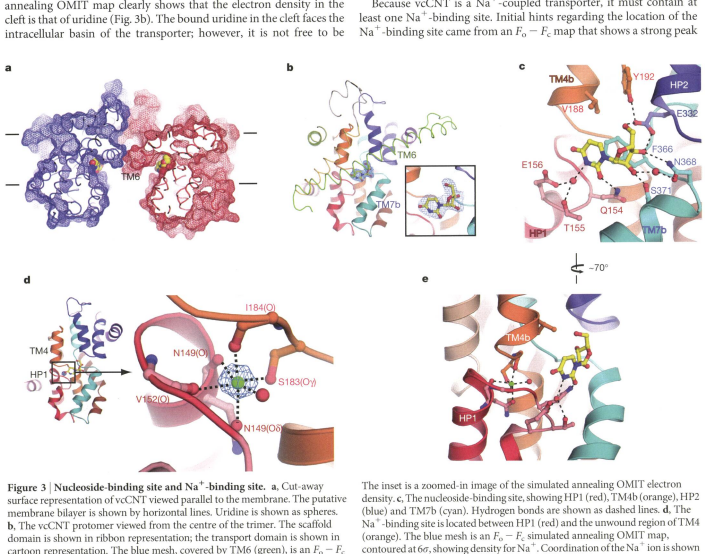


**Figure 3 | Nucleoside-binding site and $Na^+$-binding site.** **a**, Cut-away surface representation of vcCNT viewed parallel to the membrane. The putative membrane bilayer is shown by horizontal lines. Uridine is shown as spheres. **b**, The vcCNT protomer viewed from the centre of the trimer. The scaffold domain is shown in ribbon representation; the transport domain is shown in cartoon representation. The blue mesh, covered by TM6 (green), is an $F_o - F_c$ simulated annealing OMIT map, contoured at 4$\sigma$, showing density for uridine. The inset is a zoomed-in image of the simulated annealing OMIT electron density. **c**, The nucleoside-binding site, showing HP1 (red), TM4b (orange), HP2 (blue) and TM7b (cyan). Hydrogen bonds are shown as dashed lines. **d**, The $Na^+$-binding site is located between HP1 (red) and the unwound region of TM4 (orange). The blue mesh is an $F_o - F_c$ simulated annealing OMIT map, contoured at 6$\sigma$, showing density for $Na^+$. Coordination of the $Na^+$ ion is shown as dashed lines. **e**, The $Na^+$-binding site is near the nucleoside-binding site.

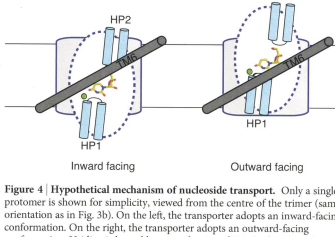


**Figure 4 | Hypothetical mechanism of nucleoside transport.** Only a single protomer is shown for simplicity, viewed from the centre of the trimer (same orientation as in Fig. 3b). On the left, the transporter adopts an inward-facing conformation. On the right, the transporter adopts an outward-facing conformation. Uridine is bound between the tips of HP1 and HP2, and TM6 (grey), serving as a hydrophobic barrier, partly covers uridine. The blue dotted lines demarcate the mobile part of the transport domain, and the grey region denotes the scaffold domain. Green circles represent sodium ions. A rigid-body motion of the nucleoside-binding site across TM6 can expose the binding site to the extracellular side.

(about 8$\sigma$) between the tip of HP1 and the unwound region of TM4. Further inspection reveals that this site is octahedrally coordinated by three backbone carbonyl groups, two side-chain hydroxyl groups and a water molecule (Fig. 3d) with the typical distances (about 2.4 Å) for $Na^+$ coordination by protein[28]. Because it is difficult to distinguish $Na^+$ from $H_2O$ on the basis of electron density alone, we performed the valence test that was used to identify the $Na^+$ sites in the crystal structure of $LeuT^{28,29}$. The result ($v = 1.02$) is consistent with $Na^+$ as the bound ion in this site. Therefore we suggest that vcCNT has at least one $Na^+$-binding site at this position between HP1 and the unwound region of TM4.

The $Na^+$-binding site is near the nucleoside-binding site, but the $Na^+$ does not interact directly with the nucleoside (Fig. 3e). What is the functional role of $Na^+$ binding at this site? Because key amino-acid residues for the interactions with the nucleoside base are localized on HP1 and TM4b, we propose that the role of $Na^+$-binding is to bring HP1 close to TM4 to complete the formation of the nucleoside-binding site.

In the field of $Na^+$-coupled secondary transporters, the prevailing model for ion-coupled transport is described by the alternating-access mechanism[30]. If we assume that the alternating-access model is used, our crystal structure probably represents an inward-facing occluded conformation (Fig. 3a and Supplementary Fig. 6). On the basis of our crystal structure, previous accessibility studies of hCNTs, and studies of the $Na^+$-coupled aspartate transporter $Glt_{Ph}$, which shares certain structural features with vcCNT (Supplementary Fig. 7), we propose a hypothetical model to explain $Na^+$-coupled nucleoside transport by vcCNT (Fig. 4). A rigid-body movement of the transport domain across TM6 while the scaffold domain is held in place could permit the transition from an inward-facing to an outward-facing conformation. Our reasoning in proposing this mechanism is provided in Supplementary Information.

The crystal structure provides an important step towards understanding the mechanism of nucleoside transport by the CNT family. However, many important issues remain to be elucidated, including the structural basis for nucleoside and nucleoside-drug specificity and the conformational changes associated with each step along the transport cycle.

## METHODS SUMMARY

vcCNT was expressed in *E. coli* C41 cells. Cells were lysed and protein was solubilized with dodecyl maltoside. Protein was purified by $Co^{2+}$-affinity chromatography followed by gel-filtration chromatography in the presence of decyl maltoside and uridine.

vcCNT was crystallized in the presence of 100 mM $CaCl_2$, 37–42% PEG400 and 100 mM Tris-HCl pH 9.0 or 100 mM glycine pH 9.5. Platinum derivatives were prepared by soaking the crystals in $K_2Pt(CNS)_6$. A partial poly-Ala model was built with phases to 5.0 Å from single isomorphous replacement with anomalous scattering (SIRAS). A complete model was built by combining phases from single anomalous dispersion using a new platinum derivative with molecular replacement phases from the partial model (MR–SAD) to 3.5 Å. Structure refinement was then performed against the 2.4-Å native data. The final model is of good quality with good Ramachandran statistics (98% favoured and 2% allowed). The model contains residues 2–416 (residues 230–240 missing), a uridine, 5 decylmaltosides (1 full and 4 partial), a $Na^+$ ion and 43 bound waters. Disordered residues Lys 226 and Glu 345 were modelled as Ala.

For the flux assay, protein was reconstituted into lipid vesicles and then vesicles were diluted into buffer containing either choline chloride or NaCl. Flux was initiated by the addition of 2.4 μM [5,6-$^3$H]uridine and 1 μM valinomycin.

**Full Methods** and any associated references are available in the online version of the paper at www.nature.com/nature.

**Received 24 August 2011; accepted 20 January 2012.**
**Published online 11 March 2012.**

1. King, A. E., Ackley, M. A., Cass, C. E., Young, J. D. & Baldwin, S. A. Nucleoside transporters: from scavengers to novel therapeutic targets. *Trends Pharmacol. Sci.* **27,** 416–425 (2006).
2. Rose, J. B. & Coe, I. R. Physiology of nucleoside transporters: back to the future. *Physiology (Bethesda)* **23,** 41–48 (2008).
3. Cano-Soldado, P. *et al.* Compensatory effects of the human nucleoside transporters on the response to nucleoside-derived drugs in breast cancer MCF7 cells. *Biochem. Pharmacol.* **75,** 639–648 (2008).
4. Damaraju, V. L. *et al.* Nucleoside anticancer drugs: the role of nucleoside transporters in resistance to cancer chemotherapy. *Oncogene* **22,** 7524–7536 (2003).
5. Jordheim, L. P. & Dumontet, C. Review of recent studies on resistance to cytotoxic deoxynucleoside analogues. *Biochim. Biophys. Acta* **1776,** 138–159 (2007).
6. Errasti-Murugarren, E. & Pastor-Anglada, M. Drug transporter pharmacogenetics in nucleoside-based therapies. *Pharmacogenomics* **11,** 809–841 (2010).
7. Mackey, J. R., Baldwin, S. A., Young, J. D. & Cass, C. E. Nucleoside transport and its significance for anticancer drug resistance. *Drug Resist. Updat.* **1,** 310–324 (1998).
8. Mackey, J. R. *et al.* Immunohistochemical variation of human equilibrative nucleoside transporter 1 protein in primary breast cancers. *Clin. Cancer Res.* **8,** 110–116 (2002).
9. Mackey, J. R. *et al.* Functional nucleoside transporters are required for gemcitabine influx and manifestation of toxicity in cancer cell lines. *Cancer Res.* **58,** 4349–4357 (1998).
10. Nagai, K., Nagasawa, K. & Fujimoto, S. Uptake of the anthracycline pirarubicin into mouse M5076 ovarian sarcoma cells via a sodium-dependent nucleoside transport system. *Cancer Chemother. Pharmacol.* **55,** 222–230 (2005).
11. Pastor-Anglada, M., Felipe, A. & Casado, F. J. Transport and mode of action of nucleoside derivatives used in chemical and antiviral therapies. *Trends Pharmacol. Sci.* **19,** 424–430 (1998).
12. Pastor-Anglada, M. *et al.* Nucleoside transporters in chronic lymphocytic leukaemia. *Leukemia* **18,** 385–393 (2004).
13. Zhang, J. *et al.* The role of nucleoside transporters in cancer chemotherapy with nucleoside drugs. *Cancer Metastasis Rev.* **26,** 85–110 (2007).
14. Gray, J. H., Owen, R. P. & Giacomini, K. M. The concentrative nucleoside transporter family, SLC28. *Pflugers Arch.* **447,** 728–734 (2004).
15. Molina-Arcas, M., Casado, F. J. & Pastor-Anglada, M. Nucleoside transporter proteins. *Curr. Vasc. Pharmacol.* **7,** 426–434 (2009).
16. Ritzel, M. W. *et al.* Molecular identification and characterization of novel human and mouse concentrative $Na^+$-nucleoside cotransporter proteins (hCNT3 and mCNT3) broadly selective for purine and pyrimidine nucleosides (system cib). *J. Biol. Chem.* **276,** 2914–2927 (2001).
17. Loewen, S. K. *et al.* Functional characterization of a $H^+$/nucleoside co-transporter (CaCNT) from *Candida albicans*, a fungal member of the concentrative nucleoside transporter (CNT) family of membrane proteins. *Yeast* **20,** 661–675 (2003).
18. Loewen, S. K. *et al.* Transport of physiological nucleosides and anti-viral and anti-neoplastic nucleoside drugs by recombinant *Escherichia coli* nucleoside-$H^+$ cotransporter (NupC) produced in *Xenopus laevis* oocytes. *Mol. Membr. Biol.* **21,** 1–10 (2004).
19. Xiao, G., Wang, J., Tangen, T. & Giacomini, K. M. A novel proton-dependent nucleoside transporter, CeCNT3, from *Caenorhabditis elegans*. *Mol. Pharmacol.* **59,** 339–348 (2001).
20. Hamilton, S. R. *et al.* Subcellular distribution and membrane topology of the mammalian concentrative $Na^+$-nucleoside cotransporter rCNT1. *J. Biol. Chem.* **276,** 27981–27988 (2001).
21. Slugoski, M. D. *et al.* Substituted cysteine accessibility method analysis of human concentrative nucleoside transporter hCNT3 reveals a novel discontinuous region of functional importance within the CNT family motif (G/A)XKX3NEFVA(Y/M/F). *J. Biol. Chem.* **284,** 17281–17292 (2009).
22. Zhang, J. *et al.* Cysteine-accessibility analysis of transmembrane domains 11–13 of human concentrative nucleoside transporter 3. *Biochem. J.* **394,** 389–398 (2006).

23. Cao, Y. *et al.* Crystal structure of a phosphorylation-coupled saccharide transporter. *Nature* **473,** 50–54 (2011).
24. Yernool, D., Boudker, O., Jin, Y. & Gouaux, E. Structure of a glutamate transporter homologue from *Pyrococcus horikoshii*. *Nature* **431,** 811–818 (2004).
25. Loewen, S. K. *et al.* Identification of amino acid residues responsible for the pyrimidine and purine nucleoside specificities of human concentrative $Na^+$ nucleoside cotransporters hCNT1 and hCNT2. *J. Biol. Chem.* **274,** 24475–24484 (1999).
26. Slugoski, M. D. *et al.* Conserved glutamate residues Glu-343 and Glu-519 provide mechanistic insights into cation/nucleoside cotransport by human concentrative nucleoside transporter hCNT3. *J. Biol. Chem.* **284,** 17266–17280 (2009).
27. Yao, S. Y. *et al.* Conserved glutamate residues are critically involved in $Na^+$/nucleoside cotransport by human concentrative nucleoside transporter 1 (hCNT1). *J. Biol. Chem.* **282,** 30607–30617 (2007).
28. Nayal, M. & Di Cera, E. Valence screening of water in protein crystals reveals potential $Na^+$ binding sites. *J. Mol. Biol.* **256,** 228–234 (1996).
29. Yamashita, A., Singh, S. K., Kawate, T., Jin, Y. & Gouaux, E. Crystal structure of a bacterial homologue of $Na^+/Cl^-$-dependent neurotransmitter transporters. *Nature* **437,** 215–223 (2005).
30. Krishnamurthy, H., Piscitelli, C. L. & Gouaux, E. Unlocking the molecular secrets of sodium-coupled transporters. *Nature* **459,** 347–355 (2009).

**Supplementary Information** is linked to the online version of the paper at www.nature.com/nature.

**Acknowledgements** Data for this study were collected at beamlines SER-CAT BM22/ID22 and NE-CAT ID 24-C at the Advanced Photon Source. We thank R. MacKinnon and J. Butterwick for critical reading; R. Lefkowitz and A. Shukla for providing access and technical support for the radioactive flux assay; S. Lockless for advice on experiments; and C. Pemble for help with remote data collection. This work was supported by start-up funds from the Duke University Medical Center, the McKnight Endowment Fund for Neuroscience, the Alfred P. Sloan Foundation, the Klingenstein Fund, the Mallinckrodt foundation, the Basil O'Connor Starter Scholar Research Award 5-FY10-473 from the March of Dimes Foundation, and the National Institutes of Health Director's New Innovator Award 1 DP2 OD008380-01 (all to S.-Y.L.).

**Author Contributions** Z.J. expressed, purified and crystallized vcCNT. Z.J. performed radioactive flux and crosslinking experiments. C.-G.C. participated in part of the vcCNT crystallization and generated mutants for crystallization and functional studies. Z.J. and S.-Y.L. collected and processed the data, solved the structure, and wrote the paper. S.-Y.L. designed the study. All authors discussed the results and commented on the manuscript.

**Author Information** Atomic coordinates and structure factors for the reported crystal structure are deposited in the Protein Data Bank under accession code 3TU. Reprints and permissions information is available at www.nature.com/reprints. The authors declare no competing financial interests. Readers are welcome to comment on the online version of this article at www.nature.com/nature. Correspondence and requests for materials should be addressed to S.-Y.L. (sylee@biochem.duke.edu).

LETTER

doi:10.1038/nature10881

# Identification and characterization of a bacterial hydrosulphide ion channel

Bryan K. Czyzewski[1,2] & Da-Neng Wang[1,3]

**The hydrosulphide ion ($HS^-$) and its undissociated form, hydrogen sulphide ($H_2S$), which are believed to have been critical to the origin of life on Earth[1], remain important in physiology and cellular signalling[2]. As a major metabolite in anaerobic bacterial growth, hydrogen sulphide is a product of both assimilatory and dissimilatory sulphate reduction[2–4]. These pathways can reduce various oxidized sulphur compounds including sulphate, sulphite and thiosulphate. The dissimilatory sulphate reduction pathway uses this molecule as the terminal electron acceptor for anaerobic respiration, in which process it produces excess amounts of $H_2S$ (ref. 4). The reduction of sulphite is a key intermediate step in all sulphate reduction pathways. In *Clostridium* and *Salmonella*, an inducible sulphite reductase is directly linked to the regeneration of $NAD^+$, which has been suggested to have a role in energy production and growth, as well as in the detoxification of sulphite[3]. Above a certain concentration threshold, both $H_2S$ and $HS^-$ inhibit cell growth by binding the metal centres of enzymes and cytochrome oxidase[5], necessitating a release mechanism for the export of this toxic metabolite from the cell[5–9]. Here we report the identification of a hydrosulphide ion channel in the pathogen *Clostridium difficile* through a combination of genetic, biochemical and functional approaches. The $HS^-$ channel is a member of the formate/nitrite transport family, in which about 50 hydrosulphide ion channels form a third subfamily alongside those for formate[10,11] (FocA) and for nitrite[12] (NirC). The hydrosulphide ion channel is permeable to formate and nitrite as well as to $HS^-$ ions. Such polyspecificity can be explained by the conserved ion selectivity filter observed in the channel's crystal structure. The channel has a low open probability and is tightly regulated, to avoid decoupling of the membrane proton gradient.**

Because $H_2S$ is a weak acid with a $pK_a$ of 6.8 and a second $pK_a$ of 19, in a biological system more than 80% of it will exist in its ionized form as $HS^-$ (refs 2, 13). To account for membrane permeation of intracellularly produced $H_2S$ (refs 6, 9), a channel for $HS^-$ or $H_2S$ has been suggested[2,7], with the water channel aquaporins as possible candidates[4]. Whereas studies in planar lipid bilayers indicate that the aquaporin from *Archaeoglobus fulgidus* is not permeable to $H_2S$ and that the lipid bilayer provides little resistance to $H_2S$ permeation[9], in the vent worm *Riftia pachyptila* it has been shown that $HS^-$ ions, but not $H_2S$, are selectively transported through its outer epithelium into its vasculature[5].

Despite the high permeability of $H_2S$ across the lipid bilayer, we argue that its weak acidity necessitates a release mechanism for its ionized form, $HS^-$ (Fig. 1a). As a weak acid with a $pK_a$ of 6.8, $H_2S$ can diffuse readily across the lipid bilayer. Therefore, the distribution of $H_2S$ and $HS^-$ on the two sides of the cell membrane is directly proportional to the pH differential as described by the Henderson–Hasselbalch equation[14]. Because cellular pH is kept at neutral levels, and extracellular pH is typically one to two units more acidic, at equilibrium the $HS^-$ concentration will be 10–100-fold greater on the inside of the cell than on the outside in the absence of a release mechanism for the $HS^-$ anions. Therefore, given its significant toxicity, it would be beneficial to directly expel this ion across the membrane by the quickest mechanism available: an ion channel.

Recently, a novel family of anion channels for short-chain acids has been functionally characterized[11,15,16]. Members of the formate/nitrite transport (FNT) family transport various anions during anaerobic bacterial growth[10,12,17]. Judging from sequence homology, however, only about half of its 2,000 identified members clearly belong to either the FocA or the NirC subfamily (Figs 1b, c and Supplementary Figs 1 and 2). Notably, for both FocA and NirC, each channel gene is genetically linked to its reductase partner: *focA* to the formate reductase *pflB*[10] and *nirC* to the nitrate reductase *nirBD*[12] (Fig. 1b). Our phylogenetic analysis of bacterial genes suggests the existence of additional

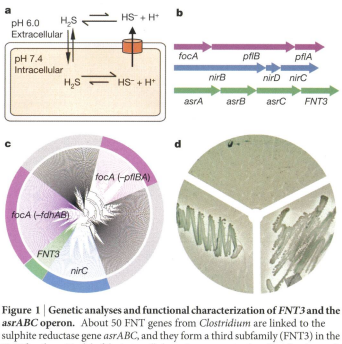


**Figure 1 | Genetic analyses and functional characterization of *FNT3* and the *asrABC* operon.** About 50 FNT genes from *Clostridium* are linked to the sulphite reductase gene *asrABC*, and they form a third subfamily (FNT3) in the FNT family. **a**, Model of the intracellular anion concentrative effect for the weak acid $H_2S$. **b**, Genomic organization of three types of FNT gene and their metabolically related reductase genes. Representatives are shown for *focA*, *nirC* and *FNT3* with their respective linked operons. **c**, Phylogenetic tree of 474 bacterial and archaeal members of the FNT family. Branches are coloured on the basis of genetic linkage to metabolic enzymes: genes linked to pyruvate formate lyase (*pflBA*) or formate dehydrogenase (*fdhABγ fdhA* and *fdhB* also known as *selA* and *selD*, respectively) are coloured pink, genes linked to nitrite reductase (*nirBD*) are coloured blue and genes linked to sulphite reductase (*asrABC*) are coloured green. The FocA protein in archaea is encoded by *fdhC* (*selC*). The grey areas represent FNT family members with no assigned function based on genetic linkage. **d**, Bismuth sulphite agar plate assay: vector control (top); *asrA*, *asrB* and *asrC* (left); *asrA*, *asrB*, *asrC* and *FNT3* (right).

[1]The Helen L. and Martin S. Kimmel Center for Biology and Medicine at the Skirball Institute of Biomolecular Medicine, New York University School of Medicine, 540 First Avenue, New York, New York 10016, USA. [2]Molecular Biophysics Graduate Program, New York University School of Medicine, 540 First Avenue, New York, New York 10016, USA. [3]Department of Cell Biology, New York University School of Medicine, 540 First Avenue, New York, New York 10016, USA.

channel subfamilies in the FNT family (Fig. 1c and Supplementary Fig. 1). One such subfamily is a group of ~50 homologous genes, temporarily termed FNT3, found in various species of *Clostridium* that are major human pathogens grown under strictly anaerobic conditions. As it is linked to a reductase gene, the *asrABC* operon[18] (Fig. 1b), we proposed that FNT3 genes might encode a channel for $HS^-$ or related ions. AsrABC reduces sulphite ($SO_3^{-2}$) to sulphide ($S^{-2}$), which is rapidly converted into $H_2S$ and $HS^-$ under physiological conditions.

*Salmonella asrABC* is the only such operon that has been characterized thus far. Its overexpression in *Escherichia coli*, which lacks this biochemical pathway, was previously shown to reduce $SO_3^{-2}$ to $H_2S$ (ref. 19). To verify first whether the homologous *asrABC* operon from *C. difficile* also encodes an $SO_3^{-2}$ reductase, we tested the growth of *E. coli* transformed with the *C. difficile asrABC* genes, plated on bismuth sulphite agar[19,20]. When *C. difficile asrABC* was induced, *E. coli* was able to overcome the expected growth inhibition by reducing $SO_3^{-2}$ to $H_2S$ (Fig. 1d and Supplementary Fig. 3). Darkening along the edges of the colonies, formed by the precipitation of bismuth and iron sulphide, further indicated that $H_2S$ gas was being produced. This showed that the *asrABC* genes from *C. difficile* do indeed encode for an $SO_3^{-2}$ reductase, which in turn supports the notion that the FNT3 gene (*'FNT3'*) in the *asrABC* operon may encode a channel for $SO_3^{-2}$ or for its reduced product, $HS^-$.

To determine whether the FNT3 protein from *C. difficile* functions as a channel for $HS^-$ or $SO_3^{-2}$, we then carried out whole-cell transport, ion–protein binding in solution and transport-inhibition assays in reconstituted proteoliposomes. First we transformed sulphide-producing *Salmonella typhimurium*, which lacks an $HS^-$ channel, with the *C. difficile FNT3*. In $SO_3^{-2}$-supplemented minimal medium, the *FNT3*-expressing *S. typhimurium* released a high concentration of $HS^-$ ions into the culture medium (Fig. 2a and Supplementary Fig. 4). This increase in extracellular $HS^-$ was specific to $HS^-$ produced by the endogenous cytoplasmic AsrABC; when the other sulphide-producing reductase in the cell, the periplasmic thiosulphate reductase, was engaged with its substrate thiosulphate, little effect on the extracellular concentration of $HS^-$ was observed. This indicates that the measured $HS^-$ was generated by $SO_3^{-2}$ reduction by the cytoplasmic AsrABC and then exported. Such an FNT3-linked increase in $HS^-$ production in *S. typhimurium* can be attributed to either increased import of $SO_3^{-2}$ or increased export of $HS^-$ from the cell. It follows that an FNT3 protein could be an ion channel for $SO_3^{-2}$ or $HS^-$.

An ion channel protein is often stabilized by its permeating ions through their direct interaction with its selectivity filter[21]. Therefore, we tested whether purified FNT3 protein interacts with the monovalent $HS^-$ or the divalent $SO_3^{-2}$. Using size-exclusion chromatography of purified protein samples incubated at different temperatures, we found that at pH 8.0 the presence of $HS^-$ ions was able to increase the nominal melting temperature of the FNT3 protein by 8 °C, whereas $SO_3^{-2}$ had little effect (Fig. 2b and Supplementary Table 1). This result is consistent with the hypothesis that FNT3 protein functions as an $HS^-$ channel but is probably impermeable to $SO_3^{-2}$. Notably, three other monovalent anions, formate, nitrite and chloride, also increased the melting temperature of the FNT3 protein, but to a lesser degree (3–4 °C).

We went on to identify the permeable ions of the FNT3 protein *in vitro*. As channels in the FNT family are expected to have low conductance rates[11], we measured the transport activity of FNT3 protein using a concentrative uptake assay[11,22]. Given that $HS^-$ ions at concentrations needed to set up a sufficient electrochemical gradient (~150 mM) are severely disruptive to the membrane, we chose to measure the permeability of FNT3 protein using another interacting ion, formate (Fig. 2b). Proteoliposomes reconstituted at pH 8.0 from purified *C. difficile* FNT3 protein were found to be permeable to formate, although at a lower rate than FocA from *Vibrio cholerae* (Fig. 2c). This permeability to formate by FNT3 protein allowed us to search for other ions that directly compete with formate for transport. Indeed, when $HS^-$ or nitrite was present in the buffer outside the proteoliposomes,

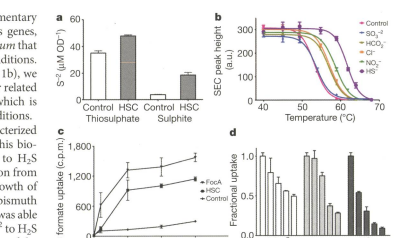


**Figure 2 | Binding and transport activity of HSC in reconstituted proteoliposomes. a**, Measurements of sulphide concentrations in the media of *Salmonella* transformed with vector control or vector encoding HSC. Minimal media were supplemented with either sulphite or thiosulphate to induce the production of hydrogen sulphide from either periplasmic thiosulphate reductase or cytoplasmic sulphite reductase. OD, optical density. **b**, Binding of detergent-solubilized and purified HSC to various anions was determined by using thermostability coupled size-exclusion chromatography. Peak heights of recovered samples are plotted against temperature and fitted to a Boltzmann sigmoidal model to determine nominal melting temperatures. **c**, Radiolabelled formate uptake in proteoliposomes reconstituted with purified HSC at pH 8.0 was monitored in a concentrative uptake assay and compared with FocA activity or vesicle controls. c.p.m., counts per minute. **d**, Inhibition of radiolabelled concentrative uptake of formate by the addition of various anions at increasing concentrations. The graph shows the amount of radiolabelled formate measured at the 10-min time point for each concentration of anion tested. The concentrations of the competing anions were 0, 0.15, 0.6, 3 and 15 mM (left to right). Error bars, s.e.m. ($N = 3$).

the uptake of formate was drastically inhibited (Fig. 2d). In the physiological sulphide concentration range (1–2 mM), ~70% inhibition was observed, whereas at the highest concentration tested (15 mM), $HS^-$ and nitrite inhibited the uptake of formate by 90% and 70%, respectively.

Such direct competitive inhibition (Fig. 2c), coupled with whole-cell transport assays (Fig. 2a) and *in vitro* binding assays (Fig. 2b), collectively indicates that the FNT3 protein from *C. difficile* is likely to be a channel for the hydrosulphide ion, $HS^-$. Although the channel is also permeable to formate and nitrite ions, the FNT3 gene is directly linked to the *asrABC* sulphite reductase operon (Fig. 1b); we have therefore tentatively named the FNT3 protein a hydrosulphide ion channel (HSC). A definite understanding of the physiological role of these channels will need to be confirmed by *in vivo* experiments such as genetic deletion studies.

To understand the transport mechanism of the HSC protein from *C. difficile* (Supplementary Fig. 5), we determined its crystal structure at high pH (pH 9.0) to a resolution of 2.2 Å (Fig. 3a and Supplementary Table 2). The HSC adopts the aquaporin/FocA fold[11,23] and forms a pentamer like FocA, with the five protomers having the same structure (Supplementary Figs 6–8). The two-fold inverted symmetry between the two halves of the protein is greater than that observed in FocA and extends to the pore-lining transmembrane helices TM2b and TM5b (Supplementary Fig. 8b), two salt-bridge triads on the periplasmic and the cytoplasmic sides (Lys 148-Glu 200-Asn 205 and Lys 16-Glu 81-Asn 86) (Fig. 4a–c), and the two short helices parallel to the membrane (helix P on the periplasmic surface and helix N at the amino terminus on the cytoplasmic surface) (Supplementary Fig. 8b). This helix N, by means of the Lys 16-Glu 81-Asn 86 salt-bridge triad, buttresses TM2b and TM5a, making the cytoplasmic side of the protein more closed and rigid than that in FocA[11].

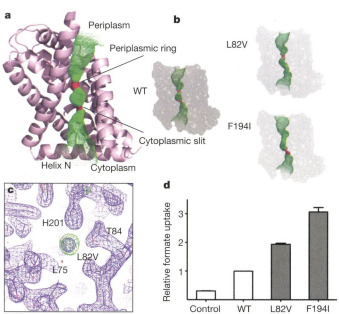


**Figure 3 | Structural and functional characterization of the ion permeation pathway. a**, Structure of a protomer of HSC overlaid with the pore diameter calculations made using HOLE, coloured to indicate permeability to water: green, permeable; red, impermeable. Transmembrane helix 2 has been removed for clarity. **b**, Pore diameter calculations from HOLE of the crystal structures for each of the two permeation pathway mutations, Leu 82 Val and Phe 194 Ile and wild type (WT). **c**, Close-up of the electron density observed at the selectivity filter for the Leu 82 Val mutant. The $2F_o - F_c$ electron density map contoured at $1.1\sigma$ is coloured purple and the $F_o - F_c$ difference density map contoured at $3\sigma$ is coloured green. **d**, Relative uptake of proteoliposomes reconstituted with purified HSC and pathway mutations. The graph shows the 10-min time point of each concentrative uptake experiment. Error bars, s.e.m. ($N = 3$).

The pore for ion permeation, which is located at the centre of each protomer, contains the selectivity filter formed by a cytoplasmic slit and a periplasmic ring in the middle of the membrane (Fig. 3a, b). The radius of the cytoplasmic slit is 0.8 Å, which is too small for an $HS^-$ ion (radius, 1.7 Å; ref. 24) to pass through (Supplementary Figs 9–11).

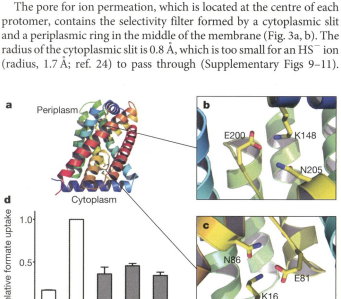


**Figure 4 | Structural and functional characterization of possible gating mechanisms. a**, Structure of the HSC protomer representing possible gating regions. The structure is coloured to show the two-fold inverted topology. **b**, **c**, The Glu-Lys-Asn salt-bridge triads, related by a pseudo-two-fold symmetry, help to stabilize helix P at the periplasmic side (**b**) and helix N at the cytoplasmic side (**c**) of the protein. The rotamer that each residue adopts is conserved. **d**, Relative uptake of proteoliposomes reconstituted with purified HSC and gating mutations. The graph shows the 10-min time point of each concentrative uptake experiment. Error bars, s.e.m. ($N = 3$).

Therefore, the HSC protein in the crystal structure is probably in a closed state. As expected from the sequence similarity between HSC and FocA in the selectivity filter (Supplementary Fig. 2), the positions or orientations of key residues changed only slightly in HSC (Supplementary Fig. 10). Such conservation explains the permeability of HSC to $HS^-$, as well as to formate and nitrite. When a residue at the cytoplasmic slit or the periplasmic ring is mutated into a smaller residue, for example Leu 82 to Val or Phe 194 to Ile, the pore size is increased, as shown in the crystal structures of the mutant protein (Fig. 3b and Supplementary Table 2), and the formate transport rate of the channel is significantly increased (Fig. 3d). We note that in the crystal structure of the Leu 82 Val mutant, electron density was observed in the cytoplasmic slit (Fig. 3c). This density, which is greater than that of a water molecule—as inferred from a B-factor fourfold lower than those of the surrounding atoms—could be accounted for by a $Cl^-$ or an $HS^-$ ion. Owing to their similar sizes and chemical properties, it has been previously observed that $Cl^-$ and $HS^-$ ions often bind to the same site in protein crystal structures[25].

The observed polyspecificity of HSC is typical for anion channels[26–28], and is most probably shared by the FocA and NirC channels as well. Such polyspecific anion recognition is at least partly due to the diffuse nature of the electron cloud of anions[29]. By contrast, cation channels often show a high degree of selectivity, which is made possible by the point-like charge properties of such ions. Because different FNT channels in this ancient protein family are coupled with their specific metabolic pathways, each channel is expected to have its own preference for permeating ions, and that preference is probably due to the small structural variations in the selectivity filter that we observed here (Supplementary Fig. 10).

The expulsion of toxic concentrations of $HS^-$ from the cytoplasm through HSC needs to be balanced against the potential risk of the uncoupling of the membrane proton gradient. Freely diffusible $H_2S$ and other weak, short-chain acids will dissociate into an anion and a proton in the cytoplasm (Fig. 1a). As the anion is expelled, there will be an intracellular net accumulation of protons. Therefore, the ground state of HSC is likely to be closed and its opening tightly regulated.

Indeed, the HSC structure we determined at high pH is in its closed state (Fig. 3 and Supplementary Figs 9–11). We then considered how easily the channel could be opened. Because the homologous FocA channel can be gated by an appropriate change in pH or cytoplasmic formate concentration[11,16], we first investigated possible pH-dependent structural changes of HSC by determining its crystal structure at pH 7.5 (resolution, 3.2 Å) and at pH 4.5 (3.0 Å) (Supplementary Table 2). The protein structures obtained at these neutral and low pH values were the same as the structure at 2.2 Å and pH 9.0 (Supplementary Fig. 12), and the channel remained closed. We then studied the two salt-bridge triads, both of which contain a glutamate residue that could potentially function as a pH sensor (Fig. 4a–c). When either of the salt bridges was broken, by mutating Lys 16 to Ser or Lys 148 to Glu, the HSC crystal structure did not change and the channel still remained closed (Supplementary Fig. 13 and Supplementary Table 2). Consistent with these structural results, the transport rates of these mutants did not increase (Fig. 4d).

To determine whether HSC is gated by anion concentration in a similar manner to *V. cholerae* FocA[11], in which the competition of formate with Thr 90 from the Ω-loop for hydrogen bonding to His 208 in the selectivity filter opens the channel, we mutated the equivalent threonine in HSC, Thr 84, to an Ala and determined its crystal structure at 2.4 Å (Supplementary Table 2). This mutant structure did not differ from the closed wild-type channel, and no increase in transport was detected (Fig. 4d and Supplementary Fig. 14). Because Thr 84, Lys 16 and Lys 148 all line the ion permeation pathway, mutation of these residues slightly reduced the ion permeation rate of the channel. Therefore, we conclude that the opening of HSC is indeed tightly regulated and the channel has a much lower open probability than FocA[11,16].

The low open probability of HSC observed here is consistent with its physiological role in the cell. The opening of HSC probably requires significant movement of TM2b. As TM2b is 'held' in space by the cytoplasmic helix N (Fig. 4a), the movement of the latter, for example by direct interaction with a cytoplasmic enzyme in the same metabolic pathway, can trigger the opening of the channel. We have no evidence for such a hypothesis, and it can be validated only by further experimentation, which we expect would reveal greater variations in both the gating mechanism and the anionic preference of FNT channels.

## METHODS SUMMARY

**Bismuth sulphite agar plate assay.** *FNT3* was isolated from *C. difficile* strain 630. *Escherichia coli* BL21(DE3) transformed with vector pCDFduet-1-asrA-asrB, pACYCduet-1-asrC, or pACYCduet-1-asrC-FNT3 were plated on bismuth sulphite agar[20] and allowed to develop for 48 h.

**Whole-cell *in vivo* transport.** *Salmonella typhimurium* transformed with pBAD-FNT3 were assayed for their ability to generate sulphide from either thiosulphate or sulphite using a silver–sulphide probe following modification of a previously published protocol[19].

**Proteoliposome reconstitution and *in vitro* transport assay.** Proteoliposomes were formed from *E. coli* total lipids and $Ni^{+2}$-NTA-purified proteins and assayed by a method modified from a previously published concentrative uptake assay[11,22].

**Protein–ion interaction assay.** Ion-induced thermostability of HSC was monitored using analytical size-exclusion chromatography. Purified protein was incubated at increasing temperatures and its recovery was monitored by size-exclusion chromatography using a high-performance liquid chromatograph. Candidate permeating ions were incubated at a concentration of 20 mM and protein was monitored for thermostabilization.

**Protein purification and crystallization and structure determination.** HSC was expressed as a carboxy-terminal FLAG–10×His fusion in *E. coli* BL21. The protein was purified using $Ni^{+2}$-NTA affinity chromatography, followed by size-exclusion chromatography. The protein was crystallized by hanging-drop vapour diffusion and the crystal structure was solved by molecular replacement.

**Full Methods** and any associated references are available in the online version of the paper at www.nature.com/nature.

**Received 2 August 2011; accepted 20 January 2012.**
**Published online 11 March 2012.**

1. Wächtershäuser, G. Groundworks for an evolutionary biochemistry: the iron-sulphur world. *Prog. Biophys. Mol. Biol.* **58,** 85–201 (1992).
2. Kabil, O. & Banerjee, R. Redox biochemistry of hydrogen sulfide. *J. Biol. Chem.* **285,** 21903–21907 (2010).
3. Dhillon, A., Goswami, S., Riley, M., Teske, A. & Sogin, M. Domain evolution and functional diversification of sulfite reductases. *Astrobiology* **5,** 18–29 (2005).
4. Rabus, R., Hansen, T. & Widdel, F. in *The Prokaryotes: Ecophysiology and Biochemistry* Vol. 2 (eds Dworkin, M. *et al.*) 659–768 (Springer, 2006).
5. Goffredi, S. K., Childress, J. J., Desaulniers, N. T. & Lallier, F. J. Sulfide acquisition by the vent worm *Riftia pachyptila* appears to be via uptake of $HS^-$, rather than $H_2S$. *J. Exp. Biol.* **200,** 2609–2616 (1997).
6. Jacques, A. G. The kinetics of penetration: XII. Hydrogen sulfide. *J. Gen. Physiol.* **19,** 397–418 (1936).
7. Freytag, J. K. *et al.* A paradox resolved: sulfide acquisition by roots of seep tubeworms sustains net chemoautotrophy. *Proc. Natl Acad. Sci. USA* **98,** 13408–13413 (2001).
8. Lee, J. K. *et al.* Structural basis for conductance by the archaeal aquaporin AqpM at 1.68 Å. *Proc. Natl Acad. Sci. USA* **102,** 18932–18937 (2005).
9. Mathai, J. C. *et al.* No facilitator required for membrane transport of hydrogen sulfide. *Proc. Natl Acad. Sci. USA* **106,** 16633–16638 (2009).
10. Suppmann, B. & Sawers, G. Isolation and characterization of hypophosphite–resistant mutants of *Escherichia coli*: identification of the FocA protein, encoded by the pfl operon, as a putative formate transporter. *Mol. Microbiol.* **11,** 965–982 (1994).
11. Waight, A. B., Love, J. & Wang, D. N. Structure and mechanism of a pentameric formate channel. *Nature Struct. Mol. Biol.* **17,** 31–37 (2010).
12. Jia, W., Tovell, N., Clegg, S., Trimmer, M. & Cole, J. A single channel for nitrate uptake, nitrite export and nitrite uptake by *Escherichia coli* NarU and a role for NirC in nitrite export and uptake. *Biochem. J.* **417,** 297–304 (2009).
13. Hughes, M. N., Centelles, M. N. & Moore, K. P. Making and working with hydrogen sulfide: the chemistry and generation of hydrogen sulfide *in vitro* and its measurement *in vivo*: a review. *Free Radic. Biol. Med.* **47,** 1346–1353 (2009).
14. Hirshfield, I. N., Terzulli, S. & O'Byrne, C. Weak organic acids: a panoply of effects on bacteria. *Sci. Prog.* **86,** 245–269 (2003).
15. Wang, Y. *et al.* Structure of the formate transporter FocA reveals a pentameric aquaporin-like channel. *Nature* **462,** 467–472 (2009).
16. Lu, W. *et al.* pH-dependent gating in a FocA formate channel. *Science* **332,** 352–354 (2011).
17. Das, P., Lahiri, A. & Chakravortty, D. Novel role of the nitrite transporter NirC in *Salmonella* pathogenesis: SPI2-dependent suppression of inducible nitric oxide synthase in activated macrophages. *Microbiology* **155,** 2476–2489 (2009).
18. Crane, B. R. & Getzoff, E. D. The relationship between structure and function for the sulfite reductases. *Curr. Opin. Struct. Biol.* **6,** 744–756 (1996).
19. Hallenbeck, P. C., Clark, M. A. & Barrett, E. L. Characterization of anaerobic sulfite reduction by *Salmonella typhimurium* and purification of the anaerobically induced sulfite reductase. *J. Bacteriol.* **171,** 3008–3015 (1989).
20. Wilson, W. J. & Blair, E. M. M.'v. A combination of bismuth and sodium sulphite affording an enrichment and selective medium for the typhoid-paratyphoid groups of bacteria. *J. Pathol. Bacteriol.* **29,** 310–311 (1926).
21. Doyle, D. A. *et al.* The structure of the potassium channel: molecular basis of $K^+$ conduction and selectivity. *Science* **280,** 69–77 (1998).
22. Middleton, R. E., Pheasant, D. J. & Miller, C. Purification, reconstitution, and subunit composition of a voltage-gated chloride channel from *Torpedo* electroplax. *Biochemistry* **33,** 13189–13198 (1994).
23. Savage, D. F., O'Connell, J. D. III, Miercke, L. J., Finer-Moore, J. & Stroud, R. M. Structural context shapes the aquaporin selectivity filter. *Proc. Natl Acad. Sci. USA* **107,** 17164–17169 (2010).
24. Feth, S., Gibbs, G. V., Boisen, M. B., Jr & Myers, R. H. Promolecule radii for nitrides, oxides, and sulfides. A comparison with effective ionic and crystal radii. *J. Phys. Chem.* **97,** 11445–11450 (1993).
25. Tai, C. H. *et al.* Characterization of the allosteric anion-binding site of O-acetylserine sulfhydrylase. *Biochemistry* **40,** 7446–7452 (2001).
26. Hille, B. *Ionic Channels of Excitable Membranes* 362–389 (Sinauer, 1992).
27. Yasui, M. *et al.* Rapid gating and anion permeability of an intracellular aquaporin. *Nature* **402,** 184–187 (1999).
28. Rychkov, G. Y., Pusch, M., Roberts, M. L., Jentsch, T. J. & Bretag, A. H. Permeation and block of the skeletal muscle chloride channel, ClC-1, by foreign anions. *J. Gen. Physiol.* **111,** 653–665 (1998).
29. Simons, J. & Jordan, K. D. Ab initio electronic structure of anions. *Chem. Rev.* **87,** 535–555 (1987).

**Supplementary Information** is linked to the online version of the paper at www.nature.com/nature.

**Acknowledgements** We are grateful the staff at beamlines X25 and X29 of the National Synchrotron Light Source at Brookhaven National Laboratory and at beamline 23ID of the Advanced Photon Source at Argonne National Laboratory for assistance in X-ray diffraction experiments. We thank A. B. Waight for suggesting the project; J. J. Marden for assistance with cloning of mutants; T. Neubert and S. Blais for mass spectrometry measurements; the 2010 CCP4 Workshop for assistance in processing diffraction data; and A. David, H. Jackson, N. K. Karpowich, J. J. Marden, R. L. Mancusso, Y. Pan and M. Zhou for discussions. This work was financially supported by the NIH (R01-GM093825, R01-DK073973, R01-MH083840 and U54-GM075026). B.K.C. was partly supported by an NIH Supplement Grant to Promote Diversity in Health-Related Research (R01-DK053973-08A1S1) and an NIH pre-doctoral fellowship (F31-AI086072).

**Author Contributions** B.K.C. did the experiments. B.K.C. and D.-N.W. wrote the manuscript.

**Author Information** The atomic coordinates and structure factors of HSC for high, medium and low pH have been deposited in the Protein Data Bank under accession codes 3TDO, 3TDR and 3TDP, respectively, and those of the Lys 16 Ser, Leu 82 Val, Thr 84 Ala, Lys 148 Glu and Phe 194 Ile mutants have been deposited under the codes 3TE2, 3TDX, 3TE1, 3TE0 and 3TDS, respectively. Reprints and permissions information is available at www.nature.com/reprints. The authors declare no competing financial interests. Readers are welcome to comment on the online version of this article at www.nature.com/nature. Correspondence and requests for materials should be addressed to D.N.W. (wang@saturn.med.nyu.edu).

CORRIGENDUM
doi:10.1038/nature10976

# Corrigendum: Functional complementation between FADD and RIP1 in embryos and lymphocytes

Haibing Zhang, Xiaohui Zhou, Thomas McQuade, Jinghe Li, Francis Ka-Ming Chan & Jianke Zhang

*Nature* **471,** 373–376 (2011)

In Fig. 3b of this Letter, the plot for the NP205 epitope response in the *Fadd*$^{-/-}$*Rip1*$^{-/-}$ double-knockout (DKO) splenocytes was a duplicate of that for the NP38 epitope response. The correct figure panel is shown below. The panel has been corrected in the HTML and PDF versions online.

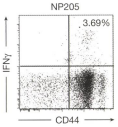


**Figure 1 | This is the correct panel from Fig. 3b of the original Letter.**

# CAREERS

**TURNING POINT** Climate scientist devises mission statement for her lab **p.501**

**ACADEMIA** Private and public US faculty receive higher pay rise this year **p.501**

**NATUREJOBS** For the latest career listings and advice **www.nature.com/naturejobs**

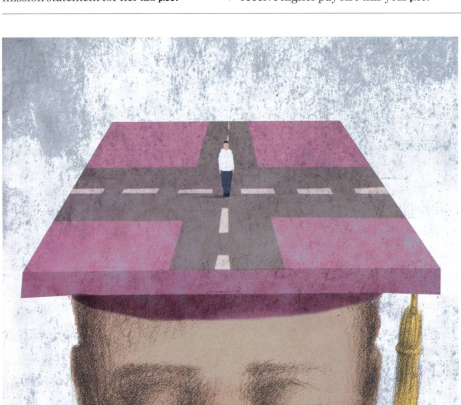

IMAGES.COM/CORBIS

RESEARCH

# Postdoc or not?

*Life-sciences graduates interested in academic research typically need to do at least one postdoc. For physics students, there are multiple caveats to consider.*

**BY KAREN KAPLAN**

Björn Flatt had always assumed that he would become an academic physicist. After earning his PhD in particle physics from Johannes Gutenberg University Mainz in Germersheim, Germany, he was happy to land a postdoctoral fellowship at Stanford University in Palo Alto, California.

But things deteriorated rapidly. The two-year fellowship was extended by a further two years so that Flatt could complete time-intensive experiments, but the delay hampered his efforts to break into the permanent-job market. By the time he started looking for an academic position in 2009, the effect of the recession was already widespread. He received no interview offers.

Flatt came to realize that he did not want to pursue an academic career after all, and set his sights on industry. However, he could not find a permanent research post, and ended up starting another postdoc, this time in mass spectrometry and instrumentation physics at Agilent Technologies in Santa Clara, California, which was at least a way to get his foot in the door. "It wasn't exactly my field, but my theses had been on instrumentation development," Flatt says. "It was actually a pretty good match." Last March, several months before the postdoc was due to end, Flatt heard about an opening in the company for a senior research and development scientist, a permanent position. Flatt applied for it and got the job.

Today, after a year in his new post, Flatt says that his two postdocs offered little value other than confirming that he did, in fact, want to pursue industrial research. They were neither crucial for building his research portfolio nor obligatory for landing his permanent position at Agilent.

Science postgraduates, especially those in the biological sciences, often see postdocs as a way to continue and refine their research, learn to run a laboratory and develop a broad, deep collaborative network. Flatt is one of many early-career physicists in the United States who dismiss that idea. Although researchers in the biological sciences may have to take multiple postdocs before landing their first permanent post, the landscape is shifting for physicists. Nearly 70% of physicists who earned their degree in 2004 took a postdoc, but the proportion had fallen to 56% in the classes of 2007 and 2008, according to the Statistical Research Center of American Institute of Physics (AIP) in College Park, Maryland.

One reason for the decline is that fewer people with physics PhDs are pursuing an academic research career. This is in part because there are, and have been, fewer positions to pick from. Academic hiring has been flat since 2003, says Crystal Bailey, the education and careers programme manager for the American Physical Society (APS), also in College Park. Between 2006 and 2007, about 350 faculty members left their job in physics, but in 2008, about 450 people with physics PhDs were seeking positions. Of those with physics PhDs in the United States from the classes of 2007 and 2008 who did not take a postdoc directly after earning their degree, 62% accepted private-sector positions, according to the AIP Statistical Research Center. Another 10% accepted government positions, such ▶

as at one of the US Department of Energy's 21 labs and technology centres. About one-quarter accepted academic posts.

Few private-sector or industry positions require an applicant to have completed a post-doc — even if those posts involve research. Bailey says that she rarely advises physics graduate students to pursue a postdoc, unless they are certain they want a career in academia or they need a job while they consider their options. Physics postgraduates are, she says, far more likely to get full-time permanent employment in the private sector, for which a postdoc is largely irrelevant.

About 12 industrial employers in the United States are currently advertising jobs for people with physics PhDs on a members-only section of the APS website, but none of them lists a postdoc as a prerequisite.

The applied-research nature of physics-related professions often makes a stint in academia less than useful. "A lot of physicists are just as comfortable doing engineering as engineers are," says James Duderstadt, president emeritus at the University of Michigan in Ann Arbor. "If they go to work for IBM, they're going to be doing applied research. If they work at the Large Hadron Collider, they're going to be doing applied physics," says Duderstadt, who was also a member of a National Academies panel that, in 2000, analysed the US postdoctoral experience. "Overall, it is not necessary, unless they have some experimental thing they need to learn in someone's lab that they can't learn in a PhD."

A postdoc could even be a drawback for physicists considering the private sector. Many of Europe's industrial employers prefer to hire applicants who have a PhD and a 'clean slate', says Maria Allegrini, a physicist at University of Pisa in Italy and a member of the APS Committee on International Scientific Affairs. "They want to train you in their own field," she says.

Physicists with experience in US industry warn that a CV with three or more academic postdocs can create the impression that the applicant had hoped for a career in academia and does not really want one in industry. "We want to find someone who's charged up with enthusiasm to work for our company," says Jim Hollenhorst, Agilent's senior director of technology, who regularly hires physics postgraduates. "So don't do three postdocs, not find an academic job, and then apply here."

*"The applied-research nature of physics-related professions often makes postdocs less than useful."*

Having multiple industrial postdocs could also be detrimental in some cases. If a researcher completes a two- or three-year postdoc at a company — requiring a significant training commitment from a senior researcher — and then leaves to do the same thing somewhere else, he or she may be viewed negatively by subsequent industrial hiring committees. But the outlook is also employer- and location-dependent, notes Dipali Bhatt-Chauhan, international-relations manager at the Institute of Physics in London. British industrial employers often view candidates with several industrial postdocs as having greater skills and knowledge than those who have done one or none, she says. "Employers would be more likely to hire that postdoc."

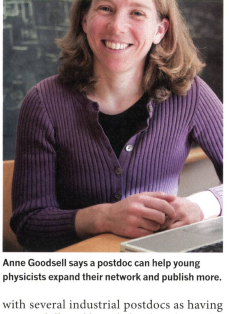

Anne Goodsell says a postdoc can help young physicists expand their network and publish more.

COURTESY

## SMART PURSUIT

The requirements are different for those seeking a government or academic research post, including at US liberal-arts colleges. Catherine Crouch, a materials physicist at Swarthmore College in Pennsylvania, completed two postdocs at Harvard University in Cambridge, Massachusetts, where she earned her PhD. In the first, she focused on physics-education research, with some teaching duties; in the second, she specialized in experimental research in a liberal-arts environment — important at Swarthmore, a liberal-arts college that heavily weights faculty research. As well as honing her research, she says, the fellowships taught her how to run a lab independently — and signalled to potential employers that she was capable of such. "When academic hiring committees are reviewing job applications, they look for a postdoc as evidence that you've had this kind of responsibility — how to run a research programme, how to pick good projects, how to decide what equipment will serve you well," she says. "There are all these meta-questions that don't necessarily come into your arena as a graduate student."

A postdoc expands young physicists' networks far beyond what they can typically achieve as a doctoral student, says Eric Jensen, chair of Swarthmore's physics and astronomy department. "It gives you the chance to build more collaborations and develop a network of colleagues at other institutions that you can be in touch with and work with," he says.

Postdocs can also be useful for those who are uncertain of their pathway or who want to pursue academia but are out of sync with the academic year hiring cycle. Anne Goodsell, an atomic and optical physicist at Middlebury College in Vermont, says that people who earn their PhD around June, for example, and are aiming for a career in academia, can generally apply for posts starting only during the following semester. In the meantime, she says, such postgraduates, as well as those who are not sure of their direction, can take a postdoc to maintain existing contacts, establish new ones, publish more, gain expertise in a subfield and sustain research momentum while waiting to apply or deciding what path to take. "It makes a lot of sense to take a post-doc to fill that gap," Goodsell says.

A postdoctoral fellowship at federal labs in Europe and the United States may sometimes lead directly to a full-time permanent position. Mary Anne With, a postdoctoral adviser at Los Alamos National Laboratory in New Mexico, says that 80–90% of the lab's technical positions are filled by former post-docs. Joseph Bernstein, an astrophysicist and postdoc at Argonne National Laboratory in Illinois, who is on his second renewal and fourth year, is considering either a consulting position or a third extension of his postdoc. The extension, he says, would be equivalent to a tenure-track assistant-professor post and is likely to lead to a permanent position at Argonne — and it pays well for a postdoc position. He declined an offer a couple of years ago for an assistant-professor position that would have meant taking a 10% pay cut. By extending his postdoc, Bernstein believes he will develop the technical computing and programming expertise necessary to become staff. "It's a good opportunity," he says.

So how does a student decide whether to pursue the postdoc path? If postgraduates are planning for a career in academia, it is still a requirement, acknowledges Bailey. But for those who remain uncertain, doing one post-doc is unlikely to damage anyone's budding career, even if they decide to head for industry, says APS executive officer Kate Kirby. "It increases the number of connections you have in your field," she says. "It makes it possible to get further letters of recommendation from a broader constituency — a tremendous advantage that can help you collaborate, get a grant or get a position." ■

**Karen Kaplan** *is assistant Careers editor at* Nature.

# TURNING POINT
# Jessica Hellman

MCASHORE

*Conservation biologist Jessica Hellman studies the effects of climate change at the University of Notre Dame in Indiana. She was inspired by her one-year fellowship from the Aldo Leopold Leadership Program in Stanford, California to do something that few scientific laboratories do — create a mission and vision statement for her research group.*

**What is the best piece of career advice you have received?**

My PhD adviser was Paul Ehrlich, a population biologist at Stanford University, and a public face of science. I studied with him because I wanted to have something to say about natural-resource management or how to deal with climate change. He was an ideal role model. But what he told me, and what I tell my students now, is "it's all about science". Concrete data, experience and knowledge are what give you a voice in the public sphere. If you bring nothing substantial to the table, you are just another voice.

**You have a fear of being labelled a 'butterfly' person. Why?**

I examine how climate change affects endangered species — an issue that has an inherent complexity because of the dynamics of temperature effects and species interactions. One of the species I've studied is the endangered Bay Checkerspot butterfly (*Euphydryas editha bayensis*), which runs out of food when high temperatures or drought cause its host plant to dry out. I don't want people to miss the point: I study butterflies not because I am more fascinated with them than with other creatures but because, with so much data available, they serve as a useful proxy for insects in general. But one thing I learned from my leadership fellowship is to be comfortable in my own skin and recognize what distinguishes me as a researcher — I'm learning to embrace my inner butterfly.

**Why are you trying to 'brand' your research?**

There are two dimensions to branding: communicating to the world who you are and what you are about, and helping you to decide what you want to be doing. I wanted to be the person to study how populations are locally adapted to climate, which my group does.

**Do you think every scientist should brand themselves?**

I think it is a worthwhile exercise. When we first hire a researcher, we want a solid idea of who they are going to be, and it is important for them to think strategically about how they can set themselves apart — so it is helpful to develop a plan that makes that clear.

**Why did you decide to write a mission and vision statement for your laboratory?**

I wanted to know who we were as a group and what we should focus on. Once you get tenure, there are a million things to do — collaborations, committees and grant applications to write. I decided that one way to be thoughtful about our work, and what to work on, would be to collectively write our mission and vision. I found some instructions and group exercises aimed at businesses, and then we had a retreat to strategically discuss how we could match our strengths, priorities and goals for making our research relevant to larger issues. We'll put a copy in the lab for new students.

**Will you continue to have retreats?**

Yes. My research group should have regular retreats. We have lab meetings to talk about science, but retreats focus on broader topics, such as professional development. I want to brainstorm with everybody about what they can be best at. Retreats are also a great way to build morale. Everybody wants to be part of something.

**Why did you start blogging and tweeting?**

I want to make science relevant to the rest of the world, be it landowners or government agencies — but I want to do it with transparency and honesty. Social media opens the shop doors a bit more. I would never tell students that their time is better spent on a blog than on a published paper, but it is a great way to be more open. ■

INTERVIEW BY VIRGINIA GEWIN

WORK-LIFE BALANCE

## Stress survey

Scientists' work obligations conflict with their personal lives three or more times a week, finds a poll of 4,225 scientists by the Association for Women in Science (AWIS) in Alexandria, Virginia. A third of respondents to the global work–life satisfaction survey said that achieving work–life balance damages their careers. "There's a lot of stress out there; it's global and not gender-specific," says AWIS past-president Joan Herbers, who blames the dissatisfaction in part on rigid tenure timelines and requirements. Extending the tenure clock to allow for birth or adoption, and asking tenure committees to rate candidates on the basis of their publications' impact rather than total number, would ease stress, says Herbers.

ACADEMIA

## Increasing salaries

Faculty members at US doctorate-granting institutions received an average 1.7% salary increase for 2011–2012, 41.7% higher than the average 1.2% the previous year, according to a survey of 224,693 faculty members at 813 four-year colleges and universities. The survey conducted by the College and University Professional Association for Human Resources in Knoxville, Tennessee, found that faculty members at public doctoral institutions received a 1.2% average pay rise for 2011–2012, three times higher than the year before. Private institutions awarded a 2.4% rise for 2011–2012, up from last year's 2.2%. Assistant professors in biology and biomedicine earned US$59,907 in 2011–2012, and those in physical sciences earned $58,771, up 2% and 2.3%, respectively.

RESEARCH

## NASA to award grants

As part of an inaugural space-technology research programme, NASA is seeking grant proposals from early-career scientists. Ten researchers in areas such as communication and navigation systems; materials, structures and mechanical systems; and human health, life support and habitation systems will receive up to US$200,000 per year for up to three years. The programme aims to improve its future space-exploration and discovery capabilities by focusing on early-stage research and seeding innovation, says a NASA spokesperson. Notices of intent to submit are due on 30 March and the deadline for final proposals is 3 May.

Weill Cornell Medical College in Qatar

# POSTDOCTORAL POSITION

In a pioneering international initiative, Cornell University and Weill Cornell Medical College established the Weill Cornell Medical College in Qatar (WCMC-Q) through a unique partnership with the Qatar Foundation for Education, Science and Community Development. Located in Doha, Qatar, and in its tenth year of operation, WCMC-Q seeks candidates for a postdoctoral associate position in Doha in:

## NEXTGEN SEQUENCE ANALYSIS

The Bioinformatics Core and Suhre Lab (http://qatar-weill.cornell.edu/research/laboratories/bioinformatics.html) at WCMC-Q invites applications for a postdoctoral associate position in the area of next generation sequence analysis and bioinformatics. The candidate will investigate the genetic basis of monogenic as well as of complex disorders that are relevant to the Middle East population. With the advent of cheap whole genome sequencing, translating huge genome data sets into clinically relevant applications is a major challenge. The successful applicant will identify and apply adequate computational tools from the NextGen field to original biological data generated at WCMC-Q's genomics core. De-novo software development will be limited. Focus is on the biological interpretation of the computational results in a clinical relevant setting.

Candidates must hold a Ph.D. degree, ideally in computational biology or bioinformatics. Applicants with a strong background in scientific computing from unrelated fields (e.g. high-energy physics), but who are willing to train in genomics, will also be considered. Proficiency in Linux scripting and one major programming language are a must.

WCMC-Q is located in Education City among other American universities in Doha, a rapidly growing research hub. The WCMC-Q research program offers a collaborative, multidisciplinary team environment, endowed with a comprehensive support infrastructure. Details regarding the WCMC-Q research program and facilities can be accessed at **http://qatar-weill.cornell.edu/research/index.html.**

WCMC-Q postdoctoral associates and research associates are appointed by the academic departments at Weill Cornell Medical College. Salary is commensurate with experience and is accompanied by an attractive foreign-service benefits package, including paid housing and a car allowance.

Qualified applicants are invited to submit a letter of application, which should outline their interest in the position, along with their curriculum vitae including the names and contact details of three referees to:

**http://job.qatar-med.cornell.edu**

*Positions are open until filled. Please note that, due to the high volume of applications, only short-listed candidates will be contacted.*

Cornell University is an equal opportunity, affirmative action educator and employer.

NW222906R

# Assistant/Associate Professor of Plant Breeding & Genetics (Tenure Track)

## Molecular Breeding & Genetics for Nutritional Quality – Research 60%; Teaching 40%

**Dept. of Plant Breeding & Genetics - NY State College of Agriculture & Life Sciences - Cornell University - Ithaca, NY**

Great universities depend on the **talents** of great people

*Cornell University fosters the pursuit of knowledge and inspires excellence. Join our global community that teaches tomorrow's thought leaders to think otherwise.*

***Responsibilities:*** Advances in biochemistry, metabolomics, and metabolic engineering, and the availability of genomic sequences for food crop species are opening new and valuable research opportunities for plant breeding. This molecular breeding position will have responsibility for conducting innovative research exploring genetic/epigenetic/quantitative variation in plants and the association with phenotypic variation in traits relating to human and animal health and nutrition made accessible by the latest technologies. These efforts could be applied to traditional or specialty crops chosen specifically for their unique attributes. The range of possible outcomes would span foods with new nutritional and health-promoting functions or bioavailability, to the chemistry of flavors and texture to new bioactive food components. Because this is part of a cluster hire, preference will be given to candidates interested in forming collaborations with other faculty with complementary expertise in nutritional sciences, food science, and animal science, among others. Appointee will be expected to develop an externally funded research program; release novel lines, germplasm or genetic stocks; supervise graduate students; teach courses at both the undergraduate and graduate levels related to plant breeding, plant genetics and genomics; and contribute to specialized courses, seminars, and team-taught courses, as well as to graduate training in plant breeding/plant genetics/genomics/plant molecular biology. We are seeking highly motivated individuals with strong research and teaching credentials. Strength in quantitative genetics/statistics is highly desirable. This position will have a 60:40 research and teaching responsibility. For more information visit our web site **http://plbrgen.cals.cornell.edu**.

***Qualifications:***

- Ph.D. in plant breeding, plant genetics/genomics, or plant molecular biology
- Experience in teaching, student advising, and research related to this position, either post-doctoral or pre-doctoral
- Evidence of ability to work with other researchers in interdisciplinary inquiry
- Evidence of ability to attract extramural support and lead an innovative research/breeding program
- Postdoctoral and/or other relevant experience desirable

***Salary:*** Competitive and commensurate with background and experience. An attractive fringe benefits package is available.

***Applications:*** Candidates are requested to submit a letter of application; detailed resume; a personal statement of research and teaching experience, leadership efforts, and contribution to diversity; copies of university transcripts; copies of one or two publications; and names and contact information for three references combined into a single file in pdf format. Send by e-mail to **Ms. Michelle Steigerwald (md464@cornell.edu) or by mail to Department of Plant Breeding and Genetics, 240 Emerson Hall, Cornell University, Ithaca, NY 14853.** Applications are reviewed as received and will continue until a suitable applicant is identified. Inquiries may be sent to Mark Sorrells, 240 Emerson Hall, Cornell University, Ithaca, NY.

Find us online at http://hr.cornell.edu/jobs or Facebook.com/CornellCareers

*Cornell University is an Affirmative Action Equal Opportunity Employer and Educator*

NW222909R

# Weill Cornell Medical College in Qatar

## TYPE 2 DIABETES SENIOR INVESTIGATOR

**BIOMEDICAL RESEARCH PROGRAM** **FACULTY POSITION**

**Weill Cornell Medical College in Qatar (WCMC-Q), a branch of Weill Medical College of Cornell University, seeks a Type 2 Diabetes Senior Investigator to join its biomedical research program.**

WCMC-Q is presently in its 10th year of operations and continues to pursue excellence in education, research, and clinical care. In a pioneering international initiative, the WCMC-Q research program was established in partnership with the Qatar Foundation for Education, Science and Community Development to address the most pressing health challenges in Qatar and the region by employing an integrated basic, translational and clinical approach.

WCMC-Q seeks a highly qualified candidate at the associate or full-professor level with an established research program in the cellular/molecular basis of Type 2 Diabetes. The successful candidate will have a stellar track record of research accomplishments and an enthusiasm for building new research initiatives. Candidates must have an MD and/or PhD degree and must be willing to relocate to Doha, which is rapidly growing as a research hub. The level of appointment will be commensurate with credentials and experience. A comprehensive and highly competitive salary and foreign service benefits package and a competitive start-up package will be provided.

The WCMC-Q research program offers a collaborative, multidisciplinary team environment, endowed with a comprehensive support infrastructure. The successful applicant will be able to draw on state-of-the-art facilities, including genomics, proteomics, imaging, and computational and biostatistics cores. Details regarding the WCMC-Q research program and facilities can be accessed at **http://qatar-weill.cornell.edu/research/index.html**.

Qualified applicants are invited to submit a letter of application, which should outline their interest in the position and a description of research interests and future research plans (3-5 pages), along with their curriculum vitae to:

**http://job.qatar-med.cornell.edu**

Applications may be submitted until June 30, 2012. Please note that, due to the high volume of applications, only short-listed candidates will be contacted.

*Cornell University is an equal opportunity, affirmative action educator and employer.*

Weill Cornell Medical College in Qatar

Education City Qatar Foundation

W/W2098AR

---

UNIVERSITY OF CAMBRIDGE

A world of opportunities

**www.cam.ac.uk/jobs/**

## Post-Doctoral Research Associate in Biological Image Analysis

Department of Genetics

Limit of tenure: Two years from date of appointment

Applications are invited for a Postdoctoral Researcher to join an interdisciplinary research group and participate in a European Research Council (ERC) funded project on the dynamics of gene expression during stem cell differentiation. You should have experience in biological image analysis and knowledge of software tool development, with a focus on usability, and an interest in working with experimentalists. Knowledge of microscopy will be an advantage.

Informal enquiries to Prof Martinez-Arias - ama11@cam.ac.uk

**Applications, which should consist of a completed CHRIS/6 application form (Parts I and III) - see http://www.admin.cam.ac.uk/offices/hr/forms/chris6/ - a full CV and covering letter describing your research interests, should be sent to Mrs A Read, Dept of Genetics, Downing St, Cambridge CB2 3EH. e-mail: jobs@gen.cam.ac.uk**

**Quote reference: PC14171. Closing date: 20 April 2012.**

**The University values diversity and is committed to equality of opportunity.**

U222731R

---

"Thank you for assisting in advertising the 6x 'Research Associate' positions on the Naturejobs website. I was advised thoroughly on the inventory that would be the best for our organisation and the web inventory worked. We received a huge response and will contact you for future advertisements."

**Nanda Rahman, Bio Nano Consulting, UK**

naturejobs

---

climate risk analysis **mudelsee**

MARIE CURIE ACTIONS

Climate Risk Analysis (CRA) is an expanding research company working on risk quantification of extreme climate/weather events. CRA is seeking a **computing scientist** to work in an international, EU-funded project on interacting networks in climate.

## Researcher in Climate & Computing

**YOUR QUALIFICATIONS**

- Degree in computing, statistics or physics
- Between four and five years full-time work experience
- Transnational and intersectorial mobilities
- Excellent communication skills (English)

**YOUR POSITION IN THE PROJECT**

- Industry-standard software development (parallelization, GUIs)
- Adaptation of statistical algorithms
- Support for statistics/computer course
- Training of project partners (in-house and travel)
- Starting date: summer 2012 (duration two years)
- Place: Hannover, Germany
- Gaining competence in climate time series and risk analysis
- Salary ca. 50,000 EUR/year, family allowance, bonuses
- Extensive covering of research, training and relocation costs

**YOUR APPLICATION**

- Cover letter, CV, reference contacts
- PDF format (one single file)
- Send by 12 May 2012 to **jobs@climate-risk-analysis.com** under subject 'JO-01/12'

**CONTACT AND MORE INFORMATION**

**www.climate-risk-analysis.com**

Dr. Manfred Mudelsee, Phone +49-511-7003 2891

CRA is devoted to excellence in research and does not discriminate against persons on the basis of ethnicity, family status, gender, medical condition, nationality or religion.

W/2033R

LMU LUDWIG-MAXIMILIANS-UNIVERSITÄT MÜNCHEN

FACULTY OF PHYSICS

The **Faculty of Physics** of the Ludwig-Maximilians-Universität München (LMU) invites applications for a

## Professorship (W2) for Experimental Physics – Biophysics

### (6 years/tenure track)

commencing as soon as possible.

The successful candidate is expected to represent the entire field of Biophysics in research and teaching at the university.

Possible fields of research include proteomics, gene regulation, enzymatic networks and bio-molecule based strategies for renewable energy. Participation in the interdisciplinary activities of the "Center for NanoScience" (CeNS), the cluster of excellence "Nanosystems Initiative Munich" (NIM) as well as in local collaborative research programs is possible. For additional information on ongoing activities see http://www.nano-initiative-munich.de and www.cens.de.

Prerequisites for this position are a university degree, a doctoral degree, teaching skills at university level and additional academic achievements.

The position is also particularly suitable for highly qualified junior academics.

The initial appointment will be for six years. After a minimum of three years it may be converted to tenure pending a positive evaluation of the candidate's aptitude for teaching and research as well as the candidate's pedagogical and personal aptitude if all legal conditions are met. In exceptional cases involving candidates with outstanding qualifications, a tenured position may be offered from the outset.

Candidates for this position should be aged 51 or under at the time of appointment. Exceptions thereto may be considered in the case of outstanding candidates.

The LMU is an equal opportunity employer and aims to increase the number of female faculty members. Therefore, applications from female candidates are explicitly encouraged.

Disabled candidates with essentially equal qualifications will be given preference.

The LMU supports dual career couples.

Please, submit your application comprising a curriculum vitae, academic records, a list of publications, as well as a two-page summary of planned research activities to the **Dekan der Fakultät für Physik der Ludwig-Maximilians-Universität München, Schellingstr. 4, 80799 München, Germany**, not later than **June 15th 2012**.

W222874R

naturejobs

Read our Postdoc articles and news in the **News and Comment** section of **naturejobs.com**

- Helpful advice
- Real life experiences
- Follow the highs and lows of postdoc life

naturejobs

**How can you make more informed career or hiring decisions?**

Follow the blog on naturejobs.com to keep up-to-date with the latest scientific employment news from around the world.

**What do you think about the news stories affecting scientific careers?**

Start sharing your opinions today on the *Naturejobs* blog.

**www.naturejobs.com**

# naturejobs

**European Head Office, London** naturejobs@nature.com
The Macmillan Building, 4 Crinan Street, London N1 9XW, UK
Tel: +44 (0) 20 7843 4961 Fax: +44 (0) 20 7843 4996

**European Manager:**
Nils Moeller; +44 (0) 20 7843 4953 n.moeller@nature.com
**Southwest UK/RoW:**
Emma Hare; +44 (0) 20 7843 4944 e.hare@nature.com
**Northeast UK/Ireland:**
Matthew Ward, +44 (0) 20 7014 4059 m.ward@nature.com
**France/Switzerland/Belgium:**
Julie Aramburu, +44 (0) 20 7843 4994 j.aramburu@nature.com
**Scandinavia/Spain/Portugal/Italy:**
Megan Ball, +44 (0) 20 7843 4973 m.ball@nature.com
**North Germany/The Netherlands/Eastern Europe:**
Kristin Doelling, +44 (0) 20 7843 4970 k.doelling@nature.com
**South Germany/Austria:**
Maria Kubalova, +44 (0) 20 7014 4084 m.kubalova@nature.com
**Natureevents:**
Matthew Clare, +44 (0) 20 7014 4015 m.clare@nature.com
**Business Development Manager, Middle East:**
Jon Giuliani, +44 (0) 20 7843 4922 j.giuliani@nature.com

**USA Head Office, New York** naturejobs@us.nature.com
75 Varick Street, 9th Floor, New York, NY 10013-1917
Tel: +1 800 989 7718 Fax: +1 800 989 7103

**US Sales Manager:**
Ken Finnegan, +1 212 726 9248 k.finnegan@us.nature.com

**Japan Head Office, Tokyo**
Chiyoda Building, 2-37 Ichigayatamachi, Shinjuku-ku, Tokyo 162-0843
Tel: +81 3 3267 8751, Fax: +81 3 3267 8746

**Asia-Pacific Sales & Business Development Manager:**
Yuki Fujiwara, +81-3-3267-8765 y.fujiwara@natureasia.com
**Business Development Manager, Greater China/Singapore:**
Gloria To, +852 2811 7191 g.to@natureasia.com

**India**
3a, 4th Floor, DLF Corporate Park, Gurgaon, 122 002, India

**Advertisement Sales:**
Vikas Chawla, +91 1242881057 v.chawla@nature.com

JAGIELLONIAN UNIVERSITY MEDICAL COLLEGE

omicron

The Jagiellonian University Medical College in Krakow, Poland has a long history of promoting high quality education through research as well as exchanging information between international institutions. It owes its exceptional position both to tradition, that stretches back over a period of six hundred years, and to its significant present-day achievements. The Faculty of Medicine is the leading faculty among the three of which the Jagiellonian University Medical College consist of. It offers an outstanding opportunity in conducting multidisciplinary research by providing state of the art facilities in molecular biology and genetics within the OMICRON Project (founded by the European Union, grant number 286038).

**Position description:** The Jagiellonian University Medical College is actively seeking bright, highly motivated candidates for postdoctoral positions (part-time positions will be considered) for a period of 27 months, while offering a competitive salary, in the fields of metabolic diseases, stem cells, vascular and cardiovascular research and oncology. The start date of employment: October 1st 2012.

Position requirements include a doctoral degree in medicine, molecular biology, cell biology, genetics or related discipline. Potential candidates are required to be proficient in English.

**Required application documents:** full Curriculum Vitae, consisting of a publication record in international journals, a description of research and laboratory work experience and three reference letters with contact information.

Applications will be accepted until **May 31st 2012.** Please, send all of the documents via e-mail to **omicron@cm.uj.edu.pl**.

Please visit the following web sites for further information: www.cm-uj.krakow.pl, www.omicron.cm.uj.edu.pl.

W222881R

## Manchester Collaborative Centre for Inflammation Research

### A Partnership between
### The University of Manchester, GlaxoSmithKline and AstraZeneca

## Professorial/Senior Fellow Positions

Ref: LSX-00905

The Manchester Collaborative Centre for Inflammation Research (MCCIR) is a new collaboration between the University of Manchester, GlaxoSmithKline and AstraZeneca to establish a world-leading translational centre for inflammatory research. The Centre, directed by Professor Tracy Hussell, starts with an initial investment of £5M from each partner and has strong links within the Faculties of Medical & Human Sciences and Life Sciences.

The MCCIR seeks to recruit professorial leaders in areas relating to basic aspects of inflammation. Candidates are expected to have an established group, a track record of independent funding and agenda-setting publications. We particularly encourage individuals already holding independent senior fellowships in a relevant area to apply. All successful appointments will be provided with additional personnel supported from core funding.

Subjects of particular interest include (but are not limited to) macrophage differentiation and activation, T cell subset regulation, neutrophil biology, dendritic cell subsets, mucosal immunology, immune modulatory peptides and proteins, and epigenetic regulation of inflammation.

As part of your application you are invited to describe your research plans and how you would contribute to the vision of the MCCIR.

Please submit your application form, research plan and curriculum vitae by 30th April 2012. http://www.manchester.ac.uk/aboutus/jobs/

Further information about these roles and the Centre is available from tracy.hussell@manchester.ac.uk or +44 (0)20 7594 3184

AstraZeneca gsk GlaxoSmithKline MANCHESTER 1824 The University of Manchester

U222965R

HOWARD HUGHES MEDICAL INSTITUTE

# HHMI Investigator Competition

The Howard Hughes Medical Institute (HHMI) invites applications for investigator positions from scientists who have demonstrated originality and substantial accomplishments in biomedical research and who show exceptional promise for future achievement and leadership in research. The Institute seeks to appoint 20 to 30 outstanding scientists to its flagship investigator program.

**Eligibility**

- Ph.D. and/or M.D. (or the equivalent)
- Tenured or tenure-track position as an assistant professor or higher academic rank (or the equivalent) at an eligible U.S. institution
- More than 5 but no more than 15 years of experience since appointment as an assistant professor or equivalent position
- Principal investigator on one or more active national peer-reviewed research grants with a duration of at least 3 years

This HHMI investigator competition is open to scientists who study significant biological problems in all of the biomedical disciplines as well as in adjacent fields such as biophysics, chemical biology, biomedical engineering, and computational biology. Plant scientists, experimental evolutionary biologists, and patient-oriented researchers are welcome to apply to this competition.

**Application information:**

**www.hhmi.org/inv2013/nat**

Deadline to establish eligibility: **May 1, 2012, 3 PM ET**

Deadline to submit all application materials: **June 13, 2012, 3 PM ET**

HHMI
HOWARD HUGHES MEDICAL INSTITUTE

*The Howard Hughes Medical Institute is an equal opportunity employer.*

NW222210R

# gairdner

LES PRIX CANADA GAIRDNER AWARDS

## CONGRATULATIONS TO THE 2012 CANADA GAIRDNER AWARD RECIPIENTS

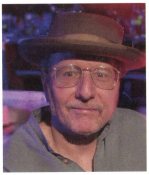

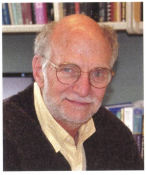

**For their pioneering discoveries concerning the biological clock responsible for circadian rhythms.**

CANADA GAIRDNER INTERNATIONAL AWARD
**JEFFREY C. HALL** PhD

Professor of Biology Emeritus, Brandeis University, Waltham, MA

CANADA GAIRDNER INTERNATIONAL AWARD
**MICHAEL ROSBASH** PhD

Investigator, Howard Hughes Medical Institute and Professor of Biology, Brandeis University, Waltham, MA

CANADA GAIRDNER INTERNATIONAL AWARD
**MICHAEL W. YOUNG** PhD

Richard and Jeanne Fisher Professor, VP Academic Affairs, Head, Laboratory of Genetics, The Rockefeller University, NY, NY

CANADA GAIRDNER INTERNATIONAL AWARD
**THOMAS M. JESSELL** PhD

Professor of Neuroscience; Investigator, Howard Hughes Medical Institute, Columbia University, NY, NY

**For research in defining the genetic and molecular pathways leading to the complex development of the spinal cord, with implications for therapeutic applications.**

CANADA GAIRDNER INTERNATIONAL AWARD
**JEFFREY V. RAVETCH** PhD MD

Theresa and Eugene Lang Professor, and Head, Leonard Wagner Laboratory of Molecular Genetics and Immunology, The Rockefeller University, NY, NY

**For his seminal work in identifying the Fc receptors of antibodies, which play a key role in the immune response, and for establishing their critical role in autoimmune diseases and cancer.**

CANADA GAIRDNER GLOBAL HEALTH AWARD
**BRIAN M. GREENWOOD** MD

London School of Hygiene & Tropical Medicine, London, UK

**For contributions to significantly reducing mortality in children due to meningitis and acute respiratory infection and for contributions to malaria prevention.**

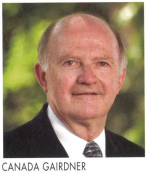

CANADA GAIRDNER WIGHTMAN AWARD
**LORNE A. BABIUK** OC SOM PhD DSc FRSC

Vice-President (Research), University of Alberta, Edmonton, AB

**For his extraordinary national and international leadership in vaccine development and research on human and veterinary infectious disease control.**

Gairdner recognizes the world's most creative and accomplished biomedical scientists.
Join our growing community at **www.gairdner.org**

THIS ANNOUNCEMENT IS SUPPORTED BY Ontario

NW221529R

# HEPTARES therapeutics

An exciting opportunity to join one of Europe's leading drug discovery companies in a senior strategic and operational role.

Heptares Therapeutics discovers and develops new medicines targeting GPCRs (G-protein-coupled receptors), a super-family of drug targets linked to a wide range of human diseases. The Company is well-funded and has established R&D collaborations with leading pharmaceutical companies.

Heptares is an industry pioneer in GPCR structure-based drug design and has built a unique capability for discovering novel molecules that modulate historically undruggable or challenging GPCRs. The Company's integrated discovery platform includes proprietary technologies for engineering stabilised GPCRs in their natural pharmacological conformations, identifying previously unknown chemistries for GPCR protein-drug interactions, and deploying advanced fragment-based approaches to GPCR target space for the first time. Using this approach, Heptares is generating a broad pipeline of drug candidates for serious CNS and metabolic disorders.

## Head of Pharmacology

**Role Specification**

- Part of the Heptares Management Team, which is responsible for developing the strategy and vision of the company.
- Line Manager of the Pharmacology Team with responsibility for all in vitro pharmacology, supporting Heptares Drug Discovery programmes.
- To manage external CROs responsible for additional in vitro and in vivo pharmacology.
- Work closely with the Medicinal Chemistry Team.
- Work closely with Development Project Teams in order to progress Heptares advanced projects to the clinic.
- Project leadership of CNS and Metabolic targets.
- Work with industry partners.

**Qualifications**

The successful candidate should have:

- A PhD or equivalent in biological sciences and at least 10 years' experience of Drug Discovery within the Pharmaceutical/ Biotechnology Industry.
- Comprehensive knowledge of in vitro assays and receptor kinetics for GPCRs.
- A track-record of working in drug discovery programmes and of progressing compounds to the development stage.
- Experience of the neurology, psychiatry and preferably metabolic therapeutic areas.
- Excellent verbal and written communication skills.
- Track record of innovation and discovery, coupled with a strong sense of practical execution.
- Demonstrated ability to define, prioritise and clearly articulate research objectives.
- Strong interpersonal skills: to work within the company as well as with partners, consultants and CROs.
- A record of building and leading productive teams and collaborations.
- Excellent line management skills.

U222947R

**Further information can be found on our website.**

**Applications should be sent to hr@heptares.com quoting reference number 2012/1P.**

**BioPark, Broadwater Road, Welwyn Garden City, Hertfordshire AL7 3AX, UK.**

**www.heptares.com**

KYUSHU UNIVERSITY

i²CNER wpi

# INTERNATIONAL INSTITUTE FOR CARBON-NEUTRAL ENERGY RESEARCH

*The International Institute for Carbon-Neutral Energy Research (I²CNER) at Kyushu University, Japan is actively seeking candidates for open-rank faculty and post-doctoral research associates.*

**OUTLINE:** The International Institute for Carbon-Neutral Energy Research (I²CNER) is a member of the World Premier International Research Center Initiative established by the Japanese Ministry of Education, Culture, Science and Technology (MEXT). Faculty members and researchers associated with I²CNER are dedicated to the Institute's mission to contribute to the creation of a sustainable and environmentally friendly society by advancing fundamental science to reduce $CO_2$ emissions and the realization of a hydrogen economy. The ITO Campus of the Kyushu University houses extensive state-of-the-art experimental and computational facilities.

**QUALIFICATIONS & CURRENT OPENINGS:** I²CNER is currently accepting applications in the following research areas:

1) Hydrogen embrittlement (Mechanics, Fatigue and Fracture, Materials, Tribology )
2) Chemistry for efficient material transformation
3) Basic science issues underlying $CO_2$ separation/concentration
4) Applied (and/or basic) science issues underlying geologic/sub-seabed/ocean CCS ($CO_2$ capture and storage )
5) Thermophysical Properties, Heat and Mass Transfer, Thermal Engineering for Highly Efficient Energy Utilization
6) Solar/Chemical Hydrogen Production ( including Steam Electrolysis )
7) Energy Analysis

All faculty members are expected to initiate and sustain vigorous research programs that both advance and are relevant to I²CNER's the mission. Candidates for senior faculty positions must have achieved national and international recognition for their research accomplishments. Post-doctoral research associates will join research groups relevant to their field of expertise and education.

**APPLICATION PROCESS:** Applicants must provide 1) Cover Letter; 2) Application Form (located on website); 3) Curriculum vitae that details research experience and interests; 4) Research Proposal (located on website); 5) List of publications; 6) Names and contact information of four references.
* All materials must be submitted in English.

**SALARY & STARTING DATE:** Salary will be commensurate with qualifications and experience. The starting date will be as soon as possible after the closing date.

**APPLICATION DEADLINE:** Wednesday, June 6, 2012, 17:00 (Japan Time); Interviews may take place prior to closing date; however, no final decisions will be made until after this time.

**FOR MORE INFORMATION:** http://i2cner.kyushu-u.ac.jp/en/recruit/recruit.php

**Send Inquiries to: wpi-office@i2cner.kyushu-u.ac.jp**

International Institute for Carbon-Neutral Energy Research (I²CNER), Kyushu University
744 Motooka, Nishi-ku, Fukuoka Postal Code 819-0395, JAPAN

TEL: +81-(0)92-802-6932 FAX: +81-(0)92-802-6939

JPSD282681

## International Research Institute of Disaster Science (IRIDeS), Tohoku University

### Website: http://www.tohoku.ac.jp/english/
### Location: Sendai, Japan

### New Research Institute in April 2012:

Having experienced the catastrophic disaster in 2011, Tohoku University has founded the International Research Institute of Disaster Science (IRIDeS). Together with collaborating organizations from many countries and with broad areas of specialization, the IRIDeS conducts world-leading research on natural disaster science and disaster mitigation. Based on the lessons from the 2011 Great East Japan (Tohoku) earthquake and tsunami disaster, the IRIDeS aims to become a world centre for the study of the disasters and disaster mitigation, learning from and building upon past lessons in disaster management from Japan and around the world. Throughout, the IRIDeS will contribute to on-going recovery/reconstruction efforts in the affected areas, conducting action-oriented research, and pursuing effective disaster management to build sustainable and resilient societies, the IRIDeS innovates the past paradigm of Japan's and world's disaster management to catastrophic natural disasters, hence to become a foundation stone of disaster reduction management and sciences.

All qualified candidates are encouraged to apply. Tohoku University is strongly committed to equal employment and to recruiting a diverse faculty and staff. The University encourages applications from all qualified candidates. We seek faculty position in the following field;

(1) Disaster Science Division
Global-scale Natural Disaster Research Field
Type: Professor or Associate Professor
Deadline for applications: April 25 2012

Website:
http://www.dcrc.tohoku.ac.jp/jobs/IRIDeS06_e.html

(2) Disaster Medical Science Division
Disaster-related Public Health Field
Type: Professor
Deadline for applications: April 13 2012

Website:
http://www.dcrc.tohoku.ac.jp/jobs/IRIDeS07_e.html

JP222741R

## CSIR-CENTRAL DRUG RESEARCH INSTITUTE
**(Council of Scientific & Industrial Research)**
Chattar Manzil Palace, Post Box No. 173, Lucknow - 226001 (U.P.)

### ADVERTISEMENT NO. 1/2012

**CSIR-Central Drug Research Institute,** Lucknow is a premier R&D Institute under the aegis of the Council of Scientific and Industrial Research (CSIR), New Delhi which is an autonomous body under Department of Scientific and Industrial Research, Government of India, invites applications for the following scientific posts :-

**SCIENTIST: 09 POSTS :**

**Pay : Pay Band PB-3, Rs.15,600-39,100 with Grade Pay of Rs.6,600/- (Gross Emoluments approximately Rs. 49,321/- p.m.); Age limit :** 32 Years.

**Post Code: 01 : Discipline:** Parasitology **(01 post)** (Unreserved)
**Post Code : 02: Discipline:** Molecular & Structural Biology **(01 post)** (Unreserved)
**Post Code: 03: Discipline:** Molecular & Structural Biology **(01 post)** (Unreserved)
**Post Code: 04: Discipline:** S&T Management **(01 post)** (Reserved for PWD- Locomotor Disability or Cerebral Palsy)
**Post Code: 05: Discipline:** Lab. Animals **(01 post)** (Reserved for ST)
**Post Code:06 : Discipline** : Pharmacology (Reserved for PWD - Hearing Impairment)
**Post Code : 07 : Discipline** : Business Development (Reserved for OBC)
**Post Code : 08 : Discipline** : Academic Affairs (Reserved for OBC)
**Post Code : 09 :** Library (Reserved for SC)

**SENIOR SCIENTIST:**
**11 POSTS (UNRESERVED) :**

**Pay: Pay Band PB-3 Rs.15,600-39,100 with Grade Pay of Rs.7,600/- (Gross Emoluments approximately Rs. 56,968/- p.m.) : Age limit :** 37 Years.

**Post Code: 10 : Discipline:** Pharmacology **(01 Post)**
**Post Code: 11 : Discipline:** Pharmacology **(01 post)**
**Post Code: 12: Discipline:** Pharmacology **(01 post)**
**Post Code: 13: Discipline** : Pharmacology **(01 post)**
**Post Code:14: Discipline:** Parasitology **(01 post)**
**Post Code:15 : Discipline:** Parasitology **(01 post)**
**Post Code: 16: Discipline:** Fungal/Microbial **(01 Post)**
**Post Code 17: Discipline:** Microbiology **(01 post)**
**Post Code: 18: Discipline:** Medicinal & Process Chemistry **(01 Post)**
**Post Code: 19: Discipline:** Medicinal & Process Chemistry **(01 Post)**
**Post Code: 20: Discipline:** Endocrinology **(01 Post)**

For complete advertisement and other details like qualifications, experience and terms & conditions please visit our Website : **http://www.cdriindia.org/situationv.asp**

RW222704R

UNIVERSITY OF JYVÄSKYLÄ

## University of Jyväskylä, Finland

University of Jyväskylä is one of the leading universities in Finland in the fields of Humanities and Natural Sciences. The Department of Biological and Environmental Science is an internationally recognized research and teaching unit. The department covers Aquatic Sciences, Ecology and Evolutionary Biology, Cell and Molecular Biology, and Environmental Science and Technology. The department houses the Finnish Centre of Excellence in Biological Interactions. The department enjoys an outstanding environment, occupying modern buildings on the shore of Lake Jyväsjärvi. The department has well-equipped laboratories, as well as specialist facilities including a bioimaging suite, a molecular genetics laboratory and a stable isotope analysis facility, and modern equipment for analysing environmental samples.

The department is currently seeking to recruit staff for the following senior positions:

**Professor in Environmental Science and Technology**
More details, and the link to the electronic application forms can be found at:

http://www.nature.com/naturejobs/science/jobs/252949-Professor-in-Environmental-Science-and-Technology

**Professor in Biochemistry**
More details, and the link to the electronic application forms can be found at: :

http://www.nature.com/naturejobs/science/jobs/252944-Professor-in-Biochemistry

It is hoped that the starting date for both roles will be 1st August 2012, or as soon as possible thereafter and the closing date for applications is **27 April 2012.**

http://www.jyu.fi/bioenv/en

W222961R

**Infectious career articles each week**
Career advice
you can't put down.
naturejobs

MRC Laboratory of Molecular Biology

**Cambridge, UK**

## Programme Leaders in Neurobiology

Coinciding with the move of the MRC Laboratory of Molecular Biology (LMB) into a new state-of-the-art research building in October 2012 (http://www2.mrc-lmb.cam.ac.uk/about-lmb/new-building), the Division of Neurobiology wishes to recruit talented scientists interested in developing an independent programme of research. We are particularly interested in individuals working on the function of neural circuits using electrophysiological or imaging techniques, and we envisage that such work would make use of organisms open to genetic manipulation. Current interests in the Division include visual and olfactory processing, circadian rhythms, mechanisms of synaptic transmission and protein misfolding in relation to neurodegenerative diseases (www2.mrc-lmb.cam.ac.uk/NB/). Scientific excellence and potential for major impact are paramount. Synergy with existing research programmes would be an advantage.

The LMB provides an excellent environment for hands-on research. Core-funding by the Medical Research Council provides long-term support for ambitious projects, while administrative duties are minimal and no teaching is required. Interactions across the four Divisions of the Laboratory are encouraged. There is extensive central support, including electronic and instrumentation workshops, imaging and transgenic mouse facilities. The University of Cambridge and affiliated institutions form a vibrant Neuroscience community (http://www.neuroscience.cam.ac.uk/).

Candidates should have a PhD and/or MD and will have completed a period of postdoctoral training or equivalent, with an excellent track record, and show outstanding potential for independent research. You will lead a small team and substantial funding will be available.

These appointments will be made at either Programme Leader or Programme Leader-track level, depending on achievements and experience. Candidates for Programme Leader positions should have a strong international track record of relevant independent research and a proven ability to lead a research team, pursuing original approaches to long-term research goals. Programme Leader-track appointments will be made for those who demonstrate the potential to develop into Programme Leaders within six years. Candidates with appropriate levels of experience may be given responsibility for oversight of core scientific activities within the LMB. Salaries are competitive (Programme Leader-track £35,935 - £48,000 per annum; Programme Leader £45,213 - £70,000 per annum).

These positions will remain open until they are filled; applications received by 6th April 2012 will be given priority.

Informal enquiries can be addressed to Michel Goedert (mg@mrc-lmb.cam.ac.uk).

Applications should include a covering letter and full CV, an outline of current research interests (1 page) and a proposal for future research (up to 2 pages), along with the names and addresses of three professional referees who have agreed to be contacted prior to interview. Applications for this post must be made online at https://ext.ssc.rcuk.ac.uk inputting the reference IRC47968. If you do not have access to the internet, or experience technical difficulties, please contact 01793 867003.

This position is subject to pre-employment screening.

**For further information about the MRC visit www.mrc.ac.uk**

The Medical Research Council is an Equal Opportunities Employer

U222895R

European Research Council erc

MRC Laboratory of Molecular Biology

**Cambridge**

## Three Positions in Neural Circuits and Behaviour

The MRC Laboratory of Molecular Biology, Cambridge, is a world-famous institution with excellent infrastructure, a collegial environment and a strong track-record in training postdoctoral fellows who have gone on to become leading scientists.

Our lab, within the Neurobiology Division of the LMB, is studying the neural circuits that transform raw sensory information into behaviour. We use the olfactory system of Drosophila as a model and apply a variety of tools including molecular genetics, computational neuroanatomy, confocal and multiphoton microscopy, electrophysiology, optogenetics and behavioural analysis. Specific projects include the neural basis of 1) sex differences in olfactory behaviour 2) innate responses to different classes of general odours 3) integration of food and pheromone information.

We are looking for two Post-Doctoral Scientists and a Research Assistant to join the lab to extend our physiological and anatomical studies.

For the Post-Doctoral positions, a PhD is required in a relevant biological subject (or a relevant experimental discipline in the physical sciences). Experience with one or more of the core techniques mentioned above is strongly preferred but all applicants will be considered carefully. One of these positions is funded by an ERC Starting Grant (currently scheduled to run until 31st August 2013) and the other position is jointly funded by ERC and the MRC for 3 years in the first instance.

**The salary for these positions will be in the range of £26,022 - £31,758 depending on experience and suitability for the position. To apply for these positions, please quote reference IRC47684 and/or IRC47704.**

For the Research Assistant position we will consider an appointment either of a more experienced researcher or a more recent graduate. Dependent on the experience of the successful candidate the qualification level will be either an undergraduate or postgraduate degree in a science or engineering subject. This position is funded by the ERC Starting Grant until 31st August 2013.

**The salary for this position will be in the range of £20,074 - £31,758 depending on experience and suitability for the position. To apply, please quote reference IRC47924.**

Successful candidates for all positions will be independent, creative and motivated researchers, capable of working efficiently within a friendly, tight-knit team.

Further information about the lab is available from our website (http://jefferislab.org) or directly from Gregory Jefferis (jefferis@mrc-lmb.cam.ac.uk).

Your salary will be supported by 30 days annual leave entitlement, an optional MRC final salary pension scheme and excellent on-site sports and social facilities.

Applications are handled by the RCUK Shared Services Centre; to apply please visit our job board at https://ext.ssc.rcuk.ac.uk and complete an online application form. Applicants who would like to receive this advert in an alternative format (e.g. large print, Braille, audio or hard copy), or who are unable to apply online should contact us by telephone on 01793 867003.

**Closing date: 5 April 2012**

**Final appointments will be subject to a pre employment screening**

The Medical Research Council is an Equal Opportunities Employer

U222896R

You don't have to look this hard to find a job with Naturejobs.

nature jobs
making science work

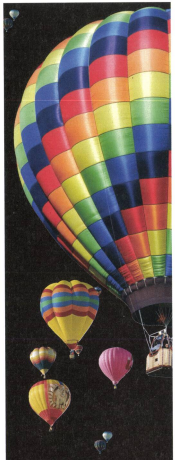

HIGHER & HIRE!

Post all your vacancies for FREE on the largest dedicated job board for the scientific community:

naturejobs.com

nature publishing group npg

dkfz. GERMAN CANCER RESEARCH CENTER IN THE HELMHOLTZ ASSOCIATION

Medizinische Fakultät Heidelberg

At the Deutsches Krebsforschungszentrum (DKFZ, German Cancer Research Center) the position of a

# Endowed Professorship (W3)

## for X-Ray Imaging and Computed Tomography

(Ref-No. 48/2012)

is available.

The Deutsches Krebsforschungszentrum (DKFZ) and the Faculty of Medicine of the Heidelberg University are jointly recruiting a scientist as head of a research group in the department Medical Physics in Radiology within the research program Imaging and Radiooncology at DKFZ.

Applicants should have obtained 'Habilitation' or equivalent scientific achievements. We expect an outstanding scientific record in x-ray computed tomography (CT) with a special focus on the development of new methods and the optimization of existing methods. The candidate should further have profound knowledge in motion-compensated image reconstruction to enable dose efficient 4D imaging in radiation oncology from sparsely sampled data. Expertise in interventional CT imaging and CT fluoroscopy is desired. Spectral CT with energy-resolved detectors and static CT (without rotating mechanics) for organ-specific sequences with highest temporal resolution are requested new research areas. The applicant should pursue and evaluate innovative methodological developments and the advance of applications of oncological imaging, molecular imaging and biophysical methods in close collaboration with the other departments of the research program at DKFZ and the radiology groups at the Heidelberg University Hospital.

We offer an excellent infrastructure including a clinical dual source dual energy spiral CT, a flat detector CT system with continuously rotating gantry, and a small animal micro-CT system as well as sufficient compute capability dedicated to running sophisticated image reconstruction algorithms.

*The German Cancer Research Center is determined to increase the number of female scientists and encourages female scientists to apply. DKFZ is an equal opportunity employer, and handicapped candidates with comparable qualifications will be favoured.*

Applications should include a curriculum vitae, a list of publications and references. Please submit your application to Prof. Dr. C. R. Bartram, Dean, Medical Faculty of the University of Heidelberg, Im Neuenheimer Feld 672, 69120 Heidelberg and to Prof. Dr. O. D. Wiestler, Chairman and Scientific Director, Deutsches Krebsforschungszentrum, Im Neuenheimer Feld 280, 69120 Heidelberg.

Zertifikat seit 2005 audit berufundfamilie

W222962R

Want the best of the global market?

Make nature jobs making science work your first choice.

# MARTIN-LUTHER-UNIVERSITÄT HALLE-WITTENBERG

An der **Medizinischen Fakultät** der Martin-Luther-Universität Halle-Wittenberg ist zum frühestmöglichen Zeitpunkt die neu geschaffene Stelle eines/einer

## W3-Professors/-in „Funktionelle Genomik“

zu besetzen.

Der/Die Stelleninhaber/in soll das Institut für Funktionelle Genomik, welches eng mit dem 2011 gegründeten Krukenberg-Krebszentrum Halle zusammenarbeitet, leiten. Schwerpunkt der Professur soll die Identifizierung und Evaluierung neuer Marker besonders im Bereich Onkologie sein. Sie soll Kompetenzen aus den Bereichen klinische Forschung, Humangenetik, Pathologie/Gewebebank, Pharmakologie und Epidemiologie integrieren und in gemeinsame Drittmitteleinwerbungen in Kooperations- und Verbundprojekten umsetzen. Von dem/der Stelleninhaber/in wird weiterhin erwartet, dass er/sie mit Arbeitsgruppen aus dem Bereich Molekulare Medizin sowie aus den Naturwissenschaftlichen Fakultäten der Universität kooperiert. Neben der Onkologie sind Kooperationen und Aktivitäten in den Bereichen Herz-Kreislaufforschung, Dermatologie, Neurologie und Psychiatrie erwünscht. Bei entsprechenden Voraussetzungen kann eine Phase I Unit eingerichtet werden.

Die Lehraufgaben sind in den Studiengängen Medizin und Zahnmedizin, in der Graduiertenschule Medizin sowie im Rahmen interfakultärer Kooperationen zu erbringen.

Einstellungsvoraussetzungen sind ein abgeschlossenes Hochschulstudium im Bereich Medizin oder Naturwissenschaften, die Promotion und Habilitation oder gleichwertige wissenschaftliche Leistungen. Nachweis der erfolgreichen Einwerbung von Drittmitteln sowie didaktische Fähigkeiten und Lehrerfahrung.

Zu den Aufgaben des/der Stelleninhabers/-in gehören außerdem die weiteren in § 34 des Hochschulgesetzes des Landes Sachsen-Anhalt genannten Verpflichtungen. Ggf. wahrgenommene Aufgaben in der Krankenversorgung werden entsprechend des Beschlusses der Kultusministerkonferenz vom 19. November 1999 in einem gesonderten Vertrag mit dem Universitätsklinikum Halle (Saale) geregelt.

Die Martin-Luther-Universität strebt eine Erhöhung des Anteils von Frauen am wissenschaftlichen Personal an und fordert daher Frauen nachdrücklich auf, sich zu bewerben. Die Martin-Luther-Universität Halle-Wittenberg bietet gute Möglichkeiten, Beruf und Familie zu vereinbaren. Schwerbehinderten Bewerbern/-innen wird bei gleicher Eignung der Vorzug gegeben.

Bewerbungen mit Lebenslauf, wesentlichen Zeugnissen, beglaubigten Kopien aller Urkunden, Darstellung des beruflichen und wissenschaftlichen Werdegangs, einer strukturierten Liste der wissenschaftlichen Arbeiten, Liste von längerfristig geplanten Forschungszielen, Nachweis der Lehrtätigkeit, Lehrkonzept, zusammengefassten Bewerbungsbogen (abrufbar unter: www.medizin.uni-halle.de → Medizinische Fakultät → Berufungen) sowie maximal zehn Sonderdrucken werden unter Angabe der Dienst- und Privatanschrift **innerhalb von sechs Wochen nach Erscheinen** dieser Anzeige an folgende Adresse erbeten: **Martin-Luther-Universität Halle-Wittenberg, Dekan der Medizinischen Fakultät, 06097 Halle (Saale).**

Zertifikat seit 2009 audit familiengerechte hochschule

W222823R

---

UNIVERSITY OF CAMBRIDGE

A world of opportunities

**www.cam.ac.uk/jobs/**

## University Lectureship

Department of Pharmacology

£37,012 - £46,846 pa

Applications are invited for a University Lectureship in the Department of Pharmacology with effect from 1 October 2012 or as soon as possible thereafter. The Department offers excellent facilities for teaching and research and has particular interests in cell signalling, neurobiology, membrane transporters and ion channels. Priority will be given to applications from candidates with research interests within the broad field of genetic approaches to Pharmacology (including but not limited to pharmacogenomics, opto-genetics, novel approaches using transgenic animal models and application of approaches from structural biology, si RNA, mRNA splicing to pharmacological problems).

**Appointments will be made at University Lecturer level with a probationary period of five years, with appointment to the retiring age thereafter. A full description of the teaching and research activities in the Department can be found at www.phar.cam.ac.uk Prospective candidates may contact the Head of Department, Professor Peter McNaughton, to discuss the post Tel: (01223) 334012, email: pam42@cam.ac.uk**

**Applications, to include a CV, cover sheet (CHRIS/6, Parts I and III only) including the names and addresses of three referees, a brief statement (two sides maximum) of future research plans and a list of publications, should be submitted to the Departmental Administrator, Dr Jo Dekkers, Department of Pharmacology, Tennis Court Road, Cambridge, CB2 1PD, Tel: (01223) 334002, e-mail: recruitment@phar.cam.ac.uk Quote Reference: PL14492. Closing date: 16 April 2012. Interview date(s): Early May 2012**

**The University values diversity and is committed to Equality of Opportunity.**

U222948R

---

University of St Andrews

# Scottish Oceans Institute, School of Biology Director

**University Marine Biological Station, Millport**

The Scottish Oceans Institute at the University of St Andrews is recruiting a leading marine scientist as the Director for the Biological Station Millport (UMBSM). This opportunity arises from a joint venture between the Universities of London and St Andrews and sits within the MASTS community. You will be expected to develop the academic potential of UMBSM as part of a range of successful research units and research centres already operating within the Scottish Oceans Institute. New investment in infrastructure is being made at the UMBSM as part of its development plan. This is an opportunity for a high achieving individual to lead a strong research - and teaching-led agenda in marine science and to integrate this within the substantial opportunities presented by the collaboration and resources presented by two of the UK's leading academic institutions. If you would like to express an interest in this position then please contact Professor Ian Boyd, Director of the Scottish Oceans Institute (ilb@st-andrews.ac.uk).

**Closing date: 30 April 2012.**
**Please quote ref: SK1107**

**We encourage applicants to apply online https://www.vacancies.st-andrews.ac.uk/welcome.aspx however if you are unable to do this, please call +44 (0)1334 462571 for an application pack.**

The University of St Andrews is a charity registered in Scotland (No SC013532).

**www.st-andrews.ac.uk**

University of St Andrews

**The University is committed to equality of opportunity**

U222828R

---

Bringing jobseekers and recruiters together.

**Academic • Industry • Government**

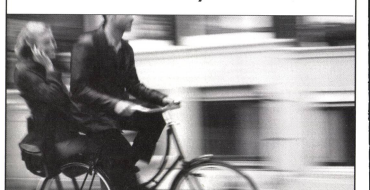

Search now at **naturejobs.com**

naturejobs

making science work

Philipps Universität Marburg

synmikro

MPI

The Philipps-Universität Marburg and the Max Planck Institute for Terrestrial Microbiology have recently established a center for Synthetic Microbiology, SYNMIKRO. Supported by the state of Hessen within its excellence program LOEWE, SYNMIKRO focuses on basic research in synthetic biology on all levels of microbial function, ranging from the development of regulatory circuits, genetic codes and metabolic pathways to the synthesis of new minimal cells and microbial communities.

In its next phase of expansion, SYNMIKRO invites applications for

## Independent Research Group Leader positions (E15 TV-H) in the areas:
## Quantitative analysis of metabolic networks
## Development of synthetic circuits
## Reprogramming of the genetic code
## Molecular evolution, metagenomics and prokaryotic biodiversity

at the Philipps-Universität Marburg. We seek individuals with an outstanding track record in the listed research areas. Successful candidates are expected to pursue research projects connected to the activities of Synmikro as described at **www.synmikro.de.**

We provide attractive start-up packages and research funding, and offer teaching associations within the faculties of biology or chemistry, depending on the successful candidate's background.

The appointment is limited for a period of 4 years, with a 1-year extension after a positive evaluation in the third year and offers the opportunity for further scientific qualification - within the scope of the assigned tasks.

Informal inquiries can be directed to Prof. Dr. Bruno Eckhardt, Director SYNMIKRO, Philipps-Universität Marburg, **director@synmikro.uni-marburg.de.**

We support women and particularly invite them to apply. Applicants with children are welcome - the Philipps-University is certified as a family friendly university. Sharing a full-time position (§ 8 Abs. 2 Satz 1 HGlG) as well as a reduction of working time is possible. Applicants with a disability as described in SGB IX (§ 2 Abs. 2, 3) will be preferred in case of equal qualifications.

Please submit your application preferentially in one PDF file since application documents will not be returned.

**Applications should be submitted by, April 10th, 2012 to info@synmikro.uni-marburg.de. The application should contain the following information in a single pdf-document: (1) cover letter, (2) curriculum vitae, including a list of publications, (3) summary of research achievements, (4) research plan, (5) statement of teaching interests and experience, if applicable, (6) previous and current funding, if applicable, (7) names and contact details of five referees.**

W222803R

Philipps Universität Marburg

synmikro

MPI

The Philipps-Universität Marburg and the Max Planck Institute for Terrestrial Microbiology have recently established a center for Synthetic Microbiology, SYNMIKRO. Supported by the state of Hessen within its excellence program LOEWE, SYNMIKRO focuses on basic research in synthetic biology on all levels of microbial function, ranging from the development of regulatory circuits, genetic codes and metabolic pathways to the synthesis of new minimal cells and microbial communities.

In its next phase of expansion, SYNMIKRO invites applications for an

## Independent Research Group Leader position (E15 TV-H) in the areas:
## Computational Biology / Mathematical modeling of microbial systems

at the Philipps-Universität Marburg. We seek a person with an outstanding track record in the quantitative analysis and modeling of biological systems. Successful candidates are expected to pursue research projects connected to the activities of Synmikro as described at **www.synmikro.de.** Experimental work will be encouraged and opportunities will be offered.

We provide an attractive start-up package and research funding, and offer teaching associations with the faculties of mathematics and computer science, biology, or physics, depending on the successful candidate's background.

The appointment is limited for a period of 4 years, with a 1-year extension after a positive evaluation in the third year and offers the opportunity for further scientific qualification - within the scope of the assigned tasks.

Informal inquiries can be directed to Prof. Dr. Bruno Eckhardt, Director SYNMIKRO, Philipps-Universität Marburg, **director@synmikro.uni-marburg.de.**

We support women and particularly invite them to apply. Applicants with children are welcome - the Philipps-University is certified as a family friendly university. Sharing a full-time position (§ 8 Abs. 2 Satz 1 HGlG) as well as a reduction of working time is possible. Applicants with a disability as described in SGB IX (§ 2 Abs. 2, 3) will be preferred in case of equal qualifications.

Please submit your application preferentially in one PDF file since application documents will not be returned.

**Applications should be submitted by, April 10th, 2012 to info@synmikro.uni-marburg.de. The application should contain the following information in a single pdf document: (1) cover letter, (2) curriculum vitae, including a list of publications, (3) summary of research achievements, (4) research plan, (5) statement of teaching interests and experience, if applicable, (6) previous and current funding, if applicable, (7) names and contact details of five referees.**

W222802R

**Small cog, big machine?**

Jobs that make a difference.

Each week. *Naturejobs.*

naturejobs

## GROUP LEADER – APPLIED STATISTICS

An experienced Applied Statistician is required at Rothamsted Research to collaborate with scientists and to develop statistical applications and methodology required by Rothamsted's research programmes. These cover a very wide range of different scientific approaches and generate quantitative data from many different experimental platforms including our established long-term agricultural and ecology experiments and the latest high throughput molecular biology technologies such as Next Generation Sequencing. Our projects require varying levels of statistical input including multivariate methods, quantitative genetics and parameter estimation.

The post holder will collaborate with colleagues on areas of statistical research and will lead a small group of applied statisticians. This group works closely with scientists across the Institute, providing introductory statistical training for staff and PhD students as well as statistical consultancy. The post holder would have both a managerial role in the applied statistics group and provide technical expertise as well as undertaking more challenging applied statistical problems arising from research projects. The post holder will also be responsible for investigating and establishing new collaborations both within and outside Rothamsted.

The ideal candidate will have considerable experience in applying statistical methods to scientific data, preferably in the area of crop/agricultural sciences and agro-ecology and be familiar with the challenges of analysing field and laboratory data. A strong track record of publishing in applied statistics and making statistical contributions to published high profile biological research is essential. Applicants should have a PhD in Applied Statistics or related subject or be able to demonstrate (through publications) that they have equivalent experience.

The post is an indefinite full time appointment with a starting salary normally in the region of £42,769 to £47,521 per annum.

***Apply by application form only, available with further particulars from www.rothamsted.ac.uk or from the HR Group, Rothamsted Research, Harpenden, Herts AL5 2JQ, rres.hr@rothamsted.ac.uk Please quote reference 1181.***

***Closing date: 20 April 2012***

An Equal Opportunities Employer.

As users of the disability symbol, Rothamsted Research guarantees to interview all disabled applicants who meet the minimum criteria for our vacancies.

ROTHAMSTED RESEARCH

U222953R

## UNIVERSITY OF MINNESOTA

### Department Head of Pharmacology University of Minnesota Medical School

The University of Minnesota Medical School seeks applications from exceptional scientists and academic leaders for the position of **Head of the Department of Pharmacology**. The successful candidate will be responsible for the functions of the Department that include its research, educational, and service activities that support the mission of the Medical School and University. As Head of the Department, the successful candidate will also have the opportunity to recruit outstanding faculty in basic and translational aspects of pharmacology and to develop collaborations and connections to other Departments, Institutes and Centers across the Academic Health Center. The Department Head will report to the Dean of the Medical School.

All candidates must have a PhD and /or MD degree and qualify for appointment as a tenured professor of the University. Candidates will have an internationally recognized research program and strong record of extramural support. The candidate must also have an outstanding record of academic leadership as well as excellent interpersonal, team building and communications skills. Candidates must have a strong commitment to graduate, undergraduate and professional medical education and be dedicated to enhancing and supporting diversity within the Department.

For details about the Department please consult: http://www.pharmacology.med.umn.edu/.

Please apply online at employment.umn.edu/applicants/Central?quickFind=101682. Please attach a cover letter, curriculum vitae and statement (1-page) on academic leadership and its role in public higher education. For questions please contact Ms. Jennifer Skar (skar0049@umn.edu). Applications will be reviewed continuously until the position is filled.

The University of Minnesota is an Equal Opportunity Educator and Employer. The Department of Pharmacology strongly encourages all individuals to apply regardless of gender, ethnicity or background and is committed to a diverse research and teaching environment.

NW222914R

## THE HONG KONG UNIVERSITY OF SCIENCE AND TECHNOLOGY

### Division of Life Science
### Faculty Positions

HKUST is a publicly-funded research university with strong graduate programs. The Division of Life Science (http://life-sci.ust.hk/) was established in 2010 through the integration of the Departments of Biochemistry and Biology with the goal of raising life science teaching and research at HKUST to a new level of excellence. The Division currently has 29 faculty members representing a broad range of significant expertise including cellular regulation and signalling, cancer biology, developmental biology, molecular and cellular neuroscience, macromolecular structure and function, marine and environmental science, and biotechnology and medicinal biochemistry. This newly formed Division is expected to grow substantially in terms of academic staff, programs, resources and facilities in the next five years.

Applications are invited for two tenure-track positions at Assistant Professor and Associate Professor ranks, specifically in the following areas:

(a) Developmental Biology/Immunology: candidates using model organisms such as fly, worm and zebrafish are preferred;
(b) Environmental Biology/Marine Biology/Ecology: candidates working on the marine environments at the organismic level or above are preferred.

Applicants of exceptional qualifications and prominence at full Professor rank in areas that complement and enhance existing strengths of the Division will also be considered. The appointees are expected to establish an internationally competitive independent research program. Teaching responsibilities include undergraduate and postgraduate courses.

Starting salary will be commensurate with qualifications and experience. Fringe benefits including medical/dental benefits and annual leave will be provided. Housing benefits will also be provided where applicable. Initial appointment will normally be on a three-year contract, renewable subject to mutual agreement. A gratuity will be payable upon successful completion of contract.

Applications indicating the areas of expertise [in area (a) or (b) as listed above], together with a curriculum vitae, a short statement on research interests and the names and addresses of three referees should be sent to the **Chair of the Life Science Search and Appointments Committee (Prof. Yung Hou Wong), c/o The Secretary of LIFS S&A Committee, Division of Life Science, The Hong Kong University of Science and Technology, Clear Water Bay, Kowloon, Hong Kong** (email: lifssearch@ust.hk) before **30 April 2012**. Review of applications will start in May 2012 and will continue until the positions are filled.

*(Information provided by applicants will be used for recruitment and other employment-related purposes.)*

JP222790R


**Stay in touch** with the latest scientific news and research, anytime, anywhere

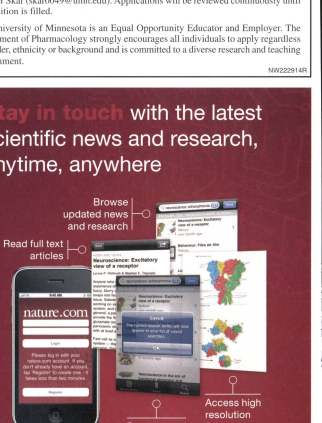
Browse updated news and research
Read full text articles
Neuroscience: Excitatory view of a receptor
nature.com
Set up saved searches
Access high resolution figures

**With the new nature.com mobile app you can read scholarly content quickly and comfortably wherever you are**

Download now at **nature.com/mobileapps**

Available on the App Store

iPhone is a trademark of Apple Inc.

nature publishing group npg

## Professor and Chair
## Department of Statistics
## The University of Nebraska-Lincoln

The University of Nebraska-Lincoln invites applications for the position of Professor and Chair, Department of Statistics. This is a full-time, 12-month appointment responsible for the academic leadership of the research, teaching and service activities in the Department of Statistics as well as for the professional development of the faculty and staff. In this position, you will have a primary focus on the continued development of the Department as an internationally recognized program in statistics along with the opportunity and expectation for developing a high level, internationally recognized campus-wide bioinformatics and computational biology initiative. The Department Chair reports to the Dean of the College of Arts and Sciences (CAS), and deans of the College of Agricultural Sciences and Natural Resources (CASNR) and the Agricultural Research Division (ARD) within the Institute of Agriculture and Natural Resources (IANR) on matters related to the department.

To succeed in this role, you will need an earned doctoral degree in Statistics or closely related field; must meet qualifications for appointment as a tenured professor; and have a record of excellent interpersonal, organizational, and leadership skills. Previous administrative experience is preferred.

If this sounds like the job for you, please access the web site http://employment.unl.edu. Search for requisition number 120174. Complete the faculty academic administrative information form. Attach a letter of application, curriculum vitae, and contact information for three professional references.

Review of applications will begin May 15, 2012, and will continue until the position is filled or the search is closed.

The University of Nebraska has an active National Science Foundation ADVANCE gender equity program, and is committed to a pluralistic campus community through affirmative action, equal opportunity, and dual careers.

NW222901R

SCHOOL OF MEDICINE
CASE WESTERN RESERVE UNIVERSITY

## Chair and Professor
## Department of Genetics and Genome Sciences
## Case Western Reserve University

The School of Medicine at Case Western Reserve University invites applications and nominations for the position of Chair of the Department of Genetics and Genome Sciences. The Department has a long- standing history of success, and is looking for an outstanding faculty member with the leadership and vision necessary to develop and strengthen an innovative research program that integrates basic genetics and genomics research with clinical and translational research. The Department has outstanding graduate programs, training both Ph.D. and genetic counseling students as well as a Clinical Genetics program run in collaboration with our main hospital affiliate, University Hospitals. The new chair will be supported by a highly competitive recruitment package.

The unified campus at CWRU facilitates collaborative interactions among scientists in the Schools of Medicine, Engineering, and Arts and Sciences, and with researchers in nearby affiliated hospitals and the Cleveland Center for Membrane and Structural Biology. Research missions are supported by excellent core facilities, including behavioral testing, whole animal imaging, confocal/multi-photon imaging, structural biology, proteomics, next-generation sequencing, bioinformatics, pluripotent stem cells, and a recently expanded and renovated animal facility that maintains a state-of-the-art transgenic core.

Applicants for this position must have a Ph.D. and/or an M.D. degree with a distinguished record of scientific achievement, demonstrated leadership skills, and a commitment to education and mentorship of students and faculty. Appointment as Professor of Genetics and Genome Sciences with tenure is anticipated and requires evidence of a productive and excellent research program recognized at the national/international level.

Please submit a CV and letter of interest addressing research, educational, administrative and leadership goals and vision to K. Palczewski Ph.D., Genetics and Genome Sciences Chair Search Committee, c/o Cami Thompson (Cami@case.edu).

In employment, as in education, Case Western Reserve University is committed to Equal Opportunity and Diversity. Women, veterans, members of underrepresented minority groups, and individuals with disabilities are encouraged to apply.

Case Western Reserve University provides reasonable accommodations to applicants with disabilities. Applicants requiring a reasonable accommodation for any part of the application and hiring process should contact the Office of Inclusion, Diversity and Equal Opportunity at 216-368-8877 to request a reasonable accommodation. Determinations as to granting reasonable accommodations for any applicant will be made on a case-by-case basis.

http://genetics.case.edu

NW222864R

**REPROGRAPHICS: CTT**, London E17 6BU UK and **The Charlesworth Group,** Wakefield, UK.
**PRINTED BY: William Gibbons & Sons Ltd,** UK; **Publishers Press**, Lebanon Junction, Ky, USA and **Obun Printing Co. Inc,** Tokyo, Japan

# VISITING BOB

*Life insurance.*

BY JOHN GILBEY

One of the great advantages of being a writer is the fascinating folk you meet. Take Bob, for example. I first talked to him in Palo Alto about eight years ago. We chatted, got on, shared some bizarre and unlikely anecdotes — but like so many chance encounters, I didn't think much more about it. Then, out of the blue, I was invited to write Bob's biography. He'd read my published stuff, liked it, and asked me to document his career in the Valley. To say I was pleased would be a major understatement.

A week later I was ensconced in a wood-panelled corner office at Bob's host institute, overlooking the coffee shops of University Avenue, with an expenses-paid contract to extract from Bob all his tales of the old days that were fit to print — a constraint that probably reduced the size of the book by half. It was one of the most enjoyable and intriguing jobs I've ever had.

Bob and I hadn't talked for several months when the call came, and I felt a sinking feeling when I realized that the caller wasn't Bob but Emily, one of the cloud of crazily bright postdocs that he employs as assistants. Like all of us, Bob wasn't getting any younger.

"Hi John, I thought I'd better call you about Bob…" Here it comes, I thought. "He's got some fairly serious health problems, and he's been asking for you."

I thought about this. "Can't you put him on the line?" There was a regretful, apologetic pause. "I'm afraid not, he can't interpret low-bandwidth AV now. Would you be able to visit him?" I was still pondering when she added: "Just one thing, don't leave it too long…"

After the ten-hour flight, what I really wanted was beer, food and sleep. At a pinch, I'd skip the food. Emily, however, was insistent that I talk to Bob first. Looking into his room from an observation window, it seemed more chaotic than I remembered, but it was the primal waft of organic decay — nauseating even from the next room — that shocked me. I glanced across at Emily, who gave a slow nod of the head.

"Hi, Bob, how are you doing?" The response was slow, like someone waking from an anaesthetic. "John? Is that you?" The voice was stretched and blurred, but the sensory unit rotated and waddled towards the window like an inebriated desk lamp.

"I really appreciate you coming over," muttered Bob. "As you can see, things aren't going too well… I don't know how much Emily has told you, but it looks like I only have a month or so left. I've already lost some peripheral stuff — that's why I can't use remote comms — but it is creeping into my long-term memory and… heck, I'm scared.

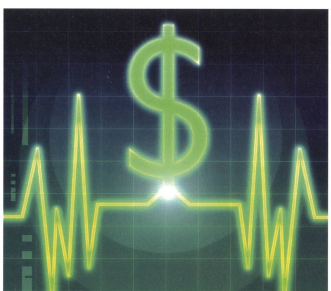

JACEY

"I need you to buy me a few more years… Just a few…" His voice faded. "Sorry, I'm going to have to rest for a while now — just follow the money…" When I looked round, I found that Emily had tears in her eyes — which made two of us.

"What does he need?" I asked Emily. She sighed and referred to an internal list — a long one. Many of Bob's systems were well beyond their technical 'end of life': the organic wet-ware circuits that formed most of his unique design were literally rotting, and had only ever been made as research tools, not production systems. No one seemed to know whether the technology could be replicated with the skills now available — or even if it would be legal — but there seemed no way that Bob's consciousness could be ported to another infrastructure.

➲ **NATURE.COM**
Follow Futures on Facebook at:
go.nature.com/mtoodm

We found a bar, drank several beers, and tried to sketch out a budget for a rebuild. The numbers were astronomical, and it was clear from Emily's terse analysis that all attempts to gather funding through the usual channels had failed.

Sleep wasn't an option. As headlights panned across the ceiling of my motel room I fought to find a solution. "Follow the money," Bob had said. Bob — the 'Bucket of Brains' they used to call him, much to his annoyance. There were no physical brains in the system. Instead, the reasoning power of 20 top scientists of the day had been distilled into a semi-organic structure that — to everyone's surprise — had fought schizophrenia and paranoia to emerge as the composite personality of Bob. The first, and last, of his kind. "Follow the money." Easy to say, but why me?

The coffee was so strong that my vision took on the character of a shaky film noir — but it fought the jet lag. Emily toyed with her green tea and tried not to look concerned. I asked the critical question: "When I was here last, I left a set of notebook files — stuff that Bob wouldn't let me use in the book, or even have copies of. Are they still here?"

Emily shrugged slightly. "We never throw anything away, that's part of our culture."

I smiled with relief, thinking of all the doors — and bank accounts — that were about to open.

Emily looked puzzled. "I'll have to check," I qualified carefully, "but from memory, those notes cover every major scandal — personal, corporate and political — in the Valley between 2015 and 2035. Bob's component consciousnesses were deeply involved — more to the point, the other folk implicated are now in very senior posts and definitely won't want this stuff made public…'Follow the money…'"

The mug of tea dropped to the table top. "You mean, he wants to blackmail people to raise the money?" Emily exclaimed in shock.

"It certainly looks like it," I replied with a smile. "I'm just beginning to realize how human Bob is." ■

**John Gilbey** *(gilbey@bcs.org.uk) is a writer who knows a thing or two about mysterious inner rottings — but not blackmail, honest…*

UltraMAB™

# The Ultra Specific IHC Antibodies

## Validated against >10,000 human antigens

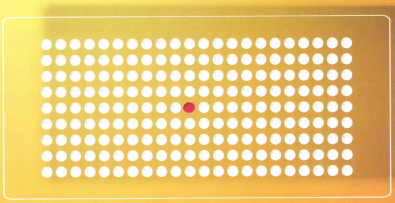

Visit Us at USCAP 2012 Booth #827

## Seeing is Believing

Through the use of high-density protein microarray technology developed by OriGene, our team is working to provide a new generation of monoclonal antibodies for use in IHC evaluations and pathology.

UltraMAB™ monoclonal antibodies are the industry's only specificity-verified reagents that have been validated against >10,000 human protein antigens. These unique tools are produced from mammalian protein antigens and quality checked for specificity, guaranteeing superior performance and exclusive specificity to their intended target. Accelerate your research and try UltraMAB today!

ORIGENE
Your Gene Company
origene.com/UltraMAB

ZS-BIO is the exclusive distributor of UltraMAB in China.

The products presented on this page are intended for research purposes only. These products are not intended to be used for therapeutic or diagnostic purposes in human or animals.
UltraMAB™ is a trademark of OriGene Technologies Inc. 2012

Cancer
Development
Endocrinology
Glycobiology
Immunology
Neuroscience
Proteases
Signal Transduction
Stem Cells

# immunoLOGICAL

Infiltration of tumors by regulatory T (Treg) cells suppresses anti-tumor immune responses and promotes tumor growth. As a result, mechanisms to inhibit Treg cell differentiation, expansion, recruitment, and function are being widely explored. With over 25 years of experience developing and manufacturing immunology-related research reagents, R&D Systems is the logical choice for products you can trust.

- More than **200** different antibodies for Treg cell research
- Treg Cell Selection & Multi-color Flow Cytometry Kits
- Bioactive proteins for Treg cell differentiation & functional studies

Inhibition of T Cell Proliferation by LRRC32

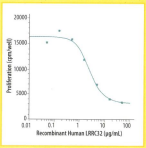


LAP Suppresses TGF-β-induced Inhibition of Mouse T helper Cells

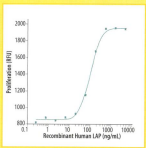


CTA-4 Inhibition of B7-1/CD80-induced IL-2 Secretion

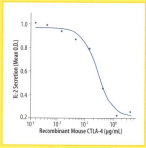


**Visit our website at www.RnDSystems.com/Treg**

**R&D Systems, Inc.** www.RnDSystems.com
**R&D Systems Europe, Ltd.** www.RnDSystems.co.uk
**R&D Systems China Co., Ltd.** www.RnDSystemsChina.com.cn

For research use only. Not for use in diagnostic procedures.

R&D SYSTEMS®